frontiers | Research Topics

Pharmacological actions of drugs in the brain: Exploring the intricacies and potential therapeutic applications

Edited by
Christina Dalla, Giuseppe Di Giovanni, Tanya Calvey and Nouria Lakhdar-Ghazal

Published in
Frontiers in Pharmacology
Frontiers in Neuroscience

ISSN 1664-8714
ISBN 978-2-8325-5469-2
DOI 10.3389/978-2-8325-5469-2

About Frontiers

Frontiers is more than just an open access publisher of scholarly articles: it is a pioneering approach to the world of academia, radically improving the way scholarly research is managed. The grand vision of Frontiers is a world where all people have an equal opportunity to seek, share and generate knowledge. Frontiers provides immediate and permanent online open access to all its publications, but this alone is not enough to realize our grand goals.

Frontiers journal series

The Frontiers journal series is a multi-tier and interdisciplinary set of open-access, online journals, promising a paradigm shift from the current review, selection and dissemination processes in academic publishing. All Frontiers journals are driven by researchers for researchers; therefore, they constitute a service to the scholarly community. At the same time, the *Frontiers journal series* operates on a revolutionary invention, the tiered publishing system, initially addressing specific communities of scholars, and gradually climbing up to broader public understanding, thus serving the interests of the lay society, too.

Dedication to quality

Each Frontiers article is a landmark of the highest quality, thanks to genuinely collaborative interactions between authors and review editors, who include some of the world's best academicians. Research must be certified by peers before entering a stream of knowledge that may eventually reach the public - and shape society; therefore, Frontiers only applies the most rigorous and unbiased reviews. Frontiers revolutionizes research publishing by freely delivering the most outstanding research, evaluated with no bias from both the academic and social point of view. By applying the most advanced information technologies, Frontiers is catapulting scholarly publishing into a new generation.

What are Frontiers Research Topics?

Frontiers Research Topics are very popular trademarks of the *Frontiers journals series*: they are collections of at least ten articles, all centered on a particular subject. With their unique mix of varied contributions from Original Research to Review Articles, Frontiers Research Topics unify the most influential researchers, the latest key findings and historical advances in a hot research area.

Find out more on how to host your own Frontiers Research Topic or contribute to one as an author by contacting the Frontiers editorial office: frontiersin.org/about/contact

Pharmacological actions of drugs in the brain: Exploring the intricacies and potential therapeutic applications

Topic editors

Christina Dalla — National and Kapodistrian University of Athens, Greece
Giuseppe Di Giovanni — University of Magna Graecia, Italy
Tanya Calvey — University of Cape Town, South Africa
Nouria Lakhdar-Ghazal — Mohammed V University, Morocco

Citation

Dalla, C., Di Giovanni, G., Calvey, T., Lakhdar-Ghazal, N., eds. (2024). *Pharmacological actions of drugs in the brain: Exploring the intricacies and potential therapeutic applications*. Lausanne: Frontiers Media SA. doi: 10.3389/978-2-8325-5469-2

Table of contents

frontiers | Frontiers in Pharmacology

TYPE Editorial
PUBLISHED 11 September 2024
DOI 10.3389/fphar.2024.1486719

OPEN ACCESS

EDITED AND REVIEWED BY
Nicholas M. Barnes,
University of Birmingham, United Kingdom

*CORRESPONDENCE
Giuseppe Di Giovanni,
giuseppe.digiovanni@unicz.it

RECEIVED 26 August 2024
ACCEPTED 05 September 2024
PUBLISHED 11 September 2024

CITATION
Dalla C, Lakhdar-Ghazal N, Calvey T and Di Giovanni G (2024) Editorial: Pharmacological actions of drugs in the brain: exploring the intricacies and potential therapeutic applications.
Front. Pharmacol. 15:1486719.
doi: 10.3389/fphar.2024.1486719

Editorial: Pharmacological actions of drugs in the brain: exploring the intricacies and potential therapeutic applications

Christina Dalla[1], Nouria Lakhdar-Ghazal[2], Tanya Calvey[3,4] and Giuseppe Di Giovanni[5]*

[1]Second Department of Obstetrics - Gynecology, Aretaieio Hospital, School of Medicine, National and Kapodistrian University of Athens, Athens, Greece, [2]Mohammed V University Rabat, Rabat, Morocco, [3]Department of Human Biology, Faculty of Health Sciences, University of Cape Town, Cape Town, South Africa, [4]Neuroscience Institute, University of Cape Town, Cape Town, South Africa, [5]Department of Medical and Surgical Sciences, University of Magna Graecia, Catanzaro, Italy

KEYWORDS

neuropharmacology, brain-drug interactions, therapeutic applications, neurological disorders, signal pathways

Editorial on the Research Topic
Pharmacological actions of drugs in the brain: exploring the intricacies and potential therapeutic applications

The brain's intricate and dynamic nature has made it a focal point of pharmacological research, with the goal of understanding how various drugs interact with its complex systems (Agid et al., 2007). This Research Topic, "Pharmacological Actions of Drugs in the Brain: Exploring the Intricacies and Potential Therapeutic Applications," brings together a diverse Research Topic of 13 articles, each shedding light on different aspects of this field. Notably, this Research Topic is part of a Research Topic dedicated to the Mediterranean Neuroscience Society Conference 2023, held in Tunis, Tunisia (MNS, 2023). These studies explore the mechanisms by which drugs modulate brain activity and behavior, offering insights into potential therapeutic avenues for a range of neurological and psychiatric conditions.

The first study in this Research Topic by Maric et al. explores the neural substrate for ghrelin's effects on ingestive, motivated, and anxiety-like behaviors, tracing its journey from the stomach to the locus coeruleus. This study highlights the complexity of gut-brain interactions and the potential of targeting such pathways for therapeutic interventions in conditions such as anxiety and eating disorders, with a degree of sex divergence.

In another significant contribution, Karimi et al. investigate the effects of umbelliprenin, a natural coumarin product, on mitigating autistic-like behaviors in a mouse model of maternal separation stress. The study's findings, which involve the modulation of MECP2 expression and oxidative stress, underscore the therapeutic potential of targeting epigenetic and oxidative pathways in autism spectrum disorders.

Traditional Chinese medicine (TCM) has long been a source of pharmacological exploration, and the review by Lv et al. investigates into the pharmacological mechanisms of antidepressant active ingredients in TCM. By focusing on adult hippocampal neurogenesis, this review provides a comprehensive overview of how ancient medicinal practices could be integrated within modern neuroscience, in order to address depression.

Anesthesia, a cornerstone of modern medicine, also features prominently in this Research Topic. Huang et al.'s brief research report reveals how propofol-induced anesthesia directly inhibits glutamatergic neurons in the lateral hypothalamus, offering new insights into the neural mechanisms underlying anesthetic states and their potential long-term effects on brain function.

The role of oxidative stress in brain pathology is further explored by Zhu et al., who demonstrate the protective effects of Edaravone dexborneol in experimental subarachnoid hemorrhage. This study contributes to the growing body of evidence supporting the Keap1/Nrf2 signaling pathway as a target for neuroprotective strategies.

Depression, a leading cause of disability worldwide, is examined in the context of gut-brain interactions by Li et al., who show how quercetin reshapes gut microbiota and modulates brain metabolism to regulate depression-like behaviors. This research underscores the importance of considering the gut-brain axis in developing novel antidepressant therapies.

The neurobiological effects of drugs also extend to substance abuse, as demonstrated by Govender et al., who investigate the impact of ibogaine on myelination markers following morphine administration. Their findings suggest a potential role for ibogaine in addressing the neurobiological underpinnings of addiction and its associated neural changes.

Hudetz's study on macrostimulation and anesthetic state-dependent, effective connectivity of cortical neurons offers a novel approach to understanding how anesthesia alters neural circuits, with implications for improving anesthesia techniques and patient outcomes.

The therapeutic potential of natural compounds is further explored in the mini review by Wang et al., which examines the antidepressant activity of mushroom and fungus extracts in rodent models. This scoping review highlights the promise of these natural products in developing new treatments for depression.

Alotaibi et al. investigate the neurotoxic effects of pyrethroids and the protective role of chitosan-encapsulated curcumin nanoparticles, using a combination of morphometric, immunofluorescence, and *in silico* approaches. Their study provides valuable insights into the potential of nanoparticle-based therapies in neurodegenerative diseases.

The complex pharmacological effects of stimulant medications in adults with ADHD are explored by Thunberg et al., who provide a nuanced analysis of the categorical and dimensional aspects of these effects. Their work contributes to a better understanding of how stimulants affect brain function in both affected and healthy populations.

Finally, Yang et al. present a systematic review on the roles and mechanisms of natural herbal extracts in treating cerebral ischemia, offering a comprehensive overview of how these extracts can be harnessed to protect the brain from ischemic damage.

Closing this Research Topic, Li et al. explore the neuroprotective effects of lutein, demonstrating its ability to inhibit glutamate-induced apoptosis in HT22 cells via the Nrf2/HO-1 signaling pathway. This study reinforces the potential of targeting oxidative stress pathways in developing therapies for neurodegenerative diseases.

Together, these 13 articles not only deepen our understanding of the pharmacological actions of drugs in the brain, but also highlight the potential for developing new therapeutic strategies to address a range of neurological and psychiatric disorders. The insights gained from these studies are poised to inform future research and clinical practice, paving the way for more effective treatments and better patient outcomes.

We hope that more discussion and insights will be presented at the next Mediterranean Neuroscience Society Conference 2025, held in Crete, Greece. For more details, please visit https://www.medneuroscisociety.org/.

Author contributions

CD: Writing–original draft, Writing–review and editing. NL-G: Writing–original draft, Writing–review and editing. TC: Writing–original draft, Writing–review and editing. GD: Writing–original draft, Writing–review and editing.

Conflict of interest

The authors declare that the research was conducted in the absence of any commercial or financial relationships that could be construed as a potential conflict of interest.

The author(s) declared that they were an editorial board member of Frontiers, at the time of submission. This had no impact on the peer review process and the final decision.

Publisher's note

References

Agid, Y., Buzsáki, G., Diamond, D., Frackowiak, R., Giedd, J., Girault, J. A., et al. (2007). How can drug discovery for psychiatric disorders be improved?. *Nat Rev Drug Discov* 6, 189–201. doi:10.1038/nrd2217

MNS (2023). Available at: https://www.medneuroscisociety.org/Interview-with-Prof-Giuseppe-Di-Giovanni-President-of-the-Mediterranean-Neuroscience-Society_A_44.html (August 26, 2024).

frontiers | Frontiers in Pharmacology

TYPE Original Research
PUBLISHED 13 November 2023
DOI 10.3389/fphar.2023.1286805

OPEN ACCESS

EDITED BY
Christina Dalla,
National and Kapodistrian University of Athens, Greece

REVIEWED BY
Patricia De Gortari,
National Institute of Psychiatry Ramon de la Fuente Muñiz (INPRFM), Mexico
Mario Perello,
National Scientific and Technical Research Council (CONICET), Argentina
Andreas Stengel,
University Hospital Tübingen, Germany

*CORRESPONDENCE
Karolina P. Skibicka,
kps5783@psu.edu

RECEIVED 31 August 2023
ACCEPTED 23 October 2023
PUBLISHED 13 November 2023

CITATION
Maric I, López-Ferreras L, Bhat Y, Asker M, Börchers S, Bellfy L, Byun S, Kwapis JL and Skibicka KP (2023), From the stomach to locus coeruleus: new neural substrate for ghrelin's effects on ingestive, motivated and anxiety-like behaviors.
Front. Pharmacol. 14:1286805.
doi: 10.3389/fphar.2023.1286805

From the stomach to locus coeruleus: new neural substrate for ghrelin's effects on ingestive, motivated and anxiety-like behaviors

Ivana Maric[1,2], Lorena López-Ferreras[1], Yashaswini Bhat[2], Mohammed Asker[1], Stina Börchers[1,2], Lauren Bellfy[3,4], Suyeun Byun[2], Janine L. Kwapis[3,4] and Karolina P. Skibicka[1,2,4]*

[1]Institute for Neuroscience and Physiology, University of Gothenburg, Gothenburg, Sweden, [2]Department of Nutritional Sciences, Pennsylvania State University, State College, PA, United States, [3]Department of Biology, Pennsylvania State University, State College, PA, United States, [4]Huck Institutes of the Life Sciences, Pennsylvania State University, State College, PA, United States

Ghrelin, a stomach-derived orexigenic hormone, has a well-established role in energy homeostasis, food reward, and emotionality. Noradrenergic neurons of the locus coeruleus (LC) are known to play an important role in arousal, emotion, cognition, but recently have also been implicated in control of feeding behavior. Ghrelin receptors (the growth hormone secretagogue receptor, GHSR) may be found in the LC, but the behavioral effects of ghrelin signaling in this area are still unexplored. Here, we first determined whether GHSR are present in the rat LC, and demonstrate that GHSR are expressed on noradrenergic neurons in both sexes. We next investigated whether ghrelin controls ingestive and motivated behaviors as well as anxiety-like behavior by acting in the LC. To pursue this idea, we examined the effects of LC GHSR stimulation and blockade on food intake, operant responding for a palatable food reward and, anxiety-like behavior in the open field (OF) and acoustic startle response (ASR) tests in male and female rats. Our results demonstrate that intra-LC ghrelin administration increases chow intake and motivated behavior for sucrose in both sexes. Additionally, females, but not males, exhibited a potent anxiolytic response in the ASR. In order to determine whether activation of GHSR in the LC was necessary for feeding and anxiety behavior control, we utilized liver-expressed antimicrobial peptide 2 (LEAP2), a newly identified endogenous GHSR antagonist. LEAP2 delivered specifically into the LC was sufficient to reduce fasting-induced chow hyperphagia in both sexes, but food reward only in females. Moreover, blockade of GHSR in the LC increased anxiety-like behavior measured in the ASR test in both sexes. Taken together, these results indicate that ghrelin acts in the LC to alter ingestive, motivated and anxiety-like behaviors, with a degree of sex divergence.

KEYWORDS

ghrelin, hindbrain, locus coeruleus (LC), food motivation, anxiety-like behavior, LEAP2

1 Introduction

The orexigenic peptide ghrelin is mainly produced by the stomach and acts on the brain to promote feeding behavior (Wren et al., 2000). Ghrelin acts via the growth hormone secretagogue receptor (GHSR), which is abundantly expressed in brain regions known to regulate homeostatic and hedonic feeding (Kojima et al., 1999). For example, the receptor is found in the hypothalamus and brainstem areas, as well as areas within the mesolimbic pathway (Zigman et al., 2006). Peripherally administered ghrelin has consistently been shown to increase appetite in satiated rodents and humans, and ghrelin injections into discrete regions such as the arcuate nucleus (Arc), lateral hypothalamus (LH), ventral tegmental area (VTA) or the nucleus of the solitary tract (NTS) are potently orexigenic (Tschop et al., 2000; Abizaid et al., 2006; Faulconbridge et al., 2008; Egecioglu et al., 2010; Skibicka and Dickson, 2011; López-Ferreras et al., 2017; Hyland et al., 2020; Barrile et al., 2023; Wald et al., 2023). Furthermore, ghrelin signaling at the level of the mesolimbic system enhances the motivation for food as well as substances of abuse (Jerlhag et al., 2009; Skibicka et al., 2011; You et al., 2022a; You et al., 2022b). Thus, ghrelin has a well-established role in maintaining energy homeostasis and driving motivated behaviors beyond nutritional needs (Andrews, 2011; Skibicka and Dickson, 2011; Menzies et al., 2013).

Ghrelin release is stimulated by metabolic stress and negative energy status, however psychological stressors such as restraint and social defeat have been demonstrated to also trigger ghrelin secretion (Asakawa et al., 2001; Cummings et al., 2001; Kristenssson et al., 2006; Patterson et al., 2013; McKay et al., 2021). Ghrelin is therefore suggested to be the interface between metabolic disorders and stress response-related mood disorders such as anxiety and depression (Chuang and Zigman, 2010). In line with this, calorie restriction and exogenous ghrelin injections have both been shown to be anxiolytic (Lutter et al., 2008; Alvarez-Crespo et al., 2012; Toufexis et al., 2016; Borchers et al., 2022a). Although some contradictory reports indicate an anxiogenic effect following ghrelin administration (Asakawa et al., 2001; Carlini et al., 2002), implying that there might be a bidirectional effect depending on experimental conditions, namely, the access to food, it is clear that the ghrelin system is a key component of emotionality responses. The precise mechanisms by which ghrelin controls mood remains unknown, but several brain regions important for regulation of emotional reactivity express the ghrelin receptor (Zigman et al., 2006; Alvarez-Crespo et al., 2012). Moreover, microinjections of ghrelin targeting the amygdala, hippocampus or dorsal raphe nucleus affect anxiety-like behaviors (Carlini et al., 2004).

Locus coeruleus (LC), however, is an unexplored substrate for ghrelin's effects on behavior. One previous study mapping out brain nuclei accessible to ghrelin present in the cerebrospinal fluid (CSF) reported uptake of fluorescein-labeled ghrelin in the LC (Cabral et al., 2013). The LC is a small nucleus located deep in the brain stem, well-established as the major source of norepinephrine (NE) in the brain and critically involved in arousal, cognition and emotionality control (Poe et al., 2020). Yet, more recent work has also put forth the idea that the LC is involved in control of feeding behavior - LC activity is suppressed during feeding and in turn, LC stimulation suppresses food intake in mice (Sciolino et al., 2022). While this work puts LC on the map of brain substrates of food intake control, it remains to be shown which metabolic or endocrine signals feed into this brain region to allow its participation in food intake control. Given the role of LC in regulation of emotionality and feeding behavior control, along with the key role of ghrelin in both processes, and the fact that at least CSF ghrelin can access the nucleus, LC emerges as a potential direct brain target of ghrelin. To our knowledge, however, the ability of ghrelin to directly act in the rat LC and functional implications of this action have not yet been reported. In the present study, we investigated the LC as a potential novel target for ghrelin's behavioral effects linked to appetite control, motivated behavior and emotional reactivity in male and female rats. We first sought to confirm the presence of GHSR in the LC of both sexes. Next, we determined the effects of LC GHSR pharmacological activation on food intake and motivated behavior for sucrose in male and female rats. Moreover, we determined whether ghrelin signaling in the LC modulates anxiety-like behavior, in both sexes. Finally, in order to determine whether LC GHSR activity is necessary for feeding and anxiety behavior control, we evaluated whether blockade of ghrelin receptors in the LC alters feeding, motivated, and anxiety behaviors. To increase the endogenous and physiological relevance of this question we utilized the newly identified endogenous GHSR antagonist - liver-expressed antimicrobial peptide 2 (LEAP2) (Ge et al., 2018; Schalla and Stengel, 2019). Endogenous LEAP2 levels in plasma are modulated by feeding status, such that they decrease during fasting and rise after feeding (Mani et al., 2019). It is a competitive antagonist and an inverse agonist of GHSR (Wang et al., 2019; M'Kadmi et al., 2019), making it a potent inhibitor of ghrelin signaling, yet still relatively unexplored.

2 Materials and methods

2.1 Animals

Female and male Sprague Dawley rats (8 weeks old upon arrival; Charles River Laboratories, Wilmington, MA and Charles River Laboratories, Italy) were individually housed on a 12-h light/dark cycle with *ad libitum* access to chow (PicoLab Rodent Diet 5053) and water. Drug injections and testing were performed during the light cycle. In the agonist experiments food was removed from the home cage at the time of drug injection, based on our previous findings that ghrelin's anxiolytic effect may be abolished if rats are allowed to feed between ghrelin administration and anxiety testing (Alvarez-Crespo et al., 2012). In the antagonist experiments where overnight fasting was applied, the animals were food deprived at the onset of the dark cycle prior to drug injection and behavioral testing. After behavioral testing, rats were returned to their home cage with free access to chow, and food intake was measured 1 or 24 h after being returned. To test the effect of intra-LC ghrelin on the intake of palatable food, a high-fat high-sugar diet (HFHS, in-house made by mixing equal weight of lard and sugar) was offered together with chow and measured after 24 h. All procedures conformed to and received approval by Institutional Animal Care and Use Committee at the Pennsylvania State University and the Animal Welfare Committee of the University of Gothenburg, Sweden, Ethical permit # 137/15.

2.2 Stereotaxic surgery

Animals were anesthetized with an intraperitoneal injection of an anesthetic cocktail composed of ketamine (90 mg/kg), acepromazine (0.64 mg/kg), and xylazine (2.7 mg/kg). Analgesia (carprofen, 5 mg/kg) and local anesthesia (bupivacaine, 2.5 mg/kg) were administered subcutaneously prior to surgery. Guide cannula (26 gauge, 3 mm CC; P1 Technologies) targeting the LC were implanted (±1.3 mm from midline, 9.8 mm posterior to bregma, 5.2 mm ventral to skull, with injector aimed 7.2 mm ventral to skull; Paxinos and Watson, 2005) and affixed to the skull with bone screws and dental cement. Rats were given at least 1 week to recover from surgery before the start of behavioral testing.

2.3 *In situ* hybridization using RNAscope

In situ hybridization (ISH) using RNAscope™ Multiplex Fluorescent v2 kit (Advanced Cell Diagnostics) was utilized to determine presence of *Ghsr* (RNAscope™ Probe-Rn-Ghsr1a-C2, 431,991-C2) and *Th* (RNAscope™ Probe-Rn-Th, 314,651) mRNA in brain sections. To allow detection of colocalization, the two target probes were assigned to different probe channels and fluorophores. Fresh frozen brains were sectioned, and 12 µm thick coronal sections containing LC were collected and fixed in 4% formalin for 15 min at 4°C. Following two quick washes in PBS, brain slices were dehydrated in 50%, 70% and 2 × 100% ethanol (5 min each). Hydrogen peroxide was dropped on the slides and washed off after 10 min. Treatment with protease IV followed (30 min) and was washed away with PBS for a total time of 15 min. Target probes and negative control probes were applied directly on the sections to cover them completely and incubated at 40°C for 2 h in a hybridization oven. Following, slides were incubated with preamplifier and amplifier probes (AMP1, 40°C for 30 min; AMP2, 40°C for 15 min). Next, the HRP signal was developed (HRP-C1 and Opal dye 520; HRP-C2 and Opal dye 570). Finally, brain sections were incubated for 30 s with DAPI and followed by mounting medium for fluorescence (Vectashield). Slides were imaged with Olympus BX53 fluorescent microscope with cellSens imaging software.

2.4 RNA extraction and gene expression

Total RNA was extracted from the LC using the RNeasy Micro kit (Qiagen). cDNA was synthesized using the High-Capacity cDNA Reverse Transcription kit (Applied Biosystems). TaqMan gene expression kits and PCR reagents were used to quantify relative mRNA levels of GHSR (*Ghsr*, Rn00821417_m1) relative to rat β-actin (*Actb*, Rn00667869_m1). Relative mRNA expression was calculated using the comparative ΔΔCt method as previously described (Livak and Schmittgen, 2001).

2.5 Drugs

Ghrelin (Tocris) and rat LEAP2 (Phoenix Pharmaceuticals) were dissolved in artificial CSF (aCSF; Tocris), which was also used for the vehicle condition. Aliquots were stored at −20°C. Drugs were infused into the LC at a volume of 0.3 µL (flow rate 0.5 µL/min) and behavioral testing was conducted 20 min later, throughout the study. Ghrelin (1 µg) was administered unilaterally to *ad libitum*-fed rats at a dose that has previously been shown effective at increasing feeding behavior when injected into discrete brain sites (Schéle et al., 2016; López-Ferreras et al., 2017; Le May et al., 2019). LEAP2 (2.5 µg per hemisphere) was administered bilaterally to rats that were fasted overnight. The dose was derived from one of the few papers published with central injection of LEAP2, and a pre-print confirming the effectiveness on food intake based on a dose-response study (Islam et al., 2020; Tufvesson-Alm et al., 2023). We used low volumes for our parenchymal injection to the LC to prevent diffusion to the adjacent fourth ventricle, and spread to other brain areas that could be important for the observed behavioral effects. The antagonist (LEAP2) was injected bilaterally so that the activity from one hemisphere would not compensate for the loss of activity in the other. For all the experiments carried out in this study, rats were returned to their home cage with free access to chow after the behavioral testing. Acute food intake was measured after 1 h in the cage. In the case of all behavioral tests (operant conditioning, OF, ASR), drug injections were performed according to a cross-over balanced experimental design for each treatment separately. All conditions were separated by a minimum of 48 h wash out period and run in a counterbalanced manner (each rat received all conditions on separate testing days).

2.6 Operant conditioning

One distinctive aspect of reward is the motivation to self-administer or work for the reward (i.e., "wanting" the reward). The motivation to obtain a sucrose pellet (45 mg, Bio-serv) was assessed using the progressive ratio (PR) operant conditioning procedure (Hodos, 1961), a test measuring the number of lever presses that a rat is willing to execute to acquire a food reward. To prevent neophobia, rats were offered 3 sucrose pellets in their home cage the day before training was initiated. Training and testing were conducted in rat conditioning chambers (Med Associates) as described previously (Dickson et al., 2012). Rats were first trained on a 30-min fixed ratio schedules (FR1 followed by FR3 and FR5), where the cost of receiving one pellet equaled to 1, 3 and 5 presses on the active lever respectively. A minimum of 30 presses on the active lever per session was required for advancement to the next schedule. Finally, the rats were trained in 60-min PR conditioning sessions where the response requirement increased according to the following equation: response ratio = [5e(0.2 × infusion number)]—5 through the following series: 1, 2, 4, 9, 12, 15, 20, 25, 32, 40, 50, 62, 77, 95, 118, 145, 178, 219, 268, 328. The effect of drugs on food motivated behavior was tested with the PR schedule. Horizontal activity was measured with the use of infrared beams in the operant chambers. Food-seeking was measured by infrared beams that were responding to head entries into the pellet receptacle. The effect of ghrelin injection on food motivation was tested in *ad libitum* fed rats, while the effect of LEAP2 was tested in overnight fasted rats. This to ensure that the antagonist is applied when endogenous ghrelin levels are higher.

2.7 Open field

The open field test (OF) is based on the animal's conflicting innate tendencies to avoid the open spaces and explore the novel environment. Administration of anxiolytics has been shown to increase time spent in the center of the open field, and decrease thigmotaxis (Walf and Frye, 2007). Here, rats were placed in the center of a brightly lit arena with dark walls (43.2 × 43.2 cm; Med Associates) and allowed to explore freely during 30 min. The animal's position and movement were detected by a grid of photocells covering the arena, and the behavior was scored automatically using Med-Associates Activity Monitor software.

2.8 Acoustic startle response

The startle reflex is a primitive motor response to a sudden, intense stimulus, which is amplified in states of anxiety and diminished with anxiolytic drugs. In contrast to the open field test, the acoustic startle procedure can assess anxiety-like behavior without the influence of exploratory behavior and locomotor activity, components which may be affected by energy status and sex, and confound the interpretation of the results (Borchers et al., 2022). Testing was conducted in the SR-LAB startle response system (San Diego Instruments), a soundproof chamber with a cylindrical animal enclosure connected to a piezoelectric motion sensor that records the startle response. Rats were placed in the acrylic cylinder (9 cm in diameter) and habituated with a background white noise (50 dB) for 5 min. Following habituation, the SR Lab Software delivered acoustic stimuli bursts of 90, 95 or 105 dB (50 ms each) in a randomized pattern (10 times for each intensity) with inter stimulus intervals ranging between 20 and 40 s. Chambers were brightly lit during testing (500 lux illumination), as bright light acts as an unconditioned anxiogenic stimulus in rats (Walker and Davis, 1997). The peak amplitude response (in millivolts) to each sound stimulus (in dB) was averaged across the 10 repetitions and used as the dependent measure.

2.9 Tissue collection

Male and female rats were decapitated after light isoflurane anesthesia, and brains were rapidly removed, flash-frozen in isopentane, and stored at −80°C until processing. Half of the rats were fasted overnight prior to the euthanasia, while the other half had free access to chow, the groups were matched by body weight. Using a cryostat, coronal sections (12 µm thick) at the level of the LC were collected and slide-mounted for RNAscope *in situ hybridization*, micropunches of the LC were collected in test tubes for gene expression analysis, and sections were examined to ensure correct cannula placement. The rats that had cannulas placed outside of the LC in either hemisphere, were excluded from all behavioral analyses. For *Ghsr* expression studies, in addition to brains from rats used for behavioral testing, brains were also collected from a separate animal cohort matched for age, in order to increase the number of samples for reliable gene analysis.

2.10 Statistical analysis

All data are presented as mean ± SEM. Statistical significance was analyzed by two-factor repeated measures ANOVA with *post hoc* Holm–Sidak's multiple comparison test when appropriate (GraphPad Prism 8 Software, Inc). To control for total locomotor activity in the OF, an analysis of covariance (ANCOVA) was performed using the *car* package for R (v. 4.3.1). *p*-values lower than 0.05 were considered statistically significant.

3 Results

3.1 Fluorescent *in situ* hybridization and qPCR show *Ghsr* expression in the rat LC

To determine the presence of *Ghsr* in the LC and the presence of *Ghsr1a* transcript on LC noradrenergic neurons we performed RNAscope *in situ* hybridization (Figure 1A; representative image of a coronal brain section 9.8 mm posterior to bregma). Expression of *Ghsr* mRNA (green) was observed throughout the LC (Figures 1B, C). *Ghsr* was present on LC neurons that express tyrosine hydroxylase mRNA (*Th*) (magenta) in female (Figure 1B) and male (Figure 1C) rats, indicating presence of the ghrelin receptor on noradrenergic neurons. Moreover, we utilized real time quantitative PCR to measure the mRNA levels of *Ghsr* in *ad libitum* fed and fasted male and female rats. The gene expression analysis revealed that there was no effect of fasting on *Ghsr* expression, in either sex. However, the expression was sexually dimorphic, such that males had higher levels of ghrelin receptors in the LC [two-factor ANOVA: interaction $F_{(1,\ 79)} = 0.001968$, $p = 0.9647$, effect of fasting $F_{(1,\ 79)} = 0.04919$, $p = 0.8250$, effect of sex $F_{(1,\ 79)} = 5.118$, $p = 0.0264$; Figure 1D].

3.2 Pharmacological activation of LC GHSR stimulates food intake and food motivation in male and female rats

Acute intra-LC ghrelin injection (1 µg) led to a significant increase in chow intake 1 h post injection [two-factor ANOVA for acute chow intake: interaction $F_{(1,\ 15)} = 1.199$, $p = 0.2909$, effect of drug $F_{(1,\ 15)} = 9.161$, $p = 0.0085$, effect of sex $F_{(1,\ 15)} = 2.227$, $p = 0.1563$, Figure 2A]. This hyperphagia persisted longer in females, which still had a greater chow intake at 24 h post ghrelin injection. Two-factor ANOVA revealed no significant effect of drug or sex, but a significant interaction between these two factors [two-factor ANOVA for 24 h food intake: interaction $F_{(1,\ 17)} = 8.890$, $p = 0.0084$, effect of drug $F_{(1,\ 17)} = 3.228$, $p = 0.0902$, effect of sex $F_{(1,\ 17)} = 1.587$, $p = 0.2248$; Figure 2B]. The effects of ghrelin on food intake were measured in a free choice paradigm, hence the animals were offered a palatable HFHS diet together with the chow. Here, ghrelin treatment did not affect HFHS-diet intake at any of the measured time points in either sex; [two-factor ANOVA for acute HFHS intake: interaction $F_{(1,\ 17)} = 0.2277$, $p = 0.6393$, effect of drug $F_{(1,\ 17)} = 0.1358$, $p = 0.7171$, effect of sex $F_{(1,\ 15)} = 0.0019$, $p = 0.9654$, Figure 2C], [two-factor ANOVA for 24 h HFHS intake: interaction $F_{(1,\ 17)} = 0.0295$, $p = 0.8655$, effect of drug $F_{(1,\ 17)} = 0.0738$, $p = 0.7890$, effect of sex $F_{(1,\ 17)} = 0.5072$, $p = 0.4860$, Figure 2D].

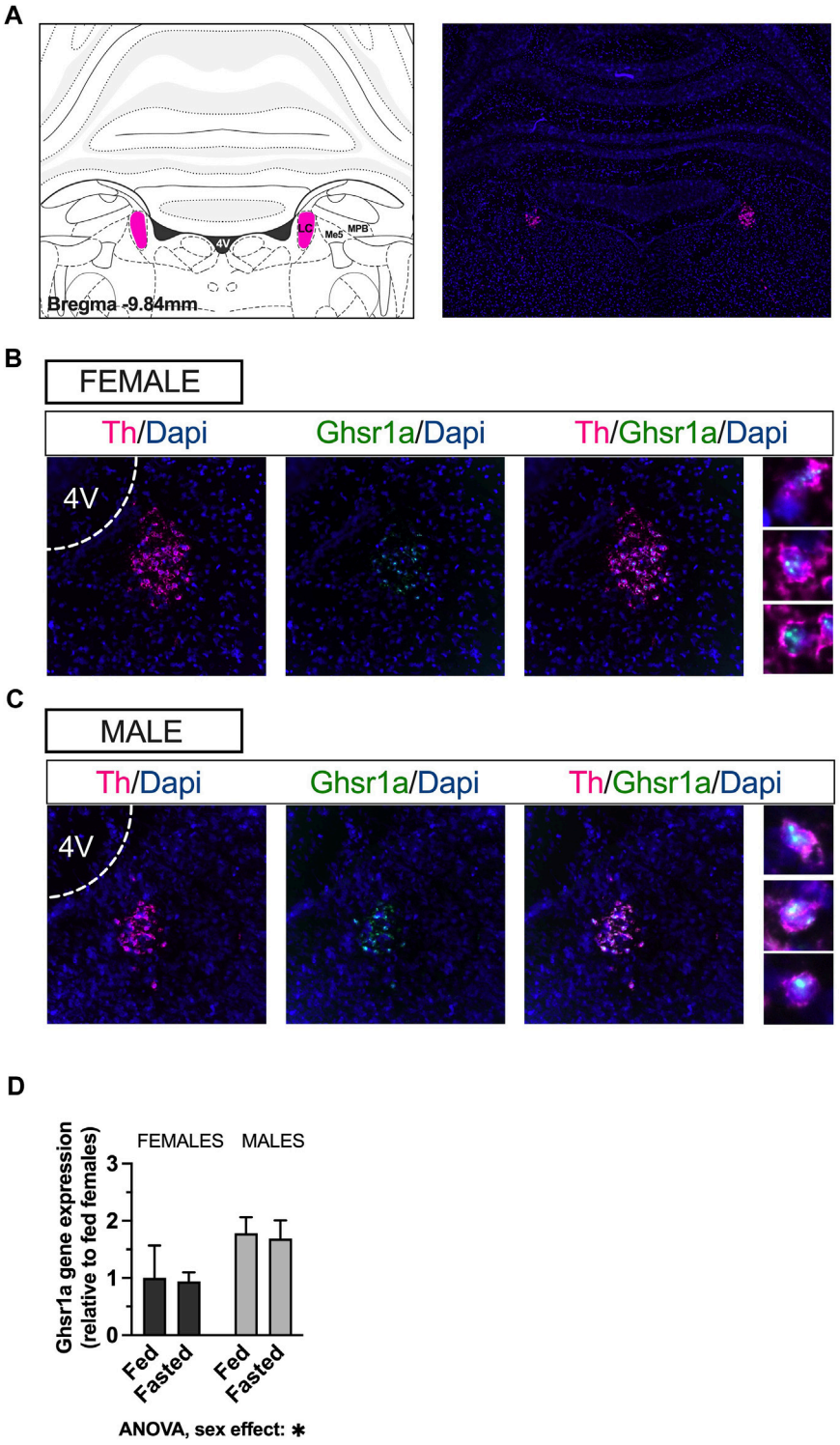

FIGURE 1
Ghsr are expressed in male and female LC, on noradrenergic neurons. RNAscope *in-situ* hybridization was used to determine expression of the *Ghsr* on *Th* neurons in LC. Representative image of *Th* mRNA (magenta) and cell nuclei (blue; DAPI) at the level of the LC in coronal brain sections of rats **(A)**. Co-localization indicates expression of GHSR1 (green) on *Th*-expressing cells (magenta) in the LC of female **(B)** and male **(C)** rats. qPCR performed on LC micropunches of *ad libitum* fed and fasted animals revealed that males expressed more *Ghsr* in the LC, but that the expression was unaffected by feeding status in both sexes **(D)**. Image corresponds to bregma –9.84 in Paxinos and Watson's Rat Brain Atlas, fifth edition. LC, locus coeruleus; Me5, mesencephalic trigeminal nucleus; MPB, medial parabrachial nucleus; Th, tyrosine hydroxylase; Dapi, 4′,6-diamidino-2-phenylindole; Ghsr1a, growth hormone secretagogue receptor 1a; 4V, fourth ventricle.

10.3389/fphar.2023.1286805

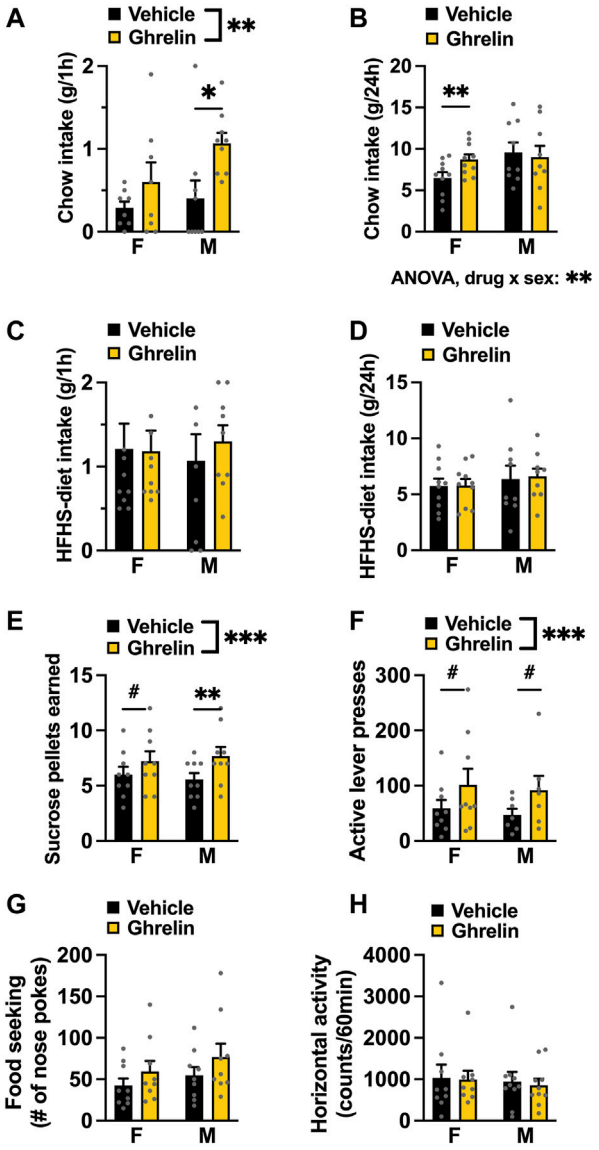

FIGURE 2
Ghrelin acts in the LC to increase chow intake and food reward in both female and male rats. Intra-LC administration of ghrelin (1 μg) ghrelin increased chow intake acutely in both males and females **(A)**, while at 24 h only females consumed more chow **(B)**. HFHS-diet intake remained unchanged 1 h **(C)** and 24 h **(D)** after ghrelin injection. In a progressive ratio operant schedule, ghrelin increased the amount of sucrose rewards earned **(E)** and the number of active lever presses to obtain the reward **(F)**, without changing food seeking **(G)** or locomotor activity **(H)** in either sex. F, females; M, males; HFHS diet, high-fat high-sugar diet. Data are expressed as mean ± SEM. #$p < 0.1$, *$p < 0.05$, **$p < 0.01$, ***$p < 0.001$, ****$p < 0.0001$.

Applying ghrelin to the LC in *ad libitum* fed rats increased motivated behavior for a food reward–as evidenced by the higher amount of sucrose pellets earned [two-factor ANOVA: interaction $F_{(1, 16)} = 1.174$, $p = 0.2946$, effect of drug $F_{(1, 16)} = 16.51$, $p = 0.0009$, effect of sex $F_{(1, 16)} = 0.000$, $p > 0.999$; Figure 2E) due to the increased effort (active lever presses) rats were willing to expend for the reward [two-factor ANOVA: interaction $F_{(1, 14)} = 0.003$, $p = 0.9549$, effect of drug $F_{(1, 14)} = 9.263$, $p = 0.0088$, effect of sex $F_{(1, 14)} = 0.141$, $p = 0.7125$; Figure 2F]. The effect was specific to motivated behavior, as food seeking (Figure 2G) and locomotor activity (Figure 2H) were not affected, although there was a trend for effect of ghrelin on food seeking behavior [two-factor ANOVA: effect of drug $F_{(1, 16)} = 3.214$, $p = 0.0919$]. Both male and female rats responded to a similar extent as there was no significant drug-sex interaction for any parameters measured during operant testing.

3.3 Blocking LC GHSR suppresses food intake and food motivation with a different latency in male and female rats

Acute intra-LC LEAP2 injection (2.5 μg per hemisphere) in overnight fasted rats, significantly reduced feeding in both males and females when chow was offered to them 1 h after the antagonist administration and measured 1 h later [two-factor ANOVA: interaction $F_{(1, 18)} = 0.1608$, $p = 0.6932$ effect of drug $F_{(1, 18)} = 11.27$, $p = 0.0035$, effect of sex $F_{(1, 18)} = 4.103$, $p = 0.0579$; Figure 3A]. However, in a separate experiment when the pellets were returned to the animals 2 h after injection, *post hoc* analysis revealed that this hypophagia was only present in females [two-factor ANOVA: interaction $F_{(1, 17)} = 1.786$, $p = 0.1991$, effect of drug $F_{(1, 17)} = 3.753$, $p = 0.0695$, effect of sex $F_{(1, 17)} = 17.13$, $p = 0.00079$; Figure 3B]. At 24 h post injection, there were no effects of LEAP2 on chow intake [two-factor ANOVA: interaction $F_{(1, 17)} = 1.473$, $p = 0.2414$, effect of drug $F_{(1, 17)} = 0.7907$, $p = 0.3863$, effect of sex $F_{(1, 17)} = 21.69$, $p = 0.0002$; Figure 3C]. Intra-LC LEAP2 injection reduced motivated behavior in females as indicated by fewer sucrose rewards earned [two-factor ANOVA: interaction $F_{(5, 30)} = 0.5021$, $p = 0.7722$, effect of drug $F_{(1, 6)} = 6.442$, $p = 0.0442$, effect of time $F_{(5, 30)} = 13.33$, $p < 0.0001$; Figure 3D] throughout the entire test. There was a trend to reduction of lever presses [two-factor ANOVA: interaction $F_{(5, 30)} = 1.195$, $p = 0.3354$, effect of drug $F_{(1, 6)} = 4.046$, $p = 0.0910$, effect of time $F_{(5, 30)} = 8.772$, $p < 0.0001$; Figure 3E]. The interval between the number of presses required for each consecutive reward is amplified, creating a large variability for this parameter. However, since there was a clear reduction in the number of rewards that the females were willing to work for, we conclude that there was a drug effect on motivated behavior. Food seeking was not affected [two-factor ANOVA: interaction $F_{(5, 30)} = 0.8984$, $p = 0.4949$, effect of drug $F_{(1, 6)} = 0.1929$, $p = 0.6759$, effect of time $F_{(5, 30)} = 21.51$, $p < 0.0001$; Figure 3F]. Locomotor activity was also unaltered by the drug [two-factor ANOVA: interaction $F_{(5, 30)} = 1.514$, $p = 0.2152$, effect of drug $F_{(1, 6)} = 3.184$, $p = 0.1246$, effect of time $F_{(5, 30)} = 18.39$, $p < 0.0001$; Figure 3G]. In contrast to the consistent effect in females, behavior of LEAP2-injected male rats in the progressive ratio operant test was not significantly affected [two-factor ANOVA for rewards earned: interaction $F_{(5, 40)} = 1.908$, $p = 0.1146$, effect of drug $F_{(1, 8)} = 0.9255$, $p = 0.3642$, effect of time $F_{(5, 40)} = 10.48$, $p < 0.0001$; Figure 3H; two-factor ANOVA for lever presses: interaction $F_{(5, 40)} = 1.228$, $p = 0.3141$, effect of drug $F_{(1, 8)} = 0.2433$, $p = 0.6351$, effect of time $F_{(5, 40)} = 8.664$, $p < 0.0001$; Figure 3I; two-factor ANOVA for food seeking: interaction $F_{(5, 40)} = 1.415$, $p = 0.2371$, effect of drug $F_{(1, 8)} = 1.246$, $p = 0.2932$, effect of time $F_{(5, 40)} = 11.89$, $p < 0.0001$; Figure 3J]. Horizontal locomotor activity was not affected either [two-factor ANOVA: interaction $F_{(5, 40)} = 1.114$, $p = 0.3539$, effect of drug $F_{(1, 8)} = 0.9553$, $p = 0.3539$, effect of time $F_{(5, 40)} = 27.87$, $p < 0.0001$, Figure 3K].

10.3389/fphar.2023.1286805

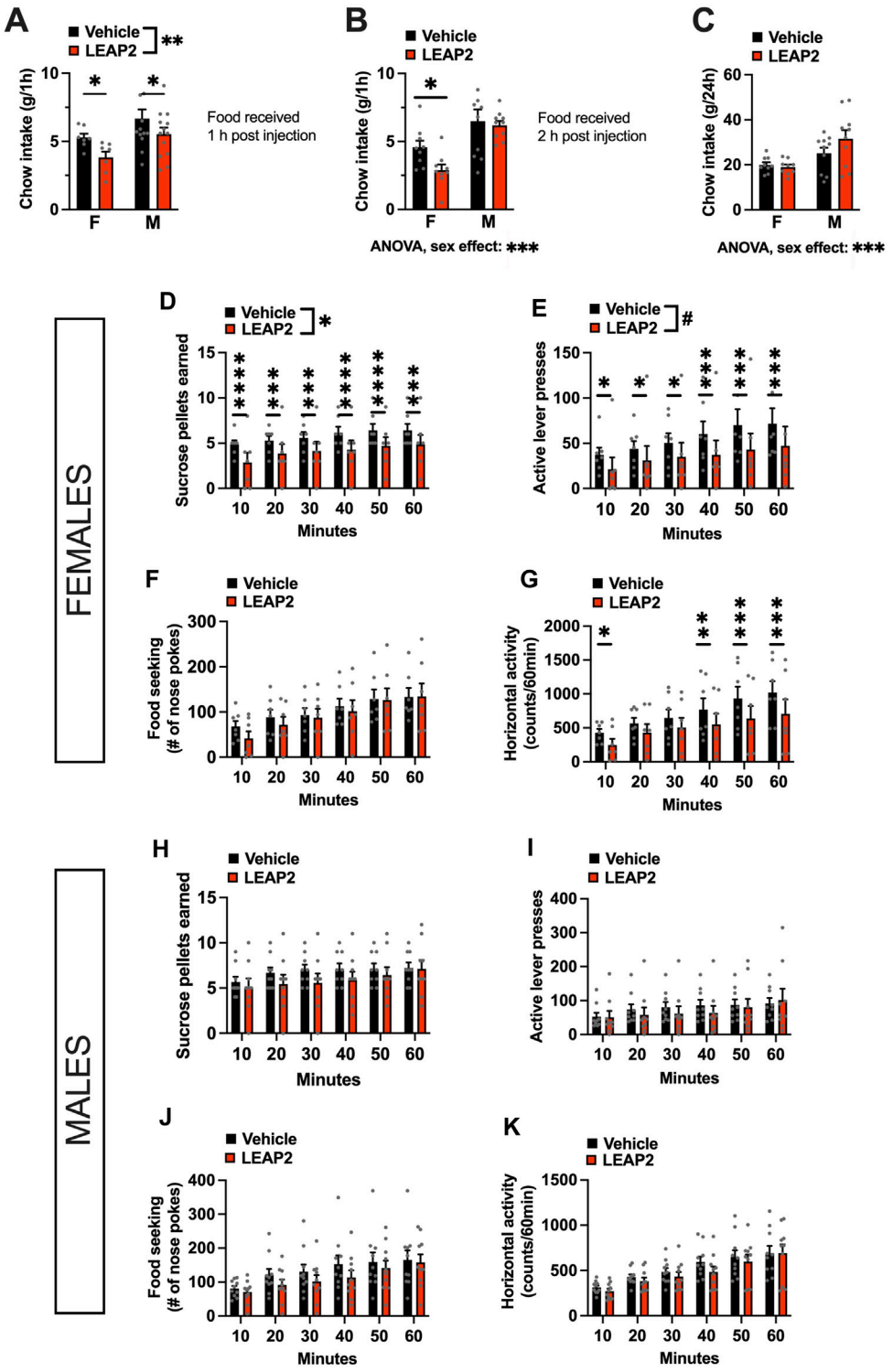

FIGURE 3
Acute pharmacological blockade of ghrelin signaling in the LC decreases food intake in both sexes, but food reward only in females. LEAP2 is anorexic in both sexes when chow is offered within 1 h post intra-LC injection **(A)**, but reduces chow intake in females only, when offered 2 hours post injection **(B)**. The anorexic effect of LEAP2 is absent in both sexes 24 h post intra-LC injection **(C)**. In females, intra-LC microinjection of LEAP2 (5 μg) decreased the number of sucrose pellets earned **(D)** and the number of lever presses for the rewards in a 60-min progressive ratio operant test **(E)**. Food seeking **(F)** was unchanged while locomotor activity was significantly reduced during the first 10 min and last 30 min of the test **(G)**. In contrast to females, acute pharmacological blockade of LC GHSR did not affect the number of sucrose pellets earned **(H)** or active lever presses **(I)** in males. Food seeking was also not significantly altered **(J)**. Locomotor activity in males was also not affected by the drug, **(K)**. LEAP2 = liver-expressed antimicrobial peptide 2. Data are expressed as mean ± SEM. #$p < 0.1$, *$p < 0.05$, **$p < 0.01$, ***$p < 0.001$, ****$p < 0.0001$.

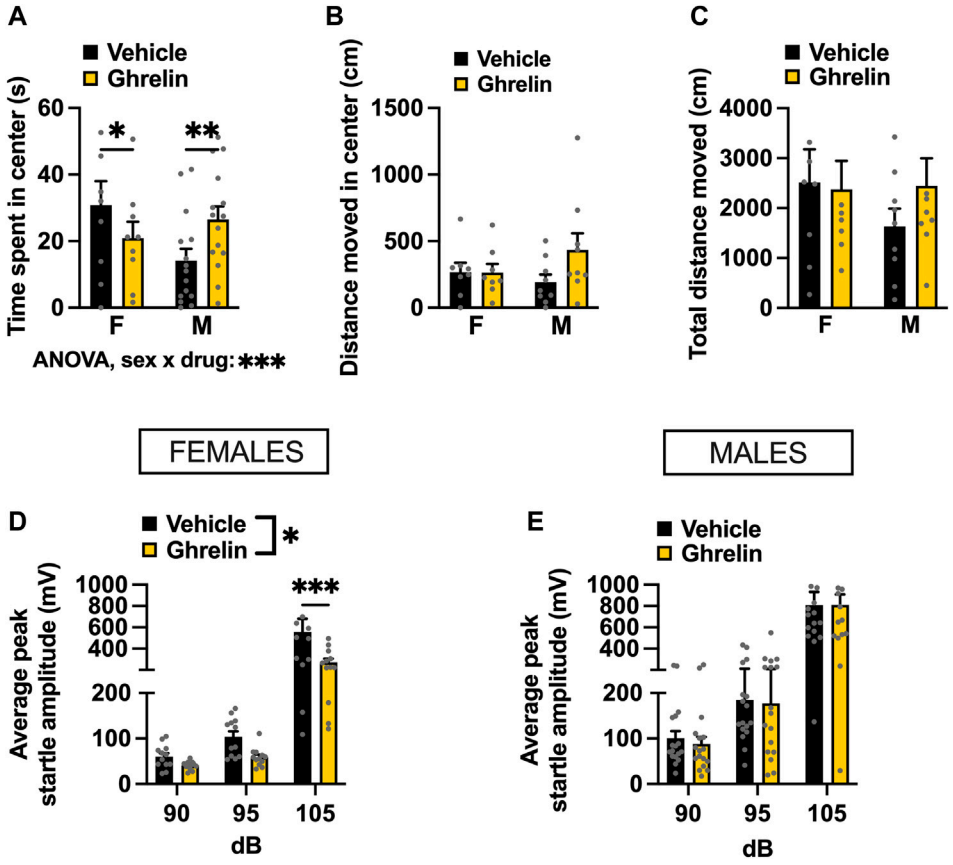

FIGURE 4
Ghrelin delivered to the LC alters anxiety-like behavior in a context-specific and sex-divergent manner. Intra-LC administration of ghrelin (1 μg) decreased the time females spent in the center, and conversely increased the time males spent in the center of the OF **(A)**. Distance moved in center **(B)** and total distance moved **(C)** remained unchanged, although a non-significant trend was detected in males. An anxiolytic effect of ghrelin was detected in the ASR test, where startle amplitude was significantly lower in ghrelin treated females **(D)** at the highest sound intensity. The treatment did not alter the startle response in males at any sound intensity **(E)**. LEAP2, liver-expressed antimicrobial peptide 2; F, females; M, males. Data are expressed as mean ± SEM. #$p < 0.1$, *$p < 0.05$, **$p < 0.01$, ***$p < 0.001$, ****$p < 0.0001$.

3.4 Activation of LC GHSR alters anxiety-like behavior in a sex-specific manner

Initially, OF was used to determine the effects of intra-LC injection of ghrelin on anxiety-like behavior. In our paradigm, we withheld chow from the animals immediately before the drug injection, and did not return it until after behavioral testing, as our previous work indicates that offering food after ghrelin injections confounds the effect of this peptide on anxiety (Alvarez-Crespo et al., 2012). Interestingly, ghrelin treated females showed a potentially heightened anxiety-like behavior, based on less time spent in the center of the OF (Holm Šídák's multiple comparisons test: $p = 0.0259$ Figure 4A). Males on the other hand, spent more time in the center of the OF after ghrelin injection, indicating a decreased anxiety-like behavior (Holm Šídák's multiple comparisons test: $p = 0.0018$, Figure 4A). Two-factor ANOVA indicated a significant interaction between sex and drug effect [$F_{(1, 22)} = 17.97$, $p = 0.0003$], and no effect of drug [$F_{(1, 22)} = 0.2143$, $p = 0.6479$] or sex [$F_{(1, 22)} = 0.7939$, $p = 0.3826$] separately. While there was no significant change in locomotor activity in either sex, male rats appeared to move more, suggesting that the time spent in the center might be confounded by changes in general locomotor activity rather than emotional reactivity. Two-factor ANOVA indicated no significant effects for distance moved in center [two-factor ANOVA: interaction $F_{(1, 15)} = 2.298$, $p = 0.1503$, effect of drug $F_{(1, 15)} = 2.166$, $p = 0.1618$, effect of sex $F_{(1, 15)} = 0.284$, $p = 0.6018$; Figure 4B], nor total distance moved [two-factor ANOVA: interaction $F_{(1, 15)} = 0.6912$, $p = 0.4188$, effect of drug $F_{(1, 15)} = 0.3461$, $p = 0.5651$, effect of sex $F_{(1, 15)} = 0.6594$, $p = 0.4295$; Figure 4C]. To explore the influence of locomotion on anxiety behavior in OF statistically, we performed an ANCOVA and determined the relationship between the total distance travelled in the arena and time in the center of the open field. In males, the covariate, total distance did influence time spent in the center of the open field [$F_{(1,21)} = 12.863$, $p < 0.001$]. There was no significant effect of the treatment on the time spent in the center after controlling for the effect of total locomotor activity [$F_{(1,21)} = 0.010$, $p = 0.9204$]. In females on the other hand, neither total locomotor activity nor treatment had a significant relationship to the time spent in the center with $F_{(1,13)} = 0.997$, $p = 0.3362$ and $F_{(1,13)} = 0.897$, $p = 0.3606$, respectively. Overall, the ANCOVA results indicated that the effect of treatment was not significant after controlling for total activity in both sexes. In order to further separate potential influence of locomotion from assessment of anxiety-like behavior we performed the ASR test. The ASR clearly revealed an anxiolytic effect of ghrelin in females, and

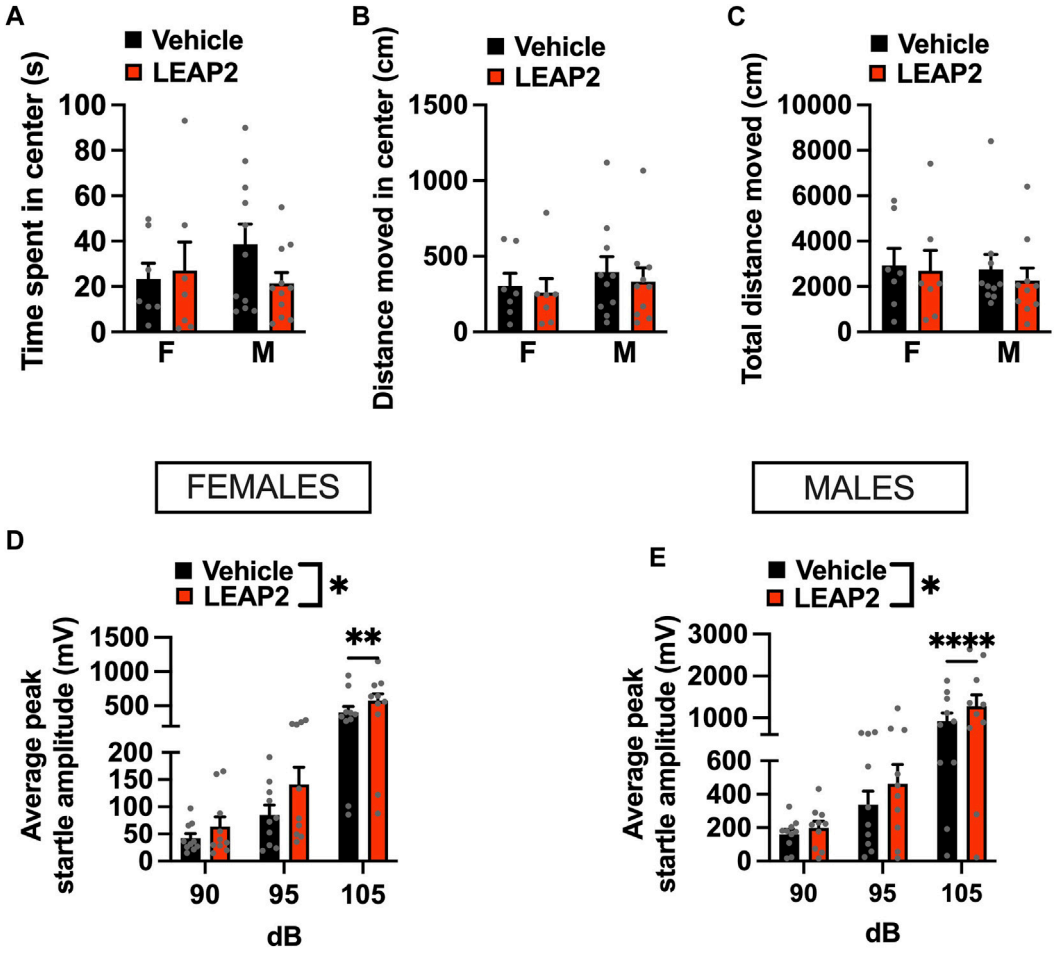

FIGURE 5
Acute pharmacological blockade of GHSR increases anxiety-like behavior in male and female rats. Intra-LC microinjection of LEAP2 (5 μg) did not change time spent in center **(A)**, locomotor activity in center **(B)**, or total distance moved **(C)** in the OF test. However, an anxiogenic effect of ghrelin receptor blockade in LC was detected in the ASR test, where startle amplitude, was significantly increased in LEAP2 treated females **(D)** and males **(E)**. LEAP2 = liver-expressed antimicrobial peptide 2; F, females; M, males. Data are expressed as mean ± SEM. #$p < 0.1$, *$p < 0.05$, **$p < 0.01$, ***$p < 0.001$, ****$p < 0.0001$.

as expected an effect of the increasing sound intensity, which plays the role of an anxiogenic stimulus in the ASR test [two-factor ANOVA: interaction $F_{(2, 22)} = 5.092$, $p = 0.0152$, effect of drug $F_{(1, 11)} = 8.003$, $p = 0.0164$, effect of sound $F_{(2, 22)} = 26.270$, $p < 0.0001$; Figure 4D]. In males, there was no drug effect at any sound intensity [two-factor ANOVA: interaction $F_{(2, 32)} = 0.0119$, $p = 0.9881$, effect of drug $F_{(1, 16)} = 0.0201$, $p = 0.8890$, effect of sound $F_{(2, 32)} = 60.03$ $p < 0.0001$; Figure 4E].

3.5 Intra-LC administration of LEAP2 exerts an anxiogenic effect

To determine if ghrelin signaling in the LC is necessary for anxiety-like behavior, we exposed fasted rats to the OF and ASR tests after LEAP2 administration. LEAP2 did not alter time spent in the center [interaction $F_{(1, 16)} = 2.285$, $p = 0.1502$, effect of drug $F_{(1, 16)} = 0.939$, $p = 0.3468$, effect of sex $F_{(1, 16)} = 0.241$, $p = 0.6301$; Figure 5A], distance moved in center [interaction $F_{(1, 15)} = 0.0407$, $p = 0.8428$, effect of drug $F_{(1, 15)} = 1.637$, $p = 0.2202$, effect of sex $F_{(1, 15)} = 0.395$, $p = 0.5388$; Figure 5B] nor total distance moved in the OF [interaction $F_{(1, 15)} = 0.124$, $p = 0.7294$, effect of drug $F_{(1, 15)} = 0.918$, $p = 0.3531$, effect of sex $F_{(1, 15)} = 0.106$, $p = 0.7484$; Figure 5C].

As fasting and manipulating ghrelin signaling may influence locomotor activity, we performed an ANCOVA for time spent in the center with total distance travelled in the open field as a covariate. The covariate, total locomotion, was significantly related to the time males spent in the center of the OF ($F_{(1,17)} = 14.139$, $p < 0.001$). After controlling for locomotion, there was no significant effect of LEAP2 on the time spent in the center of the OF ($F_{(1,17)} = 0.024$, $p = 0.8783$). Similar to males, an effect of total locomotion on time spent in the open areas of the OF ($F_{(1,11)} = 42.03$, $p < 0.0001$) was found in females. LEAP2 treatment had no effect on the time spent in the center of the OF after controlling for locomotion ($F_{(1,11)} = 0.849$, $p = 0.3764$). Therefore, LEAP2 did not have an effect on anxiety-like behavior in the OF after adjusting for locomotion, in either sex.

In contrast, LEAP2 was clearly anxiogenic in both females (Figure 5D) and males (Figure 5E) when tested in the ASR. A two-factor repeated measures ANOVA for the female data indicated

an effect of sound intensity [$F_{(2, 18)} = 26.23$, $p < 0.0001$], drug [$F_{(1, 9)} = 10.50$, $p < 0.0101$] and a strong trend for an interaction between the two factors [$F_{(2, 18)} = 3.371$, $p < 0.0571$]. In males, two-factor repeated measures ANOVA revealed an effect of sound intensity [$F_{(2, 18)} = 8.914$, $p < 0.002$], drug [$F_{(1, 9)} = 8.882$, $p < 0.0154$] and a significant interaction [$F_{(2, 18)} = 8.914$, $p < 0.002$].

4 Discussion

In the present study, we set out to determine whether ghrelin action in the LC is necessary and sufficient for control of ingestive, motivated, and emotionality behaviors. To achieve this, we investigated the behavioral outputs of pharmacological activation and inhibition of ghrelin receptors in the LC. We found that GHSR are present on noradrenergic cells in the LC of male and female rats, with higher levels in males. We show that intra-LC-injected ghrelin acutely increases food intake and also motivated behavior for sucrose. In contrast, blockade of GHSR, by intra-LC LEAP2 microinjections performed in fasted rats in order to ensure high levels of endogenously produced circulating ghrelin, resulted in decreased feeding and reduced food reward in females, while males only presented with transiently suppressed food intake. Activation of LC ghrelin receptors was anxiolytic in female rats, as indicated by decreased startle responses in the ASR test. Conversely, blockade of LC ghrelin receptors was anxiogenic in females. In males, activation of LC ghrelin receptors had no effect on behavior in the ASR test, however blockade was anxiogenic. These data indicate that the LC is a novel brain area key to ghrelin's effects on ingestive, motivated, and emotionality behavior, with some sex divergence in these effects.

Ghrelin has a well-established orexigenic effect, consistently demonstrated in the literature by peripheral injections and direct application to a variety of GHSR expressing brain areas (Faulconbridge et al., 2008; Egecioglu et al., 2010; Skibicka and Dickson, 2011; Mason et al., 2014; Wald et al., 2023). Here, we show that exogenous ghrelin increases chow intake and food motivated behavior at the level of LC as well. Acutely, we find no sex differences in chow intake measured over 1 h, nor motivated behavior for a sucrose pellet. Surprisingly, at 24 h post injection our analysis indicates an interaction between sex and treatment for the orexigenic effect, as females still had a significantly higher chow intake when measured the day after intra-LC injection. According to studies done in male rodents, most of ghrelin's hyperphagic effect takes place within 3 h, and central injection of ghrelin is reported to have no effect on feeding at 24 h post drug application in males (Faulconbridge et al., 2003; Skibicka et al., 2012). The more persistent effect on food intake that we describe in the current study is unusual but consistent with data from ghrelin injections into the LH, which exert a female-specific hyperphagia 24 h after administration (López-Ferreras et al., 2017). In contrast to the current results, we previously found the expression of *Ghsr* in the LH is higher in females (Börchers et al., 2022b). Notably, while intra-LC ghrelin increased the motivation to work for a sucrose pellet, it did not induce HFHS-intake in a free choice paradigm. Previous reports have demonstrated that central injection of ghrelin mainly induces a preference for chow over lard and sucrose (Schéle et al., 2016), and increases motivated behavior similarly for regular chow and palatable treats (Bake et al., 2019). Results of ghrelin receptor blockade at the level of LC unveiled further differences between sexes. While LEAP2 was effective in reducing fasting-induced intake and fasting-potentiated food reward in females at all tested time points, it had a transient effect on ingestive behavior in males. Moreover, motivated behavior was not significantly affected by LEAP2 in males, suggesting that the ghrelin system is necessary in females but not males in LC for control of food motivated behavior. It is likely that in males, fasting-induced activity at other ghrelin receptor-expressing brain sites is sufficient to compensate for the blocked ghrelinergic signaling from the LC (Zigman et al., 2006; Skibicka et al., 2011; Mason et al., 2014; Uriarte et al., 2019), or that there may be sex differences in one or several of the molecular components of the ghrelin-axis at the level of LC. Previous work from our group, and others, suggests that the ghrelin axis is sexually dimorphic in rats–females have much higher circulating ghrelin levels at baseline and after overnight fasting, less hepatic LEAP2, and higher ghrelin receptor expression in emotionality-influencing brain areas (Borchers et al., 2022a; Smith et al., 2022). Here, we demonstrate sex differences in *Ghsr* expression in the LC, with higher levels expressed in males, providing a potential explanation and molecular basis to the observed behavioral differences in response to LEAP2. The ghrelin receptor has a high constitutive activity, allowing it to maintain energy homeostasis without ghrelin binding (Fernandez et al., 2018). LEAP2 is a competitive antagonist and an inverse agonist of the GHSR, and sexually dimorphic expression of the receptor in the LC is very likely to influence pharmacological response at this site (M'Kadmi et al., 2019). However, a future dose-response study is needed to confirm this hypothesis, along with complementary analysis of the other components of the ghrelin axis.

Consistently with the sex divergent effects on feeding, we show a female-specific anxiolysis after intra-LC administration of ghrelin as indicated by the ASR test. This supports the hypothesis that female rats are more sensitive to the anxiolytic effects of ghrelin signaling, as a survival mechanism during periods of negative energy balance (Borchers et al., 2022a). The ability of the brain to integrate internal physiological drives, such as hunger, with external stimuli is essential for survival. LC is important for regulation of arousal, and is activated by unexpected sensory events to direct attention to potentially threatening stimuli in the environment (Aston-Jones and Cohen, 2005). Psychiatric disorders linked to stress and hyperarousal, namely, post-traumatic stress disorder (PTSD), anxiety and major depression are more prevalent in women than men (McLean et al., 2011; Olff, 2017; Li et al., 2022). Interestingly, there are well-established sex differences in the anatomy and physiology of the LC, biasing female rodents towards increased arousal and dysregulation by stress (Bangasser et al., 2016). Hunger state has been shown to affect LC response to unexpected stimuli, as a light flash evoked a greater activation of LC-NE neurons in fasted mice compared to satiated mice (Sciolino et al., 2022). Additionally, the LC has been implicated in the control of fear-induced suppression of eating through co-release of NE and glutamate in response to threatening stimuli (Yang et al., 2021). It is therefore conceivable that ghrelin, the circulating hunger hormone, modulates LC activity to address hunger rather than fear when appropriate, and that sensitivity in this system is higher in females.

Some studies indicate that plasma ghrelin may not access many of the brain regions expressing GHSR (Cabral et al., 2014; Perello et al., 2019). However, the ability of endogenous ghrelin to reach its receptors at the LC level is supported by its location next to the fourth ventricle, along with the finding that systemic ghrelin administration increases CSF ghrelin (Uriarte et al., 2019), and one previous report showing the uptake of CSF ghrelin in the LC (Cabral et al., 2013). Our *in-situ* hybridization and qPCR results confirm that *Ghsr* mRNA is present in the LC. The *Ghsr*-expressing cells were distributed within the entire nucleus and lacked any evident cluster organization in both sexes. Importantly, we show that *Ghsr* is co-expressed with *Th*, placing the receptor on norepinephrine-producing cells in the LC. The LC is the major source of noradrenergic ascending fibers to the forebrain, but investigations into the role of brain NE circuits in feeding have not conveyed uniform results. For instance, catecholamine projections from the (NTS) to the (Arc) were shown to stimulate feeding, while activating projections to the parabrachial nucleus (PBN) suppress feeding (Roman et al., 2016; Aklan et al., 2020). Moreover, lesions of the ventral noradrenergic bundle result in hyperphagia, while the effect on ingestive behavior following the interruption of projections of the dorsal noradrenergic bundle is less clear (Ahlskog and Hoebel, 1973; Sahakian et al., 1983). One previous study indirectly supports a potential functional interaction of ghrelin with catecholaminergic neurons: Chuang *et al.* found that ghrelin signaling in *Th*-expressing neurons was sufficient to mediate ghrelin's orexigenic, antidepressant-like, and stress-induced food-reward behavior (Chuang et al., 2011). The authors discuss the probable involvement of GHSR in VTA for the effects observed in their *Th-cre* mouse model, however the exact neural site responsible for the phenotype was not investigated in this study. Put together with our results, it is intriguing to speculate that the direct action of ghrelin on GHSR-TH neurons in the LC could be mediating this stress-associated feeding behavior. However, Sciolino *et al.* recently demonstrated that activation of noradrenergic neurons in the LC attenuates food intake, and identified a circuit from the LC to LH that modulates feeding and anxiety-like behavior (Sciolino et al., 2022). It is possible that ghrelin receptors and ghrelin provide an upstream signal suppressing noradrenergic neurons and the LC-LH circuits. Future studies using viral tracing could indicate whether GHSR can be found on these specific neurons. However, given the broad and relatively uniform distribution of *Ghsr* expression throughout the LC it is likely that ghrelin indeed controls this circuit. The central role of the LC in integrating physiological drives and external stimuli, underscores its position as a pivotal brain structure in orchestrating complex behaviors necessary for survival. Here, we identify the LC as a novel target site for ghrelin's influence on the brain. Our investigation sheds light on how the stomach, through the actions of ghrelin, can exert direct effect on behaviors that the LC governs, providing an important link between energy homeostasis and emotional states. Ghrelin-signaling pathways also affect motivation and ingestion of artificial rewards (Jerlhag et al., 2009; Jerlhag et al., 2010), and the LC plays an important role in substance abuse disorder (Van Bockstaele et al., 2010), making it compelling to speculate that GHSR signaling in the LC could also mediate reward for substances of abuse. Importantly, our study highlights sex-specific responses to ghrelin signaling in the LC, offering a framework for further investigation into the underlying neural circuitry and the molecular pathways driving these divergent effects. Given the involvement of both ghrelin and LC-NE in stress-related psychiatric disorders, along with the presence of sex-specific differences in these systems, it is crucial to gain a comprehensive understanding of their interaction. This knowledge could potentially contribute to the development of sex-tailored therapies for eating- and anxiety disorders.

Data availability statement

The raw data supporting the conclusion of this article will be made available by the authors, without undue reservation.

Ethics statement

The animal study was approved by the Institutional Animal Care and Use Committee at the Pennsylvania State University and the Animal Welfare Committee of the University of Gothenburg. The study was conducted in accordance with the local legislation and institutional requirements

Author contributions

IM: Conceived and designed of the study, Carried out the experiments, Sample collection, Processed the experimental data and performed the analysis, Drafted the manuscript and designed the figures. LL-F: Carried out the experiments, Processed the experimental data and performed the analysis. YB: Carried out the experiments, Sample collection. MA: Sample collection. STB: Performed the analysis of covariance. LB: Sample collection. SUB: Sample collection. JK: Methodology and resources. KS: Conceived and designed of the study, Processed the experimental data and performed the analysis, Drafted the manuscript and designed the figures. All authors contributed to manuscript revision, read, and approved the submitted version.

Funding

The author(s) declare financial support was received for the research, authorship, and/or publication of this article. This research was funded by the Swedish Research Council (2018-00660, to KS), and the National Institutes of Health R01DK129321 to KS.

Conflict of interest

The authors declare that the research was conducted in the absence of any commercial or financial relationships that could be construed as a potential conflict of interest.

Publisher's note

References

Abizaid, A., Liu, Z. W., Andrews, Z. B., Shanabrough, M., Borok, E., Elsworth, J. D., et al. (2006). Ghrelin modulates the activity and synaptic input organization of midbrain dopamine neurons while promoting appetite. *J. Clin. Invest* 116, 3229–3239. doi:10.1172/JCI29867

Ahlskog, J. E., and Hoebel, B. G. (1973). Overeating and obesity from damage to a noradrenergic system in the brain. *Science* 182, 166–169. doi:10.1126/science.182.4108.166

Aklan, I., Sayar Atasoy, N., Yavuz, Y., Ates, T., Coban, I., Koksalar, F., et al. (2020). NTS catecholamine neurons mediate hypoglycemic hunger via medial hypothalamic feeding pathways. *Cell Metab.* 31, 313–326. doi:10.1016/j.cmet.2019.11.016

Alvarez-Crespo, M., Skibicka, K. P., Farkas, I., Molnár, C. S., Egecioglu, E., Hrabovszky, E., et al. (2012). The amygdala as a neurobiological target for ghrelin in rats: neuroanatomical, electrophysiological and behavioral evidence. *PLoS One* 7, e46321. doi:10.1371/journal.pone.0046321

Andrews, Z. B. (2011). Central mechanisms involved in the orexigenic actions of ghrelin. *Peptides* 32, 2248–2255. doi:10.1016/j.peptides.2011.05.014

Asakawa, A., Inui, A., Kaga, T., Yuzuriha, H., Nagata, T., Fujimiya, M., et al. (2001). A role of ghrelin in neuroendocrine and behavioral responses to stress in mice. *Neuroendocrinology* 74, 143–147. doi:10.1159/000054680

Aston-Jones, G., and Cohen, J. D. (2005). An integrative theory of locus coeruleus-norepinephrine function: adaptive gain and optimal performance. *Annu. Rev. Neurosci.* 28, 403–450. doi:10.1146/annurev.neuro.28.061604.135709

Bake, T., Edvardsson, C. E., Cummings, C. J., and Dickson, S. L. (2019). Ghrelin's effects on food motivation in rats are not limited to palatable foods. *J. Neuroendocrinol.* 31, e12665. doi:10.1111/jne.12665

Bangasser, D. A., Wiersielis, K. R., and Khantsis, S. (2016). Sex differences in the locus coeruleus-norepinephrine system and its regulation by stress. *Brain Res.* 1641, 177–188. doi:10.1016/j.brainres.2015.11.021

Barrile, F., Cassano, D., Fernandez, G., De Francesco, P. N., Reynaldo, M., Cantel, S., et al. (2023). Ghrelin's orexigenic action in the lateral hypothalamic area involves indirect recruitment of orexin neurons and arcuate nucleus activation. *Psychoneuroendocrinology* 156, 106333. doi:10.1016/j.psyneuen.2023.106333

Borchers, S., Krieger, J. P., Asker, M., Maric, I., and Skibicka, K. P. (2022). Commonly-used rodent tests of anxiety-like behavior lack predictive validity for human sex differences. *Psychoneuroendocrinology* 141, 105733. doi:10.1016/j.psyneuen.2022.105733

Borchers, S., Krieger, J. P., Maric, I., Carl, J., Abraham, M., Longo, F., et al. (2022a). From an empty stomach to anxiolysis: molecular and behavioral assessment of sex differences in the ghrelin Axis of rats. *Front. Endocrinol. (Lausanne)* 13, 901669. doi:10.3389/fendo.2022.901669

Börchers, S., Krieger, J. P., Maric, I., Carl, J., Abraham, M., Longo, F., et al. (2022b). From an empty stomach to anxiolysis: molecular and behavioral assessment of sex differences in the ghrelin Axis of rats. *Front. Endocrinol. (Lausanne)* 13, 901669. doi:10.3389/fendo.2022.901669

Cabral, A., Fernandez, G., and Perello, M. (2013). Analysis of brain nuclei accessible to ghrelin present in the cerebrospinal fluid. *Neuroscience* 253, 406–415. doi:10.1016/j.neuroscience.2013.09.008

Cabral, A., Valdivia, S., Fernandez, G., Reynaldo, M., and Perello, M. (2014). Divergent neuronal circuitries underlying acute orexigenic effects of peripheral or central ghrelin: critical role of brain accessibility. *J. Neuroendocrinol.* 26, 542–554. doi:10.1111/jne.12168

Carlini, V. P., Monzón, M. E., Varas, M. M., Cragnolini, A. B., Schiöth, H. B., Scimonelli, T. N., et al. (2002). Ghrelin increases anxiety-like behavior and memory retention in rats. *Biochem. biophysical Res. Commun.* 299, 739–743. doi:10.1016/s0006-291x(02)02740-7

Carlini, V. P., Varas, M. M., Cragnolini, A. B., Schiöth, H. B., Scimonelli, T. N., and de Barioglio, S. R. (2004). Differential role of the hippocampus, amygdala, and dorsal raphe nucleus in regulating feeding, memory, and anxiety-like behavioral responses to ghrelin. *Biochem. biophysical Res. Commun.* 313, 635–641. doi:10.1016/j.bbrc.2003.11.150

Chuang, J.-C., Perello, M., Sakata, I., Osborne-Lawrence, S., Savitt, J. M., Lutter, M., et al. (2011). Ghrelin mediates stress-induced food-reward behavior in mice. *J. Clin. Investigation* 121, 2684–2692. doi:10.1172/JCI57660

Chuang, J. C., and Zigman, J. M. (2010). Ghrelin's roles in stress, mood, and anxiety regulation. *Int. J. Pept.* 2010, 460549. doi:10.1155/2010/460549

Cummings, D. E., Purnell, J. Q., Frayo, R. S., Schmidova, K., Wisse, B. E., and Weigle, D. S. (2001). A preprandial rise in plasma ghrelin levels suggests a role in meal initiation in humans. *Diabetes* 50, 1714–1719. doi:10.2337/diabetes.50.8.1714

Dickson, S. L., Shirazi, R. H., Hansson, C., Bergquist, F., Nissbrandt, H., and Skibicka, K. P. (2012). The glucagon-like peptide 1 (GLP-1) analogue, exendin-4, decreases the rewarding value of food: a new role for mesolimbic GLP-1 receptors. *J. Neurosci.* 32, 4812–4820. doi:10.1523/JNEUROSCI.6326-11.2012

Egecioglu, E., Jerlhag, E., Salomé, N., Skibicka, K. P., Haage, D., Bohlooly-Y, M., et al. (2010). Ghrelin increases intake of rewarding food in rodents. *Addict. Biol.* 15, 304–311. doi:10.1111/j.1369-1600.2010.00216.x

Faulconbridge, L. F., Cummings, D. E., Kaplan, J. M., and Grill, H. J. (2003). Hyperphagic effects of brainstem ghrelin administration. *Diabetes* 52, 2260–2265. doi:10.2337/diabetes.52.9.2260

Faulconbridge, L. F., Grill, H. J., Kaplan, J. M., and Daniels, D. (2008). Caudal brainstem delivery of ghrelin induces fos expression in the nucleus of the solitary tract, but not in the arcuate or paraventricular nuclei of the hypothalamus. *Brain Res.* 1218, 151–157. doi:10.1016/j.brainres.2008.04.068

Fernandez, G., Cabral, A., Andreoli, M. F., Labarthe, A., M'Kadmi, C., Ramos, J. G., et al. (2018). Evidence supporting a role for constitutive ghrelin receptor signaling in fasting-induced hyperphagia in male mice. *Endocrinology* 159, 1021–1034. doi:10.1210/en.2017-03101

Ge, X., Yang, H., Bednarek, M. A., Galon-Tilleman, H., Chen, P., Chen, M., et al. (2018). LEAP2 is an endogenous antagonist of the ghrelin receptor. *Cell metab.* 27, 461–469. doi:10.1016/j.cmet.2017.10.016

Hodos, W. (1961). Progressive ratio as a measure of reward strength. *Science* 134, 943–944. doi:10.1126/science.134.3483.943

Hyland, L., Park, S. B., Abdelaziz, Y., and Abizaid, A. (2020). Ghrelin infused into the dorsomedial hypothalamus of male mice increases food intake and adiposity. *Physiol. Behav.* 220, 112882. doi:10.1016/j.physbeh.2020.112882

Islam, M. N., Mita, Y., Maruyama, K., Tanida, R., Zhang, W., Sakoda, H., et al. (2020). Liver-expressed antimicrobial peptide 2 antagonizes the effect of ghrelin in rodents. *J. Endocrinol.* 244, 13–23. doi:10.1530/JOE-19-0102

Jerlhag, E., Egecioglu, E., Dickson, S. L., and Engel, J. A. (2010). Ghrelin receptor antagonism attenuates cocaine- and amphetamine-induced locomotor stimulation, accumbal dopamine release, and conditioned place preference. *Psychopharmacol. Berl.* 211, 415–422. doi:10.1007/s00213-010-1907-7

Jerlhag, E., Egecioglu, E., Landgren, S., Salomé, N., Heilig, M., Moechars, D., et al. (2009). Requirement of central ghrelin signaling for alcohol reward. *Proc. Natl. Acad. Sci. U. S. A.* 106, 11318–11323. doi:10.1073/pnas.0812809106

Kojima, M., Hosoda, H., Date, Y., Nakazato, M., Matsuo, H., and Kangawa, K. (1999). Ghrelin is a growth-hormone-releasing acylated peptide from stomach. *Nature* 402, 656–660. doi:10.1038/45230

Kristenssson, E., Sundqvist, M., Astin, M., Kjerling, M., Mattsson, H., Dornonville de la Cour, C., et al. (2006). Acute psychological stress raises plasma ghrelin in the rat. *Regul. Pept.* 134, 114–117. doi:10.1016/j.regpep.2006.02.003

Le May, M. V., Hume, C., Sabatier, N., Schéle, E., Bake, T., Bergström, U., et al. (2019). Activation of the rat hypothalamic supramammillary nucleus by food anticipation, food restriction or ghrelin administration. *J. Neuroendocrinol.* 31, e12676. doi:10.1111/jne.12676

Li, S., Xu, Y., Zheng, L., Pang, H., Zhang, Q., Lou, L., et al. (2022). Sex difference in global burden of major depressive disorder: findings from the global burden of disease study 2019. *Front. Psychiatry* 13, 789305. doi:10.3389/fpsyt.2022.789305

Livak, K. J., and Schmittgen, T. D. (2001). Analysis of relative gene expression data using real-time quantitative PCR and the 2(-Delta Delta C(T)) Method. *methods* 25, 402–408. doi:10.1006/meth.2001.1262

López-Ferreras, L., Richard, J. E., Anderberg, R. H., Nilsson, F. H., Olandersson, K., Kanoski, S. E., et al. (2017). Ghrelin's control of food reward and body weight in the lateral hypothalamic area is sexually dimorphic. *Physiology Behav.* 176, 40–49. doi:10.1016/j.physbeh.2017.02.011

Lutter, M., Sakata, I., Osborne-Lawrence, S., Rovinsky, S. A., Anderson, J. G., Jung, S., et al. (2008). The orexigenic hormone ghrelin defends against depressive symptoms of chronic stress. *Nat. Neurosci.* 11, 752–753. doi:10.1038/nn.2139

Mani, B. K., Puzziferri, N., He, Z., Rodriguez, J. A., Osborne-Lawrence, S., Metzger, N. P., et al. (2019). LEAP2 changes with body mass and food intake in humans and mice. *J. Clin. Invest* 129, 3909–3923. doi:10.1172/JCI125332

Mason, B. L., Wang, Q., and Zigman, J. M. (2014). The central nervous system sites mediating the orexigenic actions of ghrelin. *Annu. Rev. Physiol.* 76, 519–533. doi:10.1146/annurev-physiol-021113-170310

McKay, N. J., Giorgianni, N. R., Czajka, K. E., Brzyski, M. G., Lewandowski, C. L., Hales, M. L., et al. (2021). Plasma levels of ghrelin and GLP-1, but not leptin or amylin, respond to a psychosocial stressor in women and men. *Horm. Behav.* 134, 105017. doi:10.1016/j.yhbeh.2021.105017

McLean, C. P., Asnaani, A., Litz, B. T., and Hofmann, S. G. (2011). Gender differences in anxiety disorders: prevalence, course of illness, comorbidity and burden of illness. *J. Psychiatr. Res.* 45, 1027–1035. doi:10.1016/j.jpsychires.2011.03.006

Menzies, J. R., Skibicka, K. P., Leng, G., and Dickson, S. L. (2013). Ghrelin, reward and motivation. *Endocr. Dev.* 25, 101–111. doi:10.1159/000346058

M'Kadmi, C., Cabral, A., Barrile, F., Giribaldi, J., Cantel, S., Damian, M., et al. (2019). N-terminal liver-expressed antimicrobial peptide 2 (LEAP2) region exhibits inverse

agonist activity toward the ghrelin receptor. *J. Med. Chem.* 62, 965–973. doi:10.1021/acs.jmedchem.8b01644

Olff, M. (2017). Sex and gender differences in post-traumatic stress disorder: an update. *Eur. J. Psychotraumatol* 8 (4), 1351204. doi:10.1080/20008198.2017.1351204

Patterson, Z. R., Khazall, R., Mackay, H., Anisman, H., and Abizaid, A. (2013). Central ghrelin signaling mediates the metabolic response of C57BL/6 male mice to chronic social defeat stress. *Endocrinology* 154, 1080–1091. doi:10.1210/en.2012-1834

Perello, M., Cabral, A., Cornejo, M. P., De Francesco, P. N., Fernandez, G., and Uriarte, M. (2019). Brain accessibility delineates the central effects of circulating ghrelin. *J. Neuroendocrinol.* 31, e12677. doi:10.1111/jne.12677

Poe, G. R., Foote, S., Eschenko, O., Johansen, J. P., Bouret, S., Aston-Jones, G., et al. (2020). Locus coeruleus: a new look at the blue spot. *Nat. Rev. Neurosci.* 21, 644–659. doi:10.1038/s41583-020-0360-9

Roman, C. W., Derkach, V. A., and Palmiter, R. D. (2016). Genetically and functionally defined NTS to PBN brain circuits mediating anorexia. *Nat. Commun.* 7, 11905. doi:10.1038/ncomms11905

Sahakian, B. J., Winn, P., Robbins, T. W., Deeley, R. J., Everitt, B. J., Dunn, L. T., et al. (1983). Changes in body weight and food-related behaviour induced by destruction of the ventral or dorsal noradrenergic bundle in the rat. *Neuroscience* 10, 1405–1420. doi:10.1016/0306-4522(83)90122-7

Schalla, M. A., and Stengel, A. (2019). LEAP2: a novel regulator of food intake and body weight? *Nat. Rev. Gastroenterology Hepatology* 16, 711–712. doi:10.1038/s41575-019-0224-9

Schéle, E., Bake, T., Rabasa, C., and Dickson, S. L. (2016). Centrally administered ghrelin acutely influences food choice in rodents. *PLoS One* 11, e0149456. doi:10.1371/journal.pone.0149456

Sciolino, N. R., Hsiang, M., Mazzone, C. M., Wilson, L. R., Plummer, N. W., Amin, J., et al. (2022). Natural locus coeruleus dynamics during feeding. *Sci. Adv.* 8, eabn9134. doi:10.1126/sciadv.abn9134

Skibicka, K. P., and Dickson, S. L. (2011). Ghrelin and food reward: the story of potential underlying substrates. *Peptides* 32, 2265–2273. doi:10.1016/j.peptides.2011.05.016

Skibicka, K. P., Hansson, C., Alvarez-Crespo, M., Friberg, P. A., and Dickson, S. L. (2011). Ghrelin directly targets the ventral tegmental area to increase food motivation. *Neuroscience* 180, 129–137. doi:10.1016/j.neuroscience.2011.02.016

Skibicka, K. P., Hansson, C., Egecioglu, E., and Dickson, S. L. (2012). Role of ghrelin in food reward: impact of ghrelin on sucrose self-administration and mesolimbic dopamine and acetylcholine receptor gene expression. *Addict. Biol.* 17, 95–107. doi:10.1111/j.1369-1600.2010.00294.x

Smith, A., Woodside, B., and Abizaid, A. (2022). Ghrelin and the control of energy balance in females. *Front. Endocrinol. (Lausanne)* 13, 904754. doi:10.3389/fendo.2022.904754

Toufexis, D., Lipatova, O., Johnson, A., and Abizaid, A. (2016). Food-restriction lowers the acoustic startle response in both male and female rats, and, in combination with acute ghrelin injection, abolishes the expression of fear-potentiated startle in male rats. *J. Neuroendocrinol.* 28. doi:10.1111/jne.12436

Tschop, M., Smiley, D. L., and Heiman, M. L. (2000). Ghrelin induces adiposity in rodents. *Nature* 407, 908–913. doi:10.1038/35038090

Tufvesson-Alm, M., Zhang, Q., Aranäs, C., Blid Sköldheden, S., Edvardsson, C. E., and Jerlhag, E. (2023). Decoding the influence of central LEAP2 on hedonic food intake and its association with dopaminergic reward pathways. *bioRxiv*, 555294. 2008.2029. doi:10.1101/2023.08.29.555294

Uriarte, M., De Francesco, P. N., Fernandez, G., Cabral, A., Castrogiovanni, D., Lalonde, T., et al. (2019). Evidence supporting a role for the blood-cerebrospinal fluid barrier transporting circulating ghrelin into the brain. *Mol. Neurobiol.* 56, 4120–4134. doi:10.1007/s12035-018-1362-8

Van Bockstaele, E. J., Reyes, B. A., and Valentino, R. J. (2010). The locus coeruleus: a key nucleus where stress and opioids intersect to mediate vulnerability to opiate abuse. *Brain Res.* 1314, 162–174. doi:10.1016/j.brainres.2009.09.036

Wald, H. S., Ghidewon, M. Y., Hayes, M. R., and Grill, H. J. (2023). Hindbrain ghrelin and liver-expressed antimicrobial peptide 2, ligands for growth hormone secretagogue receptor, bidirectionally control food intake. *Am. J. physiology. Regul. Integr. Comp. physiology* 324, R547–R555. doi:10.1152/ajpregu.00232.2022

Walf, A. A., and Frye, C. A. (2007). The use of the elevated plus maze as an assay of anxiety-related behavior in rodents. *Nat. Protoc.* 2, 322–328. doi:10.1038/nprot.2007.44

Walker, D. L., and Davis, M. (1997). Anxiogenic effects of high illumination levels assessed with the acoustic startle response in rats. *Biol. Psychiatry* 42, 461–471. doi:10.1016/S0006-3223(96)00441-6

Wang, J. H., Li, H. Z., Shao, X. X., Nie, W. H., Liu, Y. L., Xu, Z. G., et al. (2019). Identifying the binding mechanism of LEAP2 to receptor GHSR1a. *Febs J.* 286, 1332–1345. doi:10.1111/febs.14763

Wren, A., Small, C. J., Ward, H. L., Murphy, K. G., Dakin, C. L., Taheri, S., et al. (2000). The novel hypothalamic peptide ghrelin stimulates food intake and growth hormone secretion. *Endocrinology* 141, 4325–4328. doi:10.1210/endo.141.11.7873

Yang, B., Sanches-Padilla, J., Kondapalli, J., Morison, S. L., Delpire, E., Awatramani, R., et al. (2021). Locus coeruleus anchors a trisynaptic circuit controlling fear-induced suppression of feeding. *Neuron* 109, 823–838.e6. doi:10.1016/j.neuron.2020.12.023

You, Z.-B., Galaj, E., Alén, F., Wang, B., Bi, G. H., Moore, A. R., et al. (2022b). Involvement of the ghrelin system in the maintenance and reinstatement of cocaine-motivated behaviors: a role of adrenergic action at peripheral β1 receptors. *Neuropsychopharmacology* 47, 1449–1460. doi:10.1038/s41386-021-01249-2

You, Z.-B., Gardner, E. L., Galaj, E., Moore, A. R., Buck, T., Jordan, C. J., et al. (2022a). Involvement of the ghrelin system in the maintenance of oxycodone self-administration: converging evidence from endocrine, pharmacologic and transgenic approaches. *Mol. Psychiatry* 27, 2171–2181. doi:10.1038/s41380-022-01438-5

Zigman, J. M., Jones, J. E., Lee, C. E., Saper, C. B., and Elmquist, J. K. (2006). Expression of ghrelin receptor mRNA in the rat and the mouse brain. *J. Comp. Neurology* 494, 528–548. doi:10.1002/cne.20823

frontiers | Frontiers in Pharmacology

TYPE Review
PUBLISHED 12 December 2023
DOI 10.3389/fphar.2023.1307746

OPEN ACCESS

EDITED BY
Christina Dalla,
National and Kapodistrian University of Athens, Greece

REVIEWED BY
Jacopo Zasso,
Human Technopole, Italy
Zhe Shi,
Hunan University of Chinese Medicine, China

*CORRESPONDENCE
Jing Teng,
60170099@sdutcm.edu.cn

RECEIVED 05 October 2023
ACCEPTED 04 December 2023
PUBLISHED 12 December 2023

CITATION
Lv S, Zhang G, Huang Y, Zhong X, Yi Y, Lu Y, Li J, Ma Y and Teng J (2023), Adult hippocampal neurogenesis: pharmacological mechanisms of antidepressant active ingredients in traditional Chinese medicine. *Front. Pharmacol.* 14:1307746. doi: 10.3389/fphar.2023.1307746

Adult hippocampal neurogenesis: pharmacological mechanisms of antidepressant active ingredients in traditional Chinese medicine

Shimeng Lv[1], Guangheng Zhang[1], Yufei Huang[2], Xia Zhong[1], Yunhao Yi[3], Yitong Lu[1], Jiamin Li[1], Yuexiang Ma[3] and Jing Teng[1]*

[1]Department of First Clinical Medical College, Shandong University of Traditional Chinese Medicine, Jinan, China, [2]Ruijin Hospital Affiliated to Shanghai Jiaotong University School of Medicine, Shanghai, China, [3]College of Traditional Chinese Medicine, Shandong University of Traditional Chinese Medicine, Jinan, China

Depression is characterized by prominent indicators and manifestations, such as anhedonia, which refers to the inability to experience pleasure, and persistent feelings of hopelessness. In clinical practice, the primary treatment approach involves the utilization of selective serotonin reuptake inhibitors (SSRIs) and related pharmacological interventions. Nevertheless, it is crucial to recognize that these agents are associated with significant adverse effects. Traditional Chinese medicine (TCM) adopts a multifaceted approach, targeting diverse components, multiple targets, and various channels of action. TCM has potential antidepressant effects. Anomalies in adult hippocampal neurogenesis (AHN) constitute a pivotal factor in the pathology of depression, with the regulation of AHN emerging as a potential key measure to intervene in the pathogenesis and progression of this condition. This comprehensive review presented an overview of the pharmacological mechanisms underlying the antidepressant effects of active ingredients found in TCM. Through examination of recent studies, we explored how these ingredients modulated AHN. Furthermore, we critically assessed the current limitations of research in this domain and proposed novel strategies for preclinical investigation and clinical applications in the treatment of depression in future.

KEYWORDS

depression, traditional Chinese medicine, antidepressant, adult hippocampal neurogenesis, pharmacological mechanism

1 Introduction

Major depressive disorder (MDD), widely known as depression, represents a psychiatric condition characterized by enduring mood deterioration and diminished capacity for experiencing pleasure. It stands as a significant contributor to global suicide rates. The World Health Organization reports that over 350 million individuals worldwide currently suffer from depression, with an average global incidence rate of approximately 4.4%. By 2030, depression is projected to become the leading disease in terms of global medical burden and serves as the largest non-fatal health loss factor universally (Rehm and Shield, 2019; Bayes et al., 2020). Primary treatment approaches for depression in clinical practice involve the utilization of selective serotonin reuptake inhibitors (SSRIs), which specifically inhibit the reabsorption of 5-hydroxytryptamine (5-HT; serotonin), thereby prolonging and enhancing

the effects of serotonin, resulting in an antidepressant response (Perez-Caballero et al., 2014; Bi et al., 2022). However, SSRIs are associated with adverse reactions, including nausea, headaches, sexual dysfunction, and weight gain. Additionally, most treatments encounter issues such as delayed effects and high non-response rates (Wang et al., 2019; Qu et al., 2021; Wei et al., 2022). Therefore, the development of more effective and safer antidepressants has become an urgent concern. Traditional Chinese medicine (TCM) exhibits characteristics such as a multi-component, multi-targeted, and multifaceted nature, making it highly suitable for depression treatment. Certain active ingredients derived from TCM have demonstrated significant antidepressant effects with minimal toxic side effects (Chi et al., 2019), indicating their potential for further research in the field of anti-depression.

Adult hippocampal neurogenesis (AHN) encompasses the entire process of neural stem cell (NSC) proliferation and division within the hippocampus, leading to the formation of neural progenitor cells (NPCs). These NPCs migrate to specific functional regions, undergo plasticity changes and differentiation, and establish synaptic connections with other neurons, ultimately promoting the production of neural function (Kuhn et al., 2018). The relationship between AHN and MDD is of considerable importance, and investigating antidepressant treatments that target the regulation of AHN holds promise for future advancements in antidepressant therapies (Sahay and Hen, 2007). Therefore, it is meaningful to design new treatment strategies for MDD patients and developing depression treatments to regulate AHN.

This review was aimed to provide an academic exposition on the physiological process of AHN and its association with the pathological mechanism of MDD. Additionally, it was also aimed to summarize and analyze the underlying mechanisms through which currently utilized active ingredients in TCM regulate AHN for the treatment of MDD. The objective of this review is to establish a scientific foundation for further basic research and clinical applications in this field.

2 Adult hippocampal neurogenesis

The hippocampus is closely intertwined with brain regions implicated in emotion, such as the amygdala and anterior cingulate cortex, and plays a fundamental role in regulating the hypothalamic-pituitary-adrenal (HPA) axis. It is crucial for emotional regulation and for understanding the development of depression (Schumacher et al., 2018; Tartt et al., 2022). Under normal physiological conditions, at least two parts of the adult mammalian brain exhibit sustained neurogenesis. They are the sub vehicular zone (SVZ) located in the later vehicle and the sub granular zone (SGZ) situated in the dentate gyrus (DG) of the hippocampus. Adult hippocampal SGZ NSCs are mainly located between the DG gate and the granulosa cell layer, and are usually in a resting state. When neural stem cells are stimulated, they gradually develop into immature neurons. After a series of processes, they develop into mature neurons, establish synaptic connections with adjacent neurons, and ultimately integrate into the functional neural circuits reflected in the hippocampus (Christian et al., 2014; Yao et al., 2016).

From a microscopic perspective, In the adult hippocampus, NSCs are responsible for generating new neurons. In rodents, NSCs in the hippocampus possess characteristics similar to astrocytes, with radiating protrusions extending to the DG granular cell layer. Therefore, these hippocampal NSCs are commonly referred to as radial glial-like cells (RGL, Type 1 cells). Activation of Type 1 cells results in the production of intermediate progenitors (Type 2 cells). Type 2 cells then differentiate into neuroblast-like cells (Type 3 cells). After several weeks or even months of maturation, Type 3 cells gradually develop into functional granular neurons (Kempermann et al., 2015; Llorens-Martín et al., 2016; Moss et al., 2016; Sánchez-Huerta et al., 2016; Pilz et al., 2018; Li et al., 2021).

3 Pathological connection between AHN and MDD

3.1 Hippocampal abnormalities

Pathological abnormalities in the hippocampus have been extensively investigated in relation to MDD (Belleau et al., 2019). A study conducted a comparative analysis of Magnetic Resonance Imaging (MRI) results between MDD patients and a healthy control group, unveiling a reduction in the volume of the left hippocampal CA3 and CA4 regions, alongside an elevation in the volume of the right hippocampal amygdala transition area (HATA) (Sun et al., 2023). Another report identified hippocampal atrophy in MDD patients experiencing anhedonia, specifically in the left CA1 and DG subfields, which may be associated with the lack of pleasure endemic to MDD (Wu et al., 2023). Furthermore, MDD patients exhibit diminished Gray Matter Volume (GMV) in the left hippocampus (Brosch et al., 2022). In this investigation, multimodal MRI techniques were employed to scrutinize connectivity patterns in individuals diagnosed with MDD. The findings revealed a significant decrease in the strength of connections within the right hippocampal sub-regional network and the temporal cortex, extending into the insula and basal ganglia. Additionally, the study observed a negative correlation between the degree of depression and functional connectivity (FC) in various brain regions, including the right cornu ammonis 1, right fusion, right HATA, and bilateral basal ganglia (Shengli et al., 2022). Nevertheless, hippocampal volume atrophy is intrinsically linked to a decline in neurogenesis, degeneration of cellular dendrites, and damage to granulosa cell dendrites (Schoenfeld et al., 2017). MDD-related atrophy in hippocampal volume manifests in the brain tissue, resulting in a reduction of hippocampal granule neurons and a decline in the extent of the neurogenic niche. As the brain region of AHN, pathological damage in the hippocampus plays a pivotal role in the progression of MDD. Furthermore, neuropathological damage within the hippocampus serves as a foundation for neurogenic impairment, while angiogenesis and an upsurge in hippocampal volume are vital physiological processes contributing to AHN occurrence (Berger et al., 2020).

3.2 Stress and adult hippocampal neurogenesis

Stress is widely acknowledged as a characteristic physiological and psychological response to both favorable and unfavorable circumstances. Prolonged stress constitutes a significant contributing factor in the development of mental disorders, including depression (Mahar et al., 2014). In rodent models, chronic stress is often employed as a model for depression due to its capacity to induce depression-like behaviors such as learned helplessness, anhedonia, and social withdrawal (Schoenfeld et al., 2017). Additionally, stress can inflict damage upon hippocampal neurons (Liu et al., 2021) and cause inflammatory cell infiltration within the hippocampus (Yan et al., 2021), directly or indirectly participating in depression onset. Studies have reported that severe and intense stress can impede AHN within the brain (Cameron and Glover, 2015), while acute or chronic stress during adulthood can hinder the regeneration and survival of new neurons within the DG region of the hippocampus (Garza et al., 2012). Moreover, stress can disrupt AHN by activating the HPA axis pathway and increasing the expression of stress-related hormones (Petrik et al., 2012). Activation of AHN can regulate excessive secretion of the HPA axis and alleviate the stress response (Snyder et al., 2011).

3.3 Neuroinflammation and adult hippocampal neurogenesis

Neuroinflammation refers to the inflammatory response occurring within the central nervous system, which can originate from various pathological injuries, including stress, infection, trauma, and ischemia. This process involves the production of pro-inflammatory cytokines, such as interleukin-1β (IL-1β), interleukin-6 (IL-6), and tumor necrosis factor-α (TNF-α), along with reactive oxygen species from innate immune cells within the central nervous system (Leng and Edison, 2021). Neuroinflammation represents a significant pathogenic factor in MDD, as substantial evidence supports the association between depression and the inflammatory process. Inflammation amplifies susceptibility to depression, and the usage of pro-inflammatory drugs heightens the risk of depression among individuals with the disorder (Kohler et al., 2016). Studies have demonstrated that administration of antidepressants reduces peripheral levels of inflammatory cytokines in individuals diagnosed with depression (Liu et al., 2020). The abnormal activation of microglia, resident macrophages within the central nervous system, is responsible for the production of several inflammatory and cytotoxic mediators associated with neuronal dysfunction and brain damage (Woodburn et al., 2021). Microglia express various receptors, including Toll-like receptors (TLRs), with TLR4 being the primary receptor for lipopolysaccharide (LPS). The activation of TLR4 induces downstream transcription factors such as nuclear factor (NF-κB) and the Nod-like receptor pyrin domain 3 (NLRP3), resulting in an increased expression of proinflammatory cytokines and the onset of neuroinflammation (Colonna and Butovsky, 2017). Neuroinflammation can regulate every step of adult neurogenesis, including cell proliferation, differentiation, migration, survival of newborn neurons, maturation, synaptogenesis, and neuritogenesis, when triggered by various immune components such as activated glia, cytokines, chemokines, and reactive oxygen species. Pro-inflammatory cytokines, including IL-6, IL-1β, and TNF-α, can influence the regulation of proliferation, neuronal cell fate, and neuronal differentiation in the context of hippocampal neurogenesis (Green and Nolan, 2014). Additionally, impaired AHN function is closely intertwined with microglial polarization. Stress-induced abnormal activation of microglia can impair the physiological process of neurogenesis, thereby leading to depression-like behavior. Reducing excessive neuroinflammation can ameliorate impaired neurogenesis and serve as a treatment for depression (Amanollahi et al., 2023; Chen et al., 2023).

3.4 Role of HPA axis in adult hippocampal neurogenesis

The HPA axis, a pivotal component of the neuroendocrine system orchestrating stress responses, plays a crucial role in the regulation of AHN. Activation of the HPA axis triggers the release of corticotropin-releasing hormone (CRH) from the paraventricular nucleus (PVN) in the hypothalamus, which in turn stimulates the secretion of corticotropin (ACTH) from the anterior pituitary gland. Subsequently, ACTH prompts the adrenal cortex to release cortisol (CORT) into the bloodstream (Frankiensztajn et al., 2020). In patients with depressive symptoms, an overactive HPA axis is associated with elevated levels of CRH, ACTH, and glucocorticoids (GCs), resulting in disrupted negative feedback and consequent pituitary and adrenal gland enlargement, as well as hypercortisolemia (Wang et al., 2021). Research indicates that the excessive activity of the HPA axis inhibits AHN through the activation of glucocorticoid receptors (GRs) and mineralocorticoid receptors by released GCs. However, antidepressant treatments have shown the ability to regulate HPA axis activity and promote AHN (Anacker et al., 2011; Anacker et al., 2013).

3.5 Autophagy and adult hippocampal neurogenesis

Autophagy, the principal intracellular degradation mechanism responsible for delivering cytoplasmic components to lysosomes for breakdown, serves a broader purpose than mere material removal. It acts as a dynamic circulatory system that generates fresh building blocks and energy, vital for cellular regeneration and maintenance of homeostasis (Mizushima and Komatsu, 2011). Dysregulation of autophagy pathways has been observed in the development of depression, indicating its significant involvement in the pathology of nervous system disorders. Promising results from clinical and preclinical studies targeting autophagy regulation have been reported (Jia and Le, 2015; Gassen and Rein, 2019). Notably, autophagy is closely intertwined with AHN in depression models, wherein chronic stress-induced decline in AHN is mediated by autophagic death of NSCs (Jung et al., 2020). The intervention of CORT triggers the upregulation of autophagy-related gene 5 (ATG5), leading to excessive neuronal autophagy in the DG. It results in heightened degradation of brain-derived neurotrophic

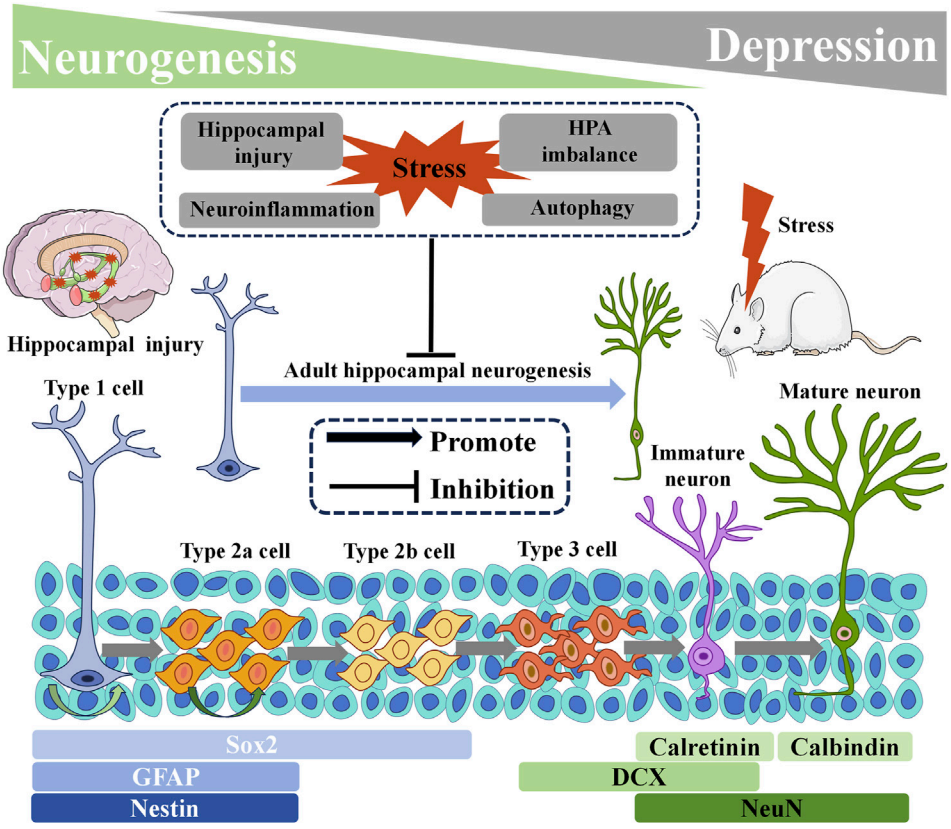

FIGURE 1
Adult Hippocampal Neurogenesis and Its Relationship with Depression. Below are markers that highlight the specificity of neurogenic processes. HPA: hypothalamic-pituitary-adrenal. DCX: doublecortin. GFAP: glial fibrillary acid protein. NeuN: neuronal nuclei. Sox2: sex determining region Y-box2.

factor (BDNF) and a significant reduction in the proliferation of NSCs, NPCs, and neuroblasts. Consequently, the survival and migration of new immature and mature neurons within the DG are impaired. Conversely, downregulation of neuron ATG5 promotes AHN and ameliorates depressive-like behavior in mice (Zhang et al., 2023). Furthermore, the absence of nuclear receptor binding factor 2 (NRBF2), an autophagy-related factor, disrupts autophagy flux in adult NSCs, compromising AHN and inducing a depression-like phenotype. On the contrary, overexpression of NRBF2 in adult NSCs within the DG region mitigates AHN impairment and treats depression (Zhang et al., 2023) (Figure 1).

3.6 Effects of antidepressant therapy on adult hippocampal neurogenesis

The hippocampus, as a NSC niche, facilitates neurogenesis throughout adulthood. Dysfunction of the hippocampus due to aging, injury, depression, or neurodegenerative diseases can lead to cognitive decline, significantly affecting the quality of life for individuals. Antidepressant treatments hold promise in directly or indirectly promoting AHN and alleviating depressive symptoms (Kot et al., 2022). SSRIs, commonly prescribed antidepressants, exert their effects by selectively blocking the reuptake of 5-HT, thereby prolonging and enhancing its activity (Perez-Caballero et al., 2014; Bi et al., 2022). Physical activity is another intervention capable of regulating emotional responses and effectively alleviating adverse emotions, including depression (Pearce et al., 2022). Both SSRIs and physical activity have been shown to promote AHN, contributing to their antidepressant mechanisms (Micheli et al., 2018). Recent studies have demonstrated that exercise improves anxiety performance in postmenopausal mice by fostering nerve regeneration in the DG region (Kang et al., 2023). Fluoxetine, a selective SSRI is widely used in clinical practice, ameliorates depression-like behavior by enhancing neurogenesis in a mouse model of Parkinson's disease (Mendonça et al., 2022a). Additionally, fluoxetine regulates negative behavior during the mouse estrus cycle by increasing AHN (Yohn et al., 2020). Importantly, when normal AHN processes were disrupted using genetic and radiological methods, the therapeutic effect of fluoxetine significantly diminished, highlighting the indispensable role of AHN in antidepressant treatment (Santarelli et al., 2003; Perera et al., 2011). Metformin, a first-line treatment for type 2 diabetes, controls blood sugar levels by suppressing liver gluconeogenesis and affecting glucose metabolism through various mechanisms (LaMoia and Shulman, 2021). It has also been explored for its potential in treating depression. Previous reports suggest that metformin can modulate gut microbiota and autophagy, offering therapeutic benefits for depression. Compared to other oral

hypoglycemic drugs, metformin demonstrates a reduced risk of depression and potential efficacy as an antidepressant (Yu et al., 2022; Mendonça et al., 2022b; Yang et al., 2022). Recent studies have revealed that metformin improves depressive-like behavior by promoting AHN (Lv et al., 2023).

In conclusion, a strong correlation exists between AHN and multiple pathogenic pathways associated with MDD. Impaired AHN functionality plays a pivotal role in the development and progression of MDD. Approaches aimed at promoting AHN have exhibited significant therapeutic benefits in preclinical trials for intervening in MDD. Consequently, enhancing AHN has emerged as a prominent area of study for advancing antidepressant medications.

4 Mechanism of active ingredients of TCM in promoting AHN in antidepressants

4.1 Regulation of the BDNF signaling pathway

BDNF is a growth factor extensively investigated for its involvement in neuronal maturation, synapse development, and synaptic plasticity within the brain (Björkholm and Monteggia, 2016). According to the neurotrophic hypothesis, reduced BDNF expression leads to neuronal atrophy, diminished synaptic plasticity, and contributes to the pathogenesis of depression (van Zutphen et al., 2019). Conversely, optimizing BDNF levels enhances synaptic plasticity and remodeling, mitigates neuronal damage, and ameliorates depressive symptoms (Phillips, 2017). The BDNF/tyrosine kinase receptor B (TrkB) signaling pathway plays a critical role in antidepressant interventions. BDNF facilitates AHN through TrkB regulation, promoting the differentiation and maturation of cortical progenitor cells into neurons during embryonic development (Bartkowska et al., 2007; Donovan et al., 2008). Several studies have reported on the modulation of the BDNF signaling pathway by bioactive components of TCM that foster AHN and alleviate depression.

Oroxylin A, the primary active compound extracted from *Scutellariae radix* (Sajeev et al., 2022), intricately regulates the BDNF/TrKB pathway, fostering AHN and exerting an antidepressant effect (Wu et al., 2022). Camellia assamica var. Kucha (Kucha), a Chinese tea cultivated in Yunnan Province, contains theacrine, a caffeine-like compound and the principal purine alkaloid. It manifests its antidepressant properties by precisely modulating the phosphodiesterase-4 (PDE4)/cyclic adenosine monophosphate (cAMP)/cAMP response element-binding (CREB)/BDNF/TrKB signaling pathway, thereby promoting AHN (Sheng et al., 2020; Ouyang et al., 2021).

Cucurbitacin B, primarily derived from *Cucumis melo L* (Dai et al., 2023), exhibits an antidepressant effect by ameliorating depression-like behavior in mice. Mechanistic investigations have unveiled its involvement in promoting BDNF/TrKB pathway activity and neurogenesis (Ge et al., 2023). Quercetin, abundantly present in various vegetables and fruits, possesses diverse beneficial pharmacological effects (Di Petrillo et al., 2022). In a murine model of depression induced by chronic unpredictable cold stress (CUMS), quercetin administration fosters AHN and treats depression through the Forkhead box transcription factor G1 (FoxG1)/BDNF/TrKB signaling pathway (Ma et al., 2021).

Xanthoceraside, a triterpenoid saponin extracted from *Xanthoceras sorbifolia Bunge* (Zhou et al., 2022), activates the BDNF signaling pathway and AHN, thus alleviating CUMS-induced depression (Guan et al., 2021). Water extracts of Panax ginseng and Polygala tenuifolia also exhibit antidepressant effects by modulating the BDNF/TrKB signaling pathway and promoting AHN (Jiang et al., 2021a). Chronic social distress (CSDS) is often employed in preclinical studies to induce animal models of depression that resemble human depressive mood (Yoshida et al., 2021). Recent reports have demonstrated that CSDS inhibits AHN by impairing the BDNF/TrKB signaling pathway in the hippocampus of mice. However, intervention with Ginsenoside Rb1 can alleviate these pathological phenomena (Jiang et al., 2021b). Another active compound derived from *Panax ginseng C.A. Meyer*, Ginsenoside Rh2, improves depressive behavior in mice by positively modulating the BDNF/TrKB signaling pathway (Shi et al., 2022).

Paeonia lactiflora Pall, a commonly used antidepressant in TCM, contains the water-soluble monoterpene glycoside paeoniflorin, which exhibits various pharmacological activities (Zhou et al., 2020). Recent studies have unveiled that paeoniflorin alleviates CUMS-induced inhibition of AHN by promoting the expression of the BDNF/TrKB signaling pathway (Chen et al., 2019). Echinacoside, a natural phenylethanoid glycoside extracted from *Cistanche Tubulosa* (Li et al., 2022), exerts an antidepressant effect by augmenting the activity of the BDNF/TrKB signaling pathway, regulating M1/M2 polarization of microglia, and inhibiting neuroinflammation (Lu et al., 2023).

Cryptotanshinone, a natural quinone diterpenoid extracted from *Salvia miliorrhiza*, employs the BDNF/TrKB and NFκB signaling pathways to promote AHN and inhibit neuroinflammation[], thus exerting its antidepressant mechanism (Wang et al., 2021). Naringin, a bioflavonoid identified from *Tangerine Peel*, promotes AHN and treats depression by activating the CREB signaling pathway (Gao et al., 2022). Pterostilbene, an active ingredient derived from Dragon's blood, fosters AHN through the BDNF/extracellular signal-regulated kinase (ERK)/CREB signaling pathway, thereby improving depressive-like behavior in mice subjected to chronic unpredictable stress (CUS) (Yang et al., 2019).

4.2 Inhibition of neuroinflammation

Neuroinflammation plays a pivotal role in the pathogenesis of MDD. Excessive neuroinflammatory responses have been shown to hinder AHN, while inhibiting neuroinflammation promotes AHN and ameliorates depressive-like behavior. Thymoquinone, a bioactive compound found in Nigella sativa, effectively suppresses neuroinflammation in the hippocampus and amygdala, promoting AHN and restoring BDNF levels, thus facilitating neurogenesis (Nazir et al., 2022). Hesperidin, a flavanone glycoside abundantly present in citrus fruits such as lemon, sweet orange (Citrus sinensis), and grapefruits (Hajialyani et al., 2019), exerts antidepressant effects through its

anti-inflammatory and antioxidant properties, stress reduction, attenuation of cell apoptosis, and enhancement of neurogenesis (Kwatra et al., 2020). Porphyran, an active component isolated from *Porphyra haitanensis*, mitigates exaggerated inflammation induced by LPS in the hippocampus, restores the activity of the BDNF signaling pathway, fosters AHN, and improves depressive behavior in mice (Yi et al., 2021). Patchouli alcohol, the principal active ingredient of Patchouli, inhibits NLRP3 inflammasomes and ameliorates microglia-mediated disturbances in neurogenesis (He et al., 2023). Akebia saponin D, a triterpenoid saponin derived from the rhizome of *Dipsacus asper* (Yang et al., 2021), reprograms neurogenic microglia via the peroxisome proliferator-activated receptor-gamma (PPAR-γ) pathway, rescues hippocampal neurogenesis impaired by Chronic Mild Stress (CMS), and enhances AHN (Zhang et al., 2023). Ginsenoside Rg1 and Ginsenoside Rb1, major components of Panax ginseng C.A. Meyer, exert their antidepressant effects by downregulating neuroinflammation and promoting AHN (Jiang et al., 2020). Similarly, Ginsenoside Rb1 utilizes PPAR-γ mediated activation of microglia to improve AHN in depression treatment (Zhang et al., 2021). Silymarin, a derivative derived from *milk thistle seeds*, has long been used in the treatment of hepatic ailments (Gillessen and Schmidt, 2020). In the treatment of depression, empirical data suggests that Silymarin and Silymarin nanoparticles may exert their therapeutic effects through their antioxidant and anti-inflammatory mechanisms, while also promoting neurogenesis in the prefrontal cortex and hippocampus (Ashraf et al., 2019). Berberine, an isoquinoline alkaloid extracted from the Chinese herb *Coptis chinensis* and various *Berberis* plants, (Song et al., 2020), inhibits NLRP3 inflammasomes to mitigate neuroinflammatory responses, enhances synaptic plasticity and neurogenesis, and improves neuronal degeneration, thereby exhibiting its antidepressant effect (Qin et al., 2023).

4.3 Regulation of the HPA axis

The HPA axis, a vital component of the neuroendocrine system, is closely associated with AHN and the pathophysiology of depression. Formononetin, a phytoestrogen obtained from the Chinese medicinal herb *Red Clover* (Yu et al., 2022), promotes AHN by modulating serum CORT levels and hippocampal GR expression in a mouse model of CORT-induced depression (Zhang et al., 2022). Puerarin, a phytoestrogen extracted from *Pueraria* plants (Zhang et al., 2019), holds potential for treating depression-like behavior induced by ovariectomy, with mechanisms involving the inhibition of HPA axis hyperactivity, regulation of BDNF expression, and promotion of AHN (Tantipongpiradet et al., 2019). The Ethanol Extract of Dipterocarpus alatus alleviates HPA axis hyperactivity induced by Unpredictable CMS (UCMS) and regulates BDNF and CREB expression levels (Daodee et al., 2019). The Flower Essential Oil of Tagets Minuta promotes neurogenesis through the modulation of the HPA axis and the BDNF/protein kinase B (Akt)/ERK2 pathway (Birmann et al., 2022). Leonurine, a prominent bioactive constituent derived from *Herba leonuri* (Zhao et al., 2021), promotes axonal growth and neurotrophic activity in cultured PC12 cells through the regulation of the GR/SGK1 signaling pathway (Meng et al., 2019).

4.4 Adjustment of the PI3K/Akt signaling pathway

The Phosphatidylinositol 3-kinase (PI3K)/protein kinase B (Akt) signaling pathway represents a crucial regulatory cascade governing cell growth, proliferation, migration, metabolism, and survival (Wang et al., 2022). Targeted modulation of the PI3K/Akt signaling pathway has shown antidepressant effects, as both patients with MDD and animal models exhibit downregulation of PI3K and Akt expression. Moreover, targeted regulation of the PI3K/Akt signaling pathway demonstrates an antidepressant effect (Zhang et al., 2021). Furthermore, this pathway plays a role in promoting AHN by facilitating cellular growth and survival in response to growth factors (Chen et al., 2020). *Xiaoyaosan*, a compound widely employed in TCM, serves as an exemplary representative due to its multiple targets and pathways that contribute to its antidepressant properties (Chen et al., 2022). In a recent study, it was discovered that the ethyl acetate fraction of *Xiaoyaosan* can treat depression by regulating the PI3K/Akt signaling pathway, reducing neuronal apoptosis, and fosters neurogenesis, thereby effectively treating depression (Zeng et al., 2022). The PI3K/Akt signaling pathway also mediates the neuroprotective effect of Akebia saponin D and the antidepressant effects of Baicalin by safeguarding neural stem/precursor cells against inflammatory effects mediated by microglia and stimulating their proliferation and neuronal differentiation, respectively (Liu et al., 2022). *Baicalin*, isolated from *Scutellaria baicalensis*, possesses antidepressant properties due to its association with hippocampal neurogenesis. Previous studies have demonstrated that Baicalin has the ability to modulate the PI3K/Akt/glycogen synthase kinase-3β (GSK3β)/β-catenin pathway, thereby stimulating AHN and eliciting antidepressant effects (Zhao et al., 2020). Moreover, Baicalin has been shown to promote AHN, and alleviate inflammation-induced pain-related depression through Akt-mediated AHN (Fang et al., 2020). Additionally, Baicalin facilitates neuronal differentiation and survival through the Akt/FoxG1 pathway, contributing to its antidepressant effects (Zhang et al., 2019).

4.5 Regulation of the microbiota-gut-brain axis

The gut microbiota, an intricate internal metabolic organ comprised of over 10^{14} bacteria and weighing approximately 0.3% of an individual's body weight, has garnered recognition for its significant role. Emerging research highlights a profound correlation between the gut microbiota and the central nervous system (Xiao et al., 2020). The bidirectional communication between the brain and gut microbiota has captivated scientific interest due to its disruption being identified as a pivotal driver in the development of depression (Du et al., 2020). Notably, the microbiota-gut-brain axis exerts influence on hippocampal neurogenesis by modulating serum metabolite levels (Siopi et al.,

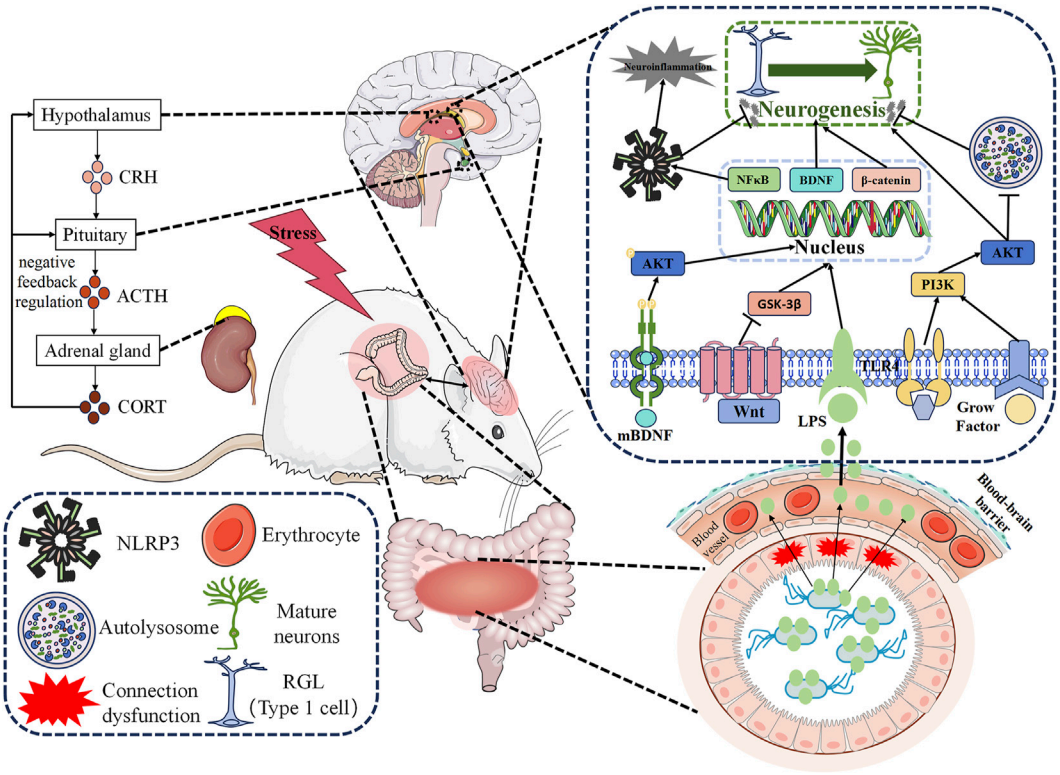

FIGURE 2
Mechanism of Regulating Adult Hippocampal Neurogenesis by Active Ingredients of Traditional Chinese Medicine in Antidepressant. Active ingredients extracted from Traditional Chinese Medicine promote AHN by regulating various signaling pathways, such as BDNF signaling pathway, PI3K/Akt signaling pathway, and Wnt/β-catenin signaling pathway, as well as by inhibiting neuroinflammation and modulating the HPA axis and microbiota-gut-brain axis. BDNF: Brain-derived neurotrophic factor. PI3K: Phosphatidylinositol 3-kinase. Akt: Protein kinase B. AHN: Adult hippocampal neurogenesis. NF-κB: Transcription factor nuclear factor. NLRP3: Nod-like receptor thermal protein domain 3. CRH: Corticotropin releasing hormone. ACTH: Corticotropin. CORT: Cortisol. LPS: Lipopolysaccharide. RGL: Radial glial-like cells. HPA: hypothalamic-pituitary-adrenal.

2020), while antidepressants have demonstrated efficacy through this axis (Bi et al., 2022).

Eucommia cortex polysaccharides represent the principal active constituents derived from Eucommia cortex (Sun et al., 2022). In a recent preclinical investigation, it was discovered that Eucommia cortex polysaccharides mitigate the release of bacterial-derived LPS, inhibit the TLR4/NFκB/MAPK signaling pathway mediated by microglia, and promote AHN (Wang et al., 2023). Inulin, originally extracted from *Inula helenium*, bestows various beneficial effects upon the body (Illippangama et al., 2022). In a mouse model of chronic unpredictable mild stress (CUMS)-induced depression, disruptions in intestinal microbiota, compromised intestinal barrier integrity, altered levels of short-chain fatty acids (SCFAs), and elevated circulating LPS were observed, resulting in excessive activation of neuroinflammation, impairment of hippocampal neurogenesis, and synaptic plasticity. Inulin intervention ameliorated these pathological phenomena and reversed the depression-like behavior induced by CUMS (Wang et al., 2023). Diosgenin, one of the primary bioactive compounds found in fenugreek seeds (Arya and Kumar, 2021), shows promise in rectifying gut microbiota imbalances, regulating HPA axis secretion levels, upregulating hippocampal BDNF signaling pathway expression, promoting AHN, and treating depression (Cui et al., 2023). Consequently, the microbiota-gut-brain axis assumes a pivotal role for antidepressant interventions, mediating the augmentation of AHN through active ingredients found in TCM.

4.6 Regulation of the Wnt/β-catenin signaling pathway

The Wnt/β-catenin pathway plays a critical role in the process of embryonic development and the maintenance of tissue equilibrium in adult organisms. Dysregulation of Wnt/β-catenin signal transduction often accompanies major disorders (Liu et al., 2022). It is widely postulated that Wnt signaling exerts influence on the delicate balance between NSC proliferation and differentiation through transcriptional co-activators, particularly β-catenin, during brain development and adult tissue homeostasis maintenance. Alterations in Wnt signaling have been implicated in developmental abnormalities and neurological diseases. Employing the Wnt/β-catenin pathway as a therapeutic approach for depression and the facilitation of AHN has yielded promising outcomes (Gao et al., 2021).

Crocin, a hydrophilic carotenoid synthesized in the flowers of the Crocus genus (Boozari and Hosseinzadeh, 2022), has

TABLE 1 Mechanism of action of active ingredients in traditional Chinese medicine.

Active ingredients of TCM	CAS NO.	Molecular formula	Main sources	Modeling method	Behavioral testing evaluation	Mechanism of action/ main indicators	References
Oroxylin A	480-11-5	$C_{16}H_{12}O_5$	*Scutellariae radix*	CUMS	OFT, FST, TST, SPT	BDNF/TrkB system participates in promoting AHN and antidepressant processes	Sajeev et al. (2022), Wu et al. (2022)
Theacrine	2309-49-1	$C_9H_{12}N_4O_3$	*Camellia assamica var. Kucha*	CWIRS + CUMS	FST, TST, SPT, SMAT	Regulating the PDE4/cAMP/CREB/BDNF/TrkB pathway to promote AHN	Sheng et al. (2020), Ouyang et al. (2021)
Cucurbitacin B	6199-67-3	$C_{32}H_{46}O_8$	*Cucumis melo L*	CUMS	OFT, FST, TST, SPT	Promote BDNF/TrkB pathway activity and neurogenesis	Dai et al. (2023), Ge et al. (2023)
Quercetin	117-39-5	$C_{15}H_{10}O_7$	*Widely distributed in fruits and vegetables*	CUMS	OFT, SPT, TST	Regulating the FoxG1/CREB/BDNF pathway to promote AHN	Ma et al. (2021), Di Petrillo et al. (2022)
Ginsenoside Rb1	41753-43-9	$C_{54}H_{92}O_{23}$	*Panax ginseng C.A. Meyer*	CSDS	SIT, SPT, FST	Enhancing BDNF signaling cascade and promoting AHN	Jiang et al. (2021b)
Ginsenoside Rh2	78214-33-2	$C_{36}H_{62}O_8$	*Panax ginseng C.A. Meyer*	CUMS	FST, TST, OFT	Positive regulation of BDNF/TrKB signaling pathway	Shi et al. (2022)
paeoniflorin	23180-57-6	$C_{23}H_{28}O_{11}$	*Paeonia lactiflora Pall*	CUMS	SPT	Promote the expression of BDNF/TrKB signaling pathway to alleviate AHN inhibition caused by CUMS	Chen et al. (2019), Zhou et al. (2020)
Echinacoside	82854-37-3	$C_{35}H_{46}O_{20}$	*Cistanche tubulosa*	CUMS	OFT, FST, TST, SPT	Enhance the activity of BDNF/TrKB signaling pathway and regulate M1/M2 polarization of microglia and inhibit neuroinflammation	Li et al. (2022), Lu et al. (2023)
Cryptotanshinone	35825-57-1	$C_{19}H_{20}O_3$	*Salvia miltiorrhiza*	CUS	SPT, FST, FUST, LAT	Through BDNF/TrKB and NFκB signaling pathway to promote AHN and inhibit neuroinflammation	Wang et al. (2021b)
Naringin	10236-47-2	$C_{27}H_{32}O_{14}$	*Tangerine peel*	CORT	TST, OFT, FST	Activating the CREB signaling pathway to promote AHN	Gao et al. (2022)
Pterostilbene	537-42-8	$C_{16}H_{16}O_3$	*Dragon's blood*	CUS	SPT, OFT, FST, NSFT	Promoting AHN through the BDNF/ERK/CREB signaling pathway	Yang et al. (2019)
Thymoquinone	490-91-5	$C_{10}H_{12}O_2$	*Nigella sativa*	UCMS	FST, EPM, SIT, NSFT	Inhibiting neuroinflammation in the hippocampus and amygdala and restoring BDNF levels	Nazir et al. (2022)
Hesperidin	520-26-3	$C_{28}H_{34}O_{15}$	*lemon, sweet orange (Citrus sinensis), and grapefruits*	RS + LPS	EPM, OFT, TST, FET, SPT	Anti inflammation, antioxidant stress, alleviating cell apoptosis, and promoting neurogenesis	Hajialyani et al. (2019), Kwatra et al. (2020)
Porphyran	11016-36-7	$C_{26}H_{44}O_{27}S_2^{-2}$	*Porphyra haitanensis*	LPS	FST, TST, OFT	Suppress NFκB/NLRP3 inflammatory signaling pathway, restores BDNF signaling pathway activity, promotes AHN	Yi et al. (2021)
Patchouli alcohol	5986-55-0	$C_{15}H_{26}O$	*patchouli*	CMS	SPT, TST, FST, OFT, LAT, Coat score	Inhibition of NLRP3 inflammasome and improvement of microglia mediated neurogenic disorders	Lee et al. (2020), He et al. (2023)

(Continued on following page)

TABLE 1 (*Continued*) Mechanism of action of active ingredients in traditional Chinese medicine.

Active ingredients of TCM	CAS NO.	Molecular formula	Main sources	Modeling method	Behavioral testing evaluation	Mechanism of action/ main indicators	References
Akebia saponin D	39524-08-8	$C_{47}H_{76}O_{18}$	*Dipsacus asper*	CMS	SPT, OFT, FST	Through PPAR-γ Pathway reprogramming of neurogenic microglia to restore hippocampal neurogenesis	Yang et al. (2021), Zhang et al. (2023c)
Ginsenoside Rg1	22427-39-0	$C_{42}H_{72}O_{14}$	*Panax ginseng C.A. Meyer*	CSDS	SIT, SPT, TST, FST	Downregulation and upregulation of neuroinflammation in neurogenesis	Jiang et al. (2020)
Ginsenoside Rb1	41753-43-9	$C_{54}H_{92}O_{23}$	*Panax ginseng C.A. Meyer*	CMS	TST, FST	Through PPAR-γ Mediated activation of microglia and improvement of AHN	Zhang et al. (2021a)
Berberine	2086-83-1	$C_{20}H_{18}NO_4^+$	*Coptis chinensis*	CORT	OFT, TST, FST, SPT	Inhibiting the activation of NLRP3 inflammasomes reduces neuroinflammatory responses and improves neuronal degeneration by promoting synaptic plasticity and neurogenesis	Song et al. (2020), Qin et al. (2023)
Formononetin	485-72-3	$C_{16}H_{12}O_4$	*Herb Red Clover*	CORT	SPT, FST, LAT	Reduced serum corticosterone levels, upregulated protein expression levels of GR and BDNF in the hippocampus, and promoted neurogenesis in the hippocampus	Yu et al. (2022b), Zhang et al. (2022)
Puerarin	3681-99-0	$C_{21}H_{20}O_9$	*Pueraria plants*	Ovariectomy	TST, FST	Relieve excessive activation of HPA axis and regulate BDNF expression level, promoting AHN	Zhang et al. (2019a), Tantipongpiradet et al. (2019)
Leonurine	24697-74-3	$C_{14}H_{21}N_3O_5$	*Herba leonuri*	CORT	Not Applicable	Regulating the GR/ SGK1 signaling pathway	Meng et al. (2019), Zhao et al. (2021)
Xiaoyaosan ethyl acetate fraction	Not Applicable	Not Applicable	*Xiaoyaosan*	CUMS	SPT, ST, NFST, TST	Promote hippocampal neurogenesis, reduce neuronal apoptosis, and regulate PI3K/Akt pathway activity	Zeng et al. (2022)
Akebia saponin D	39524-08-8	$C_{47}H_{76}O_{18}$	*Dipsacus asper*	LPS	SPT, FST, EPM, NORT, MWM	Neuroprotective effects are mediated through the PI3K/ Akt signaling pathway, protecting neural stem/ precursor cells from the inflammatory effects mediated by microglia and stimulating their proliferation and neuronal differentiation	Liu et al. (2022a)
Baicalin	21967-41-9	$C_{21}H_{18}O_{11}$	*Scutellaria baicalensis*	CORT	SPT, OFT, TST, FST, NSFT	Activating AHN and antidepressant effects through the PI3K/AKT/ GSK3β/β-catenin pathway	Zhao et al. (2020)
Baicalin	21967-41-9	$C_{21}H_{18}O_{11}$	*Scutellaria baicalensis*	CFA	SPT, TST, Splash test	Alleviation of inflammatory pain related depression through Akt mediated adult hippocampal neurogenesis	Fang et al. (2020)
Baicalin	21967-41-9	$C_{21}H_{18}O_{11}$	*Scutellaria baicalensis*	CUMS	SPT, OFT, TST	Promoting neuronal differentiation and survival through the Akt/ FOXG1 pathway, thereby exerting antidepressant effects	Zhang et al. (2019b)

(Continued on following page)

TABLE 1 (*Continued*) Mechanism of action of active ingredients in traditional Chinese medicine.

Active ingredients of TCM	CAS NO.	Molecular formula	Main sources	Modeling method	Behavioral testing evaluation	Mechanism of action/ main indicators	References
Inulin	9005-80-5	Not Applicable	*Inula helenium*	CUMS	TST, FST, OFT, EPM, MBT	Regulate intestinal microbiota disorder and SCFAs levels, protect intestinal barrier, inhibit neuroinflammation, promote AHN, and restore synaptic plasticity	Illippangama et al. (2022), Wang et al. (2023b)
Diosgenin	512-04-9	$C_{27}H_{42}O_3$	*Fenugreek seeds*	CRS	SPT, FST	Improve intestinal microbiota imbalance, regulate HPA axis secretion level, upregulate hippocampal BDNF signaling pathway expression, and promote AHN	Arya and Kumar (2021), Cui et al. (2023)
Crocin	42553-65-1	$C_{44}H_{64}O_{24}$	*Crocus genus*	CUMS	SPT, FST, TST	Through Wnt/β-catenin signaling pathway promotes AHN and exerts antidepressant effects	Boozari and Hosseinzadeh (2022), Tao et al. (2023)
Baicalin	21967-41-9	$C_{21}H18O_{11}$	*Scutellaria baicalensis*	CUMS	TST, EPM, SPT	Adjusting Wnt/β-catenin signaling pathway, activating AHN	Xiao et al. (2021)

Note:CUMS, chronic unpredictable mild stress; CWIRS, chronic water immersion restraint stress; CSDS, Chronic social defeat stress; CUS, Chronic unpredictable stress; RS, Restraint stress; LPS, Lipopolysaccharide; CFA, Freund's adjuvant; CRS, Chronic restraint stress; SIT, Social Interaction Test; LAT, Locomotor activity test; NSFT, Novelty-suppressed feeding test; ST, Splash test; NORT, Novel object recognition test; MWM, Morris water maze; MBT, Marble burying test; OFT, Open field test; TST, Tail suspension test; FST, Forced swimming test; SPT, Sucrose preference test; SMAT, Spontaneous Motor Activity Test; BDNF, Brain-derived neurotrophic factor; TrKB, tyrosine kinase B; AHN, Adult hippocampal neurogenesis; PDE4, Phosphodiesterase-4; cAMP, Cyclic adenosine mono—Phosphate; CREB, cAMP response-element binding; FoxG1, Forkhead box transcription factor G1; EPM, Elevated Plus Maze; NF-κB, Nuclear transcription factor-κB; NLRP3, Nucleotide-binding oligomerization domain-like receptor protein 3; PPAR-γ, Peroxisome proliferator-activated receptor-gamma; GR, Glucocorticoid receptor; SGK1, Serum-inducible and glucocorticoid-inducible kinase 1; PI3K, Phosphatidylinositol 3-kinase; Akt, Protein kinase B; GSK3β, Glycogen synthase kinase-3b; HPA, Hypothalamic-pituitary-adrenal; SCFAs, Short-chain fatty acids; TCM, traditional chinese medicine.

exhibited the capacity to enhance AHN and induce antidepressant effects by modulating the Wnt/β-catenin signaling pathway (Tao et al., 2023). Similarly, Baicalin has demonstrated its ability to counteract depression-like behavior induced by CUMS in mice by finely modulating the Wnt/β-catenin signaling pathway and promoting AHN (Xiao et al., 2021) (Figure 2; Table 1).

5 Discussion

MDD is a debilitating, chronic, and recurrent mental illness characterized by profound emotional distress, feelings of inadequacy, somatic discomfort, disturbances in sleep or appetite, and an elevated susceptibility to suicidal attempts and actions (Xia et al., 2023). Despite its substantial impact on individuals and society, the pathophysiology of MDD remains enigmatic, and effective interventions are limited, posing an enduring challenge in contemporary medicine (Chen et al., 2022). TCM encompasses a myriad of components, targets, and pathways that harbor potential therapeutic benefits. Moreover, bioactive constituents derived from TCM possess the capacity to engender AHN through diverse signaling pathway, including BDNF, PI3K/Akt, and Wnt/β-catenin, as well as via the modulation of neuroinflammation and the intricate interplay within the HPA and microbiota-gut-brain axes. These bioactive entities hold immense promise for the treatment of MDD.

Nevertheless, current research predominantly relies on animal or cellular models, lacking sufficient exploration into the clinical efficacy of TCM active ingredients in alleviating depression among MDD patients. Additionally, numerous bioactive compounds sourced from TCM encounter challenges such as instability, poor solubility, and limited ability to traverse the blood-brain barrier. The precise targeting of organs implicated in MDD by these bioactive agents also remains uncertain. Furthermore, several Chinese herbal medicines lack well-defined quality control standards, impeding the assurance of chemical component stability and consistency, thereby constraining their clinical utility and hindering the investigation of their pharmacological mechanisms. Most notably, there exists a paucity of research pertaining to the specificity of TCM active ingredients in relation to AHN, warranting further scrutiny to ascertain the ability of these bioactive moieties to efficaciously target AHN.

Therefore, future research endeavors should concentrate on expanding clinical observations regarding the efficacy and adverse reactions of TCM active ingredients in treating MDD patients, while concurrently ameliorating the quality control standards of TCM. Moreover, considerable efforts ought to be devoted to enhancing the exploration of targeted delivery systems for TCM that augment drug concentration and duration of action

within the central nervous system, thereby heightening the therapeutic effects of bioactive constituents in target organs. Additionally, the integration of multiple omics techniques can enrich our understanding of the intricate pathways involved in the promotion of AHN by TCM active ingredients, thus fortifying the connection between AHN and MDD. Finally, the incorporation of antagonists or reverse validation methods, such as gene knockout strategies, can facilitate the elucidation of the mechanisms through which Chinese herbal active ingredients regulate AHN. Extensive work would be required in clinical and preclinical studies to unravel the underlying mechanisms by which antidepressant treatments regulate AHN. It is of great significance for the development of TCM as a therapeutic modality for MDD.

Author contributions

SL: Writing–original draft, Writing–review and editing. GZ: Writing–review and editing. YH: Writing–review and editing. XZ: Writing–review and editing. YY: Writing–review and editing. YL: Writing–review and editing. JL: Writing–review and editing. YM: Writing–review and editing. JT: Writing–review and editing.

Funding

The author(s) declare financial support was received for the research, authorship, and/or publication of this article. This study was supported by a study on the Shandong Province Special Disease Prevention Project of Integrated Traditional Chinese and Western Medicine (YXH2019ZXY006).

Conflict of interest

The authors declare that the research was conducted in the absence of any commercial or financial relationships that could be construed as a potential conflict of interest.

Publisher's note

References

Amanollahi, M., Jameie, M., Heidari, A., and Rezaei, N. (2023). The dialogue between neuroinflammation and adult neurogenesis: mechanisms involved and alterations in neurological diseases. *Mol. Neurobiol.* 60 (2), 923–959. doi:10.1007/s12035-022-03102-z

Anacker, C., Cattaneo, A., Luoni, A., Musaelyan, K., Zunszain, P. A., Milanesi, E., et al. (2013). Glucocorticoid-related molecular signaling pathways regulating hippocampal neurogenesis. *Neuropsychopharmacology* 38 (5), 872–883. doi:10.1038/npp.2012.253

Anacker, C., Zunszain, P. A., Cattaneo, A., Carvalho, L. A., Garabedian, M. J., Thuret, S., et al. (2011). Antidepressants increase human hippocampal neurogenesis by activating the glucocorticoid receptor. *Mol. Psychiatry* 16 (7), 738–750. doi:10.1038/mp.2011.26

Arya, P., and Kumar, P. (2021). Diosgenin a steroidal compound: an emerging way to cancer management. *J. Food Biochem.* 45 (12), e14005. doi:10.1111/jfbc.14005

Ashraf, A., Mahmoud, P. A., Reda, H., Mansour, S., Helal, M. H., Michel, H. E., et al. (2019). Silymarin and silymarin nanoparticles guard against chronic unpredictable mild stress induced depressive-like behavior in mice: involvement of neurogenesis and NLRP3 inflammasome. *J. Psychopharmacol.* 33 (5), 615–631. doi:10.1177/0269881119836221

Bartkowska, K., Paquin, A., Gauthier, A. S., Kaplan, D. R., and Miller, F. D. (2007). Trk signaling regulates neural precursor cell proliferation and differentiation during cortical development. *Development* 134 (24), 4369–4380. doi:10.1242/dev.008227

Bayes, J., Schloss, J., and Sibbritt, D. (2020). Effects of polyphenols in a mediterranean diet on symptoms of depression: a systematic literature review. *Adv. Nutr.* 11 (3), 602–615. doi:10.1093/advances/nmz117

Belleau, E. L., Treadway, M. T., and Pizzagalli, D. A. (2019). The impact of stress and major depressive disorder on hippocampal and medial prefrontal cortex morphology. *Biol. Psychiatry* 85 (6), 443–453. doi:10.1016/j.biopsych.2018.09.031

Berger, T., Lee, H., Young, A. H., Aarsland, D., and Thuret, S. (2020). Adult hippocampal neurogenesis in major depressive disorder and alzheimer's disease. *Trends Mol. Med.* 26 (9), 803–818. doi:10.1016/j.molmed.2020.03.010

Bi, C., Guo, S., Hu, S., Chen, J., Ye, M., and Liu, Z. (2022). The microbiota-gut-brain axis and its modulation in the therapy of depression: comparison of efficacy of conventional drugs and traditional Chinese medicine approaches. *Pharmacol. Res.* 183, 106372. doi:10.1016/j.phrs.2022.106372

Birmann, P. T., Casaril, A. M., Zugno, G. P., Acosta, G. G., Severo Sabedra Sousa, F., Collares, T., et al. (2022). Flower essential oil of *Tagetes minuta* mitigates oxidative stress and restores BDNF-Akt/ERK2 signaling attenuating inflammation- and stress-induced depressive-like behavior in mice. *Brain Res.* 1784, 147845. doi:10.1016/j.brainres.2022.147845

Björkholm, C., and Monteggia, L. M. (2016). BDNF - a key transducer of antidepressant effects. *Neuropharmacology* 102, 72–79. doi:10.1016/j.neuropharm.2015.10.034

Boozari, M., and Hosseinzadeh, H. (2022). Preventing contrast-induced nephropathy (CIN) with herbal medicines: a review. *Phytother. Res.* 36 (10), 1130–1146. doi:10.1002/ptr.6880

Brosch, K., Stein, F., Schmitt, S., Pfarr, J. K., Ringwald, K. G., Thomas-Odenthal, F., et al. (2022). Reduced hippocampal gray matter volume is a common feature of patients with major depression, bipolar disorder, and schizophrenia spectrum disorders. *Mol. Psychiatry* 27 (10), 4234–4243. doi:10.1038/s41380-022-01687-4

Cameron, H. A., and Glover, L. R. (2015). Adult neurogenesis: beyond learning and memory. *Annu. Rev. Psychol.* 66, 53–81. doi:10.1146/annurev-psych-010814-015006

Chen, J., Lei, C., Li, X., Wu, Q., Liu, C., Ma, Q., et al. (2022). Research progress on classical traditional Chinese medicine formula xiaoyaosan in the treatment of depression. *Front. Pharmacol.* 13, 925514. doi:10.3389/fphar.2022.925514

Chen, L. B., Qiu, F. M., Zhong, X. M., Hong, C., and Huang, Z. (2019). Promoting neurogenesis in hippocampal dentate gyrus of chronic unpredictable stress-induced depressive-like rats with paeoniflorin. *J. Integr. Neurosci.* 18 (1), 43–49. doi:10.31083/j.jin.2019.01.116

Chen, X., Chen, H., He, Y., Fu, S., Liu, H., Wang, Q., et al. (2020). Proteomics-guided study on buyang huanwu decoction for its neuroprotective and neurogenic mechanisms for transient ischemic stroke: involvements of EGFR/PI3K/Akt/Bad/14-3-3 and jak2/stat3/cyclin D1 signaling cascades. *Mol. Neurobiol.* 57 (10), 4305–4321. doi:10.1007/s12035-020-02016-y

Chen, X., Cui, Q. Q., Hu, X. H., Ye, J., Liu, Z. C., Mei, Y. X., et al. (2023). CD200 in dentate gyrus improves depressive-like behaviors of mice through enhancing hippocampal neurogenesis via alleviation of microglia hyperactivation. *J. Neuroinflammation* 20 (1), 157. doi:10.1186/s12974-023-02836-4

Chi, X., Wang, S., Baloch, Z., Zhang, H., Li, X., Zhang, Z., et al. (2019). Research progress on classical traditional Chinese medicine formula Lily Bulb and Rehmannia Decoction in the treatment of depression. *Biomed. Pharmacother.* 112, 108616. doi:10.1016/j.biopha.2019.108616

Christian, K. M., Song, H., and Ming, G. L. (2014). Functions and dysfunctions of adult hippocampal neurogenesis. *Annu. Rev. Neurosci.* 37, 243–262. doi:10.1146/annurev-neuro-071013-014134

Colonna, M., and Butovsky, O. (2017). Microglia function in the central nervous system during health and neurodegeneration. *Annu. Rev. Immunol.* 35, 441–468. doi:10.1146/annurev-immunol-051116-052358

Cui, J. J., Huang, Z. Y., Xie, Y. H., Wu, J. B., Xu, G. H., Li, C. F., et al. (2023). Gut microbiota mediated inflammation, neuroendocrine and neurotrophic functions involved in the antidepressant-like effects of diosgenin in chronic restraint stress. *J. Affect Disord.* 321, 242–252. doi:10.1016/j.jad.2022.10.045

Dai, S., Wang, C., Zhao, X., Fu, K., and Liu, Y. (2023). Cucurbitacin B: a review of its pharmacology, toxicity, and pharmacokinetics. *Pharmacol. Res.* 187, 106587. doi:10.1016/j.phrs.2022.106587

Daodee, S., Monthakantirat, O., Ruengwinitwong, K., Gatenakorn, K., Maneenet, J., Khamphukdee, C., et al. (2019). Effects of the ethanol extract of Dipterocarpus alatus leaf on the unpredictable chronic mild stress-induced depression in ICR mice and its possible mechanism of action. *Molecules* 24 (18), 3396. doi:10.3390/molecules24183396

Di Petrillo, A., Orrù, G., Fais, A., and Fantini, M. C. (2022). Quercetin and its derivates as antiviral potentials: a comprehensive review. *Phytother. Res.* 36 (1), 266–278. doi:10.1002/ptr.7309

Donovan, M. H., Yamaguchi, M., and Eisch, A. J. (2008). Dynamic expression of TrkB receptor protein on proliferating and maturing cells in the adult mouse dentate gyrus. *Hippocampus* 18 (5), 435–439. doi:10.1002/hipo.20410

Du, Y., Gao, X. R., Peng, L., and Ge, J. F. (2020). Crosstalk between the microbiota-gut-brain axis and depression. *Heliyon* 6 (6), e04097. doi:10.1016/j.heliyon.2020.e04097

Fang, A., Li, Y., Wu, X., Wu, B., and Zhang, Y. (2020). Baicalin attenuates inflammatory pain associated depressive symptoms via Akt-mediated adult hippocampal neurogenesis. *Metab. Brain Dis.* 35 (7), 1085–1093. doi:10.1007/s11011-020-00599-y

Frankiensztajn, L. M., Elliott, E., and Koren, O. (2020). The microbiota and the hypothalamus-pituitary-adrenocortical (HPA) axis, implications for anxiety and stress disorders. *Curr. Opin. Neurobiol.* 62, 76–82. doi:10.1016/j.conb.2019.12.003

Gao, C., Wu, M., Du, Q., Deng, J., and Shen, J. (2022). Naringin mediates adult hippocampal neurogenesis for antidepression via activating CREB signaling. *Front. Cell Dev. Biol.* 10, 731831. doi:10.3389/fcell.2022.731831

Gao, J., Liao, Y., Qiu, M., and Shen, W. (2021). Wnt/β-Catenin signaling in neural stem cell homeostasis and neurological diseases. *Neuroscientist* 27 (1), 58–72. doi:10.1177/1073858420914509

Garza, J. C., Guo, M., Zhang, W., and Lu, X. Y. (2012). Leptin restores adult hippocampal neurogenesis in a chronic unpredictable stress model of depression and reverses glucocorticoid-induced inhibition of GSK-3β/β-catenin signaling. *Mol. Psychiatry* 17 (8), 790–808. doi:10.1038/mp.2011.161

Gassen, N. C., and Rein, T. (2019). Is there a role of autophagy in depression and antidepressant action? *Front. Psychiatry* 10, 337. doi:10.3389/fpsyt.2019.00337

Ge, J. B., Jiang, B., Shi, T. S., Li, W. Y., Chen, W. J., Zhu, B. L., et al. (2023). Cucurbitacin B exerts significant antidepressant-like effects in a chronic unpredictable mild stress model of depression: involvement of the hippocampal BDNF-TrkB system. *Int. J. Neuropsychopharmacol.* 26, 680–691. doi:10.1093/ijnp/pyad052

Gillessen, A., and Schmidt, H. H. (2020). Silymarin as supportive treatment in liver diseases: a narrative review. *Adv. Ther.* 37 (4), 1279–1301. doi:10.1007/s12325-020-01251-y

Green, H. F., and Nolan, Y. M. (2014). Inflammation and the developing brain: consequences for hippocampal neurogenesis and behavior. *Neurosci. Biobehav Rev.* 40, 20–34. doi:10.1016/j.neubiorev.2014.01.004

Guan, W., Gu, J. H., Ji, C. H., Liu, Y., Tang, W. Q., Wang, Y., et al. (2021). Xanthoceraside administration produces significant antidepressant effects in mice through activation of the hippocampal BDNF signaling pathway. *Neurosci. Lett.* 757, 135994. doi:10.1016/j.neulet.2021.135994

Hajialyani, M., Hosein Farzaei, M., Echeverría, J., Nabavi, S. M., Uriarte, E., and Sobarzo-Sánchez, E. (2019). Hesperidin as a neuroprotective agent: a review of animal and clinical evidence. *Molecules* 24 (3), 648. doi:10.3390/molecules24030648

He, H., Xie, X., Zhang, J., Mo, L., Kang, X., Zhang, Y., et al. (2023). Patchouli alcohol ameliorates depression-like behaviors through inhibiting NLRP3-mediated neuroinflammation in male stress-exposed mice. *J. Affect Disord.* 326, 120–131. doi:10.1016/j.jad.2023.01.065

Illippangama, A. U., Jayasena, D. D., Jo, C., and Mudannayake, D. C. (2022). Inulin as a functional ingredient and their applications in meat products. *Carbohydr. Polym.* 275, 118706. doi:10.1016/j.carbpol.2021.118706

Jia, J., and Le, W. (2015). Molecular network of neuronal autophagy in the pathophysiology and treatment of depression. *Neurosci. Bull.* 31 (4), 427–434. doi:10.1007/s12264-015-1548-2

Jiang, N., Huang, H., Zhang, Y., Lv, J., Wang, Q., He, Q., et al. (2021b). Ginsenoside Rb1 produces antidepressant-like effects in a chronic social defeat stress model of depression through the BDNF-trkb signaling pathway. *Front. Pharmacol.* 12, 680903. doi:10.3389/fphar.2021.680903

Jiang, N., Lv, J., Wang, H., Huang, H., Wang, Q., Lu, C., et al. (2020). Ginsenoside Rg1 ameliorates chronic social defeat stress-induced depressive-like behaviors and hippocampal neuroinflammation. *Life Sci.* 252, 117669. doi:10.1016/j.lfs.2020.117669

Jiang, N., Wang, H., Li, C., Zeng, G., Lv, J., Wang, Q., et al. (2021a). The antidepressant-like effects of the water extract of Panax ginseng and Polygala tenuifolia are mediated via the BDNF-TrkB signaling pathway and neurogenesis in the hippocampus. *J. Ethnopharmacol.* 267, 113625. doi:10.1016/j.jep.2020.113625

Jung, S., Choe, S., Woo, H., Jeong, H., An, H. K., Moon, H., et al. (2020). Autophagic death of neural stem cells mediates chronic stress-induced decline of adult hippocampal neurogenesis and cognitive deficits. *Autophagy* 16 (3), 512–530. doi:10.1080/15548627.2019.1630222

Kang, Y., Yao, J., Gao, X., Zhong, H., Song, Y., Di, X., et al. (2023). Exercise ameliorates anxious behavior and promotes neuroprotection through osteocalcin in VCD-induced menopausal mice. *CNS Neurosci. Ther.* 29, 3980–3994. doi:10.1111/cns.14324

Kempermann, G., Song, H., and Gage, F. H. (2015). Neurogenesis in the adult Hippocampus. *Cold Spring Harb. Perspect. Biol.* 7 (9), a018812. doi:10.1101/cshperspect.a018812

Kohler, O., Krogh, J., Mors, O., and Benros, M. E. (2016). Inflammation in depression and the potential for anti-inflammatory treatment. *Curr. Neuropharmacol.* 14 (7), 732–742. doi:10.2174/1570159x14666151208113700

Kot, M., Neglur, P. K., Pietraszewska, A., and Buzanska, L. (2022). Boosting neurogenesis in the adult Hippocampus using antidepressants and mesenchymal stem cells. *Cells* 11 (20), 3234. doi:10.3390/cells11203234

Kuhn, H. G., Toda, T., and Gage, F. H. (2018). Adult hippocampal neurogenesis: a coming-of-age story. *J. Neurosci.* 38 (49), 10401–10410. doi:10.1523/JNEUROSCI.2144-18.2018

Kwatra, M., Ahmed, S., Gawali, B., Panda, S. R., and Naidu, V. (2020). Hesperidin alleviates chronic restraint stress and lipopolysaccharide-induced Hippocampus and Frontal cortex damage in mice: role of TLR4/NF-κB, p38 MAPK/JNK, Nrf2/ARE signaling. *Neurochem. Int.* 140, 104835. doi:10.1016/j.neuint.2020.104835

LaMoia, T. E., and Shulman, G. I. (2021). Cellular and molecular mechanisms of metformin action. *Endocr. Rev.* 42 (1), 77–96. doi:10.1210/endrev/bnaa023

Lee, J., Kong, B., and Lee, S. H. (2020). Patchouli alcohol, a compound from *Pogostemon cablin*, inhibits obesity. *J. Med. Food* 23 (3), 326–334. doi:10.1089/jmf.2019.0182

Leng, F., and Edison, P. (2021). Neuroinflammation and microglial activation in Alzheimer disease: where do we go from here? *Nat. Rev. Neurol.* 17 (3), 157–172. doi:10.1038/s41582-020-00435-y

Li, J., Yu, H., Yang, C., Ma, T., and Dai, Y. (2022). Therapeutic potential and molecular mechanisms of echinacoside in neurodegenerative diseases. *Front. Pharmacol.* 13, 841110. doi:10.3389/fphar.2022.841110

Li, W., Wang, S., He, H., Qin, J., Cheng, X., Zhao, H., et al. (2021). Expression and function of Ndel1 during the differentiation of neural stem cells induced by hippocampal exosomesticle. *Stem Cell Res. Ther.* 12 (1), 51. doi:10.1186/s13287-020-02119-2

Liu, C., Ying, Z., Li, Z., Zhang, L., Li, X., Gong, W., et al. (2021). Danzhi xiaoyao powder promotes neuronal regeneration by downregulating notch signaling pathway in the treatment of generalized anxiety disorder. *Front. Pharmacol.* 12, 772576. doi:10.3389/fphar.2021.772576

Liu, J., Xiao, Q., Xiao, J., Niu, C., Li, Y., Zhang, X., et al. (2022b). Wnt/β-catenin signalling: function, biological mechanisms, and therapeutic opportunities. *Signal Transduct. Target Ther.* 7 (1), 3. doi:10.1038/s41392-021-00762-6

Liu, J. J., Wei, Y. B., Strawbridge, R., Bao, Y., Chang, S., Shi, L., et al. (2020). Peripheral cytokine levels and response to antidepressant treatment in depression: a systematic review and meta-analysis. *Mol. Psychiatry* 25 (2), 339–350. doi:10.1038/s41380-019-0474-5

Liu, Q., Zhang, J., Xiao, C., Su, D., Li, L., Yang, C., et al. (2022a). Akebia saponin D protects hippocampal neurogenesis from microglia-mediated inflammation and ameliorates depressive-like behaviors and cognitive impairment in mice through the PI3K-Akt pathway. *Front. Pharmacol.* 13, 927419. doi:10.3389/fphar.2022.927419

Llorens-Martín, M., Rábano, A., and Ávila, J. (2016). The ever-changing morphology of hippocampal granule neurons in physiology and pathology. *Front. Neurosci.* 9, 526. doi:10.3389/fnins.2015.00526

Lu, R., Zhang, L., Wang, H., Li, M., Feng, W., and Zheng, X. (2023). Echinacoside exerts antidepressant-like effects through enhancing BDNF-CREB pathway and inhibiting neuroinflammation *via* regulating microglia M1/M2 polarization and JAK1/STAT3 pathway. *Front. Pharmacol.* 13, 993483. doi:10.3389/fphar.2022.993483

Lv, H., Gao, Z., Wang, Y., Chen, S., Liu, P., Xie, Y., et al. (2023). Metformin improves comorbid depressive symptoms in mice with allergic rhinitis by reducing olfactory bulb damage. *Neurochem. Res.* 48, 3639–3651. doi:10.1007/s11064-023-04012-9

Ma, Z. X., Zhang, R. Y., Rui, W. J., Wang, Z. Q., and Feng, X. (2021). Quercetin alleviates chronic unpredictable mild stress-induced depressive-like behaviors by promoting adult hippocampal neurogenesis via FoxG1/CREB/BDNF signaling pathway. *Behav. Brain Res.* 406, 113245. doi:10.1016/j.bbr.2021.113245

Mahar, I., Bambico, F. R., Mechawar, N., and Nobrega, J. N. (2014). Stress, serotonin, and hippocampal neurogenesis in relation to depression and antidepressant effects. *Neurosci. Biobehav Rev.* 38, 173–192. doi:10.1016/j.neubiorev.2013.11.009

Mendonça, I. P., de Paiva, I. H. R., Duarte-Silva, E. P., de Melo, M. G., da Silva, R. S., do Nascimento, M. I. X., et al. (2022b). Metformin improves depressive-like behavior in experimental Parkinson's disease by inducing autophagy in the substantia nigra and hippocampus. *Inflammopharmacology* 30 (5), 1705–1716. doi:10.1007/s10787-022-01043-6

Mendonça, I. P., Paiva, I. H. R., Duarte-Silva, E. P., Melo, M. G. D., Silva, R. S. D., Oliveira, W. H. D., et al. (2022a). Metformin and fluoxetine improve depressive-like behavior in a murine model of Parkinsońs disease through the modulation of neuroinflammation, neurogenesis and neuroplasticity. *Int. Immunopharmacol.* 102, 108415. doi:10.1016/j.intimp.2021.108415

Meng, P., Zhu, Q., Yang, H., Liu, D., Lin, X., Liu, J., et al. (2019). Leonurine promotes neurite outgrowth and neurotrophic activity by modulating the GR/SGK1 signaling pathway in cultured PC12 cells. *Neuroreport* 30 (4), 247–254. doi:10.1097/WNR.0000000000001180

Micheli, L., Ceccarelli, M., D'Andrea, G., and Tirone, F. (2018). Depression and adult neurogenesis: positive effects of the antidepressant fluoxetine and of physical exercise. *Brain Res. Bull.* 143, 181–193. doi:10.1016/j.brainresbull.2018.09.002

Mizushima, N., and Komatsu, M. (2011). Autophagy: renovation of cells and tissues. *Cell* 147 (4), 728–741. doi:10.1016/j.cell.2011.10.026

Moss, J., Gebara, E., Bushong, E. A., Sánchez-Pascual, I., O'Laoi, R., El M'Ghari, I., et al. (2016). Fine processes of Nestin-GFP-positive radial glia-like stem cells in the adult dentate gyrus ensheathe local synapses and vasculature. *Proc. Natl. Acad. Sci. U. S. A.* 113 (18), E2536–E2545. doi:10.1073/pnas.1514652113

Nazir, S., Farooq, R. K., Nasir, S., Hanif, R., and Javed, A. (2022). Therapeutic effect of Thymoquinone on behavioural response to UCMS and neuroinflammation in hippocampus and amygdala in BALB/c mice model. *Psychopharmacol. Berl.* 239 (1), 47–58. doi:10.1007/s00213-021-06038-9

Ouyang, S. H., Zhai, Y. J., Wu, Y. P., Xie, G., Wang, G. E., Mao, Z. F., et al. (2021). Theacrine, a potent antidepressant purine alkaloid from a special Chinese tea, promotes adult hippocampal neurogenesis in stressed mice. *J. Agric. Food Chem.* 69 (25), 7016–7027. doi:10.1021/acs.jafc.1c01514

Pearce, M., Garcia, L., Abbas, A., Strain, T., Schuch, F. B., Golubic, R., et al. (2022). Association between physical activity and risk of depression: a systematic review and meta-analysis. *JAMA Psychiatry* 79 (6), 550–559. doi:10.1001/jamapsychiatry.2022.0609

Perera, T. D., Dwork, A. J., Keegan, K. A., Thirumangalakudi, L., Lipira, C. M., Joyce, N., et al. (2011). Necessity of hippocampal neurogenesis for the therapeutic action of antidepressants in adult nonhuman primates. *PLoS One* 6 (4), e17600. doi:10.1371/journal.pone.0017600

Perez-Caballero, L., Torres-Sanchez, S., Bravo, L., Mico, J. A., and Berrocoso, E. (2014). Fluoxetine: a case history of its discovery and preclinical development. *Expert Opin. Drug Discov.* 9 (5), 567–578. doi:10.1517/17460441.2014.907790

Petrik, D., Lagace, D. C., and Eisch, A. J. (2012). The neurogenesis hypothesis of affective and anxiety disorders: are we mistaking the scaffolding for the building? *Neuropharmacology* 62 (1), 21–34. doi:10.1016/j.neuropharm.2011.09.003

Phillips, C. (2017). Brain-derived neurotrophic factor, depression, and physical activity: making the neuroplastic connection. *Neural Plast.* 2017, 7260130. doi:10.1155/2017/7260130

Pilz, G. A., Bottes, S., Betizeau, M., Jörg, D. J., Carta, S., Simons, B. D., et al. (2018). Live imaging of neurogenesis in the adult mouse hippocampus. *Science* 359 (6376), 658–662. doi:10.1126/science.aao5056

Qin, Z., Shi, D. D., Li, W., Cheng, D., Zhang, Y. D., Zhang, S., et al. (2023). Berberine ameliorates depression-like behaviors in mice via inhibiting NLRP3 inflammasome-mediated neuroinflammation and preventing neuroplasticity disruption. *J. Neuroinflammation* 20 (1), 54. doi:10.1186/s12974-023-02744-7

Qu, S. Y., Li, X. Y., Heng, X., Qi, Y. Y., Ge, P. Y., Ni, S. J., et al. (2021). Analysis of antidepressant activity of huang-lian jie-du decoction through network pharmacology and metabolomics. *Front. Pharmacol.* 12, 619288. doi:10.3389/fphar.2021.619288

Rehm, J., and Shield, K. D. (2019). Global burden of disease and the impact of mental and addictive disorders. *Curr. Psychiatry Rep.* 21 (2), 10. doi:10.1007/s11920-019-0997-0

Sahay, A., and Hen, R. (2007). Adult hippocampal neurogenesis in depression. *Nat. Neurosci.* 10 (9), 1110–1115. doi:10.1038/nn1969

Sajeev, A., Hegde, M., Girisa, S., Devanarayanan, T. N., Alqahtani, M. S., Abbas, M., et al. (2022). Oroxylin A: a promising flavonoid for prevention and treatment of chronic diseases. *Biomolecules* 12 (9), 1185. doi:10.3390/biom12091185

Sánchez-Huerta, K., García-Martínez, Y., Vergara, P., Segovia, J., and Pacheco-Rosado, J. (2016). Thyroid hormones are essential to preserve non-proliferative cells of adult neurogenesis of the dentate gyrus. *Mol. Cell Neurosci.* 76, 1–10. doi:10.1016/j.mcn.2016.08.001

Santarelli, L., Saxe, M., Gross, C., Surget, A., Battaglia, F., Dulawa, S., et al. (2003). Requirement of hippocampal neurogenesis for the behavioral effects of antidepressants. *Science* 301 (5634), 805–809. doi:10.1126/science.1083328

Schoenfeld, T. J., McCausland, H. C., Morris, H. D., Padmanaban, V., and Cameron, H. A. (2017). Stress and loss of adult neurogenesis differentially reduce hippocampal volume. *Biol. Psychiatry* 82 (12), 914–923. doi:10.1016/j.biopsych.2017.05.013

Schumacher, A., Villaruel, F. R., Ussling, A., Riaz, S., Lee, A. C. H., and Ito, R. (2018). Ventral hippocampal CA1 and CA3 differentially mediate learned approach-avoidance conflict processing. *Curr. Biol.* 28 (8), 1318–1324. doi:10.1016/j.cub.2018.03.012

Sheng, Y. Y., Xiang, J., Wang, Z. S., Jin, J., Wang, Y. Q., Li, Q. S., et al. (2020). Theacrine from *Camellia kucha* and its health beneficial effects. *Front. Nutr.* 7, 596823. doi:10.3389/fnut.2020.596823

Shengli, C., Yingli, Z., Zheng, G., Shiwei, L., Ziyun, X., Han, F., et al. (2022). An aberrant hippocampal subregional network, rather than structure, characterizes major depressive disorder. *J. Affect Disord.* 302, 123–130. doi:10.1016/j.jad.2022.01.087

Shi, L. S., Ji, C. H., Liu, Y., Gu, J. H., Tang, W. Q., Zhang, W., et al. (2022). Ginsenoside Rh2 administration produces crucial antidepressant-like effects in a CUMS-induced mice model of depression. *Brain Behav.* 12 (8), e2705. doi:10.1002/brb3.2705

Siopi, E., Chevalier, G., Katsimpardi, L., Saha, S., Bigot, M., Moigneu, C., et al. (2020). Changes in gut microbiota by chronic stress impair the efficacy of fluoxetine. *Cell Rep.* 30 (11), 3682–3690. doi:10.1016/j.celrep.2020.02.099

Snyder, J. S., Soumier, A., Brewer, M., Pickel, J., and Cameron, H. A. (2011). Adult hippocampal neurogenesis buffers stress responses and depressive behaviour. *Nature* 476 (7361), 458–461. doi:10.1038/nature10287

Song, D., Hao, J., and Fan, D. (2020). Biological properties and clinical applications of berberine. *Front. Med.* 14 (5), 564–582. doi:10.1007/s11684-019-0724-6

Sun, P., Wang, M., Li, Z., Wei, J., Liu, F., Zheng, W., et al. (2022). *Eucommiae cortex* polysaccharides mitigate obesogenic diet-induced cognitive and social dysfunction via modulation of gut microbiota and tryptophan metabolism. *Theranostics* 12 (8), 3637–3655. doi:10.7150/thno.72756

Sun, Y., Hu, N., Wang, M., Lu, L., Luo, C., Tang, B., et al. (2023). Hippocampal subfield alterations in schizophrenia and major depressive disorder: a systematic review and network meta-analysis of anatomic MRI studies. *J. Psychiatry Neurosci.* 48 (1), E34–E49. doi:10.1503/jpn.220086

Tantipongpiradet, A., Monthakantirat, O., Vipatpakpaiboon, O., Khampukdee, C., Umehara, K., Noguchi, H., et al. (2019). Effects of puerarin on the ovariectomy-induced depressive-like behavior in ICR mice and its possible mechanism of action. *Molecules* 24 (24), 4569. doi:10.3390/molecules24244569

Tao, W., Ruan, J., Wu, R., Zhao, M., Zhao, T., Qi, M., et al. (2023). A natural carotenoid crocin exerts antidepressant action by promoting adult hippocampal neurogenesis through Wnt/β-catenin signaling. *J. Adv. Res.* 43, 219–231. doi:10.1016/j.jare.2022.02.015

Tartt, A. N., Mariani, M. B., Hen, R., Mann, J. J., and Boldrini, M. (2022). Dysregulation of adult hippocampal neuroplasticity in major depression: pathogenesis and therapeutic implications. *Mol. Psychiatry* 27 (6), 2689–2699. doi:10.1038/s41380-022-01520-y

van Zutphen, E. M., Rhebergen, D., van Exel, E., Oudega, M. L., Bouckaert, F., Sienaert, P., et al. (2019). Brain-derived neurotrophic factor as a possible predictor of electroconvulsive therapy outcome. *Transl. Psychiatry* 9 (1), 155. doi:10.1038/s41398-019-0491-9

Wang, J., Hu, K., Cai, X., Yang, B., and He, Q. (2022). Targeting PI3K/AKT signaling for treatment of idiopathic pulmonary fibrosis. *Acta Pharm. Sin. B* 12 (1), 18–32. doi:10.1016/j.apsb.2021.07.023

Wang, K., Zhai, Q., Wang, S., Li, Q., Liu, J., Meng, F., et al. (2021b). Cryptotanshinone ameliorates CUS-induced depressive-like behaviors in mice. *Transl. Neurosci.* 12 (1), 469–481. doi:10.1515/tnsci-2020-0198

Wang, L., Wang, Z., Lan, Y., Tuo, Y., Ma, S., and Liu, X. (2023b). Inulin attenuates blood-brain barrier permeability and alleviates behavioral disorders by modulating the TLR4/MyD88/NF-κB pathway in mice with chronic stress. *J. Agric. Food Chem.* 71 (36), 13325–13337. doi:10.1021/acs.jafc.3c03568

Wang, M., Sun, P., Li, Z., Li, J., Lv, X., Chen, S., et al. (2023a). Eucommiae cortex polysaccharides attenuate gut microbiota dysbiosis and neuroinflammation in mice exposed to chronic unpredictable mild stress: beneficial in ameliorating depressive-like behaviors. *J. Affect Disord.* 334, 278–292. doi:10.1016/j.jad.2023.04.117

Wang, X. L., Feng, S. T., Wang, Y. T., Chen, N. H., Wang, Z. Z., and Zhang, Y. (2021a). Paeoniflorin: a neuroprotective monoterpenoid glycoside with promising anti-depressive properties. *Phytomedicine* 90, 153669. doi:10.1016/j.phymed.2021.153669

Wang, Y. S., Shen, C. Y., and Jiang, J. G. (2019). Antidepressant active ingredients from herbs and nutraceuticals used in TCM: pharmacological mechanisms and prospects for drug discovery. *Pharmacol. Res.* 150, 104520. doi:10.1016/j.phrs.2019.104520

Wei, Y., Chang, L., and Hashimoto, K. (2022). Molecular mechanisms underlying the antidepressant actions of arketamine: beyond the NMDA receptor. *Mol. Psychiatry* 27 (1), 559–573. doi:10.1038/s41380-021-01121-1

Woodburn, S. C., Bollinger, J. L., and Wohleb, E. S. (2021). The semantics of microglia activation: neuroinflammation, homeostasis, and stress. *J. Neuroinflammation* 18 (1), 258. doi:10.1186/s12974-021-02309-6

Wu, C., Jia, L., Mu, Q., Fang, Z., Hamoudi, H. J. A. S., Huang, M., et al. (2023). Altered hippocampal subfield volumes in major depressive disorder with and without anhedonia. *BMC Psychiatry* 23 (1), 540. doi:10.1186/s12888-023-05001-6

Wu, Z. H., Fan, H., Gao, S. Y., Jin, Y. F., Cheng, C., Jiang, B., et al. (2022). Antidepressant-like activity of oroxylin A in mice models of depression: a behavioral and neurobiological characterization. *Front. Pharmacol.* 13, 921553. doi:10.3389/fphar.2022.921553

Xia, C. Y., Guo, Y. X., Lian, W. W., Yan, Y., Ma, B. Z., Cheng, Y. C., et al. (2023). The NLRP3 inflammasome in depression: potential mechanisms and therapies. *Pharmacol. Res.* 187, 106625. doi:10.1016/j.phrs.2022.106625

Xiao, Q., Shu, R., Wu, C., Tong, Y., Xiong, Z., Zhou, J., et al. (2020). Crocin-I alleviates the depression-like behaviors probably via modulating "microbiota-gut-brain" axis in mice exposed to chronic restraint stress. *J. Affect Disord.* 276, 476–486. doi:10.1016/j.jad.2020.07.041

Xiao, Z., Cao, Z., Yang, J., Jia, Z., Du, Y., Sun, G., et al. (2021). Baicalin promotes hippocampal neurogenesis via the Wnt/β-catenin pathway in a chronic unpredictable mild stress-induced mouse model of depression. *Biochem. Pharmacol.* 190, 114594. doi:10.1016/j.bcp.2021.114594

Yan, Z. Y., Jiao, H. Y., Chen, J. B., Zhang, K. W., Wang, X. H., Jiang, Y. M., et al. (2021). Antidepressant mechanism of traditional Chinese medicine formula xiaoyaosan in CUMS-induced depressed mouse model via RIPK1-RIPK3-MLKL mediated necroptosis based on network pharmacology analysis. *Front. Pharmacol.* 12, 773562. doi:10.3389/fphar.2021.773562

Yang, J., Zhang, Z., Xie, Z., Bai, L., Xiong, P., Chen, F., et al. (2022). Metformin modulates microbiota-derived inosine and ameliorates methamphetamine-induced anxiety and depression-like withdrawal symptoms in mice. *Biomed. Pharmacother.* 149, 112837. doi:10.1016/j.biopha.2022.112837

Yang, L., Ran, Y., Quan, Z., Wang, R., Yang, Q., Jia, Q., et al. (2019). Pterostilbene, an active component of the dragon's blood extract, acts as an antidepressant in adult rats. *Psychopharmacol. Berl.* 236 (4), 1323–1333. doi:10.1007/s00213-018-5138-7

Yang, S., Hu, T., Liu, H., Lv, Y. L., and Zhang, W. (2021). Akebia saponin D ameliorates metabolic syndrome (MetS) via remodeling gut microbiota and attenuating intestinal barrier injury. *Biomed. Pharmacother.* 138, 111441. doi:10.1016/j.biopha.2021.111441

Yao, B., Christian, K. M., He, C., Jin, P., Ming, G. L., and Song, H. (2016). Epigenetic mechanisms in neurogenesis. *Nat. Rev. Neurosci.* 17 (9), 537–549. doi:10.1038/nrn.2016.70

Yi, L. T., Zhang, M. M., Cheng, J., Wan, H. Q., Li, C. F., Zhu, J. X., et al. (2021). Antidepressant-like effects of degraded porphyran isolated from Porphyra haitanensis. *Mol. Nutr. Food Res.* 65 (9), e2000869. doi:10.1002/mnfr.202000869

Yohn, C. N., Shifman, S., Garino, A., Diethorn, E., Bokka, L., Ashamalla, S. A., et al. (2020). Fluoxetine effects on behavior and adult hippocampal neurogenesis in female C57BL/6J mice across the estrous cycle. *Psychopharmacol. Berl.* 237 (5), 1281–1290. doi:10.1007/s00213-020-05456-5

Yoshida, K., Drew, M. R., Kono, A., Mimura, M., Takata, N., and Tanaka, K. F. (2021). Chronic social defeat stress impairs goal-directed behavior through dysregulation of ventral hippocampal activity in male mice. *Neuropsychopharmacology* 46 (9), 1606–1616. doi:10.1038/s41386-021-00990-y

Yu, H., Yang, R., Wu, J., Wang, S., Qin, X., Wu, T., et al. (2022a). Association of metformin and depression in patients with type 2 diabetes. *J. Affect Disord.* 318, 380–385. doi:10.1016/j.jad.2022.09.015

Yu, L., Zhang, Y., Chen, Q., Zhou, H., and Wan, H. (2022b). Formononetin protects against inflammation associated with cerebral ischemia-reperfusion injury in rats by targeting the JAK2/STAT3 signaling pathway. *Biomed. Pharmacother.* 149, 112836. doi:10.1016/j.biopha.2022.112836

Zeng, J., Ji, Y., Luan, F., Hu, J., Rui, Y., Liu, Y., et al. (2022). Xiaoyaosan ethyl acetate fraction alleviates depression-like behaviors in CUMS mice by promoting hippocampal neurogenesis via modulating the IGF-1Rβ/PI3K/Akt signaling pathway. *J. Ethnopharmacol.* 288, 115005. doi:10.1016/j.jep.2022.115005

Zhang, C., Zhu, L., Lu, S., Li, M., Bai, M., Li, Y., et al. (2022). The antidepressant-like effect of formononetin on chronic corticosterone-treated mice. *Brain Res.* 1783, 147844. doi:10.1016/j.brainres.2022.147844

Zhang, J., Liu, Q., Su, D., Li, L., Xiao, C., He, H., et al. (2023c). Akebia saponin D acts via the PPAR-gamma pathway to reprogramme a pro-neurogenic microglia that can restore hippocampal neurogenesis in mice exposed to chronic mild stress. *CNS Neurosci. Ther.* 29 (9), 2555–2571. doi:10.1111/cns.14196

Zhang, K., Wang, F., Zhai, M., He, M., Hu, Y., Feng, L., et al. (2023a). Hyperactive neuronal autophagy depletes BDNF and impairs adult hippocampal neurogenesis in a corticosterone-induced mouse model of depression. *Theranostics* 13 (3), 1059–1075. doi:10.7150/thno.81067

Zhang, L., Tang, M., Xie, X., Zhao, Q., Hu, N., He, H., et al. (2021a). Ginsenoside Rb1 induces a pro-neurogenic microglial phenotype via PPARγ activation in male mice exposed to chronic mild stress. *J. Neuroinflammation* 18 (1), 171. doi:10.1186/s12974-021-02185-0

Zhang, R., Ma, Z., Liu, K., Li, Y., Liu, D., Xu, L., et al. (2019b). Baicalin exerts antidepressant effects through Akt/FOXG1 pathway promoting neuronal differentiation and survival. *Life Sci.* 221, 241–248. doi:10.1016/j.lfs.2019.02.033

Zhang, S., Lu, Y., Chen, W., Shi, W., Zhao, Q., Zhao, J., et al. (2021b). Network pharmacology and experimental evidence: PI3K/AKT signaling pathway is involved in the antidepressive roles of chaihu shugan san. *Drug Des. Devel Ther.* 15, 3425–3441. doi:10.2147/DDDT.S315060

Zhang, S. Q., Deng, Q., Zhu, Q., Long, L. H., and Wu, P. F. (2023b). Cell type-specific NRBF2 orchestrates autophagic flux and adult hippocampal neurogenesis in chronic stress-induced depression. *Cell Discov.* 9 (1), 90. doi:10.1038/s41421-023-00583-7

Zhang, Y., Yang, X., Ge, X., and Zhang, F. (2019a). Puerarin attenuates neurological deficits via Bcl-2/Bax/cleaved caspase-3 and Sirt3/SOD2 apoptotic pathways in subarachnoid hemorrhage mice. *Biomed. Pharmacother.* 109, 726–733. doi:10.1016/j.biopha.2018.10.161

Zhao, B., Peng, Q., Poon, E. H. L., Chen, F., Zhou, R., Shang, G., et al. (2021). Leonurine promotes the osteoblast differentiation of rat BMSCs by activation of autophagy via the PI3K/Akt/mTOR pathway. *Front. Bioeng. Biotechnol.* 9, 615191. doi:10.3389/fbioe.2021.615191

Zhao, F., Tao, W., Shang, Z., Zhang, W., Ruan, J., Zhang, C., et al. (2020). Facilitating granule cell survival and maturation in dentate gyrus with Baicalin for antidepressant therapeutics. *Front. Pharmacol.* 11, 556845. doi:10.3389/fphar.2020.556845

Zhou, H., Zhao, J., Liu, C., Zhang, Z., Zhang, Y., and Meng, D. (2022). Xanthoceraside exerts anti-Alzheimer's disease effect by remodeling gut microbiota and modulating microbial-derived metabolites level in rats. *Phytomedicine* 98, 153937. doi:10.1016/j.phymed.2022.153937

Zhou, Y. X., Gong, X. H., Zhang, H., and Peng, C. (2020). A review on the pharmacokinetics of paeoniflorin and its anti-inflammatory and immunomodulatory effects. *Biomed. Pharmacother.* 130, 110505. doi:10.1016/j.biopha.2020.110505

frontiers | Frontiers in Pharmacology

TYPE Original Research
PUBLISHED 08 January 2024
DOI 10.3389/fphar.2023.1300310

OPEN ACCESS

EDITED BY
Tanya Calvey,
University of Cape Town, South Africa

REVIEWED BY
Nelly Maritza Vega Rivera,
National Institute of Psychiatry Ramon de la Fuente Muñiz (INPRFM), Mexico
Ben A. Chindo,
Kaduna State University, Nigeria

*CORRESPONDENCE
Hossein Amini-Khoei,
aminikhoyi@gmail.com,
aminikhoyi.h@skums.ac.ir

RECEIVED 23 September 2023
ACCEPTED 04 December 2023
PUBLISHED 08 January 2024

CITATION
Karimi P, Ghahfarroki MS, Lorigooini Z, Shahrani M and Amini-Khoei H (2024), Umbelliprenin via increase in the *MECP2* and attenuation of oxidative stress mitigates the autistic-like behaviors in mouse model of maternal separation stress.
Front. Pharmacol. 14:1300310.
doi: 10.3389/fphar.2023.1300310

Umbelliprenin via increase in the *MECP2* and attenuation of oxidative stress mitigates the autistic-like behaviors in mouse model of maternal separation stress

Parnian Karimi, Mehryar Shahgholian Ghahfarroki, Zahra Lorigooini, Mehrdad Shahrani and Hossein Amini-Khoei*

Medical Plants Research Center, Basic Health Sciences Institute, Shahrekord University of Medical Sciences, Shahrekord, Iran

Introduction: Autism spectrum disorder (ASD) is a complex neurodevelopmental condition. Maternal separation (MS) stress is an early-life stress factor associated with behaviors resembling Autism. Both *MECP2* and oxidative stress are implicated in the pathophysiology of Autism. Umbelliprenin (UMB) is a coumarin compound with various pharmacological properties. Our study aimed to investigate the potential effects of UMB in mitigating autistic-like behaviors in a mouse model subjected to MS stress, focusing on probable alterations in *MECP2* gene expression in the hippocampus.

Methods: MS paradigm was performed, and mice were treated with saline or UMB. Behavioral tests consisting of the three-chamber test (evaluating social interaction), shuttle box (assessing passive avoidance memory), elevated plus-maze (measuring anxiety-like behaviors), and marble-burying test (evaluating repetitive behaviors) were conducted. Gene expression of *MECP2* and measurements of total antioxidant capacity (TAC), nitrite level, and malondialdehyde (MDA) level were assessed in the hippocampus.

Results: The findings demonstrated that MS-induced behaviors resembling Autism, accompanied by decreased *MECP2* gene expression, elevated nitrite, MDA levels, and reduced TAC in the hippocampus. UMB mitigated these autistic-like behaviors induced by MS and attenuated the adverse effects of MS on oxidative stress and *MECP2* gene expression in the hippocampus.

Conclusion: In conclusion, UMB likely attenuated autistic-like behaviors caused by MS stress, probably, through the reduction of oxidative stress and an increase in *MECP2* gene expression.

KEYWORDS

maternal separation stress, Autism spectrum disorder, umbelliprenin, MeCP2, oxidative stress

Introduction

Autism spectrum disorder (ASD) encompasses a diverse range of neurodevelopmental disorders characterized by challenges in social communication and interaction, as well as repetitive and restricted patterns of behavior and interests (Wen et al., 2017). Various factors such as epigenetic, metabolic, and environmental conditions are ASD pathogenic factors (Faras et al., 2010). Previous studies have determined that neonatal exposure to psychosocial difficulties, such as maternal separation (MS) stress, significantly disrupts brain development, consequently increasing susceptibility to neuropsychiatric disorders (Amiri et al., 2016; Amini-Khoei et al., 2019). Ample evidence has been demonstrated that MS could lead to neurotransmission, neuroendocrine, and neurostructural alterations in the central nervous system (CNS) (Gildawie et al., 2021). It has been well-determined that MS via neurotransmission and neurostructural modifications in the brain provoked autistic-like behaviors in rodents, indicating that the MS paradigm could be considered as an experimental model of Autism in rodents (Mansouri et al., 2021; Farzan et al., 2023; Khaledi et al., 2023; Moghaddam et al., 2023; Yadollahi-Farsani et al., 2023). MS, with its abovementioned changes in the hippocampus, causes mood-behavioral disorders (Arabi et al., 2021). Studies on autistic patients represented irregular hippocampal patterns (Xu et al., 2020). Studies on the experimental models have determined hippocampal alterations in Autism, indicating the pivotal role of the hippocampus in the pathophysiology of ASD (Zhong et al., 2020; Lee et al., 2023). Methyl-CpG-Binding Protein 2 (*MECP2*) regulates neurons that modulate social interactions (Pejhan and Rastegar, 2021). Some cases of neurodevelopmental disorders like Autism and Rett syndrome may be linked to mutations or dysregulation of the *MECP2* gene (Zoghbi, 2005; Calfa et al., 2011), suggesting that *MECP2* is involved in the pathophysiology of Autism (Neul, 2022). *MECP2* regulates neurophysiological functions implicated in developing neurons and synaptic plasticity (Sánchez-Lafuente et al., 2022). Specifically, researchers have observed that methylation at a specific region of the *MECP2* gene, which causes a decrease in the level of *MECP2* protein in the brain, is associated with Autism (Neul, 2022). Preclinical studies have determined that hippocampal *MECP2* knockdown provoked autistic-like behaviors in rats (Choi et al., 2022). Thus, *MECP2* could consider as a new target to introduce new agents as well as explore the efficacy of therapeutics in ASD.

Coumarins are natural benzopyrene derivatives abundantly present in various plant sources (Iranshahi et al., 2009; Shakeri et al., 2014). They possess a wide range of pharmacological activities.

Umbelliprenin (UMB) is a sesquiterpene Coumarin compound found in Ferula species. Extensive research has demonstrated that UMB possesses various pharmacological properties (Hashemzaei et al., 2020). Numerous studies have confirmed its diverse effects, including antioxidative, neuroprotective, proapoptotic, and anti-inflammatory properties (Hashemzaei et al., 2015). Researchers have investigated its impact on neuropathic pain and found that it effectively mitigates oxidative stress while providing neuroprotection (Shahraki et al., 2020). Additionally, UMB has shown anti-inflammatory properties and acts as a modulator of cytokine secretion (Khaghanzadeh et al., 2017).

In this study, we aimed to investigate the potential of UMB to mitigate autistic-like behaviors in a mouse model of MS stress, with a specific focus on assessing its effect on the alterations of *MECP2* gene expression in the hippocampus.

Materials and methods

Animals and maternal separation paradigm

Pregnant Naval Medical Research Institute (NMRI) mice were obtained from the Institute Pasteur in Iran. The animals were housed in laboratory conditions with standard parameters, including a 12-hour light/dark cycle (with lights turned on at 8:00 a.m.), a consistent temperature of 21°C ± 2 °C, and free access to food and water. The birthday (pups with an average weight of about 3 g) was designated as postnatal day (PND) 0. From PND2, the neonates were separated from their mothers for 3 h each day (from 10 a.m. to 1 p.m.) until PND14. Subsequently, the neonates were returned to their mothers' cages until PND25 (Lorigooini et al., 2020a). To avoid the litter effect, pups of each mouse were accidentally numbered on PND 25 and were randomly assigned to the experimental groups. Forty-five maternally separated male mice were randomly divided into three groups (n = 15). Additionally, fifteen NMRI male mice not exposed to the MS model were selected as the control group. By establishing a bilateral alpha of 0.05 and a confidence interval of 90%, 15 mice were considered for each experimental group based on a sample size calculation formula (Chen et al., 2022).

Study design

All agents were administered via the intraperitoneal (i.p.) route for seven consecutive days from PND 51–53 until PND 58–60. The behavioral experiments related to autistic-like behaviors were conducted immediately after the treatments were completed and carried out between 09:00 a.m. and 05:00 p.m. (light phase). Finally, the mice were sacrificed under deep anesthesia using diethyl ether, and their hippocampi were dissected for molecular analysis (Lorigooini et al., 2021). The dose and administration time were selected based on previous studies and our pilot study (Rashidi et al., 2018; Shahraki et al., 2020).

The control group (Group 1) received normal saline (1 mL/kg). The second to fourth groups consisted of the MS mice treated with normal saline (1 mL/kg), UMB (12.5 mg/kg), and UMB (25 mg/kg), respectively. It has been established that animals display low subject-to-subject variation (Jiang et al., 2017). To minimize animal suffering and diminish the number of mice used, based on the formula introduced by Charan et al., five mice in each group is the satisfactory limit and, therefore, can be considered an adequate sample size to see the effect of the drug in animal studies (Charan and Kantharia, 2013). Since behavioral tests impose different levels of stress on animals, to minimize the impact of stress reactivity, from 15 mice in each experimental group, five mice were subjected to the three-chamber sociability test, five mice were subjected to the shuttle box test, and five mice subjected to the EPM and MBT (7).

Behavioral tests

Evaluation of sociability and social preference indexes

The three-chamber test was employed to assess social behaviors. A plexiglass box was divided into three chambers: a central section

and two side chambers. During the habituation, sociability, and social preference phases, mice freely explored the box. In the habituation phase, mice were placed in the central chamber for 5 min to acclimatize to the environment. Two cylindrical wire cages were placed in the two side chambers for the sociability phase. In the next step, one wire cage contained a stranger of the same sex and age mouse (novel mouse 1 or social stimulus 1), and the time spent exploring each chamber was measured for 10 min. The other wire cage remained empty. The time spent directly interacting with the social stimulus and the empty chamber (non-social stimulus) was recorded. The sociability index (SI) was calculated as (social stimulus 1 - non-social stimulus)/(social stimulus 1 + non-social stimulus). For the social preference index (SPI), another unfamiliar mouse (new mouse 2 or social stimulus 2) was placed in a different empty wire cage, and the time spent in each chamber was recorded for 10 min. The SPI was determined using the following formula: (social stimulus 2 - social stimulus 1)/(social stimulus 2 + social stimulus 1) (Amini et al., 2023; Pang et al., 2023).

Evaluation of passive avoidance memory

The shuttle box is a device used to assess passive avoidance memory. The mice were placed in the box, and adaptation of the mice was completed over the first 2 days. Mice were allowed to explore the apparatus for 5 min. On the third day, the mice were placed in the bright chamber, and after 2 min, the door was opened. The door was closed when the mice entered the dark section, and an electrical shock (1 mA/second) was administered. The dark chamber latency was recorded as the initial latency (T1). The same procedure was repeated on the fourth day without the electrical shock, and the second latency was recorded (T2) (Farzan et al., 2023).

Evaluation of repetitive behaviors

The Marble Burying Test (MBT) assessed repetitive behaviors in rodents. For the test, each mouse was placed in a clean cage containing 20 marbles arranged in a uniform grid pattern on fresh, unscented mouse bedding material with a depth of 5 cm and allowed to explore for 20 min. The number of marbles buried (covered with at least two-thirds of the bedding) was then calculated and recorded for each mouse. To avoid any potential bias, the test cage and marbles were carefully cleaned with 70% ethanol between each test, and fresh bedding material was used for each test (Farzan et al., 2023).

Evaluation of anxiety-like behavior

The Elevated Plus Maze (EPM) is an appropriate test for assessment of rodents' anxiety-like behavior. The maze was constructed from black opaque Plexiglas and consisted of two open arms (30 × 5 cm) and two closed arms (30 × 5 × 15 cm), which were connected by a central platform (5 × 5 cm). During the test, each mouse was individually placed in the center of the maze, facing one of the closed arms, for 5 min, allowing it to explore the maze. The time spent in each arm, including the open and closed arms, and the number of entries into each arm were recorded. An arm entry was defined as placing all four paws into an arm (Sadeghi et al., 2023). In addition, the anxiety index was calculated as follows: Anxiety Index = 1 − ([Open arm time/Test duration] + [Open arms entries/Total number of entries]/2) (Moreno-Martínez et al., 2022). After each trial, the maze was cleaned with 70% ethanol to eliminate any odor cues left by the mice. The test was conducted in a quiet environment with controlled lighting conditions to minimize external disturbances.

Nitrite assay

Initially, the mice were anesthetized with diethyl ether and sacrificed, and the hippocampus was removed and immediately placed into liquid nitrogen. The Griess reaction method was used to assess the nitrite level. Hippocampal homogenates were prepared, and nitrite concentrations were determined using a colorimetric assay based on the Griess reaction. In brief, 100 µL of samples were loaded into each well and mixed with 100 µL of Griess reagent. After 10 minutes of incubation at room temperature, the automated plate reader measured the absorbance at 540 nm. The nitrite level was determined using a standard curve of sodium nitrite (Sigma, United States of America) and reported as micromole per mg protein (Wopara et al., 2021).

Measurement of malondialdehyde (MDA) level

The MDA level in the hippocampus was measured using the previously described method. To do this, 100 µL of hippocampus supernatant aliquots were mixed with 900 µLs of Tris-KCl buffer, and then 500 µL of 30% TCA was added. Afterward, 500 µL of thiobarbituric acid (TBA) (0.75%) was added and permitted to be heated in a water bath at 80 C for 45 min. The mixture was centrifuged (3,000 rpm g, 5 min), and the supernatant's absorbance was read at 562 nm using an ELISA reader. The MDA level is reported as a nanomole of MDA per mg protein (Nagababu et al., 2010).

Measurement of total antioxidant capacity (TAC)

The ferric-reducing ability of plasma (FRAP) method was used to determine the TAC in the hippocampus. This method measured TAC in the hippocampal samples using the previously reported method at 37°C and pH 3.6. After 30 min, absorbance was measured and registered as a percentage of the combined ferric reducing/antioxidant potency of the antioxidants in protein, with the findings given as micromol Fe2+/mg protein (Benzie and Strain, 1999; Nasiri-Boroujeni et al., 2021).

Quantitative Real-Time polymerase chain reaction (qRT-PCR)

The gene expression of *MECP2* in the hippocampus was measured using Real-Time PCR. After collecting the hippocampal tissue, total RNA was extracted using RNX-plus. The RNA was then reverse-transcribed into cDNA using a PrimeScript RT reagent kit (Takara Bio, Inc., Otsu, Japan). Gene-specific primers and a fluorescent probe for *MECP2* were designed and optimized. Real-time PCR was done on the cDNA samples using a light cycler instrument (Roche Diagnostics, Mannheim, Germany) (Takara Bio). The results were analyzed using the $2^{-\Delta\Delta CT}$ method to calculate the relative gene expression levels of *MECP2* in the hippocampus. The housekeeping gene B2M was used as a reference gene to normalize the gene expression levels (Omidi-Ardali et al., 2019; Lorigooini et al., 2021). Table 1 presents primer sequences.

Data analysis

Kolmogorov–Smirnov test was applied to evaluate the normal distribution of data, resulting in parametric data. Brown-Forsythe test was used for the evaluation of data homogeneity. Data were

TABLE 1 primer sequences.

Gene	Forward	Reverse
MECP2	TGTATGATGACCCCACCT TGCC	TCCCTCTCCCAGTTACCG TGAA
B2m	CGTGATCTTTCTGGTGCT TGTC	GGAAGTTGGGCTTCC CATTCT

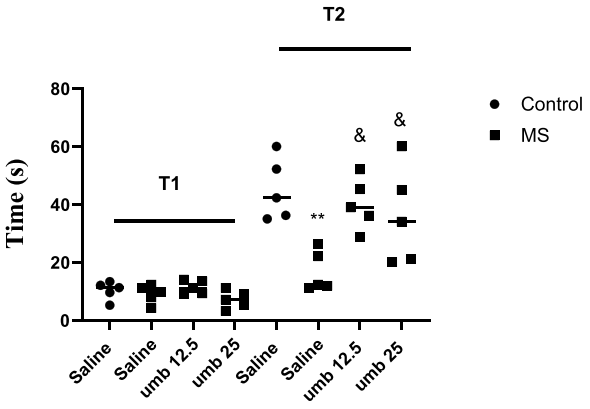

FIGURE 1
The effect of UMB on the initial and step-through latencies in the passive avoidance response in the shuttle box test. Values were calculated for a sample of 5 mice and reported as the mean ± S.E.M. The statistical analysis employed a one-way ANOVA followed by Tukey's post-test. $^{**}p < 0.001$ in compared to the control group, $^{\delta}p < 0.05$ in compared to the saline-treated MS group.

expressed as mean ± S.E.M and analyzed with one-way variance analysis (ANOVA) followed by Tukey's *post hoc* test. Results were deemed statistically significant at $p < 0.05$.

Results

Effects of UMB on passive avoidance memory in the shuttle box test

The results indicated no notable difference among the experimental groups in the initial phase (T1) of the shuttle box test. However, in the second phase of the test (T2), the results showed a marked reduction in the MS group compared to the control group ($p < 0.01$). We observed that UMB at doses of 12.5 and 25 mg/kg significantly increased T2 compared to the saline-treated MS group ($p < 0.05$) (Figure 1).

Effects of UMB on repetitive behavior in the marble burying test

The study's findings revealed that the MS group had a significantly higher number of buried marbles than the control group ($p < 0.001$). However, the number of marbles buried was decreased considerably in the MS mice treated with UMB at a dose of 12.5 mg/kg ($p < 0.01$) and UMB at a dose of 25 mg/kg ($p < 0.001$) compared to the saline-treated MS mice (Figure 2).

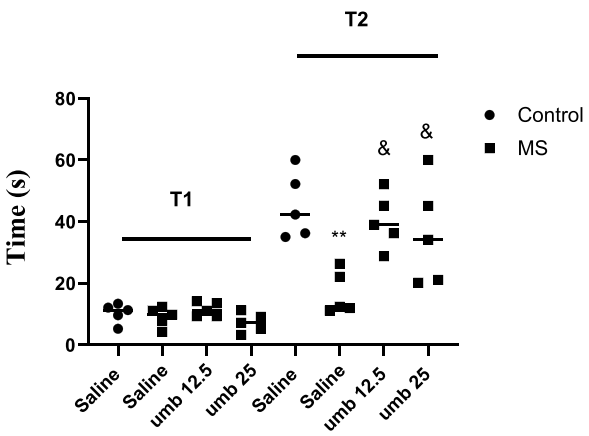

FIGURE 2
The effect of UMB on the number of marbles buried. The values were calculated for a sample of 5 mice and reported as the mean ± S.E.M. The statistical analysis employed a one-way ANOVA followed by Tukey's post-test. $^{***}p < 0.001$ compared to the control group and $^{\delta\delta}p < 0.01$ and $^{\delta\delta\delta}p < 0.001$ compared to the saline-treated MS group.

Effects of UMB on sociability and social preference indexes in the three-chamber test

Findings showed that the MS group exhibited a significant reduction in their SI ($p < 0.01$) compared to the control group. However, when MS groups were treated with UMB at doses of 12.5 and 25 mg/kg, their SI improved significantly ($p < 0.01$) compared to the saline-received MS mice (Figure 3). Additionally, we observed that SPI was decreased considerably in the MS group compared to the control group ($p < 0.001$). When MS groups were treated with UMB at doses of 12.5 and 25 mg/kg, their SPI significantly increased compared to the saline-treated MS animals ($p < 0.05$).

Effects of UMB on the open arms entries and time in the EPM test

The findings from the EPM test are presented in Figure 4. The MS group demonstrated a pronounced reduction in open-arm entries compared to the control group ($p < 0.01$). Treatment of the MS group with UMB at doses of 12.5 mg/kg ($p < 0.05$) and 25 mg/kg ($p < 0.01$) resulted in a significant increase in the number of open-arm entries compared to the saline-treated MS mice. Additionally, the time spent in open arms was significantly lower in the MS group compared to the control group ($p < 0.001$). However, administering UMB at a dose of 12.5 mg/kg ($p < 0.01$) and 25 mg/kg ($p < 0.05$) to the MS group resulted in a significant increase in the time spent in open arms compared to the saline-treated MS mice. Furthermore, results showed that the MS group had a higher anxiety index compared to the control mice ($p < 0.001$). Treatment of MS mice with UMB at doses of 12.5 ($p < 0.01$) and 25 mg/kg ($p < 0.001$) significantly decreased anxiety index compared to the saline-treated MS mice.

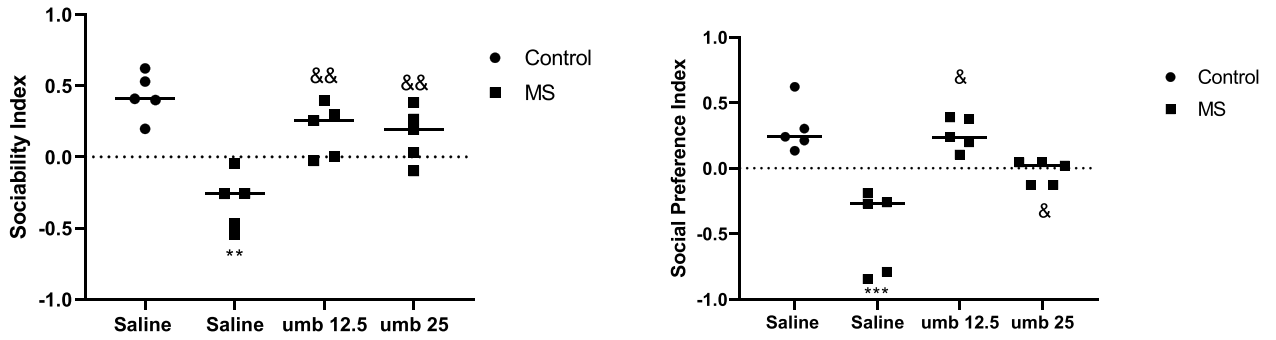

FIGURE 3
The effect of UMB on sociability index and social preference index. The values were calculated for a sample of 5 mice and reported as the mean ± S.E.M. The statistical analysis employed a one-way ANOVA followed by Tukey's post-test. $^{**}p < 0.01$ and $^{***}p < 0.001$ compared to the control group and $^{\delta}p < 0.05$ and $^{\delta\delta}p < 0.01$ compared to the saline-treated MS group.

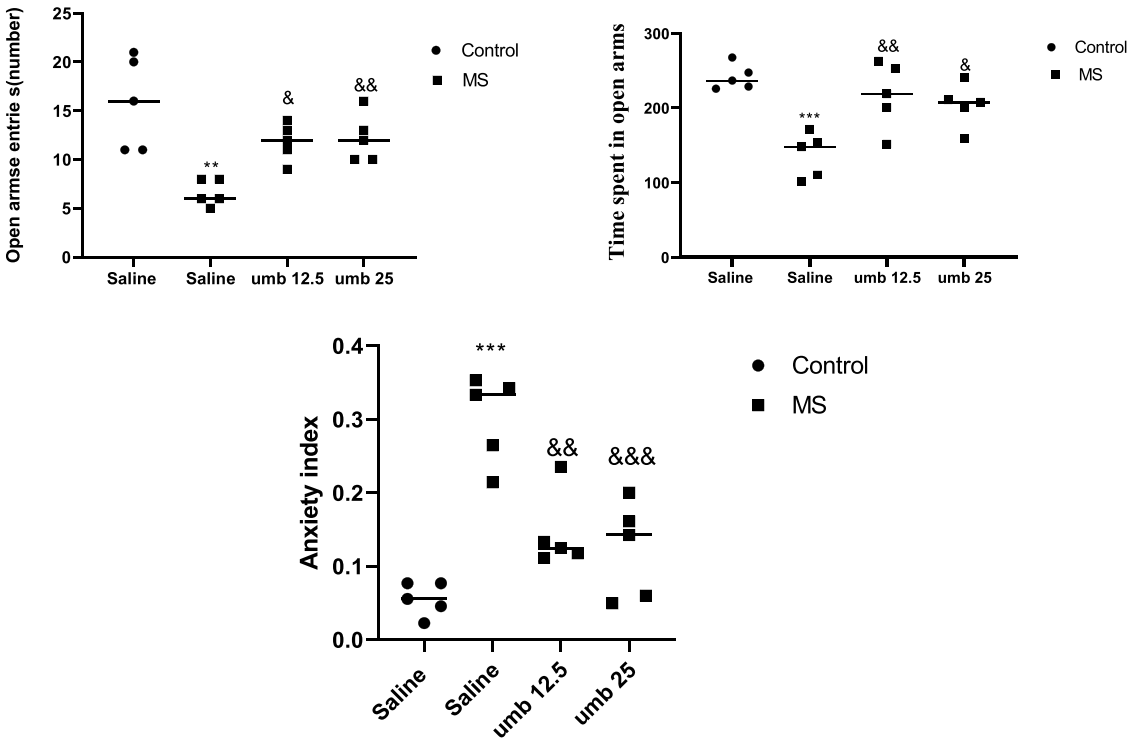

FIGURE 4
The effect of UMB on the open arms entries and time spent in open arms in the EPM. Values were calculated for a sample of 5 mice and reported as the mean ± S.E.M. The statistical analysis employed a one-way ANOVA followed by Tukey's post-test. $^{**}p < 0.01$ and $^{***}p < 0.001$ in comparison to the control group, $^{\delta}p < 0.05$, $^{\delta\delta}p < 0.01$ and $^{\delta\delta\delta}p < 0.001$ in comparison to the saline-treated MS group.

Effects of UMB on nitrite levels in the hippocampus

The results indicated a significant increase in nitrite levels in the hippocampus tissue of the MS group compared to the control group ($p < 0.05$). Treatment of MS mice with UMB at a dose of 12.5 mg/kg ($p < 0.05$) and UMB at a dose of 25 mg/kg ($p < 0.01$) resulted in a significant decrease in nitrite levels compared to the saline-treated MS mice (Figure 5).

Effects of UMB on MDA levels in the hippocampus

Based on the results shown in Figure 6, the MDA level of the hippocampus was significantly increased in the MS group compared to the control group ($p < 0.05$). Treatment of MS mice with UMB at doses of 12.5 and 25 mg/kg ($p < 0.05$) resulted in a significant decrease in the MDA levels compared to the saline-treated MS mice.

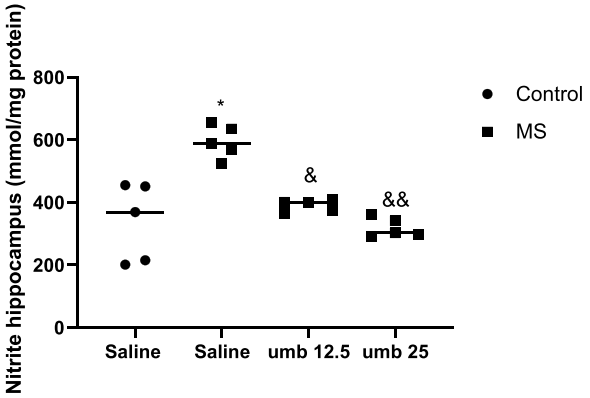

FIGURE 5
The effect of UMB on the nitrite levels in the hippocampus. Values were calculated for a sample of 5 mice and reported as the mean ± S.E.M. The statistical analysis employed a one-way ANOVA followed by Tukey's post-test. *$p < 0.05$ compared to the control group, $^{\&}p < 0.05$ and $^{\&\&}p < 0.01$ in compared to the saline-treated MS group.

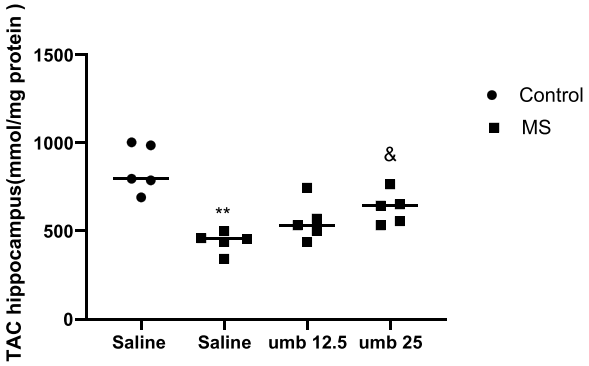

FIGURE 7
The effect of UMB on the *TAC* in the hippocampus. Values were calculated for a sample of 5 mice, reported as the mean ± S.E.M., and analyzed by one-way ANOVA followed by Tukey's *post hoc* test. **$p < 0.01$ compared to the control group and $^{\&}p < 0.05$ in compared to the saline-treated MS group.

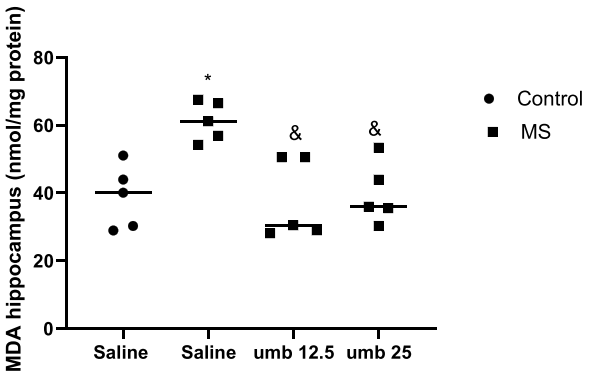

FIGURE 6
The effect of UMB on the MDA level in the hippocampus. Values were calculated for a sample of 5 mice, reported as the mean ± S.E.M., and analyzed by one-way ANOVA followed by Tukey's *post hoc* test. *$p < 0.05$ compared to the control group and $^{\&}p < 0.05$ in compared to the saline-treated MS group.

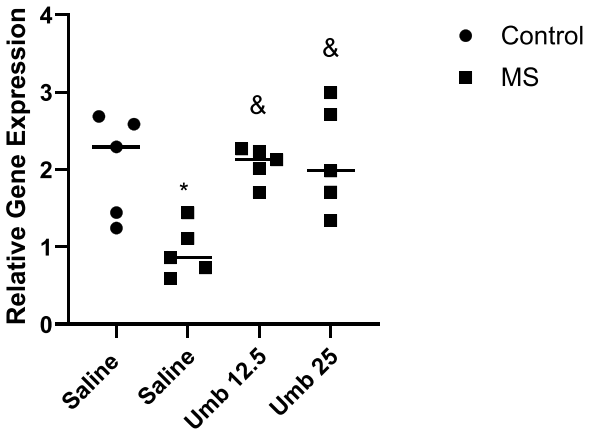

FIGURE 8
The effect of UMB on the gene expression of *MECP2* in the hippocampus. Values were calculated for a sample of 5 mice, reported as the mean ± S.E.M., and analyzed by one-way ANOVA followed by Tukey's *post hoc* test. *$p < 0.05$ compared to the control group and $^{\&}p < 0.05$ in compared to the saline-treated MS group.

Effects of UMB

on TAC in the hippocampus Results showed that the TAC in the hippocampus of the MS group significantly decreased compared to the control group ($p < 0.01$) (Figure 7). Treatment of MS mice with UMB at a dose of 25 mg/kg resulted in a significant increase in the TAC compared to the saline-treated MS mice ($p < 0.05$).

Gene expression of *MECP2* in the hippocampus following administration of UMB Figure 8 shows the effects of UMB on the gene expression of *MECP2* in the hippocampus. The results showed that the gene expression of *MECP2* in the hippocampus of the MS group significantly decreased compared to the control group ($p < 0.05$). Treatment of MS mice with UMB at doses of 12.5 and 25 mg/kg resulted in a significant increase in the gene expression of *MECP2* in the hippocampus compared to the saline-treated MS mice ($p < 0.05$).

Discussion

The present study examined the effects of UMB on the manifestations of autistic-like behaviors following the MS paradigm. Our findings revealed that MS resulted in autistic-like behavior, as evidenced by a decrease in secondary delay time in the shuttle box test, indicating impaired passive avoidance memory. There was also an increase in the number of hidden marbles in the

MBT, demonstrating repetitive behaviors. Additionally, the three-chamber test's sociability and social preference indexes were reduced, suggesting impaired social interaction. Furthermore, there was a decrease in the number and duration of entries in the EPM, reflecting anxiety-like behaviors.

Moreover, we found that autistic-like behaviors are associated with decreased MECP2 gene expression, TAC, and increased MDA and nitrite levels in the hippocampus, indicating an oxidative stress state and neurodevelopmental failure.

Investigating the potential effects of UMB, we observed that UMB significantly attenuated the autistic-like behaviors induced by MS. Furthermore, it increased *MECP2* gene expression. It mitigated oxidative stress markers in the hippocampus.

ASD encompasses a range of neurodevelopmental alterations, and its prevalence is significantly rising worldwide (Selamet and Usta, 2023). Recent studies have elucidated the involvement of multiple environmental and genetic factors in the pathogenesis of ASD (Lipkin et al., 2023). Early detection of Autism can facilitate timely interventions and treatments, improving outcomes (Juruena et al., 2020). The lack of effective treatments, alongside the fact that current therapeutic approaches exhibit partial efficacy and present notable side effects, creates a pressing need to investigate new effective and safe agents for the management of Autism (Vivanti et al., 2014).

Given the incomplete understanding of the pathophysiology of Autism, researchers are actively exploring potential pathways and mechanisms involved in this complex disorder. One pathway of interest is the *MECP2* pathway. Consequently, in this study, we investigated the therapeutic potential of UMB, aiming to elucidate its effect on autistic-like behaviors following the MS paradigm.

Recent investigations have unveiled the profound influence of early-life stress on developing neurodevelopmental abnormalities (Farzan et al., 2023). Furthermore, mounting evidence suggests that early-life stress can contribute to the manifestation of psychiatric disorders and behavioral impairments, including depression, anxiety, and Autism (Amiri et al., 2016; Lorigooini et al., 2020b; Pitsillou et al., 2020). Račekov et al. reported reduced neurogenesis across various brain regions in animals subjected to early postnatal stress (Račeková et al., 2009). In this regard, it has been determined that Autism is associated with decreased neurogenesis in the brain (Bicker et al., 2021). There is growing evidence that ELS, such as MS, is related to the development of ASD (Farzan et al., 2023; Khaledi et al., 2023; Makris et al., 2023). In this regard, it has been demonstrated that MS in animal models induces autistic-like behaviors such as repetitive behaviors, anxiety-like behaviors, memory impairment, and social interaction impairments (Mansouri et al., 2020). Chang et al. revealed an increase in the number of buried marbles in the MBT in mice exhibiting autistic-like features (Chang et al., 2017). In line with the studies mentioned earlier, we showed that maternally separated mice buried more marbles than the control group.

Furthermore, Varadinova et al. observed that in autistic mice, secondary delay in the shuttle box test decreased compared to the control group (Varadinova et al., 2019). Our result showed that maternally separated mice have a lower secondary delay time in the shuttle box than the control mice. Previous studies have reported a decrease in the number and duration of entries in the open arms of EPM for MS mice (Tallarico et al., 2023). Consistent with these findings, our study revealed that MS mice exhibited reduced time and number of entries into the open arms of the EPM. Previous studies have shown that mice with autistic-like features display diminished social interactions, such as lower sociality and social preference indexes, suggesting impaired social communication (Yin et al., 2023). In line with these findings, our study revealed that mice subjected to MS exhibited reduced social communications and connected less with their counterparts compared to the control group. Emerging evidence suggests a role of oxidative stress in the pathophysiology of various neurodevelopmental disorders like ASD (Cipolla and Lodhi, 2017) with particular relevance to ASD (Nadeem et al., 2019). Oxidative stress plays a crucial role in triggering neuroinflammation, which is considered a major contributing factor to ASD (McDougle and Carlezon, 2013). Consistent with these studies, our study revealed a significant decrease in brain antioxidant capacity, as well as an increase in nitrite and MDA levels in the hippocampus.

MECP2 alteration has been involved in a range of neurodevelopmental disorders like ASD (Wen et al., 2017; Alexander-Howden et al., 2023; Li et al., 2023). Notably, *MECP2* mutations have been extensively described in Rett syndrome, Autism, intellectual disability, and early-onset psychosis (Couvert et al., 2001; Chahrour and Zoghbi, 2007). Furthermore, functional protein alterations resulting from mutated *MECP2* have been linked to distinct neurodevelopmental impairments in Rett syndrome and ASD, which are connected with autistic characteristics (Shahbazian et al., 2002; Shibayama et al., 2004). Our findings align with these reports, demonstrating a significant reduction in *MECP2* gene expression in the hippocampus of MS mice. One limitation of our study is that we only evaluated *MECP2* at the gene level. Assessing *MECP2* at the protein level using Western blotting, *IHC, or ELISA* is suggested for future studies. Another limitation of this study is that we did not examine the effects of umbelliprenin in autistic-like behaviors following MS in female mice.

UMB, a member of the coumarin family, has been determined to exert neuroprotective effects through its antioxidative properties (Sharifi et al., 2020; Fiorito et al., 2022). Recent studies have elucidated its anti-inflammatory, anticancer, immune-modulatory, analgesic, and neuroprotective attributes (Hashemzaei et al., 2015; Rashidi et al., 2018). Ample evidence has corroborated its antioxidative and anti-inflammatory effects (Shakeri et al., 2014).

In the present study, we found that the administration of UMB to the MS mice led to the attenuation of autistic-like behaviors, as indicated by an increase in the social preference index and sociability index in the three-chamber test, an increase in the time and number of entrances to the open arm in the EPM test, an increase in the second delay in the shuttle box test, and a decrease in the number of buried marbles in the MBT. These behavioral tests showed that, at least partially, UMB mitigated autistic-like behaviors following MS. Furthermore, we found that following the administration of UMB, the levels of nitrite and MDA significantly decreased in the hippocampus of the MS mice. In addition, UMB significantly increased total antioxidant capacity in the hippocampus of MS mice. In the case of *MECP2* gene expression, our results showed that UMB significantly increased the gene expression of *MECP2* in the hippocampus of MS mice. However, further studies are warranted to evaluate the exact mechanism underlying the effects of UMB in autistic-like behaviors.

Conclusion

In conclusion, our results suggest that an increase in the oxidative stress markers and a decrease in the gene expression of *MECP2* in the hippocampus contributes, at least partly, to the manifestation of autistic-like behaviors observed following the MS paradigm. We concluded that UMB probably, partially at least, via attenuation of oxidative stress and increase in the gene expression of *MECP2* in the hippocampus attenuated the autistic-like behaviors following MS stress in male mice.

Data availability statement

The original contributions presented in the study are included in the article/Supplementary Material, further inquiries can be directed to the corresponding author.

Ethics statement

The animal study was approved by Shahrekord University of Medical Sciences (Ethics code: IR.SKUMS.AEC.1400.002). The study was conducted in accordance with the local legislation and institutional requirements.

Author contributions

PK: Methodology, Writing–original draft. MG: Methodology, Writing–original draft. ZL: Data curation, Formal Analysis, Investigation, Software, Writing–original draft. MS: Methodology, Writing–original draft. HA-K: Conceptualization, Funding acquisition, Investigation, Methodology, Project administration, Resources, Supervision, Validation, Visualization, Writing–original draft, Writing–review and editing.

Funding

The author(s) declare financial support was received for the research, authorship, and/or publication of this article. This study was supported by a research grant (3846) from Shahrekord University of Medical Sciences, Shahrekord, Iran.

Acknowledgments

The authors appreciate Mrs. Elham Bijad's contribution to this study.

Conflict of interest

The authors declare that the research was conducted in the absence of any commercial or financial relationships that could be construed as a potential conflict of interest.

Publisher's note

References

Alexander-Howden, B., Zhang, L., van der Sloot, A. M., Tollis, S., St-Cyr, D. J., Sicheri, F., et al. (2023). A screen for MeCP2-TBL1 interaction inhibitors using a luminescence-based assay. *Sci. Rep.* 13 (1), 3868. doi:10.1038/s41598-023-29915-z

Amini, F., Amini-Khoei, H., Haratizadeh, S., Setayesh, M., Basiri, M., Raeiszadeh, M., et al. (2023). Hydroalcoholic extract of Passiflora incarnata improves the autistic-like behavior and neuronal damage in a valproic acid-induced rat model of autism. *J. Traditional Complementary Med.* 13, 315–324. doi:10.1016/j.jtcme.2023.02.005

Amini-Khoei, H., Haghani-Samani, E., Beigi, M., Soltani, A., Mobini, G. R., Balali-Dehkordi, S., et al. (2019). On the role of corticosterone in behavioral disorders, microbiota composition alteration and neuroimmune response in adult male mice subjected to maternal separation stress. *Int. Immunopharmacol.* 66, 242–250. doi:10.1016/j.intimp.2018.11.037

Amiri, S., Amini-Khoei, H., Mohammadi-Asl, A., Alijanpour, S., Haj-Mirzaian, A., Rahimi-Balaei, M., et al. (2016). Involvement of D1 and D2 dopamine receptors in the antidepressant-like effects of selegiline in maternal separation model of mouse. *Physiology Behav.* 163, 107–114. doi:10.1016/j.physbeh.2016.04.052

Arabi, M., Nasab, S. H., Lorigooini, Z., Boroujeni, S. N., Mortazavi, S. M., Anjomshoa, M., et al. (2021). Auraptene exerts protective effects on maternal separation stress-induced changes in behavior, hippocampus, heart and serum of mice. *Int. Immunopharmacol.* 93, 107436. doi:10.1016/j.intimp.2021.107436

Benzie, I. F. F., and Strain, J. J. (1999). Ferric reducing/antioxidant power assay: direct measure of total antioxidant activity of biological fluids and modified version for simultaneous measurement of total antioxidant power and ascorbic acid concentration. *Methods Enzym.* 299, 15–27. doi:10.1016/s0076-6879(99)99005-5

Bicker, F., Nardi, L., Maier, J., Vasic, V., and Schmeisser, M. J. (2021). Criss-crossing autism spectrum disorder and adult neurogenesis. *J. Neurochem.* 159 (3), 452–478. doi:10.1111/jnc.15501

Calfa, G., Percy, A. K., and Pozzo-Miller, L. (2011). Experimental models of Rett syndrome based on Mecp2 dysfunction. *Exp. Biol. Med.* 236 (1), 3–19. doi:10.1258/ebm.2010.010261

Chahrour, M., and Zoghbi, H. Y. (2007). The story of Rett syndrome: from clinic to neurobiology. *Neuron* 56 (3), 422–437. doi:10.1016/j.neuron.2007.10.001

Chang, Y. C., Cole, T. B., and Costa, L. G. (2017). Behavioral phenotyping for autism spectrum disorders in mice. *Curr. Protoc. Toxicol.* 72 (1), 11. doi:10.1002/cptx.19

Charan, J., and Kantharia, N. (2013). How to calculate sample size in animal studies? *J. Pharmacol. Pharmacother.* 4 (4), 303–306. doi:10.4103/0976-500X.119726

Chen, Y., Cai, W., Li, C., Su, Z., Guo, Z., Li, Z., et al. (2022). Sex differences in peripheral monoamine transmitter and related hormone levels in chronic stress mice with a depression-like phenotype. *PeerJ* 10, e14014. doi:10.7717/peerj.14014

Choi, M., Ko, S. Y., Seo, J. Y., Kim, D. G., Lee, H., Chung, H., et al. (2022). Autistic-like social deficits in hippocampal MeCP2 knockdown rat models are rescued by ketamine. *BMB Rep.* 55 (5), 238–243. doi:10.5483/BMBRep.2022.55.5.038

Cipolla, C. M., and Lodhi, I. J. (2017). Peroxisomal dysfunction in age-related diseases. *Trends Endocrinol. Metabolism* 28 (4), 297–308. doi:10.1016/j.tem.2016.12.003

Couvert, P., Bienvenu, T., Aquaviva, C., Poirier, K., Moraine, C., Gendrot, C., et al. (2001). MECP2 is highly mutated in X-linked mental retardation. *Hum. Mol. Genet.* 10 (9), 941–946. doi:10.1093/hmg/10.9.941

Faras, H., Al Ateeqi, N., and Tidmarsh, L. (2010). Autism spectrum disorders. *Ann. Saudi Med.* 30 (4), 295–300. doi:10.4103/0256-4947.65261

Farzan, M., Farzan, M., Amini-Khoei, H., Shahrani, M., Bijad, E., Anjomshoa, M., et al. (2023). Protective effects of vanillic acid on autistic-like behaviors in a rat model of maternal separation stress: behavioral, electrophysiological, molecular and

histopathological alterations. *Int. Immunopharmacol.* 118, 110112. doi:10.1016/j.intimp.2023.110112

Fiorito, S., Preziuso, F., Sharifi-Rad, M., Marchetti, L., Epifano, F., and Genovese, S. (2022). Auraptene and umbelliprenin: a review on their latest literature acquisitions. *Phytochem. Rev.* 21, 317–326. doi:10.1007/s11101-020-09713-5

Gildawie, K. R., Ryll, L. M., Hexter, J. C., Peterzell, S., Valentine, A. A., and Brenhouse, H. C. (2021). A two-hit adversity model in developing rats reveals sex-specific impacts on prefrontal cortex structure and behavior. *Dev. Cogn. Neurosci.* 48, 100924. doi:10.1016/j.dcn.2021.100924

Hashemzaei, M., Dousti, T., Tsarouhas, K., Bagheri, G., Nikolouzakis, T. K., Rezaee, R., et al. (2020). Effect of umbelliprenin on blood pressure in high-fat diet hypertensive rats. *Farmacia* 68 (3), 447–452. doi:10.31925/farmacia.2020.3.9

Hashemzaei, M., SadeghiBonjar, M. A., Tabrizian, K., Iranshahi, M., Iranshahy, M., and Rezaee, R. (2015). Evaluation of the analgesic effect of Umbelliprenin and Umbelliprenin-morphine co-administration on the acute, chronic and neuropathic pain. *Indian J. Pharm. Educ.* 49 (2), 121–125. doi:10.5530/ijper.49.2.7

Iranshahi, M., Askari, M., Sahebkar, A., and Hadjipavlou, L. D. (2009). Evaluation of antioxidant, anti-inflammatory and lipoxygenase inhibitory activities of the prenylated coumarin umbelliprenin. *DARU J. Pharm. Sci.* 17, 99–103.

Jiang, Z.-D., Alexander, A., Ke, S., Valilis, E. M., Hu, S., Li, B., et al. (2017). Stability and efficacy of frozen and lyophilized fecal microbiota transplant (FMT) product in a mouse model of *Clostridium difficile* infection (CDI). *Anaerobe* 48, 110–114. doi:10.1016/j.anaerobe.2017.08.003

Juruena, M. F., Eror, F., Cleare, A. J., and Young, A. H. (2020). The role of early life stress in HPA axis and anxiety. *Anxiety Disord. Rethink. Underst. recent Discov.* 1191, 141–153. doi:10.1007/978-981-32-9705-0_9

Khaghanzadeh, N., Samiei, A., Mojtahedi, Z., Ramezani, M., Hosseinzadeh, M., and Ghaderi, A. (2017). Umbelliprenin induced both anti-inflammatory and regulatory cytokines in C57/BL6 mice. *Iran. J. Basic Med. Sci.* 20 (7), 829–834. doi:10.22038/IJBMS.2017.9021

Khaledi, F., Dehkordi, H. T., Zarean, E., Shahrani, M., and Amini-Khoei, H. (2023). Possible role of NO/NMDA pathway in the autistic-like behaviors induced by maternal separation stress in mice. *Plos one* 18 (10), e0292631. doi:10.1371/journal.pone.0292631

Lee, K. Y., Wang, H., Yook, Y., Rhodes, J. S., Christian-Hinman, C. A., and Tsai, N.-P. (2023). Tumor suppressor p53 modulates activity-dependent synapse strengthening, autism-like behavior and hippocampus-dependent learning. *Mol. Psychiatry* 2023, 1–13. doi:10.1038/s41380-023-02268-9

Li, X., Nie, Y., Qiu, Z., and Wang, S. (2023). Human MECP2 transgenic rats show increased anxiety, severe social deficits, and abnormal prefrontal neural oscillation stability. *Biochem. Biophysical Res. Commun.* 648, 28–35. doi:10.1016/j.bbrc.2023.01.057

Lipkin, W. I., Bresnahan, M., and Susser, E. (2023). Cohort-guided insights into gene–environment interactions in autism spectrum disorders. *Nat. Rev. Neurol.* 19 (2), 118–125. doi:10.1038/s41582-022-00764-0

Lorigooini, Z., Boroujeni, S. N., Sayyadi-Shahraki, M., Rahimi-Madiseh, M., Bijad, E., and Amini-Khoei, H. (2021). Limonene through attenuation of neuroinflammation and nitrite level exerts antidepressant-like effect on mouse model of maternal separation stress. *Behav. Neurol.* 2021, 2021–2028. doi:10.1155/2021/8817309

Lorigooini, Z., Nouri, A., Mottaghinia, F., Balali-Dehkordi, S., Bijad, E., Dehkordi, S. H., et al. (2020b). Ferulic acid through mitigation of NMDA receptor pathway exerts anxiolytic-like effect in mouse model of maternal separation stress. *J. Basic Clin. Physiology Pharmacol.* 32 (1), 20190263. doi:10.1515/jbcpp-2019-0263

Lorigooini, Z., Sadeghi Dehsahraei, K., Bijad, E., Habibian Dehkordi, S., and Amini-Khoei, H. (2020a). Trigonelline through the attenuation of oxidative stress exerts antidepressant-and anxiolytic-like effects in a mouse model of maternal separation stress. *Pharmacology* 105 (5-6), 289–299. doi:10.1159/000503728

Makris, G., Eleftheriades, A., and Pervanidou, P. (2023). Early life stress, hormones, and neurodevelopmental disorders. *Hormone Res. Paediatr.* 96 (1), 17–24. doi:10.1159/000523942

Mansouri, M., Pouretemad, H., Roghani, M., Wegener, G., and Ardalan, M. (2020). Autistic-like behaviours and associated brain structural plasticity are modulated by oxytocin in maternally separated rats. *Behav. Brain Res.* 393, 112756. doi:10.1016/j.bbr.2020.112756

Mansouri, M., Pouretemad, H., Wegener, G., Roghani, M., Afshari, M., Mallard, C., et al. (2021). Dual profile of environmental enrichment and autistic-like behaviors in the maternal separated model in rats. *Int. J. Mol. Sci.* 22 (3), 1173. doi:10.3390/ijms22031173

McDougle, C. J., and Carlezon, W. A., Jr (2013). Neuroinflammation and autism: toward mechanisms and treatments. *Neuropsychopharmacology* 38 (1), 241–242. doi:10.1038/npp.2012.174

Moghaddam, A. H., Eslami, A., khanjani Jelodar, S., Ranjbar, M., and Hasantabar, V. (2023). Preventive effect of quercetin-Loaded nanophytosome against autistic-like damage in maternal separation model: the possible role of Caspase-3, Bax/Bcl-2 and Nrf2. *Behav. Brain Res.* 441, 114300. doi:10.1016/j.bbr.2023.114300

Moreno-Martínez, S., Tendilla-Beltrán, H., Sandoval, V., Flores, G., and Terrón, J. A. (2022). Chronic restraint stress induces anxiety-like behavior and remodeling of dendritic spines in the central nucleus of the amygdala. *Behav. Brain Res.* 416, 113523. doi:10.1016/j.bbr.2021.113523

Nadeem, A., Ahmad, S. F., Attia, S. M., Al-Ayadhi, L. Y., Al-Harbi, N. O., and Bakheet, S. A. (2019). Dysregulated enzymatic antioxidant network in peripheral neutrophils and monocytes in children with autism. *Prog. Neuro-Psychopharmacology Biol. Psychiatry* 88, 352–359. doi:10.1016/j.pnpbp.2018.08.020

Nagababu, E., Rifkind, J. M., Boindala, S., and Nakka, L. (2010). Assessment of antioxidant activity of eugenol *in vitro* and *in vivo*. *Free radicals Antioxid. Protoc.* 610, 165–180. doi:10.1007/978-1-60327-029-8_10

Nasiri-Boroujeni, S., Rahimi-Madiseh, M., Lorigooini, Z., Piroti, K., Rafieian-Koupaei, M., and Amini-Khoei, H. (2021). NMDA receptor mediates the anticonvulsant effect of hydroalcoholic extract of *Artemisia persica* in PTZ-induced seizure in mice. *Evidence-Based Complementary Altern. Med.* 2021, 6422451. doi:10.1155/2021/6422451

Neul, J. L. (2022). The relationship of Rett syndrome and MECP2 disorders to autism. *Dialogues Clin. Neurosci.* 14, 253–262. doi:10.31887/DCNS.2012.14.3/jneul

Omidi-Ardali, H., Lorigooini, Z., Soltani, A., Balali-Dehkordi, S., and Amini-Khoei, H. (2019). Inflammatory responses bridge comorbid cardiac disorder in experimental model of IBD induced by DSS: protective effect of the trigonelline. *Inflammopharmacology* 27, 1265–1273. doi:10.1007/s10787-019-00581-w

Pang, R., Yan, S., Tu, Y., Qian, S., Yu, H., Hu, X., et al. (2023). Transient hearing abnormalities precede social deficits in a mouse model of autism. *Behav. Brain Res.* 437, 114149. doi:10.1016/j.bbr.2022.114149

Pejhan, S., and Rastegar, M. (2021). Role of DNA methyl-CpG-binding protein MeCP2 in Rett syndrome pathobiology and mechanism of disease. *Biomolecules* 11 (1), 75. doi:10.3390/biom11010075

Pitsillou, E., Bresnehan, S. M., Kagarakis, E. A., Wijoyo, S. J., Liang, J., Hung, A., et al. (2020). The cellular and molecular basis of major depressive disorder: towards a unified model for understanding clinical depression. *Mol. Biol. Rep.* 47, 753–770. doi:10.1007/s11033-019-05129-3

Račeková, E., Lievajová, K., Danko, J., Martončíková, M., Flešárová, S., Almašiová, V., et al. (2009). Maternal separation induced alterations of neurogenesis in the rat rostral migratory stream. *Cell. Mol. Neurobiol.* 29, 811–819. doi:10.1007/s10571-009-9362-x

Rashidi, M., Khalilnezhad, A., Amani, D., Jamshidi, H., Muhammadnejad, A., Bazi, A., et al. (2018). Umbelliprenin shows antitumor, antiangiogenesis, antimetastatic, anti-inflammatory, and immunostimulatory activities in 4T1 tumor-bearing Balb/c mice. *J. Cell. Physiology* 233 (11), 8908–8918. doi:10.1002/jcp.26814

Sadeghi, M. A., Hemmati, S., Yousefi-Manesh, H., Fekrvand, S., Foroutani, L., Nassireslami, E., et al. (2023). Neuronal nitric oxide synthase inhibition accelerated the removal of fluoxetine's anxiogenic activity in an animal model of PTSD. *Behav. Brain Res.* 437, 114128. doi:10.1016/j.bbr.2022.114128

Sánchez-Lafuente, C. L., Kalynchuk, L. E., Caruncho, H. J., and Ausió, J. (2022). The role of MeCP2 in regulating synaptic plasticity in the context of stress and depression. *Cells* 11 (4), 748. doi:10.3390/cells11040748

Selamet, E., and Usta, M. B. (2023). Mitochondrial dysfunction and mTOR in autism spectrum disorders. *Psikiyatr. Güncel Yaklaşımlar.* 15 (4), 697–704. doi:10.18863/pgy.1205786

Shahbazian, M. D., Antalffy, B., Armstrong, D. L., and Zoghbi, H. Y. (2002). Insight into Rett syndrome: MeCP2 levels display tissue-and cell-specific differences and correlate with neuronal maturation. *Hum. Mol. Genet.* 11 (2), 115–124. doi:10.1093/hmg/11.2.115

Shahraki, J., Rezaee, R., Mohammadzehi Kenar, S., Setoodeh Nezhad, S., Bagheri, G., Jahantigh, H., et al. (2020). Umbelliprenin relieves paclitaxel-induced neuropathy. *J. Pharm. Pharmacol.* 72 (12), 1822–1829. doi:10.1111/jphp.13365

Shakeri, A., Iranshahy, M., and Iranshahi, M. (2014). Biological properties and molecular targets of umbelliprenin–a mini-review. *J. Asian Nat. Prod. Res.* 16 (8), 884–889. doi:10.1080/10286020.2014.917630

Sharifi, S. F. F. P. M., Marchetti, R. L., and Genovese, F. E. S. (2020). Auraptene and umbelliprenin: a review on their latest literature acquisitions. *Phytochem. Rev.* 21, 317–326.

Shibayama, A., Cook, E. H., Jr, Feng, J., Glanzmann, C., Yan, J., Craddock, N., et al. (2004). MECP2 structural and 3′-UTR variants in schizophrenia, autism and other psychiatric diseases: a possible association with autism. *Am. J. Med. Genet. Part B Neuropsychiatric Genet.* 128 (1), 50–53. doi:10.1002/ajmg.b.30016

Tallarico, M., Leo, A., Russo, E., Citraro, R., Palma, E., and De Sarro, G. (2023). Seizure susceptibility to various convulsant stimuli in the BTBR mouse model of autism spectrum disorders. *Front. Pharmacol.* 14, 1155729. doi:10.3389/fphar.2023.1155729

Varadinova, M., Bogdanov, G., and Markova, P. (2019). Effects of risperidone on learning and memory parameters in experimental model of autism. *Trakia J. Sci.* 17 (3), 203–207. doi:10.15547/tjs.2019.03.002

Vivanti, G., Prior, M., Williams, K., and Dissanayake, C. (2014). Predictors of outcomes in autism early intervention: why don't we know more? *Front. Pediatr.* 2, 58. doi:10.3389/fped.2014.00058

Wen, Z., Cheng, T.-L., Li, G.-z., Sun, S.-B., Yu, S.-Y., Zhang, Y., et al. (2017). Identification of autism-related MECP2 mutations by whole-exome sequencing and functional validation. *Mol. autism* 8 (1), 43–10. doi:10.1186/s13229-017-0157-5

Wopara, I., Modo, E. U., Adebayo, O. G., Mobisson, S. K., Nwigwe, J. O., Ogbu, P. I., et al. (2021). Anxiogenic and memory impairment effect of food color exposure: upregulation of oxido-neuroinflammatory markers and acetyl-cholinestrase activity in the prefrontal cortex and hippocampus. *Heliyon* 7 (3), e06378. doi:10.1016/j.heliyon.2021.e06378

Xu, Q., Zuo, C., Liao, S., Long, Y., and Wang, Y. (2020). Abnormal development pattern of the amygdala and hippocampus from childhood to adulthood with autism. *J. Clin. Neurosci.* 78, 327–332. doi:10.1016/j.jocn.2020.03.049

Yadollahi-Farsani, Y., Vanani, V. R., Lorigooini, Z., Farahzad, A., and Amini-Khoei, H. (2023). Anethole via increase in the gene expression of PI3K/AKT/mTOR mitigates the autistic-like behaviors induced by maternal separation stress in mice. *IBRO Neurosci. Rep.* 28, 457–472. doi:10.1016/j.ibneur.2023.11.009

Yin, B., Li, H., Zhao, P., Zhao, Y., Zheng, R., Feng, P., et al. (2023). GM1 reduced the symptoms of autism spectrum disorder by suppressing α-syn through activating autophagy. *J. Mol. Neurosci.* 73 (4), 287–296. doi:10.1007/s12031-023-02110-5

Zhong, H., Xiao, R., Ruan, R., Liu, H., Li, X., Cai, Y., et al. (2020). Neonatal curcumin treatment restores hippocampal neurogenesis and improves autism-related behaviors in a mouse model of autism. *Psychopharmacology* 237, 3539–3552. doi:10.1007/s00213-020-05634-5

Zoghbi, H. Y. (2005). MeCP2 dysfunction in humans and mice. *J. child neurology* 20 (9), 736–740. doi:10.1177/08830738050200090701

frontiers | Frontiers in Neuroscience

TYPE Brief Research Report
PUBLISHED 12 January 2024
DOI 10.3389/fnins.2024.1327293

OPEN ACCESS

EDITED BY
Giuseppe Di Giovanni,
University of Malta, Malta

REVIEWED BY
Thomas Heinbockel,
Howard University, United States
Qianzi Yang,
Air Force Medical University, China
Yi Zhang,
Zunyi Medical University, China

*CORRESPONDENCE
Weixing Ding
✉ dwx466145142@163.com
Feng Cai
✉ 1551305579@qq.com

†These authors have contributed equally to this work

RECEIVED 24 October 2023
ACCEPTED 02 January 2024
PUBLISHED 12 January 2024

CITATION
Huang Y, Xiao Y, Li L, Feng X, Ding W and Cai F (2024) Propofol-induced anesthesia involves the direct inhibition of glutamatergic neurons in the lateral hypothalamus.
Front. Neurosci. 18:1327293.
doi: 10.3389/fnins.2024.1327293

Propofol-induced anesthesia involves the direct inhibition of glutamatergic neurons in the lateral hypothalamus

Yan Huang[1†], Yong Xiao[2†], Linji Li[1], Xinglong Feng[1], Weixing Ding[3*] and Feng Cai[4*]

[1]Department of Anesthesiology, Nanchong Central Hospital, Second Clinical Medical College of North Sichuan Medical College, Nanchong, China, [2]Emergency Department of the General Hospital of the Tibet Military Region, Lhasa, China, [3]Qujing Secend Peopie's Hospital, Department of Pain, Qujing, Yunnan, China, [4]Department of Urologyand Neurocardiothoracic Surgery, 927 Hospital of the Joint Logistics Support Force of the Chinese People's LiberationArmy, Puer, China

Propofol is the most widely used intravenous general anesthetic; however, the neuronal circuits that mediate its anesthetic effects are still poorly understood. Glutamatergic neurons in the lateral hypothalamus have been reported to be involved in maintenance of arousal and consciousness. Using Vglut2-Cre transgenic mice, we recorded this group of cells specifically and found that propofol can directly inhibit the glutamatergic neurons, and enhance inhibitory synaptic inputs on these cells, thereby reducing neuronal excitability. Through chemogenetic interventions, we found that inhibition of these neurons increased the duration of propofol-induced anesthesia and reduced movement in the animals after the recovery of right reflex. In contrast, activating this group of cells reduced the duration of propofol anesthesia and increased the animals' locomotor activity after the recovery of right reflex. These results suggest that propofol-induced anesthesia involves the inhibition of glutamatergic neurons in the lateral hypothalamus.

KEYWORDS

anesthesia, propofol, lateral hypothalamus, glutamatergic neurons, hM4Di receptors

Introduction

Intravenous general anesthetics are of great significance to modern surgical operation. Propofol is the most widely used intravenous anesthetic and is characterized by its favorable recovery profile (Choi et al., 2017; Mehta et al., 2017). A great deal of effort has gone into dissecting the neural circuitry and molecular targets underlying the effects of intravenous general anesthetics including propofol. Many studies have reported that propofol functions directly through generating a wide range of inhibitory impacts on neocortical regions, such as frontal cortex and entorhinal cortex (Li et al., 2016; Kobayashi and Oi, 2017; Luo et al., 2019). It is widely considered that these inhibitory effects might be attributed to that propofol could activate γ-aminobutyric acid type A receptors ($GABA_A$Rs) and thus increase the inhibitory inputs (Reine et al., 1992; Chen et al., 1999; Jeong et al., 2011). Despite the pioneering work, the neuronal circuits and molecular targets that

mediate anesthetic effects of propofol are still not completely understood. A systematic understanding of the anesthetic mechanism of propofol will contribute to the development of new anesthetics.

It has been reported that the cortical activities are tightly regulated by multiple subcortical arousal- and sleep-promoting brain regions. In fact, general anesthetics may act either by inhibiting subcortical arousal- promoting systems or activating sleep-promoting systems in the brain. For example, sevoflurane could inhibit the wakefulness-promoting neurons, such as dopamine D1 receptor-positive neurons in the nucleus accumbens (Bao et al., 2021), hypocretinergic neurons in the lateral hypothalamus (LH) (Kelz et al., 2008) and medial parabrachial neurons (Xu et al., 2020). Additionally, general anesthetics including dexmedetomidine, isoflurane, ketamine and propofol also activate sleep-promoting neurons such as the supraoptic nucleus to contribute to their anesthetic action (Jiang-Xie et al., 2019; Hua et al., 2020).

It should be noted that glutamatergic neurons in the LH have been reported to be involved in maintenance of arousal. Chemogenetic activation of LH glutamatergic neurons induced an increase in arousal that lasted for 6 h. In contrast, suppression of LH glutamatergic neuronal activity caused a reduction in wakefulness (Wang et al., 2021). Although the crucial role of the glutamatergic neurons in the LH in the maintenance of wakefulness has been established, it is still unclear whether propofol affects the activity of these neurons. Here, we have discovered a direct inhibition of glutamatergic neurons in the LH by propofol, which is involved in its anesthetic action. These results unveil a novel neural mechanism underlying the anesthetic effects of propofol and provide the targets for research and development of new anesthetic drugs.

Results

Propofol generates hyperpolarization of the wakefulness-related glutamatergic neurons in the LH

To visualize glutamatergic neurons in the LH, AAV2/9-EF1α-DIO- mCherry was injected into the LH of vGlut2-Cre mice to label the glutamatergic neurons with the mCherry. To further validate the specificity of the mCherry expression, we used fluorescence *in situ* hybridization (FISH) to detect the vesicular glutamate transporter 2 (VGLUT2, encoded by *Slc17a6*), and found that mCherry is selectively expressed in *Slc17a6*-positive neurons (**Figures 1A, B**).

We initially explored the effect of the propofol on the glutamatergic neurons in the LH (**Figure 1C**). The glutamatergic neurons were specifically recorded from the brain slices. The voltage-clamp recordings were performed to test the effects of propofol on the holding currents of glutamatergic neurons. Bath application (1–50 μM, 1 min) of propofol induced outward currents in the recorded glutamatergic neurons. The amplitude of outward currents induced by propofol was concentration-dependent (**Figures 1C, D**).

Next, we investigated whether propofol directly affects membrane intrinsic properties. To test this, the hold currents were recorded in the presence of tetrodotoxin (TTX, 1 μM) to block action potentials-dependent synaptic transmissions. Under this condition, we found that propofol still induced outward currents in the glutamatergic neurons (**Figure 1E**), suggesting that propofol directly influences the membrane properties of the glutamatergic neurons.

Additionally, propofol (10 μM) significantly reduced the firing rates of these neurons in response to inward current stimuli (**Figures 1F, G**). In sum, these data suggest that propofol suppresses the excitability of the glutamatergic neurons in the LH.

Propofol enhances the GABAergic inhibitory inputs on glutamatergic neurons

The activity of individual neurons as well as neural network is tightly controlled by the synaptic transmissions. Thus, we next explored whether propofol influences the synaptic transmissions of the glutamatergic neutrons in the LH. We firstly recorded the spontaneous excitatory postsynaptic currents (SEPSCs) in the presence of $GABA_A$ receptor antagonist bicuculline. The glutamatergic neurons of the LH exhibited a continuous level of fast excitatory synaptic events. Bath application of propofol did not affect the amplitude and frequency of SEPSCs in these glutamatergic neurons (**Figures 2A, B**).

To test the regulation of $GABA_A$ receptor-mediated spontaneous inhibitory postsynaptic currents (SIPSCs) by propofol, we blocked the ionotropic glutamate receptors by using 6-cyano-7-nitroquinoxaline-2, 3-dione (CNQX) and DL-2-amino-5-phosphonopentanoic acid (AP5). After recording stable baseline of SIPSCs, bath application of propofol remarkably increased the frequency and amplitude of these currents (**Figures 2C, D**). These results indicate that propofol increases inhibitory inputs of the glutamatergic neurons without affecting their excitatory inputs.

Chemogenetic inhibition of glutamatergic neurons in the LH facilitates induction of and prolongs emergence from propofol anesthesia

To investigate the behavioral consequences of chemogenetic inhibition of glutamatergic neurons in the LH, AAV-DIO-hM4Di-mCherry was injected into the LH of vGlut2-Cre mice to inhibit glutamatergic neurons. Whole-cell recordings of hM4Di-mCherry-positive glutamatergic neurons from acute brain slices showed a decreased number of action potentials with bath-applied clozapine N-oxide (CNO), implying that CNO was sufficient to inhibit hM4Di-mCherry-positive neurons in the LH (**Figures 3A, B**). The hM4Di-mCherry and mCherry were restrictedly expressed in the LH (**Figures 3C, D**). Compared with those in the vehicle group, chemogenetic inhibition of glutamatergic neurons in the LH decreased the duration of propofol (10 mg/kg, i.v.)-induced loss of right reflex (LORR) (**Figures 3E, F**). Even after they recovered from LORR, the locomotion of the mice with CNO injection was impaired for several minutes following propofol

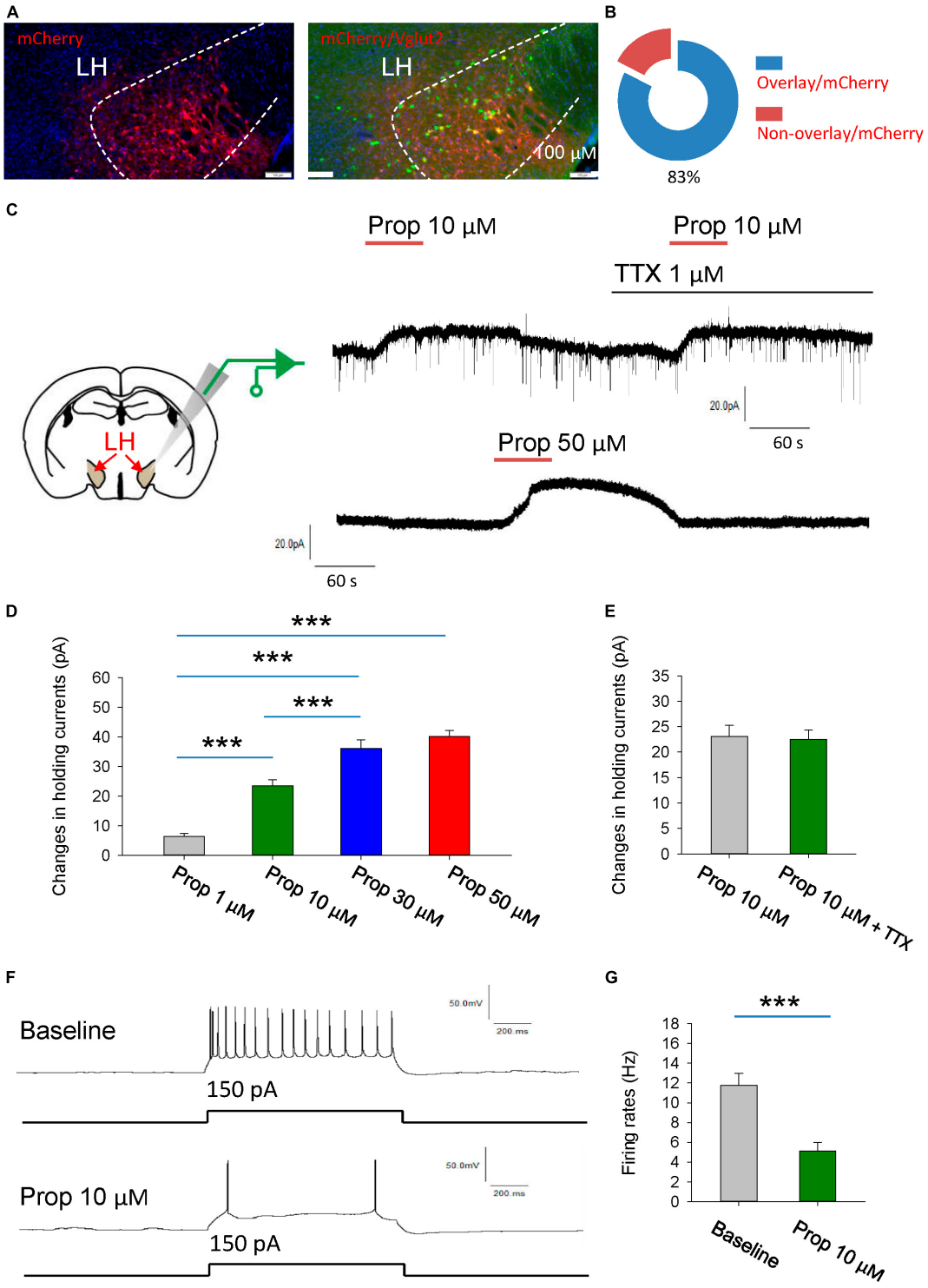

FIGURE 1
Propofol induces hyperpolarization of the glutamatergic neurons in the LH. **(A,B)** Fluorescence *in situ* hybridization (FISH) to detect the vesicular glutamate transporter 2 (VGLUT2, encoded by *Slc17a6*), noting that mCherry is selectively expressed in *Slc17a6*-positive neurons. **(C)** Schematic diagram for recording glutamatergic neurons in the LH (Left). Example electrophysiological traces before, during and after bath application of the 10 and 50 μM propofol (Right). **(D)** Effects of propofol on the holding currents of glutamatergic neurons in the LH. **(E)** Effects of propofol on the holding currents in the presence of TTX (1 μM) to block action potentials-dependent synaptic transmissions. **(F,G)** Effects of propofol on the firing rates of glutamatergic neurons in response to inward current stimuli. ***$P < 0.001$.

injection compared with control group (Figure 3G). These results suggest that glutamatergic neurons in the LH are involved in the propofol anesthesia.

We further detected the changes in neuronal activity in the LH region by c-Fos staining. Compared with the mCherry group, when LH glutamatergic neurons were inhibited by CNO during

10.3389/fnins.2024.1327293

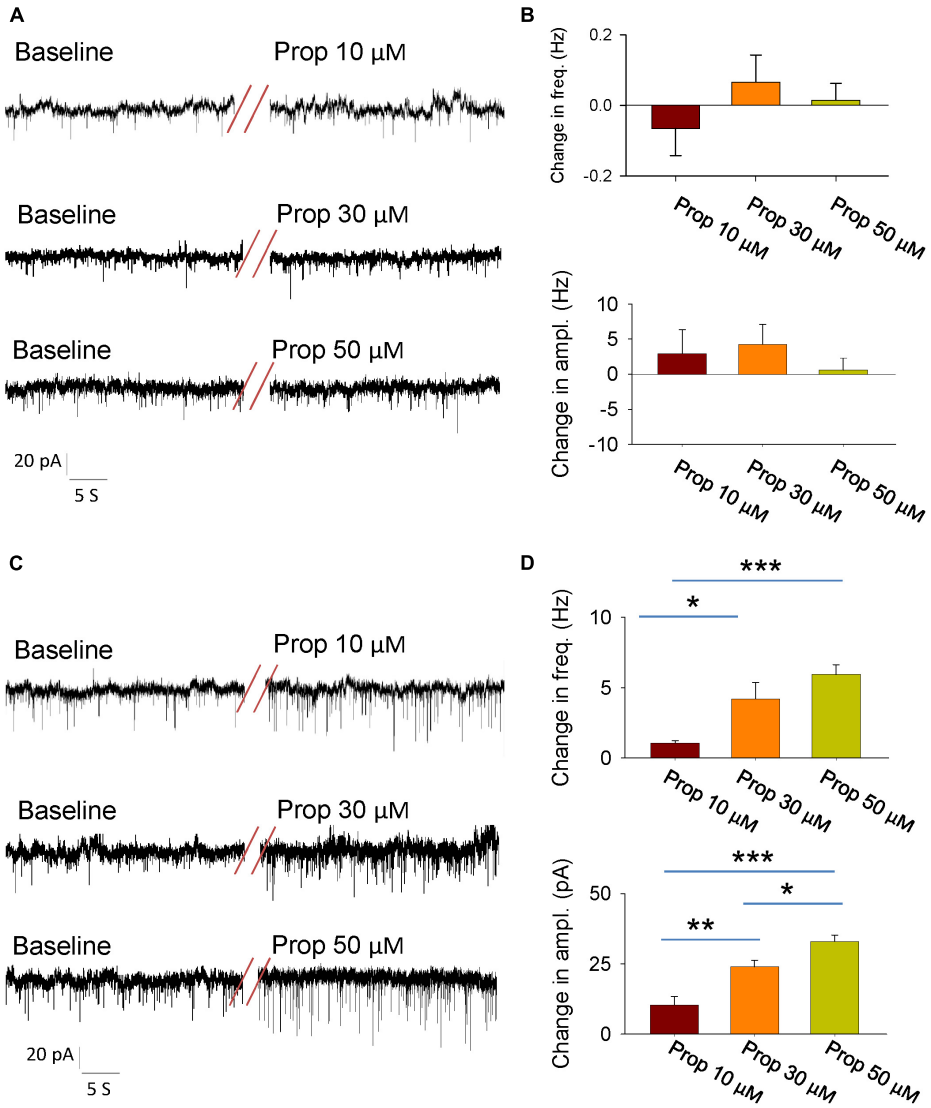

FIGURE 2
Effects of propofol synaptic transmissions of the glutamatergic neurons in the LH. **(A)** An example electrophysiological trace showing the SEPSCs of the glutamatergic neurons before and during bath application of the propofol. **(B)** Effects of propofol (10, 30, and 50 μM) on the frequency (top) and amplitude (down) of the SEPSCs. **(C)** An example electrophysiological trace showing the SIPSCs the of glutamatergic neurons before and during bath application of the propofol. **(D)** Effects of propofol (10, 30, and 50 μM) on the frequency (top) and amplitude (down) of the SIPSCs. *,**,***$P < 0.001$.

anesthesia, c-Fos positive neurons were significantly reduced (Figures 3H, I). These results further suggest that chemogenetic intervention affecting propofol anesthesia may indeed be inhibiting the neural activity in the LH region.

Activation of the glutamatergic neurons in the LH delays induction of and accelerates emergence from propofol anesthesia

Next, we want to know the behavioral effects of chemogenetic activation of glutamatergic neurons in the LH on the propofol anesthesia. Using whole-cell recordings in the acute brain slices, bath-applied CNO increased the firing rates of hM3D-mCherry-positive glutamatergic neurons, implying that CNO can activate hM3D-mCherry-positive neurons (Figures 4A, B). AAV-DIO-hM3D-mCherry and AAV-DIO-mCherry were restrictedly injected into the LH of vGlut2-Cre mice (Figures 4C, D). At the behavioral level, chemogenetic activation of glutamatergic neurons in the LH increased the duration of propofol-induced LORR (Figures 4E, F). Additionally, the locomotion with CNO injection in the mice with expression of hM3D-mCherry was also enhanced after they recovered from LORR compared with mCherry group (Figure 4G). In particular, there was a 57 and 26% increase in motor speed at 3 min (mCherry: 1.4 m/min; hM3D-mCherry: 2.2 m/min) and 5 min (mCherry: 3.8 m/min, hM3D-mCherry: 4.8 m/min) after recovery of the righting reflex, respectively. These data suggest that activation of the glutamatergic neurons in the LH delay the propofol anesthesia.

10.3389/fnins.2024.1327293

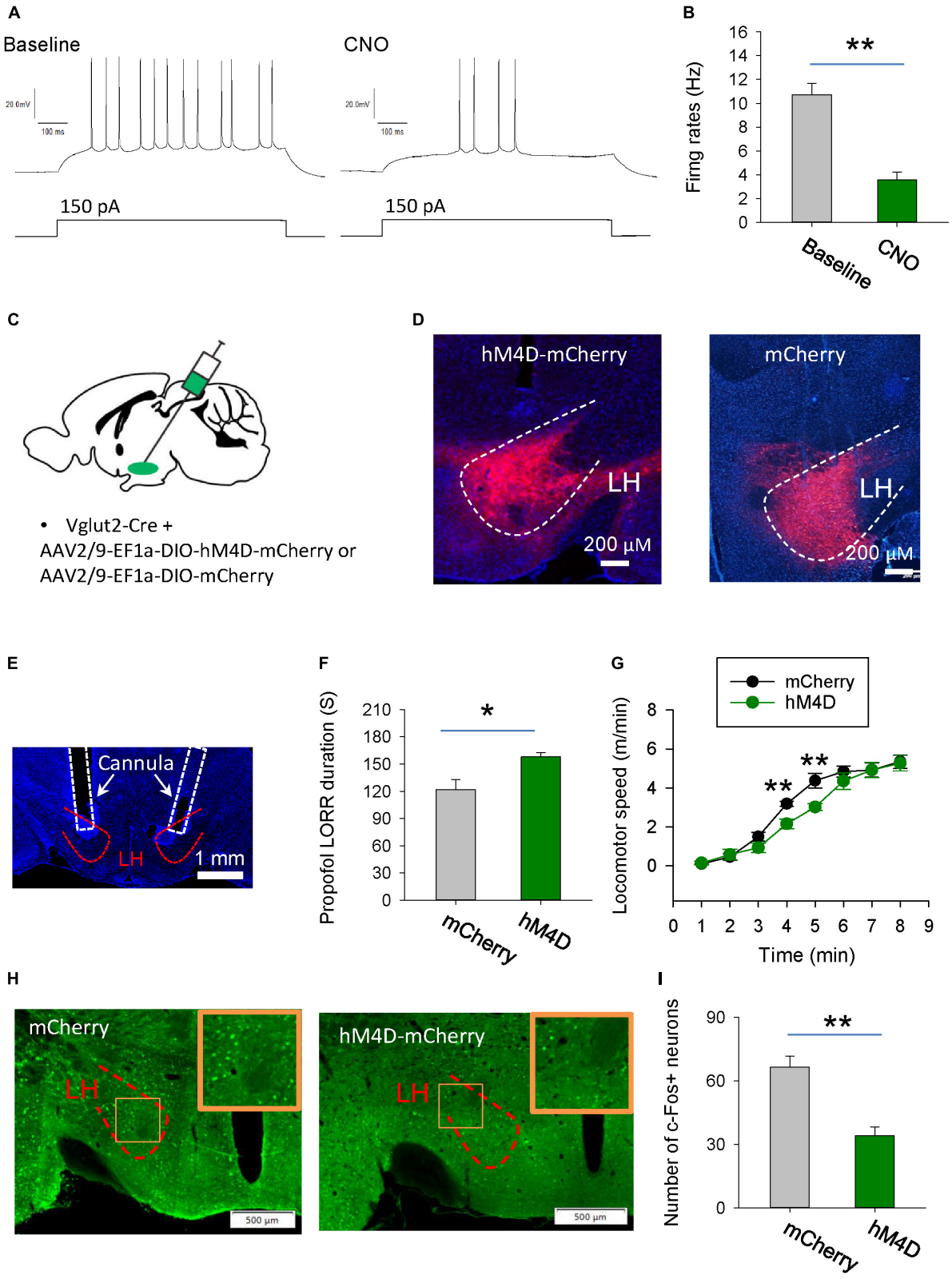

FIGURE 3
Chemogenetic inhibition of glutamatergic neurons in the LH facilitates induction of propofol anesthesia. **(A,B)** Effect of CNO on the firing rates of the hM4D-mCherry-positive neurons in the LH. **(C)** Bilateral injection of viruses into the LH region of vglut2-Cre mice. **(D)** Expression of the hM4D-mCherry and mCherry was restricted to cells in the LH. **(E)** A representative image showing the cannula implanted in the LH. **(F)** Chemogenetic inhibition of glutamatergic neurons in the LH decreased the duration of propofol (10 mg/kg, i.v.)-induced loss of LORR. **(G)** Effect of chemogenetic inhibition of glutamatergic neurons on locomotion of the mice following recovery of the LORR. **(H)** Representative images showing the c-Fos expression in the LH after application of CNO in the mCherry and hM4D-mCherry groups. The inset is an enlarged view of c-Fos expression in the LH. **(I)** Effect of chemogenetic inhibition on the c-Fos expression in the LH. *,**$P < 0.001$.

10.3389/fnins.2024.1327293

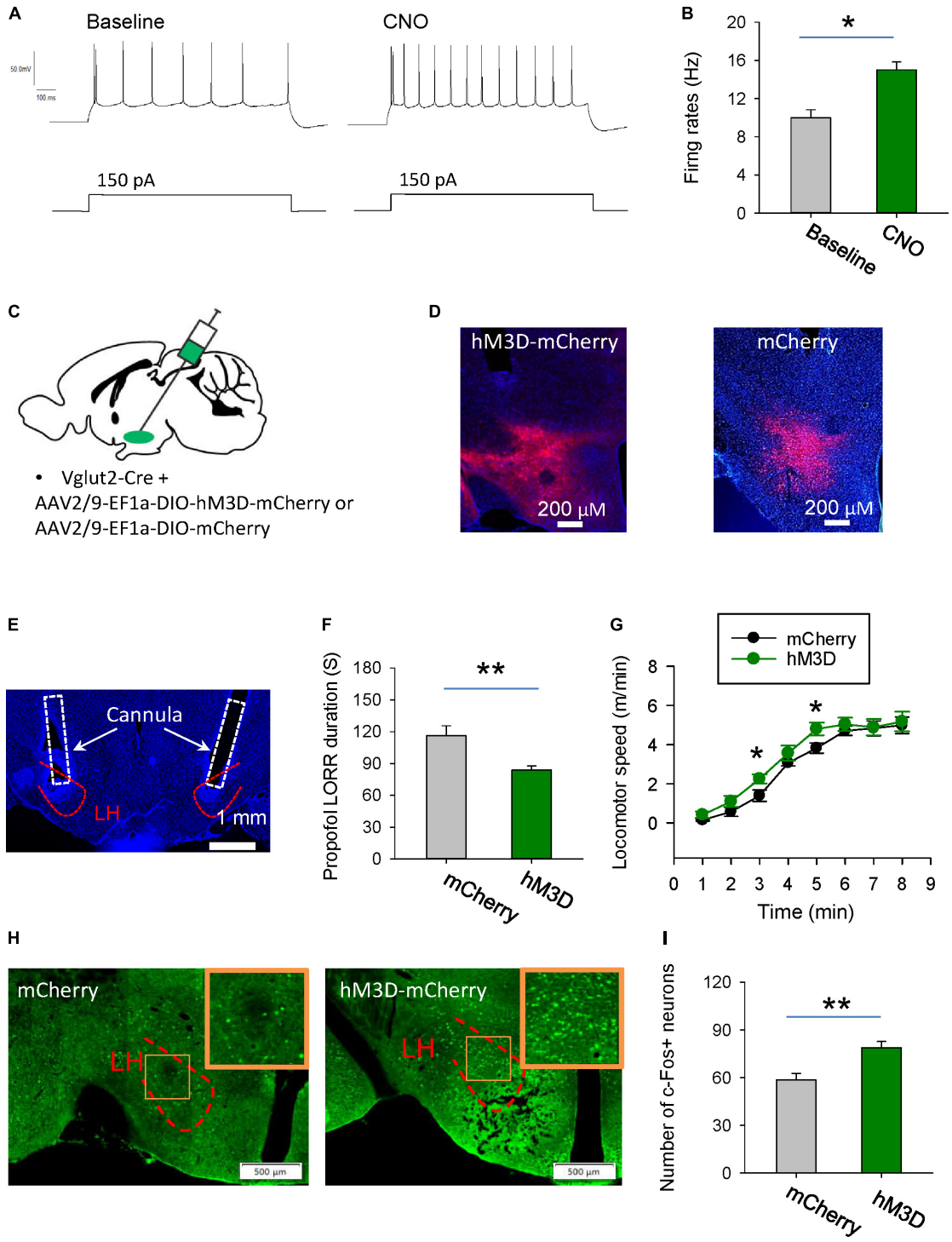

FIGURE 4
Stimulation of glutamatergic neurons in the LH delays induction of propofol anesthesia. **(A,B)** Effects of CNO on the firing rates of the hM3D-mCherry-positive neurons in the LH. **(C)** Bilateral injection of viruses into the LH region of vglut2-Cre mice. **(D)** Representative images illustrating the expression of the hM3D-mCherry and mCherry in the LH. **(E)** The cannula for application of CNO implanted within the LH. **(F)** Activation of glutamatergic neurons by CNO in the LH decreased the duration of propofol (10 mg/kg, i.v.)-induced loss of LORR. **(G)** Effects of chemogenetic activation of glutamatergic neurons on locomotion of the mice following recovery of the LORR. **(H)** Representative images showing the c-Fos expression in the mCherry and hM3D-mCherry groups. The inset is an enlarged view of c-Fos expression in the LH. **(I)** Effect of chemogenetic activation of glutamatergic neurons on the c-Fos expression in the LH. *,**$P < 0.001$.

The changes in neuronal activity in the LH were also detected by c-Fos staining. After chemogenetic activation of LH glutamatergic neurons during anesthesia, c-Fos positive neurons were significantly increased (Figures 4H, I). These data imply that chemogenetic activation of LH neurons might affect the propofol anesthesia.

Discussion

Glutamatergic neurons in the LH play an important role in maintenance of wakefulness (Wang et al., 2021). Propofol-anesthetic effects are associated with the glutamatergic neurons in the LH, as chemogenetic inhibition of these neurons increases the duration of propofol-induced LORR and vice versa. These effects of propofol were partially mediated by its inhibitory effects on the glutamatergic neurons in the LH. In sum, these findings may provide novel mechanisms underlying the anesthetic effect of propofol.

In the neocortex and subcortical hippocampus, propofol exerts a direct effect on the cell bodies of excitatory neurons, leading to neuronal hyperpolarization and downregulation of excitability (Xu et al., 2014; Li et al., 2016; Kobayashi and Oi, 2017; Luo et al., 2019). Additionally, propofol can enhance inhibitory inputs, thereby suppressing the activity of these brain regions (Chen et al., 1999; Jeong et al., 2011; Wakita et al., 2013). Consistently, we observed that propofol also inhibits glutamatergic neurons in the LH through both direct and indirect mechanisms. However, further investigation is needed to identify how propofol affects ion channels in the LH. In addition, we mainly used mice to study the effects of propofol. The investigation of propofol's mechanism of action via the LH in humans necessitates further research.

The wakefulness is regulated by multiple subcortical arousal-promoting systems, such as the acetylcholinergic neurons in the basal forebrain, serotonin neurons in the dorsal raphe, noradrenergic neurons in the locus ceruleus, dopaminergic neurons in the ventral tegmental area and lateral hypothalamus (Brown et al., 2012; Zeitzer, 2013; Venner et al., 2016; Horner and Peever, 2017; Scammell et al., 2017). While the sleep-promoting systems, such as the ventrolateral preoptic nucleus and supraoptic nucleus, inhibit the wakefulness-promoting nuclei and consequently induce the transitions from wakefulness to sleep (Szymusiak et al., 2007; Szymusiak and McGinty, 2008; Brown et al., 2012). It has been reported that anesthetics could inhibit the wakefulness-promoting neurons, including dopamine D1 receptor-positive neurons in the nucleus accumbens, orexinergic neurons in the hypothalamus and medial parabrachial neurons contribute to its anesthetic action (Kelz et al., 2008; Xu et al., 2020; Bao et al., 2021). It should be noted that propofol also inhibited the release of wakefulness-promoting neurotransmitters such as dopamine and acetylcholine during anesthesia (Gamou et al., 2010). Additionally, propofol suppresses the excitability of cholinergic neurons in basal forebrain and noradrenergic neurons in the locus ceruleus (Chen et al., 1999, 2018). The present study demonstrates that propofol inhibits the wakefulness-promoting glutamatergic neurons in the LH effectively and contributes to it anesthetic action. These findings combined with previous research support that wakefulness-promoting systems serve as crucial targets for propofol to induce anesthesia.

The LH contains several types of neurons, forming complex microcircuits. The local neural circuits mainly consist of hypocretinergic neurons-glutamatergic neurons-hypocretinergic neurons, which increases the output of hypocretinergic neurons to promote arousal by positive feedback, and hypocretinergic neurons-GABAergic neurons-melanin-concentrating hormone neurons (Li et al., 2002; Bonnavion et al., 2016). Propofol inhibits glutamate neurons, and may indirectly reduce the activity of hypocretinergic neurons, thereby reducing arousal levels. Of course, the effect of propofol on other neurons has not been reported, and further research is needed in the future. Additionally, the present study did not compare the effects of local injection of saline and CNO in the LH brain region on animal behavior, and the role of local injection of CNO remains to be investigated.

Materials and methods

Animal surgery

All mouse care and experimental procedures were approved by the North Sichuan Medical College Guide for the Care and Use of Laboratory Animals. Male adult vGlut2-Cre C57/BL6 mice were used in patch-clamp and behavioral experiments. Vglut2-Cre mice (Stock No: 016963) were obtained from the Jackson Laboratory (USA). All mice were housed in an environment with 12 h light/dark cycle and food and water *ad libitum*. Mice were anesthetized with isoflurane and placed in the stereotaxic apparatus. For pharmacological application of the CNO, a cannula was implanted into separately in the LH region on each side (bregma: AP = −1.50 mm; ML = ± 1.15 mm; DV = −4.7 mm). The cannulas were affixed to the skull by dental cement, and the incision was closed.

For chemogenetic inhibition and activation experiments, Cre-inducible AAV2/9-EF1α-DIO-hM3D-mCherry (BrainVTA Technology Co. Ltd., China) and AAV2/9-EF1α-DIO-hM4D-mCherry (BrainVTA Technology Co. Ltd., China) were bilaterally injected into the LH (bregma: AP = −1.50 mm; ML = ± 1.15 mm; DV = −4.8 mm) of the vGlut2-Cre mice, respectively, with a total volume of about 200 nL. hM4D and hM3D are mutant of G_i-coupled M4 muscarinic receptors and G_q-coupled M3 muscarinic receptors, which are selectively stimulated by the CNO, but not the endogenous acetylcholine, and thus lead to inhibit and activate the neurons, respectively.

Drug application *in vivo*

The method for drug microinjection was line with the previous study (He et al., 2016). CNO (5 μM, 200 nl) and saline were administrated by an inserted cannula and the syringe pump (Harvard apparatus) with a rate of 100 nl/min. After injection, the inserted cannula was left for additional 2 min to allow for diffusion. Propofol (10 mg/kg, i.v.) was administrated via tail-vein injection. Propofol was injected at 18:00, during which mice spent most time in wakefulness.

Behavioral tests

Mice were tested for LORR by gently placing them on their backs. Mice were assessed as positive for LORR if they made no

obvious attempt to right themselves. During anesthesia, behavioral videos of the animals were recorded. The animals' movement speed was calculated by employing a customized Matlab script for offline tracking of their body, thereby providing insights into their locomotor activity.

Histological identification

After completion of the behavioral tests, mice were anesthetized and perfused with saline followed by 4% paraformaldehyde. The brains were placed in 30% sucrose and 4% paraformaldehyde solution for dehydration. Brain sections were prepared and stained with DAPI, and the track of cannula and viral expressions can be identified. The mice with incorrect injection sites were excluded from data analysis. For FISH experiments, brains were sectioned into 14 μm coronal slices, and FISH was carried out by using RNAscope Multiplex Fluorescent Assays V2 (Advanced Cell Diagnostics). The probe Slc17a6 (319171, ACD) was used for detecting vGlut2.

Brains were sectioned into 40 μm coronal slices using a freezing microtome (CM 3050S, Leica). Sections containing the LH were incubated in blocking solution (Beyotime, China) with 1% Triton X-100 at 37°C for 25 min. After that, the sections were incubated in primary antibodies at 4°C overnight. Primary antibody (rabbit anti-c-fos, 1:1000, ab190289, Abcam) were applied. Then, the sections were washed with PBS, transferred into secondary antibody (Alexa Flour 488 donkey anti-rabbit IgG, 1:500, Invitrogen) in PBS and incubated at room temperature for 2 h. Fluorescence images were taken using a microscope digital slide scanner (SlideView VS 200, Olympus). The number of c-Fos positive neurons were counted in the LH region.

Whole-cell patch clamp recordings

vGlut2-Cre transgenic mice were used in patch camp recordings. Brains were removed after decapitation and placed into solution containing 110 mM NMDG, 110 mM HCl, 2.5 mM KCl, 1.2 mM NaH_2PO_4, 25 mM $NaHCO_3$, 25 mM Glucose, 10 mM $MgSO_4$, 0.5 mM $CaCl_2$ (pH 7.2–7.4, saturated with 95% O_2 and 5% CO_2). A total 350 μm-thick sections containing LH were cut by an oscillating tissue slicer. Sections were incubated for 15 min at 32°C cutting solution and then transferred to ACSF (120 mM NaCl, 2.5 mM KCl, 1.2 mM NaH_2PO_4, 25 mM $NaHCO_3$, 25 mM Glucose, 10 mM $MgSO_4$, 2 mM $CaCl_2$, adjusted to pH 7.2–7.4) saturated with 95% O_2 and 5% CO_2 before recording (30°C). Sections were removed to the recording chamber, where the oxygenated ACSF was continuously perfused during the whole-cell recording sessions.

Whole-cell recording was carried out in mCherry-expressing cells of LH. Glutamatergic cells were identified by a microscope equipped with differential contrast optics and an infrared video imaging camera. Recordings were performed with glass pipettes (4–6 MΩ) filled with an solution containing 125 mM potassium gluconate, 20 mM KCl, 10 mM Hepes, 1 mM EGTA, 2 mM $MgCl_2 \bullet 6H_2O$, 4 mM ATP (pH 7.2–7.4). HEKA EPC-10 amplifier was used for recording of the signals with digitalizing at 10 kHz and filtering at 2 kHz. Data were further acquired and analyzed by using PATCHMASTER and IGOR 5.0 software.

To test the effects of propofol on activity of glutamatergic neurons in the LH, inward currents were injected to depolarize the membrane potential to −55 mV and evoke tonic firing. After recording baseline, propofol was perfused for 1 min and followed with washed out.

Data analysis

Data were presented as the means ± S.E.M. Student's *t*-test, one-way repeated-measures' analysis of variance, two-way repeated-measures' analysis of variance, and Fisher's protected least significant difference *post-hoc* testing were conducted for statistical analyses. Significant differences were accepted as $P < 0.05$.

Data availability statement

The raw data supporting the conclusions of this article will be made available by the authors, without undue reservation.

Ethics statement

The animal studies were approved by the North Sichuan Medical College Guide for the Care and Use of Laboratory Animals. The studies were conducted in accordance with the local legislation and institutional requirements. Written informed consent was obtained from the owners for the participation of their animals in this study.

Author contributions

WD: Conceptualization, Funding acquisition, Project administration, Supervision, Writing – original draft, Writing – review and editing. YH: Investigation, Writing – original draft. YX: Investigation, Methodology, Writing – review and editing. LL: Investigation, Writing – review and editing. XF: Investigation, Writing – review and editing. FC: Conceptualization, Supervision, Validation, Writing – original draft, Writing – review and editing.

Funding

The author(s) declare that no financial support was received for the research, authorship, and/or publication of this article.

Conflict of interest

The authors declare that the research was conducted in the absence of any commercial or financial relationships that could be construed as a potential conflict of interest.

Publisher's note

References

Bao, W. W., Xu, W., Pan, W., Wang, G. J., Han, T. X., Qu, Y., et al. (2021). Nucleus accumbens neurons expressing dopamine D1 receptors modulate states of consciousness in sevoflurane anesthesia. *Curr. Biol.* 31, 1893–1902.e5. doi: 10.1016/j.cub.2021.02.011

Bonnavion, P., Mickelsen, L. E., Fujita, A., de Lecea, L., and Jackson, A. C. (2016). Hubs and spokes of the lateral hypothalamus: Cell types, circuits and behaviour. *J. Physiol.* 594, 6443–6462. doi: 10.1113/JP271946

Brown, R. E., Basheer, R., McKenna, J. T., Strecker, R. E., and McCarley, R. W. (2012). Control of sleep and wakefulness. *Physiol. Rev.* 92, 1087–1187.

Chen, C. L., Yang, Y. R., and Chiu, T. H. (1999). Activation of rat locus coeruleus neuron GABA(A) receptors by propofol and its potentiation by pentobarbital or alphaxalone. *Eur. J. Pharmacol.* 386, 201–210.

Chen, L., Yang, Z. L., Cheng, J., Zhang, P. P., Zhang, L. S., Liu, X. S., et al. (2018). Propofol decreases the excitability of cholinergic neurons in mouse basal forebrain via GABAA receptors. *Acta Pharmacol. Sin.* 40, 755–761. doi: 10.1038/s41401-018-0168-6

Choi, G. J., Kang, H., Baek, C. W., Jung, Y. H., and Lee, J. J. (2017). Comparison of bolus versus continuous infusion of propofol for procedural sedation: A meta-analysis. *Curr. Med. Res. Opin.* 33, 1935–1943. doi: 10.1080/03007995.2017.1370419

Gamou, S., Fukuda, S., Ogura, M., Sakamoto, H., and Morita, S. (2010). Microinjection of propofol into the perifornical area induces sedation with decreasing cortical acetylcholine release in rats. *Anesth. Analg.* 111, 395–402. doi: 10.1213/ANE.0b013e3181e24776

He, C., Luo, F., Chen, X., Chen, F., Li, C., Ren, S., et al. (2016). Superficial layer-specific histaminergic modulation of medial entorhinal cortex required for spatial learning. *Cereb. Cortex* 26, 1590–1608. doi: 10.1093/cercor/bhu322

Horner, R. L., and Peever, J. H. (2017). Brain circuitry controlling sleep and wakefulness. *Continuum* 23, 955–972.

Hua, T., Chen, B., Lu, D., Sakurai, K., Zhao, S., Han, B., et al. (2020). General anesthetics activate a potent central pain-suppression circuit in the amygdala. *Nat. Neurosci.* 23, 854–868. doi: 10.1038/s41593-020-0632-8

Jeong, J. A., Kim, E. J., Jo, J. Y., Song, J. G., Lee, K. S., Kim, H. W., et al. (2011). Major role of GABA(A)-receptor mediated tonic inhibition in propofol suppression of supraoptic magnocellular neurons. *Neurosci. Lett.* 494, 119–123. doi: 10.1016/j.neulet.2011.02.072

Jiang-Xie, L., Yin, L., Zhao, S., Prevosto, V., Han, B., Dzirasa, K., et al. (2019). A common neuroendocrine substrate for diverse general anesthetics and sleep. *Neuron* 102, 1053–1065 e4. doi: 10.1016/j.neuron.2019.03.033

Kelz, M. B., Sun, Y., Chen, J., Meng, Q. C., Moore, J. T., Veasey, S. C., et al. (2008). An essential role for orexins in emergence from general anesthesia. *Proc. Natl. Acad. Sci. U.S.A.* 105, 1309–1314. doi: 10.1073/pnas.0707146105

Kobayashi, M., and Oi, Y. (2017). Actions of propofol on neurons in the cerebral cortex. *J. Nippon Med. Sch.* 84, 165–169.

Li, X., Pan, K., Zhu, D., Li, Y., and Tao, G. (2016). Propofol postsynaptically suppresses stellate neuron excitability in the entorhinal cortex by influencing the HCN and TREK-2 channels. *Neurosci. Lett.* 619, 54–59. doi: 10.1016/j.neulet.2016.03.014

Li, Y., Gao, X. B., Sakurai, T., and van den Pol, A. N. (2002). Hypocretin/Orexin excites hypocretin neurons via a local glutamate neuron-A potential mechanism for orchestrating the hypothalamic arousal system. *Neuron* 36, 1169–1181. doi: 10.1016/s0896-6273(02)01132-7

Luo, L., Zhang, X., Xiang, T., Yuan, J., Tang, J., and Yu, Q. (2019). Propofol inhibited the excitability of pyramidal neurons in the orbitofrontal cortex by influencing the delayed rectifier K+ channels and gamma-aminobutyric acid type A receptors. *Neuroreport* 30, 102–107. doi: 10.1097/WNR.0000000000001167

Mehta, P., Sundaram, S. S., Furuta, G. T., Pan, Z., Atkins, D., and Markowitz, S. (2017). Propofol use in pediatric patients with food allergy and eosinophilic esophagitis. *J. Pediatr. Gastroenterol. Nutr.* 64, 546–549. doi: 10.1097/MPG.0000000000001291

Reine, G., Samuel, D., Nieoullon, A., and Kerkerian-Le Goff, L. (1992). Effects of lesion of the cholinergic basal forebrain nuclei on the activity of glutamatergic and GABAergic systems in the rat frontal cortex and hippocampus. *J Neural Transm. Gen. Sect.* 87, 175–192. doi: 10.1007/BF01245364

Scammell, T. E., Arrigoni, E., and Lipton, J. O. (2017). Neural circuitry of wakefulness and sleep. *Neuron* 93, 747–765.

Szymusiak, R., and McGinty, D. (2008). Hypothalamic regulation of sleep and arousal. *Ann. N. Y. Acad. Sci.* 1129, 275–286.

Szymusiak, R., Gvilia, I., and McGinty, D. (2007). Hypothalamic control of sleep. *Sleep Med.* 8, 291–301.

Venner, A., Anaclet, C., Broadhurst, R. Y., Saper, C. B., and Fuller, P. M. (2016). A novel population of wake-promoting GABAergic neurons in the ventral lateral hypothalamus. *Curr. Biol.* 26, 2137–2143. doi: 10.1016/j.cub.2016.05.078

Wakita, M., Kotani, N., Nonaka, K., Shin, M. C., and Akaike, N. (2013). Effects of propofol on GABAergic and glutamatergic transmission in isolated hippocampal single nerve-synapse preparations. *Eur. J. Pharmacol.* 718, 63–73. doi: 10.1016/j.ejphar.2013.09.018

Wang, R., Guo, H., Jiang, S., Liu, Z., Qu, W., Huang, Z., et al. (2021). Control of wakefulness by lateral hypothalamic glutamatergic neurons in male mice. *J. Neurosci. Res.* 99, 1689–1703.

Xu, W., Wang, L., Yuan, X., Wang, T., Li, W., Qu, W., et al. (2020). Sevoflurane depresses neurons in the medial parabrachial nucleus by potentiating postsynaptic GABAA receptors and background potassium channels. *Neuropharmacology* 181:108249. doi: 10.1016/j.neuropharm.2020.108249

Xu, X., Tian, Y., Wang, G., and Tian, X. (2014). Inhibition of propofol on single neuron and neuronal ensemble activity in prefrontal cortex of rats during working memory task. *Behav. Brain Res.* 270, 270–276. doi: 10.1016/j.bbr.2014.05.034

Zeitzer, J. M. (2013). Control of sleep and wakefulness in health and disease. *Prog. Mol. Biol. Transl. Sci.* 119, 137–154.

frontiers | Frontiers in Pharmacology

TYPE Original Research
PUBLISHED 26 March 2024
DOI 10.3389/fphar.2024.1362464

OPEN ACCESS

EDITED BY
Giuseppe Di Giovanni,
University of Malta, Malta

REVIEWED BY
Sebastiano Alfio Torrisi,
University of Catania, Italy
Zhe Shi,
Hunan University of Chinese Medicine, China

*CORRESPONDENCE
Can Yan,
yc1970@gzucm.edu.cn
Li-Li Wu,
wulili@gzucm.edu.cn

†These authors have contributed equally to this work and share first authorship

RECEIVED 28 December 2023
ACCEPTED 20 February 2024
PUBLISHED 26 March 2024

CITATION
Li B, Yan Y, Zhang T, Xu H, Wu X, Yao G, Li X, Yan C and Wu L-L (2024), Quercetin reshapes gut microbiota homeostasis and modulates brain metabolic profile to regulate depression-like behaviors induced by CUMS in rats. *Front. Pharmacol.* 15:1362464. doi: 10.3389/fphar.2024.1362464

Quercetin reshapes gut microbiota homeostasis and modulates brain metabolic profile to regulate depression-like behaviors induced by CUMS in rats

Bozhi Li†, Yuqi Yan†, Tiange Zhang, Hanfang Xu, Xiaofeng Wu, Gaolei Yao, Xingze Li, Can Yan* and Li-Li Wu*

Integrative Medicine Research Center, School of Basic Medical Sciences, Guangzhou University of Chinese Medicine, Guangzhou, China

Quercetin, an abundant flavonoid compound in plants, is considered a novel antidepressant; however, its mechanisms of action are poorly understood. This study aimed to investigate the therapeutic effects of quercetin on chronic unpredictable mild stress (CUMS)-induced depression-like behaviors in rats and explore the underlying mechanisms by combining untargeted metabolomics and 16S rRNA sequencing analysis of brain tissue metabolites and gut microbiota. Gut microbiota analysis revealed that at the phylum level, quercetin reduced *Firmicutes* and the *Firmicutes/Bacteroidetes (F/B)* ratio and enhanced *Cyanobacteria*. At the genus level, quercetin downregulated 6 and upregulated 14 bacterial species. Metabolomics analysis revealed that quercetin regulated multiple metabolic pathways, including glycolysis/gluconeogenesis, sphingolipid metabolism, the pentose phosphate pathway, and coenzyme A biosynthesis. This modulation leads to improvements in depression-like phenotypes, anxiety-like phenotypes, and cognitive function, highlighting the therapeutic potential of quercetin in treating depression.

KEYWORDS

depression, quercetin, brain metabolomics, gut microbiota, microbiota-gut-brain axis

Introduction

Depression is a complex mental disorder that causes 10% of global disability. Its primary symptoms include low mood, anxiety, anhedonia, and cognitive impairment (Cruz-Pereira et al., 2020). Recently, notably during the COVID-19 pandemic, the incidence and mortality rates of depression have continuously increased, becoming an increasingly heavy burden on individuals and society. Depression is linked to reductions in brain monoamine neurotransmitters (serotonin, norepinephrine, and dopamine), changes in brain neurotrophic factor levels, abnormal activation of the hypothalamic-pituitary-adrenal axis, and immune system dysregulation. In addition to these factors, many recent studies have found that abnormalities in the gut microbiota are significant factors in developing depression (Jiang et al., 2015; Averina et al., 2020; Huang and Wu, 2021). The gut, known as the "second brain," can regulate human emotions and feelings through the

gut-brain axis. The gut microbiota, known as the "second genome" of the body, functions in symbiosis with the host and has major impacts. Therefore, regulating the gut microbiota is an innovative therapy for complex central nervous system (CNS) disorders, although the precise mechanism of the brain-gut axis remains to be elucidated.

Clinical depression treatment in clinical practice mainly relies on medication, with numerous antidepressants applied since the introduction of the first antidepressant in the 1950s (Hammen, 2018). However, these antidepressant drugs often fail to alleviate depression symptoms completely and may lead to severe drug dependence and side effects (Bschor et al., 2014; Solem et al., 2017). Plant-derived compounds are being evaluated for clinical depression treatment. Quercetin is a neuroprotective flavonoid found in flowers, leaves, and fruits. It is primarily transformed in the gut by the gut microbiota and absorbed by the human body (Russo et al., 2012). Research has revealed that quercetin can improve gut microbiota dysbiosis, promote gut microbial balance, restore gut barrier structure and function, and exhibit biological activities such as anti-inflammatory, antioxidant, and antiviral effects (Horowitz and Zunszain, 2015; Suganthy et al., 2016; Babaei et al., 2018; Ulusoy and Sanlier, 2020). It also demonstrates potential pharmacological activities against mental disorders (Chen et al., 2022). Moreover, compared to traditional antidepressants, quercetin has several advantages: 1) Multiple mechanisms of action: Numerous studies have reported that quercetin may exert its antidepressant effects via various mechanisms, such as antioxidation, anti-inflammation, neuroprotection, and modulation of the neurotransmitter system (Sah et al., 2011; Yang et al., 2020; Zhang et al., 2020; Şahin et al., 2020; Ma et al., 2021); 2) Fewer side effects and non-addictive: Quercetin is associated with fewer side effects and lacks the addictive potential of traditional antidepressants, which are often linked to significant side effects (Bschor et al., 2014; Solem et al., 2017). As a natural compound, quercetin is generally considered safer, has milder side effects, and there are no reported cases of addiction, making it potentially a safer option for long-term use (Kashyap et al., 2019; Ulusoy and Sanlier, 2020); 3) Additional health benefits: In addition to its potential antidepressant properties, quercetin offers a range of other health advantages, such as lowering the risk of cardiovascular diseases, exhibiting anticancer effects, and boosting immune function (Li et al., 2016; Rauf et al., 2018; Hosseini et al., 2021). However, how quercetin modulates the "microbiota-gut-brain" axis to treat depression remains unknown. Consequently, it is essential to further investigate the regulatory effects of quercetin on the brain and gut microbiota and explore its antidepressant mechanism.

Metabolomics is a novel technology that utilizes various modern analytical techniques to determine dynamic changes in small-molecule metabolites in biological organisms, thereby characterizing and deciphering the status of life activities. It can more accurately and directly reflect the terminal and phenotypic information of biological systems, providing a new perspective for understanding the multi-factor mechanisms of diseases and comprehensively evaluating drug effects (Gu and Tong, 2020). Herein, 16S rRNA full-length sequencing and liquid chromatography-mass spectrometry (LC-MS) were employed to conduct untargeted metabolomic analysis of brain tissue metabolites and microbiota analysis of gut microbiota in rats to investigate the mechanism by which quercetin acts on the microbiota–gut–brain axis to regulate gut microbiota and brain metabolism and alleviate depression (Figure 1A).

Materials and methods

Experimental animals

Adult male Wistar rats (weighing 180–220 g) with specific pathogen-free (SPF) status were acquired from the Experimental Animal Center of the Southern Medical University in Guangzhou, China (license number: SCXK 2016-0041). All experiments involving animals adhered to the guidelines outlined in the "Regulations on the Management of Laboratory Animals" issued by the Ministry of Science and Technology of the People's Republic of China. Ethical approval for this research was obtained from the Animal Experiment Ethics Committee of Guangzhou University of Chinese Medicine.

Animal model

Prior to the commencement of the experiment, the rats were subjected to a 1-week acclimatization period in a controlled environment. This environment was maintained under a 12-h light/dark cycle, at a constant temperature of 23°C ± 2°C and a relative humidity of 60% ± 5%. To mitigate stress responses, rats were allowed unrestricted access to food and water. Subsequently, all rats underwent the sucrose preference (SP) test (SPT) to determine their individual responsiveness. Rats with aberrant baseline sucrose consumption were systematically removed from further analyses based on specific criteria. These criteria included low (<60%) SP, positional preference (showing a pronounced inclination to drink from a specific location), minimal water intake (indicating a lack of preference between sucrose solution and pure water), and excessive water intake (total water consumption exceeding twice the mean water intake of all rats). All rats were housed individually throughout the SPT to ensure isolation and accurate data collection. After SPT, the rats were randomly allocated to the control (CON), model (chronic unpredictable mild stress [CUMS]), and quercetin (QUE) groups, each consisting of 12 rats. The rats in the CON group were provided unrestricted access to both food and water, adhering to a 12-h light/dark cycle where the lights were illuminated from 8:00 to 20:00). Furthermore, the rats in the CON group were maintained at a temperature of 23°C ± 2°C, and any supplementary stressors were intentionally eliminated from the experimental conditions experienced by the rats. These rats were housed in cages with four rats per cage and accommodated in Room A to facilitate breeding. However, the rats belonging to the experimental groups, excluding the CON group, were exposed to the 12 stressors constituting the CUMS protocol. To ensure individualized housing, each rat was placed in a separate cage and subsequently transferred to Room B. The stressors included in the experimental design involved various challenges. These conditions included food deprivation (12 h), water deprivation (12 h), simultaneous deprivation of both food and water (24 h),

10.3389/fphar.2024.1362464

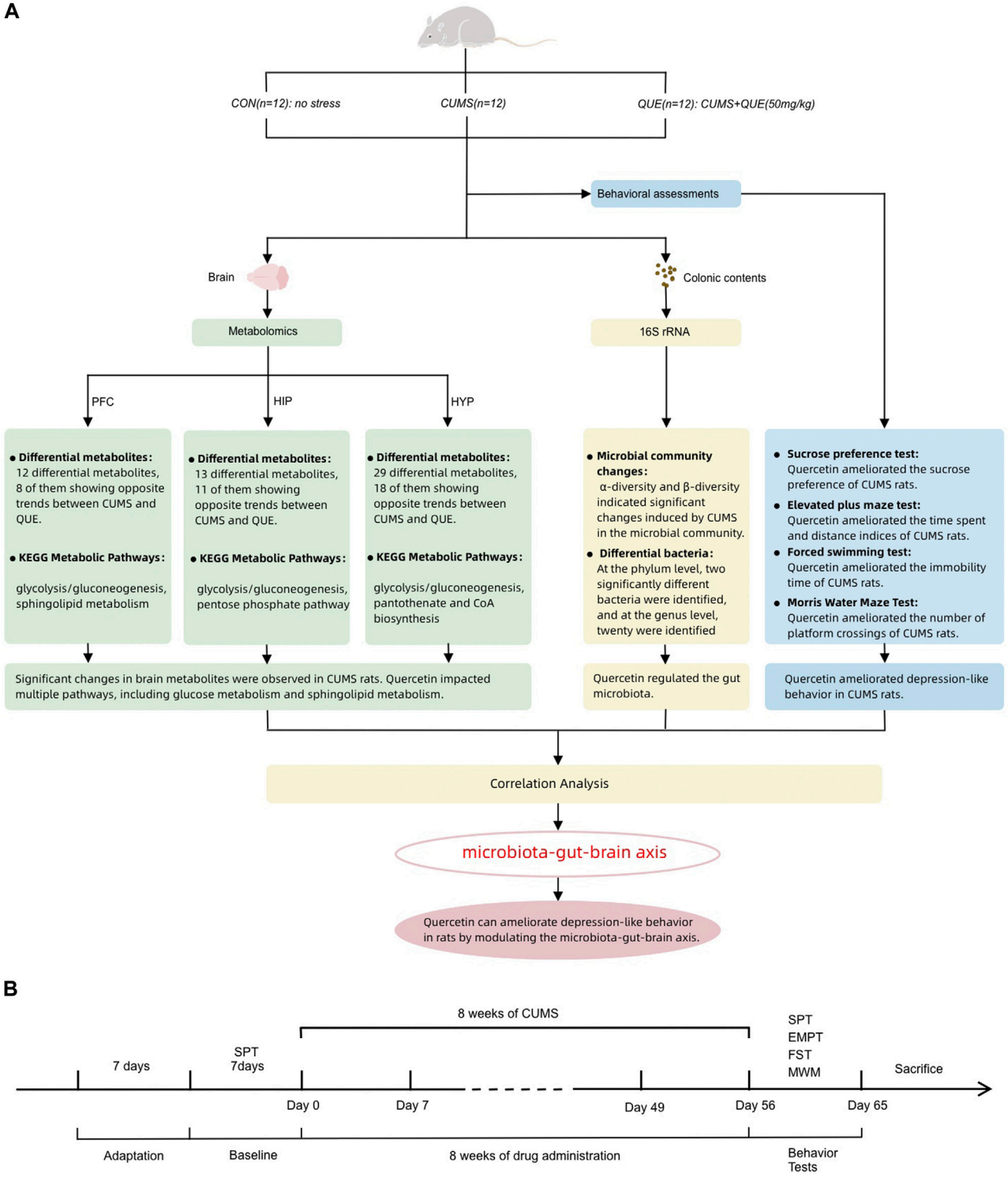

FIGURE 1
Summary of experimental procedure and results **(A)** Overview of behavioral analysis, gut microbiota analysis, and brain metabolism (prefrontal cortex, hippocampus, and hypothalamus) analysis in the CON, CUMS, and QUE groups of rats. CON, Control; QUE, Quercetin; CUMS, Chronic Unpredictable Mild Stress; SPT, Sucrose Preference Test; EPMT, Elevated Plus-Maze Test; FST, Forced Swim Test; MWM, Morris WaterMaze. **(B)** Experimental rat modeling and behavioral test workflow.

imposition of restraint stress (12 h), exposure to damp bedding (10 h), engagement in overcrowded conditions (10 h), exposure to overnight intermittent light (300 times/min, 5 h), white noise exposure (85 dB, 5 h), engagement in thermal swimming (45°C, 5 min), engagement in cold swimming (4°C, 5 min), exposure to foot shocks (1 mA, 2 s per trial, ten trials in 5 min), and continuous light

exposure during the night (20:00 to 8:00, 12 h). The stressors were randomly administered as 1-2 types daily, without repetition, within 3 days and continued for 8 weeks. The entire stress process is illustrated in Figure 1B.

Administration method

From the day the stress application commenced, the rats in each group received intragastric administration for 8 weeks and ceased when the stress application was terminated. Rats in CON and CUMS groups received a daily dose of 5 mL/kg of pure water via intragastric administration. In contrast, rats in the QUE group received a daily dose of 50 mg/kg quercetin via intragastric administration.

Behavioral tests

SPT

The SPT test was utilized to assess anhedonia, a key manifestation of depression-like behaviors, by examining the preference of rats for sucrose solution *versus* water. To maintain controlled conditions, all rats were individually housed during the experiment. The SPT involved four phases: 48-h sucrose training, 36-h baseline test, 24-h phase of food and water deprivation, and 12-h session dedicated to the actual SPT. In the final phase of the experiment, the rats were given unrestricted access to equal volumes of pure water and 1% sucrose solution for 12 h. The calculation of basic SP was conducted using the following formula: sucrose consumption/total liquid consumption × 100%. To assess SP, an SPT was performed in the model group after an 8-week duration. The model group was subjected to SPT for 12 h after a 24-h period of food and water deprivation.

Elevated plus-maze test

The EPMT is a critical tool for assessing anxiety-like behaviors in rodents. This methodology involved measuring the duration of stay and the number of entries into the open and closed arms of the maze, thereby facilitating a detailed analysis of anxiety-related behaviors. The maze was composed of a central area measuring 15 × 15 cm, from which two open arms measuring 15 × 48 cm and two closed arms measuring 15 × 48 × 40 cm. The experimental setup involved raising the apparatus to a height of 36 cm above the ground. For the testing process, the rat was positioned in a specific orientation to face the designated side of the maze. The open arms, positioned in the central area, were the focus of the test. The movements of the rats were recorded for 5 min using a camera. Multiple parameters were systematically measured to assess the anxiety-like levels exhibited by each rat. These parameters consisted of the following: 1) the time spent and percentage of time spent in the open arms, indicating the duration of the rat stay in the open arms and the percentage of the total testing period allocated to the open arms; 2) the distance traveled and percentage of the distance covered in open arms, denoting the total distance covered by the rat along with the percentage of that distance covered in the open arms; 3) the number of entries and percentage of entries made by the rat into the open arms, representing the total number of entries made by the rat into the open arms and the corresponding percentage of total entries during the test.

Forced swimming test

The FST was used to evaluate depression-like behaviors in rats by measuring their immobility time in water. The test was conducted in a transparent cylindrical tank as the swimming chamber and was characterized by the following dimensions: 30 cm in diameter, 100 cm in height, and a water depth of 35 cm. To ensure consistency, the water temperature was maintained at 25°C ± 1°C. To facilitate acclimatization to the laboratory environment, the rats were positioned in the apparatus room for 1 h before the experiment. The order of testing was randomized for each group. During the test, the experimenter gently held the rat by the tail, approximately two-thirds of the base, and slowly placed it into the swimming chamber. The behavior of each rat was recorded using a camera for 6 min. Subsequently, the experimenters, who were unaware of the group assignments, manually recorded the immobility time of each rat during the last 5 min of the test. Immobility manifests when a rat assumes a floating position on the water surface, displaying a lack of limb movement or subtle paddling motions with its forepaws and tail to sustain the head above the water.

Morris water maze test

The evaluation of spatial learning and memory in rats was conducted by applying the MWM test. This experimental approach involved quantifying the time and path chosen by the rats while navigating through a water maze to locate a hidden platform. The test had two stages: the acquisition navigation trial and the spatial probe trial, which lasted 6 days at 25°C. The water pool was uniformly partitioned into four quadrants, and the platform was strategically positioned at the center of one of the quadrants. The camera system displayed above the maze recorded rat movement trajectories synchronously. The acquisition navigation test was used to evaluate the capacity of rats to acquire spatial learning and memory in the water maze. This evaluation was conducted over 5 days, with four daily training sessions and a 30-min interval between sessions. Throughout the training sessions, a single quadrant was randomly selected as the starting point for the rat, which was subsequently placed in water. Upon successful ascent onto the hidden platform, the rat was afforded 10 s to remain there. Conversely, if the rat could not locate the platform within 120 s, appropriate guidance was provided to direct the rat towards the platform, thereby allowing it to stay there for 10 s. An image-tracking system was utilized to document the latency period of the rats in successfully locating the platform during the experiment. The spatial probe trial measured rats' spatial memory retention to find the platform after learning. On the 6th day of the experiment, the hidden platform was extracted from the water, and the rat was submerged with its orientation directed towards the pool wall at a randomly chosen entry point. To assess its performance, the number of crossings of the platform of the rat within 120 s, the time spent and distance traveled in each specific quadrant with the platform, and the time and distance percentages in each specific quadrant were measured during the test.

Z-score calculation of behavioral analysis

We utilized the standard z-score method to normalize the raw behavioral data. Z-scores serve as a statistical representation indicating the number of standard deviations (σ) that a given observation (X) deviates from the mean (μ) of the control group. Mathematically, the Z-score can be calculated using the formula $Z = (X-\mu)/\sigma$ (Guilloux et al., 2011). Many research efforts have utilized Z-scores to explore emotional behaviors in rodent models (Labots et al., 2016; Labots et al., 2018; Torrisi et al., 2021). Based on behavioral observations of rats at different time points and across sexes, Jean-Philippe Guilloux and colleagues have suggested that Z-scores of rodent emotions might be one of the most direct indicators reflective of human emotional states (Guilloux et al., 2011). The CON group served as the control group, and Z-scores were calculated for all the groups. The directionality of the scores was adjusted to ensure that an increase in the score values reflected an increase in the corresponding dimension. Z_{SPT} refers to SP, which measures the preference for sucrose. Z_{EPMT} represents the Z-score for EPMT results, including measures of time and distance in the open arms, the number of entries into the open arms, and their corresponding ratios. Z_{FST} is the Z-score of FST, which measures immobility time. Z_{MWM} indicates the Z-score for the MWM test results, including the total distance traveled, platform crossings, time and distance spent in the target quadrant, and their respective ratios. $Z_{depression} = (-Z_{SPT} + Z_{FST})/2$ was used to assess depression-like behaviors in rats. $Z_{anxiety} = -Z_{EPMT}$ used to evaluate anxiety-like levels in rats. $Z_{cognize} = Z_{MWM}$ used to assess cognitive function in rats.

Collection of fresh samples of Rat hippocampus, prefrontal cortex, hypothalamus tissues, and colonic content

1) Preparation: The rats were subjected to intraperitoneal administration of 1% pentobarbital sodium (0.3 mL/100 g) for anesthesia. 2) Dissection: After anesthesia, the chest and abdominal cavities of the rats were dissected to fully expose the heart. Following perfusion with physiological saline through the heart, the rats were decapitated, the rats' brains were quickly removed from the skull and immediately placed on an ice tray. 3) Identification of Brain Regions: The three brain regions of interest were identified based on anatomical landmarks consistent with established brain atlases. The HIP was located using its distinct C-shape structure, the PFC was identified by its anterior position relative to the frontal lobe, and the HYP was located using key anatomical landmarks such as the optic chiasm at the anterior end, the mammillary bodies at the posterior end, and the hypothalamic sulci at the lateral boundaries. 4) Region Isolation: Each brain region was carefully dissected out. The tissue was then rapidly frozen using liquid nitrogen to halt any enzymatic activity. Simultaneously, colonic contents were collected. All samples were immediately placed to 2 mL EP tubes and promptly frozen using liquid nitrogen. Subsequently, the samples were securely stored at −80°C for future use.

DNA extraction and 16S rRNA gene sequence analysis

Total microbial genomic DNA from colonic content samples was extracted using the E.Z.N.A.® Soil DNA Kit according to the protocol provided by the manufacturer's instructions (Omega Bio-Tek, Norcross, GA, United States). To assess the quality and concentration of DNA, a combination of methods was employed, including 1.0% agarose gel electrophoresis and a NanoDrop® ND-2000 spectrophotometer (Thermo Scientific, United States). Subsequently, the DNA samples were securely stored at −80°C for subsequent use. A PCR thermocycler, specifically the ABI GeneAmp® 9700 model manufactured by ABI (CA, United States), was utilized to amplify the hypervariable region V3-V4 of the bacterial 16S rRNA gene. This amplification was performed using specific primer pairs 338F (5′-ACTCCTACGGGAGGCAGCAG-3′) and 806R (5′-GGACTACHVGGGTWTCTAAT-3′) (Liu et al., 2016). The PCR reaction was conducted in triplicate with a reaction mixture composed of 5 × Fast Pfu buffer (4 μL), 2.5 mM dNTPs (2 μL), each primer at a concentration of 5 μM (0.8 μL), Fast Pfu polymerase (0.4 μL), template DNA (10 ng), and sufficient ddH_2O to reach a final volume of 20 μL. Each sample was amplified in triplicate. The PCR product was extracted from a 2% agarose gel and purified using an AxyPrep DNA Gel Extraction Kit (Axygen Biosciences, Union City, CA, United States). The extraction process followed the precise guidelines provided by the manufacturer. Subsequently, the purified PCR product was quantified using Quantus™ Fluorometer (Promega, United States). The raw FASTQ files were de-multiplexed using an in-house Perl script, followed by the application of fastp version 0.19.6 (Chen S. et al., 2018) for quality filtering. The resulting files were subsequently merged using FLASH version 1.2.7 (Magoč and Salzberg, 2011).

Metabolite extraction and (UHPLC-MS/MS) analysis

Precise measurement of a 50 mg solid sample was conducted before proceeding with metabolite extraction. The extraction process involved using a 400 μL solution consisting of methanol and water in a ratio of 4:1 (v/v). To ensure accurate quantification, an internal reference, L-2-chlorophenylalanin, was added at a concentration of 0.02 mg/mL. The mixture was allowed to settle at −10°C and was subsequently treated using the high-throughput tissue crusher Wonbio-96c (Wanbo Biotechnology Co., LTD., Shanghai, China) at a frequency of 50 Hz for 6 min. To further enhance the extraction process, ultrasound was performed at 40 kHz for 30 min at 5°C. The samples were carefully stored at −20°C for 30 min to facilitate protein precipitation. After centrifugation for 15 min at 13,000 g and 4°C, the resulting supernatant was meticulously transferred into sample vials for subsequent LC-MS/MS analysis. As an integral step in the system conditioning and quality control (QC) protocol, a pooled QC sample was prepared by uniformly combining equal volumes of all individual samples. The QC samples underwent the same disposal and testing procedures as those used for the analytical samples. These samples, which represent the entire set of samples, were injected into the system at regular intervals (every eight samples) to ensure the stability of the analysis. The UHPLC-Q Exactive system manufactured by Thermo Fisher Scientific served as the platform for LC-MS analysis. Upon the successful completion of mass spectrometry detection, the raw data obtained from LC/MS analysis were preprocessed using the specialized software

10.3389/fphar.2024.1362464

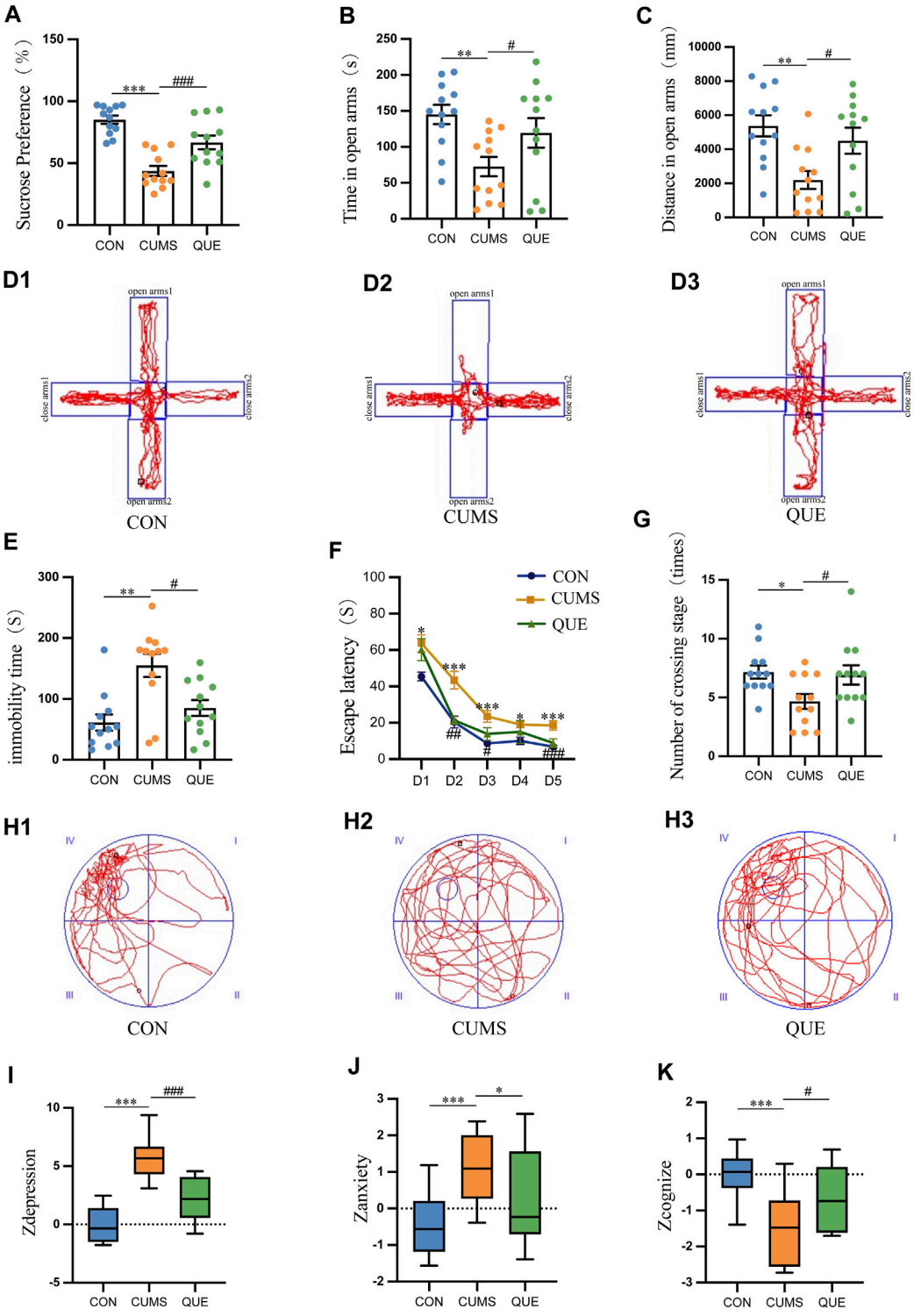

FIGURE 2
Behavioral test results in rats. **(A)** Sucrose preference (%) in SPT, $n = 12$; **(B)** Time spent in open arms (s) in EPMT, $n = 12$; **(C)** Distance traveled in open arms (mm) in EPMT, $n = 12$; **(D)** Trajectory plot in EPMT; **(E)** Immobility time (s) in FST, $n = 12$; **(F)** Escape latency (s) in MWM, $n = 12$; **(G)** Number of platform crossings in MWM; **(H)** Trajectory plot on the sixth day in MWM; **(I)** Zdepression, $n = 12$; **(J)** Zanxiety, $n = 12$; **(K)** Zcognize, $n = 12$. Data are presented as mean ± SEM. $^{*}p < 0.05$, $^{**}p < 0.01$, $^{***}p < 0.001$ compared to CON group; $\#p < 0.05$, $\#\#p < 0.01$, $\#\#\#p < 0.001$ compared to CUMS group.

Progenesis QI, developed by Waters Corporation (Milford, USA). Subsequently, a three-dimensional data matrix in CSV format was generated and exported. To identify metabolites, extensive searches were conducted using recognized databases, such as Metlin (https://metlin.scripps.edu/), HMDB (http://www.hmdb.ca/), and the Majorbio Database.

Statistical analysis

The analysis of 16S rRNA gene sequence data involved calculating rarefaction curves and measuring alpha diversity, such as Chao1 richness, Good's coverage, observed OTUs, and Shannon index. These calculations were performed using Mothur v1.30.1 (Schloss et al., 2009). To assess the similarity between microbial communities across different samples, principal coordinate analysis (PCoA) was conducted using the Vegan v2.5-3 package, with Bray-Curtis dissimilarity serving as the basis for comparison. Significant differences between sample groups were determined using the ANOSIM test. Using the Kruskal-Wallis test, along with linear discriminant analysis (LDA) effect size (LEfSe) (Segata et al., 2011) (http://huttenhower.sph.harvard.edu/LEfSe), the bacterial taxa (ranging from phylum to genera) exhibited significant variations across the various groups. The inclusion criteria for these taxa were an LDA score exceeding 2 and a *p*-value lower than 0.05.

In the analysis of metabolomics data, the R package ropls (Version 1.6.2) was employed to conduct principal component analysis (PCA) and orthogonal partial least squares-discriminant analysis (OPLS-DA). The model stability was assessed using a 7-cycle interactive validation approach. Additionally, Students' t-tests and fold difference analysis were performed to further investigate the data. Differentially abundant metabolites were identified by evaluating the variable importance in projection (VIP) values derived from the OPLS-DA model and the *p*-value derived from Student's t-test. Metabolites exhibiting VIP values exceeding 1 and *p*-values lower than 0.05 were considered to show significant differences. In addition, pathway enrichment analysis for the identified differentially abundant metabolites was performed using MetaboAnalyst 3.0 (http://www.metaboanalyst.ca/), whereas KEGG (http://www.kegg.jp) was used to identify the pathways associated with these metabolites.

The remaining data underwent statistical analysis using SPSS 22.0 software. Various statistical tests were used, such as one-way ANOVA, LSD, Welch test, Games-Howell test, Mauchly sphericity test, Greenhouse-Geisser correction, and Spearman's correlation analysis. The analysis considered data normality and homogeneity of variance using relevant statistical approaches for each case. To report the results, the mean ± SEM was used, and statistical significance was established at a *p*-value below 0.05, indicating the presence of significant differences between the groups. Co-occurrence networks were constructed to delve into the internal community connections among the samples. The co-occurrence network was established to investigate the interrelationships between the different data components. A correlation coefficient greater than 0.6 or less than −0.6 and a *p*-value less than 0.05 indicate a statistically significant and robust association between two network nodes.

Results

QUE improves depressive-like behaviors and enhances cognitive function in CUMS rats

Anhedonia, anxiety-like behaviors, and depression-like behaviors in rats were evaluated using SPT, EPMT, and FST, respectively. The experimental SPT data demonstrated a notable decline in SP among rats in the CUMS group relative to that in the CON group (p = 1.3669E-7 < 0.001). Conversely, rats in the QUE group exhibited a notable elevation in SP compared to the CUMS group (p = 0.000776 < 0.001, Figure 2A). Furthermore, the EPMT results demonstrated a significant reduction in both the time spent and distance traveled in the open arms among the rats in the CUMS group compared to those in the CON group (p = 0.003401 < 0.01, p = 0.001325 < 0.01, respectively). Nonetheless, upon QUE intervention, a notable increase was observed in both the time spent and the distance traveled in the open arms (p = 0.049647 < 0.05, p = 0.015838 < 0.05, respectively), as demonstrated in Figures 3B, C, D1–D3. The FST results revealed that rats in the CUMS group exhibited a notable increase in immobility time (p = 0.001059 < 0.01) compared to the CON group. Conversely, compared to the CUMS group, rats in the QUE group displayed a marked reduction in immobility time (p = 0.018093 < 0.05, Figure 2E).

The MWM test was used to assess the learning and spatial memory functions of the rats. In the first 5 days of the place navigation test, the data did not meet the assumption of sphericity based on Mauchly's sphericity test (p = 0.001017 < 0.001). As the training days increased, the escape latency to the platform decreased in all three groups (p = 6.9155E-16 < 0.001). During the first 5 days of the place navigation test, rats in the CUMS group took significantly more time to reach the hidden platform than those in the CON group (p = 3.8633E-7 < 0.001). However, after the QUE intervention, the time to reach the platform decreased significantly (p = 0.000046 < 0.001, Figure 2F). On the 6th day of the spatial probe test, the CUMS group displayed a substantial decrease in platform crossings (p = 0.013412 < 0.05). In contrast, after QUE treatment, the number of platform crossings in the QUE group significantly increased (p = 0.024810 < 0.05, Figures 2G, H1–H3). These results suggest that CUMS impairs spatial memory and that QUE intervention improves it in rats.

Zdepression was used to assess depression-like phenotypes in rats, Zanxiety was employed to evaluate anxiety-like phenotypes, and Zcognize was deployed to measure cognitive function. The results indicated that compared to the CON group, rats in the CUMS group displayed a significant increase in Zdepression and Zanxiety scores (p = 3.8744E-9 < 0.001 and p = 0.001302 < 0.001, respectively) and a notable decrease in Zcognize scores (p = 0.000434 < 0.001). After intervention with QUE, rats in the QUE group demonstrated a remarkable reduction in Zdepression and Zanxiety scores (p = 0.000022 < 0.001 and p = 0.044008 < 0.05, respectively), accompanied by a substantial increase in Zcognize scores (Figures 2I–K).

These results indicate that QUE effectively alleviates depressive-like and anxiety-like behaviors in rats, improves learning and spatial memory function, and enhances cognitive abilities.

Impact of quercetin intervention on brain tissue metabolic profiles

To investigate the effects of CUMS and QUE intervention on the metabolic profile of rat brain tissues, we performed an untargeted metabolomic analysis of PFC, HIP, and HYP tissues. Six multivariate OPLS-DA models were constructed, with the following parameters R^2X = 0.413, R^2Y = 0.999, Q^2 = 0.587

10.3389/fphar.2024.1362464

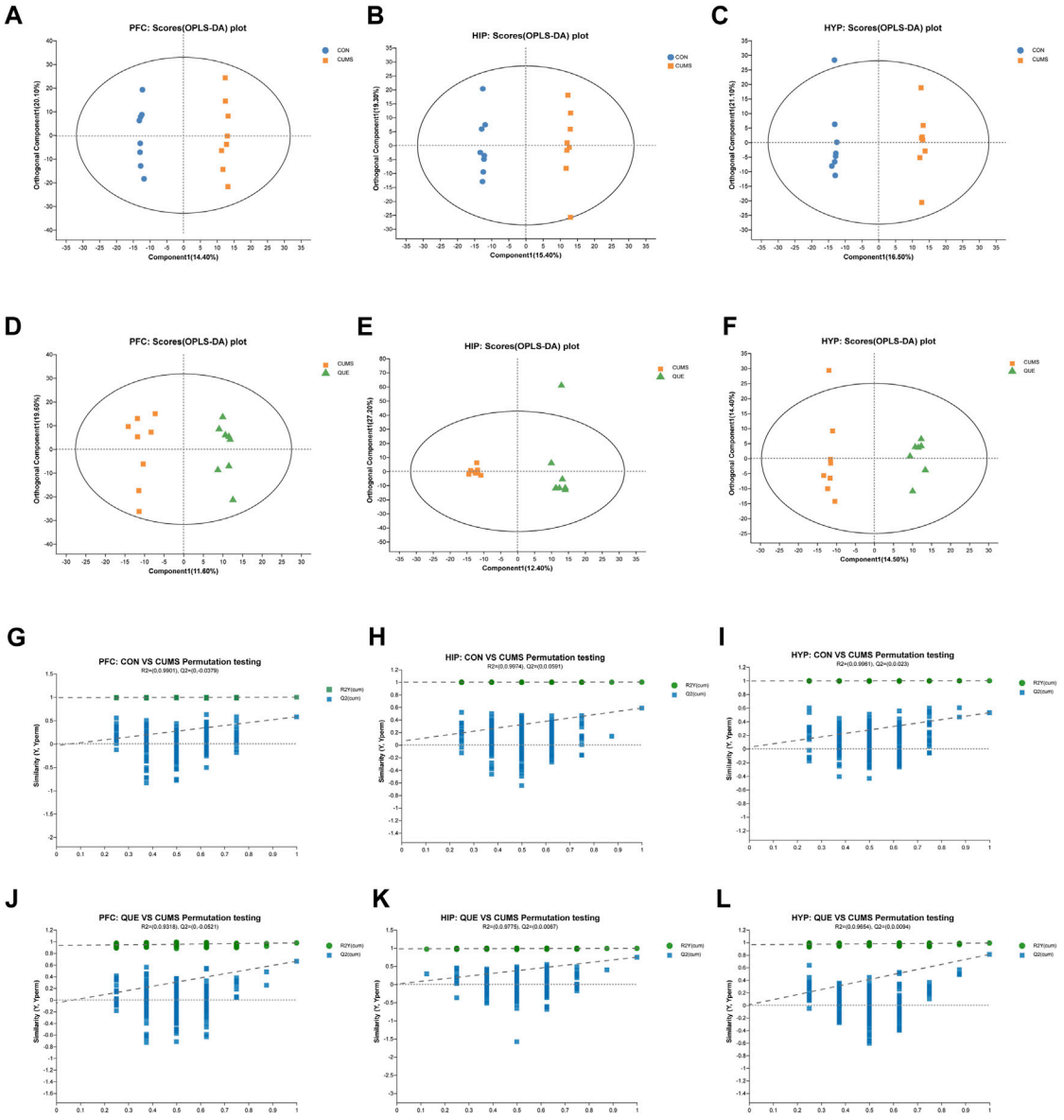

FIGURE 3
Effects of QUE on the metabolic profile of the brain in CUMS rats. **(A–F)** OPLS-DA Score Plots for CON vs. CUMS and CUMS vs. QUE in the PFC, HIP and HYP. **(G–L)** OPLS-DA replacement test (200 times) for CON vs. CUMS and CUMS vs. QUE in the PFC, HIP and HYP.

(CUMS vs. CON, HIP), $R^2X = 0.494$, $R^2Y = 0.99$, $Q^2 = 0.747$ (CUMS vs. QUE, HIP), $R^2X = 0.435$, $R^2Y = 0.999$, $Q^2 = 0.53$ (CUMS vs. CON, HYP), $R^2X = 0.289$, $R^2Y = 0.99$, $Q^2 = 0.81$ (CUMS vs. QUE, HYP), $R^2X = 0.419$, $R^2Y = 0.998$, $Q^2 = 0.577$ (CUMS vs. CON, PFC) and $^2X = 0.312$, $R^2Y = 0.976$, $Q^2 = 0.662$ (CUMS vs. QUE, PFC). These models demonstrated good stability and predictive abilities. The OPLS-DA model score plots (Figures 3A–F) displayed distinct separation of the metabolic profiles of the rat brain tissues (PFC, HIP, and HYP), indicating significant differences in the metabolites among the three groups. The permutation test results (Figures 3G–L) demonstrate that the models did not overfit.

As revealed in the volcano plots (Figures 4A–F), differential metabolites were screened based on the VIP values and Student's t-test *p*-values derived from the OPLS-DA model. Metabolites with VIP>1 and $p < 0.05$ were considered differentially expressed. In the PFC, 175 differential metabolites were identified, including 87 in the CON vs. CUMS comparison, 88 in the CUMS vs. QUE comparison, and 12 shared in the CUMS vs. CON and QUE vs. CUMS comparisons. Among these, eight metabolites exhibited opposite regulatory trends, including sphingosine, phosphoenol pyruvate, and D-glycerate 2-phosphate (Figures 4G,H, Supplementary Table S1). In HIP, 163 differential metabolites were identified, including 93 in the CON vs. CUMS comparison, 70 in the CUMS vs. QUE comparison, and 13 shared in the CUMS vs. CON and QUE vs. CUMS comparisons. Among these, 11 metabolites exhibited opposite regulatory trends, including glyceric acid and fructose 1,6-bisphosphate (Figures 4K,L, Supplementary Table S2). In the HYP, 229 differential metabolites were identified, including 99 in the CON vs. CUMS comparison, 130 in the CUMS vs. QUE comparison, and 29 shared

10.3389/fphar.2024.1362464

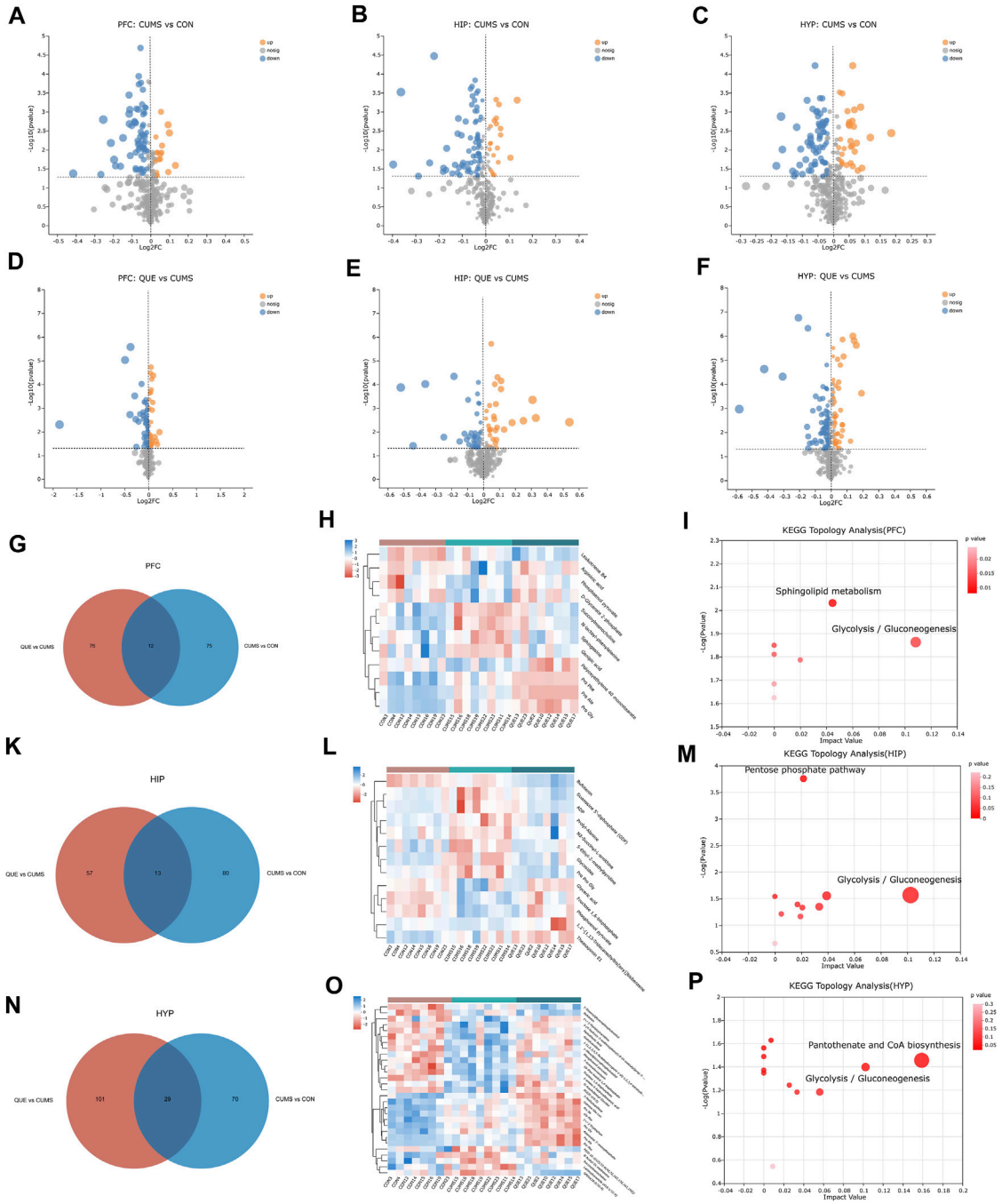

FIGURE 4
Key differential metabolites and metabolic pathways. **(A–F)** Volcano plots of differential metabolites comparing CON vs. CUMS and CUMS vs. QUE in the PFC, HIP, and HYP. **(G–I)** Venn diagrams of differential metabolites, heatmap of common differential metabolites, and KEGG topological analysis in the PFC comparing CON vs. CUMS and CUMS vs. QUE. **(K–M)** Venn diagrams of differential metabolites, heatmap of common differential metabolites, and KEGG topological analysis in the HIP comparing CON vs. CUMS and CUMS vs. QUE. **(N–P)** Venn diagrams of differential metabolites, heatmap of common differential metabolites, and KEGG topological analysis in the HYP comparing CON vs. CUMS and CUMS vs. QUE.

in the CUMS vs. CON and QUE vs. CUMS comparisons. Among these, 18 metabolites exhibited opposite regulatory trends, including fructose 1,6-bisphosphate, pantothenic acid, and phosphoenol pyruvate (Figures 4N,O, Supplementary Table S3).

To further elucidate the potential pathways affected by quercetin, we performed metabolic pathway annotations for the common differential metabolites (metabolites altered by quercetin treatment) in the CUMS vs. CON and QUE vs. CUMS groups using the KEGG and HMDB databases. Subsequently, pathway enrichment and topology analyses were conducted using the Python software package sciPy.stats, and the main metabolic pathways involving differential metabolites were identified using

10.3389/fphar.2024.1362464

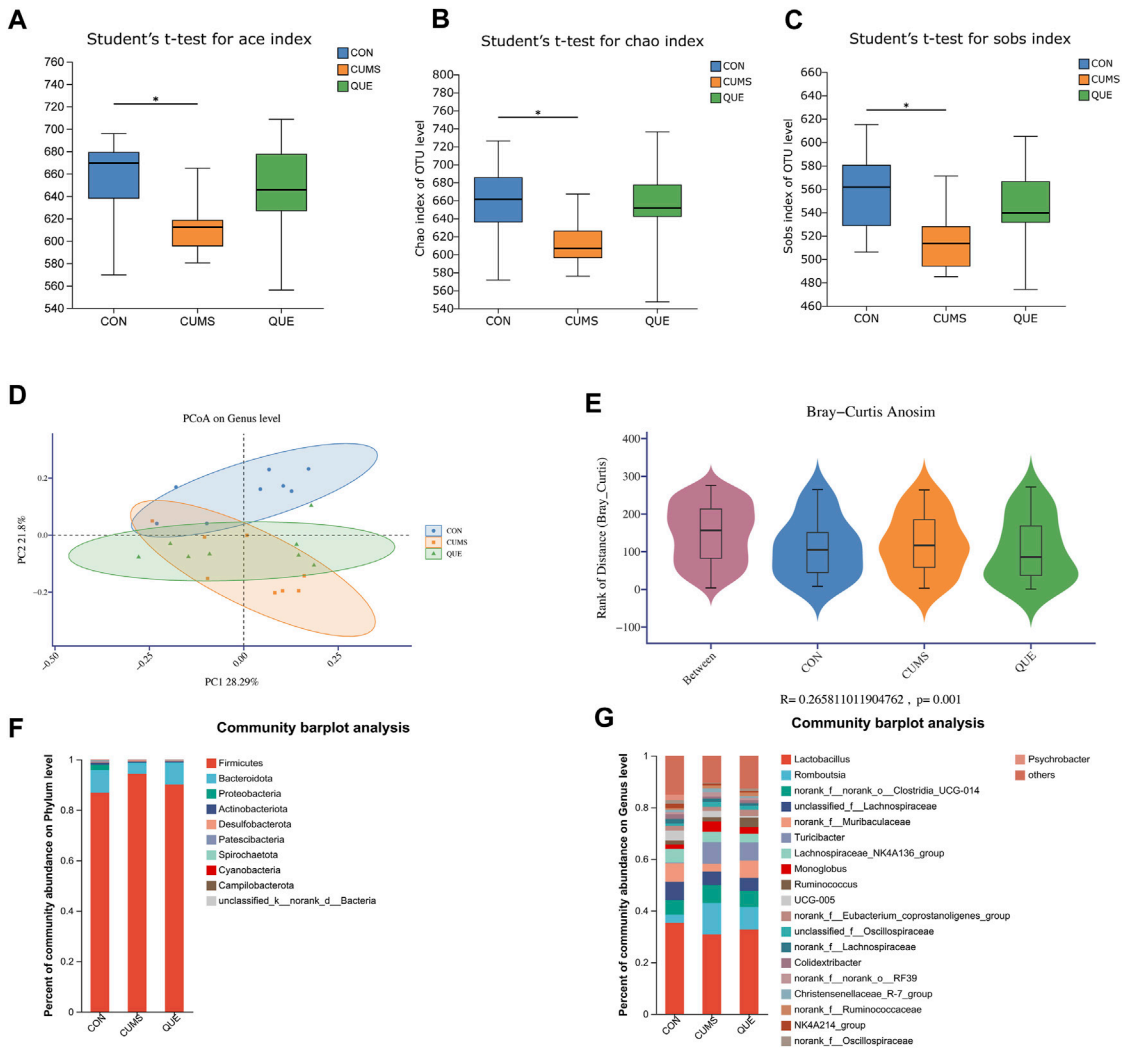

FIGURE 5
Effects of Quercetin on the Gut Microbiota of CUMS Rats. **(A)** ACE index. **(B)** Chao1 index. **(C)** Sobs index. **(D)** PCoA analysis. **(E)** In the anosim similarity analysis, R > 0 indicates larger inter-group differences than intra-group differences. **(F)** Barplot of gut microbiota abundance at the phylum level. **(G)** Barplot of gut microbiota abundance at the genus level.

Fisher's exact test. The results revealed that two metabolic pathways, glycolysis/gluconeogenesis and sphingolipid metabolism, in the PFC (Figure 4I), two metabolic pathways, glycolysis/gluconeogenesis and pentose phosphate pathway, in the HIP (Figure 4M), and two metabolic pathways, glycolysis/gluconeogenesis and pantothenate and CoA biosynthesis, were significantly perturbed in the HYP (Figure 4P). These pathways are significant targets of quercetin's activity, and their enhanced metabolites are the key differential metabolites (Supplementary Figure S2).

Regulatory effects of quercetin on the gut microbiota in depression-like rats

We used 16S rRNA gene sequencing of colonic content samples from the three rat groups to assess gut microbiota changes after CUMS modeling and quercetin administration. After sequence optimization, QC, and rarefaction, 1,111,576 feature sequences were obtained, with an average of 46,316 effective sequences per sample. These feature sequences were classified into 1,019 Operational Taxonomic Units based on 97% sequence similarity. Alpha diversity analysis results disclosed that the ace, Chao1, and Sobs indices in the gut microbiota of CUMS rats were significantly lower than those in the CON group (Figures 5A–C), indicating that CUMS intervention significantly reduced microbial community richness. The QUE group depicted an upward trend compared with the CUMS group, but the difference was not statistically significant. We further assessed the beta diversity of the microbial community using PCoA based on Bray-Curtis dissimilarity. The PCoA results (Figure 5D) and intergroup differences test (R = 0.266, $p < 0.05$, Figure 5E) demonstrated that the gut microbiota of each group clustered significantly, and significant differences existed in the microbial composition and structure among the groups. Additionally, the clustering trend of the QUE group was similar to that of the CON group, indicating that CUMS significantly changed the gut microbial community structure and that quercetin regulated the gut microbiota of CUMS rats.

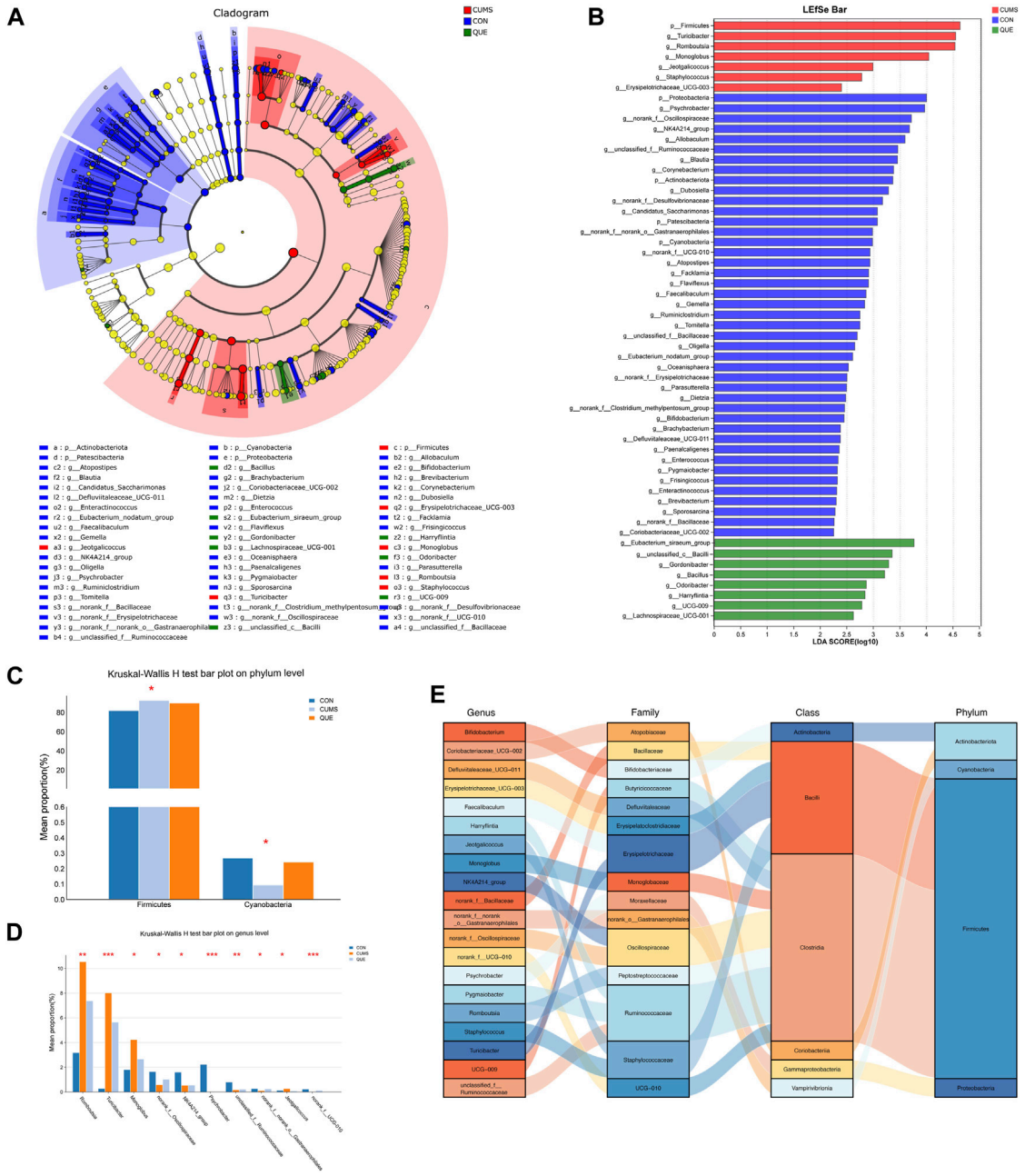

FIGURE 6
Analysis of differentially abundant bacteria in the gut microbiota of CUMS rats regulated by quercetin intervention. **(A)** Enriched microbial taxa dendrogram generated from LEfSe analysis. **(B)** Histogram depicting the distribution of differentially abundant bacteria based on LDA scores. **(C)** Significantly differentially abundant phyla with reversed abundances by quercetin intervention at the phylum level (Kruskal–Wallis H test). **(D)** Top 10 genera with reversed abundances by quercetin intervention at the genus level (Kruskal–Wallis H test). **(E)** Sankey diagram illustrating the significantly differentially abundant genera with reversed abundances by quercetin intervention at the genus level.

To further analyze the specific effects of the CUMS model and quercetin intervention on the rat gut microbiota, we examined the composition and abundance changes of gut microbial taxa in each group. At the phylum and genus levels, we retained the top 10 and 20 species with the highest abundance, respectively, to calculate the relative abundance and then plotted the relative abundance using a stacked bar chart (Figures 5F,G). At the phylum level, *Firmicutes*, *Bacteroidota*, and *Proteobacteria* were the dominant phyla, accounting for over 98% of the total relative abundance. Compared to the CON group, the gut of CUMS rats had more *Firmicutes*, less *Bacteroidota*, and a higher *Firmicutes/Bacteroidota* (F/B) ratio. Quercetin intervention reversed this trend (Figure 5F). At the genus level, changes in the gut microbial community of CUMS rats mainly involved a decrease in *Lactobacillus*, *norank_f__Muribaculaceae*, *Lachnospiraceae_NK4A136_group*, and *Psychrobacter*, and an increase in *Turicibacter*, *norank_f__norank_o__Clostridia_UCG-014*, *Romboutsia*, *UCG-005*, and *Monoglobus*. Quercetin intervention counteracted these changes (Figure 5G).

10.3389/fphar.2024.1362464

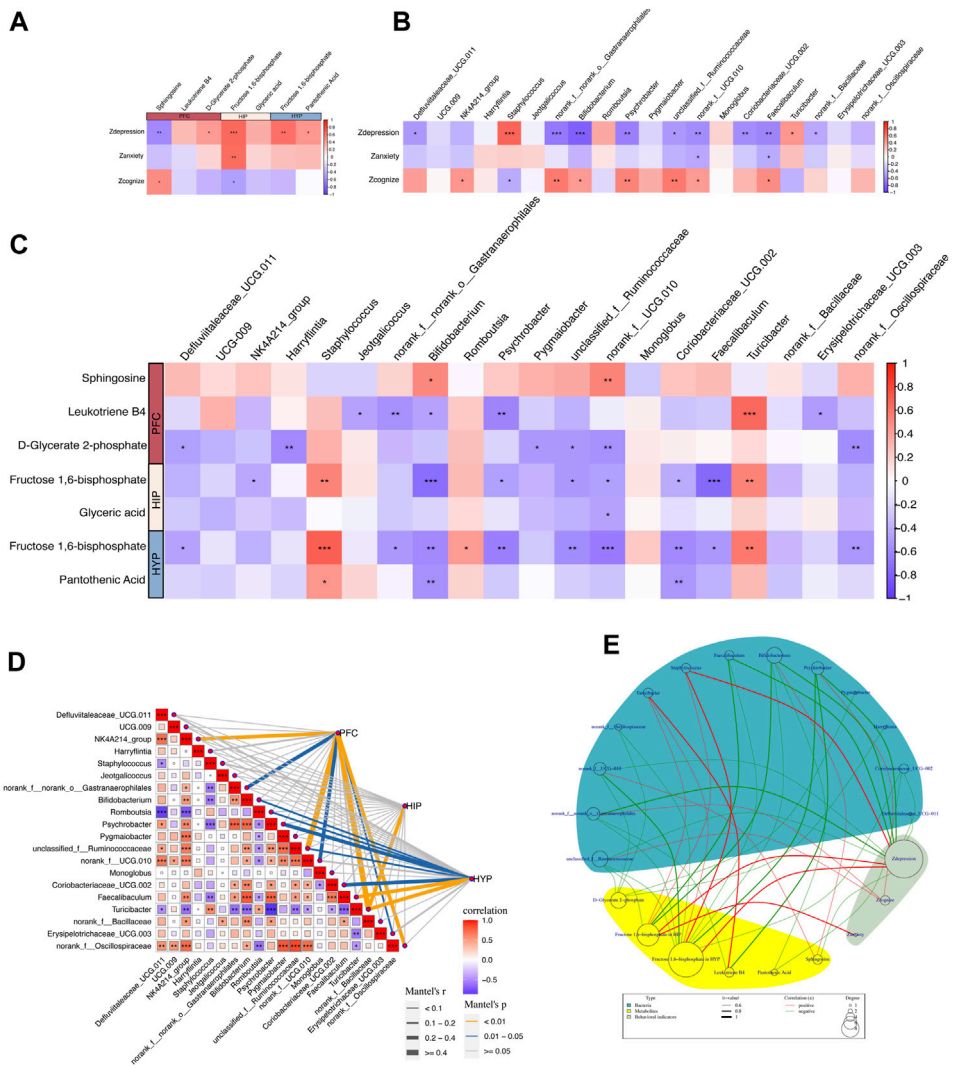

FIGURE 7
Correlation between behavioral metrics, differential metabolites, and gut differential microbiota. **(A)** Spearman's correlation analyses between the behavioral Z scores of rats and key differential metabolites in the PFC, HIP, and HYP. **(B)** Spearman's correlation analyses between the behavioral Z scores of rats and differential bacteria at the genus levels. **(C)** Spearman's correlation analyses between differential bacteria at the genus level and key differential metabolites in the PFC, HIP, and HYP. **(D)** Mantel test of the correlation between differential bacteria at the genus level and key differential metabolites in the PFC, HIP, and HYP. **(E)** Network circle of the Spearman's correlation between the behavioral Z scores of rats and key differential metabolites in the PFC, HIP, and HYP, along with differential bacteria at the genus level.

To identify statistically different biomarkers in the CUMS group and further determine the significant markers affected by quercetin intervention (QUE), we performed LEfSe and Kruskal–Wallis rank-sum test analyses. LEfSe analysis revealed 106 differentially abundant species from the phylum to the genus level (LDA score >2) (Supplementary Table S4, Figures 6A,B), with 53 species at the genus level and 5 species at the phylum level (Figures 6A,B). Based on the LEfSe analysis results, we further compared the differential markers among the CON, CUMS, and QUE groups using the Kruskal-Wallis rank sum test. At the phylum level, we identified five differentially abundant taxa with opposite trends in CON vs. CUMS and QUE vs. CUMS, among which *Firmicutes* and *Cyanobacteria* were statistically significant (Figure 6C, Supplementary Table S5). At the genus level, we identified 20 differentially abundant taxa with opposite trends in CON vs. CUMS and QUE vs. CUMS. Among these, *Romboutsia*, *Turicibacter*, *Monoglobus*, *Jeotgalicoccus*, *Staphylococcus*, and *Erysipelotrichaceae_UCG-003* were significantly increased in the CUMS group but decreased significantly after quercetin intervention. In contrast, *Bifidobacterium*, *Faecalibaculum*, and *Pygmaiobacter* decreased significantly in the CUMS group but increased significantly after quercetin intervention (Supplementary Table S6). The top 10 differentially abundant genera with statistical significance are displayed in Figure 6D. Furthermore, we categorized these 20 differentially abundant genera based on their taxonomy at the class, order, and phylum levels and depicted a Sankey plot (Figure 6E). Among them, 16 genera belonged to the phylum *Firmicutes*; two belong to the phylum *Actinobacteria*, one belongs to the phylum *Proteobacteria*, and one belongs to the phylum *Cyanobacteria*.

Correlation analysis of behavioral Z scores with key differential metabolites in brain regions and gut microbiota

To understand how quercetin regulates the "microbiota-gut-brain" axis to treat depression, we conducted a series of correlation analyses to explore the relationships among behavioral phenotypes, brain region metabolites, and gut microbiota from three dimensions: depression-like behaviors, anxiety-like behaviors, and cognitive function in rats. First, we performed Spearman's correlation analyses between the behavioral Z-scores of rats and key differential metabolites (Figure 7A) and differentially abundant taxa at the phylum (Supplementary Figure S1B) and genus levels (Figure 7B). Next, we conducted correlation analyses between the differentially abundant taxa at the phylum and genus levels and the key differential metabolites separately (Supplementary Figures S1C, S7C). Subsequently, Mantel tests were performed to analyze the correlation between differentially abundant taxa at the genus level and key differential metabolites (Figure 7D). Finally, we examined the relationships among the behavioral Z-scores, key differential metabolites, and differentially abundant taxa using Spearman's correlation analyses and constructed correlation network diagrams (Figure 7E). Correlation coefficients (r) were used to assess the degree of correlation, where $|r| > 0.6$ indicated a strong correlation, $0.4 < |r| \leq 0.6$ indicated a moderate correlation, $0.3 < |r| \leq 0.4$ indicated a weak correlation; and $|r| \leq 0.3$ indicated no correlation (Akoglu, 2018; Schober et al., 2018). We focused on results showing moderate to strong correlations (i.e., $|r| > 0.4$) in our study.

Correlation analysis of behavioral Z scores and key differential metabolites

Behavioral Z-scores were highly correlated with key differential metabolites, and several behavioral indices were highly linked to enriched differential metabolites in key pathways (Figure 7A). Specifically, Zdepression was negatively correlated with sphingosine in the PFC (r = −0.596, p = 0.002) and positively correlated with D-glycerate 2-phosphate in the PFC (r = 0.434, p = 0.033), fructose 1,6-bisphosphate in the HIP (r = 0.643, p = 0.0006), fructose 1,6-bisphosphate in the HYP (r = 0.612, p = 0.001), and pantothenic acid in the HYP (r = 0.456, p = 0.024). Zanxiety was positively correlated with fructose 1,6-bisphosphate in the HIP (r = 0.625, p = 0.001). Zcognize was positively associated with sphingosine in the PFC (r = 0.416, p = 0.042) and negatively correlated with D-glycerate 2-phosphate in the PFC (r = −0.445, p = 0.029), and fructose 1,6-bisphosphate in the HIP (r = −0.418, p = 0.041). These correlations imply potential associations between specific metabolites in different brain regions and behavioral phenotypes, highlighting the importance of these metabolites in modulating depression-like behaviors, anxiety-like behaviors, and cognitive function in rats.

Correlation analysis of behavioral Z scores and differential bacteria (phylum and genus level)

As revealed in Figure 7B, Zdepression in rats exhibited high correlations with several differential bacterial genera: Zdepression was negatively correlated with Bifidobacterium (r = −0.789, p = 4.46E-06) and Psychrobacter (r = −0.620, p = 0.001), representing nine bacterial genera; Zdepression was positively correlated with Turicibacter (r = 0.450, p = 0.027) and *Staphylococcus* (r = 0.663, p = 0.0004).

There were also correlations between Zanxiety, Zcognize, and different bacterial genera. These results suggest potential associations between specific bacterial genera and behavioral phenotypes, indicating the possible involvement of gut microbiota in modulating depression-like behaviors, anxiety-like behaviors, and cognitive function in rats.

Correlation analysis of key differential metabolites and differential bacteria (at the phylum and genus levels) in colonic contents

First, we performed a correlation analysis between key differential metabolites and taxa at the phylum level (Supplementary Figure S1C). The results demonstrated no significant correlation between the key differential metabolites and taxa at the phylum level. We then explored the correlation between the key differential metabolites and taxa at the genus level. The specific results of Spearman's correlation analysis (Figure 7C) were as follows: In the PFC, sphingosine was positively correlated with Bifidobacterium (r = 0.502, p = 0.012) and norank_f__UCG-010 (r = 0.536, p = 0.006); D-glycerate 2-phosphate was negatively correlated with Harryflintia (r = −0.580, p = 0.002), Pygmaiobacter (r = −0.507, p = 0.011), unclassified_f__Ruminococcaceae (r = −0.506, p = 0.011), norank_f__UCG-010 (r = −0.550, p = 0.005), and norank_f__Oscillospiraceae (r = −0.566, p = 0.003). In the HIP, fructose 1,6-bisphosphate was negatively correlated with Bifidobacterium (r = −0.725, p = 6.02E-05), Faecalibaculum (r = −0.747, p = 2.74E-05), NK4A214_group (r = −0.425, p = 0.038), Psychrobacter (r = −0.479, p = 0.017), unclassified_f__Ruminococcaceae (r = −0.501, p = 0.012), and norank_f__UCG-010 (r = −0.473, p = 0.019), and positively correlated with Turicibacter (r = 0.526, p = 0.008) and *Staphylococcus* (r = 0.525, p = 0.008). Glyceric acid was negatively linked to norank_f__UCG-010 (r = −0.442, p = 0.030). In the HYP, fructose 1,6-bisphosphate was negatively connected to Bifidobacterium (r = −0.587, p = 0.002), Defluviitaleaceae_UCG-011 (r = −0.459, p = 0.023), norank_f__norank_o__Gastranaerophilales (r = −0.511, p = 0.010), Psychrobacter (r = −0.627, p = 0.001), unclassified_f__Ruminococcaceae (r = −0.576, p = 0.003), norank_f__UCG-010 (r = −0.650, p = 0.0005), Coriobacteriaceae_UCG-002 (r = −0.597, p = 0.002), Faecalibaculum (r = −0.501, p = 0.012), and norank_f__Oscillospiraceae (r = −0.532, p = 0.007); it was positively correlated with Romboutsia (r = 0.423, p = 0.039), Turicibacter (r = 0.566, p = 0.003), and *Staphylococcus* (r = 0.692, p = 0.0001). Pantothenic Acid was negatively correlated with Bifidobacterium (r = −0.541, p = 0.006) and Coriobacteriaceae_UCG-002 (r = −0.522, p = 0.008) and positively correlated with *Staphylococcus* (r = 0.443, p = 0.029). Notably, fructose 1,6-bisphosphate, a key metabolite shared by HIP and HYP, was correlated with the differential taxa (Figures 7C, E). We then performed a Mantel test to assess the overall correlation between differential taxa in the gut and brain metabolites. The results demonstrated the strongest correlation between the differential taxa and metabolites in the PFC, followed by HYP, and the weakest correlation was observed in the HIP. Turicibacter was correlated with metabolites in all three brain regions (Figure 7D). Finally, we constructed a Spearman's correlation

network graph (Figure 7E) between behavioral Z-scores, key differential metabolites in the PFC, HIP, HYP, and gut differential taxa.

Discussion

Depression, a prevalent mental condition with a complex and heterogeneous pathogenesis, severely affects society. Traditional antidepressant drugs have certain limitations in treating depression and often have side effects. Consequently, the search for safer and more effective natural alternatives has become a hot topic of current research. Quercetin, a plant-based flavonoid, has been reported to have antidepressant properties; however, its mechanisms are unknown.

In this study, we established a Chronic Unpredictable Mild Stress (CUMS) rat model, renowned for its widespread use, reliability, and efficacy in chronic stress research in animals (Antoniuk et al., 2019; Lages et al., 2021). However, it is crucial to acknowledge that, similar to the human condition, not all animals subjected to the CUMS protocol develop depressive-like symptoms. (Castro et al., 2012; Marcolongo-Pereira et al., 2022). Some studies have introduced susceptible and resilient subgroups to explore the effects of these individual differences. Nonetheless, difficulties and controversies persist in empirically defining vulnerability *versus* resilience among animals (Willner, 2017), with CUMS stress potentially altering resilience in rats (Liu et al., 2023). Our study concentrated on the general modulatory effects of quercetin on depressive-like phenotypes induced by CUMS, without making specific distinctions between individual resilience and susceptibility. Further research is necessary to elucidate the specific manifestations in, and differences between, susceptible and resilient rats. We conducted metabolomics analysis of three brain regions (PFC, HIP, and HYP) and 16s rRNA sequencing analysis of the colon contents to assess the effect of quercetin on depression-like behaviors in rats. Our findings indicate that quercetin may be involved in reshaping gut microbiota, regulating brain metabolism, and thereby ameliorating depressive behaviors in rats (Supplementary Figure S2).

Increasing evidence suggests a close association between carbohydrate metabolism and depression, with abnormalities in carbohydrate metabolism being observed in the PFC (Baxter et al., 1989; Kennedy et al., 2001; Hennings et al., 2012; Li et al., 2015; Yao et al., 2023), HIP (Cherix et al., 2022), and HYP (Al-Massadi et al., 2021) of depression patients or depression-like animal models. This study found that quercetin may ameliorate depression-like behaviors in CUMS rats by modulating glycolysis/gluconeogenesis and the pentose phosphate pathway. Notably, quercetin strongly altered the glycolysis/gluconeogenesis pathway in all three brain areas. D-glycerate 2-phosphate was discovered as a critical differential metabolite in quercetin's modulation of glycolysis/gluconeogenesis in the PFC. D-glycerate 2-phosphate is an intermediate product of glycolysis that, under the catalysis of enolase, can be converted into phosphoenolpyruvate and subsequently transformed into pyruvate by pyruvate kinase, leading to ATP production and playing a crucial regulatory role in depression (Ma et al., 2018; Lin et al., 2022). In our study, the level of D-glycerate 2-phosphate was significantly elevated in CUMS rats, and quercetin intervention significantly reduced its level, suggesting that CUMS might disrupt its breakdown, causing abnormal glycolysis/gluconeogenesis and subsequent depression-like behaviors. These findings were supported by the correlation analysis (Figure 7A), which demonstrated a positive correlation between D-glycerate 2-phosphate and Zdepression and a negative correlation between D-glycerate 2-phosphate and Zcognition. In HIP and HYP, fructose 1,6-bisphosphate was identified as a key differential metabolite in quercetin's regulation of glycolysis/gluconeogenesis. In glycolysis, fructose 1,6-bisphosphate is an intermediate product that aldolase can cleave into dihydroxyacetone phosphate and glyceraldehyde 3-phosphate, which contribute to the onset and treatment of depression (Birkmayer, 1996; Demarin et al., 2004; Ma et al., 2018; Wang et al., 2021; Cho et al., 2022; Lin et al., 2022). We observed a significant increase in fructose 1,6-bisphosphate levels in the HIP and HYP of CUMS rats, which was reversed by quercetin intervention. Moreover, a strong positive correlation was observed between fructose 1,6-bisphosphate and Zdepression (Figure 7A), indicating that CUMS might induce the abnormal cleavage of fructose 1,6-bisphosphate, leading to disrupted glycolysis/gluconeogenesis and subsequent depression-like behaviors. Quercetin's regulation of fructose 1,6-bisphosphate cleavage improved abnormal glycolysis/gluconeogenesis and alleviated depression-like behaviors. Furthermore, the pentose phosphate pathway in HIP is affected by quercetin, with glycerate being a key differential metabolite. Glycerate can be converted into 2-phosphoglycerate through the action of glycerate 2-kinase, and 2-phosphoglycerate is a key compound involved in glycolysis. Through catalysis by various enzymes, 2-phosphoglycerate completes glycolysis and produces ATP, thus playing a crucial role in regulating depression (Ma et al., 2018; Cho et al., 2022; Lin et al., 2022). Quercetin significantly lowered D-glycerate 2-phosphate in the PFC, fructose 1,6-bisphosphate and glycerate in the HIP, and fructose 1,6-bisphosphate in the HYP, improving carbohydrate metabolism and alleviating depression-like behaviors.

The lipid composition of the brain may affect perception and emotional behavior, potentially causing depression and anxiety disorders (Adibhatla and Hatcher, 2008; Yadav and Tiwari, 2014; Kornhuber et al., 2015). We discovered the potential regulatory effects of quercetin on brain lipid metabolism in CUMS rats, focusing on the PFC sphingolipid metabolism pathway, in which sphingosine is a significant differential metabolite. When correlated with behavioral indicators in rats, an elevation in sphingosine levels in the PFC was associated with reduced depression-like behaviors and improved cognitive function (Figure 7A), signifying its high relevance to depression-like behaviors. Sphingosine is a crucial intermediate in the sphingolipid metabolic pathway that links ceramides and 1-phosphosphingosine. Ceramidase degrades neuroceramides into sphingosine, which sphingosine kinases phosphorylate into 1-phosphosphingosine. Recent studies have highlighted the importance of neuroceramides and 1-phosphosphingosine in brain health (van Kruining et al., 2020). Numerous studies have reported the involvement of 1-phosphosphingosine in various neurological and psychiatric disorders, including Alzheimer's disease (He et al., 2010; Asle-Rousta et al., 2013; van Kruining et al., 2020), depression, and

anxiety (Jang et al., 2011). In our study, the CUMS group exhibited a significant reduction in sphingosine levels in the PFC, indicating abnormal sphingolipid metabolism. However, quercetin administration substantially increased sphingosine levels in the PFC, further regulating neuroceramides and 1-phosphosphingosine levels, ultimately improving sphingolipid metabolism and alleviating depression-like behaviors.

Furthermore, quercetin reduced the levels of pantothenic acid in the HYP of CUMS rats, thereby modulating the biosynthesis pathway of pantothenic acid and coenzyme A (CoA). Pantothenic acid is a universal precursor of CoA, an essential cofactor in glucose, lipid, and protein metabolism (Leonardi et al., 2005; Jonczyk et al., 2008). There have been no direct reports on the association between pantothenic acid, CoA, and psychiatric disorders. However, our findings suggest that quercetin may indirectly ameliorate depression-like phenotypes by lowering hypothalamic pantothenic acid levels and improving pantothenic acid and CoA biosynthetic metabolism.

It is well known that the stability of the gut microbiota is crucial for maintaining host health, and gut dysbiosis is an important pathogenic factor in depression (Bosch et al., 2022; Radjabzadeh et al., 2022). In our study, we analyzed the changes in the gut microbiota in response to quercetin treatment in CUMS rats and the associations between gut microbiota alterations and brain metabolism changes to explore the potential mechanism by which quercetin exerts its therapeutic effects on depression-like phenotypes through the microbiota-gut-brain axis. We found that the α-diversity index of the gut microbiota in CUMS rats was significantly reduced, and quercetin treatment reversed this change (Figures 5A–C). β-Diversity analysis displayed that the microbial structure after quercetin intervention resembled that of the CON group (Figures 5D,E). These results indicate that in CUMS rats, quercetin can ameliorate gut microbiota dysbiosis and restores stability. The *Firmicutes/Bacteroidetes (F/B)* ratio, comprising the *Firmicutes* and *Bacteroidetes* phylum, affects gut microbiota homeostasis. In our study, the *Firmicutes* phylum in the colonic contents of rats significantly increased after CUMS stress, resulting in an elevated *F/B* ratio. However, quercetin intervention led to a marked decrease in the *Firmicutes* phylum and a subsequent reduction in the *F/B* ratio. The relationship between the *F/B* ratio and depression remains controversial due to the heterogeneity and complexity of depression (Jiang et al., 2015; Chen Z. et al., 2018; Barandouzi et al., 2020). Nevertheless, there is a wealth of reliable evidence that supports our findings. Jeffery et al. reported that the *F/B* ratio was significantly increased in patients with irritable bowel syndrome (IBS), obesity, and depression, accompanied by anxiety and depression-like behaviors (Jeffery et al., 2012). De Palma et al. demonstrated that transplantation of high *F/B* ratio feces induced anxiety and depression-like behaviors in mice (De Palma et al., 2017). Furthermore, at the genus level, quercetin reversed the changes in the abundance of 20 gut microbial genera in CUMS rats, which were highly correlated with depression-like phenotypes in rats (Figure 7B). Among them, 16 genera belong to the *Firmicutes* phylum, including *Romboutsia*, *Turicibacter*, and *Faecalibaculum*. Previous studies have linked *Romboutsia* and *Turicibacter* to circulating inflammation (IL-1β) and behavioral outcomes (hypersomnia and anxiety-like behavior), indicating that an increase in *Romboutsia* and *Turicibacter* exacerbates inflammation and anxiety-like behavior (Grant et al., 2021). *Faecalibaculum* produces short-chain fatty acids that are vital for improving cognitive function (D'Amato et al., 2020). Consistent with these findings, we found that quercetin significantly reduced *Romboutsia* and *Turicibacter* in the gut of CUMS rats and significantly increased *Faecalibaculum*, which reduced depression-like behaviors. Correlation analysis revealed that *Romboutsia* was positively correlated with 1,6-fructose diphosphate in HYP, *Turicibacter* was positively correlated with 1,6-fructose diphosphate in HIP and HYP, and *Faecalibaculum* was negatively correlated with 1,6-fructose diphosphate in HIP and HYP (Figure 7C). This indicates that *Romboutsia*, *Turicibacter*, and *Faecalibaculum*, regulated by quercetin, may further affect brain glucose metabolism, thereby potentially alleviating depression-like behaviors. *Bifidobacterium*, a member of the *Actinobacteria* phylum, is a well-studied probiotic known to improve depression-like behaviors in hosts (Ohland et al., 2013; Abildgaard et al., 2017a; Abildgaard et al., 2017b; Pinto-Sanchez et al., 2017). Our study found that quercetin increased *Bifidobacterium* abundance in CUMS rats, thereby potentially improving the depressive symptoms. Notably, *Bifidobacterium* was positively correlated with sphingosine in the PFC and negatively correlated with 1,6-fructose diphosphate and pantothenic acid in HIP and HYP. This suggests that quercetin may regulate the PFC sphingosine metabolism and the sugar metabolism in the HIP and HYP by modulating the *Bifidobacterium* in the gut, thereby potentially improving depression-like phenotypes. Moreover, 17 other genera, including *norank_f__UCG-010* and *Psychrobacter*, were identified as the key targets of quercetin in the gut microbiota of CUMS rats, particularly due to their strong correlation with brain metabolites (Figure 7C). However, these genera have not been thoroughly associated with depression, and their mechanisms require further studies.

In summary, our study provides new findings supporting the role of quercetin in alleviating depression-like phenotypes via multiple mechanisms. 1) Quercetin may regulate key metabolic pathways in the brain regions (PFC, HIP, and HYP) to alleviate depression-like behaviors induced by CUMS. 2) Quercetin may restore the gut microbiota balance by targeting specific bacteria (*Romboutsia*, *Turicibacter*, *Faecalibaculum*, and *Bifidobacterium*), contributing to its antidepressant effects. 3) Due to the correlation between behavioral changes, metabolite levels, and bacterial abundance in rats, quercetin may act on the microbiota-gut-brain axis to intervene in depression-like behaviors. Our findings provide information on the antidepressant potential and its possible mode of action, emphasizing the gut-brain relationship in depression treatment.

Limitations

1) We focused on the general effects of quercetin on the depressive-like phenotypes induced by CUMS in animal models, without making specific distinctions between individual resilience and susceptibility. 2) Our study utilized male rats, a choice that may not fully represent the female population. Given that depression is more prevalent in female population, it is essential that future research further incorporates considerations of gender differences. 3) This study identified potential metabolic pathways targeted by quercetin; however, the

specific mechanisms of action remain unclear. Further experimental research is required to investigate the detailed metabolic processes involved in these pathways. 4) We discovered several microbial targets that may be influenced by quercetin, including *bacteria like norank_f__UCG-010*, *Psychrobacter*, *unclassified_f__Ruminococcaceae*, and *Staphylococcus*. However, limited data are available for many of these targets, necessitating further exploration and in-depth studies. 5) Our results suggested an association between quercetin and alterations in the gut microbiota and metabolic profile; however, they did not definitively prove causation. Further research, including longitudinal studies and experimental interventions, is needed to elucidate the potential causal mechanisms underlying these observations. 6) Our attempt to explore the targets of quercetin in the microbiota-gut-brain axis is a step towards understanding the complex and multifaceted mechanisms of this axis. However, further research is needed to understand the effects of quercetin on the microbiota-gut-brain axis.

Data availability statement

The original contributions presented in the study are publicly available. The metabolomics data have been deposited in the MetaboLights database (https://www.ebi.ac.uk/metabolights/MTBLS9544), and the 16S rRNA sequencing data are available in the NCBI BioProject database (https://www.ncbi.nlm.nih.gov/bioproject/PRJNA1077291).

Ethics statement

The animal study was approved by the Guangzhou University of Chinese Medicine. The study was conducted in accordance with the local legislation and institutional requirements.

Author contributions

BL: Formal Analysis, Methodology, Software, Visualization, Writing–original draft, Writing–review and editing. YY: Data curation, Formal Analysis, Validation, Writing–original draft. TZ: Data curation, Investigation, Writing–review and editing. HX: Software, Visualization, Writing–review and editing. XW: Software, Validation, Writing–review and editing. GY: Validation, Writing–review and editing. XL: Investigation, Writing–review and editing. CY: Conceptualization, Funding acquisition, Project administration, Resources, Supervision, Writing–review and editing. L-LW: Conceptualization, Funding acquisition, Methodology, Project administration, Resources, Supervision, Writing–review and editing.

Funding

The author(s) declare that financial support was received for the research, authorship, and/or publication of this article. This work was supported by the National Natural Science Foundation of China (Nos 82174255 and 82074309) and the Major Basic Research Project of the Department of Education of Guangdong Province (2019KZDXM022). The funding source did not influence the study design, data collection, analysis, interpretation, manuscript writing, or decision to submit the article for publication.

Acknowledgments

We acknowledge support from the Integrative Medicine Research Center, School of Basic Medical Sciences, Guangzhou University of Chinese Medicine.

Conflict of interest

The authors declare that the research was conducted in the absence of any commercial or financial relationships that could be construed as a potential conflict of interest.

Publisher's note

Supplementary material

The Supplementary Material for this article can be found online at: https://www.frontiersin.org/articles/10.3389/fphar.2024.1362464/full#supplementary-material

References

Abildgaard, A., Elfving, B., Hokland, M., Lund, S., and Wegener, G. (2017a). Probiotic treatment protects against the pro-depressant-like effect of high-fat diet in Flinders Sensitive Line rats. *Brain Behav. Immun.* 65, 33–42. doi:10.1016/j.bbi.2017.04.017

Abildgaard, A., Elfving, B., Hokland, M., Wegener, G., and Lund, S. (2017b). Probiotic treatment reduces depressive-like behaviour in rats independently of diet. *Psychoneuroendocrinology* 79, 40–48. doi:10.1016/j.psyneuen.2017.02.014

Adibhatla, R. M., and Hatcher, J. F. (2008). Phospholipase A(2), reactive oxygen species, and lipid peroxidation in CNS pathologies. *BMB Rep.* 41 (8), 560–567. doi:10.5483/bmbrep.2008.41.8.560

Akoglu, H. (2018). User's guide to correlation coefficients. *Turk J. Emerg. Med.* 18 (3), 91–93. doi:10.1016/j.tjem.2018.08.001

Al-Massadi, O., Dieguez, C., Schneeberger, M., López, M., Schwaninger, M., Prevot, V., et al. (2021). Multifaceted actions of melanin-concentrating hormone on mammalian energy homeostasis. *Nat. Rev. Endocrinol.* 17 (12), 745–755. doi:10.1038/s41574-021-00559-1

Antoniuk, S., Bijata, M., Ponimaskin, E., and Wlodarczyk, J. (2019). Chronic unpredictable mild stress for modeling depression in rodents: meta-analysis of model reliability. *Neurosci. Biobehav Rev.* 99, 101–116. doi:10.1016/j.neubiorev.2018.12.002

Asle-Rousta, M., Oryan, S., Ahmadiani, A., and Rahnema, M. (2013). Activation of sphingosine 1-phosphate receptor-1 by SEW2871 improves cognitive function in Alzheimer's disease model rats. *EXCLI J.* 12, 449–461. doi:10.17877/DE290R-7354

Averina, O. V., Zorkina, Y. A., Yunes, R. A., Kovtun, A. S., Ushakova, V. M., Morozova, A. Y., et al. (2020). Bacterial metabolites of human gut microbiota correlating with depression. *Int. J. Mol. Sci.* 21 (23), 9234. doi:10.3390/ijms21239234

Babaei, F., Mirzababaei, M., and Nassiri-Asl, M. (2018). Quercetin in food: possible mechanisms of its effect on memory. *J. Food Sci.* 83 (9), 2280–2287. doi:10.1111/1750-3841.14317

Barandouzi, Z. A., Starkweather, A. R., Henderson, W. A., Gyamfi, A., and Cong, X. S. (2020). Altered composition of gut microbiota in depression: a systematic review. *Front. Psychiatry* 11, 541. doi:10.3389/fpsyt.2020.00541

Baxter, L. R., Jr., Schwartz, J. M., Phelps, M. E., Mazziotta, J. C., Guze, B. H., Selin, C. E., et al. (1989). Reduction of prefrontal cortex glucose metabolism common to three types of depression. *Arch. Gen. Psychiatry* 46 (3), 243–250. doi:10.1001/archpsyc.1989.01810030049007

Birkmayer, J. G. (1996). Coenzyme nicotinamide adenine dinucleotide: new therapeutic approach for improving dementia of the Alzheimer type. *Ann. Clin. Lab. Sci.* 26 (1), 1–9. doi:10.1016/S0065-2423(08)60428-X

Bosch, J. A., Nieuwdorp, M., Zwinderman, A. H., Deschasaux, M., Radjabzadeh, D., Kraaij, R., et al. (2022). The gut microbiota and depressive symptoms across ethnic groups. *Nat. Commun.* 13 (1), 7129. doi:10.1038/s41467-022-34504-1

Bschor, T., Bauer, M., and Adli, M. (2014). Chronic and treatment resistant depression: diagnosis and stepwise therapy. *Dtsch. Arztebl Int.* 111 (45), 766–775. doi:10.3238/arztebl.2014.0766

Castro, J. E., Diessler, S., Varea, E., Márquez, C., Larsen, M. H., Cordero, M. I., et al. (2012). Personality traits in rats predict vulnerability and resilience to developing stress-induced depression-like behaviors, HPA axis hyper-reactivity and brain changes in pERK1/2 activity. *Psychoneuroendocrinology* 37 (8), 1209–1223. doi:10.1016/j.psyneuen.2011.12.014

Chen, S., Tang, Y., Gao, Y., Nie, K., Wang, H., Su, H., et al. (2022). Antidepressant potential of quercetin and its glycoside derivatives: a comprehensive review and update. *Front. Pharmacol.* 13, 865376. doi:10.3389/fphar.2022.865376

Chen, S., Zhou, Y., Chen, Y., and Gu, J. (2018a). fastp: an ultra-fast all-in-one FASTQ preprocessor. *Bioinformatics* 34 (17), i884–i890. doi:10.1093/bioinformatics/bty560

Chen, Z., Li, J., Gui, S., Zhou, C., Chen, J., Yang, C., et al. (2018b). Comparative metaproteomics analysis shows altered fecal microbiota signatures in patients with major depressive disorder. *Neuroreport* 29 (5), 417–425. doi:10.1097/WNR.0000000000000985

Cherix, A., Poitry-Yamate, C., Lanz, B., Zanoletti, O., Grosse, J., Sandi, C., et al. (2022). Deletion of Crtc1 leads to hippocampal neuroenergetic impairments associated with depressive-like behavior. *Mol. Psychiatry* 27 (11), 4485–4501. doi:10.1038/s41380-022-01791-5

Cho, W. H., Noh, K., Lee, B. H., Barcelon, E., Jun, S. B., Park, H. Y., et al. (2022). Hippocampal astrocytes modulate anxiety-like behavior. *Nat. Commun.* 13 (1), 6536. doi:10.1038/s41467-022-34201-z

Cruz-Pereira, J. S., Rea, K., Nolan, Y. M., O'Leary Of, Dinan, T. G., and Cryan, J. F. (2020). Depression's unholy trinity: dysregulated stress, immunity, and the microbiome. *Annu. Rev. Psychol.* 71, 49–78. doi:10.1146/annurev-psych-122216-011613

D'Amato, A., Di Cesare Mannelli, L., Lucarini, E., Man, A. L., Le Gall, G., Branca, J. J. V., et al. (2020). Faecal microbiota transplant from aged donor mice affects spatial learning and memory via modulating hippocampal synaptic plasticity- and neurotransmission-related proteins in young recipients. *Microbiome* 8 (1), 140. doi:10.1186/s40168-020-00914-w

Demarin, V., Podobnik, S. S., Storga-Tomic, D., and Kay, G. (2004). Treatment of Alzheimer's disease with stabilized oral nicotinamide adenine dinucleotide: a randomized, double-blind study. *Drugs Exp. Clin. Res.* 30 (1), 27–33.

De Palma, G., Lynch, M. D., Lu, J., Dang, V. T., Deng, Y., Jury, J., et al. (2017). Transplantation of fecal microbiota from patients with irritable bowel syndrome alters gut function and behavior in recipient mice. *Sci. Transl. Med.* 9 (379), eaaf6397. doi:10.1126/scitranslmed.aaf6397

Grant, C. V., Loman, B. R., Bailey, M. T., and Pyter, L. M. (2021). Manipulations of the gut microbiome alter chemotherapy-induced inflammation and behavioral side effects in female mice. *Brain Behav. Immun.* 95, 401–412. doi:10.1016/j.bbi.2021.04.014

Gu, W., and Tong, Z. (2020). Clinical application of metabolomics in pancreatic diseases: a mini-review. *Lab. Med.* 51 (2), 116–121. doi:10.1093/labmed/lmz046

Guilloux, J. P., Seney, M., Edgar, N., and Sibille, E. (2011). Integrated behavioral z-scoring increases the sensitivity and reliability of behavioral phenotyping in mice: relevance to emotionality and sex. *J. Neurosci. Methods* 197 (1), 21–31. doi:10.1016/j.jneumeth.2011.01.019

Hammen, C. (2018). Risk factors for depression: an autobiographical review. *Annu. Rev. Clin. Psychol.* 14, 1–28. doi:10.1146/annurev-clinpsy-050817-084811

He, X., Huang, Y., Li, B., Gong, C. X., and Schuchman, E. H. (2010). Deregulation of sphingolipid metabolism in Alzheimer's disease. *Neurobiol. Aging* 31 (3), 398–408. doi:10.1016/j.neurobiolaging.2008.05.010

Hennings, J. M., Schaaf, L., and Fulda, S. (2012). Glucose metabolism and antidepressant medication. *Curr. Pharm. Des.* 18 (36), 5900–5919. doi:10.2174/138161212803523662

Horowitz, M. A., and Zunszain, P. A. (2015). Neuroimmune and neuroendocrine abnormalities in depression: two sides of the same coin. *Ann. N. Y. Acad. Sci.* 1351, 68–79. doi:10.1111/nyas.12781

Hosseini, A., Razavi, B. M., Banach, M., and Hosseinzadeh, H. (2021). Quercetin and metabolic syndrome: a review. *Phytother. Res.* 35 (10), 5352–5364. doi:10.1002/ptr.7144

Huang, F., and Wu, X. (2021). Brain neurotransmitter modulation by gut microbiota in anxiety and depression. *Front. Cell Dev. Biol.* 9, 649103. doi:10.3389/fcell.2021.649103

Jang, S., Kim, D., Lee, Y., Moon, S., and Oh, S. (2011). Modulation of sphingosine 1-phosphate and tyrosine hydroxylase in the stress-induced anxiety. *Neurochem. Res.* 36 (2), 258–267. doi:10.1007/s11064-010-0313-1

Jeffery, I. B., O'Toole, P. W., Öhman, L., Claesson, M. J., Deane, J., Quigley, E. M., et al. (2012). An irritable bowel syndrome subtype defined by species-specific alterations in faecal microbiota. *Gut* 61 (7), 997–1006. doi:10.1136/gutjnl-2011-301501

Jiang, H., Ling, Z., Zhang, Y., Mao, H., Ma, Z., Yin, Y., et al. (2015). Altered fecal microbiota composition in patients with major depressive disorder. *Brain Behav. Immun.* 48, 186–194. doi:10.1016/j.bbi.2015.03.016

Jonczyk, R., Ronconi, S., Rychlik, M., and Genschel, U. (2008). Pantothenate synthetase is essential but not limiting for pantothenate biosynthesis in Arabidopsis. *Plant Mol. Biol.* 66 (1-2), 1–14. doi:10.1007/s11103-007-9248-6

Kashyap, D., Garg, V. K., Tuli, H. S., Yerer, M. B., Sak, K., Sharma, A. K., et al. (2019). Fisetin and quercetin: promising flavonoids with chemopreventive potential. *Biomolecules* 9 (5), 174. doi:10.3390/biom9050174

Kennedy, S. H., Evans, K. R., Krüger, S., Mayberg, H. S., Meyer, J. H., McCann, S., et al. (2001). Changes in regional brain glucose metabolism measured with positron emission tomography after paroxetine treatment of major depression. *Am. J. Psychiatry* 158 (6), 899–905. doi:10.1176/appi.ajp.158.6.899

Kornhuber, J., Rhein, C., Müller, C. P., and Mühle, C. (2015). Secretory sphingomyelinase in health and disease. *Biol. Chem.* 396 (6-7), 707–736. doi:10.1515/hsz-2015-0109

Labots, M., Laarakker, M. C., Ohl, F., and van Lith, H. A. (2016). Consomic mouse strain selection based on effect size measurement, statistical significance testing and integrated behavioral z-scoring: focus on anxiety-related behavior and locomotion. *BMC Genet.* 17 (1), 95. doi:10.1186/s12863-016-0411-4

Labots, M. M., Laarakker, M. C. M., Schetters, D. D., Arndt, S. S. S., and van Lith, H. A. H. (2018). An improved procedure for integrated behavioral z-scoring illustrated with modified Hole Board behavior of male inbred laboratory mice. *J. Neurosci. Methods* 293, 375–388. doi:10.1016/j.jneumeth.2017.09.003

Lages, Y. V. M., Rossi, A. D., Krahe, T. E., and Landeira-Fernandez, J. (2021). Effect of chronic unpredictable mild stress on the expression profile of serotonin receptors in rats and mice: a meta-analysis. *Neurosci. Biobehav Rev.* 124, 78–88. doi:10.1016/j.neubiorev.2021.01.020

Leonardi, R., Zhang, Y. M., Rock, C. O., and Jackowski, S. (2005). Coenzyme A: back in action. *Prog. Lipid Res.* 44 (2-3), 125–153. doi:10.1016/j.plipres.2005.04.001

Li, C. T., Su, T. P., Wang, S. J., Tu, P. C., and Hsieh, J. C. (2015). Prefrontal glucose metabolism in medication-resistant major depression. *Br. J. Psychiatry* 206 (4), 316–323. doi:10.1192/bjp.bp.113.140434

Li, Y., Yao, J., Han, C., Yang, J., Chaudhry, M. T., Wang, S., et al. (2016). Quercetin, inflammation and immunity. *Nutrients* 8 (3), 167. doi:10.3390/nu8030167

Lin, S., Huang, L., Luo, Z. C., Li, X., Jin, S. Y., Du, Z. J., et al. (2022). The ATP level in the medial prefrontal cortex regulates depressive-like behavior via the medial prefrontal cortex-lateral habenula pathway. *Biol. Psychiatry* 92 (3), 179–192. doi:10.1016/j.biopsych.2022.02.014

Liu, C., Zhao, D., Ma, W., Guo, Y., Wang, A., Wang, Q., et al. (2016). Denitrifying sulfide removal process on high-salinity wastewaters in the presence of Halomonas sp. *Appl. Microbiol. Biotechnol.* 100 (3), 1421–1426. doi:10.1007/s00253-015-7039-6

Liu, K., Li, H., Zeng, N., Lu, W., Wu, X., Xu, H., et al. (2023). Decline of stress resilience in aging rats: focus on choroid plexus-cerebrospinal fluid-hippocampus. *World J. Biol. Psychiatry* 24 (6), 508–522. doi:10.1080/15622975.2022.2151044

Ma, J., Qi, X., Yang, C., Pan, R., Wang, S., Wu, J., et al. (2018). Calhm2 governs astrocytic ATP releasing in the development of depression-like behaviors. *Mol. Psychiatry* 23 (4), 883–891. doi:10.1038/mp.2017.229

Ma, Z. X., Zhang, R. Y., Rui, W. J., Wang, Z. Q., and Feng, X. (2021). Quercetin alleviates chronic unpredictable mild stress-induced depressive-like behaviors by promoting adult hippocampal neurogenesis via FoxG1/CREB/BDNF signaling pathway. *Behav. Brain Res.* 406, 113245. doi:10.1016/j.bbr.2021.113245

Magoč, T., and Salzberg, S. L. (2011). FLASH: fast length adjustment of short reads to improve genome assemblies. *Bioinformatics* 27 (21), 2957–2963. doi:10.1093/bioinformatics/btr507

Marcolongo-Pereira, C., Castro, F., Barcelos, R. M., Chiepe, K., Rossoni Junior, J. V., Ambrosio, R. P., et al. (2022). Neurobiological mechanisms of mood disorders: stress

vulnerability and resilience. *Front. Behav. Neurosci.* 16, 1006836. doi:10.3389/fnbeh.2022.1006836

Ohland, C. L., Kish, L., Bell, H., Thiesen, A., Hotte, N., Pankiv, E., et al. (2013). Effects of Lactobacillus helveticus on murine behavior are dependent on diet and genotype and correlate with alterations in the gut microbiome. *Psychoneuroendocrinology* 38 (9), 1738–1747. doi:10.1016/j.psyneuen.2013.02.008

Pinto-Sanchez, M. I., Hall, G. B., Ghajar, K., Nardelli, A., Bolino, C., Lau, J. T., et al. (2017). Probiotic Bifidobacterium longum NCC3001 reduces depression scores and alters brain activity: a pilot study in patients with irritable bowel syndrome. *Gastroenterology* 153 (2), 448–459. doi:10.1053/j.gastro.2017.05.003

Radjabzadeh, D., Bosch, J. A., Uitterlinden, A. G., Zwinderman, A. H., Ikram, M. A., van Meurs, J. B. J., et al. (2022). Gut microbiome-wide association study of depressive symptoms. *Nat. Commun.* 13 (1), 7128. doi:10.1038/s41467-022-34502-3

Rauf, A., Imran, M., Khan, I. A., Ur-Rehman, M., Gilani, S. A., Mehmood, Z., et al. (2018). Anticancer potential of quercetin: a comprehensive review. *Phytother. Res.* 32 (11), 2109–2130. doi:10.1002/ptr.6155

Russo, M., Spagnuolo, C., Tedesco, I., Bilotto, S., and Russo, G. L. (2012). The flavonoid quercetin in disease prevention and therapy: facts and fancies. *Biochem. Pharmacol.* 83 (1), 6–15. doi:10.1016/j.bcp.2011.08.010

Sah, S. P., Tirkey, N., Kuhad, A., and Chopra, K. (2011). Effect of quercetin on lipopolysaccharide induced-sickness behavior and oxidative stress in rats. *Indian J. Pharmacol.* 43 (2), 192–196. doi:10.4103/0253-7613.77365

Şahin, T. D., Gocmez, S. S., Duruksu, G., Yazir, Y., and Utkan, T. (2020). Resveratrol and quercetin attenuate depressive-like behavior and restore impaired contractility of vas deferens in chronic stress-exposed rats: involvement of oxidative stress and inflammation. *Naunyn Schmiedeb. Arch. Pharmacol.* 393 (5), 761–775. doi:10.1007/s00210-019-01781-5

Schloss, P. D., Westcott, S. L., Ryabin, T., Hall, J. R., Hartmann, M., Hollister, E. B., et al. (2009). Introducing mothur: open-source, platform-independent, community-supported software for describing and comparing microbial communities. *Appl. Environ. Microbiol.* 75 (23), 7537–7541. doi:10.1128/AEM.01541-09

Schober, P., Boer, C., and Schwarte, L. A. (2018). Correlation coefficients: appropriate use and interpretation. *Anesth. Analg.* 126 (5), 1763–1768. doi:10.1213/ANE.0000000000002864

Segata, N., Izard, J., Waldron, L., Gevers, D., Miropolsky, L., Garrett, W. S., et al. (2011). Metagenomic biomarker discovery and explanation. *Genome Biol.* 12 (6), R60. doi:10.1186/gb-2011-12-6-r60

Solem, S., Hagen, R., Wang, C. E., Hjemdal, O., Waterloo, K., Eisemann, M., et al. (2017). Metacognitions and mindful attention awareness in depression: a comparison of currently depressed, previously depressed and never depressed individuals. *Clin. Psychol. Psychother.* 24 (1), 94–102. doi:10.1002/cpp.1983

Suganthy, N., Devi, K. P., Nabavi, S. F., Braidy, N., and Nabavi, S. M. (2016). Bioactive effects of quercetin in the central nervous system: focusing on the mechanisms of actions. *Biomed. Pharmacother.* 84, 892–908. doi:10.1016/j.biopha.2016.10.011

Torrisi, S. A., Lavanco, G., Maurel, O. M., Gulisano, W., Laudani, S., Geraci, F., et al. (2021). A novel arousal-based individual screening reveals susceptibility and resilience to PTSD-like phenotypes in mice. *Neurobiol. Stress* 14, 100286. doi:10.1016/j.ynstr.2020.100286

Ulusoy, H. G., and Sanlier, N. (2020). A minireview of quercetin: from its metabolism to possible mechanisms of its biological activities. *Crit. Rev. Food Sci. Nutr.* 60 (19), 3290–3303. doi:10.1080/10408398.2019.1683810

van Kruining, D., Luo, Q., van Echten-Deckert, G., Mielke, M. M., Bowman, A., Ellis, S., et al. (2020). Sphingolipids as prognostic biomarkers of neurodegeneration, neuroinflammation, and psychiatric diseases and their emerging role in lipidomic investigation methods. *Adv. Drug Deliv. Rev.* 159, 232–244. doi:10.1016/j.addr.2020.04.009

Wang, X., He, H. J., Xiong, X., Zhou, S., Wang, W. W., Feng, L., et al. (2021). NAD(+) in Alzheimer's disease: molecular mechanisms and systematic therapeutic evidence obtained *in vivo*. *Front. Cell Dev. Biol.* 9, 668491. doi:10.3389/fcell.2021.668491

Willner, P. (2017). The chronic mild stress (CMS) model of depression: history, evaluation and usage. *Neurobiol. Stress* 6, 78–93. doi:10.1016/j.ynstr.2016.08.002

Yadav, R. S., and Tiwari, N. K. (2014). Lipid integration in neurodegeneration: an overview of Alzheimer's disease. *Mol. Neurobiol.* 50 (1), 168–176. doi:10.1007/s12035-014-8661-5

Yang, S., Zhou, H., Wang, G., Zhong, X. H., Shen, Q. L., Zhang, X. J., et al. (2020). Quercetin is protective against short-term dietary advanced glycation end products intake induced cognitive dysfunction in aged ICR mice. *J. Food Biochem.* 44 (4), e13164. doi:10.1111/jfbc.13164

Yao, S., Xu, M. D., Wang, Y., Zhao, S. T., Wang, J., Chen, G. F., et al. (2023). Astrocytic lactate dehydrogenase A regulates neuronal excitability and depressive-like behaviors through lactate homeostasis in mice. *Nat. Commun.* 14 (1), 729. doi:10.1038/s41467-023-36209-5

Zhang, J., Ning, L., and Wang, J. (2020). Dietary quercetin attenuates depressive-like behaviors by inhibiting astrocyte reactivation in response to stress. *Biochem. Biophys. Res. Commun.* 533 (4), 1338–1346. doi:10.1016/j.bbrc.2020.10.016

frontiers | Frontiers in Pharmacology

TYPE Original Research
PUBLISHED 01 May 2024
DOI 10.3389/fphar.2024.1388784

OPEN ACCESS

EDITED BY
Nouria Lakhdar-Ghazal,
Mohammed V University, Morocco

REVIEWED BY
Willias Masocha,
Kuwait University, Kuwait
Philippe De Deurwaerdere,
Université de Bordeaux, France

*CORRESPONDENCE
Alessandro Di Cerbo,
alessandro.dicerbo@unicam.it
Amany Abdel-Rahman Mohamed,
amanyrahman292@gmail.com

RECEIVED 20 February 2024
ACCEPTED 11 April 2024
PUBLISHED 01 May 2024

CITATION
Alotaibi BS, Abdel-Rahman Mohamed A, Abd-Elhakim YM, Noreldin AE, Elhamouly M, Khamis T, El-Far AH, Alosaimi ME, Dahran N, Alqahtani LS, Nicotra M, El-Gamal M and Di Cerbo A (2024), Exploring the link between pyrethroids exposure and dopaminergic degeneration through morphometric, immunofluorescence, and *in-silico* approaches: the therapeutic role of chitosan-encapsulated curcumin nanoparticles. *Front. Pharmacol.* 15:1388784. doi: 10.3389/fphar.2024.1388784

Exploring the link between pyrethroids exposure and dopaminergic degeneration through morphometric, immunofluorescence, and *in-silico* approaches: the therapeutic role of chitosan-encapsulated curcumin nanoparticles

Badriyah S. Alotaibi[1], Amany Abdel-Rahman Mohamed[2]*, Yasmina M. Abd-Elhakim[2], Ahmed E. Noreldin[3], Moustafa Elhamouly[4], Tarek Khamis[5,6], Ali H. El-Far[7], Manal E. Alosaimi[8], Naief Dahran[9], Leena S. Alqahtani[10], Mario Nicotra[11], Mohamed El-Gamal[12,13] and Alessandro Di Cerbo[11]*

[1]Department of Pharmaceutical Sciences, College of Pharmacy, Princess Nourah bint Abdulrahman University, Riyadh, Saudi Arabia, [2]Department of Forensic Medicine and Toxicology, Faculty of Veterinary Medicine, Zagazig University, Zagazig, Egypt, [3]Department of Histology and Cytology, Faculty of Veterinary Medicine, Damanhour University, Damanhour, Egypt, [4]Cytology and Histology Department, Faculty of Veterinary Medicine, University of Sadat City, Sadat City, Egypt, [5]Department of Pharmacology, Faculty of Veterinary Medicine, Zagazig University, Zagazig, Egypt, [6]Laboratory of Biotechnology, Faculty of Veterinary Medicine, Zagazig University, Zagazig, Egypt, [7]Department of Biochemistry, Faculty of Veterinary Medicine, Damanhour University, Damanhour, Egypt, [8]Department of Basic Health Sciences, College of Medicine, Princess Nourah bint Abdulrahman University, Riyadh, Saudi Arabia, [9]Department of Anatomy, Faculty of Medicine, University of Jeddah, Jeddah, Saudi Arabia, [10]Department of Biochemistry, College of Science, University of Jeddah, Jeddah, Saudi Arabia, [11]School of Biosciences and Veterinary Medicine, University of Camerino, Matelica, Italy, [12]Forensic Medicine and Clinical Toxicology Department, Faculty of Medicine, Mansoura University, Mansoura, Egypt, [13]Department of Biological Sciences, Faculty of Science, New Mansoura University, New Mansoura City, Egypt

Introduction: The synthetic pyrethroid derivative fenpropathrin (FNE), a commonly used insecticide, has been associated with various toxic effects in mammals, particularly neurotoxicity. The study addressed the hallmarks of the pathophysiology of Parkinson's disease upon oral exposure to fenpropathrin (FNE), mainly the alteration of dopaminergic markers, oxidative stress, and molecular docking in rat models. In addition, the protective effect of curcumin-encapsulated chitosan nanoparticles (CRM-Chs-NPs) was also assessed.

Methods: In a 60-day trial, 40 male Sprague Dawley rats were divided into 4 groups: Control, CRM-Chs-NPs (curcumin-encapsulated chitosan nanoparticles), FNE (15 mg/kg bw), and FNE + CRM-Chs-NPs.

Results: FNE exposure induced reactive oxygen species generation, ATP production disruption, activation of inflammatory and apoptotic pathways, mitochondrial function and dynamics impairment, neurotransmitter level perturbation, and mitophagy promotion in rat brains. Molecular docking analysis revealed that FNE interacts with key binding sites of dopamine synthesis and transport proteins. On the other hand, CRM-Chs-NPs mitigated FNE's toxic effects by enhancing mitochondrial dynamics, antioxidant activity, and ATP production and promoting anti-inflammatory and antiapoptotic responses.

Conclusion: In summary, FNE appears to induce dopaminergic degeneration through various mechanisms, and CRM-Chs-NPs emerged as a potential therapeutic intervention for protecting the nervous tissue microenvironment.

KEYWORDS

curcumin-encapsulated chitosan nanoparticles, dopamine, fenpropathrin, mitochondrial dynamics, antioxidant activity, anti-inflammatory activity, antiapoptotic activity

1 Introduction

Pyrethroids, widely used for their insecticidal properties, raised great concern due to their potential role in disrupting crucial cellular processes by impairing mitochondrial dynamics (Gajendiran and Abraham, 2018). The residues of pyrethroids can alter mitochondrial morphology, dynamics, and function, impairing energy production and cellular homeostasis (Jana et al., 2011). Additionally, exposure to these pesticides is associated with heightened oxidative stress, where an imbalance between reactive oxygen species (ROS) production and antioxidant defenses may trigger neurodegenerative phenomena (Mohamed et al., 2019). Moreover, pyrethroid-induced mitochondrial dysfunction is correlated with the accumulation of senescent mitochondria, impairing their clearance and contributing to cellular damage (Cui et al., 2010; Ryan et al., 2015). Mitochondrial dysfunction is also a major cause of neurodegenerative diseases, especially Parkinson's disease (PD) (Moradi Vastegani et al., 2023).

Fenpropathrin (FNE), classified as an alpha-cyano pyrethroid, is known to induce neurotoxicological responses (Weiner et al., 2009). Initially, due to its rapid metabolism and clearance, FNE was perceived as relatively harmless to mammals (Proudfoot, 2005). However, it can exert prolonged effects when introduced into aquatic environments, posing a substantial threat to fish populations by accumulating within their tissues (Brander et al., 2016). Research revealed that FNE and deltamethrin can reduce kynurenic acid (KYNA) concentration in rat cortical slices (Zielinska et al., 2005), reflecting the findings in PD patients' brain tissue and cerebrospinal fluid (Ogawa et al., 1992).

Curcumin (CRM), a bioactive compound found in the spice turmeric, has garnered significant attention for its diverse therapeutic properties. Renowned for its potent anti-inflammatory, antioxidant, and neuroprotective effects, curcumin has been extensively studied for its potential in combating various diseases and promoting overall health. Its ability to modulate multiple cellular signaling pathways makes it a promising candidate for the prevention and treatment of conditions such as cancer, neurodegenerative diseases, cardiovascular disorders, and metabolic syndrome.

Moreover, curcumin's favorable safety profile and relatively low cost further contribute to its appeal as a natural remedy. However, challenges like poor bioavailability have prompted ongoing research to enhance its efficacy through innovative delivery systems (Bavarsad et al., 2019). Various formulations have been employed to enhance the bioavailability of curcumin, a compound with neuroprotective potential (Arya et al., 2018). These innovative approaches aim to protect curcumin from chemical degradation and include methods such as encapsulation into nanoparticles or microparticles, often integrated into food or supplements. In this sense, polysaccharide-based systems, e.g., chitosan, emerged as promising tools due to their exceptional physicochemical properties (Khater et al., 2021). Chitosan (Chs), a natural polysaccharide, possesses advantageous traits, including biocompatibility, biodegradability, and mucoadhesive capabilities (Lin et al., 2022). Chitosan-encapsulated curcumin nanoparticles (CRM-Chs-NPs) have already shown improved stability of curcumin in cervical cancer cells, bioavailability, and cellular uptake. Besides, CRM-Chs-NPs demonstrated an elevated uptake in the SiHa cells regarding free CRM (Khan et al., 2018).

Neuron impairment, followed by increased ROS production (Golpich et al., 2017), can lead to the onset and worsening of PD (Abdelnour et al., 2020; Agnihotri and Aruoma, 2020). Moreover, specific genetic mutations in genes like PTEN-induced kinase 1 (*Pink1*), *Parkin*, and protein deglycase 1 (*DJ-1*) can also play a crucial role in PD if they occur in a recessive manner (Sekine and Youle, 2018). These genes are essential for maintaining a healthy balance in the mitochondria and a process called mitophagy, which helps to remove damaged mitochondria (Burbulla et al., 2017).

Additionally, neurological degeneration and PD can also be triggered by exposure to environmental toxins like 1-methyl-4-phenyl-1,2,3,6-tetrahydropyridine (MPTP), 6-hydroxydopamine hydrobromide (6-OHDA), rotenone, and FNE (Filichia et al., 2016). These pollutants can impair mitochondria function or even disrupt them. The mitochondrial complexes I-V can be directly or indirectly affected by oxidative stress resulting from exposure to FNE, leading to energy deficits, increased ROS production, mitochondrial dysfunction, and ultimately, neuronal degeneration, a central feature of PD (Tong et al., 2018). Mitochondrial complexes can have several detrimental effects, including energy deficits via reduced ATP production from damaged complexes, ROS accumulation, and oxidative stress that further damage the complexes and exacerbate oxidative damage (Sas et al., 2007; Reddy et al., 2011).

This study aimed to understand the FNE hallmarks of the pathophysiology of PD, namely, the alteration of dopaminergic

markers and oxidative stress, as well as the examination of key markers through histological and immunohistochemical staining in a rat model. Additionally, the potential benefits of CRM-Chs-NPs in counteracting the harmful effects of FNE on nerve tissue were explored. The selected dose of FNE was based on the human exposure levels as the NOAEL, identified at 300 ppm (equivalent to 15 mg/kg/bw per day), and was determined by assessing clinical indicators such as tremors, reductions in body weight, decreased blood clotting time in females, and potentially elevated alkaline phosphatase levels in both sexes at 600 ppm (equivalent to 30 mg/kg/bw per day) (Hend and Butterworth, 1976).

Additionally, the dose of CRM-Chs-NPs used in the current study was based on recent research findings, which strongly support their effectiveness and demonstrated their superior efficacy and tissue bioavailability compared to molecular curcumin in countering the harmful effects of FNE exposure on the reproductive system and hepatotoxicity (Alqahtani et al., 2023; Mohamed et al., 2023).

2 Materials and methods

2.1 Preparation and characterization of CRM-Chs nanoparticles (CRM-Chs-NPs)

CRM-Chs-NPs were prepared using the standard ionic gelation synthesis method (Kunjachan and Jose, 2010). The morphology of nanoparticles was investigated using high-resolution transmission electron microscopy (JEM-2100, JEOL, Japan, Tokyo). Zeta potential and particle size analyses were conducted using a Zeta Sizer (Nano-ZS, Malvern Instruments Ltd., Zetasizer Ver, Malvern, United Kingdom). Furthermore, the CRM-Chs-NPs surface functional groups were identified through Fourier-Transform Infrared (FTIR) spectroscopy spanning the 400–4,000 cm^{-1} range (ALPHA II Compact FT-IR spectrometer, Bruker, Germany). Notably, the distinctive characteristics of nanoparticles were previously elucidated and documented in a study (Alqahtani et al., 2023).

2.2 Animals and experimental design

A group of 40 adult male Sprague Dawley rats (10-week-old and mean weight 142 ± 0.46 g) from the Animal Housing Unit at Zagazig University's Faculty of Veterinary Medicine were enrolled. The rats were acclimated for 12 days with a 12-h light/dark cycle with unrestricted access to food and water.

Rats were randomly assigned into 4 groups: the first group (control) received corn oil (1 mL/animal) (Arma Food Industries, Egypt), the second group (CRM-Chs-Nps) received chitosan-encapsulated curcumin in distilled water at 50 mg/kg bw (Abd-Elhakim et al., 2022), the third group (FNE) received FNE at 15 mg/kg bw (Mohamed et al., 2019), and fourth group (CRM-Chs NPs + FNE) simultaneously received the chitosan-encapsulated curcumin and FNE at the same above-cited concentrations. The corn oil vehicle was used to dissolve FNE, ensuring consistency in administration across experimental groups. In our study, distilled water was not utilized as a vehicle rather it constituted a component of the preparation of CRM-Chs-NPs, tested separately from FNE. Throughout the 60-day experiment, each group was orally given the compounds via a dedicated feeding needle.

The study was approved by the Ethics Committee at Zagazig University, Egypt (Approval number: ZU-IACUC/2/F/101/2022). Procedures were conducted according to the regulations outlined in the U.K. Animals (Scientific Procedures) Act of 1986, the EU Directive 2010/63/EU on animal experimentation, and the principles and recommendations outlined in the ARRIVE guidelines (Percie du Sert et al., 2020).

2.3 Chemicals

FNE (Danitol®) was purchased from Sumitomo Chemical Co. Ltd (Saint Didier au Mont d'Or, France), CRM from Sigma Aldrich Co. (St. Louis, Missouri, United States), and low molecular weight chitosan (MW: 100–300 KDa) from Across Co. Ltd. (Chuncheon-si, South Korea). Notably, all other compounds and reagents in this analysis exhibited a ≥99.99% purity. GSH and Caspase 3 were purchased from (Cusabio Biotech Co., Ltd.) (Beutler et al., 1963), SOD, CAT, and MDA (MyBioSource, San Diego, United States) (Spitz and Oberley, 1989), ROS (Life Sciences, Mongkok Ki, Hongkong), ATP (Assay Genie, Dublin, Ireland) (Aebi, 1984), glutamate and dopamine from Biomatik (Wilmington, Delaware, United States).

2.4 Collection of samples and biochemical analysis

The rats were anesthetized by isoflurane 5% inhalation via a mask and air pump (R510–25, RWD life science, San Diego, CA) for 3 min, and then were euthanized by cervical dislocation. The two primary regions of interest for dopamine, glutamate, and oxidative stress markers analysis are the striatum and the prefrontal cortex. These brain tissue regions were included for the preparation of tissue homogenate, which was placed in 20 mL of 1X PBS and stored overnight at ≤ −20 °C. Then, each sample was centrifuged at 20,000 ×*g* for 15 min. The collected supernatant was stored for the detection of oxidative stress [malondialdehyde (MDA), ROS and adenosine triphosphate (ATP) and antioxidant (superoxide dismutase (SOD), catalase (CAT) and glutathione (GSH)] markers, neurotransmitters (dopamine, glutamate) and apoptotic indices (Caspase 3) using Enzyme-linked Immunosorbent Assay (ELISA) according to the manufacturer instructions. The samples of brain hemispheres for gene expression were frozen at −80 °C. Other tissue samples were separated in a neutral buffered formaldehyde solution for histopathological and immunohistochemical staining sections. The brain was dissected into the cerebrum, including the hippocampus and cerebellum. The cerebellum was longitudinally dissected, and the hippocampus was cross-sectionally dissected at the mammillary body and tuber cinereum level, according to Treuting et al. (2017). Cerebral samples were taken from the midbrain above the hippocampus, where dopaminergic neurons are common.

TABLE 1 Primers sequences, accession number, and product size for the quantitative RT-PCR for the analyzed genes in the brain tissue.

Target gene	Primers sequences	Accession no.	pb
Gapdh	5′-GGCACAGTCAAGGCTGAGAATG-3′	NM_017008.4	143
	3′-ATGGTGGTGAAGACGCCAGTA-5′		
Bax	5′-CGAATTGGCGATGAACTGGA-3′	NM_017059.2	109
	3′-CAAACATGTCAGCTGCCACAC-5′		
Bcl-2	5′-GACTGAGTACCTGAACCGGCATC-3′	NM_016993.1	135
	3′-CTGAGCAGCGTCTTCAGAGACA-5′		
Casp 3	5′-GAGACAGACAGTGGAACTGACGATG-3′	NM_012922.2	147
	3′-GGCGCAAAGTGACTGGATGA-5′		
Sod1	5′-TTGGCCGTACTATGG TGGTC-3′	NM_017050.1	120
	3′-GGGCAATCCCAATCA CACCA-5′		
5-Nadh oxidoreductase (Complex I)	5′-AGAGCCTCACAGACAATGGC-3′	NM_001005550.1	70
	3′-ATGGCTCCTCTACTGCCTGA-5′		
Succinate oxidoreductase (Complex II)	5′-GCTCTTGCTGAGACACATCG-3′	NM_001005534.1	191
	3′-TTGCCATGGGAAGAGACCAC-5		
Cytochrome c oxidoreductase Complex (III)	5′-CTCAGCGTGTGGACTGAATA-3′	NM_001013185.1	127
	3′-CCAGGTTCTGCAGGTGAGTT-5′		
Cytochrome c oxidase Complex (IV)	5′-GGAACCACACGCTTTTCCAC-3′	NM_012812.3	71
	3′-GAGTCTTCAAGGCTGCTCGT-5′		
ATP synthase F1 subunit alpha (Atpf1α) Complex V	5′-TGCCATTGATGGGAAGGGTC-3′	NM_023093.1	97
	3′-TGGTTCCCGCACAGAGATTC-5′		
Prkn	5′-GAACTGTGGCTGTGAGTGGA-3′	NM_020093.1	105
	3′-GGTGTTTCCCATGAGGTCGT-5′		
Mfn1	5′-CTGGGACGGAATGAGTGACC-3′	NM_138976.2	164
	3′-CATGTGAGGGGCCCAATCTT-5′		
Mfn2	5′-ACCAGCTAGAAACGAGATGTCC-3′	NM_130894.4	109
	3′-GTGCTTGAGAGGGGAAGCAT-5′		
Pink1	5′-AGGAAAAGGCCCAGATGTCG-3′	NM_001106694.1	171
	3′-CTGTTTGCTGAACCCAAGGC-5′		
Drp1	5′-GGCAACTGGAGAGGAATGCT-3′	NM_053655.3	165
	3′-CTGTTCTCGGGCAGACAGTT-5′		

Gapdh: Glyceraldehyde 3-phosphate dehydrogenase; Bax: Bcl-2-associated X protein, Bcl-2: B-cell lymphoma 2, Casp 3: Caspase 3, Sod1: Super oxide dismutase, Complex I: Nadh-ubiquinone oxidoreductase complex, Complex II: succinate dehydrogenase, Complex III: cytochrome c oxidoreductase, Complex IV: cytochrome c oxidase, Complex IV: ATP, synthase F1 subunit alpha (Atpf1α), Drp1: dynamin-related protein 1, Prkn: Parkin RBR, E3 ubiquitin protein ligase, Mfn1: Mitofusin 1, Mfn2: Mitofusin 2, Pink1: PTEN-induced kinase 1, pb: base pair.

2.5 Quantitative real-time RT-PCR (qRT-PCR)

Trizol (Invitrogen; Thermo Fisher Scientific, Waltham, MA, United States) was used for total RNA extraction from 30 mg of brain tissue. We evaluated the RNA quality to detect the A260/A280 ratio using the Nano DropVR ND-1000 Spectrophotometer (NanoDrop Technologies, Wilmington, DE, United States) for 1.5 mL of the RNA. A High-Capacity cDNA Reverse Transcription Kit cDNA Kit for cDNA synthesis (Applied Biosystems™, Waltham, MA, United States) was used. The primers were designed for the tested genes, including apoptosis genes *Casp 3, Bcl-2, Bax*, and *Sod1*), mitochondrial complex genes (*5 NADH oxidoreductase* (*Complex I*, *Succinate oxidoreductase* (*Complex II*), *Cytochrome c oxidoreductase* (*Complex III*), *Cytochrome c oxidase* (*Complex IV*), *ATP synthase F1 subunit alpha* (*ATP5F1α*), *Dynamin-related protein 1* (*Drp1*). Mitochondrial homeostasis, mitophagy-related, and mitofusins (*Mfn1* and *Mfn2*) genes were evaluated according to their manufacturer instructions (Sangon Biotech Beijing, China) as provided in

Table 1 (Kimmich et al., 1975; Mihara and Uchiyama, 1978; Yuan et al., 2006).

A thorough assessment of the primer sequences was conducted. The primer sequence was validated via blast analysis NCBI, and primer details were carefully revised. The stability of the expression of different housekeeping genes, including *Gapdh, Act-b*, and *Beta-2-macroglobulin*, and their CT values using the geNorm online software (https://genorm.cmgg.be) revealed that *Gapdh* was the most stably expressed without any significant difference among experimental groups.

2.6 Microarchitecture examination of brain tissue

Brain samples were washed in phosphate buffer saline (pH 7.4) and immersed in 10% neutral buffered formaldehyde. The conventional paraffin embedding technique was chosen for specimens (Fischer et al., 2008).

Obtained sections were stained by Hematoxylin and Eosin (H&E). The calculation was based on semiquantitative scoring of brain necrotic lesions (Gibson-Corley et al., 2013). Scoring was applied on ten randomly chosen microscopic fields at ×400 magnification and averaged. The blinded scoring of the lesions was based on the following procedure [Score scale: 0 = normal; 1 ≤ 25%; 2 = 26–50%; 3 = 51–75%; 4 = 76–100%].

2.7 Immunohistochemical and immunofluorescence staining

The antibodies used in this study were the monoclonal rabbit anti-vimentin (1:300), polyclonal rabbit anti-4-hydroxynonenal (4-HNE) (1:100), and monoclonal mouse anti-Bax (1:50), which were obtained from (Abcam, Cat Ab92547, Cambridge, United Kingdom), (Abcam, Cat Ab46545, Cambridge, United Kingdom) and (Sc-7480, Santa Cruz, CA, United States), respectively. Antigen retrieval was at 10 mM citrate buffer (pH 6.0) at 105 °C for 20 min for all markers. The procedures of immunohistochemical and immunofluorescence techniques were based on Saafan et al. (2023) and Noreldin et al. (2018). The studied micrographs were obtained with a digital camera (Leica EC3, Leica, Germany). The Fiji image analyzer (National Institutes of Health, Bethesda, MD, United States) was utilized to semi-quantitatively calculate the area percentages of the various immunostaining and immunofluorescence reactions (Schindelin et al., 2012; Buckels et al., 2022). Specific brown color images representing the immunoreactions resulting from the deconvolution of ten randomly chosen images were used for analysis. The color thresholds were unified for all analyzed micrographs to compute the different immunoreaction area percentages (Vis et al., 2000).

2.8 Molecular docking assessment

2.8.1 Instruments and tools

RCSB Protein Data Bank (RCSB PDB; https://www.rcsb.org/) and AlphaFold (https://alphafold.ebi.ac.uk/) databases, and the Molecular Operating Environment (MOE 2022.02, Chemical Computing Group, Montreal, QC, Canada) software were used for protein and ligand retrieving and molecular docking.

2.8.2 Ligand preparation

Curcumin and FNE's three-dimensional structures were obtained from the PubChem database in SDF format and opened in MOE software for energy minimization and docking with target proteins.

2.8.3 Protein preparation

The three-dimensional structures of rats' caspase 8, caspase 9, caspase 3, CAT, PINK1, NADH-ubiquinone oxidoreductase, succinate dehydrogenase complex subunit C (SDHC), coenzyme Q8A (COQ8A), ATP synthase F1 subunit alpha (ATP5F1A), protein deglycase (DJ-1), dopamine transporter (DAT), tyrosine hydroxylase proteins were retrieved from RCSB Protein Data Bank and Alpha Fold protein structure databases. Target proteins were prepared for docking using MOE software (MOE 2015.10, Chemical Computing Group, Montreal, QC, Canada) by removing water and ligand molecules in the protein structures and minimizing target protein energy.

2.8.4 Molecular docking analysis and visualization

Target proteins were docked with ligands by identifying the binding site and docking with the induced fit model. Finally, the protein-ligand interactions were visualized using the same software (Vilar et al., 2008).

2.9 Statistical analysis

All data are expressed as mean ± SEM and were analyzed using the Prism 9.0 software from GraphPad (San Diego, CA, United States). Differences among groups for mRNA expression as well as for oxidative and antioxidant enzymes, caspase 3, and neurotransmitters were analyzed using a One-Way Analysis of Variance (ANOVA) followed by Tukey's multiple range *post hoc* test, while for the scores, a Kruskal–Wallis test followed by Dunn's multiple comparisons test. A $p < 0.05$ was considered significant.

3 Results

3.1 Biochemical alterations due to exposure to FNE and/or CRM-Chs-NPs

3.1.1 Markers of antioxidant capacity, oxidative stress, and the level of ATP

The results demonstrated significant changes in various biomarkers following exposure to FNE (Table 2).

Specifically, exposure to FNE led to a substantial increase ($p < 0.001$) in ROS levels and MDA concentration in brain tissue, showing a 2.31-fold and 6.43-fold increase, respectively, compared to the control group. Conversely, there was a significant reduction ($p < 0.001$) in ATP levels by 86.53%, CAT activity by 88.13%, GSH content by 68.24%, and SOD activity by 71.01% compared to the control group.

10.3389/fphar.2024.1388784

TABLE 2 Effect of oral dosing of CRM-Chs-NPs on the brain oxidative and antioxidant enzymes, caspase-3, and neurotransmitters of adult Sprague Dawley rats exposed to FNE for 60 days.

Estimated parameters	Control	CRM-Chs-NPs	FNE	FNE + CRM-Chs-NPs
ROS (pg/mg)	184.4 ± 13.23	147.9 ± 3.37$^{£££}$	610.9 ± 22.22***	347.9 ± 27.94***,$^{£££}$
ATP (ng/mg)	23.91 ± 2.67	22.46 ± 0.4$^{£££}$	3.200 ± 0.37***	9.515 ± 1.14***,$^{£}$
GSH (ng/mg)	163.6 ± 3.21	182.9 ± 2.35*,$^{£££}$	51.96 ± 2.49***	115.7 ± 7.14***,$^{£££}$
CAT (ng/mg)	6.65 ± 0.51	8.94 ± 0.31**,$^{£££}$	0.79 ± 0.048***	3.7 ± 0.26***,$^{£££}$
MDA (nmol/mg)	1.23 ± 0.18	0.69 ± 0.054$^{£££}$	9.14 ± 0.31***	3.94 ± 0.32***,$^{£££}$
SOD (U/mg)	180.8 ± 4.29	198.4 ± 3.45$^{£££}$	52.42 ± 3.98***,$^{£££}$	142.8 ± 5.04***,$^{£££}$
Caspase-3 (ng/mg)	0.76 ± 0.07	0.62 ± 0.04$^{£££}$	7.18 ± 0.43***,$^{£££}$	4.20 ± 0.19***,$^{£££}$
Glutamate (ug/dL)	0.98 ± 0.09	1.05 ± 0.03$^{£££}$	7.92 ± 0.67***	3.01 ± 0.30*,$^{£££}$
Dopamine (DA) (ng/mg)	5.19 ± 0.24	6.29 ± 0.23$^{£££}$	0.57 ± 0.07***	2.30 ± 0.44***,$^{£}$

ROS: reactive oxygen species, ATP: Adenosine tri-phosphate, GSH: reduced glutathione, CAT: catalase, MDA: malondialdehyde, SOD: Superoxide dismutase. Means within the same row carrying different superscripts significantly differ at *$p < 0.05$ or $^{£}p < 0.05$, **$p < 0.01$ or $^{££}p < 0.01$, ***$p < 0.001$ or $^{£££}p < 0.001$. Values shown are means ± SE. n = 10 group (*) is the significance vs. control while ($^{£}$) is the difference vs. FNE, group (F_{ROS} (3, 12) = 121,7; F_{ATP} (3,12) = 46.64; F_{GSH} (3,12) = 186.6; F_{CAT} (3,12) = 117.6; F_{MDA} (3,12) = 253.5; F_{SOD} (3,12) = 236.6; $F_{Caspase\text{-}3}$ (3,12) = 169.7; $F_{Glutamate}$ (3,12) = 77.11; F_{DA} (3,12) = 65.78).

Remarkably, co-treatment of CRM-Chs-NPs and FNE (FNE + CRM-Chs-NPs group) significantly decreased ROS and MDA levels in rats' brain tissue, reducing them by 43.05% and 56.89%, respectively, compared to the FNE group ($p < 0.001$). Additionally, CRM-Chs-NPs significantly reduced oxidative stress, lowering ROS levels by 19.79% and MDA levels by 43.9% compared to the control group ($p < 0.001$).

In the CRM-Chs-NPs + FNE group, a significant enhancement in the levels of GSH, CAT, and SOD by 122.67%, 368.69%, and 172.42%, respectively, was observed compared to the FNE-exposed group ($p < 0.001$). As for ATP levels, while the FNE-exposed group experienced a significant decline (86.53%) compared to the control group ($p < 0.001$), concurrent administration of CRM-Chs-NPs with FNE significantly reversed this trend, elevating ATP content in brain tissue by 195.5% compared to the FNE group ($p < 0.05$).

Furthermore, caspase-3 protein levels in the brain tissue of the FNE-exposed group significantly increased by 842.9% compared to the control group ($p < 0.001$). However, caspase-3 was significantly reduced by 41.54% following the addition of CRM-Chs-NPs in the FNE + CRM-Chs-NPs group compared to the FNE-exposed group ($p < 0.001$).

3.1.2 The levels of dopamine and glutamate in the brain tissue

A significant increase in brain tissue levels of glutamate, reaching 7.06 times the values observed in control rats, was observed in the FNE-exposed group ($p < 0.001$). Conversely, dopamine levels in the same group exhibited a significant decrease of 89.07% compared to the control values ($p < 0.001$).

In the combined treatment group (FNE + CRM-Chs-NPs), there was a significant elevation in dopamine levels, with a 3.05-fold increase and a 62.02% compared to the FNE-treated group ($p < 0.05$). This demonstrated the beneficial effect of CRM-Chs-NPs in significantly elevating dopamine levels in the brains of exposed rats to FNE for 60 days (Table 2) ($p < 0.001$).

3.1.3 The expression pattern of estimated genes (apoptotic and antioxidant genes)

As shown in Figures 1A, B, a marked upregulation of apoptosis-related genes, namely, *Casp 3* (573.03%) and *Bax* (389.52%), was observed in the brain tissues of rats exposed to FNE, indicating a significant difference ($p < 0.001$) when compared to the control group. Conversely, the expressions of *Bcl-2* and *Sod1* exhibited substantial downregulation by 83.80% and 201.79%, respectively, compared to the control group.

Notably, the group treated with CRM-Chs-NPs displayed a noteworthy decrease ($p < 0.001$) in the mRNA expressions of *Casp 3* and *Bax* (Figures 1C, D) when compared to the FNE-exposed group, with reductions of 46.88% and 44.93%, respectively.

Furthermore, in the FNE + CRM-Chs-NPs group, there was a significant ($p < 0.001$) elevation in the mRNA expressions of *Bcl-2* and *Sod1* in brain tissues, with increases of 221.27% and 201.97%, respectively, compared to the FNE-exposed group.

3.1.4 Gene expression analysis of mitochondrial complex genes

As shown in Figures 2A–E, the rats exposed to FNE exhibited a substantial downregulation of mitochondrial *Complex* genes *I, II, III, IV*, and *V* in brain tissues, with reductions of 68.98%, 77.66%, 78.81%, 87.32%, and 69.83%, respectively, compared to the control group ($p < 0.001$).

In contrast, the brain tissue of rats subjected to combined treatment with CRM-Chs-NPs and FNE showed a significant ($p < 0.001$) upregulation of the same genes, with increases of 151.83%, 181.44%, 164.95%, 458.37%, and 157.9%, respectively, compared to the FNE-exposed group. Furthermore, when assessing the comparative effectiveness of CRM-Chs-NPs and control, a statistically significant ($p < 0.001$) improvement in the gene's activity was observed compared to the control group.

10.3389/fphar.2024.1388784

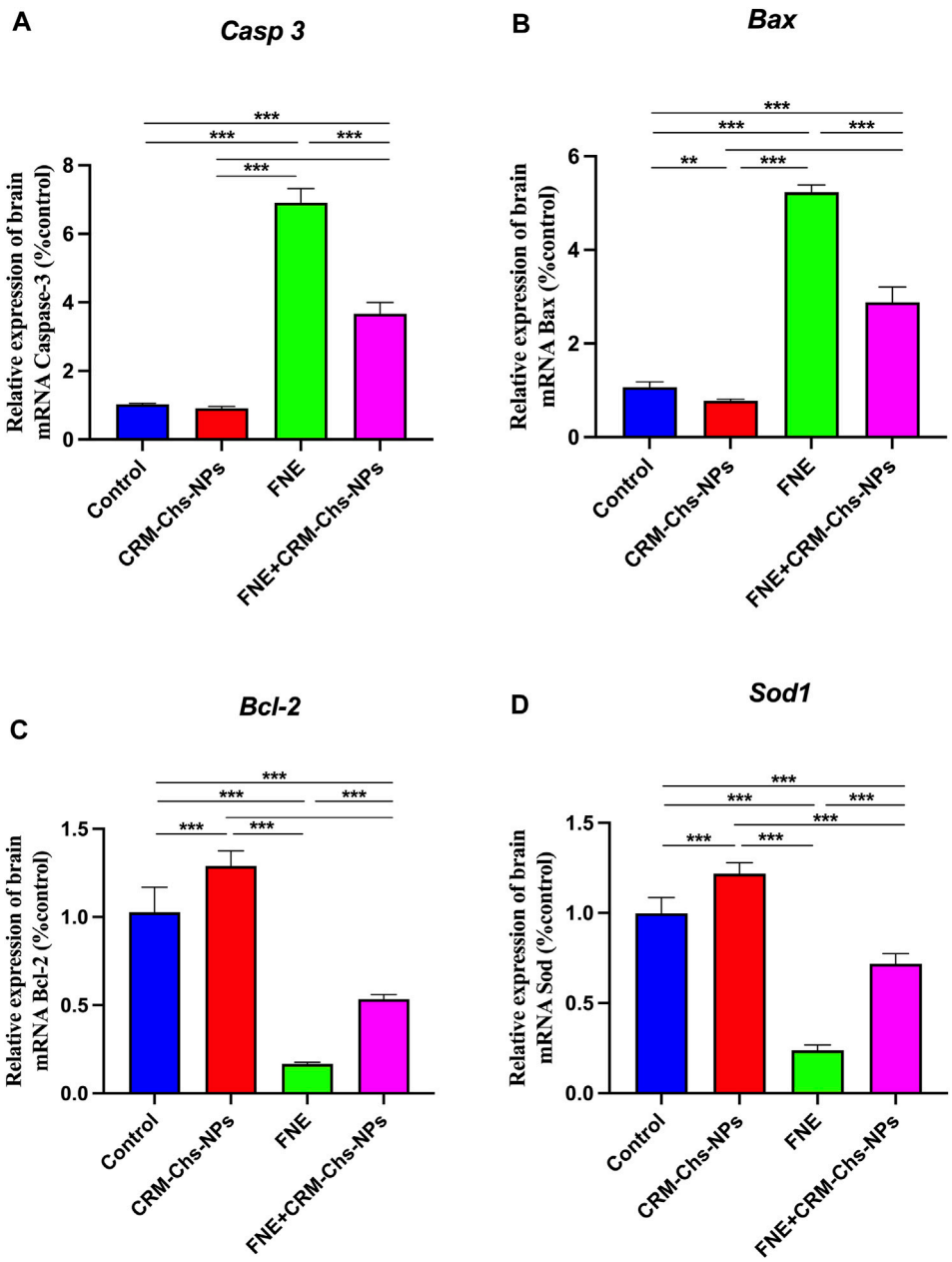

FIGURE 1
Effect of CRM-Chs-NPs oral dosing on mRNA expression of **(A)** *Casp 3*, **(B)** *Bax*, **(C)** *Bcl-2*, and **(D)** *Sod1* in the brain tissues of adult male Sprague Dawley rats exposed to FNE after 60 days. (n = 10 group), ***p < 0.01, ***p < 0.001,* [$F_{Caspase}$ (3,36) = 1,154, F_{BAX} (3,36) = 1,164, F_{Bcl-2} (3,24) = 247.8, F_{SOD} (3,36) = 463.2].

3.1.5 Gene expression analysis mitophagy and mitochondrial homeostasis-related genes

Genes associated with mitochondrial homeostasis and dynamics were also examined (Figures 3A–E).

This figure illustrates a significant downregulation ($p < 0.001$) in the expression of these genes, namely, *Pink, Drp1, Parkn, Mfn1,* and *Mfn2,* in the FNE-exposed group. The reductions were significant, 83.75%, 87.82%, 76.32%, 69.09%, and 79.08%, respectively, compared to the control group. However, when CRM-Chs-NPs were co-administered, the expression of these genes in the brain of the combined group was remarkably elevated, nearly approaching the control values compared to the FNE-exposed group. The calculated percentages are 274% in *Pink*, 293.43% in *Drp1*, 175.27% in *Parkn*, 149.84% in *Mfn1*, and 189.04% in *Mfn2* compared to the control. These findings underscore the potential of CRM-Chs-NPs to effectively mitigate the adverse effects of FNE on mitochondrial gene expression.

3.2 Microscopical findings

The study of brain histoarchitecture of negative control and CRM-Chs-NPs groups revealed normal neuropil and neurons in the brain

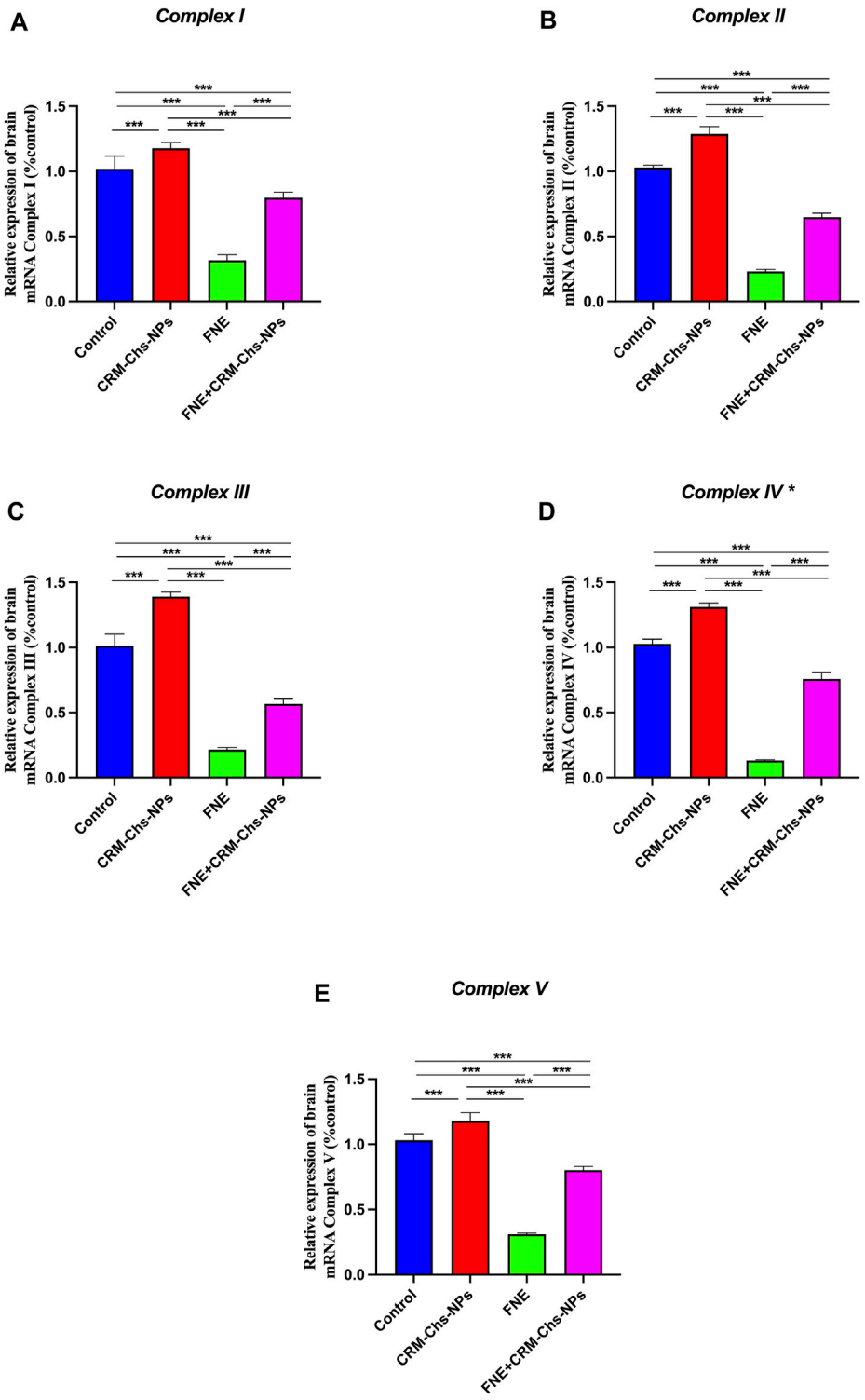

FIGURE 2
Effect of CRM-Chs-NPs oral dosing on mRNA expression of **(A)** *5-Nadh oxidoreductase* (*Complex I*), **(B)** *Succinate oxidoreductase* (*Complex II*), **(C)** *Cytochrome c oxidoreductase* (*Complex III*), and **(D)** *Cytochrome c oxidase* (*Complex IV*), **(E)** *ATP synthase F1 subunit alpha* (*Atpf1α*) (*Complex V*) in the brain tissues of adult male Sprague Dawley rats exposed to FNE for 60 days. (n = 10 group), ***$p < 0.001$, [$F_{complex\ I}$ (3, 36) = 369.2, $F_{complex\ II}$ (3, 36) = 1794, $F_{complex\ III}$ (3, 36) = 956.3, $F_{complex\ IV}$ (3, 36) = 2024, $F_{complex\ V}$ (3, 36) = 782].

areas, including cerebrum (taken from the midbrain above the hippocampus), cerebellum (longitudinally dissected), and hippocampus (cross-sectionally dissected at the level of the mammillary body and tuber cinereum) (Figures 4A, C).

However, we detected necrotic neurons in the FNE cerebrum (Figure 4B). CRM-Chs-NPs ameliorated the toxic effects of FNE on the cerebrum with few necrotic neurons (Figure 4D). These results were shown in the image-scoring analysis of brain histoarchitecture

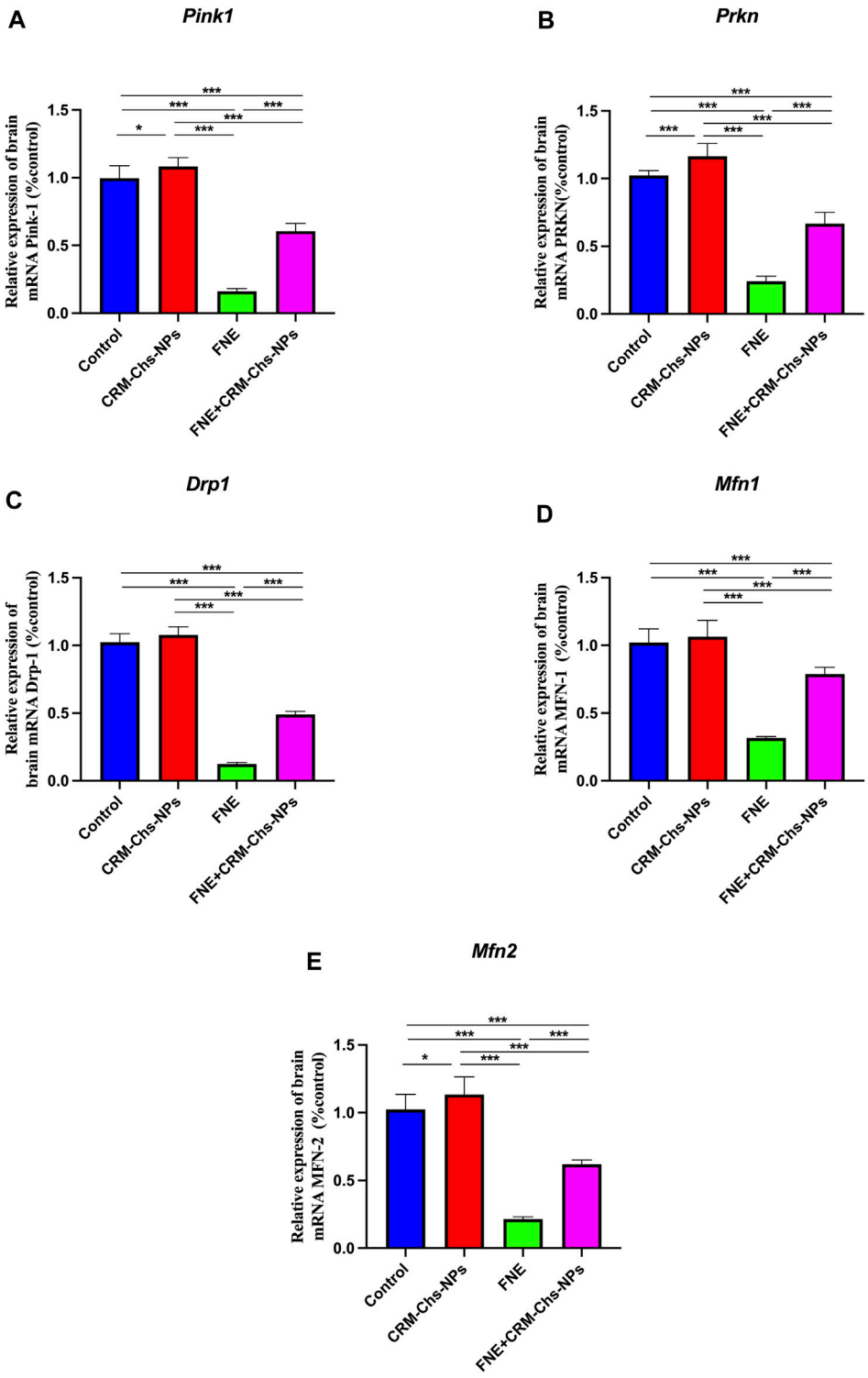

FIGURE 3
Effect of CRM-Chs-NPs oral dosing on mRNA expression of **(A)** *PTEN-induced kinase* (*Pink1*), **(B)** *Dynamin-related protein 1* (*Drp1*), **(C)** *Parkin RBR E3 ubiquitin protein ligase* (*Prkn*), **(D)** *Mitofusin 1* (*Mfn1*), and **(E)** *Mitofusin 2* (*Mfn2*) in the brain tissues of adult male Sprague Dawley rats exposed to fenpropathrin (FNE) for 60 days. (n = 10 group), *$p < 0.05$, ***$p < 0.001$, [F_{Pink1} (3, 36) = 433, F_{Drp1} (3, 36) = 1,034, F_{Prkn} (3, 36) = 357, F_{Mfn1} (3, 36) = 172.4, F_{Mfn2} (3, 36) = 230.7].

(Figure 4E). A significant increase in the FNE ($p < 0.001$) with respect to the control and CRM-Chs-NPs group ($p < 0.001$) was observed.

The hippocampal architecture revealed typical dentate gyrus in control and CRM-Chs-NPs groups (Figures 5A, C). However, the dentate gyrus displayed necrotic neurons with a few disordered

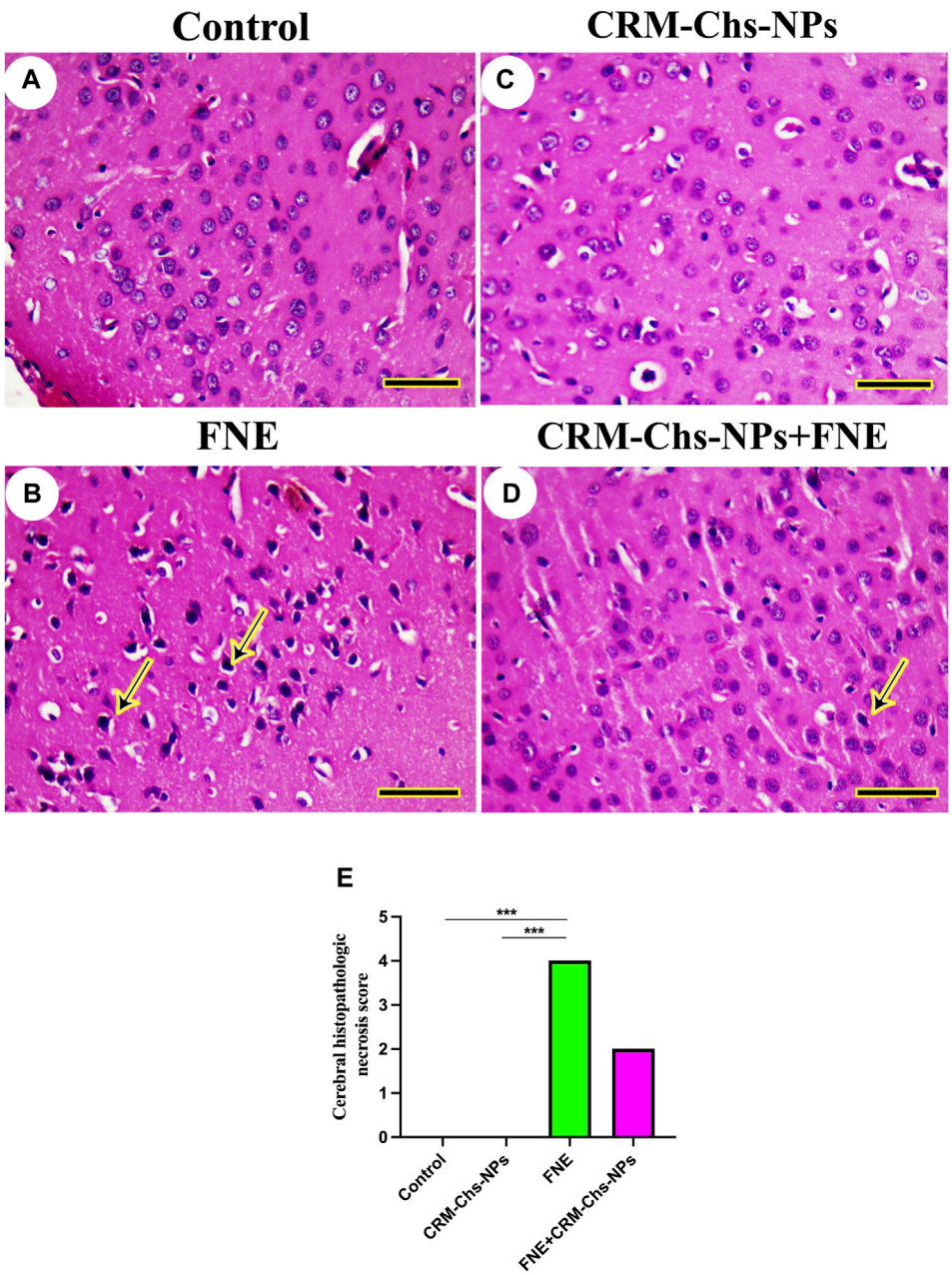

FIGURE 4
Representative photomicrograph of rat cerebrum (taken from the midbrain above the hippocampus): **(A)** control, **(B)** FNE-exposed necrotic neurons (arrow), **(C)** CRM-Chs-NPs-treated cerebrum showing normal neurons, **(D)** CRM-Chs + FNE-treated rats illustrating the improvement in cerebrum architecture with some necrotic neurons (arrow), and **(E)** graphical representation of photomicrograph score (HE, Scale bar = 50 μm). ***$p < 0.001$.

neurons in the FNE group (Figure 5B). On the other hand, CRM-Chs-NPs improved dentate gyrus structure in the CRM-Chs-NPs + FNE group (Figure 5D). These results were shown in the image-scoring analysis of hippocampal histoarchitecture (Figure 5E). A significant increase in the FNE ($p < 0.001$) and CRM-Chs-NPs + FNE ($p < 0.05$) with respect to the control and CRM-Chs-NPs group ($p < 0.001$ and $p < 0.01$, respectively) was observed.

The investigation of cerebellar histoarchitecture of control and CRM-Chs-NPs groups revealed normal neurons (Figures 6A, C). The FNE group displayed focal cavities due to lysis or loss of granules and Purkinje neurons (Figure 6B). Few pyknotic neurons could be detected on FNE cerebellar neurons following CRM-Chs-NPs administration (Figure 6D). These results were shown in the image-scoring analysis of cerebellar histoarchitecture (Figure 6E). A significant increase in the FNE ($p < 0.001$) and CRM-Chs-NPs + FNE ($p < 0.01$) with respect to the control and CRM-Chs-NPs group ($p < 0.001$ and $p < 0.01$, respectively) was observed.

3.3 Immunohistochemical staining

There was no observable BAX immunohistochemical reaction in control and CRM-Chs-NPs groups in the cerebrum (Figures 7A1,

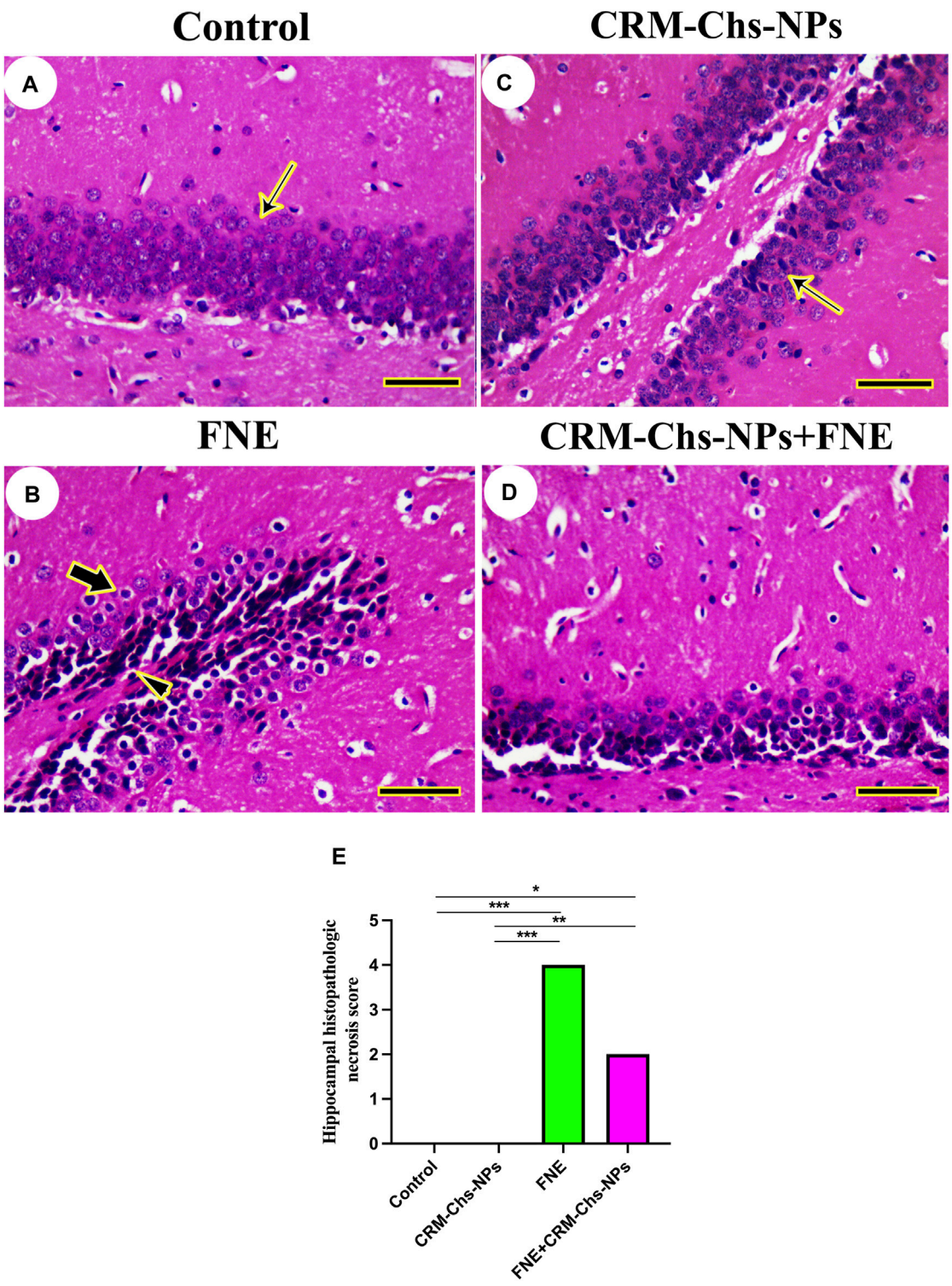

FIGURE 5
Representative photomicrograph of rat hippocampus (cross-sectionally dissected at the level of the mammillary body and tuber cinereum): **(A)** control, and **(B)** FNE reveals necrotic neurons (arrowhead) and hyperchromatic neurons (thick arrow), **(C)** CRM-Chs groups showing normal dentate gyrus (thin arrows), **(D)** CRM-Chs + FNE reveals improved hippocampal architecture, and **(E)** graphical representation of photomicrograph score (HE, *Scale bar = 50 μm*). *$p < 0.05$, **$p < 0.01$, ***$p < 0.001$.

A2), hippocampus (Figures 7B, 7B2), and cerebellum (Figures 7C1, C2), respectively. Extensive BAX reactions were detected in the nuclei of all studied brain regions of the FNE group (Figures 7A3, B3, C3). On the other hand, the co-administration of CRM-Chs-NPs to FNE decreased the BAX distribution (Figures 7A4, B4, C4). The semiquantitative analysis for the BAX area percentage revealed a

10.3389/fphar.2024.1388784

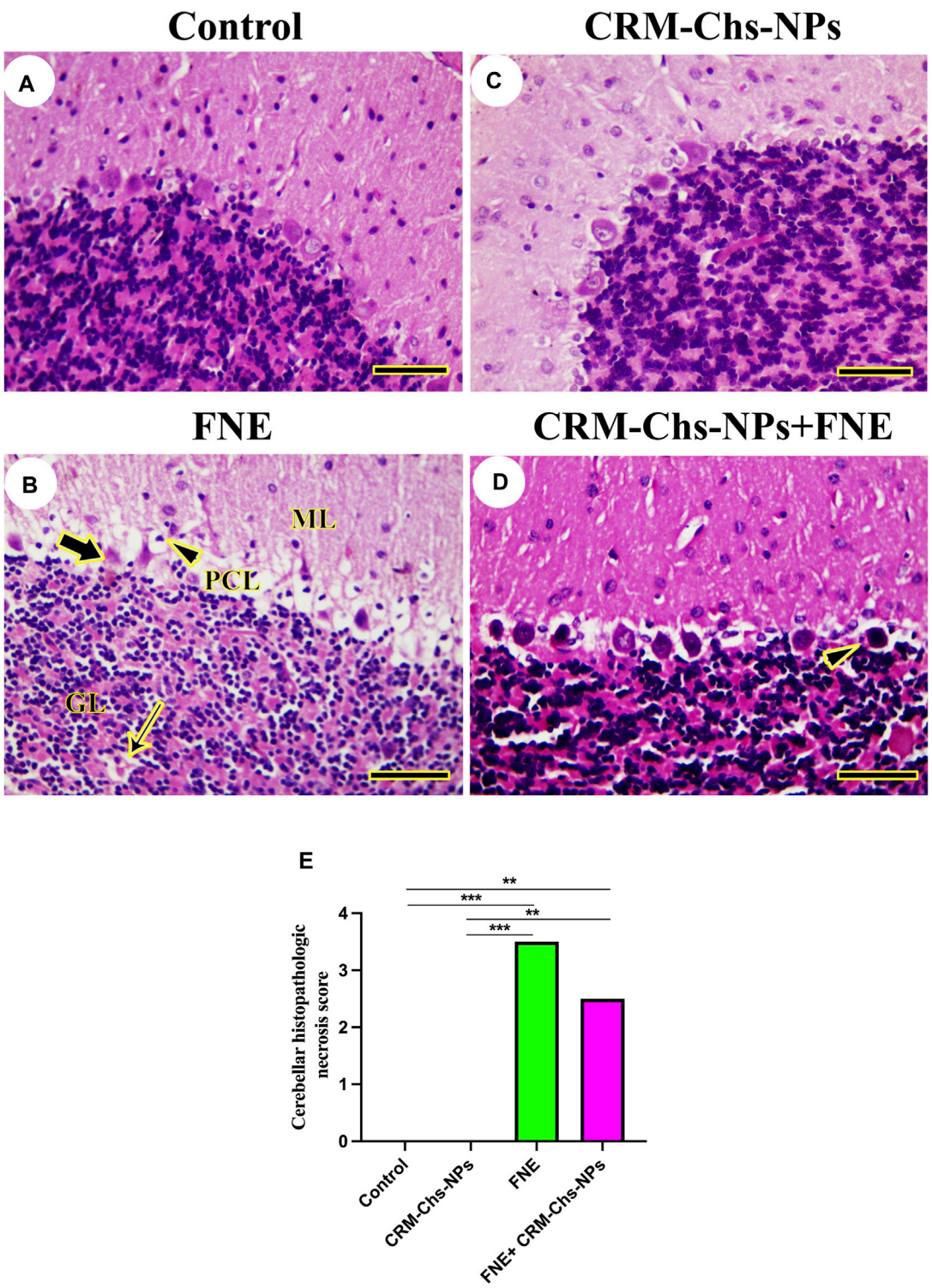

FIGURE 6
Representative photomicrograph of rat cerebellum (longitudinally dissected): **(A)** control, **(B)** FNE-treated rats revealing pyknotic Purkinje neurons (thick arrow) in the Purkinje cells layer (PCL), focal neuronal loss (thin arrow) in the granular layer (GL), and necrotic neurons (arrowhead) in the molecular layer (ML), **(C)** CRM-Chs-NPs-treated cerebellum, **(D)** CRM-Chs-NPs + FNE-treated rats showing nearly normal cerebellum with some degenerated Purkinje cells (arrowhead), and **(E)** graphical representation of photomicrograph score (HE, *Scale bar = 50 μm*). ***p < 0.01, ***p < 0.001*.

significant BAX distribution in the FNE group than in control (Figure 7A5, $p < 0.001$; B5, $p < 0.01$; C5, $p < 0.001$) and CRM-Chs-NPs (Figures 7A5, B5, C5 $p < 0.001$) groups and a significant reduction in the CRM-Chs-NPs + FNE group compared to the control group, but only for the cerebrum (Figure 7A5, $p < 0.05$). A similar trend was observed for the FNE group with respect to the

10.3389/fphar.2024.1388784

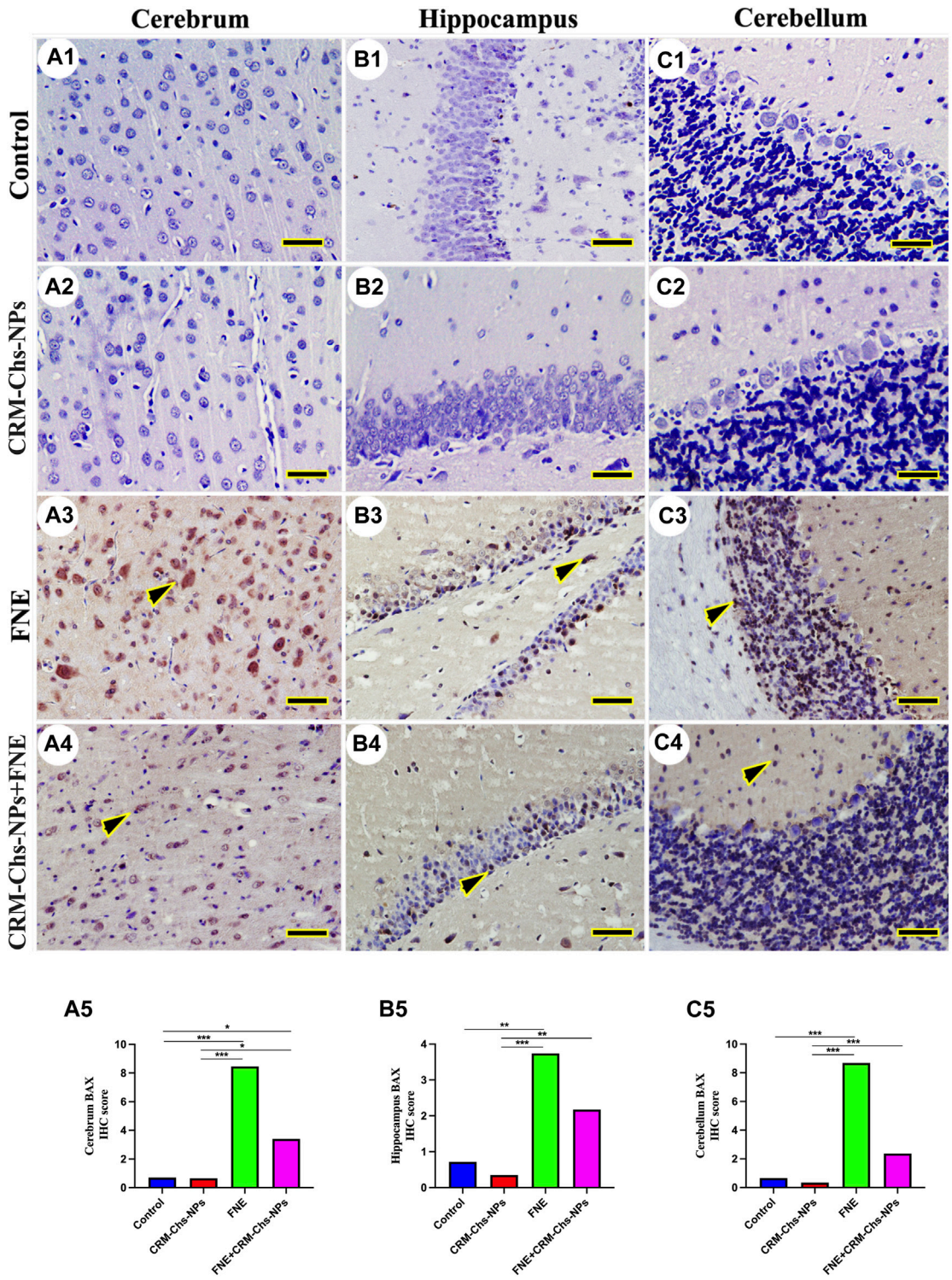

FIGURE 7
Representative photomicrograph of immunohistochemical BAX expression in the cerebrum **(A1–A5)**, hippocampus **(B1–B5)**, and cerebellum **(C1–C5)** from control **(A1,B1,C1)**, CRM-Chs-NPs **(A2,B2,C2)**, FNE **(A3,B3,C3)**, and CRM-Chs-NPs + FNE **(A4,B4,C4)** groups. Arrowheads indicate positive immune expressions (*Scale bar = 50 μm*). *$p < 0.05$, **$p < 0.01$, ***$p < 0.001$.

CRM-Chs-NPs group (Figures 8A5, B5, C5, $p < 0.001$) and for CRM-Chs-NPs + FNE compared to the CRM-Chs-NPs group (Figure 8A5, $p < 0.05$; Figure 8B5, $p < 0.01$; Figure 8C5, $p < 0.001$).

In the control and CRM-Chs-NPs groups, vimentin immunohistochemical expression showed low vimentin distribution in the cerebrum (Figures 8A1, A2), hippocampus

10.3389/fphar.2024.1388784

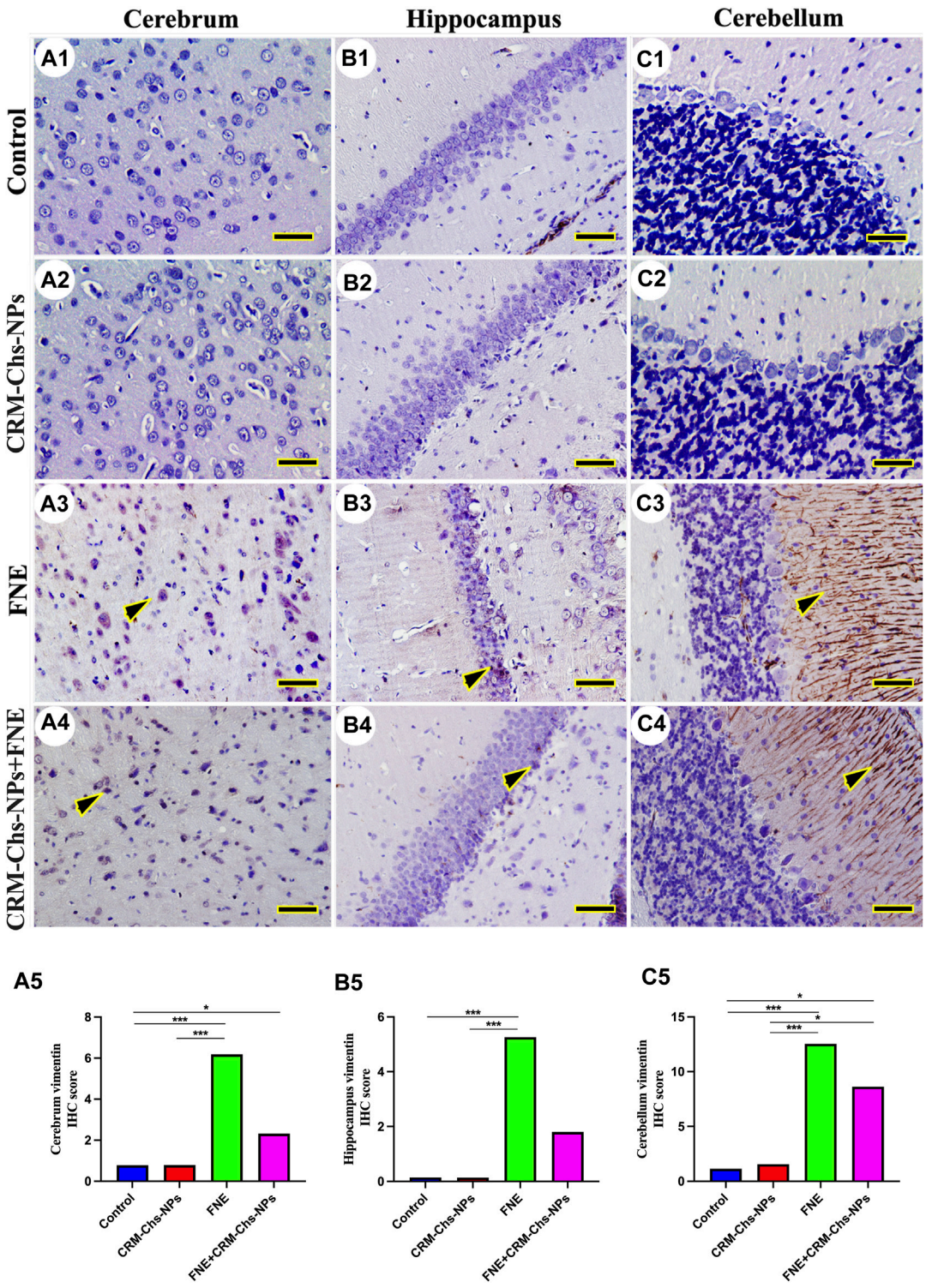

FIGURE 8
Representative photomicrograph demonstrated immunohistochemical vimentin staining in the cerebrum **(A1–A5)**, hippocampus **(B1–B5)**, and cerebellum **(C1–C5)** from negative control **(A1,B1,C1)**, CRM-Chs-NPs **(A2,B2,C2)**, FNE **(A3,B3,C3)**, and CRM-Chs-NPs + FNE **(A4,B4,C4)** groups. Arrowheads indicate positive immune expressions (*Scale bar = 50 μm*). *$p < 0.05$, ***$p < 0.001$.

(Figure 8B1B2), and cerebellum (Figures 8C1,C2). The FNE group showed extensive vimentin expression in all brain regions (Figures 8A3, B3, C3). CRM-Chs-NPs lowered vimentin distribution in the CRM-Chs-NPs + FNE group (Figures 8A4, B4, C4). The semiquantitative analysis for the vimentin area percentage revealed a more significant reaction in the FNE group than in

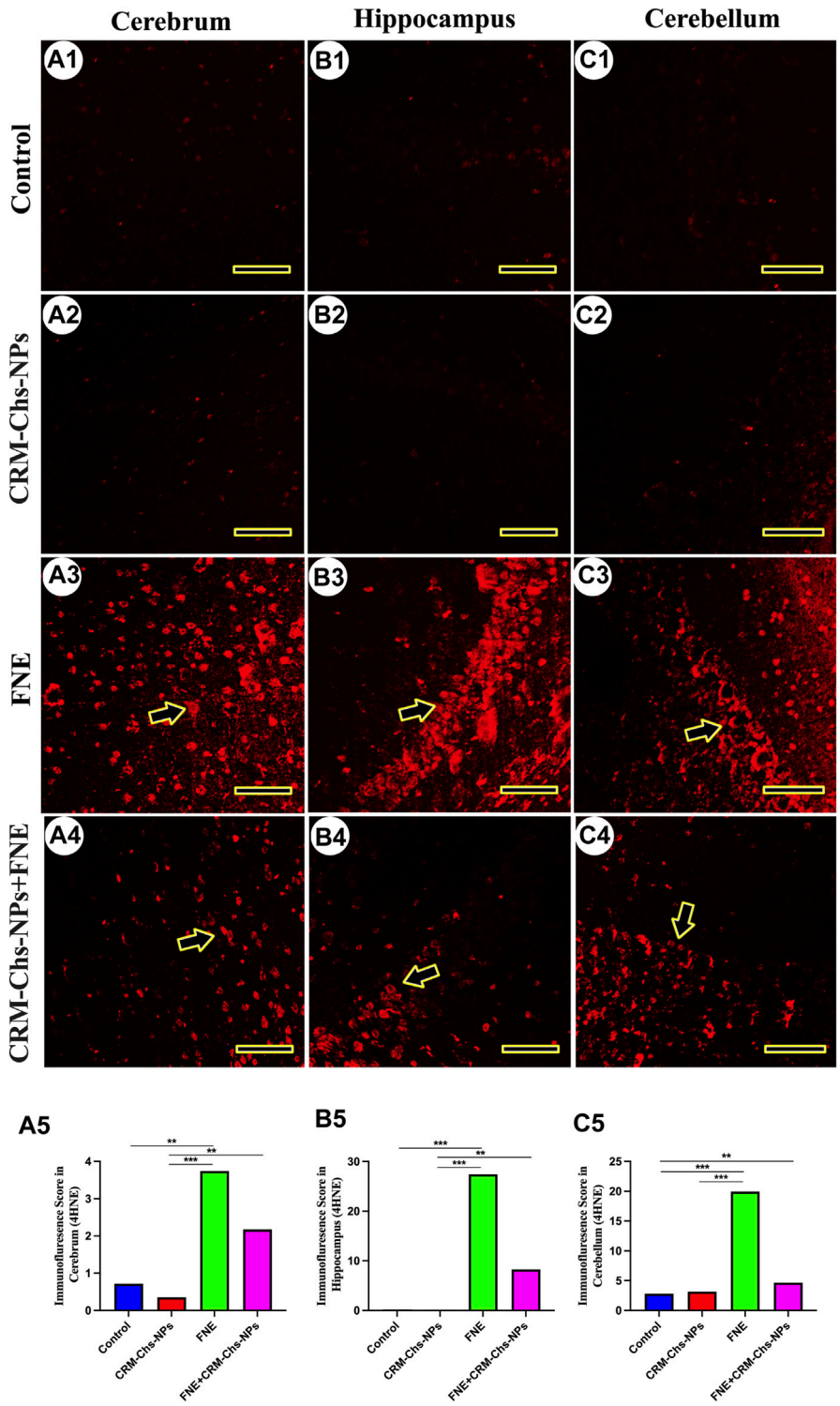

FIGURE 9
Representative photomicrograph demonstrated 4-hydroxynonenal (4-HNE) immunofluorescence in the cerebrum **(A1–A5)**, hippocampus **(B1–B5)**, and cerebellum **(C1–C5)** from negative control **(A1,B1,C1),** CRM-Chs-NPs **(A2,B2,C2)**, FNE **(A3,B3,C3)**, and CRM-Chs-NPs + FNE **(A4,B4,C4)** groups. Arrowheads indicate positive immunofluorescence expressions (*Scale bar = 50 μm*). ***p* < *0.01*, ****p* < *0.001*.

control (Figures 8A5, B5, C5, $p < 0.001$), CRM-Chs-NPs (Figures 8A5, B5, C5, $p < 0.001$), and CRM-Chs-NPs + FNE group but only for the cerebrum and the cerebellum (Figures 8A5, C5, $p < 0.05$). A similar trend was observed for the FNE group with respect to the CRM-Chs-NPs group (Figures 8A5, B5, C5, $p < 0.001$) and for CRM-Chs-NPs + FNE compared to the CRM-Chs-NPs group, but only for the cerebellum (Figure 8C5, $p < 0.05$).

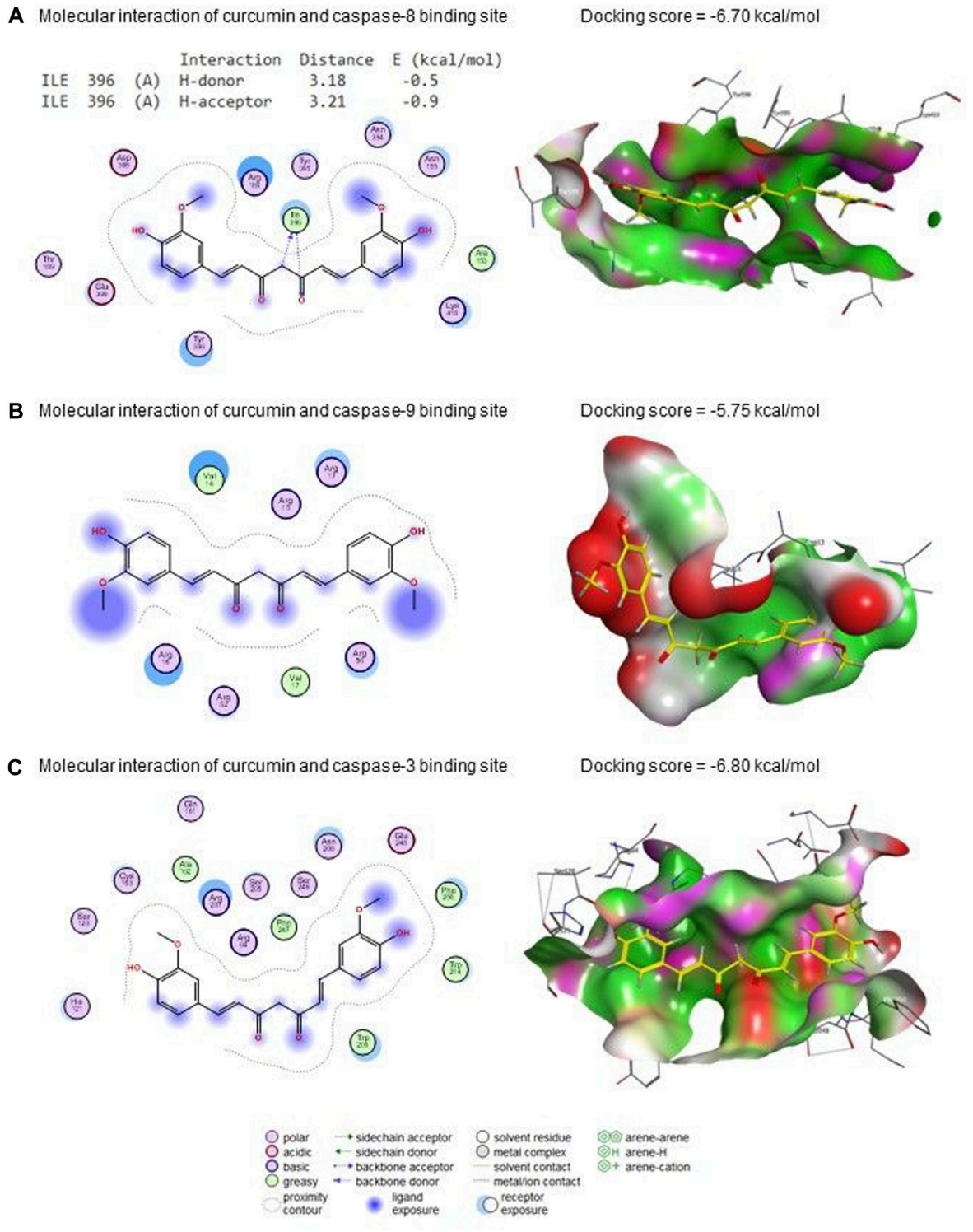

FIGURE 10
Molecular docking interaction of curcumin with **(A)** caspase 8, **(B)** caspase 9, and **(C)** caspase 3.

3.4 Immunofluorescence staining of 4-hydroxynonenal (4-HNE)

The immunofluorescence of 4HNE revealed low expression in the cerebrum (Figures 9A1, A2), hippocampus (Figures 9B1, B2), and cerebellum (Figure 9C1, C2) of the control and CRM-Chs-NPs groups. Conversely, a significant 4HNE expression was detected in all brain regions of the FNE group (Figures 9A3, B3, C3), while a low expression was detected in the brain cells of the CRM-Chs-NPs + FNE group (Figures 9A4, B4, C4). The

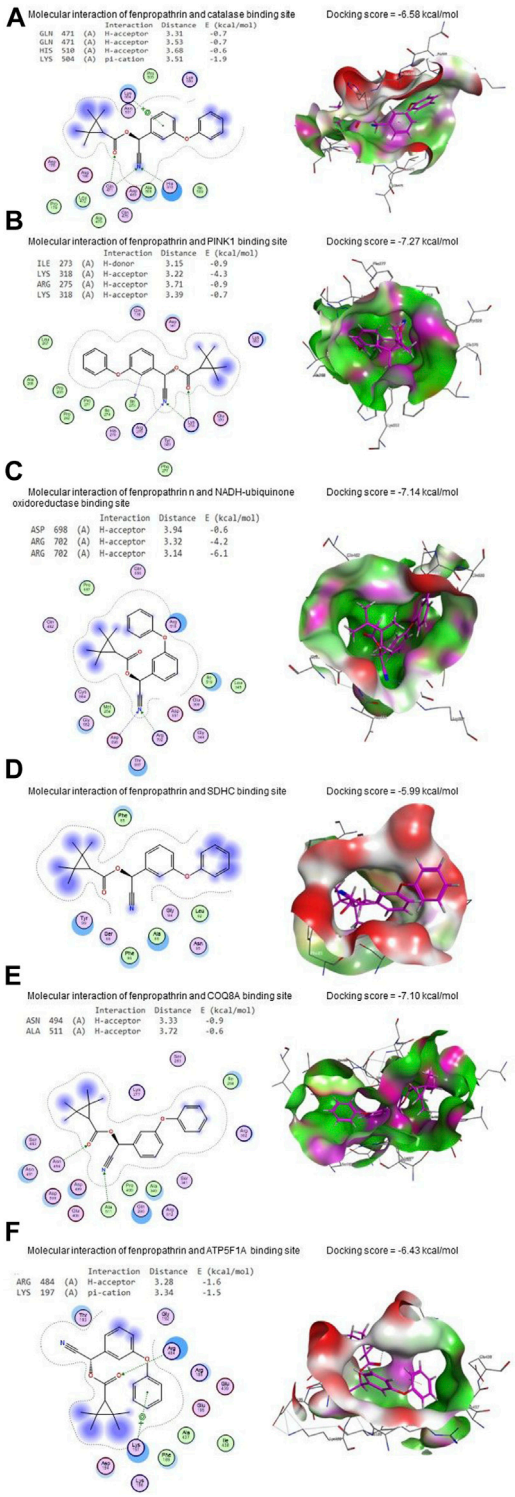

FIGURE 11
Molecular docking interaction of FNE with **(A)** CAT, **(B)** PINK1, **(C)** NADH-ubiquinone oxidoreductase, **(D)** succinate dehydrogenase complex subunit C (SDHC), **(E)** coenzyme Q8A (COQ8A), **(F)** ATP synthase F1 subunit alpha (ATP5F1A), **(G)** protein deglycase (DJ-1), **(H)** dopamine transporter (DAT), and **(I)** tyrosine hydroxylase.

semiquantitative analysis for the 4HNE area percentage revealed a significant reaction in the FNE group than in the control (Figure 9A5, $p < 0.01$; Figure 9B5, $p < 0.001$; Figure 9C5, $p < 0.01$) and CRM-Chs-NPs + FNE groups, but only for the cerebellum (Figure 9C5, $p < 0.01$).

3.5 Molecular docking

Figure 10 presents curcumin's molecular interactions and docking scores with caspase-8, caspase-9, and caspase-3 binding sites. Curcumin interacted with the ILE396 (H-donor and H-acceptor) residue in caspase-8's binding site by −6.70 kcal/mol of binding energy (Figure 10A). Also, curcumin interacted with caspase-9 (Figure 10B) and caspase-3 (Figure 10C) binding sites with energy of −5.75 and −6.80 kcal/mol, respectively.

FNE bound to GLN471 (two H-acceptors), HIS510 (H-acceptor), and LYS504 (pi-cation) residues in the CAT's binding site with an energy of −6.58 kcal/mol (Figure 11A). By the energy of −7.27 kcal/mol, FNE interacted with ILE273 (H-donor), LYS318 (two H-acceptors), and ARG275 (H-acceptor) residues in the binding site of PINK1 (Figure 11B).

Regarding NADH-ubiquinone oxidoreductase, FNE bound to ASP698 (H-acceptor) and ARG702 (two H-acceptors) residues with an energy of −7.14 kcal/mol (Figure 11C). In contrast, it interacted with SDHC's binding site with −5.99 kcal/mol of energy (Figure 11D).

As shown in Figure 11E, FNE interacted by −7.10 kcal/mol of energy with ASN494 (H-acceptor) and ALA511 (H-acceptor) residues in the binding site of COQ8A. Also, FNE is bound with ARG484 (H-acceptor) and LYS197 (pi-cation) in the binding site of ATP5F1A by an energy value of −6.43 kcal/mol (Figure 11F). By −5.73 kcal/mol of energy, FNE bound to GLU96 (H-donor), PHE119 (two H-acceptors), and GLU (pi-H) in the binding site of DJ-1, as represented in Figure 11G. The molecular interaction of the FNE and DAT binding site is represented in Figure 11H with a binding energy of −6.86 kcal/mol with ARG85 (H-acceptor) and HIS476 (H-acceptor) residues. Moreover, FNE bound to PRO327, GLY392, and SER396 residues in the binding site of tyrosine hydroxylase by an energy of −7.50 kcal/mol (Figure 11I).

4 Discussion

A failure in redox homeostasis is one of the typical hallmarks of PD (Fei et al., 2010). Research has shown that pyrethroids can cross the blood-brain barrier and affect the dopaminergic system, producing oxidative stress in PD (Nasuti et al., 2007). Hence, we investigated whether FNE increases brain oxidative stress in the present study. We detected ROS readily after FNE exposure in the brain tissue and found that its expression was significantly increased. In contrast, GSH, CAT, and total SOD levels as antioxidative indices were significantly reduced in the FNE group compared to the control. These results indicated that oxidation and reduction were dysfunctional following FNE exposure. Furthermore, the mRNA expression of the *Sod1* gene was significantly downregulated. These ROS molecules can disrupt mitochondrial function, impairing the electron transport chain and promoting mitochondrial dysfunction. Researchers have identified elevated free radicals and mitochondrial dysfunction as primary contributors to neuronal loss in PD brains (Nasuti et al., 2007).

Consequently, the expression of key mitochondrial complex genes, such as those involved in oxidative phosphorylation, can be altered. The current study confirmed this via the downregulated expression of mitochondrial *Complex* genes (*I-V*) in the brain tissue of the FNE group rather than the control. Other pyrethroids, including cypermethrin and deltamethrin, have also been documented to cause oxidative stress in cells (Mohamed et al., 2020; Rahman et al., 2022), thus confirming our findings.

However, treating FNE-intoxicated rats with CRM-Chs-NPs significantly decreased ROS and MDA levels while increasing SOD, CAT, and GSH contents and *Sod1* and mitochondrial *Complex* genes (*I-V*) expression in the brain tissues to alleviate oxidative stress, lipid peroxidation, and mitochondrial dysfunction. Similarly, CRM was observed to shield dopaminergic neurons from MPTP-induced neuronal damage (Stanic, 2017) and oxidative damage by restoring mitochondrial membrane potential, upregulating Cu-Zn superoxide dismutase, and inhibiting the production of intracellular ROS (Anand et al., 2007; Itokawa et al., 2008). CRM also inhibited GSH reduction in the brain by improving the GSH levels (Asai and Miyazawa, 2000) and reduced lipid peroxidation levels and protein carbonyl aggregates in the brain of the transgenic PD model of *Drosophila* (Kehlet et al., 2006). It has been proposed that the antioxidant properties of CRM and its nano form are mostly due to its ability to block ROS-generating enzymes such as microsomal monooxygenase, mitochondrial succinoxidase, and NADH oxidase (Alisi et al., 2018). In addition, CRM's conjugated structure and enol form can boost the activity of antioxidant enzymes and scavenge free radicals (Trujillo et al., 2013). On top of that, CRM helps keep cell membranes intact by blocking peroxidation in toxicant situations (Sankar et al., 2012).

In the current study, the molecules involved in apoptosis were upregulated in the brain tissue of FNE-administered rats via detecting the levels of Caspase 3 in the brain tissue and assessing the expression of different genes related to apoptotic cascade pathway, including *Casp 3, Bax*, and *Bcl-2*. Furthermore, the immunohistochemical reactivity scoring of BAX protein was highly enhanced, while the reaction of Bcl-2 significantly declined in the brain upon exposure to FNE. These results were previously shown in some earlier studies (Mohamed et al., 2019; Mohamed et al., 2020). Reduced complex I and cytochrome P450 activity in mitochondria (Abdou et al., 2010) and mitochondrial dysfunction (Gassner et al., 1997) have been linked to pyrethroid-induced oxidative stress. Dysregulation in these genes can further exacerbate ROS production, creating a vicious cycle of oxidative stress. This cascade of events ultimately activates apoptotic pathways, initiating programmed cell death (Cao et al., 2007; Salem et al., 2023). Environmental toxicants can cause PD by disrupting mitochondrial function or dynamics (Arya et al., 2018; Khater et al., 2021; Yin et al., 2021; Lin et al., 2022) regulated by *Mfn1*, *Mfn2,* and *Drp1* genes (Gassner et al., 1997; Reddy et al., 2011). Our results indicated that FNE administration caused downregulated expression of all these proteins, thus indicating the ability of FNE to induce the pathways related to the pathophysiological changes in PD.

Similarly, dopaminergic degeneration is caused by the neurotoxin MPTP, which specifically destroys Complex I of the mitochondrial electron transport chain. This may be a similar pattern for FNE-inducing dopaminergic degeneration and then PD. Besides, in the molecular docking assessment, FNE successfully bound to the binding sites of mitochondrial Complexes (I-V), including Pink1, DJ-1, NADH-ubiquinone oxidoreductase, SDHC, COQ8A, and ATP5F1A, which is an indication for probability to occur *in vivo* leading to mitochondrial function impairment.

On the contrary, our results indicated that co-administration of CRM-Chs-NPs + FNE reduced oxidative stress (ROS and MDA) and apoptosis molecules that enhance apoptosis in the brain tissue and activate the mitochondrial complex genes. The downregulation of *Bax* and *Caspase-3* gene expression and inhibition of the *Bcl-2* gene in the brain of rats administered FNE + CRM-Chs-NPs and CRM-Chs-NPs confirmed the protective role of CRM. These improvements could help explain the key mechanisms through which CRM-Chs-NPs counteract degenerative changes caused by FNE and decrease the likelihood of PD onset. These effects could be highly correlated to what is reported in several *in vitro* and *in vivo* investigations carried out with CRM due to its antioxidant, anti-inflammatory, antiapoptotic activities, and therapeutic potential in neurodegenerative disorders (Itokawa et al., 2008). Besides, CRM-Chs-NPs potency to attenuate mitochondrial impairments by maintaining mitochondrial integrity while reducing mitochondrial oxidative stress could contribute to its neuroprotective activity (Sandhir et al., 2014). It was also previously observed that CRM could inhibit mitophagy and regulate mitochondrial dynamics in tested cells (Maiti et al., 2019). This effect could also be interrupted by the degradability of CRM-Chs-NPs, a key solution to help maintain CRM for longer periods and act on the mitochondrial homeostatic ability (Rainey et al., 2020).

Our findings also revealed a decrease in dopamine levels and an increase in glutamate levels in the brains of rats exposed to FNE for 60 days. These outcomes align with previous research, which demonstrated a connection between dopamine turnover and the acceleration of cellular dopamine uptake in rats (Husain et al., 1994). This phenomenon is associated with the upregulation of the transcription factor *Nurr1*, resulting in an increased dopamine transporter expression (Karen et al., 2001). Furthermore, Elwan et al. (2006) reported that pyrethroids, known to block sodium channels, could enhance the transcription factor *Nurr1*. This enhancement may have contributed to our study's decrease in dopamine observed among rats exposed to FNE. It is reasonable to hypothesize that this reduction in dopamine levels may be linked to inhibited dopamine biosynthesis. This process may have occurred due to decreased synthesis of tyrosine hydroxylase and aromatic l-amino acid decarboxylase (Liu and Shi, 2006). This study also revealed a molecular interaction with average docking scores among FNE, tyrosine hydroxylase (TH), and dopamine transporter (DAT). Also, another study revealed that FNE could target the TH-positive dopamine neurons (Xiong et al., 2016). Despite this, specific staining of dopaminergic neurons and TH could explain the effect of FNE. However, it is evident from previous studies that FNE can induce PD by damaging dopaminergic neurons (Jiao et al., 2020). Thus, we focused on the toxic effects on all cerebrum, hippocampus, and cerebellum neurons and how CRM nano-formulations could ameliorate them and help prevent neurodegenerative diseases, including PD.

Besides, the reduced dopamine levels in our study, after exposure to FNE, may primarily be attributed to the loss of the biosynthesis enzyme TH. Previous research also revealed an interaction between FNE and DAT, a member of the Na^+/Cl^--dependent transporter family and a key regulator of cytosolic dopamine concentration through molecular docking (Niode et al., 2021). This interaction might have contributed to the decline in dopamine levels in FNE-exposed rats, potentially leading to increased damage to dopamine neurons (Khoshbouei et al., 2003; Yoon et al., 2004). These findings underscore the consideration of FNE as a possible neurotoxin for DA and an environmental risk factor for PD. Additionally, glutamate was significantly elevated in the brains of rats exposed to FNE, as stated in many other studies (Xiong et al., 2016; Wu et al., 2023). This could be attributed to several mechanisms, among them the ability of FNE to cause glutamate buildup and exacerbation of excitotoxicity of a ubiquitin ligase that facilitates the ubiquitination and degradation of glutamate transporter 1, which causes the accumulation of glutamate in the synapse (Cao et al., 2011). Also, it was previously confirmed that several pyrethroids, including FNE, could cause efficient alterations in Ca^{2+} influx and activation of voltage-gated calcium channels, leading to the accumulation of glutamate (Cao et al., 2011; Symington et al., 2011).

Our results also revealed increased dopamine and reduced glutamate levels in the brain tissue of rats receiving CRM-Chs-NPs + FNE. This is consistent with what was found by Pan et al. (1999), who claimed the ability of CRM to increase dopamine and TH by inhibiting the glial fibrillary acidic protein (GFAP) and iNOS protein expression. Other studies also confirmed that CRM significantly protected TH-positive cells in the *substantia nigra* and restored dopamine levels in rat model (Ireson et al., 2001) and mice model (Jagatha et al., 2008). Moreover, CRM-Chs-NPs may decrease the extracellular glutamate content at a safe physiological level through a range of buffering processes, including glutamate absorption by glial cells and its conversion by glutamate decarboxylase or glutamine synthetase to the harmless glutamine (Khalil and Khedr, 2016). Furthermore, the earlier study Lin et al. (2012) demonstrated that CRM-mediated suppression of glutamate release results in downregulation of receptor expression for both metabotropic glutamate receptors 5 (mGluR5) and N-methyl-D-aspartate receptor 2B (NMDA2B).

In addition, immunohistochemistry revealed increased levels of vimentin, an intermediate filament protein of several cell types within the central nervous system (Chen et al., 2018), in the brain tissue of rats exposed to FNE compared to the control group. Vimentin also regulates the NLRP3 inflammasome since it interacts with NLRP3 in macrophages, facilitating the assembly of proteins involved in the inflammasome, including caspase-1. This latter contributes to the maturation of IL-1β (Marandi et al., 2021) and is thus associated with neuroinflammation (Khater et al., 2022). Our study also revealed an increased immunohistochemical staining of 4HNE in response to FNE exposure. This may be linked to FNE's ability to enhance the production of ROS and induce oxidative stress, which, in turn, disrupts mitochondrial function and ATP production, leading to disrupted synaptic transmission and neuronal degeneration.

Conversely, in the CRM-Chs-NPs + FNE group, we observed a reduction in the expression of both vimentin and 4HNE in the brain tissue compared to the FNE-exposed group. This reduction could be attributed to CRM-Chs-NPs' high ROS scavenging capacity, which promotes mitochondrial stability and ATP production (Naeimi et al., 2018). These findings provide substantial evidence for the anti-inflammatory, anti-apoptotic, and stable mitochondrial dynamics exerted by CRM-Chs-NPs.

Herein, a CRM-Chs-NPs formulation has been used to increase its bioavailability by shielding it from chemical breakdown. Such a formulation has already been used to integrate bioactive components into food or dietary supplements (McClements et al., 2009). In the current study, the oral administration of CRM-Chs-NPs to rats for 60 days resulted in no side effects. Throughout the experimental period, there were no noticeable changes in the general health state of the animals. Analysis of the recorded data indicated non-significant changes in some parameters, while in others, significant improvements were observed in the CRM-Chs-NPs group compared to the control. It is known that CRM-Chs-NPs have been extensively tested in previous studies and have been reported to be safely used in both food and drug applications. These findings reinforce the safety profile of CRM-Chs-NPs and support their potential utility in various biomedical and therapeutic applications (Jagatha et al., 2008; Rafiee et al., 2019).

5 Conclusion

Our findings indicate that the FNE challenge elicited signs of compromised mitochondrial function, declined ATP generation through inhibiting mitochondrial regeneration, and enhanced mitophagy. These factors collectively resulted in disrupted synaptic transmission and neuronal degeneration, outlining the harmful effects of FNE exposure on the pathophysiology of PD. However, the concurrent administration of CRM-Chs-NPs effectively reversed these detrimental effects. CRM-Chs-NPs restored ATP production, reduced proinflammatory cytokine levels, activated antioxidant enzymes, and mitigated oxidative stress. Additionally, CRM-Chs-NPs played a crucial role in regulating the activity of the mitochondrial gene complex and mitophagy, ultimately preserving the microarchitecture of brain tissue. These results underline the therapeutic potential of CRM-Chs-NPs in mitigating FNE-induced damage to dopaminergic neurons, mitochondrial health, and brain tissue microarchitectures.

Data availability statement

The original contributions presented in the study are included in the article/supplementary materials, further inquiries can be directed to the corresponding authors.

Ethics statement

The animal study was approved by the Ethics Committee at Zagazig University, Egypt (Approval number: ZU-IACUC/2/F/101/2022). The study was conducted in accordance with the local legislation and institutional requirements.

Author contributions

BA: Validation, Writing–original draft, Writing–review and editing, Investigation, Methodology, Project administration, Visualization. AA-R: Writing–original draft, Writing–review and editing, Conceptualization, Data curation, Software, Visualization, Validation, Project administration, Methodology, Investigation. YA-E: Supervision, Writing–review and editing, Writing–original draft, Visualization, Validation, Software, Investigation. AN: Writing–review and editing, Writing–original draft, Visualization, Validation, Supervision, Software, Investigation. ME: Writing–review and editing, Writing–original draft, Visualization, Validation, Supervision, Software, Investigation. TK: Investigation, Validation, Visualization, Writing–original draft, Writing–review and editing, Methodology. AE-F: Software, Data curation, Writing–review and editing, Writing–original draft, Visualization, Validation, Methodology, Investigation. MA: Supervision, Writing–review and editing, Writing–original draft, Visualization, Validation, Software, Methodology, Investigation. ND: Formal Analysis, Writing–review and editing, Writing–original draft, Validation, Supervision, Methodology, Investigation. LA: Project administration, Visualization, Formal Analysis, Methodology, Validation, Writing–review and editing, Writing–original draft. MN: Investigation, Writing–review and editing, Writing–original draft, Visualization, Validation, Methodology. ME-G: Validation, Writing–original draft, Writing–review and editing, Conceptualization, Resources, Supervision, Visualization. AD: Software, Funding acquisition, Formal Analysis, Data curation, Supervision, Writing–review and editing, Writing–original draft, Validation.

Acknowledgement

Princess Nourah bint Abdulrahman University Researchers Supporting Project number (PNURSP2024R73), Princess Nourah bint Abdulrahman University, Riyadh, Saudi Arabia.

Conflict of interest

The authors declare that the research was conducted in the absence of any commercial or financial relationships that could be construed as a potential conflict of interest.

The author(s) declared that they were an editorial board member of Frontiers, at the time of submission. This had no impact on the peer review process and the final decision.

Publisher's note

All claims expressed in this article are solely those of the authors and do not necessarily represent those of their affiliated organizations, or those of the publisher, the editors and the reviewers. Any product that may be evaluated in this article, or claim that may be made by its manufacturer, is not guaranteed or endorsed by the publisher.

References

Abd-Elhakim, Y. M., Abdel-Motal, S. M., Malhat, S. M., Mostafa, H. I., Ibrahim, W. M., Beheiry, R. R., et al. (2022). Curcumin attenuates gentamicin and sodium salicylate ototoxic effects by modulating the nuclear factor-kappaB and apoptotic pathways in rats. *Environ. Sci. Pollut. Res. Int.* 29, 89954–89968. doi:10.1007/s11356-022-21932-1

Abdelnour, S. A., Swelum, A. A., Abd El-Hack, M. E., Khafaga, A. F., Taha, A. E., and Abdo, M. (2020). Cellular and functional adaptation to thermal stress in ovarian granulosa cells in mammals. *J. Therm. Biol.* 92, 102688. doi:10.1016/j.jtherbio.2020.102688

Abdou, R., Sasaki, K., Khalil, W., Shah, S., Murasawa, Y., and Shimoda, M. (2010). Effects of several pyrethroids on hepatic cytochrome P450 activities in rats. *J. Vet. Med. Sci.* 72, 425–433. doi:10.1292/jvms.09-0347

Aebi, H. (1984). Catalase *in vitro*. *Methods Enzymol.* 105, 121–126. doi:10.1016/s0076-6879(84)05016-3

Agnihotri, A., and Aruoma, O. I. (2020). Alzheimer's disease and Parkinson's disease: a nutritional toxicology perspective of the impact of oxidative stress, mitochondrial dysfunction, nutrigenomics and environmental chemicals. *J. Am. Coll. Nutr.* 39, 16–27. doi:10.1080/07315724.2019.1683379

Alisi, I. O., Uzairu, A., Abechi, S. E., and Idris, S. O. (2018). Evaluation of the antioxidant properties of curcumin derivatives by genetic function algorithm. *J. Adv. Res.* 12, 47–54. doi:10.1016/j.jare.2018.03.003

Alqahtani, L. S., Abd-Elhakim, Y. M., Mohamed, A. A., Khalifa, N. E., Khamis, T., Alotaibi, B. S., et al. (2023). Curcumin-loaded chitosan nanoparticles alleviate fenpropathrin-induced hepatotoxicity by regulating lipogenesis and pyroptosis in rats. *Food Chem. Toxicol.* 180, 114036. doi:10.1016/j.fct.2023.114036

Anand, P., Kunnumakkara, A. B., Newman, R. A., and Aggarwal, B. B. (2007). Bioavailability of curcumin: problems and promises. *Mol. Pharm.* 4, 807–818. doi:10.1021/mp700113r

Arya, G., Das, M., and Sahoo, S. K. (2018). Evaluation of curcumin loaded chitosan/PEG blended PLGA nanoparticles for effective treatment of pancreatic cancer. *Biomed. Pharmacother.* 102, 555–566. doi:10.1016/j.biopha.2018.03.101

Asai, A., and Miyazawa, T. (2000). Occurrence of orally administered curcuminoid as glucuronide and glucuronide/sulfate conjugates in rat plasma. *Life Sci.* 67, 2785–2793. doi:10.1016/s0024-3205(00)00868-7

Bavarsad, K., Barreto, G. E., Hadjzadeh, M.-a.-R., and Sahebkar, A. (2019). Protective effects of curcumin against ischemia-reperfusion injury in the nervous system. *Mol. Neurobiol.* 56, 1391–1404. doi:10.1007/s12035-018-1169-7

Beutler, E., Duron, O., and Kelly, B. M. (1963). Improved method for the determination of blood glutathione. *J. Lab. Clin. Med.* 61, 882–888.

Brander, S. M., Gabler, M. K., Fowler, N. L., Connon, R. E., and Schlenk, D. (2016). Pyrethroid pesticides as endocrine disruptors: molecular mechanisms in vertebrates with a focus on fishes. *Environ. Sci. Technol.* 50, 8977–8992. doi:10.1021/acs.est.6b02253

Buckels, E. J., Ross, J. M., Phua, H. H., Bloomfield, F. H., and Jaquiery, A. L. (2022). Whole-slide imaging and a Fiji-based image analysis workflow of immunohistochemistry staining of pancreatic islets. *MethodsX* 9, 101856. doi:10.1016/j.mex.2022.101856

Burbulla, L. F., Song, P., Mazzulli, J. R., Zampese, E., Wong, Y. C., Jeon, S., et al. (2017). Dopamine oxidation mediates mitochondrial and lysosomal dysfunction in Parkinson's disease. *Science* 357, 1255–1261. doi:10.1126/science.aam9080

Cao, J., Liu, Y., Jia, L., Zhou, H. M., Kong, Y., Yang, G., et al. (2007). Curcumin induces apoptosis through mitochondrial hyperpolarization and mtDNA damage in human hepatoma G2 cells. *Free Radic. Biol. Med.* 43, 968–975. doi:10.1016/j.freeradbiomed.2007.06.006

Cao, Z., Shafer, T. J., and Murray, T. F. (2011). Mechanisms of pyrethroid insecticide-induced stimulation of calcium influx in neocortical neurons. *J. Pharmacol. Exp. Ther.* 336, 197–205. doi:10.1124/jpet.110.171850

Chen, M., Puschmann, T. B., Marasek, P., Inagaki, M., Pekna, M., Wilhelmsson, U., et al. (2018). Increased neuronal differentiation of neural progenitor cells derived from phosphovimentin-deficient mice. *Mol. Neurobiol.* 55, 5478–5489. doi:10.1007/s12035-017-0759-0

Cui, M., Tang, X., Christian, W. V., Yoon, Y., and Tieu, K. (2010). Perturbations in mitochondrial dynamics induced by human mutant PINK1 can be rescued by the mitochondrial division inhibitor mdivi-1. *J. Biol. Chem.* 285, 11740–11752. doi:10.1074/jbc.M109.066662

Elwan, M. A., Richardson, J. R., Guillot, T. S., Caudle, W. M., and Miller, G. W. (2006). Pyrethroid pesticide-induced alterations in dopamine transporter function. *Toxicol. Appl. Pharmacol.* 211, 188–197. doi:10.1016/j.taap.2005.06.003

Fei, J., Qu, J. H., Ding, X. L., Xue, K., Lu, C. C., Chen, J. F., et al. (2010). Fenvalerate inhibits the growth of primary cultured rat preantral ovarian follicles. *Toxicology* 267, 1–6. doi:10.1016/j.tox.2009.10.022

Filichia, E., Hoffer, B., Qi, X., and Luo, Y. (2016). Inhibition of Drp1 mitochondrial translocation provides neural protection in dopaminergic system in a Parkinson's disease model induced by MPTP. *Sci. Rep.* 6, 32656. doi:10.1038/srep32656

Fischer, A. H., Jacobson, K. A., Rose, J., and Zeller, R. (2008). Hematoxylin and eosin staining of tissue and cell sections. *CSH Protoc.* 2008, pdb.prot4986. doi:10.1101/pdb.prot4986

Gajendiran, A., and Abraham, J. (2018). An overview of pyrethroid insecticides. *Front. Biol.* 13, 79–90. doi:10.1007/s11515-018-1489-z

Gassner, B., Wuthrich, A., Scholtysik, G., and Solioz, M. (1997). The pyrethroids permethrin and cyhalothrin are potent inhibitors of the mitochondrial complex I. *J. Pharmacol. Exp. Ther.* 281, 855–860.

Gibson-Corley, K. N., Olivier, A. K., and Meyerholz, D. K. (2013). Principles for valid histopathologic scoring in research. *Vet. Pathol.* 50, 1007–1015. doi:10.1177/0300985813485099

Golpich, M., Amini, E., Mohamed, Z., Azman Ali, R., Mohamed Ibrahim, N., and Ahmadiani, A. (2017). Mitochondrial dysfunction and biogenesis in neurodegenerative diseases: pathogenesis and treatment. *CNS Neurosci. Ther.* 23, 5–22. doi:10.1111/cns.12655

Hend, R., and Butterworth, S. (1976). *Toxicity studies on the insecticide WL 41706: a three month feeding study in rats. Unpublished report no. TLGR* 20.

Husain, R., Malaviya, M., Seth, P. K., and Husain, R. (1994). Effect of deltamethrin on regional brain polyamines and behaviour in young rats. *Pharmacol. Toxicol.* 74, 211–215. doi:10.1111/j.1600-0773.1994.tb01100.x

Ireson, C., Orr, S., Jones, D. J., Verschoyle, R., Lim, C.-K., Luo, J.-L., et al. (2001). Characterization of metabolites of the chemopreventive agent curcumin in human and rat hepatocytes and in the rat *in vivo*, and evaluation of their ability to inhibit phorbol ester-induced prostaglandin E2 production. *Cancer Res.* 61, 1058–1064.

Itokawa, H., Shi, Q., Akiyama, T., Morris-Natschke, S. L., and Lee, K. H. (2008). Recent advances in the investigation of curcuminoids. *Chin. Med.* 3, 11. doi:10.1186/1749-8546-3-11

Jagatha, B., Mythri, R. B., Vali, S., and Bharath, M. M. (2008). Curcumin treatment alleviates the effects of glutathione depletion *in vitro* and *in vivo*: therapeutic implications for Parkinson's disease explained via *in silico* studies. *Free Radic. Biol. Med.* 44, 907–917. doi:10.1016/j.freeradbiomed.2007.11.011

Jana, S., Sinha, M., Chanda, D., Roy, T., Banerjee, K., Munshi, S., et al. (2011). Mitochondrial dysfunction mediated by quinone oxidation products of dopamine: implications in dopamine cytotoxicity and pathogenesis of Parkinson's disease. *Biochim. Biophys. Acta* 1812, 663–673. doi:10.1016/j.bbadis.2011.02.013

Jiao, Z., Wu, Y., and Qu, S. (2020). Fenpropathrin induces degeneration of dopaminergic neurons via disruption of the mitochondrial quality control system. *Cell Death Discov.* 6, 78. doi:10.1038/s41420-020-00313-y

Karen, D. J., Li, W., Harp, P. R., Gillette, J. S., and Bloomquist, J. R. (2001). Striatal dopaminergic pathways as a target for the insecticides permethrin and chlorpyrifos. *Neurotoxicology* 22, 811–817. doi:10.1016/s0161-813x(01)00063-8

Kehlet, H., Jensen, T. S., and Woolf, C. J. (2006). Persistent postsurgical pain: risk factors and prevention. *Lancet* 367, 1618–1625. doi:10.1016/S0140-6736(06)68700-X

Khalil, R. M., and Khedr, N. F. (2016). Curcumin protects against monosodium glutamate neurotoxicity and decreasing NMDA2B and mGluR5 expression in rat Hippocampus. *Neurosignals* 24, 81–87. doi:10.1159/000442614

Khan, M. A., Zafaryab, M., Mehdi, S. H., Ahmad, I., and Rizvi, M. M. A. (2018). Physicochemical characterization of curcumin loaded chitosan nanoparticles: implications in cervical cancer. *Anticancer Agents Med. Chem.* 18, 1131–1137. doi:10.2174/1871520618666180412114352

Khater, S. I., Dowidar, M. F., Abdel-Aziz, A. E., Khamis, T., Dahran, N., Alqahtani, L. S., et al. (2022). β-Cell autophagy pathway and endoplasmic reticulum stress regulating-role of liposomal curcumin in experimental diabetes mellitus: a molecular and morphometric study. *Antioxidants* 11, 2400. doi:10.3390/antiox11122400

Khater, S. I., Mohamed, A. A., Arisha, A. H., Ebraheim, L. L. M., El-Mandrawy, S. a.M., Nassan, M. A., et al. (2021). Stabilized-chitosan selenium nanoparticles efficiently reduce renal tissue injury and regulate the expression pattern of aldose reductase in the diabetic-nephropathy rat model. *Life Sci.* 279, 119674. doi:10.1016/j.lfs.2021.119674

Khoshbouei, H., Wang, H., Lechleiter, J. D., Javitch, J. A., and Galli, A. (2003). Amphetamine-induced dopamine efflux. A voltage-sensitive and intracellular Na+-dependent mechanism. *J. Biol. Chem.* 278, 12070–12077. doi:10.1074/jbc.M212815200

Kimmich, G. A., Randles, J., and Brand, J. S. (1975). Assay of picomole amounts of ATP, ADP, and AMP using the luciferase enzyme system. *Anal. Biochem.* 69, 187–206. doi:10.1016/0003-2697(75)90580-1

Kunjachan, S., and Jose, S. (2010). Understanding the mechanism of ionic gelation for synthesis of chitosan nanoparticles using qualitative techniques. *Asian J. Pharm.* 4, 148. doi:10.4103/0973-8398.68467

Lin, D., Xiao, L., Qin, W., Loy, D. A., Wu, Z., Chen, H., et al. (2022). Preparation, characterization and antioxidant properties of curcumin encapsulated chitosan/lignosulfonate micelles. *Carbohydr. Polym.* 281, 119080. doi:10.1016/j.carbpol.2021.119080

Lin, T. Y., Lu, C. W., Huang, S. K., and Wang, S. J. (2012). Curcumin inhibits glutamate release from rat prefrontal nerve endings by affecting vesicle mobilization. *Int. J. Mol. Sci.* 13, 9097–9109. doi:10.3390/ijms13079097

Liu, G. P., and Shi, N. (2006). The inhibitory effects of deltamethrin on dopamine biosynthesis in rat PC12 cells. *Toxicol. Lett.* 161, 195–199. doi:10.1016/j.toxlet.2005.09.011

Maiti, P., Scott, J., Sengupta, D., Al-Gharaibeh, A., and Dunbar, G. L. (2019). Curcumin and solid lipid curcumin particles induce autophagy, but inhibit mitophagy and the PI3K-Akt/mTOR pathway in cultured glioblastoma cells. *Int. J. Mol. Sci.* 20, 399. [Online]. doi:10.3390/ijms20020399

Marandi, Y., Hashemzade, S., Tayebinia, H., Karimi, J., Zamani, A., and Khodadadi, I. (2021). NLRP3-inflammasome activation is associated with epithelial-mesenchymal transition and progression of colorectal cancer. *Iran. J. Basic Med. Sci.* 24, 483–492. doi:10.22038/ijbms.2021.52355.11835

Mcclements, D. J., Decker, E. A., Park, Y., and Weiss, J. (2009). Structural design principles for delivery of bioactive components in nutraceuticals and functional foods. *Crit. Rev. Food Sci. Nutr.* 49, 577–606. doi:10.1080/10408390902841529

Mihara, M., and Uchiyama, M. (1978). Determination of malonaldehyde precursor in tissues by thiobarbituric acid test. *Anal. Biochem.* 86, 271–278. doi:10.1016/0003-2697(78)90342-1

Mohamed, A. A., Abdellatief, S. A., Khater, S. I., Ali, H., and Al-Gabri, N. A. (2019). Fenpropathrin induces testicular damage, apoptosis, and genomic DNA damage in adult rats: protective role of camel milk. *Ecotoxicol. Environ. Saf.* 181, 548–558. doi:10.1016/j.ecoenv.2019.06.047

Mohamed, A. A., Behairy, A., Abd El-Hakim, Y. M., Metwally, M. M. M., Khamis, T., Abuzahrah, S. S., et al. (2023). Comparable bio-evaluation of curcumin and chitosan-encapsulated curcumin nanoparticles against the reprotoxic potential of fenpropathrin pyrethroid in rats: genomic and morphometric prospectives. *Food Chem. Toxicol.* 179, 113977. doi:10.1016/j.fct.2023.113977

Mohamed, A. A., Rahman, A. N. A., Mohammed, H. H., Ebraheim, L. L. M., Abo-Elmaaty, A. M. A., Ali, S. A., et al. (2020). Neurobehavioral, apoptotic, and DNA damaging effects of sub-chronic profenofos exposure on the brain tissue of *Cyprinus carpio* L.: antagonistic role of Geranium essential oil. *Aquat. Toxicol.* 224, 105493. doi:10.1016/j.aquatox.2020.105493

Moradi Vastegani, S., Nasrolahi, A., Ghaderi, S., Belali, R., Rashno, M., Farzaneh, M., et al. (2023). Mitochondrial dysfunction and Parkinson's disease: pathogenesis and therapeutic strategies. *Neurochem. Res.* 48, 2285–2308. doi:10.1007/s11064-023-03904-0

Naeimi, R., Safarpour, F., Hashemian, M., Tashakorian, H., Ahmadian, S. R., Ashrafpour, M., et al. (2018). Curcumin-loaded nanoparticles ameliorate glial activation and improve myelin repair in lyolecithin-induced focal demyelination model of rat corpus callosum. *Neurosci. Lett.* 674, 1–10. doi:10.1016/j.neulet.2018.03.018

Nasuti, C., Gabbianelli, R., Falcioni, M. L., Di Stefano, A., Sozio, P., and Cantalamessa, F. (2007). Dopaminergic system modulation, behavioral changes, and oxidative stress after neonatal administration of pyrethroids. *Toxicology* 229, 194–205. doi:10.1016/j.tox.2006.10.015

Niode, N. J., Adji, A., Rimbing, J., Tulung, M., Alorabi, M., El-Shehawi, A. M., et al. (2021). *In silico* and *in vitro* evaluation of the antimicrobial potential of Bacillus cereus isolated from Apis dorsata gut against Neisseria gonorrhoeae. *Antibiot. (Basel)* 10, 1401. doi:10.3390/antibiotics10111401

Noreldin, A. E., Elewa, Y. H. A., Kon, Y., Warita, K., and Hosaka, Y. Z. (2018). Immunohistochemical localization of osteoblast activating peptide in the mouse kidney. *Acta histochem.* 120, 323–328. doi:10.1016/j.acthis.2018.03.001

Ogawa, T., Matson, W. R., Beal, M. F., Myers, R. H., Bird, E. D., Milbury, P., et al. (1992). Kynurenine pathway abnormalities in Parkinson's disease. *Neurology* 42, 1702–1706. doi:10.1212/wnl.42.9.1702

Pan, M. H., Huang, T. M., and Lin, J. K. (1999). Biotransformation of curcumin through reduction and glucuronidation in mice. *Drug Metab. Dispos.* 27, 486–494.

Percie Du Sert, N., Hurst, V., Ahluwalia, A., Alam, S., Avey, M. T., Baker, M., et al. (2020). The ARRIVE guidelines 2.0: updated guidelines for reporting animal research. *BMC Veterinary Res.* 16, 242. doi:10.1186/s12917-020-02451-y

Proudfoot, A. T. (2005). Poisoning due to pyrethrins. *Toxicol. Rev.* 24, 107–113. doi:10.2165/00139709-200524020-00004

Rafiee, Z., Nejatian, M., Daeihamed, M., and Jafari, S. M. (2019). Application of curcumin-loaded nanocarriers for food, drug and cosmetic purposes. *Trends Food Sci. Technol.* 88, 445–458. doi:10.1016/j.tifs.2019.04.017

Rahman, A. N. A., Mohamed, A. A., Dahran, N., Farag, M. F. M., Alqahtani, L. S., Nassan, M. A., et al. (2022). Appraisal of sub-chronic exposure to lambada-cyhalothrin and/or methomyl on the behavior and hepato-renal functioning in *Oreochromis niloticus*: supportive role of taurine-supplemented feed. *Aquat. Toxicol.* 250, 106257. doi:10.1016/j.aquatox.2022.106257

Rainey, N. E., Moustapha, A., and Petit, P. X. (2020). Curcumin, a multifaceted hormetic agent, mediates an intricate crosstalk between mitochondrial turnover,

autophagy, and apoptosis. *Autophagy, Apoptosis* 2020, 3656419. doi:10.1155/2020/3656419

Reddy, P. H., Reddy, T. P., Manczak, M., Calkins, M. J., Shirendeb, U., and Mao, P. (2011). Dynamin-related protein 1 and mitochondrial fragmentation in neurodegenerative diseases. *Brain Res. Rev.* 67, 103–118. doi:10.1016/j.brainresrev.2010.11.004

Ryan, B. J., Hoek, S., Fon, E. A., and Wade-Martins, R. (2015). Mitochondrial dysfunction and mitophagy in Parkinson's: from familial to sporadic disease. *Trends Biochem. Sci.* 40, 200–210. doi:10.1016/j.tibs.2015.02.003

Saafan, S. M., Mohamed, S. A., Noreldin, A. E., El Tedawy, F. A., Elewa, Y. H. A., Fadly, R. S., et al. (2023). Rutin attenuates D-galactose-induced oxidative stress in rats' brain and liver: molecular docking and experimental approaches. *Food Funct.* 14, 5728–5751. doi:10.1039/d2fo03301a

Salem, G. A., Mohamed, A. A., Khater, S. I., Noreldin, A. E., Alosaimi, M., Alansari, W. S., et al. (2023). Enhancement of biochemical and genomic pathways through lycopene-loaded nano-liposomes: alleviating insulin resistance, hepatic steatosis, and autophagy in obese rats with non-alcoholic fatty liver disease: involvement of SMO, GLI-1, and PTCH-1 genes. *Gene* 883, 147670. doi:10.1016/j.gene.2023.147670

Sandhir, R., Yadav, A., Mehrotra, A., Sunkaria, A., Singh, A., and Sharma, S. (2014). Curcumin nanoparticles attenuate neurochemical and neurobehavioral deficits in experimental model of Huntington's disease. *Neuromolecular Med.* 16, 106–118. doi:10.1007/s12017-013-8261-y

Sankar, P., Telang, A. G., and Manimaran, A. (2012). Protective effect of curcumin on cypermethrin-induced oxidative stress in Wistar rats. *Exp. Toxicol. Pathol.* 64, 487–493. doi:10.1016/j.etp.2010.11.003

Sas, K., Robotka, H., Toldi, J., and Vecsei, L. (2007). Mitochondria, metabolic disturbances, oxidative stress and the kynurenine system, with focus on neurodegenerative disorders. *J. Neurol. Sci.* 257, 221–239. doi:10.1016/j.jns.2007.01.033

Schindelin, J., Arganda-Carreras, I., Frise, E., Kaynig, V., Longair, M., Pietzsch, T., et al. (2012). Fiji: an open-source platform for biological-image analysis. *Nat. Methods* 9, 676–682. doi:10.1038/nmeth.2019

Sekine, S., and Youle, R. J. (2018). PINK1 import regulation; a fine system to convey mitochondrial stress to the cytosol. *BMC Biol.* 16, 2. doi:10.1186/s12915-017-0470-7

Spitz, D. R., and Oberley, L. W. (1989). An assay for superoxide dismutase activity in mammalian tissue homogenates. *Anal. Biochem.* 179, 8–18. doi:10.1016/0003-2697(89)90192-9

Stanic, Z. (2017). Curcumin, a compound from natural sources, a true scientific challenge - a review. *Plant Foods Hum. Nutr.* 72, 1–12. doi:10.1007/s11130-016-0590-1

Symington, S. B., Hodgdon, H. E., Frisbie, R. K., and Clark, J. M. (2011). Binary mixtures of pyrethroids produce differential effects on Ca2+ influx and glutamate release at isolated presynaptic nerve terminals from rat brain. *Pesticide Biochem. Physiology* 99, 131–139. doi:10.1016/j.pestbp.2010.11.009

Tong, H., Zhang, X., Meng, X., Lu, L., Mai, D., and Qu, S. (2018). Simvastatin inhibits activation of NADPH oxidase/p38 MAPK pathway and enhances expression of antioxidant protein in Parkinson disease models. *Front. Mol. Neurosci.* 11, 165. doi:10.3389/fnmol.2018.00165

Treuting, P. M., Dintzis, S., and Montine, K. S. (2017). *Comparative anatomy and histology: a mouse, rat, and human atlas*. Amsterdam, Netherlands: Elsevier Science.

Trujillo, J., Chirino, Y. I., Molina-Jijón, E., Andérica-Romero, A. C., Tapia, E., and Pedraza-Chaverrí, J. (2013). Renoprotective effect of the antioxidant curcumin: recent findings. *Redox Biol.* 1, 448–456. doi:10.1016/j.redox.2013.09.003

Vilar, S., Cozza, G., and Moro, S. (2008). Medicinal chemistry and the molecular operating environment (MOE): application of QSAR and molecular docking to drug discovery. *Curr. Top. Med. Chem.* 8, 1555–1572. doi:10.2174/156802608786786624

Vis, A. N., Kranse, R., Nigg, A. L., and Van Der Kwast, T. H. (2000). Quantitative analysis of the decay of immunoreactivity in stored prostate needle biopsy sections. *Am. J. Clin. Pathol.* 113, 369–373. doi:10.1309/CQWY-E3F6-9KDN-YV36

Weiner, M. L., Nemec, M., Sheets, L., Sargent, D., and Breckenridge, C. (2009). Comparative functional observational battery study of twelve commercial pyrethroid insecticides in male rats following acute oral exposure. *Neurotoxicology* 30 (Suppl. 1), S1–S16. doi:10.1016/j.neuro.2009.08.014

Wu, Y., Qu, Q., Wan, Z., and Qu, S. (2023). Fenpropathrin induces GLT-1 ubiquitination and increases IL-6 secretion through the mdm2-p53 pathway. *ACS Chem. Neurosci.* 14, 2112–2122. doi:10.1021/acschemneuro.3c00112

Xiong, J., Zhang, X., Huang, J., Chen, C., Chen, Z., Liu, L., et al. (2016). Fenpropathrin, a widely used pesticide, causes dopaminergic degeneration. *Mol. Neurobiol.* 53, 995–1008. doi:10.1007/s12035-014-9057-2

Yin, R., Xue, J., Tan, Y., Fang, C., Hu, C., Yang, Q., et al. (2021). The positive role and mechanism of herbal medicine in Parkinson's disease. *Oxid. Med. Cell Longev.* 2021, 9923331. doi:10.1155/2021/9923331

Yoon, J. Y., Ahn, S. H., Oh, H., Kim, Y. S., Ryu, S. Y., Ho, W. K., et al. (2004). A novel Na+ channel agonist, dimethyl lithospermate B, slows Na+ current inactivation and increases action potential duration in isolated rat ventricular myocytes. *Br. J. Pharmacol.* 143, 765–773. doi:10.1038/sj.bjp.0705969

Yuan, J. S., Reed, A., Chen, F., and Stewart, C. N., Jr. (2006). Statistical analysis of real-time PCR data. *BMC Bioinforma.* 7, 85. doi:10.1186/1471-2105-7-85

Zielinska, E., Kocki, T., Saran, T., Borbely, S., Kuc, D., Vilagi, I., et al. (2005). Effect of pesticides on kynurenic acid production in rat brain slices. *Ann. Agric. Environ. Med.* 12, 177–179.

frontiers | Frontiers in Pharmacology

TYPE Original Research
PUBLISHED 30 May 2024
DOI 10.3389/fphar.2024.1342226

OPEN ACCESS

EDITED BY
Giuseppe Di Giovanni,
University of Malta, Malta

REVIEWED BY
Sivareddy Challa,
University of Illinois at Peoria, United States
Gaoxiao Zhang,
Jinan University, China

*CORRESPONDENCE
Guobiao Liang,
liangguobiao6708@163.com
Chunyong Yu,
zhengjiangning@sina.com
Pengyu Pan,
panpengyu09@sina.com

RECEIVED 21 November 2023
ACCEPTED 06 May 2024
PUBLISHED 30 May 2024

CITATION
Zhu K, Bi S, Zhu Z, Zhang W, Yang X, Li J, Liang G, Yu C and Pan P (2024), Edaravone dexborneol attenuates oxidative stress in experimental subarachnoid hemorrhage via Keap1/Nrf2 signaling pathway.
Front. Pharmacol. 15:1342226.
doi: 10.3389/fphar.2024.1342226

Edaravone dexborneol attenuates oxidative stress in experimental subarachnoid hemorrhage via Keap1/Nrf2 signaling pathway

Kunyuan Zhu[1,2], Shijun Bi[1], Zechao Zhu[1,2], Wenxu Zhang[1,2], Xinyu Yang[1,2], Jiashuo Li[2], Guobiao Liang [1]*, Chunyong Yu[1]* and Pengyu Pan [1]*

[1]Department of Neurosurgery, General Hospital of Northern Theater Command, Shenyang, China, [2]China Medical University, Shenyang, Liaoning, China

Background: Subarachnoid hemorrhage (SAH) serves as a disease characterized by high incidence rate, which is exceedingly prevalent and severe. Presently, there is no unambiguous or efficacious intervention for the neurological impairment following SAH. Administering multi-targeted neuroprotective agents to reduce oxidative stress (OS) and neuroinflammation caused by early brain injury (EBI) has been demonstrated to improve neurological function and prognosis following SAH. Edaravone dexborneol (EDB), a novel multi targeted neuroprotective medication, combines four parts edaravone (EDA) with 1 part (+)-borneol in proportion. Clinical trials conducted in China have revealed during 2 days of acute ischemic stroke (AIS), early administration of EDB leads to improved therapeutic outcomes compared to treatment in EDA monotherapy. Currently, there is no clear evidence that EDB can effectively treat SAH, therefore, our study aims to investigate its potential therapeutic effects and mechanisms on EBI after SAH.

Method: We used the intravascular threading method to establish a mouse model of SAH to explore whether EDA and EDB could produce anti-OS and anti-apoptosis effects. Behavioral assessment of mice was conducted using the balance beam experiment and the modified Garcia scoring system. Neuronal damage due to OS and Keap1/Nrf2 signaling pathway were detected through techniques of immunofluorescence, Western blotting, spectrophotometry. The group of EDA and EDB were injected intraperitoneally for 72 h after SAH.

Results: The experiment results indicated that EDB lead to remarkably positive results by significantly enhancing neurological function, reducing blood-brain barrier (BBB) injury, and effectively inhibiting neuronal apoptosis after SAH. Further examination indicated EDB significantly reduced the expression of Keap1 and increased the expression of Nrf2, and it inhibited MDA, and

Abbreviations: EDA, Edaravone; EDB, Edaravone dexborneol; SAH, Subarachnoid hemorrhage; OS, Oxidative stress; EBI, Early brain injury; AIS, Acute ischemic stroke; IAS, Intracranial aneurysms; BBB, Blood-brain barrier; ROS, Reactive oxygen species; MDA, Malondialdehyde; SOD, Superoxide dismutase; TNF-α, Tumor necrosis factor-α; IL-1β, Interleukin-1β; COX-2, Cyclooxygenase-2; Keap1, Kelch-like ECH-associated protein 1; Nrf2, Nuclear factor erythroid 2-related factor 2; ICA, Internal carotid artery; ECA, External carotid artery; CCA, Common carotid artery; ANOVA, One-way analysis of variance.

enhanced SOD activity after SAH. These outcomes surpassed the effectiveness observed in EDA monotherapy. However, the application of ML385 reversed the anti-OS effects of EDB and EDA.

Conclusion: Our experimental findings indicated that EDB could activate Keap1/Nrf2 signaling pathway to reduce OS damage, thereby protecting neurological function and enhancing behavioral abilities after SAH. These outcomes could facilitate the creation of new approaches for the clinical management of SAH.

KEYWORDS

subarachnoid hemorrhage, early brain injury, edaravone dexborneol, oxidative stress, KEAP1, Nrf2,

1 Introduction

Subarachnoid hemorrhage (SAH) is a severe neurological disorder, which result in substantial neurological impairment and potentially life-threatening complications (Claassen and Park, 2022). The primary cause is the intracranial aneurysm rupture, accounting for approximately 85% (Claassen and Park, 2022). Patients with SAH at 55 years averagely, experience a notable impact on their quality of life, health, and personal property safety (Macdonald and Schweizer, 2017). Neuronal damage after SAH can occur through various pathways, such as neuroinflammation and injury caused by oxidative stress (OS) (Xu W. et al., 2019; Zeng et al., 2021). Pathophysiological alterations, such as the disturbance of blood-brain barrier (BBB) or the occurrence of vasogenic and cytotoxic cerebral oedema, can contribute to early brain injury (EBI), ultimately resulting in deteriorating neurological impairment (Feng et al., 2022). At present, there is a lack of any recognized successful approach to tackle the neurological damage resulting from SAH. Therefore, we urgently need a new treatment with good curative effect. Research has demonstrated that multi-target neuroprotective agents, which help to reduce OS and neuroinflammation induced by EBI, can be significant interventions to improve neurological impairment and prognosis following SAH (Feng et al., 2022). The main components of edaravone dexborneol (EDB) are edaravone (EDA) and dexborneol. It was considered to be a novel neuroprotective agent (Xu J. et al., 2019). Wherein, EDA serves as free radical scavenger, safeguarding neurons by sequestering reactive oxygen species (ROS) (Suh et al., 2019). Then, by preventing lipid peroxidation, DNA damage, and vascular endothelial damage, EDA aided in reducing neuronal injury resulting from SAH (Kikuchi et al., 2013; Wu S. et al., 2014). Furthermore, the administration of EDA markedly reduced neuronal apoptosis in cases of SAH (Chen et al., 2022). Dexborneol, the primary compound in (+)-borneol, is a bicyclic monoterpenoid that is highly soluble in lipids (Liu et al., 2021). It assisted in the absorption of other medications and helped preserve the integrity of the tight junction proteins and BBB (Liu et al., 2011; Dong et al., 2018). By enhancing the superoxide dismutase (SOD) activity, reducing the malondialdehyde (MDA) level, and effectively alleviating OS harm to the body, dexborneol demonstrates its antioxidant properties (Hur et al., 2013). Furthermore, it had the potential to decrease the synthesis or conveyance of proinflammatory cytokines such as interleukin-1β (IL-1β), cyclooxygenase-2 (COX-2), and tumor necrosis factor-α (TNF-α), thereby mitigating the risk of inflammation (Chen et al., 2019). Studies evaluating the effectiveness of EDB have shown improved neurological results in patients who received EDB during 2 days of acute ischemic stroke (AIS) onset, as opposed to those treated solely with EDA (Xu J. et al., 2019; Xu et al., 2021). EDB has proposed to offer protection from AIS through various pathways, including anti-oxidative, anti-inflammatory, and inhibition of apoptosis (Hu R. et al., 2022). Studies have demonstrated that the conventional OS pathway kelch-like ECH-associated protein 1 (Keap1)/nuclear factor erythroid 2-related factor 2 (Nrf2) signaling pathway is effective in treating cerebral infarction (Zhang et al., 2023). Keap1 and Nrf2 collaborate to regulate the antioxidant reaction, presenting a possible treatment approach for inflammatory diseases. The imbalance of Keap1/Nrf2 complex decreases antioxidants and may be related to the advancement of SAH (Tu et al., 2019). After SAH, a pathophysiological process of global cerebral ischemia occurs (Sehba et al., 2013). Pathophysiological process of global cerebral ischemia after SAH. Emerging evidence indicated that EDB could diminish OS and inflammation in a cerebral infarction model through Keap1/Nrf2 signaling pathway (Yang et al., 2022). However, the efficacy of EDB in treating brain injury caused by SAH has not been conclusively established. Our hypothesis is that EDB could reduce neurological injury induced by SAH by inhibiting OS via Keap1/Nrf2. In our experiment, we evaluated the therapeutic efficacy of EDB treating SAH and elucidated the mechanisms involved, to provide a new clinical strategy for treating SAH.

2 Materials and methods

2.1 Experimental animals

The research study underwent a thorough review and approved by the Ethics Committee of the General Hospital of the Northern Theater command. A total of 410 C57BL/6 mice (adult male, aged 8–10 weeks, weighing 22–30 g) were employed for this investigation. These animals were procured from the Laboratory Animal Centre of the General Hospital of the Northern Theater command. Our experimental animals were accommodated in a standard light environment (12 h of darkness/12 h of light) within an SPF-class laboratory animal facility, ensuring they had access to sufficient food and water.

2.2 Experimental design

This experimental design contained the three parts, with the following:

Experiment 1: To examine the effectiveness of EDB and determine the optimal dosage, we allocated randomly 100 C57BL/6 mice to seven groups, namely, sham, SAH, SAH + vehicle, SAH + EDB 1.25 mg/kg, SAH + EDB 12.5 mg/kg, SAH + EDB 125 mg/kg and SAH + EDA10 mg/kg group (12 mice in each group). Neurological deficits were evaluated in each group by means of the modified Garcia and balance beam tests following SAH induction, with a sample size of six mice per group. Additionally, brain water content (left, right cerebral hemispheres, cerebellum) was measured at 24 and 72 h post-SAH to evaluate the severity of cerebral oedema, also with six mice per group. According to the aforementioned findings, we have determined that the ideal dose of EDB is 12.5 mg/kg. Then we employed EDA with 10 mg/kg as a comparative standard in this investigation. This chosen dosage will be utilized in the subsequent experiments.

Experiment 2: To examine the neuroprotective role of EDB in the context of SAH, we allocated stochastically 120 C57BL/6 mice into five distinct groups: sham, SAH, SAH + vehicle, SAH + EDB and SAH + EDA group (21 mice in each group). After inducing SAH, we quantified the permeability of Evans blue dye in the right and left cerebral hemispheres to assess BBB integrity. This assessment was carried out on a subset of six mice from each group. In addition, the levels of apoptotic proteins and signaling pathway proteins (Keap1 and Nrf2) were analysis using Western blotting ($n = 6$). Immunofluorescence staining ($n = 3$) was utilized to examine the level of apoptotic neurons in the left cerebral hemisphere subsequent to SAH. Additionally, a subset of six mice from each group were utilized to measure the content of SOD and MDA, which provide insight into brain OS level.

Experiment 3: To explore the specific mechanism of action of EDB, we allocated 190 C57BL/6 mice into six groups randomly: sham, SAH + vehicle, SAH + vehicle + EDB, SAH + ML385+EDB, SAH + vehicle + EDA and SAH + ML385+EDA group (27 mice in each group). After 24 h of inducing SAH, a subset of six mice from each group underwent several tests, included two behavioral experiment and measurements of brain water content (left, right cerebral hemisphere and cerebellum). The purpose was to evaluate neurological deficits and determine the severity of cerebral oedema. Western blotting analysis was undertaken on a subset of six mice from each group to identify apoptotic proteins and signaling pathway proteins. This analysis purpose was to examine the levels of these proteins and their potential contribution to the observed effects of EDB in relation to SAH. Immunofluorescence staining was carried out on a subset of three mice from each group to identify apoptotic neurons in the left cerebral hemisphere following SAH. Additionally, we measured SOD and MDA levels, providing insights into the degree of cerebral OS.

2.3 Drug doses

In our experiment, we administered intraperitoneal injections of EDB to mice at three different doses: a low dose of 1.25 mg/kg, a medium dose of 12.5 mg/kg, and a high dose of 125 mg/kg. The first injection was given 15 min after inducing SAH, followed by injections every 12 h until the mice died. These doses were determined according to previous studies on edaravone and our pre-experiments (Jangra et al., 2017; Herbet et al., 2019; Dang et al., 2022). On the other hand, the control group of mice received intraperitoneal injections of PBS buffer 15 min following SAH. In experiment 3, mice were intraperitoneally injected with ML385 (30 mg/kg, AbMole, Houston, United States) for 30 min before SAH based on previous studies (Singh et al., 2016; Hu Q. et al., 2022). EDA and EDB was administered after the administration of ML385 (Dang et al., 2022) (Figure 1A).

2.4 Mouse SAH model

This experimental study established the mouse SAH model on the left side using intravascular threading, as previously reported (Pan et al., 2017). Initially, mice were anaesthetized with 1% sodium pentobarbital (40 mg/kg) by intraperitoneal injection. Then the external carotid artery (ECA) was surgically separated using an operation microscope (Leica, Wetzlar, Germany), and a 2-mm incision was made at its distal end. Subsequently, insertion of a 5–0 nylon suture into the internal carotid artery (ICA) was performed through the previously made incision in the ECA until encountering a minimal degree of resistance. The suture was further advanced by an additional 2 mm to penetrate the site where the anterior cerebral and middle cerebral arteries bifurcate. Following the precise placement of the nylon suture at the intended location, it was cautiously withdrawn. To redirect blood flow from the common carotid artery (CCA) to the ICA and induce SAH, the ECA was securely ligated. The control group of mice underwent a similar procedure, nevertheless, the suture did not advance through the artery when encountering resistance. This procedure replicated the steps without inducing SAH.

2.5 Neurological function score

In the experiment, two assessment methods, namely, the modified Garcia score and the balance beam test, were utilized in a blinded method to assess the extent of neurobehavioral deficits post-SAH 24 and 72 h (Pan et al., 2020). The modified Garcia score was a comprehensive scoring system consisting of six tests, which were used to assess various aspects of neurological function. It allocated 18 points to judge the extent of neurological impairments. These tests assessed spontaneous activity, spontaneous limb movement, forepaw extension, climbing, body proprioception, and response to whisker stimulation. Each individual test in the modified Garcia score was scored from 3 to 18 points. Higher scores within this range indicate improved neurological function for that specific test. The balance beam test involved placing the mice on a beam, and their ability to walk along the beam within 1 minute was measured. The distance walked by the mice was then scored on a scale of 0–five points, with higher score indicating better motor coordination and balance.

2.6 SAH grading assessment

The experiment utilized an 18-point SAH severity grading system (Dong et al., 2016). The skull base of the mice was classified into six regions, and a grading system ranging from

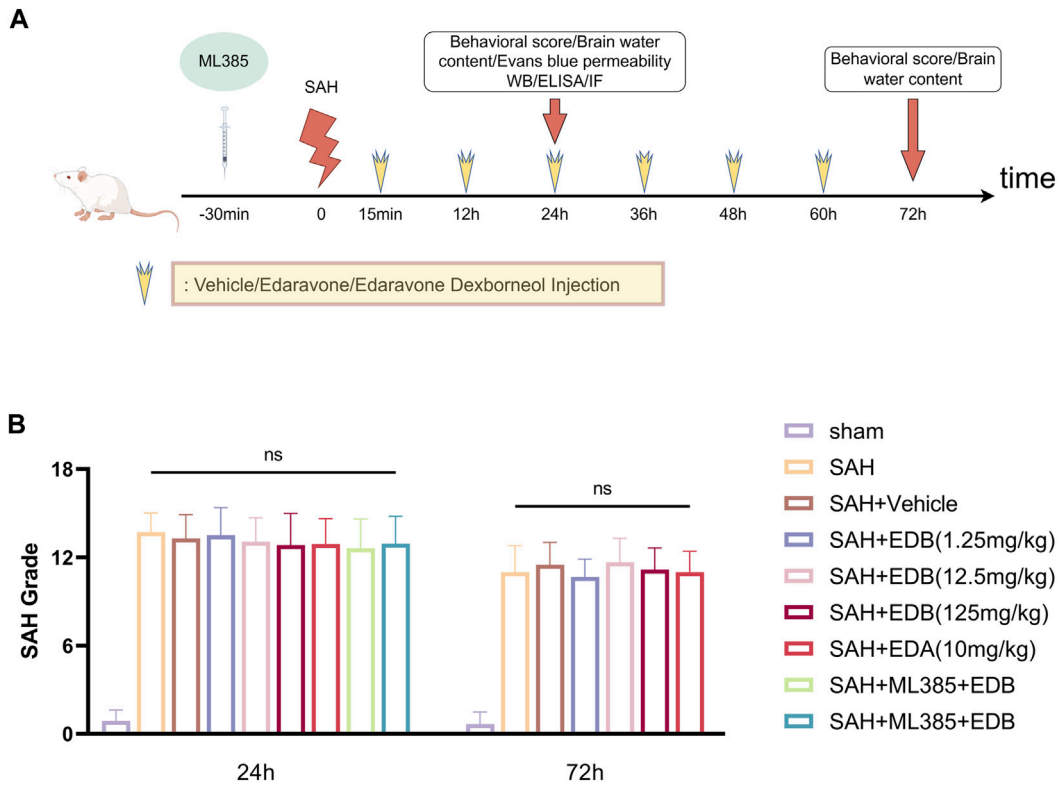

FIGURE 1
(A) Experimental flow chart; **(B)** SAH grading scores after SAH. No statistical difference in SAH grade indicated the SAH model are consistent and comparable in each group.

0 to three was applied to assess the extent of bleeding observed in each region. A score of 0 indicated no hemorrhage in that region, while a score of one indicated a small amount of hemorrhage. A score of two denoted significant hemorrhage with clear vascular morphology, and a score of three indicated a large amount of hemorrhage with unclear vascular morphology. The total score of hemorrhage severity was calculated by summing up the scores of all six regions. Scores ranging from 0 to seven indicated mild hemorrhage, scores from 8 to 12 indicated moderate hemorrhage, and scores from 13 to 18 indicated severe hemorrhage. Experiment excluded mice with SAH scores below eight points.

2.7 Brain water content

The determination method of brain water content was the same as the previous experiment (Zou et al., 2021). Mice were euthanized by cervical dislocation method, then the brain was dissected into the left, right hemispheres, as well as the cerebellum. Subsequently, the tissue was subjected to a 105°C oven for a duration of 24 h in order to thoroughly eliminate all moisture. After the completion of the drying, the weight of the brains was once again measured in order to ascertain their dry weight. The formula for calculating brain water content was as follow:

$$\text{Brain water content} = \frac{(wet\ weight - dry\ weight)}{wet\ weight} \times 100\%$$

2.8 Evans blue penetration assessment

The BBB disruption was evaluated using Evans blue dye penetration as previously reported (Han et al., 2021). At post-24 h SAH, under 1% sodium pentobarbital anesthesia, we administered a 2% concentration of Evans blue dye (4 mL/kg) via the left femoral vein, followed by a 60-min circulation. In order to eliminate any residual dye in the vessels, mice were then perfused with PBS buffer. Brain tissue was collected and homogenized in a saline solution. Afterwards, the brain tissue that had been homogenized using frozen centrifuge (Thermo, Massachusetts, United States) was subjected to centrifugation at a speed of 15,000 revolutions per minute for a duration of 30 min. The collected liquid above the sediment was obtained, and an equivalent amount of trichloroacetic acid was introduced to cause protein precipitation. After being incubated overnight at 4°C, the mixture was subjected to another round of centrifugation at 15,000 rpm to collect the ultimate supernatant. The microplate reader (Epoch, Biotek, Winooski, United States) measurement of absorbance at 620 nm was conducted in order to determine the concentration of Evans blue dye present in the supernatant.

2.9 Western blotting

We extracted the mice brains and then proteins were then harvested from the left cerebral hemisphere and analyzed via Western blotting techniques as previously described (Li et al., 2020).

10.3389/fphar.2024.1342226

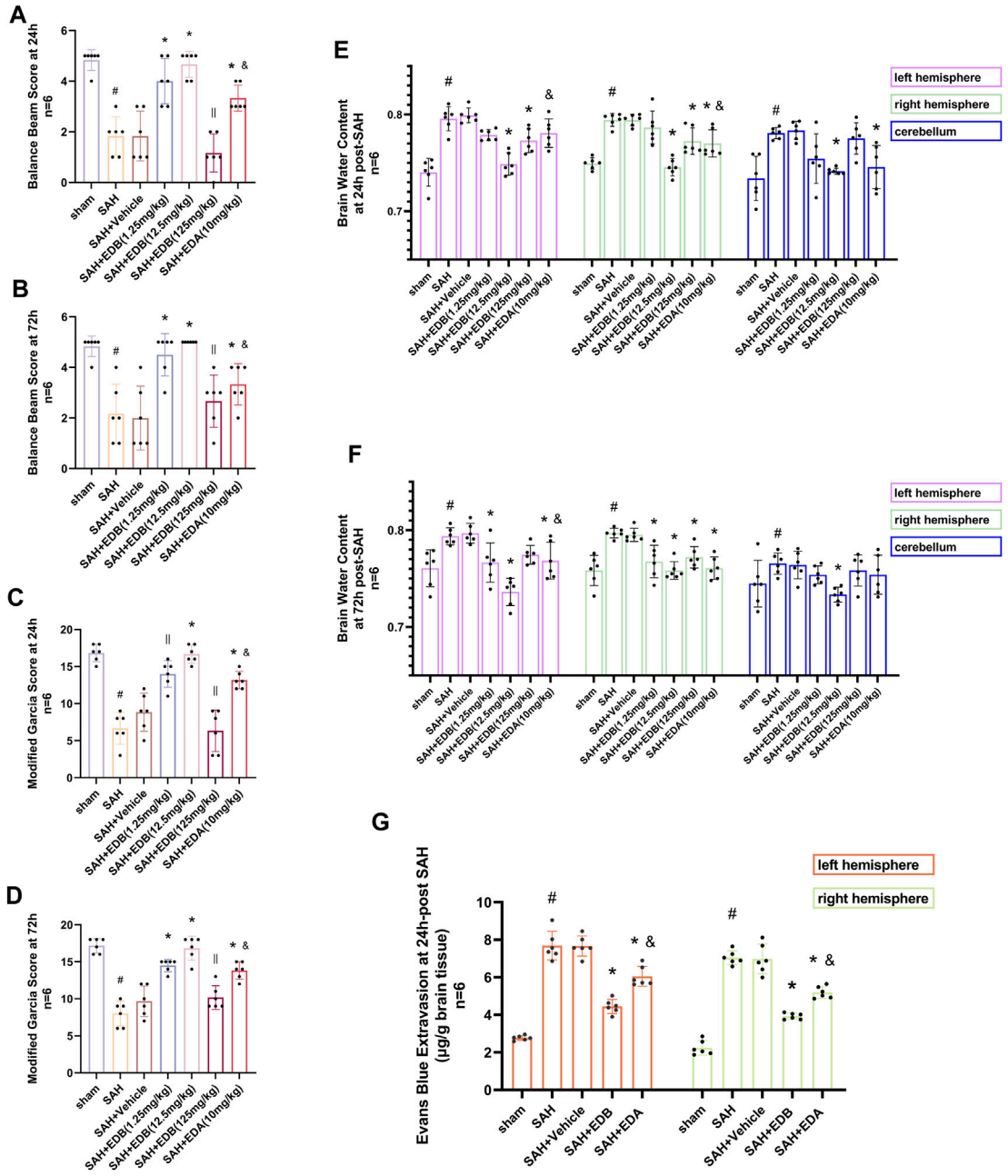

FIGURE 2
Neurological behavioral scores, brain water content of left, right hemisphere and cerebellum and Evans blue permeability after SAH. **(A and B)** Balance beam test scores at 24 and 72 h after SAH; **(C and D)** The modified Garcia scores at 24 and 72 h after SAH; **(E and F)** Brain water content at 24 h and 72 h post-SAH; **(G)** Evans blue permeability of left, right hemisphere at 24 h post-SAH. Data are presented as the mean ± SD. # $p < 0.05$ compared with sham; * $p < 0.05$ compared with SAH + vehicle; and $p < 0.05$ compared with SAH + EDB (12.5 mg/kg); || $p \geq 0.05$ compared with SAH + vehicle.

Each well on the gel was supplemented with 40 μg of protein, followed by gel electrophoresis (Bio-rad, California, United States). The proteins were subsequently transferred onto a nitrocellulose membrane and sealed with a sealing buffer at ambient temperature for a duration of 60 min. After sealing, the nitrocellulose membrane was then subjected to incubation with a diluted primary antibody overnight at a temperature of 4°C. The main primary antibody included the antibodies of Keap1 (Proteintech, Wuhan, China), Nrf2 (Proteintech, Wuhan, China), β-tubulin (Proteintech, Wuhan, China), Bax (Santa Cruz, Texas, United States), Bcl-2 (Santa Cruz, Texas, United States), caspase-3 (Santa Cruz, Texas, United States), cleaved caspase-3 (Santa Cruz, Texas, United States), Parp1 (Proteintech, Wuhan, China) and Hsp90 (Bioss, Beijing, China). Subsequently, the membrane was incubated with an appropriately diluted secondary antibody for a period of 2 h at ambient temperature. The main secondary antibody included goat anti-rabbit IgG/HRP (Bioss, Beijing, China) and goat anti-mouse IgG/HRP (Bioss, Beijing, China). Chemiluminescence imaging system (Tanon 4,600, Tanon, Shanghai, China) was used to detect the bands which were then analyzed densitometrically by ImageJ.

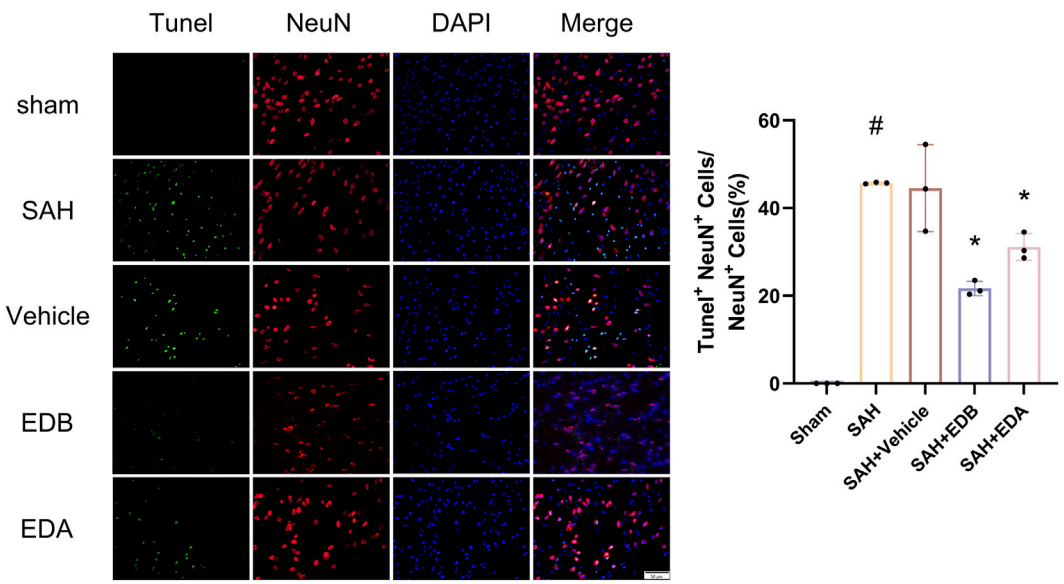

FIGURE 3
Neuronal Tunel immunofluorescence staining and ratio of Tunel-positive neurons to normal neurons. Data are presented as the mean ± SD. # $p < 0.05$ compared with sham; * $p < 0.05$ compared with SAH + vehicle.

2.10 Immunofluorescence staining

As previously, immunofluorescence staining was performed on fixed frozen section (Zhang et al., 2015). Following SAH, the mice were subjected to anesthesia using 1% sodium pentobarbital, followed by intracardial perfusion with a PBS buffer solution containing 4% PFA. Immediately euthanizing mice, and their brain tissues were gathered and immersed in 4% PFA for a duration of 24 h. Subsequently, the tissues were dehydrated in 30% sucrose for an additional 24 h. Afterwards, the specimens were quick-frozen at −35°C and coronal slices of the brain with a thickness of 8 μm were taken by using a freezing microtome (Leica, Wetzlar, Germany). To permeabilize, we used a solution of Triton X-100 at a concentration of 0.3% for 30 min at room temperature, after that, we sealed it with BSA for an additional 60 min at the same temperature. The sections were subsequently incubated with the NeuN antibody (Abcam, Cambridge, Britain) for an extended period of time at a temperature of 4°C. Following that, the sections were subjected to a fluorescent secondary antibody that corresponded to the source of the primary antibody, and this process was carried out at room temperature for a duration of 60 min. The main fluorescent secondary antibody included goat anti-mouse AF555 (Bioss, Beijing, China) and goat anti-rabbit AF555 (Bioss, Beijing, China). Next, Tunel Apoptosis Assay Kit (Beyotime, Shanghai, China) was done to detect apoptotic cells according to the manufacturer's instructions. Lastly, the sections were sealed using the fluorescence quenching agent containing DAPI (Solarbio, Beijing, China). Finally, we observed these sections using the fluorescence microscope (BX-53, Olympus, Tokyo, Japan) to analyze the localization of the molecules.

2.11 Measurement of SOD and MDA

24 h after SAH, mice brain tissue was harvested. Subsequently, the brain tissues were homogenized in chilled PBS buffer at a ratio of 20 mg tissue per 100 μL buffer. Following the process of homogenization, we centrifuged and collected the supernatant. Finally, we utilized a microplate reader for the determination of SOD and MDA using Lipid Peroxidation MDA Assay Kit (Beyotime, Shanghai, China) and SOD Activity Assay Kit (Beyotime, Shanghai, China) according to the instructions (Han et al., 2022).

2.12 Statistics and analysis

Data were presented as mean ± SD (standard deviation). All of the data were tested for normality and variance homogeneity (Brown–Forsythe test). The outcomes between the two groups were compared with independent *t*-test, and Bonferroni corrected one-way ANOVA was chosen for contrast between multiple groups. The median (interquartile range) was used to describe the neurologic score results, and Mann-Whitney U test was carried out to compare differences. Statistical analysis was conducted using GraphPad Prism 9.0 and the statistical program SPSS 22.0, with statistical significance defined as $p < 0.05$.

3 Result

3.1 Mortality

None of the sham-operated mice died, eight mice died in SAH group, and 18 mice died in SAH + vehicle group, and nine

10.3389/fphar.2024.1342226

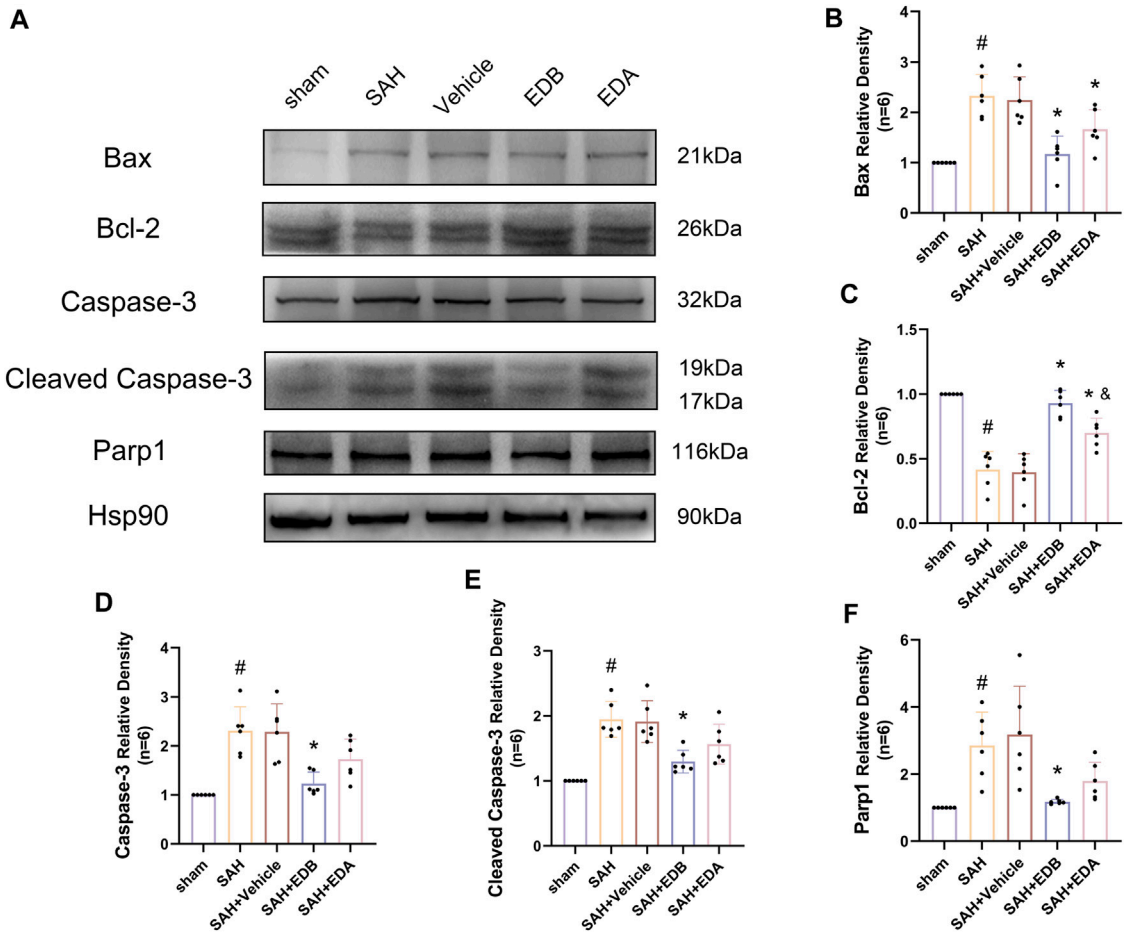

FIGURE 4
Western blotting and relative density analysis of apoptotic proteins. **(A)** The expressions of Bax, Bcl-2, caspase-3, cleaved caspase-3, Parp1 and Hsp90 were measured by Western blotting; **(B)** Bax relative density; **(C)** Bcl-2 relative density; **(D)** Caspase-3 relative density; **(E)** Cleaved caspase-3 relative density; **(F)** Parp1 relative density. Data are presented as the mean ± SD. # $p < 0.05$ compared with sham; * $p < 0.05$ compared with SAH + vehicle; and $p < 0.05$ compared with SAH + EDB.

mice died in SAH + EDA group, and 10 mice died in SAH + EDB group (3 mice in SAH + EDB 1.25 mg/kg group, five mice in SAH + EDB 12.5 mg/kg group, two mice in SAH + EDB 125 mg/kg group) and 14 mice died in SAH + ML385 group (7 mice in SAH + ML385 + EDA, seven mice in SAH + ML385+EDB) within 24 h after SAH due to severe hemorrhagic volume (Supplementary Figure S1). No mice were excluded from this study because of mild hemorrhagic volume without obvious neurological deficits (SAH grade score <8), and the SAH grade exhibited no statistical difference among each group (Figure 1B).

3.2 EDB improves neurological functions after SAH and alleviates BBB disruption

For evaluating the EDB efficacy in treating neurobehavioral impairment, our experiment utilized a neurological function scoring system for the assessment of severity. At both 24 and 72 h following SAH, the SAH and SAH + vehicle groups exhibited notable neurological impairments in contrast to the EDB group, which demonstrated substantial enhancement in behavioral assessment, particularly in 12.5 mg/kg group (Figures 2A–D). After SAH, the group receiving EDB treatment demonstrated greater superiority compared to the group receiving only EDA treatment. Additionally, we also evaluated the impact of EDB on brain oedema after SAH through quantifying brain water content post-SAH. The findings indicated notable brain oedema in left, right hemispheres as well as in the cerebellum for both the SAH and SAH + vehicle group during the first 72 h after SAH. On the other hand, both the groups treated with EDA and EDB exhibited a notable alleviation of cerebral oedema. Furthermore, the treatment with a moderate dose (12.5 mg/kg) exhibited a markedly better outcome in comparison to the remaining two groups. In the left cerebral hemisphere at 24 h and 72 h after SAH, the therapeutic performances of EDA group and EDB group were in addition to significant differences, and the degree of cerebral oedema was reduced more significantly by EDB treatment (Figures 2E,F). Meanwhile, we also assessed the extent of BBB injury after SAH by measuring the permeability of Evans blue dye. The SAH and SAH + vehicle groups exhibited a significant leakage of Evans blue, suggesting a compromised integrity of the BBB after SAH. In comparison, both EDA and EDB treatments

10.3389/fphar.2024.1342226

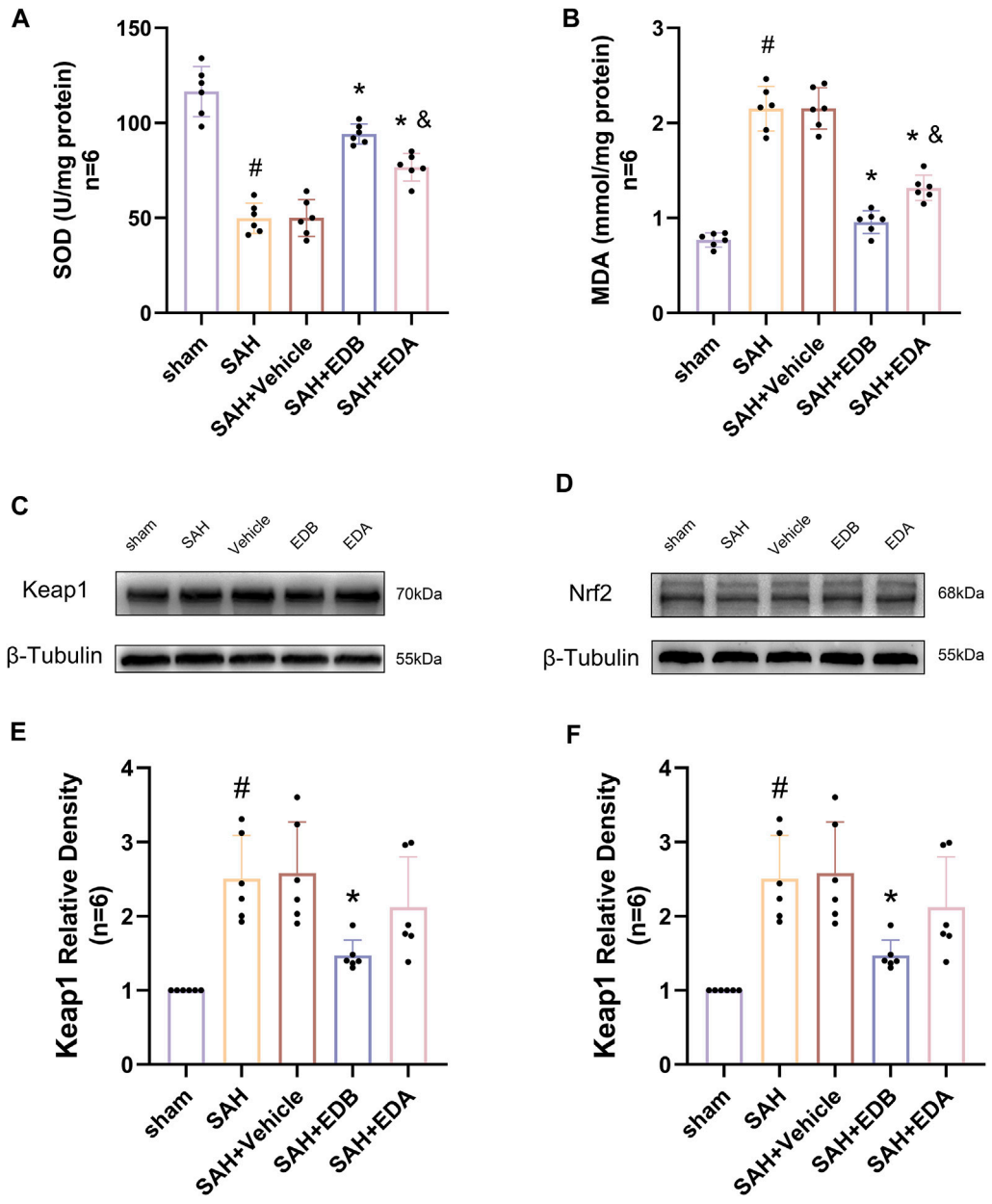

FIGURE 5
Measurement of oxidative stress indicators, Western blotting and relative density analysis of signaling pathway proteins. **(A)** The level of SOD; **(B)** The level of MDA; **(C)**The expressions of Keap1 were measured by Western blotting; **(D)** The expressions of Nrf2 were measured by Western blotting; **(E)** Keap1 relative density; **(F)** Nrf2 relative density. Data are presented as the mean ± SD. # $p < 0.05$ compared with sham; * $p < 0.05$ compared with SAH + vehicle; and $p < 0.05$ compared with SAH + EDB.

resulted in a significant reduction in Evans blue leakage, indicating attenuation of BBB damage (Figure 2G). Significantly, the effect with EDB treatment was significantly superior to the effect with EDA treatment, when compared to the EDA group. To summarize, in relation to enhancing neurobehavioral function, minimizing cerebral oedema, and reducing BBB disruption following SAH, the EDB treatment exhibited a notable therapeutic impact and outperformed the solitary use of EDA treatment. As a result of the experiment, 12.5 mg/kg EDB was found to be the optimal treatment dosage for SAH. Following a thorough analysis of the results, we opted for 12.5 mg/kg dosage of EDB for the forthcoming experiments.

3.3 EDB reduces neuro-apoptosis after SAH

To study the impact of EDB on decreasing neuronal apoptosis after SAH, our experiment employed immunofluorescence staining to assess the extent of neuronal apoptosis in brain tissue following SAH. The results obtained from both the SAH and SAH + vehicle

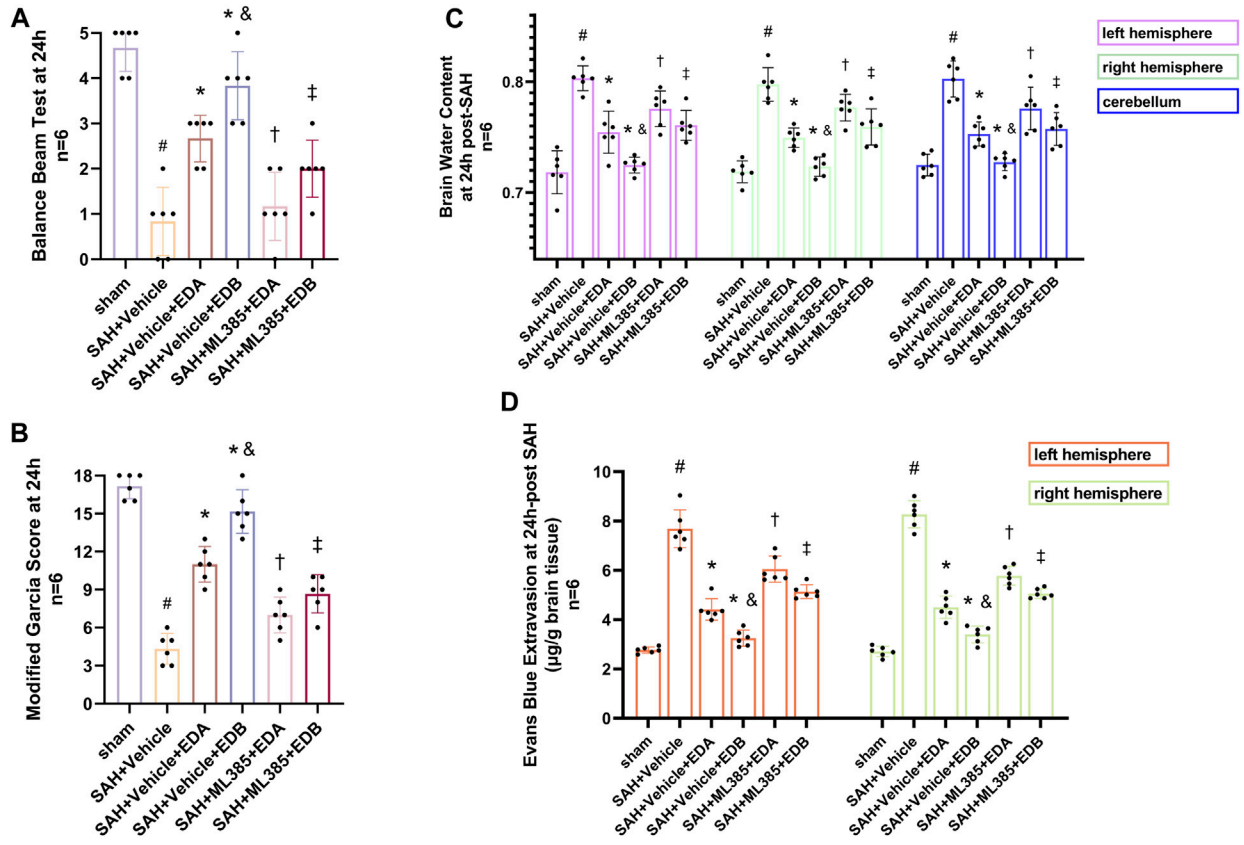

FIGURE 6
After application of the Nrf2 inhibitor (ML385) intervention, neurological behavioral scores, brain water content and Evans blue permeability after SAH. **(A)** Balance beam test scores at 24 h after SAH; **(B)** The modified Garcia scores at 24 h after SAH; **(C)** Brain water content of left, right hemisphere and cerebellum at 24 h after SAH; **(D)** Evans blue permeability after SAH. Data are presented as the mean ± SD. # $p < 0.05$ compared with sham; * $p < 0.05$ compared with SAH + vehicle; and $p < 0.05$ compared with SAH + EDA; † $p < 0.05$ compared with SAH + vehicle + EDA; ‡ $p < 0.05$ compared with SAH + vehicle + EDB.

groups demonstrated a significant elevation in the quantity of Tunel-positive neurons, suggesting a marked augmentation in neuronal apoptosis. Conversely, Tunel-positive neuron numbers in the EDA and EDB treatment groups exhibited a substantial decrease in comparison to the SAH + vehicle group, indicating the effectiveness of both EDA and EDB treatments in reducing apoptotic neurons after SAH (Figure 3). Furthermore, the EDB group exhibited a lower count of apoptotic neurons than the EDA group, suggesting the EDB treatment exhibited superiority over the EDA treatment alone. On the other hand, Western blotting was utilized to assess the levels of various proteins involved in the regulation of apoptosis. These proteins encompassed the pro-apoptotic proteins Bax, caspase3, cleaved caspase3 and Parp1, along with the anti-apoptotic protein Bcl-2 (Figure 4A). The results of the study revealed a notable reduction in Bcl-2 expression in SAH + vehicle group, while there was a noteworthy increase in the levels of Bax, caspase3, cleaved caspase3 and Parp1. However, the treatment of EDB effectively reversed these results. (Figures 4B–F). The findings demonstrated that EDB successfully decreased neural apoptosis following SAH. Moreover, the observed reduction in neuronal apoptosis after SAH exhibited a notably higher magnitude in the EDB treatment group in comparison to the EDA treatment group, suggesting EDB treatment was more effective than EDA treatment alone in reducing neuronal apoptosis.

3.4 EDB inhibits OS after SAH

To investigate the impact of EDB therapy on the prevention of OS, we conducted an analysis of its antioxidant properties by assessing the levels of SOD and MDA at SAH post-24 h. The results indicated a noteworthy increase in MDA levels, as well as a notable decline in SOD levels in both SAH and SAH + vehicle groups, indicating heightened oxidative damage. In contrast to the control group, both the EDA and EDB treatment groups exhibited a reduction in MDA expression and an elevation in SOD levels (Figures 5A,B). Furthermore, the antioxidant impact of EDB was significantly greater in comparison to the sole administration of

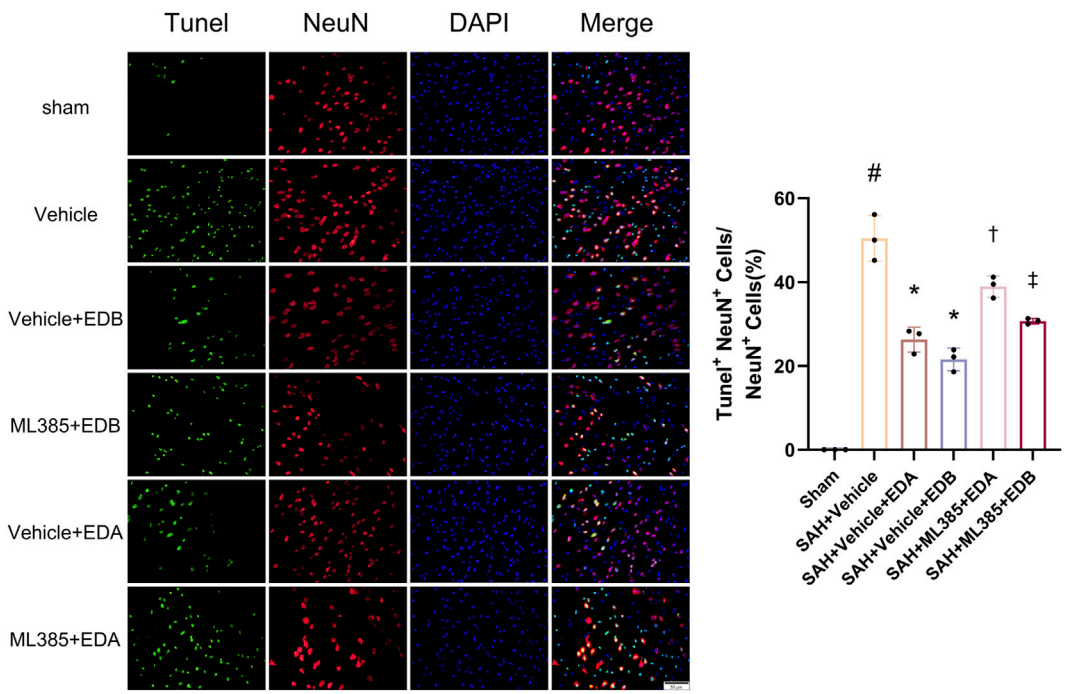

FIGURE 7
After application of the Nrf2 inhibitor (ML385) intervention, neuronal Tunel immunofluorescence staining and ratio of Tunel-positive neurons to normal neurons. Data are presented as the mean ± SD. # $p < 0.05$ compared with sham; * $p < 0.05$ compared with SAH + vehicle; † $p < 0.05$ compared with SAH + vehicle + EDA; ‡ $p < 0.05$ compared with SAH + vehicle + EDB.

EDA. In conclusion, both EDA and EDB treatments exhibited remarkable antioxidant capacity against SAH-induced neural injury. Moreover, the antioxidant potential of EDB exceeded that of EDA treatment in isolation.

3.5 EDB attenuates OS injury after SAH via the Keap1/Nrf2 signal pathway

To identify the mechanisms by which EDB mitigates OS after SAH, we conducted Western blotting to assess the levels of Keap1 and Nrf2 (Figures 5C,D). There was a notable increase in Keap1 expression in both the SAH and SAH + vehicle groups, while Nrf2 expression decreased significantly. However, the groups treated with EDA and EDB demonstrated a noteworthy reduction in Keap1 expression and a notable elevation in Nrf2 expression when compared to the control group (Figures 5E,F). Moreover, EDB treatment group exhibited a more pronounced reduction in Keap1 expression and an elevation in Nrf2 expression in comparison to the group receiving EDA alone.

3.6 Blockade of Nrf2 can abolish the anti-OS of EDB

To further evaluate the effect of Keap1/Nrf2 signaling pathway on the antioxidant effect of EDB, the Nrf2 inhibitor ML385 was applied to SAH-induced mice at 30 min prior to drug administration. Compared with the SAH + vehicle group, two behavioral experiments score of the SAH + vehicle + EDA and SAH + vehicle + EDB groups showed significant improvement, whereas both ML385-treated groups showed poorer behavioral status; the behavioral scores of SAH + ML385+EDA were worse in contrast to the SAH + ML385+EDB group (Figures 6A,B). The findings of this study indicated that the inhibition of Nrf2 hindered the antioxidant properties of EDB in relation to the behavioral aspects of mice. The SAH + vehicle + EDA and SAH + vehicle + EDB groups exhibited a significant decrease in brain water content and Evans blue permeability (Figures 6C,D), whereas both groups showed a significant increase in these measures following ML385 treatment. These findings suggested that the ability of EDB to mitigate cerebral oedema and BBB disruption was significantly impeded when Nrf2 was blocked. To investigate the impact of ML385 on mitigating SAH-induced apoptosis following the administration of EDA and EDB, we analyzed the number of Tunel-positive neurons in the brain after SAH by immunofluorescence staining. The results showed that, compared with SAH + vehicle group, the number of Tunel-positive neurons decreased significantly. After the application of ML385, these results were reversed (Figure 7). On the other hand, Western blotting results showed the groups treated with SAH + vehicle + EDA and SAH + vehicle + EDB exhibited a noteworthy reduction in Bcl-2 expression and a notable increase in the expression of Bax, caspase3, cleaved caspase3 and Parp1 (Figures 8A–F). However, the administration of ML385 effectively reversed these results. The findings of this study demonstrated that when ML385 blocked the Keap1/Nrf2 signal pathway, the anti-apoptosis effects of EDA and EDB in reducing neuronal apoptosis were hindered. To detect

10.3389/fphar.2024.1342226

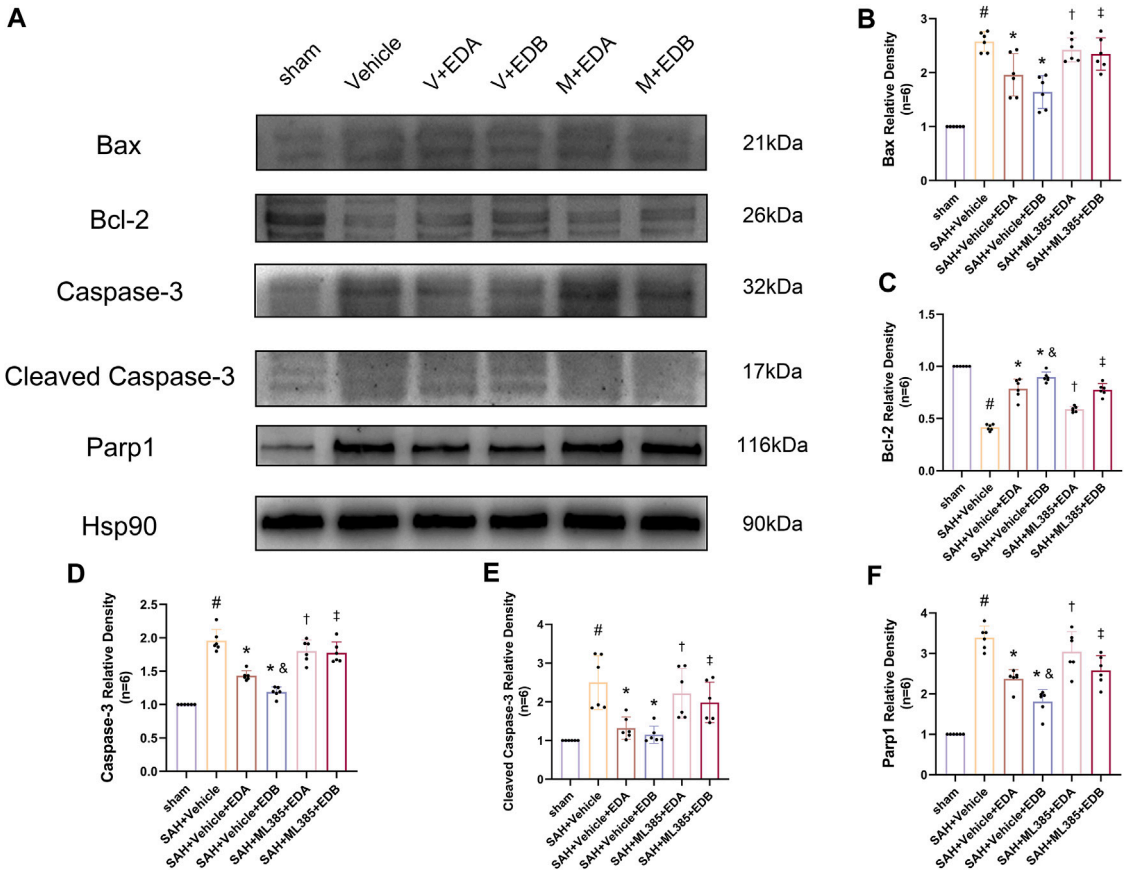

FIGURE 8
After application of the Nrf2 inhibitor (ML385) intervention, Western blotting and relative density analysis of apoptotic proteins. **(A)** The expressions of Bax, Bcl-2, caspase-3, cleaved caspase-3, Parp1 and Hsp90 were measured by Western blotting; **(B)** Bax relative density; **(C)** Bcl-2 relative density; **(D)** Caspase-3 relative density; **(E)** Cleaved caspase-3 relative density; **(F)** Parp1 relative density. Data are presented as the mean ± SD. # $p < 0.05$ compared with sham; * $p < 0.05$ compared with SAH + vehicle; and $p < 0.05$ compared with SAH + EDA; † $p < 0.05$ compared with SAH + vehicle + EDA; ‡ $p < 0.05$ compared with SAH + vehicle + EDB.

the impact of ML385 on the reduction of SAH-mediated OS following the treatment of EDA and EDB, we quantitatively analyzed SOD and MDA in the brain tissue of mice after SAH. The results showed that the level of SOD increased and the level of MDA decreased significantly compared with SAH + vehicle group. Then after the application of ML385, these results were significantly reversed (Figures 9A,B). Meanwhile, we used Western blotting to detect the signaling pathway proteins Keap1 and Nrf2 (Figures 9C,D). In comparison to the SAH + vehicle + EDA and SAH + vehicle + EDB groups, the application of ML385 resulted in an elevation of Keap1 levels and a reduction in Nrf2 levels in both groups. These results demonstrated that ML385 could block the Keap1/Nrf2 signaling pathway to inhibit the anti-oxidative effects of EDA and EDB (Figures 9E,F).

4 Discussion

Our research findings have demonstrated the beneficial effects of EDB in ameliorating the neuronal detrimental consequences of OS, reducing neuronal apoptosis, and improving prognosis within the context of SAH. Additionally, we have provided evidence to substantiate the claim that the neuroprotective advantages of EDB in SAH are attained by means of activating anti-oxidative response by the Keap1/Nrf2 signaling pathway.

EDB serves as a new neuroprotective medication with multiple targets, blending EDA and dexborneol in a 4:1 ratio (Xu J. et al., 2019). Clinical trials evaluating the effectiveness of EDB have shown that patients who received EDB during 48 h of AIS had improved neurological status compared to those received EDA solely (Xu J. et al., 2019; Xu et al., 2021). Furthermore, the safety and tolerability with EDB at different doses were found to be more advantageous in comparison to the administration of EDA alone (Wu H. Y. et al., 2014). Research has shown that EDB for treating AIS has a neuroprotective mechanism that encompasses various pathways for neuroprotection, such as OS, apoptotic injury and inflammation response (Huang et al., 2022). Nevertheless, there is currently a lack of empirical evidence regarding the efficacy of EDB for treating SAH.

AIS patients have been treated with EDA, which acts as an antioxidant by scavenging free radicals (Rothstein, 2017). Numerous experimental studies suggest that EDA may reduce brain damage in SAH through multiple mechanisms. EDA is recognized for its antioxidant characteristics and its capacity to

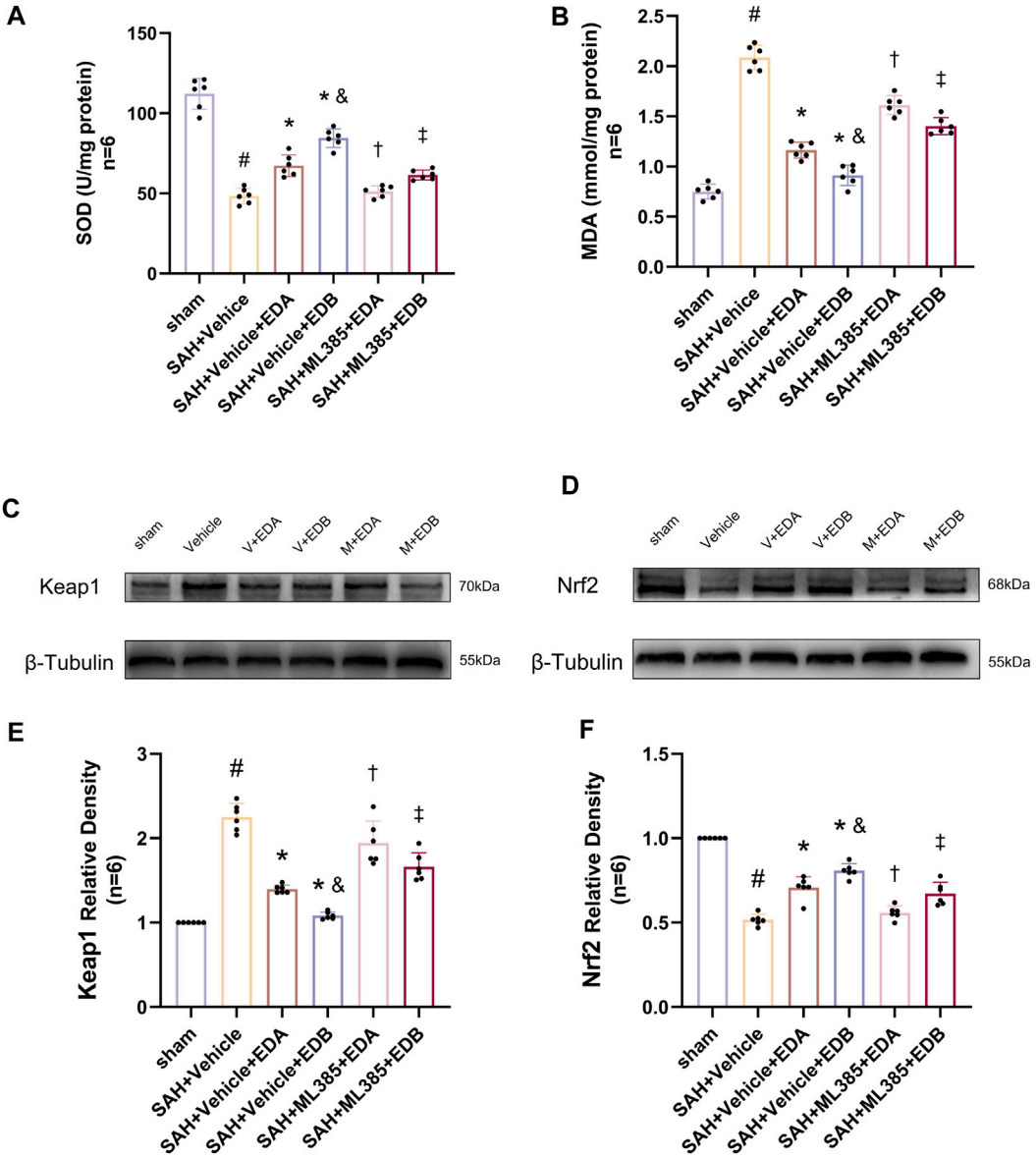

FIGURE 9
After application of the Nrf2 inhibitor (ML385) intervention, measurement of oxidative stress indicators, Western blotting and relative density analysis of signaling pathway proteins. **(A)** The level of SOD; **(B)** The level of MDA; **(C)**The expressions of Keap1 were measured by Western blotting; **(D)** The expressions of Nrf2 were measured by Western blotting; **(E)** Keap1 relative density; **(F)** Nrf2 relative density. Data are presented as the mean ± SD. # $p < 0.05$ compared with sham; * $p < 0.05$ compared with SAH + vehicle; and $p < 0.05$ compared with SAH + EDA; † $p < 0.05$ compared with SAH + vehicle + EDA; ‡ $p < 0.05$ compared with SAH + vehicle + EDB.

eliminate hydroxyl radicals, peroxyl radicals, and other ROS. This helps in decreasing OS and preventing the buildup of lipid peroxidation and oxidative DNA damage (Kikuchi et al., 2013; Wu S. et al., 2014; Suh et al., 2019). Multiple studies have provided evidence supporting the efficacy of EDA in SAH for the purpose of neuronal protection, neurological function enhancement, and mitigation of unfavorable prognostic outcomes subsequent to SAH (Yamashita and Abe, 2019). At the same time, we select EDA as a positive control drug to further explore the efficacy with EDB treatment.

Dexborneol, a bicyclic monoterpene compound, is the primary component of (+)-borneol. It assists in the uptake of other medications and protects the tight junction proteins and BBB. This protection helps prevent neurological harm in AIS (Liu et al., 2011; Dong et al., 2018; Liu et al., 2021). In addition, dexborneol has the ability to enhance SOD activity and decrease MDA levels, effectively diminishing OS harm within the body. It also suppresses the generation and manifestation of pro-inflammatory factors and associated proteins, thereby inhibiting the inflammatory response (Hur et al., 2013; Chen et al., 2019). The combination of EDA and dexborneol, known as EDB, has the potential to be more efficient compared to using EDA alone (Xu J. et al., 2019; Xu et al., 2021). Our current research examined the efficacy of SAH with EDB treatment and explored the distinctions compared to EDA therapy.

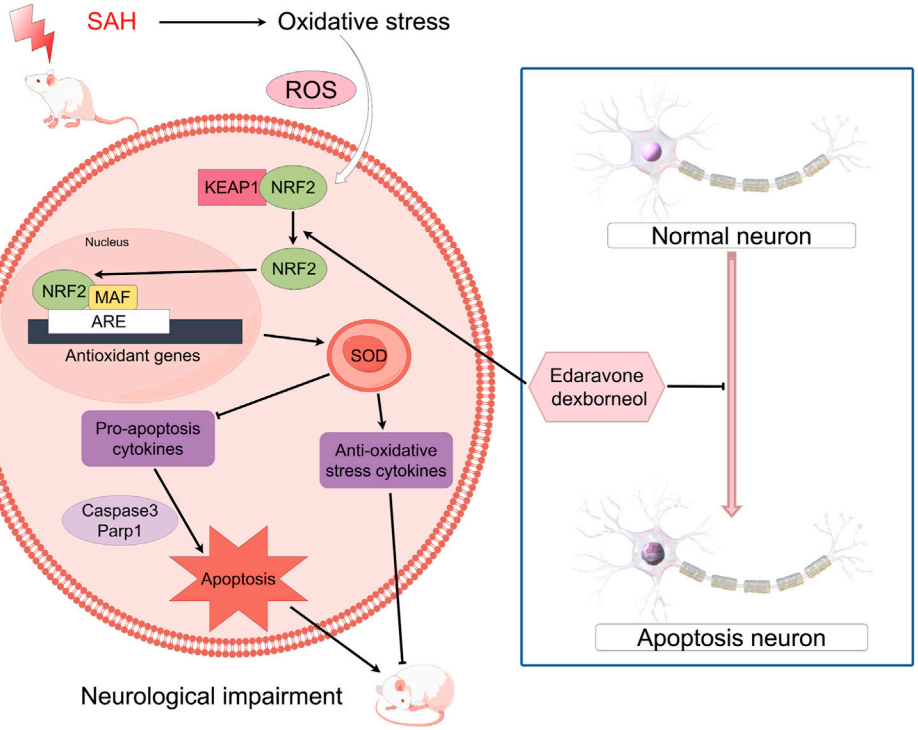

FIGURE 10
Mechanism of oxidative stress and neuronal apoptosis associated with EDB.

The findings indicated that the utilization of EDB therapy following SAH exhibited superior effectiveness and neuroprotective benefits in comparison to EDA in isolation.

SAH serves as a type of cerebrovascular event caused by blood entering the subarachnoid space from a ruptured aneurysm. There are various causes for its occurrence, with the most frequent being ruptured cerebral aneurysms and traumatic hemorrhage (Claassen and Park, 2022). EBI is a common complication that typically happens within 72 h after SAH, it is responsible for the majority of fatalities and is the primary factor contributing to unfavorable outcomes after SAH (Rass and Helbok, 2019). Studies have identified OS as an important mechanism of EBI that leads to neurological dysfunction after SAH (Mo et al., 2019). OS is a physiological condition resulting from the elevation of ROS and free radicals, potentially resulting in cellular structural damage. Additionally, OS following SAH can result in neuronal apoptosis (Forman and Zhang, 2021; Wu et al., 2021).

The Keap1/Nrf2 signaling pathway is of paramount importance in alleviating OS and exhibits a significant association with inflammatory disorders (Lu et al., 2016). Nrf2 is a prominent transcription factor implicated in OS transcription, constituting a key component within the repertoire of cell defense mechanisms (Liu et al., 2022). The role of Nrf2 is closely controlled by Keap1, a linker protein of the Cul3-based E3 ligase. In typical physiological circumstances, Keap1 engages with Nrf2 to direct the proteasome towards ubiquitin degradation (Baird and Yamamoto, 2020). When exposed to OS, Keap1 loses its activity and the process of Nrf2 ubiquitination stops (Yang et al., 2021). This leads to the buildup of newly produced Nrf2 and its subsequent activation. Consequently, Nrf2 is subsequently passed on to cell nucleus, initiating the transcription of numerous genes responsible for cellular defense, ultimately activating the defense mechanism (Adinolfi et al., 2023). In short, the Keap1/Nrf2 signaling pathway is of paramount importance in upholding cell redox equilibrium and dynamic homeostasis (Figure 10). Moreover, it actively supports anti-oxidative processes in SAH (Zhang et al., 2019). Our results showed EDA and EDB displayed strong antioxidant properties. In comparison to EDA alone, the use of EDB resulted in a greater decrease in OS-induced harm after SAH. Moreover, the combination of EDA and dexborneol exhibited increased neuroprotective properties against cell apoptosis following SAH.

The effectiveness of EDB in treating SAH was assessed in our experimental study. Moreover, we verified its ability to prevent OS and cell apoptosis while also uncovering the precise mechanism. In addition, there is also a need for research into the pivotal effect of EDB in other pathophysiological processes of SAH-mediated EBI, including neuroinflammation and vasospasm. Considering the extensive utilization of EDB in AIS, we eagerly anticipate forthcoming clinical studies involving individuals with SAH.

5 Conclusion

To summarize, this experiment demonstrates that EDB has a strong neuroprotective effect and improves behavioral function following SAH. The primary foundation of action appears to involve the initiation of the Keap1/Nrf2 signaling pathway, providing antioxidant activity as well as reducing neuronal apoptosis. These findings emphasize the potential for EDB as a neuroprotective agent with multi-target effects in mitigating

neurological damage associated with SAH. The results of this study are of significant clinical importance and make a valuable addition to the advancement of novel SAH-treatment approaches.

Data availability statement

The original contributions presented in the study are included in the article/Supplementary Materials, further inquiries can be directed to the corresponding authors.

Ethics statement

The animal study was approved by the Ethics Committee of the General Hospital of the Northern Theater command. The study was conducted in accordance with the local legislation and institutional requirements.

Author contributions

KZ: Writing–review and editing, Writing–original draft, Validation, Software, Project administration, Methodology, Investigation, Formal Analysis, Data curation, Conceptualization. SB: Writing–original draft, Investigation. ZZ: Writing–original draft, Investigation. WZ: Writing–original draft, Investigation. XY: Writing–original draft, Investigation. JL: Writing–original draft, Investigation. GL: Writing–original draft, Writing–review and editing, Visualization, Validation, Supervision, Resources, Project administration, Funding acquisition, Conceptualization. CY: Writing–original draft, Writing–review and editing, Visualization, Validation, Supervision. PP: Writing–original draft, Writing–review and editing, Visualization, Validation, Supervision, Resources, Project administration, Funding acquisition, Conceptualization.

Funding

The author(s) declare that financial support was received for the research, authorship, and/or publication of this article. This work was supported by National Natural Science Foundation of China (Grant Nos. 81971133, 82071481, and 82301487), Liaoning Province "Revitalization Talents Program" (Grant Nos. XLYC2002109), Liaoning Provincial Science and Technology Plan (Grant Nos. 2021JH2/10300059 and 2023JH2/101700096), Shenyang Science and Technology Plan (Grant Nos. 2020-20-4-017), China Stroke Society Start-up Fund.

Conflict of interest

The authors declare that the research was conducted in the absence of any commercial or financial relationships that could be construed as a potential conflict of interest.

Publisher's note

All claims expressed in this article are solely those of the authors and do not necessarily represent those of their affiliated organizations, or those of the publisher, the editors and the reviewers. Any product that may be evaluated in this article, or claim that may be made by its manufacturer, is not guaranteed or endorsed by the publisher.

Supplementary material

The Supplementary Material for this article can be found online at: https://www.frontiersin.org/articles/10.3389/fphar.2024.1342226/full#supplementary-material

SUPPLEMENTARY FIGURE S1
Figure shows the percent survival of the study mice. None of the sham-operated mice died, 8 mice died in SAH group, and 18 mice died in SAH+ Vehicle group, and 9 mice died in SAH+ EDA group, and 10 mice died in SAH+ EDB group (3 mice in SAH+ EDB 1.25 mg/kg group, 5 mice in SAH+ EDB 12.5 mg/kg group, 2 mice in SAH+ EDB 125 mg/kg group) and 14 mice died in SAH+ ML385 group (7 mice in SAH+ ML385+ EDA, 7 mice in SAH+ ML385+ EDB) within 24 h after SAH due to severe hemorrhagic volume. Survival rates were significantly lower in the SAH group than in the sham group at 24 and 72 hours after subarachnoid hemorrhage. It was able to improve after applying EDA and EDB treatment, and the improvement was more significant in EDB.

References

Adinolfi, S., Patinen, T., Jawahar Deen, A., Pitkanen, S., Harkonen, J., Kansanen, E., et al. (2023). The KEAP1-NRF2 pathway: targets for therapy and role in cancer. *Redox Biol.* 63, 102726. doi:10.1016/j.redox.2023.102726

Baird, L., and Yamamoto, M. (2020). The molecular mechanisms regulating the KEAP1-NRF2 pathway. *Mol. Cell Biol.* 40 (13), 000999-e120. doi:10.1128/MCB.00099-20

Chen, Q., Cai, Y., Zhu, X., Wang, J., Gao, F., Yang, M., et al. (2022). Edaravone dexborneol treatment attenuates neuronal apoptosis and improves neurological function by suppressing 4-HNE-associated oxidative stress after subarachnoid hemorrhage. *Front. Pharmacol.* 13, 848529. doi:10.3389/fphar.2022.848529

Chen, Z. X., Xu, Q. Q., Shan, C. S., Shi, Y. H., Wang, Y., Chang, R. C., et al. (2019). Borneol for regulating the permeability of the blood-brain barrier in experimental ischemic stroke: preclinical evidence and possible mechanism. *Oxid. Med. Cell Longev.* 2019, 2936737. doi:10.1155/2019/2936737

Claassen, J., and Park, S. (2022). Spontaneous subarachnoid haemorrhage. *Lancet* 400 (10355), 846–862. doi:10.1016/S0140-6736(22)00938-2

Dang, R., Wang, M., Li, X., Wang, H., Liu, L., Wu, Q., et al. (2022). Edaravone ameliorates depressive and anxiety-like behaviors via Sirt1/Nrf2/HO-1/Gpx4 pathway. *J. Neuroinflammation* 19 (1), 41. doi:10.1186/s12974-022-02400-6

Dong, T., Chen, N., Ma, X., Wang, J., Wen, J., Xie, Q., et al. (2018). The protective roles of L-borneolum, D-borneolum and synthetic borneol in cerebral ischaemia via modulation of the neurovascular unit. *Biomed. Pharmacother.* 102, 874–883. doi:10.1016/j.biopha.2018.03.087

Dong, Y., Fan, C., Hu, W., Jiang, S., Ma, Z., Yan, X., et al. (2016). Melatonin attenuated early brain injury induced by subarachnoid hemorrhage via regulating NLRP3 inflammasome and apoptosis signaling. *J. Pineal Res.* 60 (3), 253–262. doi:10.1111/jpi.12300

Feng, D., Zhou, J., Liu, H., Wu, X., Li, F., Zhao, J., et al. (2022). Astrocytic NDRG2-PPM1A interaction exacerbates blood-brain barrier disruption after subarachnoid hemorrhage. *Sci. Adv.* 8 (39), eabq2423. doi:10.1126/sciadv.abq2423

Forman, H. J., and Zhang, H. (2021). Targeting oxidative stress in disease: promise and limitations of antioxidant therapy. *Nat. Rev. Drug Discov.* 20 (9), 689–709. doi:10.1038/s41573-021-00233-1

Han, Y., Tong, Z., Wang, C., Li, X., and Liang, G. (2021). Oleanolic acid exerts neuroprotective effects in subarachnoid hemorrhage rats through SIRT1-mediated HMGB1 deacetylation. *Eur. J. Pharmacol.* 893, 173811. doi:10.1016/j.ejphar.2020.173811

Han, Y., Wang, C., Li, X., and Liang, G. (2022). Oleanolic acid reduces oxidative stress and neuronal apoptosis after experimental subarachnoid hemorrhage by regulating Nrf2/HO-1 pathway. *Drug Dev. Res.* 83 (3), 680–687. doi:10.1002/ddr.21899

Herbet, M., Natorska-Chomicka, D., Ostrowska, M., Gawronska-Grzywacz, M., Izdebska, M., Piatkowska-Chmiel, I., et al. (2019). Edaravone presents antidepressant-like activity in corticosterone model of depression in mice with possible role of Fkbp5, Comt, Adora1 and Slc6a15 genes. *Toxicol. Appl. Pharmacol.* 380, 114689. doi:10.1016/j.taap.2019.114689

Hu, Q., Zuo, T., Deng, L., Chen, S., Yu, W., Liu, S., et al. (2022b). β-Caryophyllene suppresses ferroptosis induced by cerebral ischemia reperfusion via activation of the NRF2/HO-1 signaling pathway in MCAO/R rats. *Phytomedicine* 102, 154112. doi:10.1016/j.phymed.2022.154112

Hu, R., Liang, J., Ding, L., Zhang, W., Liu, X., Song, B., et al. (2022a). Edaravone dexborneol provides neuroprotective benefits by suppressing NLRP3 inflammasome-induced microglial pyroptosis in experimental ischemic stroke. *Int. Immunopharmacol.* 113, 109315. doi:10.1016/j.intimp.2022.109315

Huang, Y., Zhang, X., Zhang, C., Xu, W., Li, W., Feng, Z., et al. (2022). Edaravone dexborneol downregulates neutrophil extracellular trap expression and ameliorates blood-brain barrier permeability in acute ischemic stroke. *Mediat. Inflamm.* 2022, 3855698. doi:10.1155/2022/3855698

Hur, J., Pak, S. C., Koo, B. S., and Jeon, S. (2013). Borneol alleviates oxidative stress via upregulation of Nrf2 and Bcl-2 in SH-SY5Y cells. *Pharm. Biol.* 51 (1), 30–35. doi:10.3109/13880209.2012.700718

Jangra, A., Sriram, C. S., Dwivedi, S., Gurjar, S. S., Hussain, M. I., Borah, P., et al. (2017). Sodium phenylbutyrate and edaravone abrogate chronic restraint stress-induced behavioral deficits: implication of oxido-nitrosative, endoplasmic reticulum stress cascade, and neuroinflammation. *Cell Mol. Neurobiol.* 37 (1), 65–81. doi:10.1007/s10571-016-0344-5

Kikuchi, K., Tancharoen, S., Takeshige, N., Yoshitomi, M., Morioka, M., Murai, Y., et al. (2013). The efficacy of edaravone (radicut), a free radical scavenger, for cardiovascular disease. *Int. J. Mol. Sci.* 14 (7), 13909–13930. doi:10.3390/ijms140713909

Li, G., Dong, Y., Liu, D., Zou, Z., Hao, G., Gao, X., et al. (2020). NEK7 coordinates rapid neuroinflammation after subarachnoid hemorrhage in mice. *Front. Neurol.* 11, 551. doi:10.3389/fneur.2020.00551

Liu, R., Zhang, L., Lan, X., Li, L., Zhang, T. T., Sun, J. H., et al. (2011). Protection by borneol on cortical neurons against oxygen-glucose deprivation/reperfusion: involvement of anti-oxidation and anti-inflammation through nuclear transcription factor κappaB signaling pathway. *Neuroscience* 176, 408–419. doi:10.1016/j.neuroscience.2010.11.029

Liu, S., Long, Y., Yu, S., Zhang, D., Yang, Q., Ci, Z., et al. (2021). Borneol in cardio-cerebrovascular diseases: pharmacological actions, mechanisms, and therapeutics. *Pharmacol. Res.* 169, 105627. doi:10.1016/j.phrs.2021.105627

Liu, S., Pi, J., and Zhang, Q. (2022). Signal amplification in the KEAP1-NRF2-ARE antioxidant response pathway. *Redox Biol.* 54, 102389. doi:10.1016/j.redox.2022.102389

Lu, M. C., Ji, J. A., Jiang, Z. Y., and You, Q. D. (2016). The keap1-nrf2-ARE pathway as a potential preventive and therapeutic target: an update. *Med. Res. Rev.* 36 (5), 924–963. doi:10.1002/med.21396

Macdonald, R. L., and Schweizer, T. A. (2017). Spontaneous subarachnoid haemorrhage. *Lancet* 389 (10069), 655–666. doi:10.1016/S0140-6736(16)30668-7

Mo, J., Enkhjargal, B., Travis, Z. D., Zhou, K., Wu, P., Zhang, G., et al. (2019). AVE 0991 attenuates oxidative stress and neuronal apoptosis via Mas/PKA/CREB/UCP-2 pathway after subarachnoid hemorrhage in rats. *Redox Biol.* 20, 75–86. doi:10.1016/j.redox.2018.09.022

Pan, P., Zhang, X., Li, Q., Zhao, H., Qu, J., Zhang, J. H., et al. (2017). Cyclosporine A alleviated matrix metalloproteinase 9 associated blood-brain barrier disruption after subarachnoid hemorrhage in mice. *Neurosci. Lett.* 649, 7–13. doi:10.1016/j.neulet.2017.03.050

Pan, P., Zhao, H., Zhang, X., Li, Q., Qu, J., Zuo, S., et al. (2020). Cyclophilin a signaling induces pericyte-associated blood-brain barrier disruption after subarachnoid hemorrhage. *J. Neuroinflammation* 17 (1), 16. doi:10.1186/s12974-020-1699-6

Rass, V., and Helbok, R. (2019). Early brain injury after poor-grade subarachnoid hemorrhage. *Curr. Neurol. Neurosci. Rep.* 19 (10), 78. doi:10.1007/s11910-019-0990-3

Rothstein, J. D. (2017). Edaravone: a new drug approved for ALS. *Cell* 171 (4), 725. doi:10.1016/j.cell.2017.10.011

Sehba, F. A., Pluta, R. M., and Macdonald, R. L. (2013). Brain injury after transient global cerebral ischemia and subarachnoid hemorrhage. *Stroke Res. Treat.* 2013, 827154. doi:10.1155/2013/827154

Singh, A., Venkannagari, S., Oh, K. H., Zhang, Y. Q., Rohde, J. M., Liu, L., et al. (2016). Small molecule inhibitor of NRF2 selectively intervenes therapeutic resistance in KEAP1-deficient NSCLC tumors. *ACS Chem. Biol.* 11 (11), 3214–3225. doi:10.1021/acschembio.6b00651

Suh, L. Y. K., Babu, D., Tonoyan, L., Reiz, B., Whittal, R., Tabatabaei-Dakhili, S. A., et al. (2019). Myeloperoxidase-mediated oxidation of edaravone produces an apparent non-toxic free radical metabolite and modulates hydrogen peroxide-mediated cytotoxicity in HL-60 cells. *Free Radic. Biol. Med.* 143, 422–432. doi:10.1016/j.freeradbiomed.2019.08.021

Tu, W., Wang, H., Li, S., Liu, Q., and Sha, H. (2019). The anti-inflammatory and anti-oxidant mechanisms of the keap1/nrf2/ARE signaling pathway in chronic diseases. *Aging Dis.* 10 (3), 637–651. doi:10.14336/AD.2018.0513

Wu, F., Liu, Z., Li, G., Zhou, L., Huang, K., Wu, Z., et al. (2021). Inflammation and oxidative stress: potential targets for improving prognosis after subarachnoid hemorrhage. *Front. Cell Neurosci.* 15, 739506. doi:10.3389/fncel.2021.739506

Wu, H. Y., Tang, Y., Gao, L. Y., Sun, W. X., Hua, Y., Yang, S. B., et al. (2014b). The synergetic effect of edaravone and borneol in the rat model of ischemic stroke. *Eur. J. Pharmacol.* 740, 522–531. doi:10.1016/j.ejphar.2014.06.035

Wu, S., Sena, E., Egan, K., Macleod, M., and Mead, G. (2014a). Edaravone improves functional and structural outcomes in animal models of focal cerebral ischemia: a systematic review. *Int. J. Stroke* 9 (1), 101–106. doi:10.1111/ijs.12163

Xu, J., Wang, A., Meng, X., Yalkun, G., Xu, A., Gao, Z., et al. (2021). Edaravone dexborneol versus edaravone alone for the treatment of acute ischemic stroke: a phase III, randomized, double-blind, comparative trial. *Stroke* 52 (3), 772–780. doi:10.1161/STROKEAHA.120.031197

Xu, J., Wang, Y., Wang, A., Gao, Z., Gao, X., Chen, H., et al. (2019b). Safety and efficacy of Edaravone Dexborneol versus edaravone for patients with acute ischaemic stroke: a phase II, multicentre, randomised, double-blind, multiple-dose, active-controlled clinical trial. *Stroke Vasc. Neurol.* 4 (3), 109–114. doi:10.1136/svn-2018-000221

Xu, W., Li, T., Gao, L., Zheng, J., Yan, J., Zhang, J., et al. (2019a). Apelin-13/APJ system attenuates early brain injury via suppression of endoplasmic reticulum stress-associated TXNIP/NLRP3 inflammasome activation and oxidative stress in a AMPK-dependent manner after subarachnoid hemorrhage in rats. *J. Neuroinflammation* 16 (1), 247. doi:10.1186/s12974-019-1620-3

Yamashita, T., and Abe, K. (2019). Edaravone: a new treatment for als. *Brain Nerve* 71 (11), 1245–1251. doi:10.11477/mf.1416201434

Yang, N., Sun, H., Xue, Y., Zhang, W., Wang, H., Tao, H., et al. (2021). Inhibition of MAGL activates the Keap1/Nrf2 pathway to attenuate glucocorticoid-induced osteonecrosis of the femoral head. *Clin. Transl. Med.* 11 (6), e447. doi:10.1002/ctm2.447

Yang, X., Wang, B., and Wang, Y. (2022). Keap1-Nrf2/ARE pathway-based investigation into the mechanism of edaravone dexborneol in cerebral infarction model neuroprotection. *Cell Mol. Biol. (Noisy-le-grand)* 68 (9), 102–108. doi:10.14715/cmb/2022.68.9.16

Zeng, H., Chen, H., Li, M., Zhuang, J., Peng, Y., Zhou, H., et al. (2021). Autophagy protein NRBF2 attenuates endoplasmic reticulum stress-associated neuroinflammation and oxidative stress via promoting autophagosome maturation by interacting with Rab7 after SAH. *J. Neuroinflammation* 18 (1), 210. doi:10.1186/s12974-021-02270-4

Zhang, H., Wang, L., Zhu, B., Yang, Y., Cai, C., Wang, X., et al. (2023). A comparative study of the neuroprotective effects of dl-3-n-butylphthalide and edaravone dexborneol on cerebral ischemic stroke rats. *Eur. J. Pharmacol.* 951, 175801. doi:10.1016/j.ejphar.2023.175801

Zhang, T., Su, J., Guo, B., Wang, K., Li, X., and Liang, G. (2015). Apigenin protects blood-brain barrier and ameliorates early brain injury by inhibiting TLR4-mediated inflammatory pathway in subarachnoid hemorrhage rats. *Int. Immunopharmacol.* 28 (1), 79–87. doi:10.1016/j.intimp.2015.05.024

Zhang, T., Wu, P., Budbazar, E., Zhu, Q., Sun, C., Mo, J., et al. (2019). Mitophagy reduces oxidative stress via Keap1 (Kelch-Like epichlorohydrin-associated protein 1)/nrf2 (nuclear factor-E2-related factor 2)/PHB2 (prohibitin 2) pathway after subarachnoid hemorrhage in rats. *Stroke* 50 (4), 978–988. doi:10.1161/STROKEAHA.118.021590

Zou, Z., Dong, Y. S., Liu, D. D., Li, G., Hao, G. Z., Gao, X., et al. (2021). MAP4K4 induces early blood-brain barrier damage in a murine subarachnoid hemorrhage model. *Neural Regen. Res.* 16 (2), 325–332. doi:10.4103/1673-5374.290904

frontiers | Frontiers in Pharmacology

TYPE Mini Review
PUBLISHED 03 June 2024
DOI 10.3389/fphar.2024.1387158

OPEN ACCESS

EDITED BY
Christina Dalla,
National and Kapodistrian University of Athens, Greece

REVIEWED BY
Alexia Polissidis,
Biomedical Research Foundation of the Academy of Athens (BRFAA), Greece

*CORRESPONDENCE
Alasdair M. Barr,
al.barr@ubc.ca

†These authors have contributed equally to this work to this manuscript

RECEIVED 16 February 2024
ACCEPTED 02 May 2024
PUBLISHED 03 June 2024

CITATION
Wang CK, Kim G, Aleksandrova LR, Panenka WJ and Barr AM (2024), A scoping review of the effects of mushroom and fungus extracts in rodent models of depression and tests of antidepressant activity.
Front. Pharmacol. 15:1387158.
doi: 10.3389/fphar.2024.1387158

A scoping review of the effects of mushroom and fungus extracts in rodent models of depression and tests of antidepressant activity

Catherine K. Wang[1,2‡], Gio Kim[1,2‡], Lily R. Aleksandrova[3], William J. Panenka[2,3] and Alasdair M. Barr[1,2*]

[1]Department of Anesthesiology, Pharmacology and Therapeutics, Faculty of Medicine, University of British Columbia (UBC), Vancouver, BC, Canada, [2]British Columbia Mental Health and Substance Use Services Research Institute, Vancouver, BC, Canada, [3]Department of Psychiatry, Faculty of Medicine, Canada Faculty of Pharmaceutical Sciences, UBC, Vancouver, BC, Canada

One of the most important developments in psychopharmacology in the past decade has been the emergence of novel treatments for mood disorders, such as psilocybin for treatment-resistant depression. Psilocybin is most commonly found in different species of mushroom; however, the literature on mushroom and fungus extracts with potential antidepressant activity extends well beyond just psilocybin-containing mushrooms, and includes both psychedelic and non-psychedelic species. In the current review, we systematically review the preclinical literature on mushroom and fungus extracts, and their effects of animal models of depression and tests of antidepressant activity. The PICO structure, PRISMA checklist and the Cochrane Handbook for systematic reviews of intervention were used to guide the search strategy. A scoping search was conducted in electronic databases PubMed, CINAHL, Embase and Web of Science. The literature search identified 50 relevant and suitable published studies. These included 19 different species of mushrooms, as well as seven different species of other fungi. Nearly all studies reported antidepressant-like effects of treatment with extracts. Treatments were most commonly delivered orally, in both acute and chronically administered studies to predominantly male rodents. Multiple animal models of depression were used, the most common being unpredictable chronic mild stress, while the tail suspension test and forced swim test were most frequently used as standalone antidepressant screens. Details on each experiment with mushroom and fungus species are discussed in detail, while an evaluation is provided of the strengths and weaknesses of these studies.

KEYWORDS

animal model, antidepressant, fungus, mushroom, preclinical

Introduction

Mood disorders remain among the most prevalent and disabling of all psychiatric conditions. They also represent one of the leading causes of worldwide disease burden (Friedrich, 2017; Collaborators, 2022). While many individuals affected by mood disorders respond well to treatment, a significant proportion of people show either partial or no response to antidepressant therapies (McLachlan, 2018). If an individual fails to respond to two or more trials of standard antidepressant pharmacotherapy, they may be considered "treatment-resistant" (Voineskos et al., 2020). Furthermore, many individuals may show a therapeutic response to antidepressant treatment but suffer side-effects that significantly reduce their quality of life (Teng et al., 2022), resulting in reduced treatment adherence (Hung, 2014; Rossom et al., 2016).

Clinical treatment options for those who do not respond well to standard antidepressant therapies have historically remained limited. However, in recent years, several landmark studies have reported that administration of psychedelic drugs under controlled conditions, typically in combination with psychotherapy, can significantly reduce depressive symptoms (Griffiths et al., 2016; Ross et al., 2016; Palhano-Fontes et al., 2019; Davis et al., 2021; Eisenstein, 2022; Goodwin et al., 2022). Importantly, this includes individuals with treatment-resistant depression (Carhart-Harris et al., 2016). Additionally, in clinical trials reported to-date, the side-effect profile of these compounds has appeared relatively benign (Eisenstein, 2022) with no evidence of some of the side-effects associated with other psychotropic medications, such as weight gain and metabolic dysregulation (Boyda et al., 2013; Boyda et al., 2021; Sepúlveda-Lizcano et al., 2023).

While the use of the term "psychedelic" has no official definition, it typically refers to a drug that is able to alter perception, thoughts, feelings and consciousness in humans (Hosanagar et al., 2021). Psychedelic drugs are commonly categorized as either "classical" or "atypical" (Kamal et al., 2023). The former category represents drugs with agonism or partial agonism at the serotonergic 5-HT2A receptor, and includes tryptamines (such as psilocybin and DMT), ergolines (such as LSD) and phenethylamines (such as mescaline) (Kelmendi et al., 2022). The atypical psychedelics have diverse mechanisms of action (Aleksandrova and Phillips, 2021), which are not primarily at the 5-HT2A receptor, and include drugs such as ketamine, ibogaine, muscimol and salvinorin A (Kelmendi et al., 2022). At this point, it is important to note that many compounds from both classes of psychedelic drugs have their origins in commonly available mushrooms and other fungi.

Mushrooms and other fungi

Mushrooms are generally defined as the spore-producing fruiting body of a fungus. Traditional medicine has used mushrooms, and fungi in general, in medical treatment for centuries (Yadav and Negi, 2021; Gravina et al., 2023), taking advantage of their numerous perceived therapeutic benefits. Such properties have been reported to include antimicrobial (Moussa et al., 2022), antibacterial, antioxidant, hepatoprotective (Venturella et al., 2021), and antitumor (Pandya et al., 2019) effects. More recently, researchers have investigated "medicinal" mushrooms as potential alternatives or complements to mainstream antidepressant treatments. For example, non-psychedelic species such as *Hericium erinaceus* and *Ganoderma lucidum* have been noted as having mood-improving qualities in humans (Nagano et al., 2010; Fijałkowska et al., 2022), although head-to-head trials comparing effects against standard antidepressant pharmacotherapies are lacking. Nevertheless, the increasing body of evidence which indicates that psilocybin (a psychedelic compound found in many species of mushrooms (Strauss et al., 2022)) has potent antidepressant effects, including in those with treatment-resistant depression (Haikazian et al., 2023; Simonsson et al., 2023), supports the notion that mushrooms and other fungi may hold significant therapeutic potential in this area. However, given the enormous number of potential species of mushroom and other fungi that could have antidepressant effects, measured against the tremendous costs associated with conducting clinical trials in humans, it is critical to determine which mushroom and fungus species and their derivatives represent the best preclinical leads for further development. In this context, it is vitally important to understand which species have already demonstrated efficacy in preclinical animal models of depression and specific screens for antidepressant activity. The purpose of the present scoping review is therefore to systematically identify which mushroom and fungus species have been tested for antidepressant effects in specific preclinical models, and to summarize and evaluate the results of these studies.

Materials and methods

The PICO structure, PRISMA checklist and the Cochrane Handbook (Higgins and Green, 2011) for systematic reviews of intervention were used to guide the search strategy. A scoping search was conducted in electronic databases PubMed, CINAHL (via EBSCO), Embase (via Ovid), and Web of Science, as previously (Tse et al., 2014; Yuen et al., 2021; Lian et al., 2022). One preprint source was found as a suggestion under another article and later located on Google Scholar. The latest literature search was conducted on 19 December 2023.

A combination of 26 individual search terms were used with the following keywords: "mushroom" or "mushrooms" or "fungus" and "depress*" or "antidepress*" and "animal" or "animal model". Filters excluding human studies or non-article sources were applied as needed. Searches were also conducted using specific behavioural models/tests or mushroom species as keywords. Studies were limited to those using rodent species as those reflect the expertise of the authors (Lu et al., 2005; Barr et al., 2006; Hill et al., 2007; Boyda et al., 2014); however, it is important to note that other species, such as zebrafish, represent additional valid animal models of antidepressant efficacy (Braun et al., 2024).

Studies were included if they met the following criteria: 1) studies tested a mushroom, fungus, or relevant mushroom derivative, and; 2) used a rodent model or behavioural test of depression or screen of antidepressant activity. Studies were excluded if they 1) were not published in English, or; 2) were not full text original research studies (i.e., conference abstracts, review papers).

A total of 546 articles were identified using Covidence (www.covidence.org), with 241 duplicates removed, leaving 305 articles to be screened. After title and abstract screening, 237 were deemed irrelevant, leaving 68 studies for eligibility assessment. After full text review, 18 studies were excluded, leaving 50 studies in the final database. Figure 1 outlines a PRISMA flowchart of the study selection process.

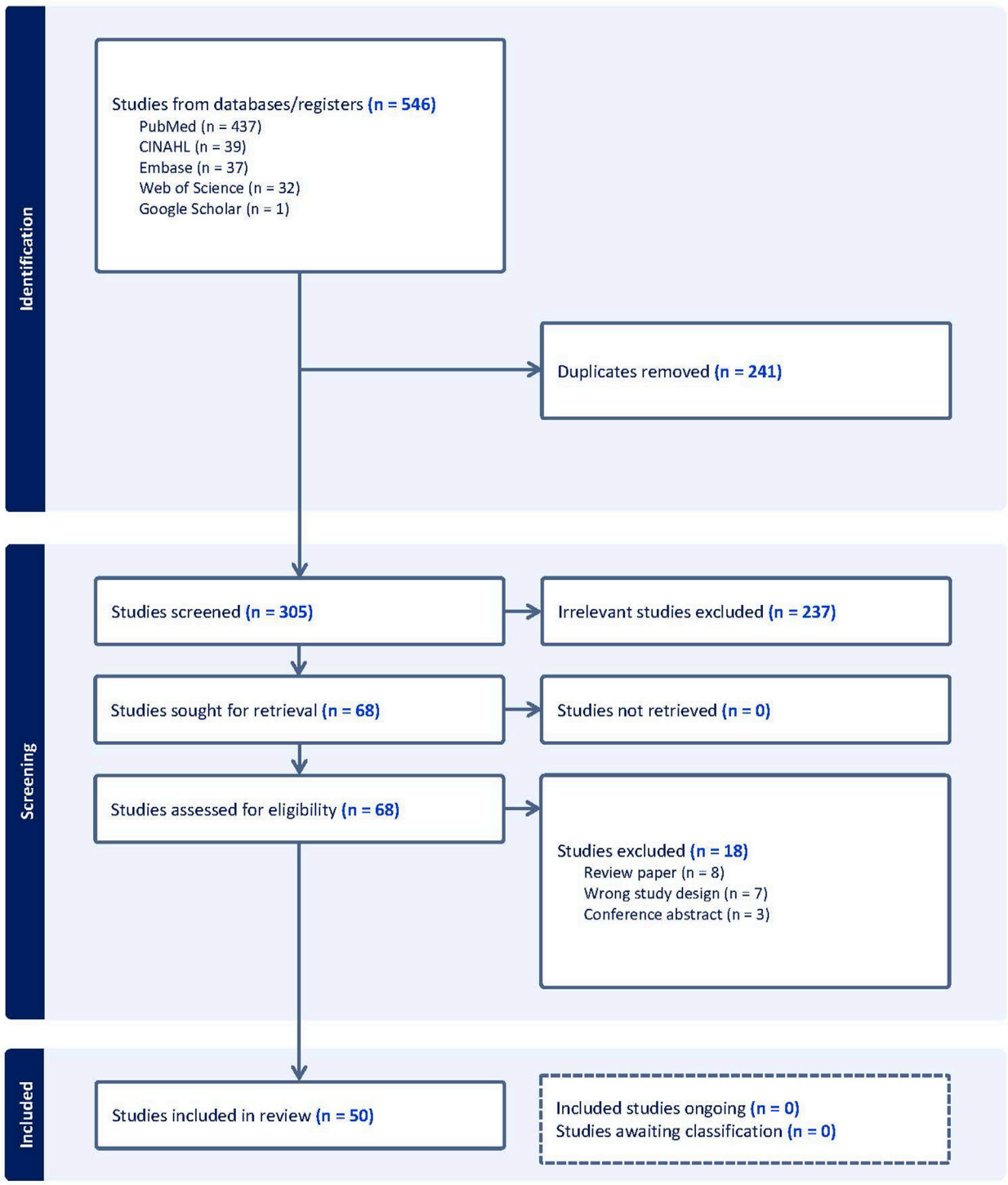

FIGURE 1
Literature review flow process.

Abstracts and full texts were screened by GK and CKW. Data was extracted independently by GK and CKW with key variables extrapolated and outlined in Supplementary Table S1. Any discrepancies throughout the process were brought to consensus by GK and CKW with the assistance of AMB if required.

Results

The literature search identified 50 relevant and suitable published studies. These included 19 different species of mushrooms see Table 1, as well as seven different species of other fungi see Table 2; there were also three studies that used compounds which are common to multiple mushroom species.

Characteristics of animals used and drug administration

The species used in all of the animal models were limited to rats and mice: we did not find instances of other rodent species that have been utilized as antidepressant screens (Kramer et al., 1998; Alo et al., 2019). Fourteen of the studies used rats (Matsuzaki et al., 2013; Minami et al., 2013; Tan et al., 2016; Liu C. et al., 2017; Song et al., 2017; Wang et al., 2017; Huang et al., 2020; Nascimento et al., 2020; Lin et al., 2021a; Zhang L. et al., 2021; Lin et al., 2021b; Anuar et al., 2022; Cheng, 2023; Rakoczy et al., 2023), while the remaining 36 studies used mice to test for antidepressant-like effects (Zhou et al., 2005; Nishizawa et al., 2007; Koo et al., 2008; Singh et al., 2014; Tianzhu et al., 2014; Socala et al., 2015; Yao et al., 2015; Gupta et al., 2016; Huang et al., 2016; Nakamichi et al., 2016; Song et al., 2016; Xu, 2016; Bao et al., 2017; Liu Y. et al., 2017; Lin et al., 2017; Chiu et al., 2018; Mahmoudi et al., 2018; Ryu et al., 2018; Jin et al., 2019; Li et al., 2019; Song et al., 2020; Li H. et al., 2021; Li TJ. et al., 2021; Zhang T. et al., 2021; Chong et al., 2021; Hossen et al., 2021; Park et al., 2021; Singh et al., 2021; Zhao et al., 2021; Chou et al., 2022; Mi et al., 2022; Xin et al., 2022; Yu et al., 2022; Ezurike et al., 2023; Zhao et al., 2023; Hernandez-Leon et al., 2024). In terms of strains, 10 of the rat studies used Sprague-Dawley, three included Wistar and one used Long-Evans rats. For the mice studies, the most commonly used strain was the C57BL/6 strain and sub-strains (12 studies), followed by Institute for Cancer Research mice (seven studies), Swiss Albino and Kunming mice (six studies each) and one study each with BALB/c, CD1, Swiss Webster and NMRI strains. Two studies did not mention the specific strains used (Li et al., 2019; Park et al., 2021). The overwhelming majority of rat studies used male rats (12 studies) compared to female rats (two studies (Minami et al., 2013; Anuar et al., 2022)). All mice studies utilized males, most of which included males only, while five studies used both male and female mice (Singh et al., 2014; Song et al., 2016; Liu Y. et al., 2017; Hossen et al., 2021; Ezurike et al., 2023), and one study did not specify sex (Park et al., 2021). Thus, only 14% of studies used female animals in their investigation.

Administration of mushroom or fungus derivatives to animals was mostly through a single route of administration, although a handful of studies used two different routes of administration (Yao et al., 2015; Huang et al., 2016; Chou et al., 2022; Yu et al., 2022; Hernandez-Leon et al., 2024). The most common route of administration was oral (*per os*, p.o.), which accounted for more than 50% of studies (29 of 55 instances of administration). Second most common was treatment by intraperitoneal (i.p.) injection (13 instances), followed by intragastric (i.g.) administration (7 instances). Extracts were administered to animals in their food in three separate studies (Nakamichi et al., 2016; Bao et al., 2017; Anuar et al., 2022), by subcutaneous (s.c.) injection in two studies (Chou et al., 2022; Yu et al., 2022), and by intravenous (i.v.) administration in one study (Zhang L. et al., 2021).

The methods of extraction of mushroom and fungus derivatives was reported in 28 studies. Methods included use of both polar and non-polar solvents, with the most common ones including water and various alcohols. For many of the studies where complex extraction procedures were involved, including with non-polar solvents, it was not possible to determine if the extracts that were administered to animals also contained traces of these solvents (e.g., (Singh et al., 2021)), which could feasibly have an effect on behaviour.

The duration of drug treatment varied significantly across the studies, from acute doses with behavioural testing 30 min later (Socala et al., 2015; Mahmoudi et al., 2018; Jin et al., 2019; Zhang T. et al., 2021; Hossen et al., 2021; Park et al., 2021; Hernandez-Leon et al., 2024), up to 92 days of continuous administration (Anuar et al., 2022). Of the 50 studies, 13 were acute (treatment over a span of <24 h) (Matsuzaki et al., 2013; Socala et al., 2015; Yao et al., 2015; Gupta et al., 2016; Lin et al., 2017; Mahmoudi et al., 2018; Jin et al., 2019; Zhang T. et al., 2021; Hossen et al., 2021; Park et al., 2021; Singh et al., 2021; Rakoczy et al., 2023; Hernandez-Leon et al., 2024), six were sub-acute (1–7 days) (Nishizawa et al., 2007; Song et al., 2016; Bao et al., 2017; Nascimento et al., 2020; Song et al., 2020; Yu et al., 2022), and the remaining 31 studies involved chronic treatment (>7 days). The mean duration of treatment for the chronic studies was 30.4 (±16.7) days for the longest treated group in each study (some studies had varying durations of treatment depending on the group). The modal and median periods of treatment for chronic studies were both 28 days. Rats were more likely to be treated chronically, with only two of the 14 rat studies involving acute treatment (Matsuzaki et al., 2013; Rakoczy et al., 2023).

Animal models of depression and tests of antidepressant activity

A variety of animal models of depression and antidepressant screens were used to examine mushroom and fungus antidepressant efficacy. By far the most common animal model used to induce a depressive-like phenotype in rodents was the unpredictable chronic mild stress paradigm (UCMS), with 14 studies implementing this model (Zhou et al., 2005; Tianzhu et al., 2014; Tan et al., 2016; Liu C. et al., 2017; Song et al., 2017; Wang et al., 2017; Li et al., 2019; Huang et al., 2020; Lin et al., 2021a; Zhang L. et al., 2021; Lin et al., 2021b; Zhao et al., 2021; Xin et al., 2022; Cheng, 2023); rats were used in the majority (9) of these studies. The second most frequent model involved the use of chronic restraint stress, in four mouse studies (Nakamichi et al., 2016; Chiu et al., 2018; Chong et al., 2021; Zhao et al., 2023). Two rat studies used ovariectomy procedures to model menopausal depression (Minami et al., 2013; Anuar et al., 2022), while high-dose corticosterone was administered to mice in two studies (Chou et al., 2022; Yu et al., 2022). Other models included the use of lipopolysaccharide (Yao et al., 2015), chronic social defeat stress (Li H. et al., 2021), maternal separation (Mi et al., 2022), ethanol binge drinking (Nascimento et al., 2020) and streptozotocin to model diabetes-induced depression (Huang et al., 2016). To determine that a depressive-like state had been induced by the

TABLE 1 Summary of rodent depression models and behavioural tests used to screen for antidepressant effects in different mushroom species. Subchronic and chronic treatment schedules include daily administration of drug unless otherwise stated.

Route	Treatment duration	Extraction method	Rodent species	Strain	Sex	Sample size	Behavioural test or model	Test duration	Test frequency	Doses tested	Combined with	Other notes	Reference number
Hericium erinaceus													
Food	Chronic (92 d)	Methanol	Rat	Wistar	Female	Sham (n = 11) OVX Model (n = 11) OVX + HE (n = 10) OVX + E_2 (n = 8)	OVX	96 d	Once	n/a	n/a	Models menopausal depression	Anuar et al. (2022)
							FST	5 min		OVX Model* 1%#			
p.o.	Chronic (28 d)	Ethanol	Mouse	ICR	Male	n = 10 per group Control CRS Model CRS + HE (Low, Medium, High)	CRS	14 d	2 h daily	n/a	Erinacine A	Mycelium	Chiu et al. (2018)
							FST	5 min	Once	CRS Model*** 100 mg/kg 200 mg/kg## 400 mg/kg##			
							TST						
i.p.	Chronic (28 d)	Ethanol	Mouse	C57BL/6	Male	n = 76 in total	CRS	14 d	6 h daily	n/a#	n/a	n/a	Chong et al. (2021)
							SPT	2 h	Once	CRS Model*** 10 mg/kg## 25 mg/kg##			
							TST	5 min		CRS Model* 10 mg/kg 25 mg/kg##			
s.c.	Chronic (21 d)	Alcohol	Mouse	SAMP8, BALB/C	Male	n = 8 per group CORT Model CORT + (Low, Medium, High) CORT + Fluoxetine	CORT	21 d	Daily	40 mg/kg	Chlorella	0.1 mL chlorella + 6 mg HE 0.2 mL chlorella + 12 mg HE 0.4 mL chlorella + 24 mg HE	Chou et al. (2022)
p.o.							FST	Last 4 min of 6 min	Once	CORT Model 0.25 mL/25 g 0.5 mL/25 g# 2.5 mL/25 g#			
p.o.	Chronic (9 d)	n/a	Mouse	C57BL/6	Male	n = 6 Control Low dose High dose	TST	15 min	Daily for 9 d	75 mg/kg 150 mg/kg % immobility increased daily over 9 d period	n/a	Mycelium; Uses TST-induced depression model, not screen	Li et al. (2021b)
p.o.	Chronic (28 d)	Ethanol	Mouse	C57BL/6	Male	n/a Control HE (Low, High)	FST	Last 4 min of 6 min	Once	20 mg/kg* 60 mg/kg*	n/a	n/a	Ryu et al. (2018)
							TST						
i.p.	Subchronic (1 d)	n/a	Mouse	C57BL/6N	Male	n = 11–12 per group Control Control + Amycenone LPS Model LPS + Amycenone	LPS	1 d	Once	n/a	n/a	Amycenone: hericenones/ hericium isolates (0.5%) and amyloban (6%) Use LPS to induce depression	Yao et al. (2015)
p.o.							FST	6 min		Non-LPS 200 mg/kg LPS LPS Model** 200 mg/kg#			
							TST	10 min		Non-LPS 200 mg/kg LPS LPS Model*** 200 mg/kg##			

(Continued on following page)

10.3389/fphar.2024.1387158

TABLE 1 (*Continued*) Summary of rodent depression models and behavioural tests used to screen for antidepressant effects in different mushroom species. Subchronic and chronic treatment schedules include daily administration of drug unless otherwise stated.

Route	Treatment duration	Extraction method	Rodent species	Strain	Sex	Sample size	Behavioural test or model	Test duration	Test frequency	Doses tested	Combined with	Other notes	Reference number
Ganoderma lucidum													
p.o.	Chronic (28 d)	Ethanol	Rat	Sprague-Dawley	Male	n = 8 per group Control UCMS Model UCMS + Gl-E (Low, Medium, High) UCMS + Fluoxetine	UCMS	28 d	Daily	n/a	n/a	Preprint; not peer-reviewed	Cheng (2023)
							SPT	3 h	Once	UCMS Model*** 0.02 g/kg 0.1 g/kg# 0.5 g/kg##			
p.o.	Chronic (28 d)	Ethanol	Mouse	Swiss Albino	Both	n = 5 per group Control EEGL (Low, Medium, High)	FST	Last 4 min of 6 min	Once	Male 100 mg/kg* 200 mg/kg** 400 mg/kg** Female 100 mg/kg* 200 mg/kg* 400 mg/kg**	n/a	n/a	Ezurike et al. (2023)
	Chronic (29 d)						TST			Male 100 mg/kg* 200 mg/kg** 400 mg/kg** Female 100 mg/kg* 200 mg/kg* 400 mg/kg*			
i.p.	n/a	n/a	Mouse	C57BL/6	Male	SPT: n = 7 per group TST: n = 8–10 per group FST: n = 9–10 per group Control Control + GLP (Low, Medium, High) CSDS Model CSDS + GLP (Medium) Imipramine	CSDS	10 d	5–10 min daily	n/a	n/a	Polysaccharide	Li et al. (2021a)
							SPT	2 h	Once	CSDS Model***			
	Subchronic (5 d)						FST	Last 4 min of 6 min		Non-CSDS 1 mg/kg 5 mg/kg*** 12.5 mg/kg CSDS 5 mg/kg###			
	Acute (60 min)						TST			Non-CSDS 1 mg/kg 5 mg/kg* 12.5 mg/kg CSDS 5 mg/kg#			
p.o.	Acute (60 min)	Water	Rat	Sprague-Dawley	Male	Control (n = 8) MAK (Low, High) (n = 6) Imipramine (n = 5)	FST	5 min	Once	0.3 g/kg 1 g/kg*	n/a	Mycelium	Matsuzaki et al. (2013)
i.p.	Chronic (21 d)	Ethanol + Ethyl Acetate	Mouse	C57BL/6J	Male	n = 11–13 per group Control Control + GLT	MS	21 d	4 h daily	n/a	n/a	Triterpenoids	Mi et al. (2022)
							SPT	24 h	Once	Non-MS 40 mg/kg			

(Continued on following page)

10.3389/fphar.2024.1387158

TABLE 1 (*Continued*) Summary of rodent depression models and behavioural tests used to screen for antidepressant effects in different mushroom species. Subchronic and chronic treatment schedules include daily administration of drug unless otherwise stated.

Route	Treatment duration	Extraction method	Rodent species	Strain	Sex	Sample size	Behavioural test or model	Test duration	Test frequency	Doses tested	Combined with	Other notes	Reference number
						MS Model MS + GLT				MS MS Model**** 40 mg/kg####			
							FST	6 min		Non-MS 40 mg/kg MS MS Model**** 40 mg/kg###			
							TST			Non-MS 40 mg/kg MS MS Model* 40 mg/kg#			
							Splash Test	5 min		Non-MS 40 mg/kg MS MS Model**** 40 mg/kg####			
							Nest Building	24 h		Non-MS 40 mg/kg MS MS Model*** 40 mg/kg####			
p.o.	Subchronic (3 d)	Water	Rat	Wistar	Male	n = 6–9 per group Control Binge Drinking (EtOH) Model Binge + AEGI	Binge Drinking	35 d	Weekly (daily administration for 3 consecutive days)	n/a	n/a	Models binge drinking induced depression	Nascimento et al. (2020)
							FST	Last 3 min of 5 min	Once	Binge Drinking Model**** 0.1 mL/100 g##			
p.o.	Acute (60 min)	Petroleum Ether, Chloroform, Methanol, and Water Methanol → Ethyl Acetate, n-Butanol, and Methanol fractions	Mouse	Swiss Albino	Male	n = 6 per group Control Extracts Pet. Ether (Low, Medium, High) Chloroform (Low, Medium, High) Methanol (Low, Medium, High) Aqueous (Low, Medium, High) Imipramine Fractions **E**: Ethyl Acetate (Very Low, Low, Medium) **N**: n-Butanol (Very Low, Low, Medium) **MF**: Methanol-soluble fraction (Low, Medium, High) Imipramine	FST	Last 4 min of 6 min	Once	Extracts 100 mg/kg* 200 mg/kg* 400 mg/kg* **(for all extracts)** Fractions 50 mg/kg – **E***, **N*** 100 mg/kg – **E***, **N**, **MF*** 200 mg/kg – **E***, **N***, **MF*** 400 mg/kg – **MF***	n/a	n/a	Singh et al. (2021)

(Continued on following page)

10.3389/fphar.2024.1387158

TABLE 1 (*Continued*) Summary of rodent depression models and behavioural tests used to screen for antidepressant effects in different mushroom species. Subchronic and chronic treatment schedules include daily administration of drug unless otherwise stated.

Route	Treatment duration	Extraction method	Rodent species	Strain	Sex	Sample size	Behavioural test or model	Test duration	Test frequency	Doses tested	Combined with	Other notes	Reference number
i.g.	Acute (30 min)	Water	Mouse	Swiss Albino	Male	n = 11–12 per group Control *G. lucidum* extract (Very Low, Low, Medium, High)	FST	Last 4 min of 6 min	Once	50 mg/kg 100 mg/kg** 200 mg/kg*** 400 mg/kg***	n/a	Mycelium	Socala et al. (2015)
p.o.	Chronic (28 d)	Water	Mouse	C57BL/6	Male	n = 10 per group Control Control + PGL (Low, Medium, High) UCMS Model UCMS + PGL (Low, Medium. High) UCMS + Fluoxetine	UCMS	56 d	Daily	n/a	n/a	Spore polysaccharide-peptide	Zhao et al. (2021)
							SPT	24 h	Once	UCMS Model** 100 mg/kg$^{\#}$ 200 mg/kg$^{\#\#}$ 400 mg/kg$^{\#\#}$			
	Acute (1 h) Chronic (28 d)						FST	Last 4 min of 6 min		<u>Acute</u> 100 mg/kg 200 mg/kg* 400 mg/kg** <u>Chronic</u> UCMS Model 100 mg/kg$^{\#}$ 200 mg/kg$^{\#}$ 400 mg/kg$^{\#\#}$			
	Acute (1 h)						TST			100 mg/kg 200 mg/kg** 400 mg/kg**			
Ganoderma applanatum													
p.o.	Acute (30 min)	Ethanol and Water	Mouse	Swiss Albino	Both	n = 5 per group Control Ethanol (Low, High) Aqueous (Low, High) Diazepam [i.p.]	TST	6 min	Once	<u>Ethanol</u> 200 mg/kg 400 mg/kg <u>Aqueous</u> 200 mg/kg 400 mg/kg	n/a	n/a	Hossen et al. (2021)
p.o.	Acute (60 min)	Petroleum Ether, Chloroform, Methanol, and Water	Mouse	Swiss Albino	Male	n = 6 per group Control <u>Extracts</u> Pet. Ether (Low, Medium, High) Chloroform (Low, Medium, High) Methanol (Low, Medium, High) Aqueous (Low, Medium, High) Imipramine	FST	Last 4 min of 6 min	Once	<u>Extracts</u> 100 mg/kg* 200 mg/kg* 400 mg/kg* **(for all extracts)**	n/a	n/a	Singh et al. (2021)
Ganoderma philippii													
p.o.	Acute (60 min)	Petroleum Ether, Chloroform, Methanol, and Water	Mouse	Swiss Albino	Male	n = 6 per group Control <u>Extracts</u> Pet. Ether (Low, Medium, High)	FST	Last 4 min of 6 min	Once	<u>Extracts</u> 100 mg/kg* 200 mg/kg* 400 mg/kg* **(for all extracts)**	n/a	n/a	Singh et al. (2021)

(Continued on following page)

10.3389/fphar.2024.1387158

TABLE 1 (*Continued*) Summary of rodent depression models and behavioural tests used to screen for antidepressant effects in different mushroom species. Subchronic and chronic treatment schedules include daily administration of drug unless otherwise stated.

Route	Treatment duration	Extraction method	Rodent species	Strain	Sex	Sample size	Behavioural test or model	Test duration	Test frequency	Doses tested	Combined with	Other notes	Reference number
						Chloroform (Low, Medium, High) Methanol (Low, Medium, High) Aqueous (Low, Medium, High) Imipramine							
Ganoderma brownii													
p.o.	Acute (60 min)	Petroleum Ether, Chloroform, Methanol, and Water	Mouse	Swiss Albino	Male	n = 6 per group Control Extracts Pet. Ether (Low, Medium, High) Chloroform (Low, Medium, High) Methanol (Low, Medium, High) Aqueous (Low, Medium, High) Imipramine	FST	Last 4 min of 6 min	Once	Extracts 100 mg/kg* 200 mg/kg* 400 mg/kg* **(for all extracts)**	n/a	n/a	Singh et al. (2021)
Ganoderma sp.													
i.v.	Chronic (21 d)	n/a	Rat	Sprague-Dawley	Male	Sham (n = 8) MCAO (n = 7) PSD Model (n = 7) PSD + GAA (Low, Medium, High) (n = 8)	PSD (UCMS)	21 d	Daily	n/a	n/a	Ganoderic acid (triterpenoid) Performs MCAO to induce stroke conditions Use UCMS to establish PSD	Zhang et al. (2021a)
							SPT	3 h	Once	PSD Model 10 mg/mL 20 mg/mL# 30 mg/mL## p̂ < 0.01 v.s. MCAO group			
Grifola frondosa													
Food	Subchronic: Cohort 1 (5 d) Cohort 2 (1 d) Cohort 3 (5 d)	n/a	Mouse	CD-1	Male	Cohort 1 (n = 14 per group) Cohort 2 (n = 14 per group) Cohort 3 (n = 10–11 per group) For each cohort: Control Low Medium High Imipramine	FST	Last 4 min of 6 min	Once	1:4 GF:chow** 1:2 GF:chow** 1:1 GF:chow***	n/a	Tested with multiple cohorts	Bao et al. (2017)
	Subchronic: Cohort 1 (1 d) Cohort 2 (5 d) Cohort 3 (1 d)					Cohort 1 (n = 14 per group) Cohort 2 (n = 13 per group) Cohort 3 (n = 11 per group)	TST			1:4 GF:chow* 1:2 GF:chow** 1:1 GF:chow**			

(Continued on following page)

10.3389/fphar.2024.1387158

TABLE 1 (*Continued*) Summary of rodent depression models and behavioural tests used to screen for antidepressant effects in different mushroom species. Subchronic and chronic treatment schedules include daily administration of drug unless otherwise stated.

Route	Treatment duration	Extraction method	Rodent species	Strain	Sex	Sample size	Behavioural test or model	Test duration	Test frequency	Doses tested	Combined with	Other notes	Reference number
						For each cohort: Control Low Medium High Imipramine							
Psilocybe cubensis													
p.o. (whole) i.p. (extracts)	Acute (30 min)	Methanol and Water	Mouse	Swiss Webster	Male	n ≥ 7 per group Control Whole Mushroom (Very High) Methanol (Low, Medium, High) Aqueous (Low, Medium, High) Fluoxetine [s.c.] Imipramine [i.p.]	FST	5 min	Once	Whole Mushroom 1000 mg/kg* Methanol 1 mg/kg 10 mg/kg** 100 mg/kg*** Aqueous 1 mg/kg** 10 mg/kg*** 100 mg/kg***	n/a	n/a	Hernandez-Leon et al. (2024)
i.p.	Acute (30 min)	Chloroform	Mouse	NMRI	Male	n = 8 per group Control PCE (Low, High) PCE (Low) + Ketamine PCE (High) + Ketamine Ketamine Fluoxetine	FST TST	Last 4 min of 6 min	Once	10 mg/kg 40 mg/kg For PCE (10 mg/kg): PCE + Ketamine (1 mg/kg)*** For PCE (40 mg/kg): PCE + Ketamine (1 mg/kg)***	Ketamine	Alkaloid extract	Mahmoudi et al. (2018)
Pleurotus eryngii													
p.o.	Chronic (84 d) Chronic (79 d)	Ethanol	Rat	Wistar	Female	Sham (n = 10) OVX Model (n = 10) OVX + *P. eryngii* (n = 8)	OVX FST	84 d 6 min	Once Once	n/a OVX Model* 500 mg/kg#	n/a	Models menopausal depression	Minami et al. (2013)
i.p.	Acute (30 min)	Ethanol	Mouse	n/a	n/a	n = 4 per group Control EtOH Extract Mixture (pellet) R2 Fraction Fluoxetine	FST	4 min	Once	EtOH Extract* Mixture (pellet)** R2 Fraction* (all 20 mg/kg)	n/a	EtOH Extract → Pellet → R2: fractions increase in purification levels	Park et al. (2021)
Pleurotus ostreatus													
Food	Subchronic (5 d) Subchronic (1 d)	n/a	Mouse	CD-1	Male	Control (n = 11) PO (n = 11) Imipramine (n = 10–11)	FST TST	Last 4 min of 6 min	Once	1:2 PO:chow	n/a	n/a	Bao et al. (2017)

(Continued on following page)

10.3389/fphar.2024.1387158

TABLE 1 (*Continued*) Summary of rodent depression models and behavioural tests used to screen for antidepressant effects in different mushroom species. Subchronic and chronic treatment schedules include daily administration of drug unless otherwise stated.

Route	Treatment duration	Extraction method	Rodent species	Strain	Sex	Sample size	Behavioural test or model	Test duration	Test frequency	Doses tested	Combined with	Other notes	Reference number
Pleurotus citrinopileatus													
Food	Chronic (21 d)	n/a	Mouse	C57BL/6J	Male	Control (n = 6) Control + 10% (n = 8) CRS Model (n = 8) CRS + 10% (n = 8)	CRS	21 d	4 h daily	n/a	n/a	Antioxidant ergothioneine (ERGO) and golden oyster mushroom extract (GOME)	Nakamichi et al. (2016)
	Chronic (14 d)					Control (n = 11) 10% GOME (n = 11) ERGO (n = 6) *Ginkgo biloba* extract (n = 6)	FST	5 min	Once	10% GOME* 120 mg/100 g ERGO*			
						Control (n = 15) 0.1% GOME (n = 6) 0.3% GOME (n = 6) 1% GOME (n = 12) 10% GOME (n = 15)	TST	First 2 min of 3 min		0.1% 0.3% 1%* 10%*			
Marasmius androsaceus													
p.o.	Subchronic (7 d)	n/a	Mouse	Kunming	Male	n = 8 per group Control MEPS1 (High) MEPS2 (Medium) MEPS3 (Low)	FST	6 min	Once	180 mg/kg 60 mg/kg* 30 mg/kg	n/a	Extracellular polysaccharide	Song et al. (2020)
							TST	5 min		180 mg/kg* 60 mg/kg** 30 mg/kg			
p.o.	Chronic (28 d)	n/a	Rat	Sprague-Dawley	Male	n = 10 per group Control UCMS Model UCMS + MEPS (Low, Medium, High)	UCMS	56 d	Daily	n/a	n/a	Exopolysaccharides	Song et al. (2017)
							SPT	1 h	Weekly for 7 weeks	UCMS Model** 6 mg/kg 30 mg/kg# 150 mg/kg## *Model: significant from day 14 to day 56* *MEPS: 30 mg/kg and 150 mgm/kg significant from day 49 to day 56*			
							FST	Last 5 min of 6 min	Once	UCMS Model*** 6 mg/kg# 30 mg/kg### 150 mg/kg###			
							TST			UCMS Model*** 6 mg/kg 30 mg/kg### 150 mg/kg###			

(Continued on following page)

10.3389/fphar.2024.1387158

TABLE 1 (*Continued*) Summary of rodent depression models and behavioural tests used to screen for antidepressant effects in different mushroom species. Subchronic and chronic treatment schedules include daily administration of drug unless otherwise stated.

Route	Treatment duration	Extraction method	Rodent species	Strain	Sex	Sample size	Behavioural test or model	Test duration	Test frequency	Doses tested	Combined with	Other notes	Reference number
p.o.	Subchronic (7 d)	n/a	Mouse	Kunming	Both	n = 10 per group Control MEPS (Low, Medium, High) Fluoxetine [i.g.]	FST	Last 5 min of 6 min	Once	10 mg/kg 50 mg/kg 250 mg/kg*	n/a	Exopolysaccharide	Song et al. (2016)
							TST	6 min		10 mg/kg 50 mg/kg* 250 mg/kg***			
i.g.	Chronic (14 d)	n/a	Mouse	C57BL/6J	Male	n = 8 per group IR CRS Model CRS + M	IR + Dp (CRS)	21 d	4 h daily	n/a	n/a	Mycelium Mice were irradiated with 13 Gy TAI to induce intestinal radiation injury CRS was used to induce depression	Zhao et al. (2023)
							FST	Last 4 min of 6 min	Once	CRS Model^{+++} CRS + M$^{\#\#}$ $^{+++}p < 0.001$ v.s. IR group			
							TST			CRS Model^{++} CRS + M$^{\#\#}$ $^{++}p < 0.01$ v.s. IR group			
Collybia maculata													
i.p.	Acute (immediate)	n/a	Mouse	C57BL/6J	Male	n = 7–10 per group Vehicle Colly	FST	6 min	Once	2 mg/kg	n/a	Colly: non-nitrogenous sesquiterpene of *C. maculata*	Gupta et al. (2016)
Poria cocos													
p.o.	Chronic (35 d)	Water	Rat	Sprague-Dawley	Male	n = 7 per group Control Control + PCW (Low, Medium, High) UCMS Model UCMS + PCW (Low, Medium, High)	UCMS	35 d	Daily	n/a	n/a	Sclerotium	Huang et al. (2020)
	Chronic (35 d)						SPT	1 h	Weekly for 5 weeks	UCMS Model* 100 mg/kg$^{\#}$ 300 mg/kg$^{\#}$ 900 mg/kg (*After 4 weeks*)			
	Chronic (28 d)						FST	5 min	Once	100 mg/kg* 300 mg/kg* 900 mg/kg*			
Lentinula edodes													
p.o.	Acute (2 h) Chronic (14 d)	n/a	Mouse	ICR	Male	n = 5 per group Control Pilopool	FST	Last 4 min of 6 min	Once	Acute 10 mL/kg* Chronic 10 mL/kg	Pilopool mixture: 30% of *L. edodes*/shiitake extract + 30% water-soluble chitosan, 30% *Allium sativum L.* extract, 0.5% of *Dioscorea batatas D.*, and 0.5% of bamboo salt	n/a	Koo et al. (2008)

(Continued on following page)

10.3389/fphar.2024.1387158

TABLE 1 (*Continued*) Summary of rodent depression models and behavioural tests used to screen for antidepressant effects in different mushroom species. Subchronic and chronic treatment schedules include daily administration of drug unless otherwise stated.

Route	Treatment duration	Extraction method	Rodent species	Strain	Sex	Sample size	Behavioural test or model	Test duration	Test frequency	Doses tested	Combined with	Other notes	Reference number
Armillaria mellea													
p.o.	Chronic (35 d)	Water	Rat	Sprague-Dawley	Male	n = 7 per group Control UCMS Model UCMS + WAM (Low, Medium, High) UCMS + Fluoxetine	UCMS	35 d	Daily	n/a	n/a	n/a	Lin et al. (2021a)
	Chronic (34 d)						SPT	1 h	Once	UCMS Model** 250 mg/kg$^{\#}$ 500 mg/kg$^{\#}$ 1000 mg/kg$^{\#}$			
	Chronic (30 d)						FST	5 min		250 mg/kg$^{\#\#\#\#}$ 500 mg/kg$^{\#\#\#\#}$ 1000 mg/kg$^{\#\#\#\#}$			
i.p.	Acute (30 min)	Ethyl Acetate	Mouse	ICR	Male	n = 10 per group Control PSAM (Lowest, Very Low, Low, Medium, High, Very High, Highest) Fluoxetine	FST	Last 4 min of 6 min	Once	0.05 mg/kg 0.1 mg/kg 0.5 mg/kg* 1 mg/kg* 5 mg/kg* 20 mg/kg 50 mg/kg	n/a	Protoilludane sesquiterpenoid aromatic esters	Zhang et al. (2021b)
							TST			0.05 mg/kg 0.1 mg/kg 0.5 mg/kg* 1 mg/kg** 5 mg/kg* 20 mg/kg* 50 mg/kg For PSAM (0.1 mg/kg): PSAM + Fluoxetine (5 mg/kg)* PSAM + Reboxetine (2.5 mg/kg)**	Fluoxetine Reboxetine		
Agaricus brasiliensis													
p.o.	Chronic (30 d)	Water	Mouse	Kunming	Male	n = 10 per group Control UCMS Model UCMS + AWE	UCMS	28 d	Daily	n/a	n/a	n/a	Xin et al. (2022)
							TST	Last 5 min of 6 min	Once	UCMS Model* 3 g/kg$^{\#}$			
Xylaria sp.													
i.g.	Chronic (28 d)	n/a	Rat	Sprague-Dawley	Male	n = 6–9 per group Control UCMS Model UCMS + Wuling powder (Low, Medium, High) UCMS + Fluoxetine	UCMS	42 d	Daily	n/a	n/a	Wuling mycelia powder	Tan et al. (2016)
							SPT	1 h	Weekly for 6 weeks	UCMS Model*** 0.5 g/kg$^{\#}$ 1 g/kg$^{\#\#\#}$ 2 g/kg$^{\#\#\#}$ *Model: significant from week 2 to week 6* *Wuling: significant from week 6*			

(Continued on following page)

10.3389/fphar.2024.1387158

TABLE 1 (*Continued*) Summary of rodent depression models and behavioural tests used to screen for antidepressant effects in different mushroom species. Subchronic and chronic treatment schedules include daily administration of drug unless otherwise stated.

Route	Treatment duration	Extraction method	Rodent species	Strain	Sex	Sample size	Behavioural test or model	Test duration	Test frequency	Doses tested	Combined with	Other notes	Reference number
Antrodia cinnamomea													
p.o.	Chronic (16 d)	n/a	Mouse	Kunming	Both	n = 24 per group Control AC (Low, Medium, High)	Weight-loaded FST	n/a	Once	0.1 g/kg 0.3 g/kg** 0.9 g/kg**	n/a	Mycelium Does not focus on depression nor use valid screen	Liu et al. (2017b)
Mushrooms (General)													
i.p.	Acute (60 min)	n/a	Mouse	ICR	Male	n = 10 per group Er, ErF, ErS, ErN (Low, High) ErN (Very Low, Low, Medium, High) Fluoxetine Er (Low) + Fluoxetine Er (Low) + Tianeptine Er (Low) + Reboxetine	FST	Last 4 min of 6 min	Once	All derivatives: 5 mg/kg – **Er*, ErF*, ErS*, ErN**** 20 mg/kg – **Er*, ErF*, ErS*, ErN**** ErN: 0.1 mg/kg* 0.5 mg/kg 1 mg/kg* 5 mg/kg** For ErN (0.5 mg/kg): ErN + Fluoxetine (5 m/g/kg) ErN + Tianeptine (15 mg/kg)** ErN + Reboxetine (2.5 mg/kg)**	Fluoxetine Tianeptine Reboxetine	Ergosterol and derivatives	Lin et al. (2017)
i.g.	Subchronic (1 d) *Injected 3 times (23.5 h, 5 h, and 1 h prior to test)*	n/a	Rat	Long Evans	Male	n = 10 per group Control Psilocybin Baeocystin Norbaeocystin Aeruginascin Fluoxetine	FST	5 min	Once	Psilocybin* Baeocystin Norbaeocystin* Aeruginascin (all 1 mg/kg)	n/a	Baeocystin, norbaeocystin, aeruginascin: tryptamine alkaloids and analogs of psilocybin Preprint; not peer-reviewed	Rakoczy et al. (2023)
s.c.	Subchronic (3 d)	n/a	Mouse	ICR	Male	n = 10 per group Control CORT Model CORT + p-CA	CORT	23 d	Daily	20 mg/kg	n/a	P-Coumaric acid (p-CA)	Yu et al. (2022)
i.p.							SPT	24 h	Once	CORT Model*** 75 mg/kg###			
							FST	Last 4 min of 6 min		CORT Model* 75 mg/kg#			

*$p < 0.05$, **$p < 0.01$, ***$p < 0.001$, ****$p < 0.0001$ compared to control.

#$p < 0.05$, ##$p < 0.01$, ###$p < 0.001$, ####$p < 0.0001$ compared to model/vehicle.

Acute (< 1 d), Subchronic (1–7 d), Chronic (> 7 d).

Abbreviations: FST = forced swim test; TST = tail suspension test; OVX = ovariectomy; UCMS = unpredictable chronic mild stress; CORT = corticosterone; SPT = sucrose preference test; CRS = chronic restraint stress; CSDS = chronic social defeat stress; PSD = post-stroke depression; MS = maternal separation; LPS = lipopolysaccharide; MCAO = middle cerebral artery occlusion; HE = *Hericium erinaceus;* Gl-E = *Ganoderma lucidum* extract; EEGL = ethanol extract of *Ganoderma lucidum;* GLP = *Ganoderma lucidum* polysaccharide; MAK = *Ganoderma lucidum* mycelia; GLT = *Ganoderma lucidum* triterpenoid; AEGI = aqueous extract of *Ganoderma lucidum;* PGL = Polysaccharide-peptide of *Ganoderma lucidum;* GAA = Ganoderic acid; PCE = *Psilocybe cubensis* extract; PO = *Pleurotus ostreatus;* EtOH = ethanol; MEPS = exopolysaccharide polysaccharide of *Marasmius androsaceus;* PCW = *Poria cocos* water extract; WAM = water extract of *Armillaria mellea;* PSAM = Protoilludane sesquiterpenoid aromatic esters from *Armillaria mellea;* AWE = *Agaricus brasiliensis* water extract; AC = *Antrodia cinnamomea;* Er = Ergosterol; IR = intestinal radiation; E_2 = 17β-estradiol; Dp = depression; i.p. = intraperitoneal; p.o. = per os (oral); i.g. = intragastric; s.c. = subcutaneous; i.v. = intravenous.

10.3389/fphar.2024.1387158

TABLE 2 Summary of rodent depression models and behavioural tests used to screen for antidepressant effects in different non-mushroom species of fungi. Subchronic and chronic treatment schedules include daily administration of drug unless otherwise stated.

Cordyceps militaris													
p.o.	Chronic (34 d)	Water	Rat	Sprague-Dawley	Male	n = 6 per group Control UCMS Model UCMS + CW (Low, Medium, High) UCMS + Fluoxetine	UCMS	34 d	Daily	n/a	n/a	n/a	Lin et al. (2021b)
							SPT	1 h	Once	UCMS Model*** 125 mg/kg### 250 mg/kg# 500 mg/kg#			
i.g.	Chronic (42 d)	n/a	Mouse	ICR	Male	n = 20 per group Control UCMS Model UCMS + COR (Low, High) UCMS + Fluoxetine	UCMS	42 d	Daily	n/a	n/a	Cordycepin (3'-deoxyadenosine): component of *C. militaris*	Tianzhu et al. (2014)
							SPT	12 h	Twice (Weeks 3 and 6)	Week 3 UCMS Model 20 mg/kg 40 mg/kg Week 6 UCMS Model** 20 mg/kg## 40 mg/kg##			
							FST	Last 4 min of 6 min	Once	UCMS Model** 20 mg/kg# 40 mg/kg##			
							TST		Twice (Weeks 3 and 6)	Week 3 UCMS Model 20 mg/kg 40 mg/kg Week 6 UCMS Model** 20 mg/kg## 40 mg/kg##			
i.g.	Chronic (28 d)	Water	Mouse	Kunming	Male	n = 12 per group Control PCM (Low, Medium, High)	Weight-loaded FST	n/a	Once	40 mg/kg* 80 mg/kg* 160 mg/kg*	n/a	Polysaccharide Does not focus on depression nor use valid screen	Xu (2016)
Cordyceps sinensis													
p.o.	Subchronic (5 d)	Supercritical Fluid and Hot Water	Mouse	C57BL/6	Male	n = 17 per group Control Supercritical (Low, Medium, High) Aqueous (Low, Medium, High)	TST	6 min	Once	Supercritical 2.5 mL/kg 5 mL/kg* 10 mL/kg* Aqueous 500 mg/kg 1000 mg/kg 2000 mg/kg	n/a	n/a	Nishizawa et al. (2007)
p.o.	Chronic (30 d)	n/a	Mouse	Swiss Albino	Both	n = 6 per group Control Natural *C. sinensis* (Low, Medium, High) Lab-cultured Mycelia (Low, Medium, High) Fluoxetine	Photoactometer	n/a	Once	NC 100 mg/kg 300 mg/kg* 500 mg/kg* LCM 100 mg/kg 300 mg/kg* 500 mg/kg*	n/a	Mycelium	Singh et al. (2014)
Paecilomyces tenuipes													
p.o.	Chronic (28 d)	Water	Rat	Sprague-Dawley	Male	n = 10 per group Control UCMS Model UCMS + PTNE (Low, Medium, High) UCMS + Fluoxetine	UCMS	56 d	Daily	n/a	n/a	Cultured mycelium	Liu et al. (2017a)
							FST	Last 5 min of 6 min	Once	UCMS Model*** 0.04 g/kg## 0.2 g/kg### 1 g/kg###			
p.o.	Chronic (21 d)	Alcohol and Water	Mouse	n/a	Male	n = 10 per group Control Control + AE (Low, Medium, High) Control + WE (Low, Medium, High)	UCMS	21 d	Daily	n/a	n/a	Mutant *P. tenuipes* strain M98 Mycelium	Li et al. (2019)
							SPT	1 h	Once	**UCMS** UCMS Model* Alcohol 0.05 g/kg 0.25 g/kg 2.5 g/kg# Water			

(Continued on following page)

TABLE 2 (*Continued*) Summary of rodent depression models and behavioural tests used to screen for antidepressant effects in different non-mushroom species of fungi. Subchronic and chronic treatment schedules include daily administration of drug unless otherwise stated.

						Control + Fluoxetine UCMS Model UCMS + AE (Low, Medium, High) UCMS + WE (Low, Medium, High) UCMS + Fluoxetine				0.04 g/kg 0.2 g/kg 2 g/kg#			
	Chronic (15 d), Chronic (21 d; UCMS)						FST	Last 4 min of 6 min		**Non-UCMS** Alcohol 0.05 g/kg 0.25 g/kg 2.5 g/kg* Water 0.04 g/kg 0.2 g/kg 2 g/kg** **UCMS** UCMS Model* Alcohol 0.05 g/kg 0.25 g/kg 2.5 g/kg# Water 0.04 g/kg# 0.2 g/kg 2 g/kg#			
							TST			**Non-UCMS** Alcohol 0.05 g/kg* 0.25 g/kg 2.5 g/kg Water 0.04 g/kg* 0.2 g/kg 2 g/kg* **UCMS** UCMS Model* Alcohol 0.05 g/kg 0.25 g/kg 2.5 g/kg Water 0.04 g/kg 0.2 g/kg# 2 g/kg#			
Paecilomyces hepiali													
p.o.	Chronic (28 d)	Water	Rat	Sprague-Dawley	Male	n = 6 per group Control UCMS Model UCMS + PHC (Low, Medium, High) UCMS + Fluoxetine	UCMS	56 d	Daily	n/a	n/a	n/a	Wang et al. (2017)
							SPT	2 h	Once	UCMS Model** 0.08 g/kg 0.4 g/kg# 2 g/kg##			
							FST	Last 5 min of 6 min		UCMS Model* 0.08 g/kg# 0.4 g/kg 2 g/kg##			
Ophiocordyceps formosana													
i.p.	Subchronic (5 d)	n/a	Mouse	C57BL/6	Male	Control (n = 6) STZ Model (n = 8) STZ + OFE (n = 8) STZ + Rosiglitazone (n = 8)	STZ	5 d	Daily	40 mg/kg	n/a	Uses STZ to induce diabetes Models diabetes-induced depression	Huang et al. (2016)
p.o.	Chronic (28 d)						TST	6 min	Once	STZ Model* 25 mg/mL#			
Penicillium sp.													
i.p.	Acute (30 min)	n/a	Mouse	ICR	Male	n = 8 per group 36 groups Control 2a–2i 3a–3r 4a–4g Fluoxetine	FST	Last 4 min of 6 min	Once	0.1 mL/20 g* *28 compounds showed significant antidepressant effect (26.23% – 89.96% decrease in immobility time vs. control)	n/a	Compounds are derivatives of *P. sp.*	Jin et al. (2019)

(Continued on following page)

TABLE 2 (*Continued*) Summary of rodent depression models and behavioural tests used to screen for antidepressant effects in different non-mushroom species of fungi. Subchronic and chronic treatment schedules include daily administration of drug unless otherwise stated.

Beauveria sp.													
i.g.	Chronic (21 d)	n/a	Mouse	Kunming	Male	n = 10 per group Control UCMS Model UCMS + BCEF (Low, Medium, High) UCMS + Moclobemide	UCMS SPT	21 d 24 h	Daily Once	n/a UCMS Model** 25 mg/kg$^{\#\#}$ 50 mg/kg$^{\#\#}$ 100 mg/kg$^{\#\#}$	n/a	BCEF0083: bioactive compound	Zhou et al. (2005)

*p < 0.05, **p < 0.01, ***p <0.001, ****p < 0.0001 compared to control

$^{\#}$p < 0.05, $^{\#\#}$p < 0.01, $^{\#\#\#}$p < 0.001, $^{\#\#\#\#}$p < 0.0001 compared to model/vehicle

Acute (< 1 d), Subchronic (1–7 d), Chronic (> 7 d)

Abbreviations: FST = forced swim test; TST, tail suspension test; UCMS, unpredictable chronic mild stress; SPT, sucrose preference test; STZ, streptozotocin(-induced diabetes); CW, *Cordyceps militaris* water extract; COR, Cordycepin; PCM = polysaccharide of *Cordyceps militaris;* PTNE = *Paecilomyces tenuipes* N45 aqueous extract; AE, alcohol extract; WE, water extract; PHC, *Paecilomyces hepiali* extract; OFE, *Ophiocordyceps formosana* extract; BCEF = bioactive compound from entomogenous fungi; i.p. = intraperitoneal; p.o. = per os (oral); i.g. = intragastric.

animal models, which could then be reversed by compounds with antidepressant activity, behavior was predominantly assessed with three main tests, which included the forced swim test (FST) (19 studies), tail suspension test (TST) (13 studies) and sucrose preference test (SPT) (16 studies)—multiple studies used two or more of these tasks. One study assessed behavior in the splash test as well as nest building (Mi et al., 2022), while one study measured locomotor activity and neuromuscular endurance (Singh et al., 2014). Twenty one of the 50 studies did not use an animal model of depression *per se*, and tested antidepressant activity solely with standalone antidepressant screens. This included 18 studies which used the FST and 10 that used the TST (seven studies used both); only two of these 21 studies used rats (Matsuzaki et al., 2013; Rakoczy et al., 2023).

Antidepressant effects of mushroom extracts

The Kingdom Fungi encompasses many known species which can be further classified into subgroups by the mechanism with which they reproduce and disseminate their spores (Boundless, 2024). Fungi subcategories include mushrooms, as well as other fungi such as moulds and yeasts. Mushrooms from the genus *Psilocybe* are of particular interest as many from the genus are known to contain the psychoactive compounds psilocybin and psilocin. This includes the species *Psilocybe cubensis*, which has been demonstrated to be able to alleviate depression and anxiety symptoms in clinical trials (Ross et al., 2016; Goodwin et al., 2022). Other mushrooms species such as *H. erinaceus* and *G. lucidum* do not necessarily contain psychoactive compounds, but are still of interest in models and studies of depression. Most research investigating the use of medicinal mushrooms and their extracts to treat depression has been in preclinical settings, rather than in clinical trials.

Of the 19 species of mushroom tested for antidepressant-like activity in the current review, the most common one was *G. lucidum*, in nine studies Table 1. Two studies used UCMS and reported 28-day treatment with doses of 100–500 mg/kg, p.o. exerted antidepressant-like effects in the SPT (Cheng, 2023) and both the SPT and FST (Zhao et al., 2021). A 5 mg/kg, i.p. dose in mice exerted antidepressant-like effects in the TST and FST after chronic social defeat stress (Li H. et al., 2021), while effects in mice subjected to the maternal separation model were reversed with a 21-day treatment with 40 mg/kg, i.p. of extract (Mi et al., 2022); 100 mg/kg, p.o. also reversed immobility in the FST in a binge-alcohol model (Nascimento et al., 2020). Antidepressant screens found positive effects with chronic doses of 100–1,000 mg/kg, p.o. in the FST and TST (Matsuzaki et al., 2013; Socala et al., 2015; Singh et al., 2021; Ezurike et al., 2023). Significant antidepressant-like effects were observed with the UCMS model with *Ganoderma* sp. extracts (21-day, 20–30 mg/kg, i.v.) (Zhang L. et al., 2021); in this study, the authors did not specify with species of *Ganoderma* the active compound ganoderic acid-a was extracted from.

Hericium erinaceus was examined in seven studies. Extracts (25 mg/kg, i.p. and 200–400 mg/kg, p.o.) for 28 days reversed the effects of chronic restraint stress in the SPT, TST (Chong et al., 2021) and FST (Chiu et al., 2018). Doses of 12–24 mg (combined with *Chlorella Vulgaris*), p.o. for 21 days significantly reversed immobility in the FST caused by treatment with high dose corticosterone (Chou et al., 2022). A single oral dose of 200 mg/kg reversed increased immobility in the FST and TST caused by lipopolysaccharide (Yao et al., 2015), while 28-day administration at 20–60 mg/kg, p.o. decreased immobility in the TST and FST (Ryu et al., 2018).

For other mushroom species examined, effects were observed with the UCMS model with *Marasmius androsaceus* (28-day, 30–150 mg/kg, p.o.), *Poria cocos* (35-day, 100–300 mg/kg, p.o.) (Huang et al., 2020), *Armillaria mellea* (35-day, 250–1,000 mg/kg, p.o.) (Lin et al., 2021a), *Agaricus brasiliensis* (30-day, 3,000 mg/kg, p.o.) (Xin et al., 2022) and *Xylaria sp*. (28-day, 500–2000 mg/kg, i.g.) (Tan et al., 2016). Other animal models included antidepressant-like effects in a model of menopausal depression (*Pleurotus eryngii*, 79-day, 500 mg/kg, p.o.) (Minami et al., 2013), chronic restraint stress (*Pleurotus citrinopileatus,* 14-day, 1,200 mg/kg, in food) (Nakamichi et al., 2016) (*M. androsaceus*, 14-day, i.g.) (Zhao et al., 2023) and high-dose corticosterone (P-coumaric acid–compound found in some mushrooms, 3-day, 75 mg/kg, i.p.) (Yu et al., 2022).

As an antidepressant screen, studies using the standalone FST and TST reported significant antidepressant-like effects with *Ganoderma applanatum*, *Ganoderma philippii,* and *Ganoderma brownii* (single dose, 100–400 mg/kg, p.o.) (Singh et al., 2021), *Grifola frondosa* (1/5-days, in a 1:1-1:4 ratio of *Griflola frondosa* powder to rat chow ratio) while *Pleurotus ostreatus* had no effect in the same study (Bao et al., 2017), *P. cubensis* (single dose. 1,000 mg/kg, p.o. (Hernandez-Leon et al., 2024), and single dose 10–40 mg/kg, i.p., combined with ketamine) (Mahmoudi et al., 2018), *P. eryngii* (single dose, 20 mg/kg, i.p.) (Park et al., 2021),

M. androsaceus (7-day, 50–250 mg/kg, p.o.) (Song et al., 2016; Song et al., 2020), *Lentinula edodes* (single dose 10 ml/kg p.o., [30% water soluble chitosan, 30% *Allium sativum* extract, 30% *L. edodes* extract, 0.5% Dioscorea Batatas extract, 0.5% bamboo salt extract]) (Koo et al., 2008), *A. mellea* (single dose, 5–20 mg/kg, i.p.) (Zhang T. et al., 2021), as well as ergosterol and derivatives (single dose, 0.1–20 mg/kg, i.p.) (Lin et al., 2017), and the mushroom extracts psilocybin and norbaeocystin (three doses over 24 h, 1 mg/kg, i.g.) (Rakoczy et al., 2023). No antidepressant effect was observed for Collybolide (a fungal metabolite; 2 mg/kg, i.p.) extract (Gupta et al., 2016).

Antidepressant effects of fungus extracts

For the seven species of fungus that do not produce mushrooms, antidepressant activity was examined using the UCMS model in six studies Table 2. Antidepressant-like effects on the SPT and/or FST were observed with *Cordyceps militaris* (34-day, 125–500 mg/kg, p.o.) (Lin et al., 2021b) and (42-day, 20–40 mg/kg, i.g.) (Tianzhu et al., 2014), *Paecilomyces tenuipes* (28-day, 40–1,000 mg/kg, p.o.) (Liu C. et al., 2017) and (21-day, 40–2,500 mg/kg, p.o.) (Li et al., 2019), *Paecilomyces hepiali* (28-day, 80–2000 mg/kg, p.o.) (Wang et al., 2017) and *Beauveria* sp. (21-day, 25–100 mg/kg, i.g.) (Zhou et al., 2005). Treatment with *Ophiocordyceps formosana* (28-day, 2.5 mg, p.o.) reversed TST deficits in a streptozotocin-induced model of diabetic depression (Huang et al., 2016). Three studies used standalone animal antidepressant screens, in which *Cordyceps sinensis* decreased immobility in the TST (5-day, 5–10 ml/kg, p.o.) (Nishizawa et al., 2007) and locomotor activity (30-day, 300–500 mg/kg, p.o.) (Singh et al., 2014), while a wide range of *Penicillium sp*. derivatives (single dose, 30 mg/kg, i.p.) were active in the FST (Jin et al., 2019).

Discussion

In the current analysis, we have summarized the main findings from a scoping review of the effects of mushroom and fungus extracts in preclinical tests of antidepressant efficacy. While this topic covers a broad range of compounds and techniques, several important themes are evident. Firstly, a large number of different species exhibit antidepressant-like activity, including 19 species of mushrooms and seven species of other fungi. For each of these, there can be multiple derivatives with their own antidepressant-like effects; for example, one study with *Penicillium sp*. identified 28 individual compounds with antidepressant-like effects in the FST (Jin et al., 2019), including some with more potent effects than the positive control fluoxetine. Thus, it appears that there is significant potential for novel compounds with antidepressant activity within these organisms. While this includes mushrooms with extracts that have traditionally been associated with psychoactive properties, such as *P. cubensis*, other novel compounds were identified with antidepressant-like effects. For example, P-coumaric acid was found to exhibit antidepressant-like effects after high dose corticosterone treatment (Yu et al., 2022); and was previously reported to exert pro-cognitive and anxiolytic effects in rodents (Scheepens et al., 2014; Kim et al., 2017; Ghaderi et al., 2022). Several of the species evaluated in this review have been tested in humans, confirming benefits for clinical depression. The antidepressant effects of psilocybin and psilocin, which are present in multiple of the current mushroom species are now well established (Griffiths et al., 2016; Ross et al., 2016; Davis et al., 2021; Eisenstein, 2022; Goodwin et al., 2022). In addition, one study showed that menopausal women experienced a reduction in depression and anxiety after 4 weeks of Hericium erinaceus intake (Nagano et al., 2010) while another showed a non-significant trend of reduced depression in women with fibromyalgia who received micromilled *G. lucidum* carpophores for 6 weeks (Pazzi et al., 2020).

Secondly, viewed as a whole, there are a number of both strengths and limitations within this literature. A positive is that the majority of studies administered compounds orally. While for many, use of oral gavage on a daily basis is technically more challenging than i.p. or s.c. drug administration in rodents (Turner et al., 2011), it strongly increases the translational validity of the studies, as human trials will be likely to use the same route of administration and be affected by similar pharmacokinetic processes, such as first-pass metabolism and low bioavailability (Bicker et al., 2020). It is also promising that antidepressant-like effects were observed across a wide duration of treatments with psychedelic and non-psychedelic-containing mushrooms and other fungi. Psychedelic compounds generally induce rapid drug tolerance upon repeated administration (Baumeister et al., 2014; Huang et al., 2022), where 5-HT2A receptor desensitization and/or downregulation leads to functional tolerance that can last several days (Buchborn et al., 2015; de la Fuente Revenga et al., 2022). However, observations of antidepressant-like effects weeks after treatment indicate that therapeutic effects may be sustained with these compounds (Aleksandrova and Phillips, 2021; Kelmendi et al., 2022). Various psychedelics have been reported to enhance neuroplasticity (synapto- and dendritogenesis) in frontocorticolimbic circuitry and increase functional connectivity in the brain, presumably reversing structural and functional deficits in depression (Aleksandrova and Phillips, 2021; Kelmendi et al., 2022). These psychedelic-induced structural and functional changes have been shown to last for weeks to months in animal models and/or humans and are thought to underlie the sustained therapeutic efficacy of these compounds (Aleksandrova and Phillips, 2021; Kelmendi et al., 2022).

While not necessarily a weakness, an extremely wide range of doses of extracts were tested in the current studies. From Tables 1, 2, these range from 1 mg/kg (Li H. et al., 2021; Rakoczy et al., 2023) to 3,000 mg/kg (Xin et al., 2022). Part of this reflects the effects of different routes of administration. Most of the extracts were administered orally, which is associated with a need for higher dosing, and therefore many of these studies included doses in the hundreds of milligrams per kilogram. But this wide range of dosing also represents the likelihood that many of the extracts were in early stage development, where the active compounds are unknown, and so whole product, heterogeneous extracts are used where the efficacy of active compounds may be modified through both pharmacodynamic (e.g., receptor antagonism) and pharmacokinetic (e.g., absorption) processes by many inactive compounds. Thus, such studies are early-stage screens as part of an iterative process (Reis et al., 2017), and in the case of positive

effects in the antidepressant screen, this will lead to refinement of extracts by further chemical analysis and result in greater potency, with a lower dose needed.

Multiple different animal models of depression and antidepressant screens were used to test for antidepressant-like effects. Although there is no universally accepted definition, animal models of depression are typically more complex and chronic than antidepressant screens, and are used to emulate some feature(s) of depression, such as its symptoms (face validity) or underlying biology (construct validity) (Geyer et al., 1995; Willner, 1984; Belzung and Lemoine, 2011; van den Berg, 2022). By contrast, antidepressant screens such as the TST and FST are acute and were originally designed to identify novel antidepressant compounds (predictive validity) without regard for similarity to the human condition (Commons et al., 2017). The most commonly used animal model of depression in the present studies was the UCMS paradigm, which is based on the development of anhedonia following exposure to chronic, variable stressors (Willner, 2017; Nollet, 2021). The model has strong theoretical appeal, based on the chronic onset of the antidepressant response, and performs well on key measures of validity (Willner, 1997). Nevertheless, the model has been criticized on both theoretical and practical grounds (Forbes et al., 1996; Barr and Phillips, 1998; Planchez et al., 2019; Markov and Novosadova, 2022), although a recent meta-analysis supported the utility of the model when specifically measuring anhedonia (Antoniuk et al., 2019). Thus, greater confidence should be placed in those studies with mushroom and fungus extracts that measured anhedonia (such as with the SPT) than those that did not. Alternate models of depression were also conducted, such as chronic social defeat stress (Li H. et al., 2021) and maternal separation (Mi et al., 2022), but typically only in a single study; given the importance of reproducibility within this field (Petković and Chaudhury, 2022), the literature will benefit from similar findings from alternate groups, or reproduction by the same groups themselves. Additionally, there are a number of other well-established and commonly used animal models of depression that should be used to assess antidepressant activity with these extracts, including surgical, pharmacological and genetic models (Barr and Phillips, 2002; Song and Leonard, 2005; Barr et al., 2011; Overstreet, 2012; Overstreet and Wegener, 2013; Vollmayr and Gass, 2013; Hendriksen et al., 2015; Czéh et al., 2016; Aleksandrova et al., 2019).

Slightly under half of the studies (22) utilized antidepressant screens such as the FST and TST, rather than models of depression. In most cases, these studies were methodologically sound, and used the appropriate controls, such as concurrent testing for locomotor activity and positive drug controls (Bogdanova et al., 2013; Yankelevitch-Yahav et al., 2015). However, several studies utilized variants of the FST, such as the "weight-loaded" FST (Xu, 2016; Liu Y. et al., 2017), whose validity is less well determined, while one study ascribed antidepressant-like effects based on changes in locomotor activity (Singh et al., 2014), which is a behavior with low specificity for depression. An additional concern was the small proportion of female animals tested, given that major depression is twice as common in women as in men: this issue is prevalent in the field of animal models of neuropsychiatric disorders as a whole (Kokras and Dalla, 2014), but future studies in this area should consider including female animals (Gobinath et al., 2018). Overall, however, the present review suggests that there is significant potential for novel antidepressant drug development with mushroom and fungus extracts provided that models and screens are conducted with high integrity.

Author contributions

CW: Conceptualization, Data curation, Formal Analysis, Investigation, Methodology, Validation, Visualization, Writing–original draft, Writing–review and editing. GK: Conceptualization, Data curation, Formal Analysis, Investigation, Methodology, Validation, Visualization, Writing–original draft, Writing–review and editing. LA: Formal Analysis, Writing–original draft, Writing–review and editing. WP: Conceptualization, Funding acquisition, Investigation, Project administration, Resources, Supervision, Writing–original draft, Writing–review and editing. AB: Conceptualization, Formal Analysis, Funding acquisition, Investigation, Methodology, Project administration, Resources, Supervision, Validation, Writing–original draft, Writing–review and editing.

Funding

The author(s) declare that financial support was received for the research, authorship, and/or publication of this article. AB was supported by a grant from NSERC. CW and GK were supported by BioTalent Canada with financial support from Translational Life Sciences.

Conflict of interest

The authors declare that the research was conducted in the absence of any commercial or financial relationships that could be construed as a potential conflict of interest.

Publisher's note

Supplementary material

The Supplementary Material for this article can be found online at: https://www.frontiersin.org/articles/10.3389/fphar.2024.1387158/full#supplementary-material

References

Aleksandrova, L. R., and Phillips, A. G. (2021). Neuroplasticity as a convergent mechanism of ketamine and classical psychedelics. *Trends Pharmacol. Sci.* 42 (11), 929–942. Epub 2021/09/28. doi:10.1016/j.tips.2021.08.003

Aleksandrova, L. R., Wang, Y. T., and Phillips, A. G. (2019). Evaluation of the Wistar-Kyoto rat model of depression and the role of synaptic plasticity in depression and antidepressant response. *Neurosci. Biobehav Rev.* 105, 1–23. Epub 2019/07/25. doi:10.1016/j.neubiorev.2019.07.007

Alo, R., Zizza, M., Fazzari, G., Facciolo, R. M., and Canonaco, M. (2019). Genistein modifies hamster behavior and expression of inflammatory factors following subchronic unpredictable mild stress. *Neuroendocrinology* 108 (2), 98–108. doi:10.1159/000495209

Antoniuk, S., Bijata, M., Ponimaskin, E., and Wlodarczyk, J. (2019). Chronic unpredictable mild stress for modeling depression in rodents: meta-analysis of model reliability. *Neurosci. Biobehav Rev.* 99, 101–116. Epub 2018/12/12. doi:10.1016/j.neubiorev.2018.12.002

Anuar, A. M., Minami, A., Matsushita, H., Ogino, K., Fujita, K., Nakao, H., et al. (2022). Ameliorating effect of the edible mushroom Hericium erinaceus on depressive-like behavior in ovariectomized rats. *Biol. Pharm. Bull.* 45 (10), 1438–1443. Epub 2022/10/03. doi:10.1248/bpb.b22-00151

Bao, H., Ran, P., Sun, L., Hu, W., Li, H., Xiao, C., et al. (2017). Griflola frondosa (GF) produces significant antidepressant effects involving AMPA receptor activation in mice. *Pharm. Biol.* 55 (1), 299–305. Epub 2016/12/13. doi:10.1080/13880209.2016.1235590

Barr, A. M., Boyda, H. N., and Procyshyn, R. M. (2011). "Withdrawal," in *Animal models of drug addiction*. Editor M. C. Olmstead (Totowa, NJ: Humana Press), 431–459.

Barr, A. M., and Phillips, A. G. (1998). Chronic mild stress has no effect on responding by rats for sucrose under a progressive ratio schedule. *Physiol. Behav.* 64 (5), 591–597. PubMed PMID: 9817568. doi:10.1016/s0031-9384(98)00060-2

Barr, A. M., and Phillips, A. G. (2002). Increased successive negative contrast in rats withdrawn from an escalating-dose schedule of D-amphetamine. *Pharmacol. Biochem. Behav.* 71 (1-2), 293–299. PubMed PMID: 11812535. doi:10.1016/s0091-3057(01)00664-5

Barr, A. M., Powell, S. B., Markou, A., and Geyer, M. A. (2006). Iloperidone reduces sensorimotor gating deficits in pharmacological models, but not a developmental model, of disrupted prepulse inhibition in rats. *Neuropharmacology* 51 (3), 457–465. PubMed PMID: 16762376. doi:10.1016/j.neuropharm.2006.04.004

Baumeister, D., Barnes, G., Giaroli, G., and Tracy, D. (2014). Classical hallucinogens as antidepressants? A review of pharmacodynamics and putative clinical roles. *Ther. Adv. Psychopharmacol.* 4 (4), 156–169. Epub 2014/08/02. doi:10.1177/2045125314527985

Belzung, C., and Lemoine, M. (2011). Criteria of validity for animal models of psychiatric disorders: focus on anxiety disorders and depression. *Biol. mood anxiety Disord.* 1 (1), 9. Epub 2011/01/01. doi:10.1186/2045-5380-1-9

Bicker, J., Fortuna, A., Alves, G., and Falcão, A. (2020). Nose-to-brain delivery of natural compounds for the treatment of central nervous system disorders. *Curr. Pharm. Des.* 26 (5), 594–619. Epub 2020/01/16. doi:10.2174/1381612826666200115101544

Bogdanova, O. V., Kanekar, S., D'Anci, K. E., and Renshaw, P. F. (2013). Factors influencing behavior in the forced swim test. *Physiol. Behav.* 118, 227–239. Epub 2013/05/21. doi:10.1016/j.physbeh.2013.05.012

Boundless (2024) Fungi reproduction: UC Davis office of the provost. Available at: https://bio.libretexts.org/Bookshelves/Introductory_and_General_Biology/Book%3A_General_Biology_(Boundless)/24%3A_Fungi/24.01%3A_Characteristics_of_Fungi/24.1C%3A_Fungi_Reproduction (updated 4/18/2024).

Boyda, H. N., Procyshyn, R. M., Pang, C. C., Hawkes, E., Wong, D., Jin, C. H., et al. (2013). Metabolic side-effects of the novel second-generation antipsychotic drugs asenapine and iloperidone: a comparison with olanzapine. *PLoS One* 8 (1), e53459. PubMed PMID: 23326434. doi:10.1371/journal.pone.0053459

Boyda, H. N., Procyshyn, R. M., Tse, L., Yuen, J. W. Y., Honer, W. G., and Barr, A. M. (2021). A comparison of the metabolic side-effects of the second-generation antipsychotic drugs risperidone and paliperidone in animal models. *PLoS One* 16 (1), e0246211. Epub 2021/01/29. doi:10.1371/journal.pone.0246211

Boyda, H. N., Ramos-Miguel, A., Procyshyn, R. M., Topfer, E., Lant, N., Choy, H. H., et al. (2014). Routine exercise ameliorates the metabolic side-effects of treatment with the atypical antipsychotic drug olanzapine in rats. *Int. J. Neuropsychopharmacol.* 17 (1), 77–90. PubMed PMID: 23953063. doi:10.1017/S1461145713000795

Braun, D., Rosenberg, A. M., Rabaniam, E., Haruvi, R., Malamud, D., Barbara, R., et al. (2024). High-resolution tracking of unconfined zebrafish behavior reveals stimulatory and anxiolytic effects of psilocybin. *Mol. Psychiatry*. Epub 2024/01/18. doi:10.1038/s41380-023-02391-7

Buchborn, T., Schröder, H., Dieterich, D. C., Grecksch, G., and Höllt, V. (2015). Tolerance to LSD and DOB induced shaking behaviour: differential adaptations of frontocortical 5-HT(2A) and glutamate receptor binding sites. *Behav. Brain Res.* 281, 62–68. Epub 2014/12/17. doi:10.1016/j.bbr.2014.12.014

Carhart-Harris, R. L., Bolstridge, M., Rucker, J., Day, C. M., Erritzoe, D., Kaelen, M., et al. (2016). Psilocybin with psychological support for treatment-resistant depression: an open-label feasibility study. *Lancet Psychiatry* 3 (7), 619–627. Epub 2016/05/24. doi:10.1016/s2215-0366(16)30065-7

Cheng, H. Y. (2023). Ganoderma lucidum ameliorated depression-like behavior in an unpredictable chronic mild stress rat model via regulation of monoamines. *Res. Square*. 10.21203/rs.3.rs-2389771/v1 Available at: https://www.researchsquare.com/article/rs-2389771/v1.

Chiu, C. H., Chyau, C. C., Chen, C. C., Lee, L. Y., Chen, W. P., Liu, J. L., et al. (2018). Erinacine A-enriched Hericium erinaceus mycelium produces antidepressant-like effects through modulating BDNF/PI3K/Akt/GSK-3β signaling in mice. *Int. J. Mol. Sci.* 19 (2), 341. Epub 2018/01/25. doi:10.3390/ijms19020341

Chong, P. S., Poon, C. H., Roy, J., Tsui, K. C., Lew, S. Y., Phang, M. W. L., et al. (2021). Neurogenesis-dependent antidepressant-like activity of Hericium erinaceus in an animal model of depression. *Chin. Med.* 16 (1), 132. Epub 2021/12/09. doi:10.1186/s13020-021-00546-8

Chou, M. Y., Ho, J. H., Huang, M. J., Chen, Y. J., Yang, M. D., Lin, L. H., et al. (2022). Potential antidepressant effects of a dietary supplement from the chlorella and lion's mane mushroom complex in aged SAMP8 mice. *Front. Nutr.* 9, 977287. Epub 2022/09/20. doi:10.3389/fnut.2022.977287

Collaborators, G. M. D. (2022). Global, regional, and national burden of 12 mental disorders in 204 countries and territories, 1990-2019: a systematic analysis for the Global Burden of Disease Study 2019. *Lancet Psychiatry* 9 (2), 137–150. Epub 2022/01/14. doi:10.1016/s2215-0366(21)00395-3

Commons, K. G., Cholanians, A. B., Babb, J. A., and Ehlinger, D. G. (2017). The rodent forced swim test measures stress-coping strategy, not depression-like behavior. *ACS Chem. Neurosci.* 8 (5), 955–960. Epub 2017/03/14. doi:10.1021/acschemneuro.7b00042

Czéh, B., Fuchs, E., Wiborg, O., and Simon, M. (2016). Animal models of major depression and their clinical implications. *Prog. Neuropsychopharmacol. Biol. Psychiatry* 64, 293–310. Epub 2015/04/22. doi:10.1016/j.pnpbp.2015.04.004

Davis, A. K., Barrett, F. S., May, D. G., Cosimano, M. P., Sepeda, N. D., Johnson, M. W., et al. (2021). Effects of psilocybin-assisted therapy on major depressive disorder: a randomized clinical trial. *JAMA psychiatry* 78 (5), 481–489. Epub 2020/11/05. doi:10.1001/jamapsychiatry.2020.3285

de la Fuente Revenga, M., Jaster, A. M., McGinn, J., Silva, G., Saha, S., and González-Maeso, J. (2022). Tolerance and cross-tolerance among psychedelic and nonpsychedelic 5-HT(2A) receptor agonists in mice. *ACS Chem. Neurosci.* 13 (16), 2436–2448. Epub 2022/07/29. doi:10.1021/acschemneuro.2c00170

Eisenstein, M. (2022). The psychedelic escape from depression. *Nature* 609 (7929), S87–S89. Epub 2022/09/29. doi:10.1038/d41586-022-02872-9

Ezurike, P. U., Odunola, E., Oke, T. A., Bakre, A. G., Olumide, O., Odetoye, O., et al. (2023). Ganoderma lucidum ethanol extract promotes weight loss and improves depressive-like behaviors in male and female Swiss mice. *Physiol. Behav.* 265, 114155. Epub 2023/03/13. doi:10.1016/j.physbeh.2023.114155

Fijałkowska, A., Jędrejko, K., Sułkowska-Ziaja, K., Ziaja, M., Kała, K., and Muszyńska, B. (2022). Edible mushrooms as a potential component of dietary interventions for major depressive disorder. *Foods (Basel, Switz.)* 11 (10), 1489. Epub 2022/05/29. doi:10.3390/foods11101489

Forbes, N. F., Stewart, C. A., Matthews, K., and Reid, I. C. (1996). Chronic mild stress and sucrose consumption: validity as a model of depression. *Physiol. Behav.* 60 (6), 1481–1484. Epub 1996/12/01. doi:10.1016/s0031-9384(96)00305-8

Friedrich, M. J. (2017). Depression is the leading cause of disability around the world. *Jama* 317 (15), 1517. Epub 2017/04/19. doi:10.1001/jama.2017.3826

Geyer, M. A., and Markou, A. (1995). "Animal models of psychiatric disorders," in *Psychopharmacology: the fourth generation of progress. Psychopharmacology: the fourth generation of progress*. Editors F. E. Bloom and D. J. Kupfer (New York: Raven Press), 787–798.

Ghaderi, S., Gholipour, P., Komaki, A., Salehi, I., Rashidi, K., Esmaeil Khoshnam, S., et al. (2022). p-Coumaric acid ameliorates cognitive and non-cognitive disturbances in a rat model of Alzheimer's disease: the role of oxidative stress and inflammation. *Int. Immunopharmacol.* 112, 109295. Epub 2022/10/05. doi:10.1016/j.intimp.2022.109295

Gobinath, A. R., Wong, S., Chow, C., Lieblich, S. E., Barr, A. M., and Galea, L. A. M. (2018). Maternal exercise increases but concurrent maternal fluoxetine prevents the increase in hippocampal neurogenesis of adult offspring. *Psychoneuroendocrinology* 91, 186–197. Epub 2018/03/27. doi:10.1016/j.psyneuen.2018.02.027

Goodwin, G. M., Aaronson, S. T., Alvarez, O., Arden, P. C., Baker, A., Bennett, J. C., et al. (2022). Single-dose psilocybin for a treatment-resistant episode of major depression. *N. Engl. J. Med.* 387 (18), 1637–1648. Epub 2022/11/03. doi:10.1056/NEJMoa2206443

Gravina, A. G., Pellegrino, R., Auletta, S., Palladino, G., Brandimarte, G., D'Onofrio, R., et al. (2023). Hericium erinaceus, a medicinal fungus with a centuries-old history: evidence in gastrointestinal diseases. *World J. gastroenterology* 29 (20), 3048–3065. Epub 2023/06/22. doi:10.3748/wjg.v29.i20.3048

Griffiths, R. R., Johnson, M. W., Carducci, M. A., Umbricht, A., Richards, W. A., Richards, B. D., et al. (2016). Psilocybin produces substantial and sustained decreases in depression and anxiety in patients with life-threatening cancer: a randomized double-blind trial. *J. Psychopharmacol.* 30 (12), 1181–1197. Epub 2016/12/03. doi:10.1177/0269881116675513

Gupta, A., Gomes, I., Bobeck, E. N., Fakira, A. K., Massaro, N. P., Sharma, I., et al. (2016). Collybolide is a novel biased agonist of κ-opioid receptors with potent antipruritic activity. *Proc. Natl. Acad. Sci. U. S. A.* 113 (21), 6041–6046. Epub 2016/05/11. doi:10.1073/pnas.1521825113

Haikazian, S., Chen-Li, D. C. J., Johnson, D. E., Fancy, F., Levinta, A., Husain, M. I., et al. (2023). Psilocybin-assisted therapy for depression: a systematic review and meta-analysis. *Psychiatry Res.* 329, 115531. Epub 2023/10/16. doi:10.1016/j.psychres.2023.115531

Hendriksen, H., Korte, S. M., Olivier, B., and Oosting, R. S. (2015). The olfactory bulbectomy model in mice and rat: one story or two tails? *Eur. J. Pharmacol.* 753, 105–113. Epub 2014/12/03. doi:10.1016/j.ejphar.2014.10.033

Hernandez-Leon, A., Escamilla-Orozco, R. I., Tabal-Robles, A. R., Martínez-Vargas, D., Romero-Bautista, L., Escamilla-Soto, G., et al. (2024). Antidepressant- and anxiolytic-like activities and acute toxicity evaluation of the Psilocybe cubensis mushroom in experimental models in mice. *J. Ethnopharmacol.* 320, 117415. Epub 2023/11/18. doi:10.1016/j.jep.2023.117415

Higgins, J. P. T., and Green, S. (2011) *Cochrane Handbook for systematic reviews of interventions*. Chichester (UK): John Wiley & Sons.

Hill, M. N., Barr, A. M., Ho, W. S., Carrier, E. J., Gorzalka, B. B., and Hillard, C. J. (2007). Electroconvulsive shock treatment differentially modulates cortical and subcortical endocannabinoid activity. *J. Neurochem.* 103 (1), 47–56. Epub 2007/06/15. doi:10.1111/j.1471-4159.2007.04688.x

Hosanagar, A., Cusimano, J., and Radhakrishnan, R. (2021). Therapeutic potential of psychedelics in the treatment of psychiatric disorders, Part 1: psychopharmacology and neurobiological effects. *J. Clin. Psychiatry* 82 (2), 20ac13786. Epub 2021/05/15. doi:10.4088/JCP.20ac13786

Hossen, S. M. M., Islam, M. J., Hossain, M. R., Barua, A., Uddin, M. G., and Emon, N. U. (2021). CNS anti-depressant, anxiolytic and analgesic effects of Ganoderma applanatum (mushroom) along with ligand-receptor binding screening provide new insights: multi-disciplinary approaches. *Biochem. biophysics Rep.* 27, 101062. Epub 2021/07/22. doi:10.1016/j.bbrep.2021.101062

Huang, C. W., Hong, T. W., Wang, Y. J., Chen, K. C., Pei, J. C., Chuang, T. Y., et al. (2016). Ophiocordyceps formosana improves hyperglycemia and depression-like behavior in an STZ-induced diabetic mouse model. *BMC Complement. Altern. Med.* 16 (1), 310. Epub 2016/08/25. doi:10.1186/s12906-016-1278-7

Huang, J., Pham, M., Panenka, W. J., Honer, W. G., and Barr, A. M. (2022). Chronic treatment with psilocybin decreases changes in body weight in a rodent model of obesity. *Front. Psychiatry* 13, 891512. Epub 2022/06/07. doi:10.3389/fpsyt.2022.891512

Huang, Y. J., Hsu, N. Y., Lu, K. H., Lin, Y. E., Lin, S. H., Lu, Y. S., et al. (2020). Poria cocos water extract ameliorates the behavioral deficits induced by unpredictable chronic mild stress in rats by down-regulating inflammation. *J. Ethnopharmacol.* 258, 112566. Epub 2020/01/14. doi:10.1016/j.jep.2020.112566

Hung, C. I. (2014). Factors predicting adherence to antidepressant treatment. *Curr. Opin. Psychiatry* 27 (5), 344–349. Epub 2014/07/18. doi:10.1097/yco.0000000000000086

Jin, Q., Fu, Z., Guan, L., and Jiang, H. (2019). Syntheses of benzo[d]Thiazol-2(3H)-One derivatives and their antidepressant and anticonvulsant effects. *Mar. drugs* 17 (7), 430. Epub 2019/07/26. doi:10.3390/md17070430

Kamal, S., Jha, M. K., and Radhakrishnan, R. (2023). Role of psychedelics in treatment-resistant depression. *Psychiatr. Clin. North Am.* 46 (2), 291–305. Epub 2023/05/07. doi:10.1016/j.psc.2023.02.004

Kelmendi, B., Kaye, A. P., Pittenger, C., and Kwan, A. C. (2022). Psychedelics. *Curr. Biol.* 32 (2), R63–R67. Epub 2022/01/26. doi:10.1016/j.cub.2021.12.009

Kim, H. B., Lee, S., Hwang, E. S., Maeng, S., and Park, J. H. (2017). p-Coumaric acid enhances long-term potentiation and recovers scopolamine-induced learning and memory impairments. *Biochem. Biophys. Res. Commun.* 492 (3), 493–499. Epub 2017/08/24. doi:10.1016/j.bbrc.2017.08.068

Kokras, N., and Dalla, C. (2014). Sex differences in animal models of psychiatric disorders. *Br. J. Pharmacol.* 171 (20), 4595–4619. Epub 2014/04/05. doi:10.1111/bph.12710

Koo, H. N., Um, J. Y., Kim, H. M., Lee, E. H., Sung, H. J., Kim, I. K., et al. (2008). Effect of pilopool on forced swimming test in mice. *Int. J. Neurosci.* 118 (3), 365–374. Epub 2008/02/27. doi:10.1080/00207450701593145

Kramer, M. S., Cutler, N., Feighner, J., Shrivastava, R., Carman, J., Sramek, J. J., et al. (1998). Distinct mechanism for antidepressant activity by blockade of central substance P receptors. *Science.* 281 (5383), 1640–1645. PubMed PMID: 9733503. doi:10.1126/science.281.5383.1640

Li, H., Xiao, Y., Han, L., Jia, Y., Luo, S., Zhang, D., et al. (2021a). Ganoderma lucidum polysaccharides ameliorated depression-like behaviors in the chronic social defeat stress depression model via modulation of Dectin-1 and the innate immune system. *Brain Res. Bull.* 171, 16–24. Epub 2021/03/12. doi:10.1016/j.brainresbull.2021.03.002

Li, T. J., Lee, T. Y., Lo, Y., Lee, L. Y., Li, I. C., Chen, C. C., et al. (2021b). Hericium erinaceus mycelium ameliorate anxiety induced by continuous sleep disturbance *in vivo*. *BMC complementary Med. Ther.* 21 (1), 295. Epub 2021/12/07. doi:10.1186/s12906-021-03463-3

Li, Y., Han, L., Lu, T., Noman, M., Qiang, W., Lan, X., et al. (2019). Antidepressant-like activities of extracts of the fungus Paecilomyces tenuipes M98. *Psychiatry Clin. Psychopharmacol.* 29 (4), 872–879. doi:10.1080/24750573.2019.1691352

Lian, L., Kim, D. D., Procyshyn, R. M., Cázares, D., Honer, W. G., and Barr, A. M. (2022). Long-acting injectable antipsychotics for early psychosis: a comprehensive systematic review. *PLoS One* 17 (4), e0267808. Epub 2022/04/30. doi:10.1371/journal.pone.0267808

Lin, M., Li, H., Zhao, Y., Cai, E., Zhu, H., Gao, Y., et al. (2017). Ergosteryl 2-naphthoate, an ergosterol derivative, exhibits antidepressant effects mediated by the modification of GABAergic and glutamatergic systems. *Mol. (Basel, Switz.)* 22 (4), 565. Epub 2017/04/01. doi:10.3390/molecules22040565

Lin, Y. E., Chen, Y. C., Lu, K. H., Huang, Y. J., Panyod, S., Liu, W. T., et al. (2021b). Antidepressant-like effects of water extract of Cordyceps militaris (Linn.) Link by modulation of ROCK2/PTEN/Akt signaling in an unpredictable chronic mild stress-induced animal model. *J. Ethnopharmacol.* 276, 114194. Epub 2021/05/12. doi:10.1016/j.jep.2021.114194

Lin, Y. E., Wang, H. L., Lu, K. H., Huang, Y. J., Panyod, S., Liu, W. T., et al. (2021a). Water extract of Armillaria mellea (Vahl) P. Kumm. Alleviates the depression-like behaviors in acute- and chronic mild stress-induced rodent models via anti-inflammatory action. *J. Ethnopharmacol.* 265, 113395. Epub 2020/09/22. doi:10.1016/j.jep.2020.113395

Liu, C., Wang, J., Xu, S., An, S., Tang, S., He, J., et al. (2017a). Paecilomyces tenuipes extract prevents depression-like behaviors in chronic unpredictable mild stress-induced rat model via modulation of neurotransmitters. *Mol. Med. Rep.* 16 (2), 2172–2178. Epub 2017/06/29. doi:10.3892/mmr.2017.6807

Liu, Y., Li, L., An, S., Zhang, Y., Feng, S., Zhao, L., et al. (2017b). Antifatigue effects of antrodia cinnamomea cultured mycelium via modulation of oxidative stress signaling in a mouse model. *Biomed. Res. Int.* 2017, 9374026. Epub 2017/04/21. doi:10.1155/2017/9374026

Lu, X., Barr, A. M., and Bartfai, T. (2005). Galanin receptors as novel drug targets for the treatment of depression and anxiety. *Drug Dev. Res.* 65 (4), 227–236. doi:10.1002/ddr.20026

Mahmoudi, E., Faizi, M., Hajiaghaee, R., and Razmi, A. (2018). Alteration of depressive-like behaviors by Psilocybe cubensis alkaloid extract in mice: the role of glutamate pathway. *Res. J. Pharmacogn.* 5 (2), 17–24. doi:10.22127/rjp.2018.58486

Markov, D. D., and Novosadova, E. V. (2022). Chronic unpredictable mild stress model of depression: possible sources of poor reproducibility and latent variables. *Biology* 11 (11), 1621. Epub 2022/11/12. doi:10.3390/biology11111621

Matsuzaki, H., Shimizu, Y., Iwata, N., Kamiuchi, S., Suzuki, F., Iizuka, H., et al. (2013). Antidepressant-like effects of a water-soluble extract from the culture medium of Ganoderma lucidum mycelia in rats. *BMC Complement. Altern. Med.* 13, 370. Epub 2013/12/29. doi:10.1186/1472-6882-13-370

McLachlan, G. (2018). Treatment resistant depression: what are the options? *Bmj* 363, k5354. Epub 2018/12/20. doi:10.1136/bmj.k5354

Mi, X., Zeng, G. R., Liu, J. Q., Luo, Z. S., Zhang, L., Dai, X. M., et al. (2022). Ganoderma lucidum triterpenoids improve maternal separation-induced anxiety- and depression-like behaviors in mice by mitigating inflammation in the periphery and brain. *Nutrients* 14 (11), 2268. Epub 2022/06/11. doi:10.3390/nu14112268

Minami, A., Matsushita, H., Horii, Y., Ieno, D., Matsuda, Y., Saito, M., et al. (2013). Improvement of depression-like behavior and memory impairment with the ethanol extract of Pleurotus eryngii in ovariectomized rats. *Biol. Pharm. Bull.* 36 (12), 1990–1995. Epub 2013/12/03. doi:10.1248/bpb.b13-00657

Moussa, A. Y., Fayez, S., Xiao, H., and Xu, B. (2022). New insights into antimicrobial and antibiofilm effects of edible mushrooms. *Food Res. Int. Ott.(Ont)* 162 (Pt A), 111982. Epub 2022/12/04. doi:10.1016/j.foodres.2022.111982

Nagano, M., Shimizu, K., Kondo, R., Hayashi, C., Sato, D., Kitagawa, K., et al. (2010). Reduction of depression and anxiety by 4 weeks Hericium erinaceus intake. *Biomed. Res. (Tokyo, Jpn.)* 31 (4), 231–237. Epub 2010/09/14. doi:10.2220/biomedres.31.231

Nakamichi, N., Nakayama, K., Ishimoto, T., Masuo, Y., Wakayama, T., Sekiguchi, H., et al. (2016). Food-derived hydrophilic antioxidant ergothioneine is distributed to the brain and exerts antidepressant effect in mice. *Brain Behav.* 6 (6), e00477. Epub 2016/05/03. doi:10.1002/brb3.477

Nascimento, C. P., Luz, D. A., da Silva, C. C. S., Malcher, C. M. R., Fernandes, L. M. P., Dalla Santa, H. S., et al. (2020). Ganoderma lucidum ameliorates neurobehavioral changes and oxidative stress induced by ethanol binge drinking. *Oxidative Med. Cell. Longev.* 2020, 2497845. Epub 2020/08/18. doi:10.1155/2020/2497845

Nishizawa, K., Torii, K., Kawasaki, A., Katada, M., Ito, M., Terashita, K., et al. (2007). Antidepressant-like effect of Cordyceps sinensis in the mouse tail suspension test. *Biol. Pharm. Bull.* 30 (9), 1758–1762. Epub 2007/09/11. doi:10.1248/bpb.30.1758

Nollet, M. (2021). Models of depression: unpredictable chronic mild stress in mice. *Curr. Protoc.* 1 (8), e208. doi:10.1002/cpz1.208

Overstreet, D. H. (2012). Modeling depression in animal models. *Methods Mol. Biol.* 829, 125–144. Epub 2012/01/11. doi:10.1007/978-1-61779-458-2_7

Overstreet, D. H., and Wegener, G. (2013). The flinders sensitive line rat model of depression--25 years and still producing. *Pharmacol. Rev.* 65 (1), 143–155. Epub 2013/01/16. doi:10.1124/pr.111.005397

Palhano-Fontes, F., Barreto, D., Onias, H., Andrade, K. C., Novaes, M. M., Pessoa, J. A., et al. (2019). Rapid antidepressant effects of the psychedelic ayahuasca in treatment-resistant depression: a randomized placebo-controlled trial. *Psychol. Med.* 49 (4), 655–663. Epub 2018/06/16. doi:10.1017/s0033291718001356

Pandya, U., Dhuldhaj, U., and Sahay, N. S. (2019). Bioactive mushroom polysaccharides as antitumor: an overview. *Nat. Prod. Res.* 33 (18), 2668–2680. Epub 2018/05/05. doi:10.1080/14786419.2018.1466129

Park, Y. S., Jang, S., Lee, H., Kang, S., Seo, H., Yeon, S., et al. (2021). Identification of the antidepressant function of the edible mushroom Pleurotus eryngii. *J. fungi (Basel, Switz.)* 7 (3), 190. Epub 2021/04/04. doi:10.3390/jof7030190

Pazzi, F., Adsuar, J. C., Domínguez-Muñoz, F. J., García-Gordillo, M. A., Gusi, N., and Collado-Mateo, D. (2020). Ganoderma lucidum effects on mood and health-related quality of life in women with fibromyalgia. *Healthc. (Basel, Switz.)* 8 (4), 520. Epub 2020/12/04. doi:10.3390/healthcare8040520

Petković, A., and Chaudhury, D. (2022). Encore: behavioural animal models of stress, depression and mood disorders. *Front. Behav. Neurosci.* 16, 931964. Epub 2022/08/26. doi:10.3389/fnbeh.2022.931964

Planchez, B., Surget, A., and Belzung, C. (2019). Animal models of major depression: drawbacks and challenges. *J. neural Transm. (Vienna)* 126 (11), 1383–1408. Epub 2019/10/05. doi:10.1007/s00702-019-02084-y

Rakoczy, R. J., Runge, G. N., Sen, A. K., Sandoval, O., Nguyen, Q., Roberts, B. R., et al. (2023). Pharmacological and behavioral effects of tryptamines present in psilocybin-containing mushrooms. *bioRxiv* 2023. doi:10.1101/2023.10.19.563138

Reis, F. S., Martins, A., Vasconcelos, M. H., Morales, P., and Ferreira, ICFR (2017). Functional foods based on extracts or compounds derived from mushrooms. *Trends Food Sci. Technol.* 66, 48–62. doi:10.1016/j.tifs.2017.05.010

Ross, S., Bossis, A., Guss, J., Agin-Liebes, G., Malone, T., Cohen, B., et al. (2016). Rapid and sustained symptom reduction following psilocybin treatment for anxiety and depression in patients with life-threatening cancer: a randomized controlled trial. *J. Psychopharmacol.* 30 (12), 1165–1180. Epub 2016/12/03. doi:10.1177/0269881116675512

Rossom, R. C., Shortreed, S., Coleman, K. J., Beck, A., Waitzfelder, B. E., Stewart, C., et al. (2016). Antidepressant adherence across diverse populations and healthcare settings. *Depress Anxiety* 33 (8), 765–774. Epub 2016/06/21. doi:10.1002/da.22532

Ryu, S., Kim, H. G., Kim, J. Y., Kim, S. Y., and Cho, K. O. (2018). Hericium erinaceus extract reduces anxiety and depressive behaviors by promoting hippocampal neurogenesis in the adult mouse brain. *J. Med. food* 21 (2), 174–180. Epub 2017/11/02. doi:10.1089/jmf.2017.4006

Scheepens, A., Bisson, J. F., and Skinner, M. (2014). p-Coumaric acid activates the GABA-A receptor *in vitro* and is orally anxiolytic *in vivo*. *Phytotherapy Res. PTR* 28 (2), 207–211. Epub 2013/03/28. doi:10.1002/ptr.4968

Sepúlveda-Lizcano, L., Arenas-Villamizar, V. V., Jaimes-Duarte, E. B., García-Pacheco, H., Paredes, C. S., Bermúdez, V., et al. (2023). Metabolic adverse effects of psychotropic drug therapy: a systematic review. *Eur. J. investigation health, Psychol. Educ.* 13 (8), 1505–1520. Epub 2023/08/25. doi:10.3390/ejihpe13080110

Simonsson, O., Carlbring, P., Carhart-Harris, R., Davis, A. K., Nutt, D. J., Griffiths, R. R., et al. (2023). Assessing the risk of symptom worsening in psilocybin-assisted therapy for depression: a systematic review and individual participant data meta-analysis. *Psychiatry Res.* 327, 115349. Epub 2023/08/01. doi:10.1016/j.psychres.2023.115349

Singh, K. P., Meena, H. S., and Negi, P. S. (2014). Enhancement of neuromuscular activity by natural specimens and cultured mycelia of Cordyceps sinensis in mice. *Indian J. Pharm. Sci.* 76 (5), 458–461. doi:10.4103/0250-474X.143105

Singh, R., Shri, R., Singh, A. P., and Dhingra, G. S. (2021). Valorization of Ganoderma species: chemical characterization and antidepressant-like activity. *Waste Biomass Valorization* 12 (4), 2025–2036. doi:10.1007/s12649-020-01157-4

Socala, K., Nieoczym, D., Grzywnowicz, K., Stefaniuk, D., and Wlaz, P. (2015). Evaluation of anticonvulsant, antidepressant-and anxiolytic-like effects of an aqueous extract from cultured mycelia of the lingzhi or reishi medicinal mushroom Ganoderma lucidum (higher basidiomycetes) in mice. *Int. J. Med. mushrooms* 17 (3), 209–218. Epub 2015/05/09. doi:10.1615/intjmedmushrooms.v17.i3.10

Song, C., and Leonard, B. E. (2005). The olfactory bulbectomised rat as a model of depression. *Neurosci. Biobehav Rev.* 29 (4-5), 627–647. Epub 2005/06/01. doi:10.1016/j.neubiorev.2005.03.010

Song, J., Geng, X., Su, Y., Zhang, X., Tu, L., Zheng, Y., et al. (2020). Structure feature and antidepressant-like activity of a novel exopolysaccharide isolated from Marasmius androsaceus fermentation broth. *Int. J. Biol. Macromol.* 165 (Pt B), 1646–1655. Epub 2020/10/12. doi:10.1016/j.ijbiomac.2020.10.015

Song, J., Wang, X., Huang, Y., Qu, Y., Teng, L., Wang, D., et al. (2017). Antidepressant-like effects of Marasmius androsaceus metabolic exopolysaccharides on chronic unpredictable mild stress-induced rat model. *Mol. Med. Rep.* 16 (4), 5043–5049. Epub 2017/08/03. doi:10.3892/mmr.2017.7145

Song, J., Xing, G., Cao, J., Teng, L., Li, C., Meng, Q., et al. (2016). Investigation of the antidepressant effects of exopolysaccharides obtained from Marasmius androsaceus fermentation in a mouse model. *Mol. Med. Rep.* 13 (1), 939–946. Epub 2015/12/10. doi:10.3892/mmr.2015.4584

Strauss, D., Ghosh, S., Murray, Z., and Gryzenhout, M. (2022). An overview on the taxonomy, phylogenetics and ecology of the psychedelic genera Psilocybe, panaeolus, pluteus and gymnopilus. *Front. For. Glob. Change* 5. doi:10.3389/ffgc.2022.813998

Tan, Y. F., Liao, Z. L., Qiu, Y. J., Zhu, J. P., and Yu, E. Y. (2016). Possible involvement of L-arginine-nitric oxide (NO)-cyclic guanosine monophosphate (cGMP) signaling pathway in the antidepressant-like effect of Wuling mycelia powder in rat. *Biomed. Pharmacother.* 78, 60–65. Epub 2016/02/24. doi:10.1016/j.biopha.2015.12.016

Teng, T., Zhang, Z., Yin, B., Guo, T., Wang, X., Hu, J., et al. (2022). Effect of antidepressants on functioning and quality of life outcomes in children and adolescents with major depressive disorder: a systematic review and meta-analysis. *Transl. psychiatry* 12 (1), 183. Epub 2022/05/05. doi:10.1038/s41398-022-01951-9

Tianzhu, Z., Shihai, Y., and Juan, D. (2014). Antidepressant-like effects of cordycepin in a mice model of chronic unpredictable mild stress. *Evidence-based complementary Altern. Med. eCAM.* 2014, 438506. Epub 2015/01/15. doi:10.1155/2014/438506

Tse, L., Procyshyn, R. M., Fredrikson, D. H., Boyda, H. N., Honer, W. G., and Barr, A. M. (2014). Pharmacological treatment of antipsychotic-induced dyslipidemia and hypertension. *Int. Clin. Psychopharmacol.* 29 (3), 125–137. PubMed PMID: 24169026. doi:10.1097/YIC.0000000000000014

Turner, P. V., Brabb, T., Pekow, C., and Vasbinder, M. A. (2011). Administration of substances to laboratory animals: routes of administration and factors to consider. *J. Am. Assoc. Laboratory Animal Sci. JAALAS.* 50 (5), 600–613.

van den Berg, H. (2022). Evaluating the validity of animal models of mental disorder: from modeling syndromes to modeling endophenotypes. *Hist. Philosophy Life Sci.* 44 (4), 59. doi:10.1007/s40656-022-00537-4

Venturella, G., Ferraro, V., Cirlincione, F., and Gargano, M. L. (2021). Medicinal mushrooms: bioactive compounds, use, and clinical trials. *Int. J. Mol. Sci.* 22 (2), 634. Epub 2021/01/14. doi:10.3390/ijms22020634

Voineskos, D., Daskalakis, Z. J., and Blumberger, D. M. (2020). Management of treatment-resistant depression: challenges and strategies. *Neuropsychiatr. Dis. Treat.* 16, 221–234. Epub 2020/02/06. doi:10.2147/ndt.s198774

Vollmayr, B., and Gass, P. (2013). Learned helplessness: unique features and translational value of a cognitive depression model. *Cell. tissue Res.* 354 (1), 171–178. Epub 2013/06/14. doi:10.1007/s00441-013-1654-2

Wang, J., Liu, Y., Li, L., Qi, Y., Zhang, Y., Li, L., et al. (2017). Dopamine and serotonin contribute to Paecilomyces hepiali against chronic unpredictable mild stress induced depressive behavior in Sprague Dawley rats. *Mol. Med. Rep.* 16 (4), 5675–5682. Epub 2017/08/30. doi:10.3892/mmr.2017.7261

Willner, P. (1984). The validity of animal models of depression. *Psychopharmacol. Berl.* 83 (1), 1–16. Epub 1984/01/01. doi:10.1007/bf00427414

Willner, P. (1997). Validity, reliability and utility of the chronic mild stress model of depression: a 10-year review and evaluation. *Psychopharmacol. Berl.* 134 (4), 319–329. Epub 1998/02/06. doi:10.1007/s002130050456

Willner, P. (2017). The chronic mild stress (CMS) model of depression: history, evaluation and usage. *Neurobiol. stress* 6, 78–93. Epub 2017/02/24. doi:10.1016/j.ynstr.2016.08.002

Xin, Y., Zhang, Y., and Zhang, X. (2022). Antidepressant effect of water extract of royal sun medicinal mushroom, Agaricus brasiliensis (agaricomycetes), in mice exposed to chronic unpredictable mild stress. *Int. J. Med. mushrooms* 24 (4), 63–73. Epub 2022/06/14. doi:10.1615/IntJMedMushrooms.2022042726

Xu, Y. F. (2016). Effect of polysaccharide from Cordyceps militaris (ascomycetes) on physical fatigue induced by forced swimming. *Int. J. Med. mushrooms* 18 (12), 1083–1092. Epub 2017/01/18. doi:10.1615/IntJMedMushrooms.v18.i12.30

Yadav, D., and Negi, P. S. (2021). Bioactive components of mushrooms: processing effects and health benefits. *Food Res. Int. Ott.(Ont)* 148, 110599. Epub 2021/09/12. doi:10.1016/j.foodres.2021.110599

Yankelevitch-Yahav, R., Franko, M., Huly, A., and Doron, R. (2015). The forced swim test as a model of depressive-like behavior. *J. Vis. Exp.* (97), 52587. Epub 2015/04/14. doi:10.3791/52587

Yao, W., Zhang, J. C., Dong, C., Zhuang, C., Hirota, S., Inanaga, K., et al. (2015). Effects of amycenone on serum levels of tumor necrosis factor-α, interleukin-10, and depression-like behavior in mice after lipopolysaccharide administration. *Pharmacol. Biochem. Behav.* 136, 7–12. Epub 2015/07/08. doi:10.1016/j.pbb.2015.06.012

Yu, X. D., Zhang, D., Xiao, C. L., Zhou, Y., Li, X., Wang, L., et al. (2022). P-coumaric acid reverses depression-like behavior and memory deficit via inhibiting AGE-RAGE-mediated neuroinflammation. *Cells* 11 (10), 1594. Epub 2022/05/29. doi:10.3390/cells11101594

Yuen, J. W. Y., Kim, D. D., Procyshyn, R. M., Panenka, W. J., Honer, W. G., and Barr, A. M. (2021). A focused review of the metabolic side-effects of clozapine. *Front. Endocrinol.* 12, 609240. Epub 2021/03/16. doi:10.3389/fendo.2021.609240

Zhang, L., Zhang, L., and Sui, R. (2021a). Ganoderic acid A-mediated modulation of microglial polarization is involved in depressive-like behaviors and neuroinflammation in a rat model of post-stroke depression. *Neuropsychiatr. Dis. Treat.* 17, 2671–2681. Epub 2021/08/24. doi:10.2147/ndt.s317207

Zhang, T., Du, Y., Liu, X., Sun, X., Cai, E., Zhu, H., et al. (2021b). Study on antidepressant-like effect of protoilludane sesquiterpenoid aromatic esters from Armillaria Mellea. *Nat. Prod. Res.* 35 (6), 1042–1045. Epub 2019/05/29. doi:10.1080/14786419.2019.1614577

Zhao, J., Zeng, X., Liu, J., Liu, X., Liu, Z., Wang, B., et al. (2023). Marasmius androsaceus mitigates depression-exacerbated intestinal radiation injuries through reprogramming hippocampal miRNA expression. *Biomed. Pharmacother.* 165, 115157. Epub 2023/07/17. doi:10.1016/j.biopha.2023.115157

Zhao, S., Rong, C., Gao, Y., Wu, L., Luo, X., Song, S., et al. (2021). Antidepressant-like effect of Ganoderma lucidum spore polysaccharide-peptide mediated by upregulation of prefrontal cortex brain-derived neurotrophic factor. *Appl. Microbiol. Biotechnol.* 105 (23), 8675–8688. Epub 2021/10/31. doi:10.1007/s00253-021-11634-y

Zhou, L. L., Ming, L., Ma, C. G., Cheng, Y., and Jiang, Q. (2005). Antidepressant-like effects of BCEF0083 in the chronic unpredictable stress models in mice. *Chin. Med. J. Engl.* 118 (11), 903–908.

Glossary

FST	forced swim test
TST	tail suspension test
OVX	ovariectomy
UCMS	unpredictable chronic mild stress
CORT	corticosterone
SPT	sucrose preference test
CRS	chronic restraint stress
CSDS	chronic social defeat stress
STZ	streptozotocin (-induced diabetes)
PSD	post-stroke depression
MS	maternal separation
LPS	lipopolysaccharide
MCAO	middle cerebral artery occlusion
HE	Hericium erinaceus
GI-E	Ganoderma lucidum extract
EEGL	ethanol extract of Ganoderma lucidum
GLP	Ganoderma lucidum polysaccharide
MAK	Ganoderma lucidum mycelia
GLT	Ganoderma lucidum triterpenoid
AEGI	aqueous extract of Ganoderma lucidum
PGL	Polysaccharide-peptide of Ganoderma lucidum
GAA	Ganoderic acid
PCE	Psilocybe cubensis extract
PO	Pleurotus ostreatus
EtOH	ethanol
MEPS	exopolysaccharide polysaccharide of Marasmius androsaceus
PCW	Poria cocos water extract
WAM	water extract of Armillaria mellea
PSAM	Protoilludane sesquiterpenoid aromatic esters from Armillaria mellea
AWE	Agaricus brasiliensis water extract
AC	Antrodia cinnamomea
Er	Ergosterol
CW	Cordyceps militaris water extract
COR	Cordycepin
PCM	polysaccharide of Cordyceps militaris
PTNE	Paecilomyces tenuipes N45 aqueous extract
AE	alcohol extract
WE	water extract
PHC	Paecilomyces hepiali extract
OFE	Ophiocordyceps formosana extract
BCEF	bioactive compound from entomogenous fungi
IR	intestinal radiation
E2	17β-estradiol
Dp	depression
i.p.	intraperitoneal
p.o.	per os (oral)
i.g.	intragastric
s.c.	subcutaneous
i.v.	intravenous

frontiers | Frontiers in Neuroscience

TYPE Original Research
PUBLISHED 05 July 2024
DOI 10.3389/fnins.2024.1387098

OPEN ACCESS

EDITED BY
Tanya Calvey,
University of Cape Town, South Africa

REVIEWED BY
Alberto L. Vazquez,
University of Pittsburgh, United States
Hirokazu Takahashi,
The University of Tokyo, Japan

*CORRESPONDENCE
Anthony G Hudetz
ahudetz@umich.edu

RECEIVED 16 February 2024
ACCEPTED 07 June 2024
PUBLISHED 05 July 2024

CITATION
Hudetz AG (2024) Microstimulation reveals anesthetic state-dependent effective connectivity of neurons in cerebral cortex. *Front. Neurosci.* 18:1387098. doi: 10.3389/fnins.2024.1387098

Microstimulation reveals anesthetic state-dependent effective connectivity of neurons in cerebral cortex

Anthony G Hudetz*

Department of Anesthesiology, Center for Consciousness Science, University of Michigan, Ann Arbor, MI, United States

Introduction: Complex neuronal interactions underlie cortical information processing that can be compromised in altered states of consciousness. Here intracortical microstimulation was applied to investigate anesthetic state-dependent effective connectivity of neurons in rat visual cortex *in vivo*.

Methods: Extracellular activity was recorded at 32 sites in layers 5/6 while stimulating with charge-balanced discrete pulses at each electrode in random order. The same stimulation pattern was applied at three levels of anesthesia with desflurane and in wakefulness. Spikes were sorted and classified by their waveform features as putative excitatory and inhibitory neurons. Network motifs were identified in graphs of effective connectivity constructed from monosynaptic cross-correlograms.

Results: Microstimulation caused early (<10 ms) increase followed by prolonged (11–100 ms) decrease in spiking of all neurons throughout the electrode array. The early response of excitatory but not inhibitory neurons decayed rapidly with distance from the stimulation site over 1 mm. Effective connectivity of neurons with significant stimulus response was dense in wakefulness and sparse under anesthesia. The number of network motifs, especially those of higher order, increased rapidly as the anesthesia was withdrawn indicating a substantial increase in network connectivity as the animals woke up.

Conclusion: The results illuminate the impact of anesthesia on functional integrity of local cortical circuits affecting the state of consciousness.

KEYWORDS

microstimulation, cortex, network, connectivity, spike, anesthesia, consciousness

Introduction

Complex neuronal interactions underlie cortical information processing from which cognitive functions and consciousness emerge. Anesthetic agents are unique tools to alter neuronal behavior with the goal to better understand the neurobiological basis of normal and altered states of consciousness. Most prior work examined changes in neuronal connectivity through recordings of spontaneous ongoing activity or sensory stimulus-evoked activity during different wakeful and anesthetized states (Hudetz et al., 2009; Andrada et al., 2012; Vizuete et al., 2012; Aasebo et al., 2017; Lee et al., 2021; Bharioke et al., 2022; Margalit et al., 2022; Aggarwal et al., 2023). However, recent studies suggest that further insight into the functional interaction of neurons may be gained through exogenous perturbation of single neurons or local neuronal populations.

Former studies proposed to employ intracortical microstimulation to probe the structure and function of intact neuronal circuits (Clark et al., 2011; Kwan and Dan, 2012; Kumar et al., 2013). This approach can help reveal the causal or "effective" connectivity of neurons (Aertsen et al., 1989) that is not directly discoverable from the recording of undisturbed, spontaneous activity alone (Clark et al., 2011; Kumar et al., 2013; Sadeh and Clopath, 2020). Microstimulation also helps mitigate the confounding effect of background activity of other neurons, in analogy with what is achieved by evoked potential averaging (Cheney et al., 2013). The effect of anatomically precise perturbation by microstimulation can propagate throughout the neuron network, generating multiple extra spikes that last for hundreds of ms (London et al., 2010; Kwan and Dan, 2012; Emiliani et al., 2015; Bernardi et al., 2021). Such spike sequences formed by forward and recurrent interactions may reflect basic information packets in the neuron network (Luczak et al., 2015). Anesthetics can also alter the spike sequences (Tanabe et al., 2023), which could inform the potential mechanism by which state-dependent cellular changes may impair neuronal information processing and consciousness (Hudetz et al., 2015; Margalit et al., 2022; Pazienti et al., 2022).

Intracortical stimulation was recently used to examine the effects of anesthesia on electroencephalographic connectivity (Arena et al., 2021) but not the connectivity of discrete neurons in local cortical circuits. To fill this gap of knowledge, this work applied intracortical microstimulation to investigate how anesthesia achieved with the inhalational agent desflurane may alter stimulus-related spiking activity and effective connectivity of discrete neurons in rat visual cortex *in vivo*. By electrically stimulating neuronal tissue at one of the sites of an intracortical microelectrode array and measuring the spiking activity of neurons at all other electrode sites, the effective connectivity of the neuronal network was estimated. We hypothesized that the anesthetic would disrupt effective connectivity of the neurons in a dose-dependent manner, implying a gradual disruption of information processing. We also examined how the anesthetic may influence the stimulus response of putative excitatory vs. inhibitory neurons. Most inhalational anesthetics suppress spontaneous neuronal activity by facilitating inhibitory synaptic transmission and suppressing excitatory synaptic transmission (Franks, 2008), but the state-dependent effects of intracortical microstimulation on excitatory vs. inhibitory neuron firing are unclear. We anticipated that the effects of anesthesia on microstimulation-induced neuron firing will also be cell type dependent. Overall, the study aimed to gain insight into how anesthesia impacts the functional integrity of cortical neuronal connectivity relevant for the loss or return of consciousness.

Materials and methods

Surgery and experimental protocol

The study was approved by the Institutional Animal Care and Use Committee in accordance with the Guide for the Care and Use of Laboratory Animals of the Governing Board of the National Research Council (National Academies of Sciences, Engineering, and Medicine, 2011). General procedures followed those described before (Lee et al., 2020) but using a different probe design. Briefly, nine adult male and female rats were chronically implanted with microelectrode arrays (Microprobes, Gaithersburg, MD, USA) into the right primary visual cortex (V1) for extracellular recording and stimulation. The probes consisted of 32 platinum/iridium (70%/30%) electrodes of 75 μm diameter and 2 mm length. They had approximately 100 kOhm impedance. The electrodes were arranged in a 6 × 6 square matrix format, omitting the corner locations. The electrode spacing was 250 μm in both directions. The stereotaxic target coordinates of the center of the array at the electrode tips were −6.75 mm anteroposterior, 3.60 mm mediolateral, and 1.50 mm deep from Bregma. The depth was chosen to target infragranular cortex (layers 5/6); this was not verified with histological analysis in this study. One corner of the electrode array was occupied by the reference electrode consisting of the same Pt/Ir composition with 10 kOhm impedance. An additional low-impedance electrode placed in the opposite corner of the array or an external bare wire tied to a stainless-steel screw in the cranium over the left cerebellum served as ground.

Several days after recovery the animals were placed unrestrained in a sealed, dark anesthesia chamber for testing. The experiment consisted of stepwise decrease of inhaled concentration of desflurane at 6, 4, 2.5 and 0% mixed to 30% oxygen-enriched air. Desflurane concentrations were chosen to cover a suitable range from light sedation to deep anesthesia. Based on our former experiments (Imas et al., 2005) with testing the righting reflex–a putative index of consciousness in rodents (Franks, 2008), 2.5% corresponds to conscious sedation, 6% unconsciousness and 4% is near the transition point. Anesthetic depth was not tested in the present experiments. Each anesthetic concentration was held for 60 min including an equilibration time of 15 min before commencing microstimulation. A typical experiment lasted for 4 h.

Stimulation parameters

Monopolar stimuli with respect to ground were delivered to each electrode site one by one in random order at 0.5 s intervals (2 Hz). The stimulation frequency was chosen to maximize the number of stimuli delivered while allowing population spike activity return to the prestimulus baseline. The same stimulation sequence was repeated 80 times, equivalent to a total of 2,560 stimuli delivered in each condition. Stimulation pulses were charge-balanced, biphasic waveforms (Merrill et al., 2005) that were initially varied with respect to cathodic-anodic temporal order and asymmetry of duration and amplitude. Preliminary tests in 4 animals with 5, 10, 20, and 40 μA stimulation currents showed that maximum response was afforded by 40 μA in agreement with other studies (Voigt and Kral, 2019; Sombeck et al., 2022; Yun et al., 2023). In all subsequent experiments a maximum stimulus current of 40 μA was used with 5:1 and 1:5 amplitude/phase duration ratios to maximize the number of similar trials within the same experimental time frame. The corresponding amplitudes and phase durations were 40 μA for 60 μs and 8 μA for 300 μs separated by 0 μA for 60 μs.

Recording system and data analysis

Extracellular potentials were recorded at all electrode sites except at the one being stimulated using the data acquisition system, Scout Processor and Nano2+Stim front end (Ripple Neuro, Salt Lake City, UT, USA), digitized at 30 kHz and band-pass filtered at 300–7,500 Hz for spike detection. Spike rasters and local field potential (LFP) traces in two conditions before and during microstimulation are shown in Figures 1A, B in one experiment as an example. The stimulus artifact was removed by template subtraction (Sombeck et al., 2022). As shown in Figure 1C, significant stimulus artifact at the non-stimulated electrodes was limited to 1 ms duration (Figure 1C). The amplitude of the subsequent slow potential was less than 1 mV and inconsequential for spike detection and classification following band-pass filtering. Electromyographic (EMG) artifacts due to motion were eliminated by rejecting data from all channels within ± 1 s of any signal exceeding 6 standard deviations of the mean. A total of 160 spiking neurons were recorded in 9 rats. Unit spikes were extracted and sorted using the software Spyking Circus (Yger et al., 2018). The number of recorded neurons in each condition in each animal is provided in Table 1. Neurons were classified off-line into putative excitatory or inhibitory type based on the half peak-width and trough-to-peak time of their spike waveform as illustrated in Figures 1D–F as done before (Lee et al., 2020).

Network analysis

Stimulus-related network connectivity was analyzed in two different ways. First, an effective connectivity map was constructed from all pairs of stimulus-neuron sites from neurons

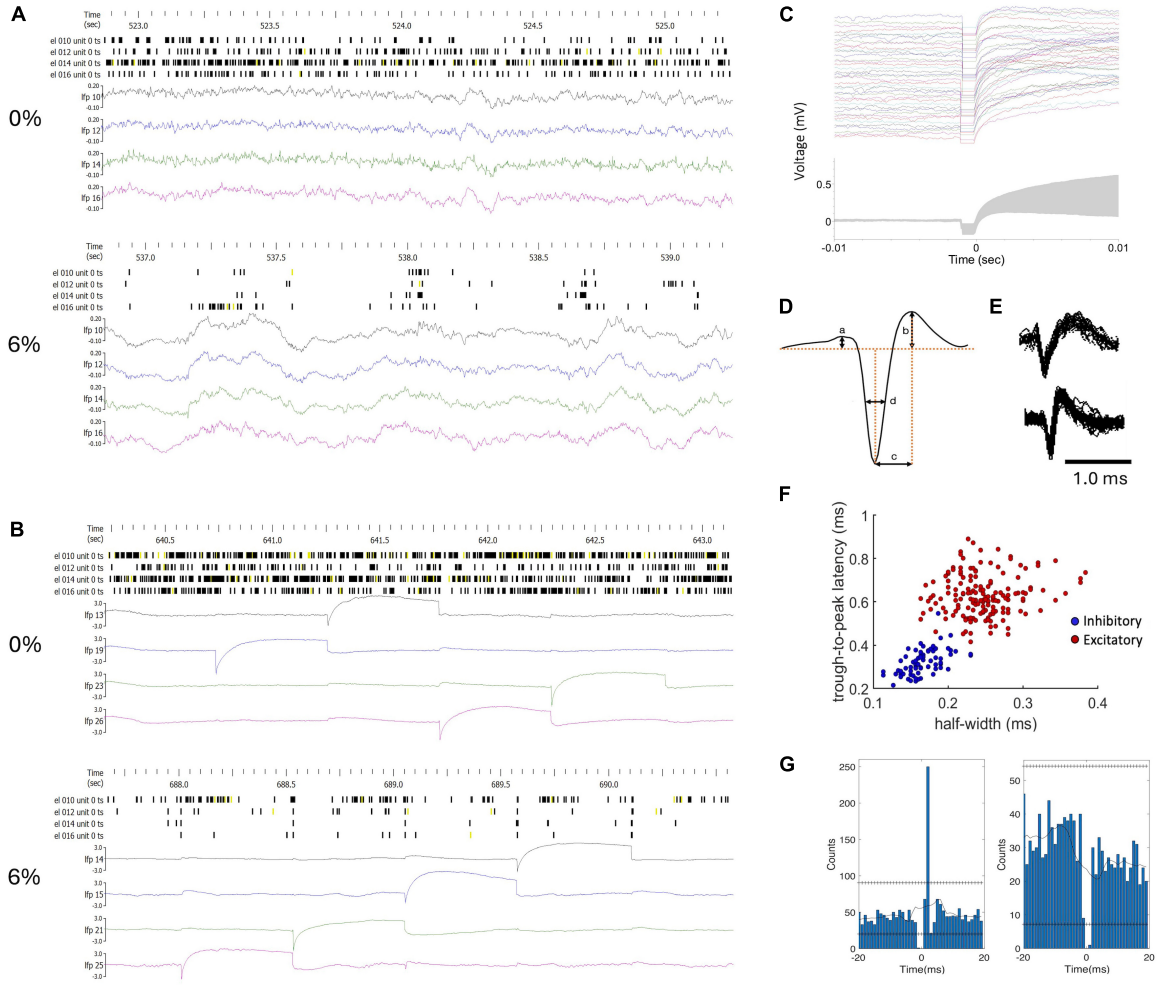

FIGURE 1
Classification of units and monosynaptic connectivity. **(A)** Example of raw spike trains (unclassified) and local field potentials (LFP) from four neurons in wakefulness (0%) and in desflurane anesthesia (6%). **(B)** Data from the same experiment during microstimulation. LFP channels were chosen to include stimulation events within the 2.5-second time window as shown. The amplitude scale of the LFP was adjusted to fit the stimulus artifact into range. **(C)** Stimulus artifacts at a selected electrode site. Top: 80 stimulus traces superimposed; Bottom: ± one standard deviation of signals around the mean (gray zone). **(D)** Features of spike waveform used for unit classification. **(E)** Examples of regular spiking excitatory neuron (top) and fast spiking inhibitory neuron (bottom). Several spike waveforms were aligned and superimposed. **(F)** Trough-to-peak time (b) and half amplitude width of the negative peak (c) provided separation of units into putative excitatory and inhibitory neurons with typical spike shapes. **(G)** Cross correlograms of neuron-pairs that indicate excitatory (left) and inhibitory (right) monosynaptic connections as an example. Horizontal lines of "+" symbols indicate high and low global confidence intervals obtained from spike-jittered average.

with a significant change in spike rate within 1–4 ms after stimulation. Spike counts from 20 trials at each stimulus site were averaged. Significant change was defined by a spike rate increase (or decrease) exceeding ± 95% confidence interval of the 200 ms pre-stimulus baseline. For each stimulation site, neurons with significantly increased firing rate were marked by a vector from the respective stimulation site. Pooling all vectors from all stimulation sites were then compiled in a directed graph. The resulting graph depicted the influence of microstimulation on all recorded neurons as a binary directed network.

Second, putative monosynaptic connections were determined from the short time lag spike cross-correlograms (CCGs) from spontaneous (pre-stimulus) and stimulation-induced activity as before (Vizuete et al., 2012; Kobayashi et al., 2019). Briefly, for each pair of neurons, CCGs were calculated at 1 ms time bins over an interval of ± 50 ms. To avoid false detection due to background fluctuations, the CCGs were also calculated from surrogate spike trains prepared by "jittering" the spike times within ± 5 ms, repeated 1,000 times to yield 1,000 surrogate data sets. The 99% confidence interval of the number of CCG counts in each time bin were obtained and their maximum and minimum were used as global thresholds. Putative excitatory or inhibitory monosynaptic connections between a pair of neurons recorded at different electrode sites were inferred by the presence of CCG peak exceeding (excitatory) or trough descending below (inhibitory) the respective global threshold within 1–4 ms time lag (Figure 1G). Each monosynaptic connection was represented by a vector between the respective electrode sites. Concatenation of such vectors were interpreted as putative polysynaptic paths. All such vectors were combined yielding a graph with its nodes being the electrode sites. The low-level structure of the graphs was analyzed by finding its 1st, 2nd and 3rd order connectivity motifs (Recanatesi et al., 2019). Motifs of each order were counted in each condition, pre- and post-stimulus. Motifs of the 2nd and 3rd order can have different variants, called unique motifs. Unique motifs are those different from all other motifs. Their number reflects motif diversity.

Statistics

Within-group effects of microstimulation and anesthetic level were tested with ANOVA followed by Tukey Honestly Significant Difference post-hoc tests. All results are presented as means and standard deviation. Some of the analyses were limited to experiments that yielded the most neurons/spikes. Some of the analyses were limited to experiments that yielded the most neurons/spikes.

Results

Simultaneous extracellular recording and electrical stimulation was performed in nine rats using 32-site microelectrode arrays in primary visual cortex at three levels of anesthesia and wakefulness. On average active neurons were found at 63% of the electrode sites which progressively dropped to 40% at 6% desflurane ($p < 0.0001$, ANOVA). Figure 1A presents an example of the firing pattern of neurons and local field potentials recorded at the same electrodes in wakefulness and anesthesia at baseline (without stimulation). As shown, the regular firing pattern in wakefulness converts to an intermittent pattern associated with slow wave activity in anesthesia.

Microstimulation was applied to each electrode site was then stimulated one by one in random order at 2 Hz repetition rate using charge-balanced biphasic pulses. We compared the effect of stimuli with different phase duration, amplitude, and temporal order on the firing response of neurons. In all stimuli, the maximum current was 40 μA with 60 μs pulse width and balanced by another phase with opposite polarity as illustrated in Figure 2. Putative excitatory and inhibitory neurons were not distinguished in this analysis. Cathodic-first charge-balanced stimuli activated more neurons than anodic-first charge-balanced stimuli, although this difference was small. All subsequent experiments were performed with asymmetric biphasic pulses with 40 μA maximum intensity and 60 μs pulse width, balanced with 8 μA intensity and 300 μs pulse width.

Figure 3 shows the time course of spike responses of putative excitatory and inhibitory neurons. Neurons were classified by their spike waveform features. Microstimulation generally caused

TABLE 1 Number of recorded neurons.

Rat	Desflurane			
	0%	2.5%	4%	6%
1	16 (2)	15 (0)	16 (0)	13 (0)
2	23 (6)	21 (7)	19 (4)	11 (0)
3	22 (3)	24 (3)	15 (2)	21 (2)
4	18 (1)	17 (1)	16 (2)	7 (1)
5	22 (2)	22 (1)	22 (2)	17 (2)
6	17 (2)	15 (1)	14 (2)	2 (0)
7	25 (2)	21 (4)	17 (3)	21 (3)
8	21 (4)	22 (4)	21 (4)	15 (2)
9	18 (2)	16 (1)	17 (1)	9 (1)

Number of inhibitory neurons in parenthesis.

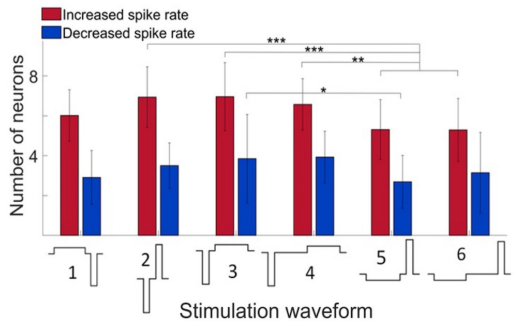

FIGURE 2
Effect of stimulus waveform on the number of neurons showing significant change in firing rate. Maximum stimulus current was 40 μA with 60 μs pulse width and charge balanced. Responses elicited from various stimulation sites were pooled. All data were obtained in wakefulness. Data are from 4 rats. Mean ± SD, *$p < 0.05$, **$p < 0.01$, ***$p < 0.001$.

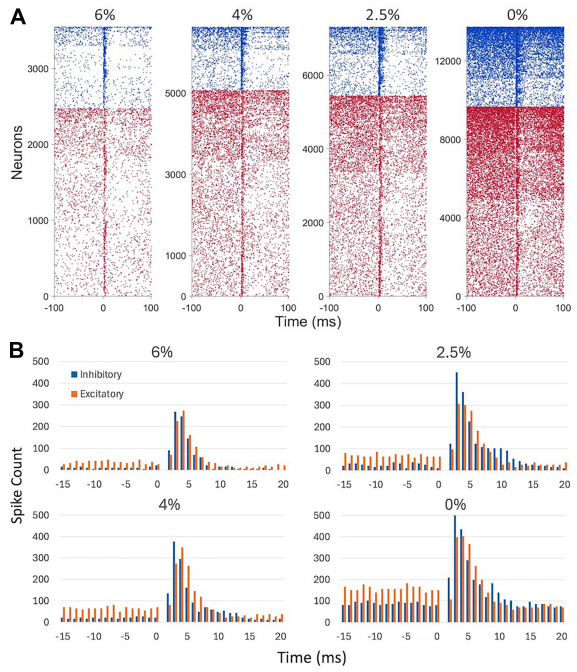

FIGURE 3
Effect of microstimulation on cortical spiking activity in four conditions. **(A)** Raster plots of putative inhibitory (blue) and excitatory (red) neuron firing. Inhaled concentration of the anesthetic desflurane is indicated on top. Each line corresponds to a neuron responding to a different trial, i.e., to stimulation at a different electrode site. Neurons with at least one spike within ± 100 ms of stimulation only were included. Neurons of both types were sorted vertically by their firing rate. Stimulus is at time 0. **(B)** Peristimulus histogram of spike counts. Spike data are absent in the 0–1 ms time bin due to stimulus artifact. Stimuli were charge-balanced, biphasic, asymmetric, cathodic-leading, pulses with 40 μA maximum intensity delivered at 2 Hz. Data are from 9 rats.

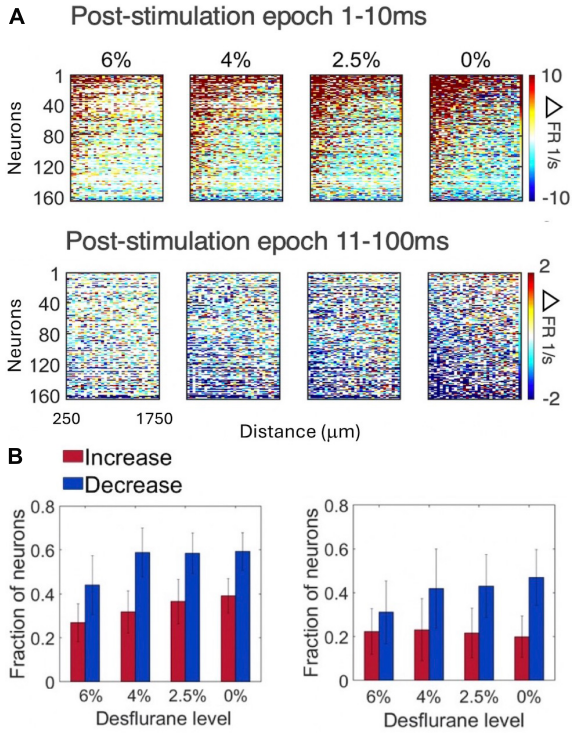

FIGURE 4
Change in firing rate as a function of distance from stimulation site in four conditions and two post-stimulus epochs. **(A)** Change in spike rate change of individual neurons. For each neuron, the 32 stimulation channels are arranged left to right in the order of increasing distance from stimulation site. Neurons are arranged top down from maximum increase (red) to maximum decrease (blue) of spike rate during the wakefulness (0%) and the same order is kept for the other three conditions. Desflurane concentrations are shown on top. Data are from 9 rats. **(B)** Fraction of neurons that produced statistically significant increase (red) or decrease (blue) in firing rate (1–10ms left, 11–100ms right). More neurons showed decrease than increase of firing rate with microstimulation ($p < 0.0001$, ANOVA), a difference qualitatively conserved across states. Stimuli were asymmetric, cathodic-leading, biphasic pulses with 40 μA maximum intensity delivered at 2 Hz.

an early increase, within 10 ms, followed by a prolonged (11–100 ms) decrease in neuron firing. Both excitatory and inhibitory neurons showed this behavior. Neurons responding to stimulation were scattered throughout the electrode array. Despite the smaller number of inhibitory neurons recorded, their total spike count was higher due to their generally higher average spike rate. The maximum spike rates attained post stimulus at 6, 4, 2, and 0% desflurane were 2.3, 4.0, 4.5, and 6.5 spikes/s, respectively, for excitatory neurons and 10.0, 15.9, 18.4, and 25.0 spikes/s, respectively, for inhibitory neurons.

Figure 4A compares the change in spike rate of each neuron as a function of distance from the stimulation site separately for the early (1–10 ms) and late (11–100 ms) response. The magnitude of spike rate increase decayed with the neuron's distance from the stimulation site. In contrast, the magnitude of spike rate decrease was essentially independent of the distance from the stimulation site. This pattern was essentially conserved across all conditions. The number of neurons responding with a significant increase or decrease in spike rate to stimulation in the two epochs is illustrated in Figure 4B. The magnitudes of the early increase and late decrease tended to increase slightly at lighter levels of anesthesia and upon waking although these effects were not statistically significant. Approximately twice as many neurons decreased than increased their spike rate following microstimulation ($p < 0.0001$, ANOVA).

We examined more closely how the early response of excitatory vs. inhibitory neurons varied as a function their distance from the stimulation site. This analysis was limited to the first 4 ms compatible with putative monosynaptic effects. As Figure 5 shows, the number of excitatory neurons that significantly increased their firing rate decayed rapidly with distance from the stimulation site. This dependence was absent for inhibitory neurons suggesting that they were stimulated in a more distributed manner.

We then examined the spatial pattern of stimulus-induced (effective) connectivity of neurons. This was done in two different ways. First, a directed graph was constructed from the vectors from each stimulation site to all neurons whose firing rate was either significantly increased or decreased by microstimulation (Figure 6A). The resulting connectivity map illustrates the overall influence of microstimulation on the spiking of all recorded neurons. Comparing different conditions, effective connectivity was sparse under anesthesia, suggesting reduced overall neuronal

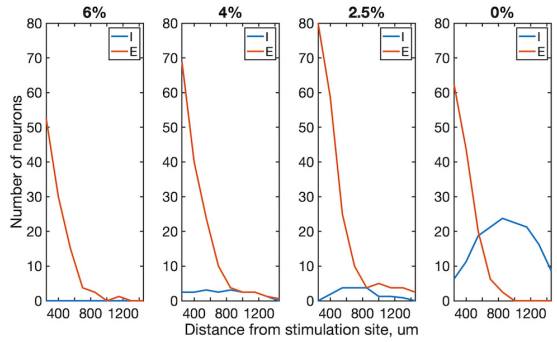

FIGURE 5
Effect of distance from stimulation site on excitatory and inhibitory neuron spiking within 1–4 ms post-stimulus interval in four conditions. The number of neurons whose firing rate exceeded 99% confidence interval of their prestimulus firing rate are plotted. Trials from all stimulus sites were combined. Data are from 4 rats. Desflurane concentrations is indicated on top. Stimuli were charge-balanced, asymmetric, biphasic, cathodic-leading pulses with 40 μA maximum intensity delivered at 2 Hz. $P < 0.0001$ (ANOVA and Tukey) for 0% vs. 2.5%, 4% and 6% for inhibitory; N.S. (ANOVA) for all excitatory neurons.

excitability. The total number of positive effects (neurons with increasing spike rates) was significantly greater as the anesthetic was withdrawn. Thus, the effective connectivity map indicated progressively stronger influence of stimulation at lighter levels of anesthesia and especially in wakefulness. Moreover, negative effects (neurons with decreasing spike rates) were almost absent at all levels of anesthesia. Second, we estimated effective connectivity from putative pair-wise monosynaptic connections as determined from spike cross-correlograms both pre- and post-stimulus. A directed graph was constructed by representing all monosynaptic connections as vectors between two respective electrode sites as graph nodes. Monosynaptic connections between neurons at different electrode sites only were considered (Figure 6B). When two or more monosynaptic connections occurred in series, their combination was interpreted as a putative polysynaptic path. As with the previous method, higher connectivity was evident in light anesthesia and wakefulness and more in the post-stimulus than pre-stimulus phase.

To further examine the structure of the effective connectivity map, we identified low-level functional motifs of the networks. A motif is a small subset of pairwise connections, representative of a unit of overall network connectivity. Pairwise connections are arranged in series or in diverging or converging patterns, leading to multiple variants of second, third and higher order motifs (Recanatesi et al., 2019). First order motifs consist of a single monosynaptic connection; second order motifs contain two connections; and third order motifs contain three connections. Second and third order motifs have multiple variants defined by their connectivity profile. The prevalence of motifs of increasing order, characterized by their relative frequency, reflects the complexity of the overall connectivity of the network and its change with stimulation and anesthetic condition. Figure 6C shows that microstimulation increased the total number of detected motifs, thus enhancing monosynaptic and putative polysynaptic connectivity at all levels of anesthesia although this effect did not reach significance at 0% desflurane in this comparison (for statistics see figure). Similar results were obtained for the number of unique

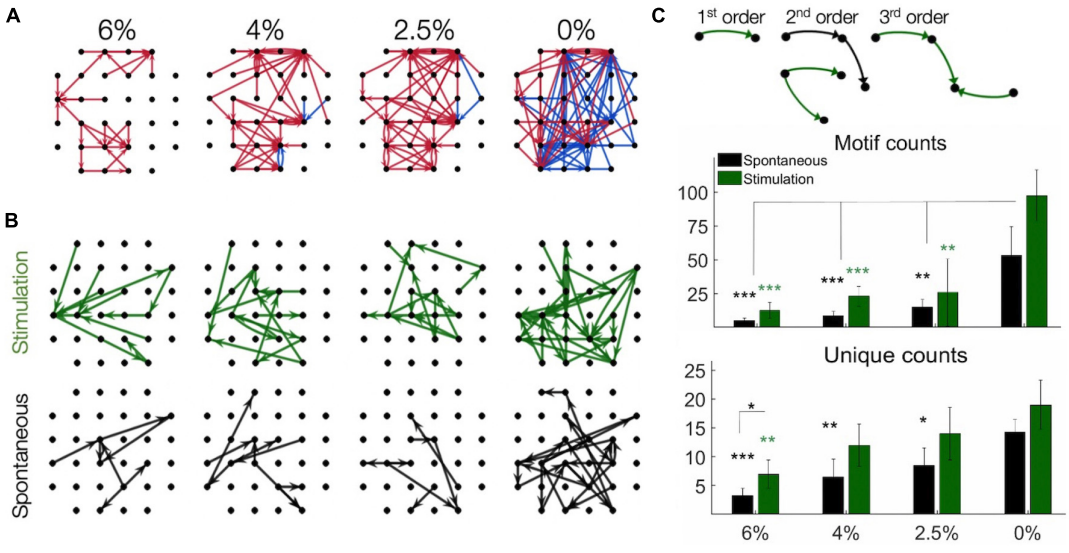

FIGURE 6
Effective connectivity of neurons determined by microsimulation. **(A)** Connectivity maps in one rat as an example. Arrows point from the site of stimulation to the site of significantly increased (red) or decreased (blue) spike rate within 1–4 ms post-stimulation (desflurane concentrations indicated on top). Desflurane concentrations is indicated on top. **(B)** Putative monosynaptic effective connectivity maps inferred from pairwise spike cross-correlograms pre-stimulus (spontaneous) and post-stimulus (stimulation). The graphs represent "multi-node" paths composed of pairwise connections. **(C)** Effect of anesthesia on the number of connectivity motifs as inferred from pairwise spike cross-correlograms before and after microstimulation. Examples of motifs of different order are illustrated on top. The counts of 1st, 2nd, and 3rd order motifs were combined. Unique counts reflect the diversity of distinct motif types. Desflurane concentration is on the horizontal axis. Data are from 4 rats. Mean ± SD, $*p < 0.05$; $**p < 0.01$; $***p < 0.001$. Stimuli were charge-balanced, asymmetric, biphasic, cathodic-leading pulses with 40 μA maximum intensity delivered at 2 Hz.

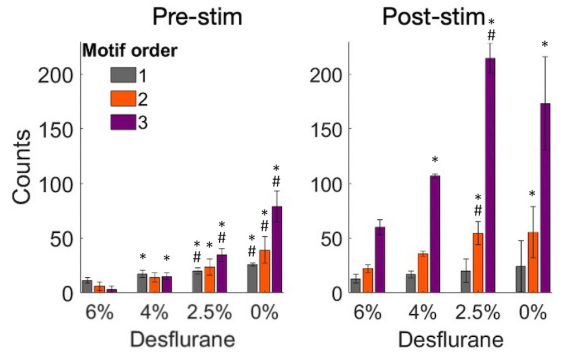

FIGURE 7
Change in the number of motifs of orders 1–3 as a function of experimental condition before and after microstimulation. Motifs were derived from pairwise spike cross-correlograms. Stimuli were charge-balanced, asymmetric, biphasic, cathodic-leading pulses with 40 μA maximum intensity delivered at 2 Hz. *$p < 0.05$ vs. at 6%, #$p < 0.05$ greater than at next higher desflurane concentration.

motifs, suggesting that the diversity of motif variants also increased after microstimulation. In addition, both the total number of motifs and their diversity significantly increased as the anesthetic was withdrawn and reached maximum in wakefulness (see figure for statistics). Figure 7 compares the change in the number of motifs of different orders separately. A progressive increase in the number of all motifs with decreasing anesthetic concentration was evident both pre-stimulus and post-stimulus ($p < 0.0001$, ANOVA), except in post-stimulus first order motifs. In addition, microstimulation increased the number of motifs of all orders ($p < 0.005$, ANOVA) with the most dramatic effect seen in motif order 3 (for pairwise statistical comparison see figure).

Discussion

The main goal of this work was to apply intracortical microstimulation to examine how anesthesia may alter effective connectivity of neurons in a local cortical circuit. Microstimulation was chosen as an effective means to modulate local neuronal activity and its propagation across adjacent and remote recording sites (Kwan and Dan, 2012; Kumar et al., 2013). Probing local circuitry by causal perturbation provides additional insight into neuronal connectivity underlying cortical information processing over that obtainable by recording spontaneous or physiological stimulus-related activity (Clark et al., 2011; Kumar et al., 2013; Cicmil and Krug, 2015; Sadeh and Clopath, 2020). Further, by investigating the concentration-dependent effect of anesthesia on intracortical stimulus-related connectivity has a unique potential to help better understand how neuronal networks function in altered states across experimentally controlled levels of consciousness (Arena et al., 2021).

Consistent with prior studies we found that intracortical microstimulation generally produced a biphasic neuronal response consisting of an early increase in firing within 10 ms followed by a transient suppression of 100 ms or so (Butovas and Schwarz, 2003; Sombeck et al., 2022; Yun et al., 2023). This biphasic pattern was conserved at all levels of anesthesia although the spike rate increases were lower during anesthesia than in the awake state. The exact duration of these phases was reported to vary with stimulus intensity (Yun et al., 2023), although this aspect was not investigated further here.

Also, as found before (McIntyre and Grill, 2000; Voigt and Kral, 2019), cathodic-leading charge-balanced stimulus waveforms were more effective in stimulating neuron firing than the reverse waveforms, although this difference in our preparation was quite small. Experimental and computational studies suggest that local cells are preferentially activated by cathodic-first asymmetrical charge-balanced biphasic stimulus waveforms, while fibers of passage is affected more by anodic-phase-first asymmetrical charge- balanced biphasic stimulus waveforms (Cogan, 2008; Voigt and Kral, 2019). However, it was also shown that stimulus polarity and asymmetry influence the probability and localization of neuron activation in an opposite manner (Stieger et al., 2022). Also, computational modeling suggests that the initial mechanism of activation is an antidromic propagation to the soma following axonal activation (Kumaravelu et al., 2022). Orthodromic propagation and synaptic transmission could then mediate the further propagation of activation. However, which of these mechanisms likely contributed to stimulation-evoked neuronal firing at the recording sites cannot be determined from the present data.

We also examined how anesthesia with desflurane modulated the stimulus response of putative excitatory vs. inhibitory neurons. Most inhalational anesthetic agents suppress spontaneous neuronal activity by facilitating inhibitory synaptic transmission and suppressing excitatory synaptic transmission (Franks, 2008) through a variety of actions on specific receptors, channels, and extrasynaptic and mitochondrial energy modulation, the relative extent of which vary with the particular anesthetic. In particular, desflurane potentiates $GABA_A$ receptor-mediated inhibition, inhibits NMDA receptor mediated excitation, inhibit voltage-gated, and to a lesser degree, inward rectifying potassium channels and kainate receptors (Nishikawa and Harrison, 2003; Alkire et al., 2008). Despite the inhibitory potentiation observed *in vitro*, in the intact cortical circuit *in vivo*, the strength of monosynaptic excitatory connections is more suppressed than that of monosynaptic inhibitory connections (Vizuete et al., 2012). Although most anesthetics affect the cortical circuits directly (Hentschke et al., 2005), this is further modulated via subcortical centers including the brainstem, thalamus, and basal forebrain (Brown et al., 2010). Due to these complexities, the effect of intracortical microstimulation on excitatory vs. inhibitory neuron activity was difficult to predict *a priori*.

To investigate this question, the early neuron spike responses were examined in 1–4 ms post-stimulus period which limits the response to monosynaptic transmission (apart from possible electrotonic conduction). Transsynaptic responses to single-pulse cortical electrical stimulation were reported in a comparable time frame (Sombeck et al., 2022). Under anesthesia very few inhibitory neurons showed monosynaptic response, whereas excitatory neurons continued to respond to stimulation. The latter could be a result of disinhibition due to the suppression of inhibitory neurons, although this possibility requires further investigation. As the anesthetic was withdrawn, substantially more inhibitory neurons responded, suggesting a normalization of the E/I balance. The spatial distributions of stimulus-responding excitatory and

inhibitory neurons were also different. Inhibitory neurons had a relatively wide distribution in wakefulness, consistent with their excitation by horizontal axonal projections that extend over 1 mm (Kisvarday, 1992). The suppression of their firing rate under anesthesia could be mediated by their dense connectivity by electrical coupling (Butovas et al., 2006). This does not seem to be the case for excitatory neurons, however. Indeed, the decay of the number of excitatory neurons with distance from stimulation site could be related to their relatively sparse connectivity (Overstreet et al., 2013). A similar spatial decay of connectivity over 1 mm was reported before (Eles et al., 2021). Alternatively, if the neuron responses to microstimulation were mediated by electrotonic excitation via field potentials, this effect would decay exponentially with distance from the stimulation site.

The main goal of this study was to determine how anesthesia altered microstimulation-induced effective connectivity of cortical neurons. The graded reduction in effective connectivity at increasing depth of anesthesia was consistent with an overall reduction in neuronal firing rate (Hudetz et al., 2009) impeding the ongoing neuronal interactions and the propagation of activity to remote sites. Moreover, the negative effects of microstimulation (neurons with decreasing spike rates) were virtually absent in anesthesia suggesting that they were at their minimum baseline activity. This is consistent with the direct effect of volatile anesthetics on cortical firing by augmenting inhibitory neurotransmission (Hentschke et al., 2005). The directed effective connectivity graphs derived from putative monosynaptic connections confirmed these findings, revealing sparser connectivity in anesthesia compared to the dense connectivity in wakefulness that was further augmented in the post-stimulus phase.

To gain further insight into network connectivity, we also analyzed the prevalence of simple network motifs in different conditions. Such motifs have been considered as building blocks of complex recurrent networks. The motifs' statistical prevalence can determine overall network properties, such as dimensionality, code compression, computational flexibility, network input-output response, and memory (Hu et al., 2014; Recanatesi et al., 2019). In the rat visual cortex, recordings of layer 5 pyramidal neurons revealed the presence of small, strongly connected network units that determine overall network connectivity (Song et al., 2005). Our analysis revealed a sharp difference in the overall number of motifs between wakefulness and anesthesia consistent with the rapid collapse of network connectivity. This difference was most expressed in the number of 3rd order motifs in the pre-stimulus condition. Although we were not able to identify motifs of higher than 3rd order due to the limited size of the electrode array, it could be surmised by extrapolation that higher order motifs would be even more affected. Because the number of 1st order motifs (monosynaptic connections) was hardly affected by the anesthetic (especially post-stimulus), the increase in higher-order motifs was probably due to network reconfiguration rather than an overall change in pair-wise connectivity. The fact that microstimulation did not significantly increase the number of motifs in the awake condition could mean that they were already at their near maximum density.

Several limitations of the current study are recognized. First, due to the sparse sampling of neuronal network, effective connectivity maps represent a small subset of true neuronal connectivity. A complete reconstruction of the neuronal network would theoretically require stimulating all single neurons and their combinations of the entire neuron network (O'Doherty et al., 2012; Kumar et al., 2013; Sadeh and Clopath, 2020). Nevertheless, the observed change in graph density in our sample should reflect the general trend of the anesthetic effect. Second, neuronal connectivity as determined here could be in part from synaptic transmission and in part from electrical fields through a mixture of antidromic and orthodromic activation (Butovas and Schwarz, 2003). The use of cathodic-leading biphasic stimuli in the present experiments presumably favored orthodromic activation, although this could not be verified with extracellular recordings. In addition, the probability of evoking excitatory responses decayed with distance rapidly, which could be due to the increasing sparsity of synaptic terminals reached or the weakening of electrical field with distance. Although cross-correlograms with short time-lag likely reflect monosynaptic spike transmission probability between pairs of neurons, they can be confounded by common inputs with comparable temporal delay. Thus, the neuron connections derived here are approximate and both the monosynaptic connections and their combinations inferred as polysynaptic connections should be considered putative. Third, extracellular microstimulation affects not a single cell but an unknown population of cells and passing axons surrounding the stimulation electrode. These difficulties could be mitigated by neuronal redundancy, i.e., that many neighboring neurons often respond to similar stimulus features, that a relatively small group of cells can drive network activity in similar fashion (Yassin et al., 2010; Kwan and Dan, 2012; Emiliani et al., 2015; Bernardi et al., 2021), and that frequently recurring neuronal firing sequences represent a small fraction of all possible patterns (Luczak et al., 2007, 2009; Luczak and Maclean, 2012). Thus, effective connectivity as derived here is best interpreted as "embeddedness," i.e., the influence of a local neuronal population on individual neurons at a distance. In fact, both experiments and computer simulations suggest that an estimation of neuronal embeddedness is a valid approach for network discovery (Vlachos et al., 2012; Kumar et al., 2013). Fourth, motifs are only a metric of the basic building blocks of the functional connectivity of a local neuron network. There are several other graph-based metrics; however, our graphs were relatively small and sparse to apply such methods to them. The use of larger electrode arrays may allow such an analysis in the future. Fifth, one could contend that the observed changes in connectivity may in part be accounted for by the anesthetic-induced decrease in overall firing rate. However, this is not thought to be the primary contributing factor of effective connectivity changes because stimulus-induced neuronal firing is often significantly elevated during anesthesia, especially at deep anesthetic levels (Hudetz and Imas, 2007). Sixth, the accuracy of electrode placement in layers 5/6 of the primary visual cortex was not histologically verified in this work. However, the exact location of the electrodes was not critical for the general conclusions of the study. Our former work supports that stereotaxic implantation provided sufficient targeting accuracy (Pillay et al., 2014). Finally, trial-to-trial variability due to ongoing activity limits the accuracy at which an invariant network can be reconstructed. Nevertheless, it is believed that the microstimulation-based perturbational approach augments the reproducibility of the mapped network by transiently suppressing background activity (Cheney et al., 2013). In the future,

optical methods that allow more precise control of the number and type of directly stimulated neurons (Cicmil and Krug, 2015; Cavelli et al., 2023) including optogenetic stimulation with micro-light emitting diodes (LEDs) (Buzsaki et al., 2015; Wu et al., 2015; Kim et al., 2020) could be used. In addition, distinct temporal patterns of stimulation pulses could also be used to control the affected neuronal population (Eles et al., 2021) and one could also target the stimulation to specific cortical layers (Voigt et al., 2017; Urdaneta et al., 2021).

In summary, the present work demonstrates the anesthetic modulation of effective connectivity in rat visual cortex as probed by microstimulation *in vivo*. The suppression of network connectivity was associated with the preferential loss of higher order network motifs. The results are relevant to understanding the mechanisms of anesthetic-induced impairment of cortical information processing and by inference, loss of consciousness.

Data availability statement

The raw data supporting the conclusions of this article will be made available by the author, without undue reservation.

Ethics statement

The animal study was approved by the Institutional Animal Care and Use Committee (IACUC) of the University of Michigan. The study was conducted in accordance with the local legislation and institutional requirements.

Author contributions

AH: Conceptualization, Data curation, Formal analysis, Funding acquisition, Methodology, Project administration, Resources, Supervision, Validation, Writing – original draft, Writing – review & editing.

Funding

The author declares that financial support was received for the research, authorship, and/or publication of this article. Research reported in this publication was supported by the National Institute of General Medical Sciences of the National Institutes of Health under award number R01-GM056398 and the Center for Consciousness Science, Department of Anesthesiology, University of Michigan Medical School, Ann Arbor, Michigan, USA.

Acknowledgments

I thank the assistance of Dr. Shiyong Wang in conducting the experiments, Jake Schut in data analysis, and Kathy Zelenock in laboratory operations.

Conflict of interest

The author declares that the research was conducted in the absence of any commercial or financial relationships that could be construed as a potential conflict of interest.

Publisher's note

Author disclaimer

The content is solely the responsibility of the author and does not necessarily represent the official views of the National Institutes of Health.

References

Aasebo, I. E. J., Lepperod, M. E., Stavrinou, M., Nokkevangen, S., Einevoll, G., Hafting, T., et al. (2017). Temporal processing in the visual cortex of the awake and anesthetized rat. *eNeuro* 4:ENEURO.0059-17.2017. doi: 10.1523/ENEURO.0059-17.2017

Aertsen, A. M., Gerstein, G. L., Habib, M. K., and Palm, G. (1989). Dynamics of neuronal firing correlation: Modulation of "effective connectivity". *J. Neurophysiol.* 61, 900–917.

Aggarwal, A., Luo, J., Chung, H., Contreras, D., Kelz, M. B., and Proekt, A. (2023). Neural assemblies coordinated by cortical waves are associated with waking and hallucinatory brain states. *bioRxiv* [Preprint]. doi: 10.1101/2023.05.22.540656

Alkire, M. T., Hudetz, A. G., and Tononi, G. (2008). Consciousness and anesthesia. *Science* 322, 876–880.

Andrada, J., Livingston, P., Lee, B. J., and Antognini, J. (2012). Propofol and etomidate depress cortical, thalamic, and reticular formation neurons during anesthetic-induced unconsciousness. *Anesth. Analg.* 114, 661–669. doi: 10.1213/ANE.0b013e3182405228

Arena, A., Comolatti, R., Thon, S., Casali, A. G., and Storm, J. F. (2021). General anesthesia disrupts complex cortical dynamics in response to intracranial electrical stimulation in rats. *eNeuro* 8:ENEURO.0343-20.2021. doi: 10.1523/ENEURO.0343-20.2021

Bernardi, D., Doron, G., Brecht, M., and Lindner, B. (2021). A network model of the barrel cortex combined with a differentiator detector reproduces features of the behavioral response to single-neuron stimulation. *PLoS Comput. Biol.* 17:e1007831. doi: 10.1371/journal.pcbi.1007831

Bharioke, A., Munz, M., Brignall, A., Kosche, G., Eizinger, M. F., Ledergerber, N., et al. (2022). General anesthesia globally synchronizes activity selectively in layer 5 cortical pyramidal neurons. *Neuron* 110:2024–2040.e10.

Brown, E. N., Lydic, R., and Schiff, N. D. (2010). General anesthesia, sleep, and coma. *N. Engl. J. Med.* 363, 2638–2650.

Butovas, S., and Schwarz, C. (2003). Spatiotemporal effects of microstimulation in rat neocortex: A parametric study using multielectrode recordings. *J. Neurophysiol.* 90, 3024–3039. doi: 10.1152/jn.00245.2003

Butovas, S., Hormuzdi, S. G., Monyer, H., and Schwarz, C. (2006). Effects of electrically coupled inhibitory networks on local neuronal responses to intracortical microstimulation. *J. Neurophysiol.* 96, 1227–1236. doi: 10.1152/jn.01170.2005

Buzsaki, G., Stark, E., Berenyi, A., Khodagholy, D., Kipke, D. R., Yoon, E., et al. (2015). Tools for probing local circuits: High-density silicon probes combined with optogenetics. *Neuron* 86, 92–105.

Cavelli, M. L., Mao, R., Findlay, G., Driessen, K., Bugnon, T., Tononi, G., et al. (2023). Sleep/wake changes in perturbational complexity in rats and mice. *iScience* 26, 106186. doi: 10.1016/j.isci.2023.106186

Cheney, P. D., Griffin, D. M., and Van Acker, G. M. III (2013). Neural hijacking: Action of high-frequency electrical stimulation on cortical circuits. *Neuroscientist* 19, 434–441. doi: 10.1177/1073858412458368

Cicmil, N., and Krug, K. (2015). Playing the electric light orchestra–how electrical stimulation of visual cortex elucidates the neural basis of perception. *Philos. Trans. R. Soc. Lond. B Biol. Sci.* 370:20140206. doi: 10.1098/rstb.2014.0206

Clark, K. L., Armstrong, K. M., and Moore, T. (2011). Probing neural circuitry and function with electrical microstimulation. *Proc. Biol. Sci.* 278, 1121–1130.

Cogan, S. F. (2008). Neural stimulation and recording electrodes. *Annu. Rev. Biomed. Eng.* 10, 275–309.

Eles, J. R., Stieger, K. C., and Kozai, T. D. Y. (2021). The temporal pattern of intracortical microstimulation pulses elicits distinct temporal and spatial recruitment of cortical neuropil and neurons. *J. Neural Eng.* 18:10. doi: 10.1088/1741-2552/abc29c

Emiliani, V., Cohen, A. E., Deisseroth, K., and Hausser, M. (2015). All-optical interrogation of neural circuits. *J. Neurosci.* 35, 13917–13926.

Franks, N. P. (2008). General anaesthesia: From molecular targets to neuronal pathways of sleep and arousal. *Nat. Rev. Neurosci.* 9, 370–386.

Hentschke, H., Schwarz, C., and Antkowiak, B. (2005). Neocortex is the major target of sedative concentrations of volatile anaesthetics: Strong depression of firing rates and increase of GABAA receptor-mediated inhibition. *Eur. J. Neurosci.* 21, 93–102. doi: 10.1111/j.1460-9568.2004.03843.x

Hu, Y., Trousdale, J., Josic, K., and Shea-Brown, E. (2014). Local paths to global coherence: Cutting networks down to size. *Phys. Rev. E Stat. Nonlin Soft. Matter. Phys.* 89:032802. doi: 10.1103/PhysRevE.89.032802

Hudetz, A. G., and Imas, O. A. (2007). Burst activation of the cerebral cortex by flash stimuli during isoflurane anesthesia in rats. *Anesthesiology* 107, 983–991. doi: 10.1097/01.anes.0000291471.80659.55

Hudetz, A. G., Vizuete, J. A., and Imas, O. A. (2009). Desflurane selectively suppresses long-latency cortical neuronal response to flash in the rat. *Anesthesiology* 111, 231–239. doi: 10.1097/ALN.0b013e3181ab671e

Hudetz, A. G., Vizuete, J. A., Pillay, S., and Ropella, K. M. (2015). Critical changes in cortical neuronal interactions in anesthetized and awake rats. *Anesthesiology* 123, 171–180.

Imas, O. A., Ropella, K. M., Ward, B. D., Wood, J. D., and Hudetz, A. G. (2005). Volatile anesthetics enhance flash-induced gamma oscillations in rat visual cortex. *Anesthesiology* 102, 937–947. doi: 10.1097/00000542-200505000-00012

Kim, K., Voroslakos, M., Seymour, J. P., Wise, K. D., Buzsaki, G., and Yoon, E. (2020). Artifact-free and high-temporal-resolution in vivo opto-electrophysiology with microLED optoelectrodes. *Nat. Commun.* 11:2063. doi: 10.1038/s41467-020-15769-w

Kisvarday, Z. F. (1992). GABAergic networks of basket cells in the visual cortex. *Prog. Brain Res.* 90, 385–405.

Kobayashi, R., Kurita, S., Kurth, A., Kitano, K., Mizuseki, K., Diesmann, M., et al. (2019). Reconstructing neuronal circuitry from parallel spike trains. *Nat. Commun.* 10:4468. doi: 10.1038/s41467-019-12225-2

Kumar, A., Vlachos, I., Aertsen, A., and Boucsein, C. (2013). Challenges of understanding brain function by selective modulation of neuronal subpopulations. *Trends Neurosci.* 36, 579–586.

Kumaravelu, K., Sombeck, J., Miller, L. E., Bensmaia, S. J., and Grill, W. M. (2022). Stoney vs. histed: Quantifying the spatial effects of intracortical microstimulation. *Brain Stimul.* 15, 141–151. doi: 10.1016/j.brs.2021.11.015

Kwan, A. C., and Dan, Y. (2012). Dissection of cortical microcircuits by single-neuron stimulation in vivo. *Curr. Biol.* 22, 1459–1467. doi: 10.1016/j.cub.2012.06.007

Lee, H., Tanabe, S., Wang, S., and Hudetz, A. G. (2021). Differential effect of anesthesia on visual cortex neurons with diverse population coupling. *Neuroscience* 458, 108–119.

Lee, H., Wang, S., and Hudetz, A. G. (2020). State-dependent cortical unit activity reflects dynamic brain state transitions in anesthesia. *J. Neurosci.* 40, 9440–9454. doi: 10.1523/JNEUROSCI.0601-20.2020

London, M., Roth, A., Beeren, L., Hausser, M., and Latham, P. E. (2010). Sensitivity to perturbations in vivo implies high noise and suggests rate coding in cortex. *Nature* 466, 123–127. doi: 10.1038/nature09086

Luczak, A., and Maclean, J. N. (2012). Default activity patterns at the neocortical microcircuit level. *Front. Integr. Neurosci.* 6:30. doi: 10.3389/fnint.2012.00030

Luczak, A., Bartho, P., and Harris, K. D. (2009). Spontaneous events outline the realm of possible sensory responses in neocortical populations. *Neuron* 62, 413–425. doi: 10.1016/j.neuron.2009.03.014

Luczak, A., Bartho, P., Marguet, S. L., Buzsaki, G., and Harris, K. D. (2007). Sequential structure of neocortical spontaneous activity in vivo. *Proc. Natl. Acad. Sci. U.S.A.* 104, 347–352.

Luczak, A., Mcnaughton, B. L., and Harris, K. D. (2015). Packet-based communication in the cortex. *Nat. Rev. Neurosci.* 16, 745–755.

Margalit, S. N., Golomb, N. G., Tsur, O., Ben Yehoshua, E., Raz, A., and Slovin, H. (2022). Spatiotemporal patterns of population response in the visual cortex under isoflurane: From wakefulness to loss of consciousness. *Cereb. Cortex* 32, 5512–5529. doi: 10.1093/cercor/bhac031

McIntyre, C. C., and Grill, W. M. (2000). Selective microstimulation of central nervous system neurons. *Ann. Biomed. Eng.* 28, 219–233.

Merrill, D. R., Bikson, M., and Jefferys, J. G. (2005). Electrical stimulation of excitable tissue: Design of efficacious and safe protocols. *J. Neurosci. Methods* 141, 171–198. doi: 10.1016/j.jneumeth.2004.10.020

National Academies of Sciences, Engineering, and Medicine. (2011). *Guide for the Care and Use of Laboratory Animals*: Eighth Edition. The National Academies Press: Washington, DC. doi: 10.17226/12910

Nishikawa, K., and Harrison, N. L. (2003). The actions of sevoflurane and desflurane on the gamma-aminobutyric acid receptor type A: Effects of TM2 mutations in the alpha and beta subunits. *Anesthesiology* 99, 678–684. doi: 10.1097/00000542-200309000-00024

O'Doherty, J. E., Lebedev, M. A., Li, Z., and Nicolelis, M. A. (2012). Virtual active touch using randomly patterned intracortical microstimulation. *IEEE Trans. Neural Syst. Rehabil. Eng.* 20, 85–93. doi: 10.1109/TNSRE.2011.2166807

Overstreet, C. K., Klein, J. D., and Helms Tillery, S. I. (2013). Computational modeling of direct neuronal recruitment during intracortical microstimulation in somatosensory cortex. *J. Neural Eng.* 10:066016. doi: 10.1088/1741-2560/10/6/066016

Pazienti, A., Galluzzi, A., Dasilva, M., Sanchez-Vives, M. V., and Mattia, M. (2022). Slow waves form expanding, memory-rich mesostates steered by local excitability in fading anesthesia. *iScience* 25:103918. doi: 10.1016/j.isci.2022.103918

Pillay, S., Vizuete, J., Liu, X., Juhasz, G., and Hudetz, A. G. (2014). Brainstem stimulation augments information integration in the cerebral cortex of desflurane-anesthetized rats. *Front. Integr. Neurosci.* 8:8. doi: 10.3389/fnint.2014.00008

Recanatesi, S., Ocker, G. K., Buice, M. A., and Shea-Brown, E. (2019). Dimensionality in recurrent spiking networks: Global trends in activity and local origins in connectivity. *PLoS Comput. Biol.* 15:e1006446. doi: 10.1371/journal.pcbi.1006446

Sadeh, S., and Clopath, C. (2020). Theory of neuronal perturbome in cortical networks. *Proc. Natl. Acad. Sci. U.S.A.* 117, 26966–26976. doi: 10.1073/pnas.2004568117

Sombeck, J. T., Heye, J., Kumaravelu, K., Goetz, S. M., Peterchev, A. V., Grill, W. M., et al. (2022). Characterizing the short-latency evoked response to intracortical microstimulation across a multi-electrode array. *J. Neural Eng.* 19:10. doi: 10.1088/1741-2552/ac63e8

Song, S., Sjostrom, P. J., Reigl, M., Nelson, S., and Chklovskii, D. B. (2005). Highly nonrandom features of synaptic connectivity in local cortical circuits. *PLoS Biol* 3:e68. doi: 10.1371/journal.pbio.0030068

Stieger, K. C., Eles, J. R., Ludwig, K. A., and Kozai, T. D. Y. (2022). Intracortical microstimulation pulse waveform and frequency recruits distinct spatiotemporal patterns of cortical neuron and neuropil activation. *J. Neural Eng.* 19:10. doi: 10.1088/1741-2552/ac5bf5

Tanabe, S., Lee, H., Wang, S., and Hudetz, A. G. (2023). Spontaneous and Visual stimulation evoked firing sequences are distinct under desflurane anesthesia. *Neuroscience* 528, 54–63. doi: 10.1016/j.neuroscience.2023.07.016

Urdaneta, M. E., Kunigk, N. G., Delgado, F., Fried, S. I., and Otto, K. J. (2021). Layer-specific parameters of intracortical microstimulation of the somatosensory cortex. *J. Neural Eng.* 18:10. doi: 10.1088/1741-2552/abedde

Vizuete, J. A., Pillay, S., Diba, K., Ropella, K. M., and Hudetz, A. G. (2012). Monosynaptic functional connectivity in cerebral cortex during wakefulness and under graded levels of anesthesia. *Front. Integr. Neurosci.* 6:90. doi: 10.3389/fnint.2012.00090

Vlachos, I., Aertsen, A., and Kumar, A. (2012). Beyond statistical significance: Implications of network structure on neuronal activity. *PLoS Comput. Biol.* 8:e1002311. doi: 10.1371/journal.pcbi.1002311

Voigt, M. B., and Kral, A. (2019). Cathodic-leading pulses are more effective than anodic-leading pulses in intracortical microstimulation of the auditory cortex. *J. Neural Eng.* 16:036002. doi: 10.1088/1741-2552/ab0944

Voigt, M. B., Hubka, P., and Kral, A. (2017). Intracortical microstimulation differentially activates cortical layers based on stimulation depth. *Brain Stimul.* 10, 684–694. doi: 10.1016/j.brs.2017.02.009

Wu, F., Stark, E., Ku, P. C., Wise, K. D., Buzsaki, G., and Yoon, E. (2015). Monolithically integrated mulEDS on silicon neural probes for high-resolution optogenetic studies in behaving animals. *Neuron* 88, 1136–1148. doi: 10.1016/j.neuron.2015.10.032

Yassin, L., Benedetti, B. L., Jouhanneau, J. S., Wen, J. A., Poulet, J. F., and Barth, A. L. (2010). An embedded subnetwork of highly active neurons in the neocortex. *Neuron* 68, 1043–1050. doi: 10.1016/j.neuron.2010.11.029

Yger, P., Spampinato, G. L., Esposito, E., Lefebvre, B., Deny, S., Gardella, C., et al. (2018). A spike sorting toolbox for up to thousands of electrodes validated with ground truth recordings in vitro and in vivo. *Elife* 7:e34518. doi: 10.7554/eLife.34518

Yun, R., Mishler, J. H., Perlmutter, S. I., Rao, R. P. N., and Fetz, E. E. (2023). Responses of cortical neurons to intracortical microstimulation in awake primates. *eNeuro* 10:ENEURO.0336-22.2023. doi: 10.1523/ENEURO.0336-22.2023

frontiers | Frontiers in Pharmacology

TYPE Original Research
PUBLISHED 10 July 2024
DOI 10.3389/fphar.2024.1412178

OPEN ACCESS

EDITED BY
Christina Dalla,
National and Kapodistrian University of Athens, Greece

REVIEWED BY
Pilar Flores,
University of Almeria, Spain
Stefania Schiavone,
University of Foggia, Italy

*CORRESPONDENCE
Mussie Msghina,
mussie.msghina@oru.se

RECEIVED 04 April 2024
ACCEPTED 24 June 2024
PUBLISHED 10 July 2024

CITATION
Thunberg P, Reingardt M, Rode J and Msghina M (2024), Categorical and dimensional aspects of stimulant medication effects in adult patients with ADHD and healthy controls. *Front. Pharmacol.* 15:1412178. doi: 10.3389/fphar.2024.1412178

Categorical and dimensional aspects of stimulant medication effects in adult patients with ADHD and healthy controls

Per Thunberg[1,2], Maria Reingardt[3,4], Julia Rode[1,5] and Mussie Msghina[3,6]*

[1]Center for Experimental and Biomedical Imaging in Örebro (CEBIO), Faculty of Medicine and Health, Örebro University, Örebro, Sweden, [2]Department of Radiology and Medical Physics, Faculty of Medicine and Health, Örebro University, Örebro, Sweden, [3]Department of Psychiatry, School of Medical Sciences, Faculty of Medicine and Health, Örebro University, Örebro, Sweden, [4]Centre for Clinical Research and Education, Central Hospital, Karlstad, Sweden, [5]School of Medical Sciences, Faculty of Medicine and Health, Örebro University, Örebro, Sweden, [6]Department of Clinical Neuroscience, Karolinska Institutet, Stockholm, Sweden

Psychiatric disorders are categorized on the basis of presence and absence of diagnostic criteria using classification systems such as the international classification of diseases (ICD) and the diagnostic and statistical manual for mental disorders (DSM). The research domain criteria (RDoC) initiative provides an alternative dimensional framework for conceptualizing mental disorders. In the present paper, we studied neural and behavioral effects of central stimulant (CS) medication in adults with attention deficit hyperactivity disorder (ADHD) and healthy controls using categorical and dimensional stratifications. AX-Continuous Performance Task (AX-CPT) was utilized for the later purpose, and participants were classified as "reactive" or "proactive" based on their baseline proactive behavioral index (PBI). Out of the 65 individuals who participated (33 healthy controls and 32 patients with ADHD), 53 were included in the final analysis that consisted of 31 healthy controls and 22 ADHD patients. For the dimensional stratification, a median split of PBI scores divided participants into "reactive" and "proactive" groups irrespective of whether they had ADHD or not. Participants performed AX-CPT in conjunction with functional magnetic resonance imaging (fMRI) before and after CS medication. We found no significant within or between group CS effect when participants were categorically assigned as healthy controls and ADHD patients. For the dimensional stratification, however, CS selectively increased activation in frontoparietal cognitive areas and induced a shift towards proactive control mode in the reactive group, without significantly affecting the proactive group. In conclusion, the neural and behavioral effects of CS were more clear-cut when participants were stratified into dimensional groups rather than diagnostic categories.

KEYWORDS

cognitive control, central stimulants, ADHD, AX-CPT, proactive behavioral index

1 Introduction

Psychiatric disorders, as a rule complex syndromes with substantial heterogeneity, are categorized into distinct diagnostic groups on the basis of presence and absence of characteristic criteria using classification systems such as the diagnostic and statistical manual for mental disorders (DSM) (American Psychiatric Association, 2013) and the international classification of disease (ICD). The research domain criteria initiative (RDoC) takes a different approach and utilizes neurobiologically informed domains of function to provide a dimensional framework for conceptualizing mental disorders (Cuthbert, 2022). In clinical settings, DSM/ICD classifications are used exclusively. However, these classification systems lead to widely heterogeneous groups within the same diagnostic category and their utility for research purposes has been questioned (Widiger and Samuel, 2005; Wardenaar and de Jonge, 2013; Borgogna, Owen, and Aita, 2023). In the present study, we compared effects of stimulant medication in healthy individuals and adults with attention deficit hyperactivity disorder (ADHD) using categorical (presence and absence of ADHD diagnosis according to DSM 5) and dimensional (RDoC cognitive control construct) stratification methods.

ADHD is a neurodevelopmental disorder, with impaired cognitive control and impulsivity/hyperactivity as core symptoms (Faraone et al., 2021). Although not part of the diagnostic criteria, there is also evidence indicating that emotional dysregulation may be a core impairment in ADHD, making ADHD an even more heterogeneous syndrome than currently clinically conceptualized (Retz et al., 2012; Shaw et al., 2014). Central stimulants (CS), which act by blocking dopamine (DA) and noradrenaline (NA) reuptake, are the mainstay of pharmacological treatment (Volkow et al., 2001; Arnsten and Dudley, 2005; Berridge et al., 2006; Faraone and Glatt, 2010), and their effect in alleviating core ADHD symptoms has been shown to be robust in the clinical setting (Faraone and Glatt, 2010; Cortese et al., 2018). Roughly 70%–80% of ADHD patients treated with CS are clinically deemed to be treatment responders (Spencer et al., 2005). CS is also used by segments of the healthy population wanting to improve cognitive performance, but the beneficial effects of CS in normal functioning adults is less clear (Repantis et al., 2010; Smith and Farah, 2011). Meta-analyses in healthy individuals showed small but significant effects of methylphenidate (MPH) on working memory, inhibitory control and processing speed (Smith and Farah, 2011; Marraccini et al., 2016). A meta-analysis that compared the effect of three cognitive enhancers in healthy individuals, MPH, modafinil and dexamphetamine, found that MPH had the strongest effect of the three, with small improvements on recall, attention and inhibitory control (Roberts et al., 2020). A recent study that evaluated the effects of CS in everyday complex tasks in healthy subjects showed that CS increased effort but reduced quality of effort, and performance across participants was reversed by CS such that above average performers ended up being below average after CS and vice versa for below average performers (Bowman et al., 2023). Effects of CS have also been shown to vary with baseline cognitive capacity (Mattay et al., 2000; Cools et al., 2008; Rostami Kandroodi et al., 2021) and baseline DA and NA levels (Cools and D'Esposito, 2011). Thus, not only effects of CS may differ between healthy subjects and ADHD patients, but they may also differ within the same group on the bases of baseline behavioral and neurochemical factors.

Cognitive control, also known as top-down control or executive control is a neuropsychological construct pertaining to the flexible regulation of goal-directed behaviour and is generally associated with the functions of lateral prefrontal cortex and posterior parietal cortex (Miller and Cohen, 2001; Friedman and Robbins, 2022). Cognitive control subconstructs such as goal selection, updating, representation, and maintenance can be studied using AX-Continuous Performance Task (AX-CPT), a paradigm that is often used to assess cognitive control (Lopez-Garcia et al., 2016). In AX-CPT, single letters (A, B, X, Y) are displayed on a screen and participants are instructed to make a target response when presented with the letter X, but only if it is preceded by the letter A. For all other letter combinations, participants are instructed to make a non-target response. To create expectancy, AX trials are generally made to occur more frequently than AY, BX and BY trials (Barch et al., 2003). Cognitive control mode during AX-CPT is assessed by the proactive behavioral index (PBI), where a proactive cognitive control mode indicates better performance on BX trials than AY trials, and the opposite being the case for reactive control mode.

In a study that made use of the dual system theory of decision-making that contrasts quick heuristic mode of decision making with a slower deliberative mode, Yechiam and Zeif found that MPH improved performance by selectively enhancing the slower deliberative mode of decision-making compared to the quicker heuristic mode (Yechiam and Zeif, 2022). A conceptually comparable dual mechanism framework (DMC) has been suggested for cognitive control, contrasting proactive and reactive control modes (Braver et al., 2009; Braver, 2012). The proactive control mode has been shown to dominate in healthy adults, while patients with psychotic (Barch et al., 2003; MacDonald and Carter, 2003) and anxiety disorders (Schmid, Kleiman, and Amodio, 2015) are more prone to employ a more reactive control mode.

In the present paper, we studied behavioral and neural effects of CS in healthy controls and individuals with ADHD using two stratification strategies, (i) categorical stratification on the bases of presence and absence of ADHD diagnosis according to DSM 5, and (ii) dimensional stratification on the basis of proactive and reactive cognitive control mode. We hypothesized that the behavioral and neural effects of CS in the categorical and dimensional groups may not always parallel each other, and that the neurobehavioral homogeneity created by dimensional stratification using RDoC cognitive control domain might reveal CS effects masked by heterogeneity in the categorical stratification using diagnosis classes.

2 Materials and methods

The study was approved by the Swedish Ethical Review Authority (Dnr 2020-02278; 2020-05590) and written consent was obtained from all participants in the study.

2.1 Participants and study outline

Thirty-three healthy controls and 32 adults with ADHD were included in the study that was conducted between December 2020 and December 2023. The ADHD group was a well-

characterized clinical cohort, who had clinically responded to CS medication and are recruited from the Neuropsychiatric Outpatient Clinic at Örebro University Hospital (Rode et al., 2023). Inclusion criteria for the ADHD cohort were (i) ADHD diagnosis after extensive neuropsychiatric evaluation by a dedicated team of psychologists and senior consultants in psychiatry according to Swedish guidelines, (ii) no ongoing psychosis, bipolar, depressive, substance use or sever autism spectrum disorder, (iii) no suicidal or aggressive tendency and (iv) no contraindication for MRI investigation. Choice of medication and treatment optimization was carried out by the treating physician and followed Swedish guidelines for the pharmacological treatment of ADHD (Läkemedelsverket, 2016). Patients had to have a minimum of 4–6 weeks of stable medication before they could be enrolled in the study. Clinical response was determined by a score of 1 or 2 using clinician and patient-rated Clinical Global Impression–Improvement (CGI-I). The control group was recruited by advertising at a university campus and hospital area. Exclusion criteria for the healthy controls were (i) current or previous psychiatric and neurological ailment including substance use, (ii) ongoing psychoactive medication use, (iii) narrow-angle glaucoma, and (iv) incompatibility with magnetic resonance imaging (MRI). The control group was also assessed for potential allergic reaction to MPH or any of its ingredients. The CS medication used by the ADHD patients was either methylphenidate (MPH) or lisdexamfetamine (LDX) as selected and dose-optimized by the treating physician.

All participants underwent MRI examinations before and after CS using the same MRI scanner and protocol settings. The first session was performed in the absence of CS and the second 1–2 h after ingestion of CS, which constituted of 30 mg short-acting MPH for the healthy controls and MPH or LDX for the ADHD group as selected and dose-optimized by the treating physician. ADHD patients were instructed to abstain from CS medication for 24 h before the start of the first MRI session. CS was ingested directly after the end of the first session, and the second session started 1–2 h later to synchronize MRI examination with peak CS concentration in brain tissue. Each MRI session included a functional MRI (fMRI) acquisition with the participants performing an AX-CPT task that lasted for 14 min and 22 s.

2.2 Cognitive control task (AX-CPT)

AX-CPT was implemented using E-Prime (Psychology Software Tools version 3.0, Pittsburgh, PA, United States) and started with a rest period of 30 s displaying a fixation cross at the center of the screen, followed by 160 AX-CPT trials. An AX-CPT trial consisted of two stimuli; a cue letter ("A" or "B") followed by a probe letter ("X" or "Y") with a blank inter-stimulus interval (ISI) in between, followed by an inter-trial interval (ITI) where a fixation cross was displayed. Participants used pistol-grips held in each hand and target-responses were made by pressing a button on the right grip and on the left grip for non-target responses. Reaction time (RT) and response were recorded from the onset of the probe to, at maximum, the end of the ITI. Duration of cue and probe was 500 msec. ISI was jittered between 900–1,100 msec with average duration of 1,000 msec and ITI was jittered between 1,500–2,500 msec with average duration of 2,000 msec. The order of the trial types was randomized, with 70% being target trials (AX) and 30% divided equally between non-target trials (AY, BX, BY). Participants got instructions about AX-CPT and practiced prior MRI until they felt sure they understood the task and could perform it with ease.

RT and responses were analyzed separately for each trial type (AX, AY, BX and AY). The proactive behavioral index (PBI) was calculated using the RTs for AY and BX according to the formula (AY-BX)/(AY + BX) (Braver et al., 2009; Gonthier et al., 2016). High PBI was interpreted as a dominance of a proactive cognitive control mode and low PBI as dominance of reactive control mode. The calculation of error rate for the different trial types was based on recorded responses (correct/incorrect) while trials without any responses were omitted.

2.3 Categorical and dimensional stratification

Participants were stratified into categorical and dimensional groups on the basis of presence and absence of ADHD diagnosis according to DSM 5 (categorical stratification), or on the basis of RDoC cognitive control domain (dimensional stratification). For the categorical stratification, the two groups thus consisted of healthy controls and ADHD patients, and for the dimensional stratification of reactive and proactive individuals irrespective of their DSM 5 diagnosis status. The two dimensional groups (reactive vs. proactive) were created by a median split of baseline PBI scores (PBI_{pre}). Participants with PBI_{pre} score less than the median value formed the reactive group and those with PBI_{pre} score equal to or greater than the median value formed the proactive group.

2.4 MRI and preprocessing of fMRI data

A 3.0T MR system (Signa Premier, GE Medical Systems, WI) and a 48-channel head coil were used for all MR examinations, which included a structural image of the brain and an fMRI acquisition during the AX-CPT task. Parameters for the structural scan (3D T1w IR-prepared fast spoiled gradient recalled echo, "BRAVO") were: TR/TE = 7.3/3.0 msec, acquired voxel size 0.9 × 0.9 × 1.2 mm, parallel imaging acceleration (ARC) factor of 2. The fMRI acquisition used a gradient echo EPI pulse sequence with TR/TE = 2000/35 msec, slice thickness 2.5 mm, acquired pixel size 2.5 × 2.5 mm, no slice gap, ARC factor of 2 and a hyperband factor of 2. Acquired images were converted to nifti-format using dcm2niix (https://github.com/rordenlab/dcm2niix).

Preprocessing of fMRI data (slice-time correction, realigning, unwarping, normalizing to MNI template, smoothing) was performed using CONN (Whitfield-Gabrieli and Nieto-Castanon, 2012). Default settings were applied except for a smoothing kernel of 6 mm instead of 8 mm. The final preprocessing step included anatomical component-based noise correction (aCompCor) based on white matter and cerebrospinal fluid (CSF), scrubbing and bandpass filtering. Further details regarding the preprocessing are provided in the supplement.

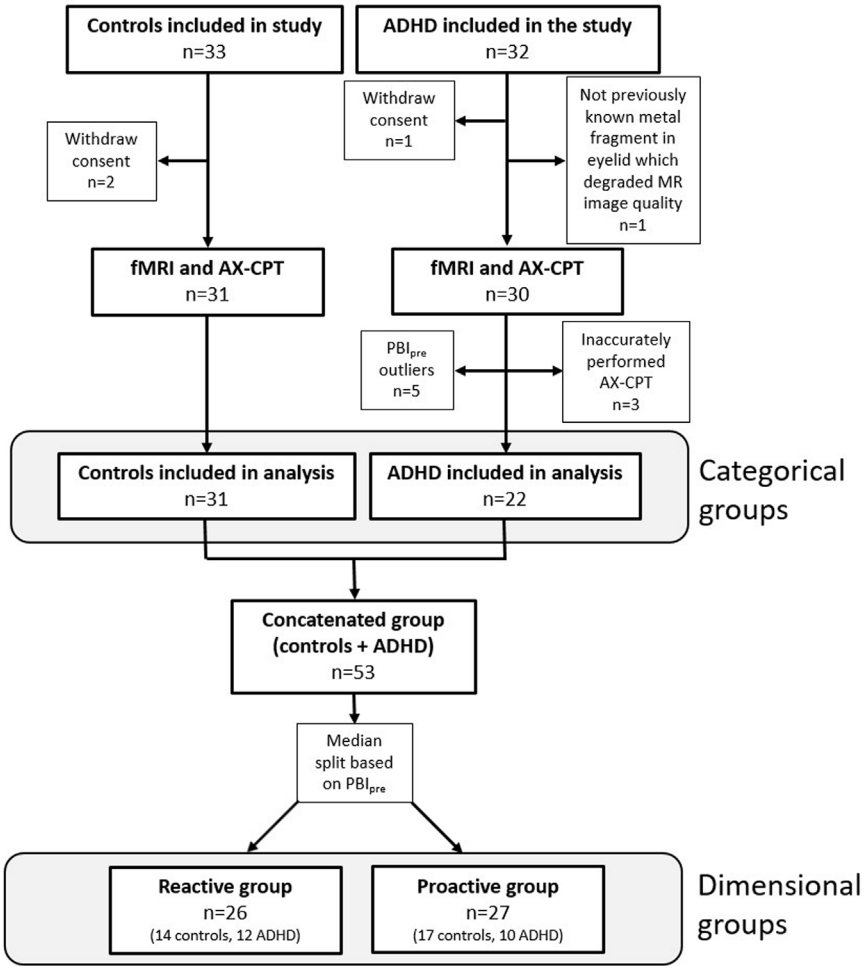

FIGURE 1
Flowchart showing inclusion and exclusion of participants in the study and the number of participants in the categorical and dimensional groups. Three participants from the ADHD group were excluded since PBI could not be calculated because they inaccurately performed the AX-CPT.

2.5 fMRI analysis

First-level analysis of each AX-CPT acquisition (pre and post CS) was performed using a general linear model (GLM) consisting of 4 regressors (AX, AY, BX and BY trials) where the onset and duration for each trial started with the presentation of the cue and lasted until the end of ITI. Group (second-level) analysis was carried out by setting up a full factorial model including beta values (i.e., BOLD signals) from the four different trials (AX, AY, BX and BY), before and after the administration of CS.

Correlations were tested between baseline PBI (PBI_{pre}) and differences in brain activity pre and post CS for the trial types (AY, BX). This was achieved by calculating a difference image (BOLD image post—BOLD image pre) for each trial type and then correlating it using PBI_{pre} as covariate.

Exploratory whole-brain analysis was performed and to correct for multiple comparisons, a pixelwise significance threshold level of $p < 0.001$ and cluster size threshold of FWE<0.05 were applied. All fMRI analyses were performed using SPM12 running on Matlab R2019b.

Labels in the Harvard-Oxford cortical structural atlas, available in FSLeyes (version 0.34.2, https://git.fmrib.ox.ac.uk/fsl/fsleyes/fsleyes), were used to provide anatomical information about significant clusters.

2.6 Statistical analysis

Behavioral data were analyzed using SPSS (IBM SPSS Statistics version 28.0), and Matlab (R2019b) was used for graphical plots. Participants with PBI_{pre} outside the range [Q1-1.5xIQR, Q3+1.5xIQR] were considered as outliers and their experimental protocol was reviewed for any outstanding issues that may explain the extreme values. (Q1 = 25th percentile, Q3 = 75th percentile, interquartile range (IQR) = Q3-Q1). Parametric tests were applied if the data could be adequately modelled according to the normal distribution, otherwise non-parametric tests were used. Two-sided p-values are reported in all cases.

TABLE 1 Baseline characteristics of study participants in the two stratification groups. Values are presented as mean ± 1 standard deviation. PBI is calculated using RT for AY and BX as PBI = (AY-BX)/(AX + BX).

		All (n = 53)	Controls (n = 31)	ADHD (n = 22)	Comparison (Controls vs. ADHD)	Reactive (n = 26)	Proactive (n = 27)	Comparison (Reactive vs. Proactive)
Age (years)		36 ± 10	37 ± 11	36 ± 9	p = 0.914	37 ± 11	36 ± 9	p = 0.689
Sex[a] (Male/ Female)		23/30	14/17	9/13	p = 0.86	15/11	8/19	p = 0.04
PBI_{pre} (a.u.)		0.15 ± 0.08	0.15 ± 0.07	0.15 ± 0.09	p = 0.957	0.09 ± 0.04	0.21 ± 0.05	p < 0.001 (due to median split)
PBI_{post} (a.u.)		0.17 ± 0.09	0.17 ± 0.09	0.17 ± 0.09	p = 0.971	0.14 ± .0.08	0.19 ± 0.09	p = 0.011
RT pre CS (msec)	AX	530 ± 139	520 ± 125	544 ± 158	p = 0.639	573 ± 155	488 ± 108	p = 0.013
	AY	631 ± 172	601 ± 134	673 ± 211	p = 0.170	665 ± 187	598 ± 153	p = 0.117
	BX	473 ± 165	457 ± 159	495 ± 174	p = 0.357	564 ± 180	385 ± 82	p < 0.001
	BY	462 ± 178	437 ± 143	499 ± 216	p = 0.209	519 ± 182	408 ± 158	p = 0.003
RT post CS (msec)	AX	505 ± 153	506 ± 147	503 ± 164	p = 0.986	534 ± 158	476 ± 145	p = 0.064
	AY	585 ± 169	588 ± 156	582 ± 190	p = 0.718	610 ± 173	561 ± 166	p = 0.24
	BX	433 ± 198	434 ± 188	431 ± 215	p = 0.871	473 ± 191	393 ± 199	p = 0.012
	BY	425 ± 190	422 ± 170	429 ± 220	p = 0.986	463 ± 177	388 ± 198	p = 0.013

CS, central stimulant medication;
a.u., arbitrary unit.
[a]Sex assigned at birth.

3 Results

3.1 Study groups and participant data

Of the 65 initial participants, 53 were included in the final analysis, which consisted of 31 healthy controls and 22 patients with ADHD (Figure 1). Five outliers were identified, and their experimental protocol carefully reviewed for any outstanding issue; in all cases circumstances could be identified that explained the extreme values and justified the exclusion of the participants. For the dimensional stratification, there were 26 individuals in the reactive group consisting of 14 healthy controls and 12 ADHD patients and 27 individuals in the proactive group consisting of 17 healthy controls and 10 ADHD patients. There was no significant difference in the number of healthy controls and ADHD patients clustering to the reactive and proactive groups (Pearson chi-square, $\chi(1) = 0.45$, p = 0.50). Baseline and behavioral data for all participants are shown in Table 1.

3.2 Cognitive control paradigm (AX-CPT)–behavioral data

The AX-CPT used in the current study resulted in the expected behavioral features, and as previously reported in the literature AY trials showed the longest reaction time and highest error rate (Table 1; Supplementary Figure S1). For the behavioral data, we analyzed potential differences in reaction time (RT) and proactive behavioral index (PBI) in the categorical and dimensional groups before and after administration of CS by evaluating interaction effects. For the categorical stratification, we found no significant interaction regarding RT or PBI between healthy controls and ADHD patients before and after CS. For the dimensional stratification, however, a 2 × 2 repeated measure ANOVA showed a significant ($F(1,51) = 8.777$, $p = 0.005$) interaction for PBI where the reactive group significantly increased its mean PBI ($p = 0.006$) compared to the proactive group, which did not show any significant change in PBI, although there was a slight decrease in this (Figure 2A). Also, there was a significant pre-post CS interaction in RT for BX [$F(1,51) = 4.516$, $p = 0.038$], where the reactive ($p = 0.004$) but not proactive group significantly decreased its RT for the BX trial (Figure 2B).

3.3 Functional brain activation data

Similar to the behavioral data, we analyzed the fMRI data for interaction effects in order to assess potential brain activation differences between groups in the categorical and dimensional stratifications before and after administration of CS. The AY and BX trials were used as regressors, as they are the basis for calculating PBI and determining reactive and proactive cognitive control mode groups.

There were no significant interaction effects between healthy controls and patients with ADHD before and after administration of

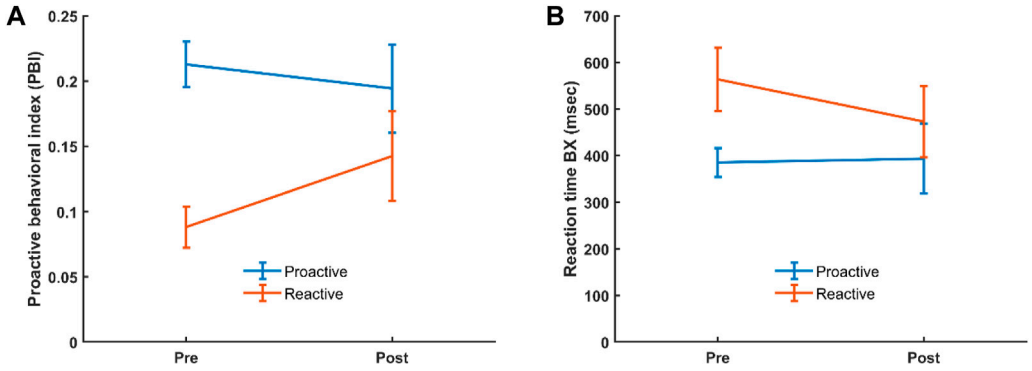

FIGURE 2
Interaction for PBI **(A)** and BX RT **(B)** in the reactive and proactive cognitive control mode groups, before and after administration of CS. Error bars show 95% confidence interval.

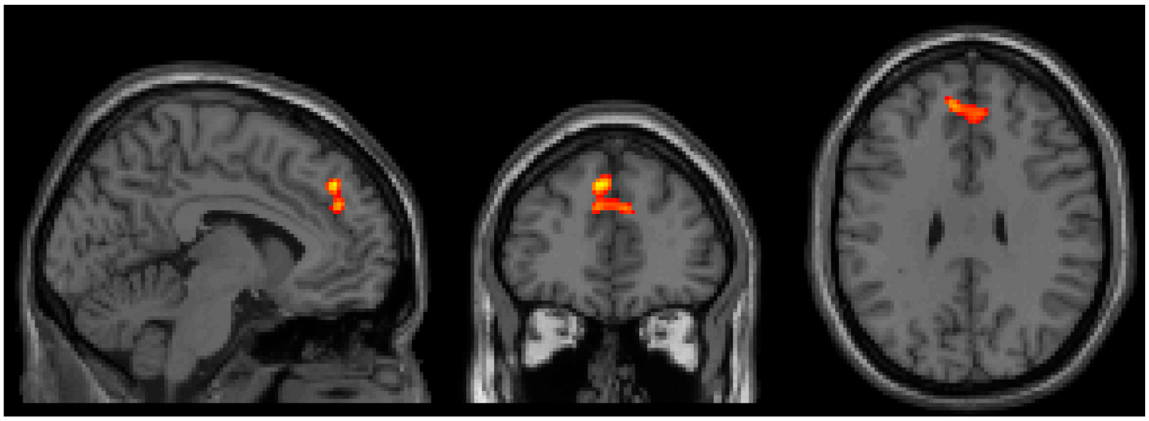

FIGURE 3
Three orthogonal slices (sagittal, coronal and axial) showing brain area where there was a significant increase of brain activity after CS for the reactive group compared to the proactive group. Images are shown using neurological orientation, i.e., subject left to the left in image.

CS in the categorical stratification. For the dimensional stratification, however, there was a significant interaction effect for BX. This interaction was noticed in a cluster located in the superior frontal and paracingulate gyri, showing that in these areas the reactive group increased its brain activation more after CS compared to the proactive group. The cluster consisted of 167 voxels (voxel size = 2 × 2 × 2 mm^3) with a peak t-statistic coordinate at (−4, 42, 40 mm) in MNI-space (Figure 3).

Correlation between baseline PBI (PBI_{pre}) and changes in brain activation for the AY and BX trials after CS was also evaluated considering all participants as one group (n = 53). There were four significant clusters showing a negative correlation between PBI_{pre} and changes in brain activation after CS for the BX trial (BX1-BX4), and one cluster (BX5) showing a positive correlation (Figure 4). We saw no significant correlations between PBI_{pre} and changes in brain activation after CS for the AY trial. A summary of all displayed clusters shown in Figure 4 is provided in Supplementary Table S1 together with anatomical information about clusters.

Figure 5 shows the correlations between PBI_{pre} and BX1-BX5 activation clusters. BX3 is virtually the same cluster obtained when comparing CS effects between the reactive and proactive groups in the dimensional stratification (Figure 3). The negative correlation indicates that reactive individuals increase brain activation in these areas after CS compared to proactive individuals, who show a decrease in brain activation after CS. For illustrative purposes, the individuals with largest increase in PBI after CS (defined as greater than the 75th percentile) are indicated in Figure 5. The majority of these individuals (11 out of 13) belong to the reactive group and most have an increase in brain activation after CS in clusters BX1-BX4 (BX1: 8/13, BX2: 8/13, BX3: 7/13, BX4: 10/13). In cluster BX5 the majority (8/13) decreased brain activity after CS. The regression lines in Figure 5 cross the *x*-axis at PBI_{pre} equal to 0.13/0.15/0.14/0.16/0.13 for clusters BX1-BX5, respectively.

4 Discussion

Psychiatric disorders are in almost all instances complex syndromes with as yet not fully established etiopathology (Insel, 2010). Diagnostic classification in clinical settings is guided by the

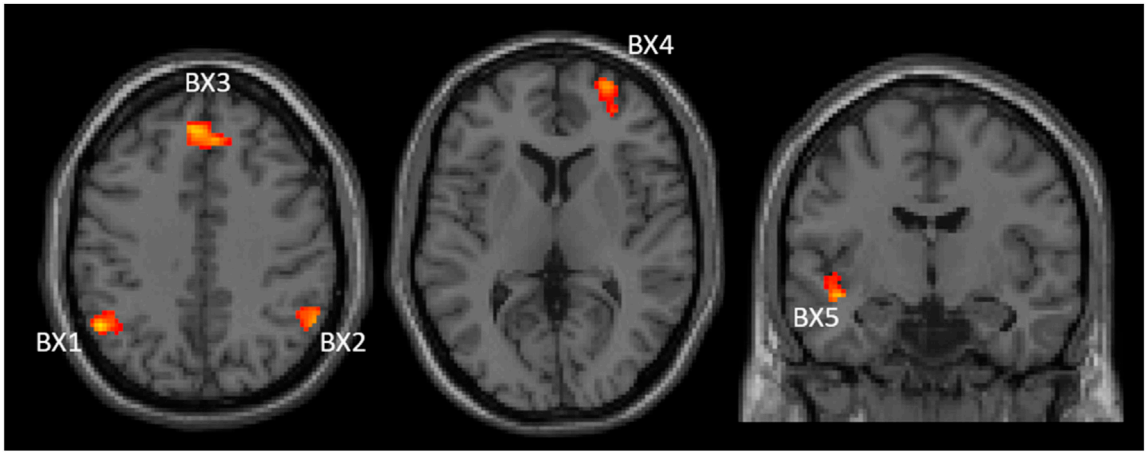

FIGURE 4
Two axial (left and middle) and one coronal (right) images showing significant clusters correlations between changes in brain activities (post-pre administration of CS) and PBI_{pre} during BX trials. The clusters are labelled (BX1-BX5) to be used for identification in text and Supplementary table S1 Images are shown using neurological orientation.

presence and absence of characteristic phenomenological criteria that in themselves remain agnostic as to the neurobiological underpinning of the disorders (American Psychiatric Association, 2013). Lately, concern has been raised pertaining to a putative lack of reproducibility in the psychiatry/psychology research fields (Open Science Collaboration, 2015). Diagnostic heterogeneity has been postulated as one possible reason behind this (Borgogna et al., 2023). The utility of these classification systems for research purposes has thus been questioned, among other things, due to the substantial within group heterogeneity between group overlap the current categorical classification systems lead to (Widiger and Samuel, 2005; Wardenaar and de Jonge, 2013; Borgogna et al., 2023). The research domain criteria initiative (RDoC), on the other hand, although not a diagnostic tool *per se*, provides a neurobiologically informed dimensional framework for conceptualizing psychiatric disorders by utilizing neurobehavioral domains of function (Insel et al., 2010). Thus, dimensional stratification by reducing within group heterogeneity (Borgogna et al., 2023) may contribute to the standardization of a study population in a such a way that intervention, control and outcome (PICO) may become reproducible when similar PICOs are studied in different research facilities. The RDoC domains that are thought to be most relevant for ADHD are cognitive control and positive valence domains, pertaining to inattention and hyperactivity/impulsivity aspects of the disorder, respectively. Paradigms that evaluate these domains include the AX Continuous Performance Task (AX-CPT) for cognitive control domains such as goal selection, goal maintenance and updating (Lopez-Garcia et al., 2016), the Go NoGo task for response selection and response inhibition (Boucher et al., 2007), and various incentive delay tasks for positive valence domains such as reward anticipation (Knutson et al., 2000).

In this study, neural and behavioral effects of CS medication during a cognitive control task (AX-CPT) were investigated using two classification strategies to stratify study participants, (i) categorical stratification using DSM 5 diagnosis and (ii) dimensional stratification using RDoC cognitive control domain irrespective of diagnosis status. Median split of proactive behavioral index (PBI) calculated from AY and BX trials of the AX-CPT (Gonthier et al., 2016) was used to divided participants into reactive and proactive groups for the dimensional stratification without paying attention to diagnosis. Based on previous studies that found the effect of CS on cognitive control to vary with baseline cognitive capacity (Mattay et al., 2000; van der Schaaf et al., 2013; Rostami Kandroodi et al., 2021), we hypothesized that dimensional stratification may be superior to categorical stratification in revealing neural and behavioral effects of CS. Also, in the categorical stratification, we expected the effects of CS to be more prominent in ADHD patients compared to healthy controls, based on previous findings that showed a robust clinical effect of CS in ADHD patients (Faraone and Glatt, 2010; Cortese et al., 2018) and a less clear-cut cognitive enhancing effects in the non-clinical population (Repantis et al., 2010; Smith and Farah, 2011).

There was, of course, the possibility that the two stratification methods would result in largely similar individuals clustering in the same groups, in a way that would undermine our study design, i.e., that most ADHD patients would cluster into the reactive group and most healthy controls into the proactive group and that there would be no meaningful difference between the two stratification methods. Contrary to our initial apprehension, however, we found an almost 50/50 clustering of patients and healthy controls into the two dimensional groups, with the median split resulting in 14 healthy controls (45.2%) and 12 ADHD patients (54.5%) clustering in the reactive group and 17 healthy individuals (54.8%) and 10 ADHD patients (45.5%) clustering in the proactive group, with no significant difference in this between healthy controls and ADHD patients. The fact that cognitive control mode cuts across diagnosis indicates that ADHD patients may not markedly differ from healthy controls in this respect, unlike, for example, psychosis patients who have been shown to employ a markedly reactive cognitive control mode compared to healthy individuals (MacDonald, 2008).

Once it was ascertained that the stratification method gave variable clustering of individuals into the categorical and

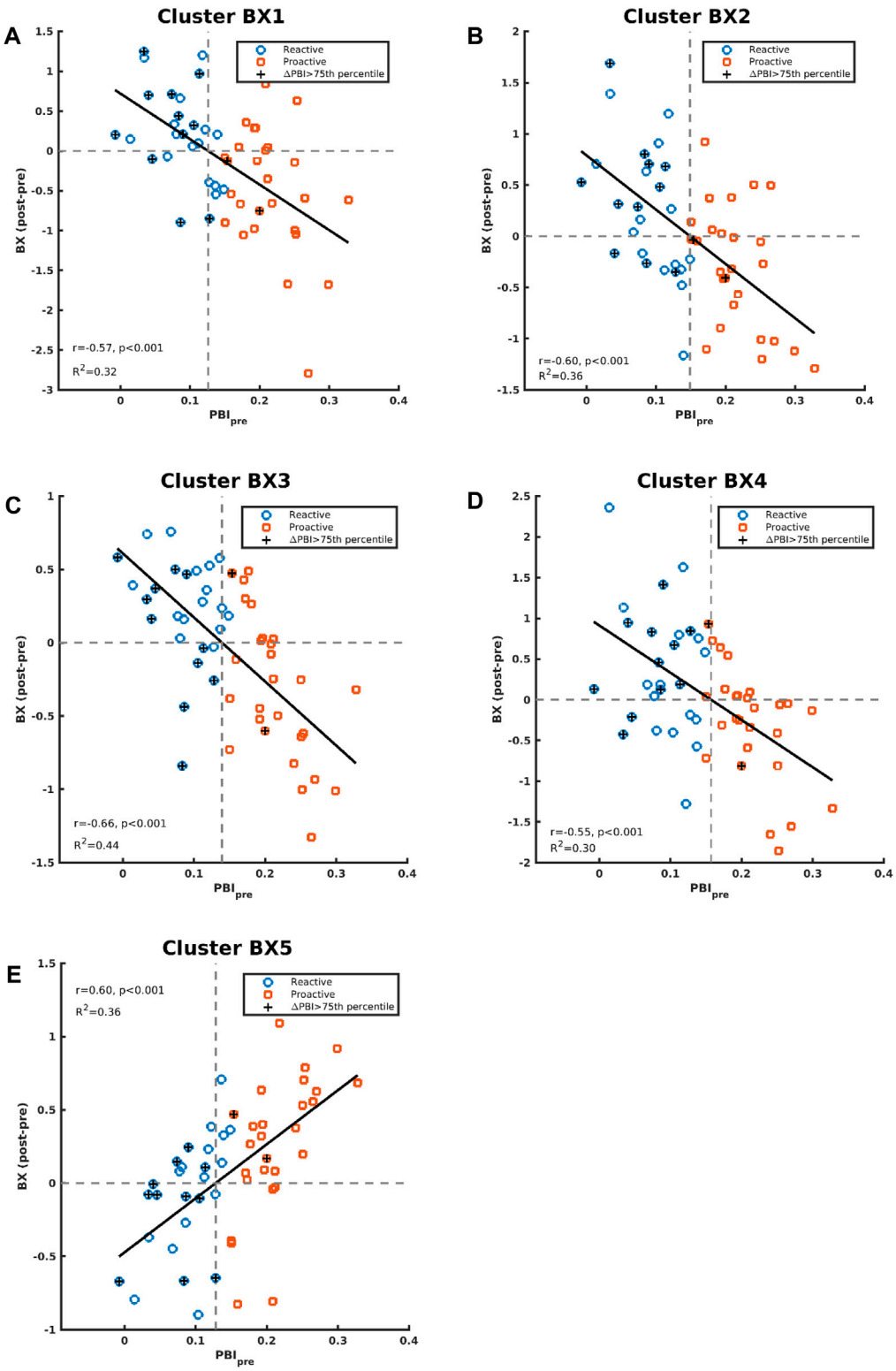

FIGURE 5
Correlations between contrast differences for BX (post-pre administration of CS) and PBI_{pre} are shown in panels **(A–E)** for cluster BX1-BX5, respectively. The individuals in the whole study who had an increase of PBI ($PBI_{post\ vs}$ PBI_{pre}) greater than the 75th percentile are indicated with "+".

dimensional groups, we went ahead to systematically evaluate the effects of CS on the groups within the two stratification strategies. When participants were categorically assigned as healthy controls and ADHD patients, on the basis of DSM 5 diagnosis, we found no significant behavioral or brain activation effects of CS in these two groups. On the other hand, when study participants were stratified

along dimensional factors into reactive and proactive cognitive control mode groups ignoring diagnosis status, CS selectively increased activation in paracingulate and superior frontal gyri in the reactive group compared to the proactive group and induced a shift towards proactive control mode in the reactive group without significantly affecting the proactive group. The shift towards proactive control mode in the reactive group was mediated by a decrease in reaction time for BX trials, without significant concomitant effects on AY trials. Besides these direct and selective effects of CS on brain activation and proactive behavioral index (PBI), we also found a significant correlation between baseline PBI and the neural effects of CS. In 4 out of the 5 active frontoparietal clusters for the BX contrast, lower baseline PBI was associated with greater post CS increase in brain activation. Clusters in frontal (frontal pole, bilateral paracingulate, right superior frontal gyrus) and parietal (bilateral angular and left supramarginal gyri) brain areas all showed increased brain activation after CS that was negatively correlated with baseline PBI scores. One left-lateralized temporo-insular cluster consisting of left insular cortex and left planum polare showed CS induced activation changes that were positively correlated to baseline PBI, i.e., the post-CS increase in these two areas was greater the higher baseline PBI score was.

Our results show that the neural and behavioral effects of CS were more clear-cut when participants were stratified along dimensional factors than diagnostic categories. In a recent study that included ADHD patients who responded and did not respond to CS treatment, we reported that saliency ("wanting") and hedonic experience ("liking"), pertaining to the positive valence RDoC domain, could predict response to CS treatment and that that the scores for "wanting" were positively correlated to resting state connectivity increase in the ventral striatum (Rode et al., 2023). Although all included patients in the present study were clinical responders to CS treatment as evaluated by clinician- and patient-rated clinical global impression–improvement (CGI-I), our results from this study indicate that cognitive control mode might also be a potential predictor of CS response in clinical the setting. In a more recent paper Hung et al., 2024 reported that striatal structural connectivity and higher pre-treatment working memory scores were correlated with greater response to CS medication in patients with ADHD (Hung et al., 2024).

As mentioned above, the effect of CS on behavioral or neural outcomes varies with baseline cognitive capacity (Mattay et al., 2000; van der Schaaf et al., 2013; Rostami Kandroodi et al., 2021), baseline DA and NA levels (Cools and D'Esposito, 2011) and rate of behavioral, physical or electrical stimulation (Sanger and Blackman, 1976). Because the proactive group had substantially lower mean RT scores for, among other things, BX and BY trials, if the proactive group were to be allowed to respond at a higher rate, this could potentially affect the results due to the rate dependency of CS effect (Sanger and Blackman, 1976). However, in the present paper, the rate of stimulus (interstimulus interval) across all subjects and conditions was constant. Thus, even though a participant had a shorter RT, this was not allowed to alter the rate of response. Furthermore, due to the low mean RT scores in the proactive group, their response to CS as far as RT is concerned could be restricted due to ceiling effects. However, when we looked at baseline RT scores across all participants, we found that both proactive and reactive individuals had baseline RT scores that ranged from low to high and did not cluster around any particular value in a way that could have imposed significant ceiling effects.

A plausible clinical implication based on the results in the current study might be that ADHD patients employing reactive cognitive control mode, as well as healthy controls who might use CS off-label, would respond better to CS than those employing a more proactive control mode. This assumes that a transition from reactive to proactive control mode is equated to being a responder of CS. Further studies are needed to elucidate this and should include groups of both CS responding and CS non-responding ADHD patients.

The lack of effect of CS in unstratified ADHD patients and unstratified healthy controls, we suspect, might be due to substantial within group heterogeneity and the known inverted U-form dose-effect curve of the signal substances dopamine and noradrenaline whose peri-synaptic levels are enhanced by CS medication. Similar lack of effect was previously reported in unstratified study participants (Cools et al., 2008), and the CS effects could be revealed when participants were stratified along baseline cognitive capacity (Cools et al., 2008) or baseline dopamine synthesis capacity (Westbrook et al., 2020).

Our implementation of the AX-CPT paradigm in this study corresponds to a low load task (Mäki-Marttunen, Hagen, and Espeseth, 2019), since it only consisted of two cue letters ("A" and "B") and two probes ("X" and "Y") and that the intra-trial interval was short. The behavioral and neural effects of the task can be expected to be larger when using a more challenging version with more cues and probes and longer intra-trial interval. However, we found such versions too difficult for some of the ADHD patients that could have led to an even greater loss of included ADHD participants, which occurred even when using this easier version (see Figure 1).

4.1 Limitations

In this study we included only ADHD patients that have clinically been judged to be responders to CS treatment. It is theoretically possible that the results may have been different had we also included ADHD patients who were CS non-responders. Another intriguing question is why ADHD patients who have clinically responded to CS medication become "non-responders" when tested with a cognitive control paradigm, if they happen to employ proactive cognitive control mode. One possible explanation for this is suggested by the recent finding of (Bowman et al., 2023), who in healthy subjects found that CS increased motivation/effort but reduced quality of effort, which suggests that CS responding ADHD patients might improve on certain but not all aspects of their impairment.

5 Conclusion

We can draw several conclusions from the current study, (i) cognitive control mode cuts across diagnostic categories and there is equal likelihood for ADHD patients to employ reactive and proactive cognitive control mode as healthy controls, (ii) dimensional stratification under our experimental condition seems to be superior to categorical stratification in revealing neural and behavioral effects of CS, and (iii) baseline cognitive

control mode might potentially be a predictor of CS treatment effect in the clinical setting.

Data availability statement

The raw data supporting the conclusions of this article will be made available by the authors, without undue reservation.

Ethics statement

The studies involving humans were approved by the Swedish Ethical Review Authority (EPM). The studies were conducted in accordance with the local legislation and institutional requirements. The participants provided their written informed consent to participate in this study.

Author contributions

PT: Conceptualization, Data curation, Formal Analysis, Methodology, Project administration, Software, Writing–original draft, Writing–review and editing. MR: Formal Analysis, Methodology, Writing–original draft, Writing–review and editing. JR: Formal Analysis, Methodology, Writing–original draft, Writing–review and editing. MM: Conceptualization, Data curation, Formal Analysis, Funding acquisition, Investigation, Methodology, Project administration, Validation, Writing–original draft, Writing–review and editing.

Funding

The author(s) declare that financial support was received for the research, authorship, and/or publication of this article. Nyckelfonden, Örebro, Sweden (OLL 935421), ALF Grants, Region Örebro län, Sweden (OLL 973230).

Conflict of interest

The authors declare that the research was conducted in the absence of any commercial or financial relationships that could be construed as a potential conflict of interest.

Publisher's note

Supplementary material

The Supplementary Material for this article can be found online at: https://www.frontiersin.org/articles/10.3389/fphar.2024.1412178/full#supplementary-material

References

American Psychiatric Association (2013). *Diagnostic and statistical manual of mental disorders*. 5th ed. American Psychiatric Association. doi:10.1176/appi.books.9780890425596

Arnsten, A. F., and Dudley, A. G. (2005). 'Methylphenidate improves prefrontal cortical cognitive function through alpha2 adrenoceptor and dopamine D1 receptor actions: relevance to therapeutic effects in Attention Deficit Hyperactivity Disorder. *Behav. Brain Funct.* 1, 2. doi:10.1186/1744-9081-1-2

Barch, D. M., Carter, C. S., MacDonald, A. W., 3rd, Braver, T. S., and Cohen, J. D. (2003). 'Context-processing deficits in schizophrenia: diagnostic specificity, 4-week course, and relationships to clinical symptoms. *J. Abnorm Psychol.* 112, 132–143. doi:10.1037/0021-843x.112.1.132

Berridge, C. W., Devilbiss, D. M., Andrzejewski, M. E., Arnsten, A. F., Kelley, A. E., Schmeichel, B., et al. (2006). Methylphenidate preferentially increases catecholamine neurotransmission within the prefrontal cortex at low doses that enhance cognitive function. *Biol. Psychiatry* 60, 1111–1120. doi:10.1016/j.biopsych.2006.04.022

Borgogna, N. C., Owen, T., and Aita, S. L. (2023). The absurdity of the latent disease model in mental health: 10,130,814 ways to have a DSM-5-TR psychological disorder. *J. Ment. Health*, 1–9. doi:10.1080/09638237.2023.2278107

Boucher, L., Palmeri, T. J., Logan, G. D., and Schall, J. D. (2007). Inhibitory control in mind and brain: an interactive race model of countermanding saccades. *Psychol. Rev.* 114, 376–397. doi:10.1037/0033-295X.114.2.376

Bowman, E., Coghill, D., Murawski, C., and Bossaerts, P. (2023). 'Not so smart? "Smart" drugs increase the level but decrease the quality of cognitive effort. *Sci. Adv.* 9, eadd4165. doi:10.1126/sciadv.add4165

Braver, T. S. (2012). The variable nature of cognitive control: a dual mechanisms framework. *Trends Cogn. Sci.* 16, 106–113. doi:10.1016/j.tics.2011.12.010

Braver, T. S., Paxton, J. L., Locke, H. S., and Barch, D. M. (2009). Flexible neural mechanisms of cognitive control within human prefrontal cortex. *Proc. Natl. Acad. Sci. U. S. A.* 106, 7351–7356. doi:10.1073/pnas.0808187106

Cools, R., and D'Esposito, M. (2011). Inverted-U-shaped dopamine actions on human working memory and cognitive control. *Biol. Psychiatry* 69, e113–e125. doi:10.1016/j.biopsych.2011.03.028

Cools, R., Gibbs, S. E., Miyakawa, A., Jagust, W., and D'Esposito, M. (2008). 'Working memory capacity predicts dopamine synthesis capacity in the human striatum. *J. Neurosci.* 28, 1208–1212. doi:10.1523/JNEUROSCI.4475-07.2008

Cortese, S., Adamo, N., Giovane, C. D., Mohr-Jensen, C., Hayes, A. J., Carucci, S., et al. (2018). Comparative efficacy and tolerability of medications for attention-deficit hyperactivity disorder in children, adolescents, and adults: a systematic review and network meta-analysis. *Lancet. Psychiatry* 5, 727–738. doi:10.1016/S2215-0366(18)30269-4

Cuthbert, B. N. (2022). Research domain criteria (RDoC): progress and potential. *Curr. Dir. Psychol. Sci.* 31, 107–114. doi:10.1177/09637214211051363

Faraone, S. V., Banaschewski, T., Coghill, D., Zheng, Y., Biederman, J., Bellgrove, M. A., et al. (2021). The world federation of ADHD international consensus statement: 208 evidence-based conclusions about the disorder. *Neurosci. Biobehav. Rev.* 128, 789–818. doi:10.1016/j.neubiorev.2021.01.022

Faraone, S. V., and Glatt, S. J. (2010). A comparison of the efficacy of medications for adult attention-deficit/hyperactivity disorder using meta-analysis of effect sizes. *J. Clin. Psychiatry* 71, 754–763. doi:10.4088/JCP.08m04902pur

Friedman, N. P., and Robbins, T. W. (2022). The role of prefrontal cortex in cognitive control and executive function. *Neuropsychopharmacology* 47, 72–89. doi:10.1038/s41386-021-01132-0

Gonthier, C., Macnamara, B. N., Chow, M., Conway, A. R., and Braver, T. S. (2016). 'Inducing proactive control shifts in the AX-CPT. *Front. Psychol.* 7, 1822. doi:10.3389/fpsyg.2016.01822

Hung, Y., Green, A., Kelberman, C., Gaillard, S., Capella, J., Rudberg, N., et al. (2024). Neural and cognitive predictors of stimulant treatment efficacy in medication-naive ADHD adults: a pilot diffusion tensor imaging study. *J. Atten. Disord.* 28, 936–944. doi:10.1177/10870547231222261

Insel, T., Cuthbert, B., Garvey, M., Heinssen, R., Pine, D. S., Quinn, K., et al. (2010). Research domain criteria (RDoC): toward a new classification framework for research on mental disorders. *Am. J. Psychiatry* 167, 748–751. doi:10.1176/appi.ajp.2010.09091379

Insel, T. R. (2010). Rethinking schizophrenia. *Nature* 468, 187–193. doi:10.1038/nature09552

Knutson, B., Westdorp, A., Kaiser, E., and Hommer, D. (2000). FMRI visualization of brain activity during a monetary incentive delay task. *Neuroimage* 12, 20–27. doi:10.1006/nimg.2000.0593

Läkemedelsverket (2016). Läkemedel vid adhd - behandlingsrekommendation. *Inf. från Läkemedelsv.* 27, 13–24.

Lopez-Garcia, P., Lesh, T. A., Salo, T., Barch, D. M., MacDonald, A. W., 3rd, Gold, J. M., et al. (2016). The neural circuitry supporting goal maintenance during cognitive control: a comparison of expectancy AX-CPT and dot probe expectancy paradigms. *Cogn. Affect Behav. Neurosci.* 16, 164–175. doi:10.3758/s13415-015-0384-1

MacDonald, A. W. (2008). Building a clinically relevant cognitive task: case study of the AX paradigm. *Schizophr. Bull.* 34, 619–628. doi:10.1093/schbul/sbn038

MacDonald, A. W., 3rd, and Carter, C. S. (2003). Event-related FMRI study of context processing in dorsolateral prefrontal cortex of patients with schizophrenia. *J. Abnorm Psychol.* 112, 689–697. doi:10.1037/0021-843X.112.4.689

Mäki-Marttunen, V., Hagen, T., and Espeseth, T. (2019). Task context load induces reactive cognitive control: an fMRI study on cortical and brain stem activity. *Cogn. Affect Behav. Neurosci.* 19, 945–965. doi:10.3758/s13415-019-00691-6

Marraccini, M. E., Weyandt, L. L., Rossi, J. S., and Gudmundsdottir, B. G. (2016). 'Neurocognitive enhancement or impairment? A systematic meta-analysis of prescription stimulant effects on processing speed, decision-making, planning, and cognitive perseveration. *Exp. Clin. Psychopharmacol.* 24, 269–284. doi:10.1037/pha0000079

Mattay, V. S., Callicott, J. H., Bertolino, A., Heaton, I., Frank, J. A., Coppola, R., et al. (2000). Effects of dextroamphetamine on cognitive performance and cortical activation. *Neuroimage* 12, 268–275. doi:10.1006/nimg.2000.0610

Miller, E. K., and Cohen, J. D. (2001). 'An integrative theory of prefrontal cortex function. *Annu. Rev. Neurosci.* 24, 167–202. doi:10.1146/annurev.neuro.24.1.167

Open Science Collaboration (2015). PSYCHOLOGY. Estimating the reproducibility of psychological science. *Science* 349 (6251), aac4716. PMID: 26315443. doi:10.1126/science.aac4716

Repantis, D., Schlattmann, P., Laisney, O., and Heuser, I. (2010). Modafinil and methylphenidate for neuroenhancement in healthy individuals: a systematic review. *Pharmacol. Res.* 62, 187–206. doi:10.1016/j.phrs.2010.04.002

Retz, W., Stieglitz, R. D., Corbisiero, S., Retz-Junginger, P., and Rosler, M. (2012). Emotional dysregulation in adult ADHD: what is the empirical evidence? *Expert Rev. Neurother.* 12, 1241–1251. doi:10.1586/ern.12.109

Roberts, C. A., Jones, A., Sumnall, H., Gage, S. H., and Montgomery, C. (2020). How effective are pharmaceuticals for cognitive enhancement in healthy adults? A series of meta-analyses of cognitive performance during acute administration of modafinil, methylphenidate and D-amphetamine. *Eur. Neuropsychopharmacol.* 38, 40–62. doi:10.1016/j.euroneuro.2020.07.002

Rode, J., Runnamo, R., Thunberg, P., and Msghina, M. (2023). Salience and hedonic experience as predictors of central stimulant treatment response in ADHD - a resting state fMRI study. *J. Psychiatric Res.* 163, 378–385. doi:10.1016/j.jpsychires.2023.05.073

Rostami Kandroodi, M., Cook, J. L., Swart, J. C., Frobose, M. I., Geurts, D. E. M., Vahabie, A. H., et al. (2021). Effects of methylphenidate on reinforcement learning depend on working memory capacity. *Psychopharmacol. Berl.* 238, 3569–3584. doi:10.1007/s00213-021-05974-w

Sanger, D. J., and Blackman, D. E. (1976). 'Rate-dependent effects of drugs: a review of the literature. *Pharmacol. Biochem. Behav.* 4, 73–83. doi:10.1016/0091-3057(76)90178-7

Schmid, P. C., Kleiman, T., and Amodio, D. M. (2015). Neural mechanisms of proactive and reactive cognitive control in social anxiety. *Cortex* 70, 137–145. doi:10.1016/j.cortex.2015.05.030

Shaw, P., Stringaris, A., Nigg, J., and Leibenluft, E. (2014). Emotion dysregulation in attention deficit hyperactivity disorder. *Am. J. Psychiatry* 171, 276–293. doi:10.1176/appi.ajp.2013.13070966

Smith, M. E., and Farah, M. J. (2011). Are prescription stimulants "smart pills"? The epidemiology and cognitive neuroscience of prescription stimulant use by normal healthy individuals. *Psychol. Bull.* 137, 717–741. doi:10.1037/a0023825

Spencer, T., Biederman, J., Wilens, T., Doyle, R., Craig, S., Prince, J., et al. (2005). 'A large, double-blind, randomized clinical trial of methylphenidate in the treatment of adults with attention-deficit/hyperactivity disorder. *Biol. Psychiatry* 57, 456–463. doi:10.1016/j.biopsych.2004.11.043

van der Schaaf, M. E., Fallon, S. J., Ter Huurne, N., Buitelaar, J., and Cools, R. (2013). 'Working memory capacity predicts effects of methylphenidate on reversal learning. *Neuropsychopharmacology* 38, 2011–2018. doi:10.1038/npp.2013.100

Volkow, N. D., Wang, G., Fowler, J. S., Logan, J., Gerasimov, M., Maynard, L., et al. (2001). Therapeutic doses of oral methylphenidate significantly increase extracellular dopamine in the human brain. *J. Neurosci.* 21, RC121. doi:10.1523/JNEUROSCI.21-02-j0001.2001

Wardenaar, K. J., and de Jonge, P. (2013). Diagnostic heterogeneity in psychiatry: towards an empirical solution. *BMC Med.* 11, 201. doi:10.1186/1741-7015-11-201

Westbrook, A., van den Bosch, R., Maatta, J. I., Hofmans, L., Papadopetraki, D., Cools, R., et al. (2020). 'Dopamine promotes cognitive effort by biasing the benefits versus costs of cognitive work. *Science* 367, 1362–1366. doi:10.1126/science.aaz5891

Whitfield-Gabrieli, S., and Nieto-Castanon, A. (2012). Conn: a functional connectivity toolbox for correlated and anticorrelated brain networks. *Brain Connect.* 2, 125–141. doi:10.1089/brain.2012.0073

Widiger, T. A., and Samuel, D. B. (2005). Diagnostic categories or dimensions? A question for the diagnostic and statistical manual of mental disorders--fifth edition. *J. Abnorm Psychol.* 114, 494–504. doi:10.1037/0021-843X.114.4.494

Yechiam, E., and Zeif, D. (2022). The effect of methylphenidate and mixed amphetamine salts on cognitive reflection: a field study. *Psychopharmacol. Berl.* 239, 455–463. doi:10.1007/s00213-021-06016-1

frontiers | Frontiers in Neuroscience

TYPE Original Research
PUBLISHED 24 July 2024
DOI 10.3389/fnins.2024.1378841

OPEN ACCESS

EDITED BY
Karen K. Szumlinski,
University of California, Santa Barbara,
United States

REVIEWED BY
Ignacio Carrera,
University of the Republic, Uruguay
Dalibor Sames,
Columbia University, United States

*CORRESPONDENCE
Tanya Calvey
✉ drcalvey@gmail.com

RECEIVED 30 January 2024
ACCEPTED 10 July 2024
PUBLISHED 24 July 2024

CITATION
Govender D, Moloko L, Papathanasopoulos M, Tumba N, Owen G and Calvey T (2024) Ibogaine administration following repeated morphine administration upregulates myelination markers 2′, 3′-cyclic nucleotide 3′-phosphodiesterase (CNP) and myelin basic protein (MBP) mRNA and protein expression in the internal capsule of Sprague Dawley rats. *Front. Neurosci.* 18:1378841. doi: 10.3389/fnins.2024.1378841

Ibogaine administration following repeated morphine administration upregulates myelination markers 2′, 3′-cyclic nucleotide 3′-phosphodiesterase (CNP) and myelin basic protein (MBP) mRNA and protein expression in the internal capsule of Sprague Dawley rats

Demi Govender[1,2], Leila Moloko[1], Maria Papathanasopoulos[3], Nancy Tumba[3], Gavin Owen[3] and Tanya Calvey[2,4]*

[1]School of Anatomical Sciences, Faculty of Health Sciences, University of the Witwatersrand, Johannesburg, South Africa, [2]Department of Human Biology, Faculty of Health Sciences, University of Cape Town, Cape Town, South Africa, [3]HIV Pathogenesis Research Unit, Faculty of Health Sciences, University of the Witwatersrand, Johannesburg, South Africa, [4]Neuroscience Institute, University of Cape Town, Cape Town, South Africa

Ibogaine is a psychedelic alkaloid being investigated as a possible treatment for opioid use disorder. Ibogaine has a multi-receptor profile with affinities for mu and kappa opioid as well as NMDA receptors amongst others. Due to the sparsity of research into ibogaine's effects on white matter integrity and given the growing evidence that opioid use disorder is characterized by white matter pathology, we set out to investigate ibogaine's effects on two markers of myelination, 2′, 3′-cyclic nucleotide 3′-phosphodiesterase (CNP) and myelin basic protein (MBP). Fifty Sprague Dawley rats were randomly assigned to five experimental groups of $n = 10$; (1) a saline control group received daily saline injections for 10 days, (2) a morphine control group received escalating morphine doses from 5 to 15 mg/kg over 10 days, (3) an ibogaine control group that received 10 days of saline followed by 50 mg/kg ibogaine hydrochloride, (4) a combination morphine and ibogaine group 1 that received the escalating morphine regime followed by 50 mg/kg ibogaine hydrochloride and (5) a second combination morphine and ibogaine group 2 which followed the same morphine and ibogaine regimen yet was terminated 72 h after administration compared to 24 h in the other groups. White matter from the internal capsule was dissected and qPCR and western blotting determined protein and gene expression of CNP and MBP. Morphine upregulated CNPase whereas ibogaine alone had no effect on CNP mRNA or protein expression. However, ibogaine administration following repeated morphine administration had an immediate effect by increasing CNP mRNA expression. This effect diminished after 72 h and resulted in a highly significant upregulation of CNPase protein at 72 h post administration. Ibogaine administration alone significantly upregulated protein expression yet downregulated MBP mRNA expression. Ibogaine administration following repeated morphine administration significantly upregulated MBP

mRNA expression which increased at 72 h post administration resulting in a highly significant upregulation of MBP protein expression at 72 h post administration. These findings indicate that ibogaine is able to upregulate genes and proteins involved in the process of remyelination following opioid use and highlights an important mechanism of action of ibogaine's ability to treat substance use disorders.

KEYWORDS

ibogaine, psychedelic medicine, white matter, opioid use disorder, oligodendrocytes

1 Introduction

Opioids continue to be the group of substances with the highest contribution to severe drug-related harm, including fatal overdoses (United Nations Office on Drugs and Crime, 2023). An estimated 60 million people engaged in non-medical opioid use in 2021. Opioids remain the leading cause of deaths from fatal overdoses. Opioids accounted for nearly 70% of the 128,000 deaths attributed to drug use disorders in 2019. Opioid use disorders (OUDs) also accounted for the majority (71% of the 18 million healthy years) of life lost owing to premature death and disability in 2019 (United Nations Office on Drugs and Crime, 2023).

Ibogaine is the primary alkaloid in *Tabernathe iboga* root bark and may have anti-addictive effects that lead to reduced drug cravings, decreased symptoms of withdrawal, and prevention of relapse (Maisonneuve et al., 1991; Sheppard, 1994; Alper et al., 1999; Mash et al., 2000, 2018; Parker and Siegel, 2001; Schenberg et al., 2014; Barsuglia et al., 2018; Calvey and Howells, 2018). Ibogaine undergoes extensive first-pass metabolism to noribogaine (the principle metabolite) by cytochrome P4502D6 in the gut wall and liver following oral administration. Ibogaine is cleared from the blood within 24 h (t1/2 = 4–6 h) depending on CYP2D6 genotype. Noribogaine, on the other hand, is eliminated over 5–7 days (t1/2 = 24–30 h; Mash, 2023).

The mechanisms of action of ibogaine continue to be explored but likely result from its multiple receptor affinities and polypharmacology. Ibogaine inhibits transport of serotonin and dopamine and is a serotonin reuptake blocker. It is a non-competitive inhibitor on nicotinic receptors such as the ganglionic and alpha-3 beta-4 subtype, a partial agonist of mu and kappa opioid receptors, and an NMDA channel blocker (Mash, 2023). Noribogaine binds to the serotonin transporter with a higher affinity (Villalba et al., 2024) and is a weak mu opioid receptor antagonist. Ibogaine is able to produce a neuroadaptive effect on endogenous opioid systems which reverses opioid tolerance (Barsuglia et al., 2018; Calvey and Howells, 2018; Corkery, 2018). Both ibogaine and noribogaine modulate the analgesic effect and physical tolerance to morphine (Calvey and Howells, 2018; Mash, 2023). Further, ibogaine possesses an opiate replacement mechanism of action as reported for compounds such as methadone possibly due to its agonism on the mu opioid receptor, however, neither ibogaine nor noribogaine produce signs and symptoms of opioid intoxication in opioid naïve persons (Mash et al., 1995; Zubaran et al., 1999; Baumann et al., 2001a,b; Barsuglia et al., 2018; Corkery, 2018).

We have conducted research on mechanisms of action of ibogaine for several years. Findings from our lab indicate that ibogaine HCl affects gene and protein expression in proteins related to substance use disorders. For example, ibogaine HCl downregulates the glutamate ionotropic receptor AMPA subunit 1 (GRIA1; Calvey et al., 2019a,b) and upregulates histone deacetylase 2,3 (HDAC2,3) which is involved in epigenetic mechanisms diminishing opioid tolerance (Moloko et al., 2019).

Of particular interest is the role of white matter on the pathology of SUDs and opioid addiction. Oligodendrocytes have been understudied with regards to drug abuse and its effects (Miguel-Hidalgo, 2018) but the effect of opioid addiction is associated with demyelination (Liu et al., 2013; Fan et al., 2018). Upadhyay et al. (2010) showed decreased anisotropy of white matter tracts specifically in the amygdala-specific tracts which suggests decreased white matter tract connectivity in brains affected by opioid addiction. This further suggests that opioid addiction causes demyelination. There are two myelin markers that have commonly been used to assess the amount of myelin present in a sample: myelin basic protein (MBP) and 2′, 3′-cyclic nucleotide 3′-phosphodiesterase (CNP) protein. Changes in expression and abundance of these proteins can be used as early markers for increased or decreased myelin (Lindner et al., 2008; Oberoi et al., 2019).

Myelin basic protein (MBP) is the second most abundant myelin sheath protein and has four main isoforms which are 21.5, 18.5, 17, and 14 kDa (Akiyama et al., 2002). It compromises 30% of the total myelin protein and is a structural protein that is essential for CNS myelin (Boggs, 2006). It is bound to the cytosolic membrane of the oligodendrocytes between the layers of cells. It is involved in the adhesion of the cytosolic surface of the myelin sheath layers (De Vries et al., 1997; Boggs, 2006). Therefore, its main function is adhesion for the myelin sheath formation and has a critical role in myelination or remyelination. CNPase is an enzyme and structural protein present in the cytoplasm of oligodendrocytes that catalyzes the hydrolysis of 2′,3′-cyclic nucleotides (Verrier et al., 2013). It is utilized during the early stages of oligodendrocyte differentiation and has been associated with compacting the myelin layers on axons as it is found on the outer layers of the cells (De Vries et al., 1997; Maier et al., 2008).

Very little is known about ibogaine's effect on white matter or its role in de- or remyelination. The pharmacology of ibogaine and noribogaine suggests potential to increase white matter. Ibogaine increases BDNF and GDNF, which has been shown to have neuroplastic effects in addiction (Carnicella and Ron, 2009; Marton et al., 2019). Ibogaine and noribogaine are partial kappa opioid

receptor agonists (Glick et al., 1997; Glick and Maisonneuve, 1998; Alper, 2001; Maillet et al., 2015; Mash, 2023). The kappa opioid receptor has been shown to influence remyelination through oligodendrocytes (Du et al., 2016; Mei et al., 2016). The kappa opioid receptor is an important regulator of oligodendrocyte differentiation and remyelination. This regulation is achieved by controlling the oligodendrocyte precursor cells (OPCs) developing into oligodendrocytes (Du et al., 2016; Mei et al., 2016). The kappa opioid receptor is expressed on OPCs and in white matter such as the corpus callosum (Mei et al., 2016). Of interest is ibogaine's dual affinity for mu and kappa opioid receptors. Several dual kappa/mu opioid receptor agonists have produced strong antinociception effects in mice while lacking the typical dysphoric or addictive properties of pure kappa- or pure mu opioid receptor agonists, respectively (Khan et al., 2022). This highlights the inter-play between the functions of these two types of opioid receptors. Very little is known about this relationship in ibogaine or in the process of myelination.

We were, therefore, interested in observing ibogaine's effect on myelination markers. Preliminary findings indicated that ibogaine administration upregulated CNPase protein expression in rats (Govender et al., 2020). We expanded the study to include analysis of both protein and gene expression of CNPase and MBP in groups of Sprague Dawley rats. The experiment was designed to indicate effects of ibogaine and morphine administration as well as the temporal mechanisms of remyelination.

2 Materials and methods

2.1 Animal experiment

The ethical approval for this study was issued by the Animal Research Ethics Committee at the University of the Witwatersrand. Fifty male Sprague-Dawley (SD) rats, post-natal days 42–45, were on a 12-h light/dark cycle with food and water access as needed. All the animals were allowed a pre-treatment acclimatization period of 1 week. Two rats were housed in 1500U Techniplast Eurostandard Type IV S cages to prevent social isolation. Animals were assigned randomly to one of five groups and weighed daily, to calculate accurate dosages of ibogaine, morphine and saline. The animals were randomly divided into five groups of 10 rats: saline control, ibogaine only, morphine only, morphine ibogaine 1 test group and morphine ibogaine 2 test group with a 3-day waiting period before termination.

The saline control group ($n = 10$) received daily 1 ml/kg subcutaneous (s.c.) saline (0.9% sodium chloride, Adcocare, Adcock Ingram Critical Care) for 10 days. The rats were terminated 24 h following the last administration.

The morphine group ($n = 10$) was administered daily morphine (s.c.) for 10 days according to an escalated morphine protocol starting at 5 mg/kg for 48 h, 7.5 mg/kg for 72 h, 10 mg/kg for 72 h, and 15 mg/kg for 48 h. The rats were terminated 24 h following the last administration.

The ibogaine group ($n = 10$) received daily saline (0.9% sodium chloride, Adcocare, Adcock Ingram Critical Care) s.c. for 10 days and a 50 mg/kg intraperitoneal (i.p.) dose of ibogaine hydrochloride (HCl; Iboga Association, Cape Town, 98% purity) on day 11 (Rezvani et al., 1995; Glick et al., 1997). Ibogaine was homogenized in 1 ml/kg saline immediately before administration. The rats were terminated 24 h following the last administration.

The first morphine-ibogaine group ($n = 10$) received the escalated morphine regime for 10 days followed by a 50 mg/kg dose of ibogaine HCl on day 11. The rats were terminated 24 h following the last administration.

The second morphine-ibogaine group ($n = 10$) received the same treatment as the first morphine-ibogaine group except the rats were terminated 72 h following the last administration. The experiment was designed for morphine-ibogaine group 1 to evaluate myelination 24 h after treatment and for morphine-ibogaine group 2 to represent myelination at 72 h post treatment which has previously been found to be peak remyelination (Skripuletz et al., 2011).

Rats were decapitated with a sharp, well-maintained guillotine on the day of termination.

2.2 White matter tissue collection from the Sprague Dawley rat brains

Brains were carefully removed from the skulls immediately following decapitation, the white matter of the internal capsule was dissected from the brains on ice, transferred to separate 1.5 mL Eppendorf tubes and flash-frozen in liquid nitrogen prior to storage at −80°C for subsequent tissue processing.

2.3 White matter sample preparation for qPCR and western blotting

The frozen brain samples were homogenized with a homogenizer in QIAzol lysis reagent (Qiagen, Netherlands) to disrupt the cells. The QIAzol RNeasy Lipid Tissue Mini Kit (Qiagen, Netherlands) was used, following the manufacturer's instructions. The kit allowed for separation of the homogenate into three phases: RNA in the upper aqueous phase, DNA in the interphase and proteins in the lower organic phase. RNA was processed as per the kit's instructions.

The protein fractions from the Qiazol lysis homogenate were added to ice cold acetone in a 1:1 ratio, centrifuged at 14,500 rpm for 10 min and the supernatant was discarded. The pellet was homogenized with 5% sodium dodecyl sulfate (SDS).

2.4 Bicinchoninic acid assay of total proteins extracted from white matter

BCA assays are used to determine the concentration of total protein in a sample. This is done using a standard curve of Bovine Serum Albumin (BSA). The protein samples that were prepared in 5% SDS were measured by diluting them with 5% SDS to 1:5, 1:10, or 1:20 depending on their concentration as the highest limit of this standard curve was 2,000 µg/ml. The Pierce™ BCA Protein Assay kit (Thermoscientific, Massachusetts, USA) was used according to manufacturer instructions. Samples and the working reagent

were added in duplicates to the plate in a 1:8 ratio of sample to working reagent. The plate was incubated at 37°C for 30 min and the absorbance read on the Biorad iMark™ microplate reader (Microplate Manager Software, Bio-Rad) at 570 nm.

2.5 Reverse transcription of extracted mRNA from white matter into cDNA

The Superscript™ III First Strand Synthesis system for RT-PCR (Invitrogen, Massachusetts, USA) was used to convert 2 μg RNA from each sample into cDNA, according to manufacturer's instructions. Final cDNA concentrations were measured with a Nanodrop™ _ND-1000 (Massachusetts, USA) spectrometer and diluted with RNase free water to 100 ng/μl. Aliquots were stored at 4°C.

2.6 qPCR protocol and data analysis

Primers are listed in Table 1 and were manufactured by Inqaba Biotec™, Pretoria, South Africa. An annealing temperature gradient test revealed that all primer sets worked efficiently at an annealing temperature of 51°C.

Quantitative PCR was done in 10 μl reactions using the 2X Fast SYBR™ Green Master Mix (Thermofischer Scientific, Massachusetts, United States) with 6 μm each of the reverse and forward primers and 100 ng of cDNA per reaction. Reactions were setup in triplicate and included the corresponding beta actin housekeeping gene on the same 96-well plate. Negative, no DNA controls were also included in triplicates for both housekeeping gene and genes of interest. The Lightcycler® 96 instrument and software (Roche Diagnostics, Indianapolis, United States of America) were used to run the reactions and extract the Cq values for each curve. Thermal cycling conditions were as follows: 95°C for 10 min, 45 cycles of 95°C for 15 s, 51°C for 20 s, and 72°C for 30 s. A melting curve was included at the end of all runs, with the following parameters: 95°C for 10 s, 65°C for 1 min and 97°C for 1 s.

Delta delta Cq value was used to calculate the fold change with the following formula:

$$\begin{aligned} \Delta\Delta Cq &= (Cq_{\text{gene of interest}} - Cq_{\beta-\text{actin}})_{\text{test group}} \\ &- (Cq_{\text{gene of interest}} - Cq_{\beta-\text{actin}})_{\text{saline group}} \\ \textit{Fold change} &= E^{-\Delta\Delta Cq} \end{aligned}$$

2.7 SDS PAGE and western blot analysis of the white matter total protein from SD rats

Sodium dodecyl sulfate polyacrylamide gel electrophoresis was used to separate the proteins in the white matter tissue before being transferred onto a nitrocellulose membrane during western blotting.

Equal amounts of protein samples were resolved by Laemmli SDS–PAGE on a 15% Tris–glycine gel (Laemmli, 1970). Proteins resolved by SDS–PAGE were then transferred to nitrocellulose membrane using blotting buffer (50 mM Tris–HCl, 200 mM glycine, pH 8.3, containing 0.1% (w/v) SDS and 20% (v/v) methanol) at 35 V overnight at 4°C in the Hoefer™ T22 mighty small transfer tank. Membranes were blocked in TBS (0.2 M NaCl and 20 mM Tris–HCl, pH 7.4) containing 0.5% (w/v) BSA (TBS-BSA) for 1 h at room temperature. Membranes were then washed 3× with TBS (5 min/wash).

Polyclonal mouse antibodies raised against the proteins investigated in the study were used to detect their levels of expression in each rat brain sample. Membranes were separately incubated for an hour at RT with solutions of the primary antibodies, each diluted in TBS-BSA as follows: the Anti-CNPase antibody (Abcam) was diluted 1:10000, Anti-Myelin Basic Protein antibody (Biolegend) was diluted 1:2000, and Anti-beta Actin antibody (Abcam) was diluted 1:2500. The Anti-beta actin was diluted in TBST-BSA (TBS-BSA with 0.1% Tween-20). The membranes were then washed with TBST (3×, 10 min/wash) and incubated with goat anti-mouse IgG secondary antibody conjugated to horseradish peroxidase (Abcam) for 1 h at room temperature. The secondary antibody was diluted in TBS-BSA at 1:5000 to detect the Anti-CNP and Anti-MBP primary antibodies, and at 1:2500 to detect the Anti-β-actin primary antibody. After washing the membranes (2×, 10 min/wash with TBST, followed by 1× for 10 min with TBS) they were incubated with the Pierce™ ECL Western Blotting Substrate (Thermofischer Scientific) for 5 min. The blots were imaged in the ChemiDoc™ MP imaging system (Bio-Rad). and the bands analyzed for peak density using the QuantityOne™ version 4.6.9 Software Programme (Bio-Rad). The data was normalized using the following formula for all proteins:

$$\textit{Samples Protein expression} = \frac{\frac{\textit{sample densitometric measurement}}{\textit{loading control from membrane}}}{\frac{\textit{actin densitometric measurement}}{\textit{loading control of actin membrane}}}$$

Each sample was analyzed by western blotting in duplicate, and the protein expression values for each replicate were averaged.

2.8 Statistical analysis

All statistical analysis was done using GraphPad Prism 9.5.0 for Windows (GraphPad Software). Shapiro-Wilk tests were run to test for normality. ANOVA, unpaired *t*-tests and Mann-Whitney tests were run to determine significance between the groups dependent on the normality of the data. Outliers were determined at 1% using the ROUT method. The data is represented by mean ± standard error of the mean (SEM).

3 Results

3.1 Effects of ibogaine and morphine on CNP

Quantitative PCR was used to evaluate the changes in the mRNA expression of CNP in the white matter of the internal capsule of SD rats (Figure 1). Three outliers were found in this analysis: 1 in the morphine control, 1 in the ibogaine control

TABLE 1 Primers for genes used in qPCR (CNP, MBP, and beta actin).

Gene	Forward primer	Reverse primer
CNP (Hattori et al., 2014)	5′-CAA CAG GAT GTG GTG AGG A-3′	5′-CTG TCT TGG GTG TCA CAA AG-3′
MBP (Ray et al., 2003)	5′-TGA AAA CCC AGT AGT CCA C-3′	5′-GGA TTA AGA GAG GGT CTG C-3′
β-actin (Ray et al., 2003)	5′-TAC AAC CTC CTT GCA GCT CC-3′	5′-GGA TCT TCA TGA GGT AGT CTG TC-3′

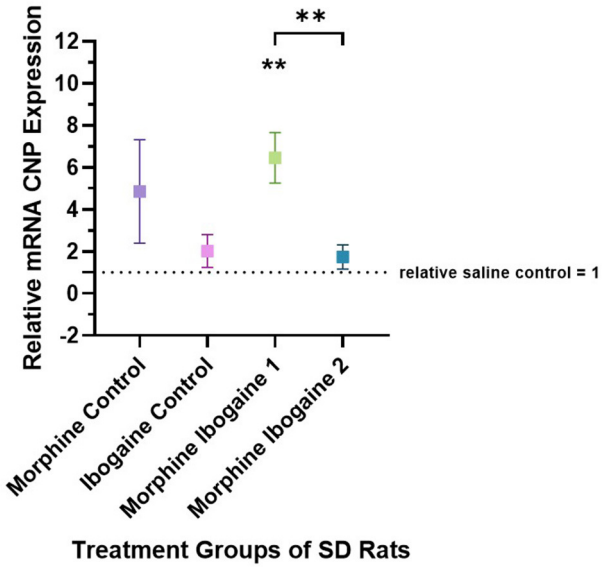

FIGURE 1
Relative mRNA expression of CNP gene in morphine control ($n = 6$), ibogaine control ($n = 8$), morphine ibogaine 1 ($n = 8$), and morphine ibogaine 2 ($n = 7$). There was an immediate increase in mRNA expression of CNP after ibogaine administration following repeated morphine administration. The data is presented as Mean ± SEM. **Shows significance ($p < 0.0021$) which is compared to saline.

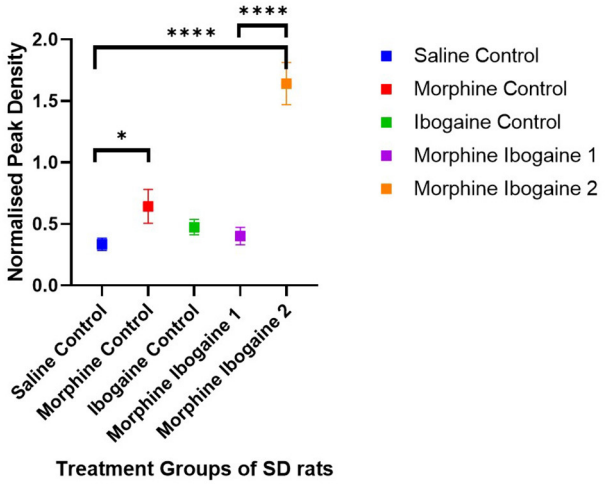

FIGURE 2
Peak density measurements of CNP protein expression of white matter in SD rats showed increased expression in morphine as well as morphine ibogaine group 2. Relative protein expression of CNP protein in saline control ($n = 8$), morphine control ($n = 7$), ibogaine control ($n = 9$), morphine ibogaine 1 ($n = 8$), and morphine-ibogaine 2 ($n = 9$). The data is presented as mean ± SEM. *Shows significance ($p < 0.05$). ****Shows significance ($p < 0.0001$).

and 1 in the morphine ibogaine 2 groups. These outliers were removed from the data set prior to analysis. Repeated morphine administration as well as ibogaine-only administration had no significant effect on CNP mRNA expression relative to the saline control. Although insignificant, morphine-only treatment trended toward increasing mRNA expression. Repeated morphine administration followed by ibogaine administration (morphine ibogaine 1) significantly increased CNP mRNA expression ($p = 0.001$). The morphine ibogaine 2 group showed no significant change in CNP mRNA expression relative to the saline control. This suggests that the immediate increase in CNP mRNA expression (24 h post administration) diminishes by 72 h post administration.

Densitometric measurements of the western blots showed that the protein expression levels of CNPase in the white matter of SD rats increased following repeated morphine administration relative to the saline control ($p = 0.046$; Figure 2). Ibogaine administration had no effect on CNPase protein expression. Repeated morphine administration followed by ibogaine had no immediate effect on CNPase (morphine ibogaine 1), however, after 72 h (morphine ibogaine 2), there was a highly significant increase in CNPase protein expression ($p = 0.0001$).

Taken together, morphine alone upregulated CNP protein expression. Ibogaine alone had no effect on mRNA or protein expression. However, in combination, there was an early upregulation of CNP mRNA that resulted in a highly significant upregulation of CNPase protein expression after 72 h.

3.2 Effects of ibogaine and morphine on MBP

Quantitative PCR was used to evaluate the changes in the mRNA expression of MBP in the white matter of the internal capsule of SD rats (Figure 3). Two outliers were found in this analysis: 1 in the ibogaine control and 1 in the morphine ibogaine 2 groups. These outliers were removed from the data set prior to analysis. Repeated morphine administration had no effect on MBP mRNA expression relative to the saline control. Ibogaine administration significantly decreased MBP mRNA expression relative to the saline control ($p < 0.0001$). The immediate effect of ibogaine administration following repeated morphine administration (morphine ibogaine 1) was to significantly increase MBP mRNA expression relative to the saline control ($p = 0.038$) and following 72 h (morphine ibogaine 2), this increase was

sustained and slightly elevated relative to the saline control ($p = 0.041$).

Western blots of the white matter from the SD rats showed two isomers of MBP with molecular weights of 21.5 and 18.5 kDa (Figure 4). There were no significant differences between the test groups for the 21.5 kDa isomer (Figure 4B). The following are group differences of the 18.5 kDa isomer (Figure 4A): Repeated morphine administration had no effect on MBP protein expression relative to the saline control. Ibogaine administration significantly increased MBP protein expression relative to the saline control ($p < 0.0021$). The immediate effect of ibogaine administration following repeated morphine administration (morphine ibogaine 1) was insignificant relative to the saline control, however, following 72 h (morphine ibogaine 2), there was a highly significant increase in MBP protein expression ($p < 0.0002$) that was elevated relative to the ibogaine.

Taken together, it appears that morphine administration alone had no effect on MBP mRNA or protein expression. Ibogaine alone significantly downregulated mRNA expression yet upregulated protein expression at the same time point. In combination (repeated morphine administration followed by ibogaine administration), there was an early upregulation of MBP mRNA expression that increased after 72 h resulting in upregulated protein expression at 72 h post administration.

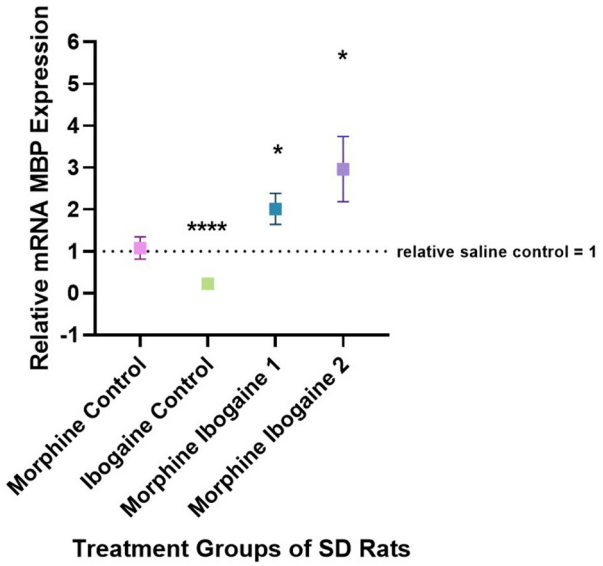

FIGURE 3
Relative mRNA expression of MBP gene in morphine control ($n = 7$), ibogaine control ($n = 8$), morphine ibogaine 1 ($n = 8$), and morphine-ibogaine 2 ($n = 7$). Relative mRNA expression of MBP is decreased after ibogaine administration and increased expression is seen in both morphine ibogaine treatment groups. The data is presented as mean ± SEM. *Shows significance ($p < 0.5$). ****Shows significance ($p < 0.0001$).

4 Discussion

Our results indicate that ibogaine alone had no effect on CNP mRNA or protein expression. Treatment with morphine-only trended toward increasing CNPase protein expression and significantly upregulated mRNA expression. In combination, ibogaine administration following repeated morphine administration had an immediate effect by significantly increasing CNP mRNA expression. This effect diminished after 72 h yet resulted in a highly significant upregulation of CNPase protein at 72 h post administration. Morphine-only treatment had no significant effect on MBP mRNA or protein expression. Ibogaine administration alone significantly upregulated protein expression yet downregulated MBP mRNA expression at the same time point. Ibogaine administration following repeated morphine administration significantly upregulated MBP mRNA expression which was elevated at 72 h post administration resulting in a highly significant upregulation of MBP protein expression at 72 h post administration.

These effects on both gene and protein expression of CNP and MBP suggest an interaction between morphine and ibogaine with regards to increasing myelination. It is also important to highlight that the interaction between morphine and ibogaine takes place after only 10 days of morphine administration. Although morphine does seem to upregulate CNPase, the combination of morphine and ibogaine augments that effect. This is shown when comparing the morphine-ibogaine groups 1 and 2 in both the mRNA and protein findings (Figures 1, 2). The mRNA is significantly upregulated 24 h post ibogaine administration (more so than the morphine control) which subsides by 72 h. The protein in morphine and ibogaine group 1 is not upregulated which, in contrast to the morphine group, confirms an interaction between morphine and ibogaine. At 72 h, CNPase shows a highly significant increase in the combination group. These findings replicate an early study we conducted where ibogaine alone had no effect on CNPase protein expression yet ibogaine administration following repeated morphine administration was significantly upregulated (Govender et al., 2020). With MBP (Figures 3, 4), the gene expression data shows a clear difference between the combination groups and the morphine- and ibogaine-only controls. The protein data is less clear but when comparing combination groups 1 and 2 in Figure 4, it is evident that combination morphine-ibogaine has less of an effect at 24 h than after 72 h. The initial mRNA upregulation results in a highly significant upregulation of the protein at 72 h which is what you would expect. Although the morphine results are unexpected and explained further in a subsequent paragraph, there is a definite augmenting effect of combination morphine and ibogaine that supersedes any substance on its own. A future experiment should include additional time points for all groups, especially morphine-only at 72 h to further clarify these findings, as this is the major limitation of the current study.

These findings also point to a possible intricate relationship between the mu and kappa opioid receptors and their roles in myelination as a possible mechanism behind the enhanced effect of the combination administration. Repeated morphine administration would downregulate the mu opioid receptor and lead to the recruitment of beta-arrestin (Valentino and Volkow, 2018). This downregulation could enhance the kappa opioid receptor mechanisms of action of ibogaine as ibogaine is a partial agonist at both kappa and mu opioid receptors. The upregulation of these myelin proteins is seen after 72 h indicating the effects are

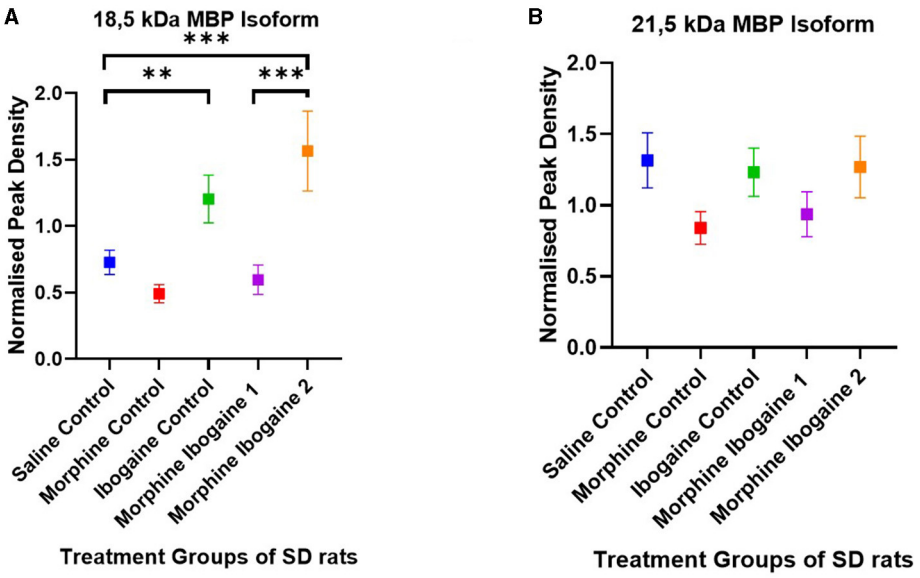

FIGURE 4
Peak density of MBP **(A)** 18.5 isoform and **(B)** 21.5 isoform in white matter of the SD rats in the saline control ($n = 8$), morphine control ($n = 6$), ibogaine control ($n = 9$), morphine ibogaine 1 ($n = 8$), and morphine-ibogaine 2 ($n = 9$). There was increased MBP expression of the 18.5 isoform after ibogaine administration and in the morphine ibogaine group 2. There was no significant differences in the peak density of the 21.5 isoform between the groups. **Shows significance ($p < 0.0021$). ***Shows significance ($p < 0.0002$).

likely due to the primary metabolite, noribogaine, with a higher kapa opioid receptor affinity (Maillet et al., 2015). Dynorphin, the endogenous kappa opioid receptor ligand, is known to be released rapidly after drug administration, activating CNS and peripheral kappa opioid receptors (Khan et al., 2022). This combined with the downregulation of mu opioid receptors could enhance ibogaine's effect on the kappa opioid receptor and, thus, its involvement in myelination.

We were also able to demonstrate an early upregulation of MBP mRNA following ibogaine as well as combined morphine-ibogaine administration leading to an upregulation of MBP protein. An early upregulation of CNP mRNA in the combination morphine-ibogaine group 1 led to a significant upregulation in CNPase at 72 h post administration. This is in line with previous studies showing CNP and MBP to be the earliest markers of remyelination with the myelin proteins being detected within 3–4 days (Skripuletz et al., 2011). Our results indicate that CNP and MBP mRNA are both upregulated early yet CNP diminishes by 72 h and MBP continues to elevate. The two isomers of MBP that were seen in the western blots were 21.5 and 18.5 kDa. The 18.5 kDa isomer was increased in the ibogaine-only and morphine-ibogaine 2 group. The 21.5 kDa isoform showed no significant changes in protein expression between the test groups. These results may indicate differing activation mechanisms of the two isomers as previous research has shown the 18.5 kDa isomer to be produced later in the remyelination process than the 21.5 kDa isoform (Harauz and Boggs, 2013). Another factor that may be involved in the timing of myelination markers following ibogaine administration which needs to be explored further is the differing effects of ibogaine and noribogaine. Ibogaine is eliminated by 24 h post-administration and noribogaine takes 5–7 days to be eliminated in humans (Mash, 2023) and both are eliminated by 24 h in the rat brain (Rodriguez et al., 2020). This may influence MBP gene expression. Further studies with either additional time points, direct administration of noribogaine, or intravenous administration of ibogaine (to decrease noribogaine formation) are required to explore this fully.

Further research is needed to identify ibogaine's exact mechanisms of action on the process of myelination yet likely involve ibogaine's influence on the mTOR signaling cascade (Ly et al., 2018), production of BDNF (Marton et al., 2019), and its affinity for the kappa opioid receptor (Du et al., 2016; Mei et al., 2016). Ibogaine also has a reversible voltage gated antagonistic effect on NMDA receptors (Popik et al., 1994; Mash, 2023). The NMDA receptors present on oligodendrocytes regulate myelination and axonal health (Saab et al., 2016). NMDA receptor activation may increase myelination and CNPase by increasing the cytosolic calcium and reactive oxygen species (Cavaliere et al., 2012). Due to ibogaine's voltage gating the cytosolic calcium will need to be at lower levels to activate the NOX-dependent generation of reactive oxygen species, which will activate the PI3K/AKT pathway (Cavaliere et al., 2012). The PI3K pathway promotes neural plasticity by activating mTOR. The sigma 1 receptor agonist affinity of ibogaine could also affect the oligodendrocyte CNPase activity, as the sigma 1 receptor regulates Ca^{2+} channels, which is important for CNPase activity and regulation of gene expression (Soriani and Kourrich, 2019).

The finding of morphine upregulating CNPase and having no effect on MBP was unexpected. We initially hypothesized that repeated morphine administration would downregulate both myelination markers as opioid addiction is known to decrease white matter integrity (Bora et al., 2012; Li et al., 2013; Fan et al., 2018). Bora et al. (2012) showed that longer drug use

correlated with increased white matter injury so a possible explanation could be that our administration regime was not long enough. Our administration protocol of 10 days, although adequate to facilitate neurobiological changes evident in the CNPase and combination morphine-ibogaine findings, does not represent a chronic morphine administration or opioid addiction model. It would be of great interest to the field to investigate these myelination markers in chronic morphine, conditioned-place preference or opioid self-administration models. The effects on myelination are likely to be augmented in the combination treatment groups and may show demyelination in the morphine-only groups. A recent study has shown morphine's effects on OPCs to be region specific whereby morphine-induced oligodendrogenesis occured specifically in the ventral tegmental area (Yalçin et al., 2024). Future research should, therefore, include additional white matter regions. These findings may also explain our differing results between morphine's effects on CNP vs. MBP. CNPase is an oligodendrocyte-related protein and MBP is only related to myelin which may be the reason we only see an increase in the morphine control with CNPase and not MBP. Maladaptive myelination in reward circuitry is propped by Yalçin et al. (2024) to represent a key neural substrate of pathological learning associated with OUD, suggesting myelination as a potential therapeutic target. This highlights the importance of ibogaine's role in remyelination.

There was a striking difference between ibogaine's effect on MBP protein vs. gene expression. The correlation between protein and mRNA expression is understudied with many conflicting results (Guo et al., 2008) and transcription factors would play a major role in the opposing findings. Sox2 has been identified as a crucial transcription factor for remyelination as it regulates OPC proliferation (Zhao et al., 2015; Zhang et al., 2018). Sox2 regulates OPC proliferation by increasing proliferation of the OPCs and inhibits their differentiation into mature oligodendrocytes (Zhao et al., 2015; Zhang et al., 2018). This would be essential for remyelination to occur. The transcription factors Olig1 and Olig2 have also been linked to remyelination (Wegener et al., 2015; Yang et al., 2017; Zhao et al., 2019). Another major transcription factor that is required for efficient remyelination and oligodendrocyte regeneration is Stat3 (Steelman et al., 2016). These factors should be investigated following ibogaine administration to fully understand these molecular relationships.

These findings indicate that ibogaine is able to upregulate genes and proteins involved in the process of remyelination and highlights an important mechanism of action of ibogaine's ability to repair brain injury (Cherian et al., 2024) and treat substance use disorders (Barsuglia et al., 2018; Mash et al., 2018; Mash, 2023). Future research should address ibogaine and noribogaine's effects on the mu and kappa opioid receptors as there is still disagreement in the literature regarding specific receptor affinities (Cameron et al., 2021; Mash, 2023). Experiments should be designed with chronic morphine and imaging protocols to uncover the full extent of the interaction between morphine and ibogaine and structural plasticity of white matter. These experiments may uncover ibogaine's mechanism of action in being able to treat opioid use disorders yet are also relevant for the numerous myelin-associated diseases such as stroke and multiple sclerosis.

Data availability statement

The raw data supporting the conclusions of this article will be made available by the authors, without undue reservation.

Ethics statement

The animal study was approved by Animal Research Ethics Committee at the University of the Witwatersrand. The study was conducted in accordance with the local legislation and institutional requirements.

Author contributions

DG: Formal analysis, Investigation, Methodology, Writing – original draft. LM: Investigation, Methodology, Writing – review & editing. MP: Resources, Writing – review & editing. NT: Formal analysis, Methodology, Supervision, Writing – review & editing. GO: Formal analysis, Methodology, Supervision, Writing – review & editing. TC: Conceptualization, Formal analysis, Funding acquisition, Investigation, Methodology, Project administration, Supervision, Writing – review & editing.

Funding

The author(s) declare financial support was received for the research, authorship, and/or publication of this article. Funding for this research was provided by grants held by TC from the International Society for Neurochemistry (ISN) and the National Research Foundation (NRF).

Conflict of interest

The authors declare that the research was conducted in the absence of any commercial or financial relationships that could be construed as a potential conflict of interest.

Publisher's note

References

Akiyama, K., Ichinose, S., Omori, A., Sakurai, Y., and Asou, H. (2002). Study of expression of myelin basic proteins (MBPs) in developing rat brain using a novel antibody reacting with four major isoforms of MBP. *J. Neurosci. Res.* 68, 19–28. doi: 10.1002/jnr.10188

Alper, K. R. (2001). Ibogaine: a review. *Alkaloids Chem. Biol.* 56, 1–38. doi: 10.1016/s0099-9598(01)56005-8

Alper, K. R., Lotsof, H. S., Frenken, G. M., Luciano, D. J., and Bastiaans, J. (1999). Treatment of acute opioid withdrawal with ibogaine. *Am. J. Addict.* 8, 234–242. doi: 10.1080/105504999305848

Barsuglia, J. P., Polanco, M., Palmer, R., Malcolm, B. J., Kelmendi, B., and Calvey, T. (2018). A case report SPECT study and theoretical rationale for the sequential administration of ibogaine and 5-MeO-DMT in the treatment of alcohol use disorder. *Progr. Brain Res.* 242, 121–158. doi: 10.1016/bs.pbr.2018.08.002

Baumann, M. H., Pablo, J., Ali, S. F., Rothman, R. B., and Mash, D. C. (2001a). Comparative neuro pharmacology of ibogaine and its O-desmethyl metabolite, noribogaine. *Alkaloids Chem. Biol.* 56, 79–113. doi: 10.1016/S0099-9598(01)56009-5

Baumann, M. H., Rothman, R. B., Pablo, J. P., and Mash, D. C. (2001b). *In vivo* neurobiological effects of ibogaine and its O-desmethyl metabolite, 12-hydroxyibogamine (noribogaine), in rats. *J. Pharmacol. Exp. Ther.* 297, 531–539.

Boggs, J. M. (2006). Myelin basic protein: a multifunctional protein. *Cell. Mol. Life Sci.* 63, 1945–1961. doi: 10.1007/s00018-006-6094-7

Bora, E., Yücel, M., Fornito, A., Pantelis, C., Harrison, B. J., Cocchi, L., et al. (2012). White matter microstructure in opiate addiction. *Addict. Biol.* 17, 141–148. doi: 10.1111/j.1369-1600.2010.00266.x

Calvey, T., and Howells, F. M. (2018). An introduction to psychedelic neuroscience. *Progr. Brain Res.* 242, 1–23. doi: 10.1016/bs.pbr.2018.09.013

Calvey, T., Woolf, J., and Dickens, C. (2019b). Ibogaine downregulates CREB1 and GRIA1 mRNA expression in the dorsal hippocampus. *J. Neurochem.* 150, 93–93.

Calvey, T., Woolf, J., Dickens, C., Polanco, M., Palmer, R., Malcolm, B., et al. (2019a). Combination psychedelic therapy to treat substance use disorders—insights from human and rodent studies. *J. Anat.* 184, P1–N5.

Cameron, L. P., Tombari, R. J., Lu, J., Pell, A. J., Hurley, Z. Q., Ehinger, Y., et al. (2021). A non-hallucinogenic psychedelic analogue with therapeutic potential. *Nature* 589, 474–479. doi: 10.1038/s41586-020-3008-z

Carnicella, S., and Ron, D. (2009). GDNF—a potential target to treat addiction. *Pharmacol. Ther.* 12:1. doi: 10.1016/j.pharmthera.2008.12.001

Cavaliere, F., Urra, O., Alberdi, E., and Matute, C. (2012). Oligodendrocyte differentiation from adult multipotent stem cells is modulated by glutamate. *Cell Death Dis* 3, e268–e268. doi: 10.1038/cddis.2011.144

Cherian, K. N., Keynan, J. N., Anker, L., Faerman, A., Brown, R. E., Shamma, A., et al. (2024). Magnesium-ibogaine therapy in veterans with traumatic brain injuries. *Nat. Med.* 2024, 1–9. doi: 10.1038/s41591-023-02705-w

Corkery, J. M. (2018). Ibogaine as a treatment for substance misuse: potential benefits and practical dangers. *Progr. Brain Res.* 242, 217–257. doi: 10.1016/bs.pbr.2018.08.005

De Vries, H., De Jonge, J. C., Schrage, C., Van Der Haar, M. E., and Hoekstra, D. (1997). Differential and cell development-dependent localization of myelin mRNAs in oligodendrocytes. *J. Neurosci. Res.* 47, 479–488. doi: 10.1002/(SICI)1097-4547(19970301)47:5<479::AID-JNR3>3.0.CO;2-E

Du, C., Duan, Y., Wei, W., Cai, Y., Chai, H., Lv, J., et al. (2016). Kappa opioid receptor activation alleviates experimental autoimmune encephalomyelitis and promotes oligodendrocyte-mediated remyelination. *Nat. Commun.* 7:11120. doi: 10.1038/ncomms11120

Fan, W., Wang, H., Zhang, Y., Loh, H. H., Law, P. Y., and Xu, C. (2018). Morphine regulates adult neurogenesis and contextual memory extinction via the PKCε/Prox1 pathway. *Neuropharmacology* 141, 126–138. doi: 10.1016/j.neuropharm.2018.08.031

Glick, S. D., and Maisonneuve, I. M. (1998). Mechanisms of antiaddictive actions of ibogaine. *Ann. N. Y. Acad. Sci.* 844, 214–226.

Glick, S. D., Maisonneuve, I. M., and Pearl, S. M. (1997). Evidence for roles of κ-opioid and NMDA receptors in the mechanism of action of ibogaine. *Brain Res.* 749, 340–343. doi: 10.1016/S0006-8993(96)01414-X

Govender, D., Woolf, J., Meulenberg, N., Owen, G., and Calvey, T. (2020). "Effects of ibogaine on CNPase in the white matter tissue of rats," in *Southern African Neuroscience Society Virtual Symposium*. Available online at: https://youtu.be/n38TY-MkKKA (accessed November 20, 2020).

Guo, Y., Xiao, P., Lei, S., Deng, F., Xiao, G. G., Liu, Y., et al. (2008). How is mRNA expression predictive for protein expression? A correlation study on human circulating monocytes. *Acta Biochim. Biophys. Sin.* 40, 426–436. doi: 10.1111/j.1745-7270.2008.00418.x

Harauz, G., and Boggs, J. M. (2013). Myelin management by the 18.5-kDa and 21.5-kDa classic myelin basic protein isoforms. *J. Neurochem.* 2013:12195. doi: 10.1111/jnc.12195

Hattori, T., Shimizu, S., Koyama, Y., Emoto, H., Matsumoto, Y., Kumamoto, N., et al. (2014). DISC1 (Disrupted-in-Schizophrenia-1) regulates differentiation of oligodendrocytes. *PLoS ONE* 9:e88506. doi: 10.1371/journal.pone.0088506

Khan, M. I. H., Sawyer, B. J., Akins, N. S., and Le, H. V. (2022). A systematic review on the kappa opioid receptor and its ligands: new directions for the treatment of pain, anxiety, depression, and drug abuse. *Eur. J. Med. Chem.* 243:114785. doi: 10.1016/j.ejmech.2022.114785

Laemmli, U. K. (1970). Cleavage of structural proteins during the assembly of the head of bacteriophage T4. *Nature* 227, 680–685. doi: 10.1038/227680a0

Li, W., Li, Q., Zhu, J., Qin, Y., Zheng, Y., Chang, H., et al. (2013). White matter impairment in chronic heroin dependence: a quantitative DTI study. *Brain Res.* 1531, 58–64. doi: 10.1016/j.brainres.2013.07.036

Lindner, M., Heine, S., Haastert, K., Garde, N., Fokuhl, J., Linsmeier, F., et al. (2008). Sequential myelin protein expression during remyelination reveals fast and efficient repair after central nervous system demyelination. *Neuropathol. Appl. Neurobiol.* 34, 105–114. doi: 10.1111/j.1365-2990.2007.00879.x

Liu, L. W., Lu, J., Wang, X. H., Fu, S. K., Li, Q., and Lin, F. Q. (2013). Neuronal apoptosis in morphine addiction and its molecular mechanism. *Int. J. Clin. Exp. Med.* 6, 540–545.

Ly, C., Greb, A. C., Cameron, L. P., Wong, J. M., Barragan, E. V., Wilson, P. C., et al. (2018). Psychedelics promote structural and functional neural plasticity. *Cell Rep.* 23, 3170–3182. doi: 10.1016/j.celrep.2018.05.022

Maier, O., Hoekstra, D., and Baron, W. (2008). Polarity development in oligodendrocytes: sorting and trafficking of myelin components. *J. Mol. Neurosci.* 35, 35–53. doi: 10.1007/s12031-007-9024-8

Maillet, E. L., Milon, N., Heghinian, M. D., Fishback, J., Schürer, S. C., Garamszegi, N., et al. (2015). Noribogaine is a G-protein biased κ-opioid receptor agonist. *Neuropharmacology* 99, 675–688. doi: 10.1016/j.neuropharm.2015.08.032

Maisonneuve, I. M., Keller, R. W. Jr., and Glick, S. D. (1991). Interactions between ibogaine, a potential anti-addictive agent, and morphine: an *in vivo* microdialysis study. *Eur. J. Pharmacol.* 199, 35–42. doi: 10.1016/0014-2999(91)90634-3

Marton, S., González, B., Rodríguez-Bottero, S., Miquel, E., Martínez-Palma, L., Pazos, M., et al. (2019). Ibogaine administration modifies GDNF and BDNF expression in brain regions involved in mesocorticolimbic and nigral dopaminergic circuits. *Front. Pharmacol.* 10, 1–13. doi: 10.3389/fphar.2019.00193

Mash, D. C. (2023). *Psychedelics as Psychiatric Medicine: Ibogaine* (Oxford: Oxford Psychiatry Library), 83.

Mash, D. C., Duque, L., Page, B., and Allen-Ferdinand, K. (2018). Ibogaine detoxification transitions opioid and cocaine abusers between dependence and abstinence: clinical observations and treatment outcomes. *Front. Pharmacol.* 9:529. doi: 10.3389/fphar.2018.00529

Mash, D. C., Kovera, C. A., Pablo, J., Tyndale, R. F., Ervin, F. D., Williams, I. C., et al. (2000). Ibogaine: complex pharmacokinetics, concerns for safety, and preliminary efficacy measures. *Ann. N. Y. Acad. Sci.* 914, 394–401. doi: 10.1111/j.1749-6632.2000.tb05213.x

Mash, D. C., Staley, J. K., Pablo, J. P., Holohean, A. M., Hackman, J. C., and Davidoff, R. A. (1995). Properties of ibogaine and its principal metabolite (12-hydroxyibogamine) at the MK-801 binding site of the NMDA receptor complex. *Neurosci. Lett.* 192, 53–56. doi: 10.1016/0304-3940(95)11608-Y

Mei, F., Mayoral, S. R., Nobuta, H., Wang, F., Desponts, C., Lorrain, D. S., et al. (2016). Identification of the kappa-opioid receptor as a therapeutic target for oligodendrocyte remyelination. *J. Neurosci.* 36, 7925–7935. doi: 10.1523/JNEUROSCI.1493-16.2016

Miguel-Hidalgo, J. J. (2018). Molecular neuropathology of astrocytes and oligodendrocytes in alcohol use disorders. *Front. Mol. Neurosci.* 2018:78. doi: 10.3389/fnmol.2018.00078

Moloko, L., Woolf, J., Dickens, C., and Calvey, T. (2019). *The Effects of Ibogaine on Histone Deacetylase in the Dorsal Hippocampus During Morphine Withdrawal* (BHSc Honours in Neuroscience Thesis). University of the Witwatersrand, Johannesburg, South Africa.

Oberoi, R., Chu, T., Mellen, N., Jagadapillai, R., Ouyang, H., Devlin, L. A., et al. (2019). Diverse changes in myelin protein expression in rat brain after perinatal methadone exposure. *Acta Neurobiol. Exp.* 79, 367–373. doi: 10.21307/ane-2019-034

Parker, L. A., and Siegel, S. (2001). Modulation of the effects of rewarding drugs by ibogaine. *Alkaloids Chem. Biol.* 56, 211–225. doi: 10.1016/s0099-9598(01)56015-0

Popik, P., Layer, R. T., and Skolnick, P. (1994). The putative anti-addictive drug ibogaine is a competitive inhibitor of [3H]MK-801 binding to the NMDA receptor complex. *Psychopharmacology* 114, 672–674. doi: 10.1007/BF02245000

Ray, S. K., Matzelle, D. D., Sribnick, E. A., Guyton, M. K., Wingrave, J. M., and Banik, N. L. (2003). Calpain inhibitor prevented apoptosis and maintained transcription of proteolipid protein and myelin basic protein genes in rat spinal cord injury. *J. Chem. Neuroanat.* 26, 119–124. doi: 10.1016/S0891-0618(03)00044-9

Rezvani, A. H., Overstreet, D. H., and Leef, Y. W. (1995). Attenuation of alcohol intake by Ibogaine in three strains of alcohol-preferring rats. *Pharmacol. Biochem. Behav.* 52, 615–620. doi: 10.1016/0091-3057(95)00152-M

Rodriguez, P., Urbanavicius, J., Prieto, J. P., Fabius, S., Reyes, A. L., Havel, V., et al. (2020). A single administration of the atypical psychedelic ibogaine or its metabolite noribogaine induces an antidepressant-like effect in rats. *ACS Chem. Neurosci.* 11, 1661–1672. doi: 10.1021/acschemneuro.0c00152

Saab, A. S., Tzvetavona, I. D., Trevisiol, A., Baltan, S., Dibaj, P., Kusch, K., et al. (2016). Oligodendroglial NMDA receptors regulate glucose import and axonal energy metabolism. *Neuron* 91, 119–132. doi: 10.1016/j.neuron.2016.05.016

Schenberg, E. E., Comis, M. A. D. C., Chaves, B. R., and Silveira, D. X. D. (2014). Treating drug dependence with the aid of ibogaine: a retrospective study. *J. Psychopharmacol.* 28, 993–1000. doi: 10.1177/0269881114552713

Sheppard, S. G. (1994). A preliminary investigation of ibogaine: case reports and recommendations for further study. *J. Subst. Abuse Treat.* 11, 379–385. doi: 10.1016/0740-5472(94)90049-3

Skripuletz, T., Gudi, V., Hackstette, D., and Stangel, M. (2011). De- and remyelination in the CNS white and grey matter induced by cuprizone: the old, the new, and the unexpected. *Histol. Histopathol.* 26, 1585–1597. doi: 10.14670/HH-26.1585

Soriani, O., and Kourrich, S. (2019). The sigma-1 receptor: when adaptive regulation of cell electrical activity contributes to stimulant addiction and cancer. *Front. Neurosci.* 2019:1186. doi: 10.3389/fnins.2019.01186

Steelman, A. J., Zhou, Y., Koito, H., Kim, S. J., Payne, H. R., Lu, Q. R., et al. (2016). Activation of oligodendroglial Stat3 is required for efficient remyelination. *Neurobiol. Dis.* 91, 336–346. doi: 10.1016/j.nbd.2016.03.023

United Nations Office on Drugs and Crime (2023). *World Drug Report*. Available online at: https://www.unodc.org/unodc/en/data-and-analysis/world-drug-report-2023.html (accessed December, 2023).

Upadhyay, J., Maleki, N., Potter, J., Elman, I., Rudrauf, D., Knudsen, J., et al. (2010). Alterations in brain structure and functional connectivity in prescription opioid-dependent patients. *Brain* 133, 2098–2114. doi: 10.1093/brain/awq138

Valentino, R. J., and Volkow, N. D. (2018). Untangling the complexity of opioid receptor function. *Neuropsychopharmacology* 43, 2514–2520. doi: 10.1038/s41386-018-0225-3

Verrier, J. D., Jackson, T. C., Gillespie, D. G., Janesko-Feldman, K., Bansal, R., Goebbels, S., et al. (2013). Role of CNPase in the oligodendrocytic extracellular 2′,3′-cAMP-adenosine pathway. *GLIA* 61, 1595–1606. doi: 10.1002/glia.22523

Villalba, S., González, B., Junge, S., Bernardi, A., González, J., Fagúndez, C., et al. (2024). 5-HT2A receptor knockout mice show sex-dependent differences following acute noribogaine administration. *Int. J. Mol. Sci.* 25:687. doi: 10.3390/ijms25020687

Wegener, A., Deboux, C., Bachelin, C., Frah, M., Kerninon, C., Seilhean, D., et al. (2015). Gain of Olig2 function in oligodendrocyte progenitors promotes remyelination. *Brain* 138, 120–135. doi: 10.1093/brain/awu375

Yalçin, B., Pomrenze, M. B., Malacon, K., Drexler, R., Rogers, A. E., Shamardani, K., et al. (2024). Myelin plasticity in the ventral tegmental area is required for opioid reward. *Nature* 7, 1–9. doi: 10.1038/s41586-024-07525-7

Yang, T., Zheng, Q., Wang, S., Fang, L., Liu, L., Zhao, H., et al. (2017). Effect of catalpol on remyelination through experimental autoimmune encephalomyelitis acting to promote Olig1 and Olig2 expressions in mice. *BMC Complement. Altern. Med.* 17, 1–15. doi: 10.1186/s12906-017-1642-2

Zhang, S., Zhu, X., Gui, X., Croteau, C., Song, L., Xu, J., et al. (2018). Sox2 is essential for oligodendroglial proliferation and differentiation during postnatal brain myelination and CNS remyelination. *J. Neurosci.* 38, 1802–1820. doi: 10.1523/JNEUROSCI.1291-17.2018

Zhao, C., Ma, D., Zawadzka, M., Fancy, S. P. J., Elis-Williams, L., Bouvier, G., et al. (2015). Sox2 sustains recruitment of oligodendrocyte progenitor cells following CNS demyelination and primes them for differentiation during remyelination. *J. Neurosci.* 35, 11482–11499. doi: 10.1523/JNEUROSCI.3655-14.2015

Zhao, H., Gao, X. Y., Liu, Z. H., Lin, J. W., Wang, S. P., Wang, D. X., et al. (2019). Effects of the transcription factor Olig1 on the differentiation and remyelination of oligodendrocyte precursor cells after focal cerebral ischemia in rats. *Mol. Med. Rep.* 20, 4603–4611. doi: 10.3892/mmr.2019.10713

Zubaran, C., Shoaib, M., Stolerman, I. P., Pablo, J., and Mash, D. C. (1999). Noribogaine generalization to the ibogaine stimulus: correlation with noribogaine concentration in rat brain. *Neuropsychopharmacology* 21, 119–126. doi: 10.1016/S0893-133X(99)00003-2

frontiers | Frontiers in Pharmacology

TYPE Systematic Review
PUBLISHED 02 August 2024
DOI 10.3389/fphar.2024.1424146

OPEN ACCESS

EDITED BY
Nouria Lakhdar-Ghazal,
Mohammed V University, Morocco

REVIEWED BY
Ahmed Elsayed Noreldin,
Damanhour University, Egypt
Yuxiang Fei,
China Pharmaceutical University, China

*CORRESPONDENCE
Jian Zheng,
zhengjian@cmu.edu.cn

RECEIVED 27 April 2024
ACCEPTED 03 July 2024
PUBLISHED 02 August 2024

CITATION
Yang J, Yu B and Zheng J (2024), Natural herbal extract roles and mechanisms in treating cerebral ischemia: A systematic review. *Front. Pharmacol.* 15:1424146. doi: 10.3389/fphar.2024.1424146

Natural herbal extract roles and mechanisms in treating cerebral ischemia: A systematic review

Jiashuo Yang, Bo Yu and Jian Zheng*

Department of Neurosurgery, Shengjing Hospital of China Medical University, Shenyang, China

Background: Stroke has been the focus of medical research due to its serious consequences and sequelae. Among the tens of millions of new stroke patients every year, cerebral ischemia patients account for the vast majority. While cerebral ischemia drug research and development is still ongoing, most drugs are terminated at preclinical stages due to their unacceptable toxic side effects. In recent years, natural herbs have received considerable attention in the pharmaceutical research and development field due to their low toxicity levels. Numerous studies have shown that natural herbs exert actions that cannot be ignored when treating cerebral ischemia.

Methods: We reviewed and summarized the therapeutic effects and mechanisms of different natural herbal extracts on cerebral ischemia to promote their application in this field. We used keywords such as "natural herbal extract," "herbal medicine," "Chinese herbal medicine" and "cerebral ischemia" to comprehensively search PubMed, ScienceDirect, ScienceNet, CNKI, and Wanfang databases, after which we conducted a detailed screening and review strategy.

Results: We included 120 high-quality studies up to 10 January 2024. Natural herbal extracts had significant roles in cerebral ischemia treatments *via* several molecular mechanisms, such as improving regional blood flow disorders, protecting the blood-brain barrier, and inhibiting neuronal apoptosis, oxidative stress and inflammatory responses.

Conclusion: Natural herbal extracts are represented by low toxicity and high curative effects, and will become indispensable therapeutic options in the cerebral ischemia treatment field.

KEYWORDS

natural herbal extract, herbs, cerebral ischemia, blood-brain barrier, flavonoids

1 Introduction

Cerebral ischemia (CI) is a complex disease in clinical medicine. To put it simply, due to various reasons, blood in brain tissue cannot support normal metabolism and function, with subsequent symptoms collectively referred to as CI. Worldwide, morbidity and mortality rates due to CI are very high. The disease is characterized by several etiologies, changeable conditions, and serious consequences, which exert extremely heavy burdens on patients and their families. The National Institutes of

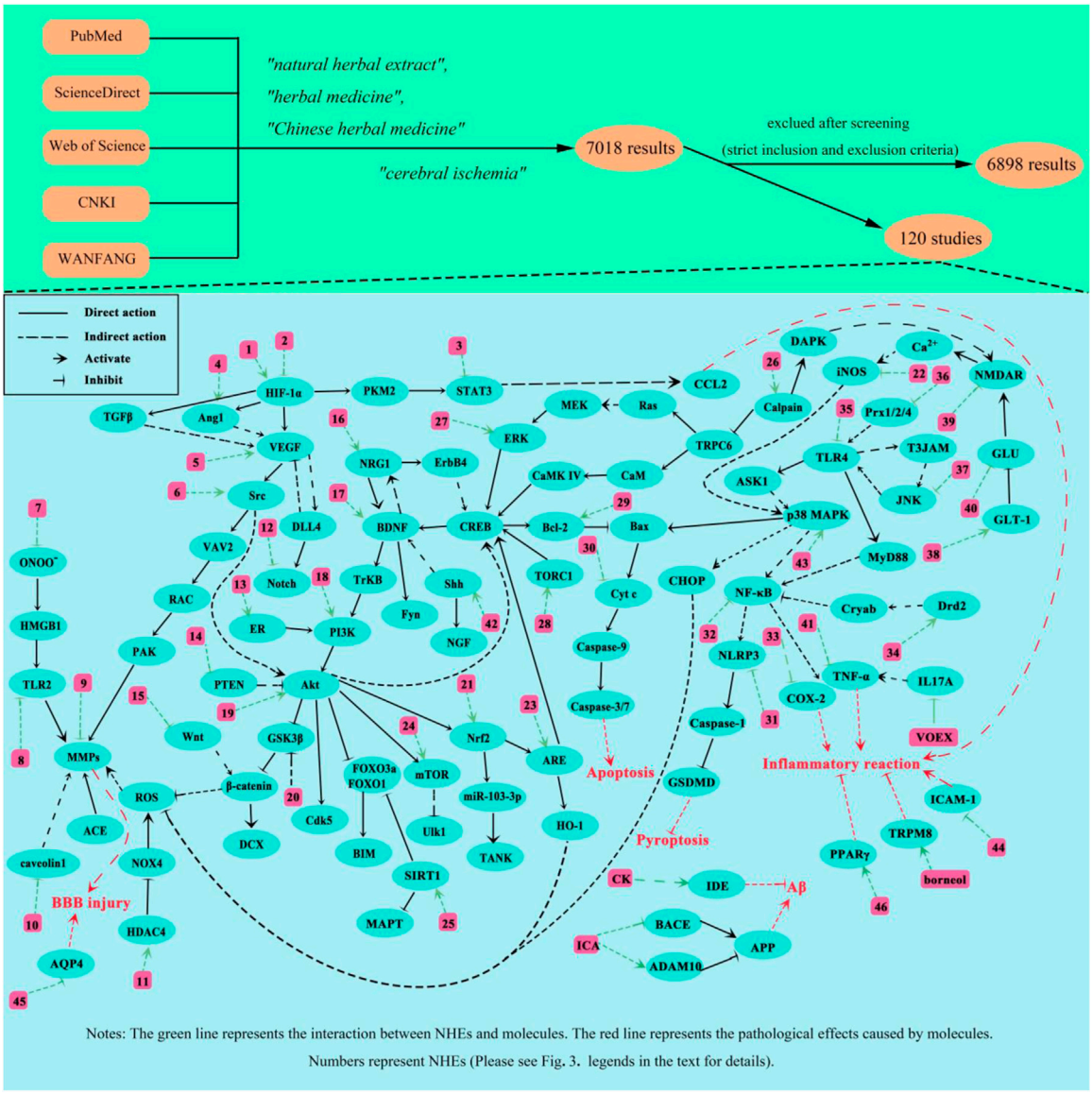

Notes: The green line represents the interaction between NHEs and molecules. The red line represents the pathological effects caused by molecules.
Numbers represent NHEs (Please see Fig. 3. legends in the text for details).

GRAPHICAL ABSTRACT

Health Stroke Scale is commonly used to assess neurological damage in patients with clinical ischemia. Even if a patient avoids death, most will experience severe neurological dysfunction. Currently, the early treatment of patients with CI mainly occurs *via* the rapid restoration of cerebral blood flow perfusion, however, this restoration increases oxidative stress and inflammatory responses in ischemic tissue, leading to reperfusion injury. One factor that determines the severity of a patient's condition is ischemia duration, which is a very important determinant when selecting treatment options for patients with acute cerebral ischemia (ACI) (Powers, 2020). Another problem that cannot be ignored is that the recombinant tissue plasminogen activator (rt-PA) drug is currently approved by the U.S. Food and Drug Administration for stroke patients, but its treatment window is very narrow and it has very serious side effects (e.g., cerebral hemorrhaging) (Dhamija and Donnan, 2007). Thus, a lack of drugs is an urgent issue for CI treatment. To remedy this, promoting low-toxicity and high-efficiency drug research and development can alleviate CI patient suffering. Our work is based on this purpose and motivation.

Herbal medicines are gifts from nature, and have helped humans solve medical problems that have plagued humankind for centuries. For example, artemisinin extracted from *Artemisia annua* L. helps alleviate malaria (Talman et al., 2019). Methanol extracts from *Allium turcicum* Özhatay and Cowley exert significant anticancer, antioxidant, and antimicrobial activities (Łpek et al., 2024). These natural herbal extracts (NHEs) have active roles in many different fields, for example, a *Chenopodium quinoa* Willd. seed extract restores photosystem II damage caused by toxic metal salts (Ganieva et al., 2023). Also, *Pistacia atlantica* Desf. extracts effectively inhibit *Fusarium oxysporum f. sp. albedinis* to rescue infected date palms (Fatiha et al., 2023). NHEs have unique structures and

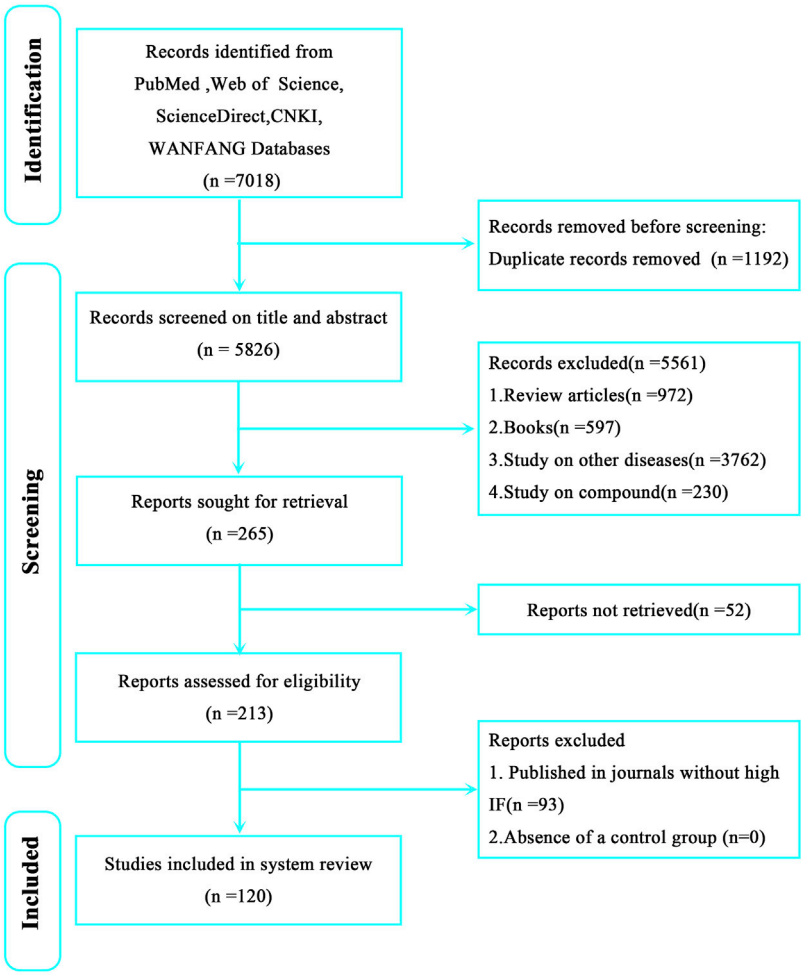

FIGURE 1
Preferred Reporting Items for Systematic Review and Meta-analysis (PRISMA) flow chart showing literature retrieval and screening in this review.

properties, and are roughly divided into alkaloids, flavonoids, polysaccharides, glycosides, organic acids, and volatile oils.

1.1 Alkaloids

Alkaloids are nitrogen-containing organic compounds mainly found in plants, which have similar chemical properties to alkalis. One common property is that they all contain nitrogen as part of their chemical structure, but not all organic compounds containing nitrogen are alkaloids. Thanks to natural herb research and exploration, nearly 10,000 alkaloids have been discovered and collected. Alkaloids are subdivided into more than 60 types, for example, *Leonurus japonicus* Houtt. total alkaloid (LHA) is an organic amine in alkaloids. LHA and kukoamine A (KuA) are common alkaloids. LHA helps protect the blood-brain barrier (BBB) and inhibits inflammatory reactions and apoptosis in ischemia-reperfusion (IR) injury (Zhang Q.-Y. et al., 2017; Li Y. et al., 2021). KuA impacts CI injury by alleviating brain edema and inhibiting oxidative stress and apoptosis (Liu et al., 2017).

1.2 Flavonoids

Flavonoids are one of the most widespread organic compounds in nature; they exist in almost all green plants, especially higher plants. In the selected studies in this review, many have investigated flavonoid NHEs, such as emodin, scutellarin, and icariin (ICA). From our research, emodin enhances cell viability and inhibits oxidative stress radicalization to alleviate IR injury (Wang et al., 2007; Leung et al., 2020); scutellarin improves neurological dysfunction in rats during IR injury by inhibiting apoptosis, focal death, and necrosis (Wang C. et al., 2023); and ICA inhibits apoptosis and protects neuronal dendrites during chronic cerebral ischemia (CCI) to improve cognitive impairment (Li W.-X. et al., 2015).

1.3 Polysaccharides

Polysaccharides are macromolecules composed of at least 10 monosaccharides, and have important roles maintaining normal life activities. Polysaccharides are divided into plant,

TABLE 1 Summary of ACI study characteristics.

In vivo		Quantity	*In vitro*		Quantity
Model			Model		
	MCAO	14		OGD	7
	PT	3		Model of cell injury induced by $COCl_2$	1
	autologous thrombotic stroke model	2	Cell types		
Species				PC12	2
	SD rats	15		N2A	1
	ICR mice	2		bEnd.3	1
	Wistar rats	1		HBMEC	1
	Tree shrews	1		Primary neurons	2
	C57BL/6 mice	1		Primary microglia	1
Drug effect				Hippocampal slices	1
	Reduce neurological deficit	15	Drug effect		
	Reduce cerebral edema	4		Enhance cell viability	7
	Inhibit oxidative stress response	4		Improve mitochondrial dysfunction	1
	Reduce infarct size	11		Protect the blood-brain barrier	1
	Inhibition inflammatory response	3		Inhibit calcium inflow	1
	Reduce cerebral thrombosis	1		Inhibit oxidative stress response	1
	Protect the blood-brain barrier	3		Inhibit apoptosis	2
	Ameliorate mitochondrial dysfunction	3		Inhibit inflammatory response	2
	Improve regional cerebral blood flow disturbance	5		Alleviate glutamate hyperexcitation injury	1
	Promote angiogenesis	2			
	Inhibit astrocyte activation and proliferation	1			

animal, and fungal polysaccharides according to extraction sources. Plant polysaccharides include ganoderma polysaccharides, lentinan, ginseng polysaccharides, and other polysaccharides beneficial to humans. Previous studies have reported that some polysaccharides may have anti-tumor effects (Zhang et al., 2021).

1.4 Glycosides

Glycosides have high medicinal value, which not only enhance immunity and antiviral effects, but also inhibit oxidative stress and enhance metabolic function in cells. Astragaloside IV (ASIV), ginsenoside, and notoginsenoside are well-known representative glycosides, especially ASIV. As an *Astragalus membranaceus* (Fisch.) Bunge extract, ASIV inhibits inflammatory reactions, promotes neurogenesis and angiogenesis, promotes neurotrophic factor expression, protects the BBB, and significantly improves neurological dysfunction caused by IR injury (Li et al., 2013; Li L. et al., 2021; Li S. et al., 2021; Shi et al., 2021). Ginsenoside has protective roles in injury caused by ACI, CCI, and IR. It not only inhibits apoptosis, increases angiogenesis, and improves local blood flow disorders, but also protects the BBB and improves cognitive dysfunction caused by CI (Zhou et al., 2014; Yang et al., 2016; Wang S. et al., 2017; Wan et al., 2017; Zhang et al., 2019; Zhang C. et al., 2020). Notoginsenoside resists injury caused by ACI and IR by alleviating brain edema, enhancing cell viability, protecting the BBB, and inhibiting apoptosis (Tu et al., 2018; Liu B. et al., 2021; Gao et al., 2022; Liu et al., 2022).

1.5 Organic acids

Organic acids are widely found in leaves, roots, and especially plant fruits. They have acidic properties, and are widely found in *Lonicera japonica* Thunb., *Schisandra chinensis* (Turcz.) Baill., *Prunus mume* Siebold & Zucc., *Rubus idaeus* L., and other herbs. Representative organic acid compounds from NHEs include salvianolic acid A (SAA) and betulinic acid (BA). In an ACI model, SAA reduces the incidence of cerebral hemorrhaging, protects the BBB, relieves vascular endothelial dysfunction, promotes neural function recovery, and induces neural progenitor cell proliferation. SAA also alleviates ischemic brain edema, inhibits inflammatory reactions, relieves oxidative stress, inhibits apoptosis, and improves long-term learning and memory

defects (Jiang et al., 2011; Chien et al., 2016; Song et al., 2019; Liu C. et al., 2021; Ling et al., 2021; Yang Y. et al., 2022). BA also inhibits neuronal autophagy against IR injury (Zhao et al., 2021).

1.6 Volatile oils

Volatile oils mainly come from aromatic traditional Chinese medicine, with many fragrant plants more or less containing these compounds. The group includes terpenoids and aromatic compounds and also their oxygen-containing derivatives such as alcohols, aldehydes, ketones, phenols, ethers, and lipids. Additionally, the group includes some nitrogen- and sulfur-containing compounds. The most common NHEs are ginkgolide and ligustilide (LIG). Seven ginkgolide species have been found: A, B, C, M, J, K, and L. Ginkgolide B (GB) exerts the greatest effects, so many pharmacological studies have focused on this compound. GB protects the BBB and improves mitochondrial respiratory function against ACI injury (Li et al., 2007). LIG alleviates neurological deficits and inhibits apoptosis, astrocyte activation and proliferation, and oxidative stress responses in a CCI model (Feng et al., 2012; Peng D. et al., 2022).

2 Search strategy

To comprehensively and systematically conduct literature retrieval and data extraction, we preliminarily searched and screened all studies from PubMed, ScienceDirect, Web of Science, CNKI, and WANFANG databases before 10 January 2024 in strict accordance with Preferred Reporting Items for Systematic Review and Meta-analysis (PRISMA) guidelines. The retrieval keywords are as follows: 1) natural herbal extracts, 2) Chinese herbal medicines, 3) herbal medicines, and 4) cerebral ischemia. Constructed retrieval expressions are (natural herbal extracts OR Chinese herbal medicines OR herbal medicines) AND cerebral ischemia. After retrieving pertinent studies (n = 7,018), we preliminarily screened (using titles, keywords, and abstracts) and comprehensively reviewed these studies. Finally, 120 studies were selected for review (Figure 1).

2.1 Inclusion and exclusion criteria

In view of the therapeutic effects and mechanisms of NHEs toward CI, and the large number of studies, we formulated the following inclusion and exclusion criteria. Inclusion criteria; 1) A cerebral ischemia model and 2) a control group are included; 3) At least one experimental group used NHEs as an intervention; and 4) Research data are published in high impact journals. Exclusion criteria; 1) Reviews or books; and 2) Studies on other diseases and compounds.

2.2 Data extraction and treatment evaluation

The authors independently extracted and summarized information from selected studies, solved any issues *via* discussion, and finally summarized the information, including; 1) NHEs; 2) The source and voucher numbers of the herbal medicine; 3) Extraction methods 4) Extraction parts and solvents; 5) Toxicity and side effects; 6) Related diseases in the study; 7) Establishing *in vitro* or *in vivo* models; 8) Animal or cell models; 9) Dose and time of treatment; 10) Main biological effects; 11) Mechanism of action; 12) Year of publication and first author; and 13) Positive controls.

2.3 Risk of bias

After discussions, the authors referred to the previous literature (Dong et al., 2023) to establish an evaluation scale of bias risk for selected studies. The following questions were posed; 1) Had the study passed peer review; 2) Were randomness principles followed when grouping models; 3) Were blinding methods applied during drug interventions and data collection; 4) Were sample sizes statistically calculated before model establishment; 5) Were animal welfare laws and regulations strictly observed in the research process; and 6) Were potential conflicts of interest between authors declared?

3 Results

From our strategy, 7,018 studies were retrieved, including 2032 Pubmed results, 1,242 Web of Science results, 3,578 ScienceDirect results, 124 CNKI results, and 42 WANFANG results. After preliminary screening and applying inclusion and exclusion, 120 studies were finally selected (Figure 1). Among these, 21 were related to ACI, 28 to CCI, and 71 to IR. In order to avoid disease subtype differences which may have affected our study results, we separately summarized the therapeutic effects of NHEs for ACI, CCI, and IR.

3.1 ACI

In the 21 ACI-related studies were 19 *in vivo* and nine *in vitro* studies, from which we summarized the characteristics of each study (Table 1). To ensure reliability, we summarized *in vivo* and *in vitro* study characteristics, separately. In the 19 *in vivo* studies, NHEs mitigated ACI-induced damage *via* different modes of action (Table 2). In nine *in vitro* studies, damaged cell models achieved varying degrees of remission after a NHE intervention (Table 3).

3.2 CCI

We included 28 studies on CCI, including 28 *in vivo* and four *in vitro* studies. We summarized CCI-related research characteristics (Table 4). NHEs alleviated damage caused by CCI and improved cognitive dysfunction caused by ischemia (Table 5). Detailed information on four studies outlining *in vitro* CCI characteristics (extracts, interventions, biological effects, and mechanisms) is shown (Table 6).

TABLE 2 NHE therapeutic effects and mechanisms in *in vivo* ACI models.

Author(Year)	Extracts	Model	Species	Interventions	Positive control	Biological effects (experimental protocol)	Mechanism	Regulation
Wang et al. (2022)	catalpol	MCAO	SD rats	catalpol(10 mg/kg) for 7 d	NA	Reduce neurological deficit (mNSS) Alleviate ischemic brain edema (water content calculation) Inhibit oxidative stress response (MDA assay) Reduce infarct size (TTC)	Nrf2/HO-1 path Bax/Bcl-2 path	Upregulated(Nrf2/HO-1 path) Downregulated(Bax/Bcl-2 path)
Zhao et al. (2017)	MO	autologous thrombotic stroke model	Wistar rats	MO(100/250/500 mg/kg) for 3 d	NA	Reduce neurological deficit (neurological deficit scores) Reduce infarct size (TTC) Reduce cerebral thrombosis (radioimmunoassay) Inhibit oxidative stress and inflammatory response (Westernblot)	6-keto-PGF1α/TXB2 Bax/Bcl-2 path	Downregulated
Li et al. (2007)	GB	PT	Tree shrews	GB(5 mg/kg)for 6 h	NA	Protect the blood-brain barrier (EB test) Improve the mitochondrial respiration (determining the oxygen consumption in an airtight chamber)	PAFR	Downregulated
Fei et al. (2017)	SCED	MCAO	SD rats	SCED(3.75/7.5/15 mg/kg) for 3 d	Ginaton(15 mg/kg)	Reduce neurological deficit (Longa) Improve regional cerebral blood flow disturbance (laser-Doppler) Alleviate ischemic brain edema (water content calculation) Reduce infarct size (TTC)	TXA2 PLC/PKC path	Downregulated
Liu et al. (2022)	NGR1	MCAO	SD rats	NGR1(20/40 mg/kg) for 24 h	Dl-3-n-Butylphthalide	Reduce neurological deficit (neurological deficit scores) Reduce infarct size (TTC) Accelerate energy metabolism (RT-qPCR)	Atp12a Atp6v1g3	Upregulated
Gao et al. (2022)	PNS	MCAO	ICR mice	PNS(50/100 mg/kg) for 3 d	minocycline	Reduce neurological deficit (Longa) Improve regional cerebral blood flow disturbance (Laser speckle imaging) Inhibit microglial activation and inflammatory response (Westernblot)	HIF-1α/PKM2/STAT3 path	Downregulated
Liu et al. (2021a)	NGR1	MCAO	SD rats	NGR1(10/20/40 mg/kg) for 12 h	Dl-3-n-Butylphthalide	Protect the blood-brain barrier (EB test)	NA	
Wang et al. (2017a)	GSRb1	PT	SD rats	GSRb1(25/50/100 mg/kg) for 1 d	nimodipine	Improve regional cerebral blood flow disturbance (laser-Doppler)	GLT-1 NMDAR Cyt-C	Upregulated(GLT-1) Downregulated(NMDAR and Cyt-C)
Liu et al. (2021b)	SAA	autologous thrombotic stroke model	SD rats	SAA(10 mg/kg) for 5 d	aspirin	Reduce neurological deficit (Longa) Protect the blood-brain barrier (EB test)	VEGFA/Src/VAV2/Rac/PAK/MMPs	Downregulated
Liu et al. (2010)	TSA	MCAO	SD rats	TSA(15/20 mg/kg) for 1 d	NA	Reduce neurological deficit (Longa) Alleviate ischemic brain edema (water content calculation)	TORC1/CREB/BDNF path	Upregulated

(Continued on following page)

10.3389/fphar.2024.1424146

TABLE 2 (*Continued*) NHE therapeutic effects and mechanisms in *in vivo* ACI models.

Author(Year)	Extracts	Model	Species	Interventions	Positive control	Biological effects (experimental protocol)	Mechanism	Regulation
Yang et al. (2016)	GSRd	MCAO	SD rats	GSRd(10 mg/kg) for 7 d	NA	Reduce neurological deficit (Longa) Reduce infarct size (TTC) Mitigate mitochondrial DNA and nuclear DNA damage (real-time analysis of mutation frequency)	NEIL1/3	Upregulated
Ma et al. (2021)	L-borneol	MCAO	SD rats	L-borneol(50/100/200 mg/kg) for 3 d	nimodipine(12 mg/kg)	Reduce neurological deficit (Longa) Reduce infarct size (TTC) Promote angiogenesis (ELISA)	Ang1/VEGF/BDNF path	Upregulated
Zhang et al. (2023b)	SHPL-49	MCAO	SD rats	SHPL-49(2.5/5/7.5/10/15 mg/kg) for 5 d	Edaravone(7.5 mg/kg)	Improve regional cerebral blood flow disturbance (laser-Doppler) Reduce infarct size (TTC) Reduce neurological deficit (Bederson)	Bax/Bcl-2/Caspase-3 path	Downregulated
Li et al. (2012a)	Galangin	MCAO	SD rats	Galangin(25/50/100 mg/kg)	EGB761(4 mg/kg)	Improve mitochondrial viability (Measurement of Mitochondrial Viability) Improve regional cerebral blood flow disturbance (laser-Doppler) Inhibit oxidative stress response (ROS assay) Reduce infarct size (TTC)	Bax/Bcl-2/Caspase-3 path	Downregulated
Liu et al. (2017)	KuA	MCAO	SD rats	KuA(5/10/20 mg/kg) for 6 h	NA	Reduce neurological deficit (neurological deficit scores) Reduce cerebral edema (water content calculation) Inhibit oxidative stress response (MDA assay) Reduce infarct size (TTC)	Bax/Bcl-2/Caspase-3 path	Downregulated
Li et al. (2015a)	T-VA	MCAO	SD rats ICR mice	T-VA(30/60/120 mg/kg) for 10 d	NA	Reduce neurological deficit (neurological deficit scores) Promote vascular endothelial cell proliferation (immunohistochemical)	VEGF	Upregulated
Liu et al. (2019a)	KRGP	MCAO	C57BL/6 mice	KRGP(100 mg/kg) for 7 d	NA	Reduce neurological deficit (neurological deficit scores) Inhibit astrocyte activation and proliferation (immunofluorescence) Ameliorate abnormal glutamate metabolism (Westernblot)	Nrf2	Upregulated
Jiang et al. (2018a)	Celastro	MCAO	SD rats	celastro	NA	Reduce neurological deficit (neurological deficit scores) Reduce infarct size (TTC) Inhibit inflammatory response (immunofluorescence)	NA	
Zhang et al. (2013)	Luteolin	MCAO	SD rats	Luteolin(4 mg/kg) for 48 h	NA	Reduce neurological deficit (Longa) Reduce infarct size (TTC)	Caspase-3 path	Downregulated

10.3389/fphar.2024.1424146

TABLE 3 NHE therapeutic effects and mechanisms in *in vivo* ACI models.

Author(Year)	Extracts	Model	Cell types	Interventions	Positive control	Biological effects (experimental protocol)	Mechanism	Regulation
Liu et al. (2022)	NGR1	OGD	N2A	NGR1 (5/10/20/100/200 μM) for 24 h	Dl-3-n-Butylphthalide	Enhance cell viability (CCK-8) Improve mitochondrial dysfunction (mitochondrial membrane potential detection)	NA	
Liu et al. (2021a)	NGR1	OGD	bEnd.3	NGR1 (200 μM)	Dl-3-n-Butylphthalide	Protect the blood-brain barrier (Westernblot)	caveolin1/MMP2/9 path	Upregulated
Liu et al. (2021b)	SAA	OGD	HBMEC	SAA (10 μM)	aspirin	Enhance cell viability (CCK-8)	VEGFA/Src/VAV2/Rac1/PAK path	Downregulated
Zhang et al. (2023b)	SHPL-49	OGD	PC12	SHPL-49 (100/200 μM) for 24 h	NA	Inhibit calcium inflow (fluorescent probe) Enhance cell viability (CCK-8) Inhibit oxidative stress response (ROS assay) Inhibit apoptosis (Hoechst staining)	Bax/Bcl-2/Caspase-3 path	Downregulated
Li et al. (2015a)	T-VA	Model of cell injury induced by $COCl_2$	PC12	T-VA (15/30/60 μM) for 36 h	NA	Enhance cell viability (MTT) Inhibit inflammatory response (immunohistochemical)	NF-κB/p65 COX-2	Downregulated
Jiang et al. (2018a)	celastro	OGD	Primary neurons、Primary microglia	Celastro (0.25/0.5/1/2 μM) for 3 h	NA	Enhance cell viability (CCK-8) Inhibit apoptosis (Flow Cytometry) Inhibit inflammatory response (Westernblot)	IL-33/ST2	Upregulated
Ferreira et al. (2023)	EDAC	OGD	Hippocampal slices	EDAC (1/10 μg/mL) for 1 h	NA	Alleviate glutamate hyperexcitation injury (Annexin V/PI assay) Protect astrocytes and oligodendrocytes (immunohistochemical)	Glutamate receptor	Downregulated
Sun et al. (2015)	Asiaticoside	OGD	Primary neurons	Asiaticoside (10/100 nM) for 24 h	NA	Enhance cell viability (MTT)	Bax/Bcl-2/Caspase-3 path	Downregulated
Zhang et al. (2013)	Luteolin	OGD	SH-SY5Y	Luteolin(10/25/50 ug/mL)	sulforaphane(10 μM)	Enhance cell viability (MTT)	Nrf2	Upregulated

10.3389/fphar.2024.1424146

TABLE 4 Summary of CCI study characteristics.

In vivo		Quantity	*In vitro*		Quantity
Model			Model		
	MCAO	2		OGD	3
	rUCCAO	1		Model of cell injury induced by H_2O_2	1
	2VO	14	Cell types		
	BCAS	3		PC12	1
	BCCAo	5		SH-SY5Y	1
	4VO	1		Primary neurons	1
	PBOCCA	2		HT-22	1
Species			Drug effect		
	SD rats	14		Enhance cell viability	1
	C57BL/6 mice	5		Inhibit apoptosis	1
	Wistar rats	9		Alleviate hypoxic damage	1
Drug effect				Ameliorate mitochondrial dysfunction	1
	Reduce neurological deficit	6			
	Induce proliferation of neural progenitor cells	1			
	Improve cognitive impairment	24			
	Inhibit activation and proliferation of astrocytes	2			
	Inhibit oxidative stress response	5			
	Inhibit apoptosis	1			
	Inhibit inflammatory response	3			
	Inhibit neuronal demyelination	3			
	Protect neuronal dendrites	1			
	Inhibit microglial activation	1			
	Improve regional cerebral blood flow disturbance	1			
	Reduce infarct size	1			

3.3 Cerebral IR

Of the 71 cerebral IR-related studies, 68 were *in vivo* and 31 were *in vitro* based. A summary of study characteristics is shown (Table 7), and then we describe the studies *in vivo* and *in vitro*, separately. Studies showed that NHEs had therapeutic roles in *in vivo* brain IR models (Supplementary Table S1). NHEs also reduced IR damage in *in vitro* models (Table 8).

4 Quality evaluation of selected studies

Using our bias risk assessment scale, bias risk assessments were conducted on the 120 studies. All were peer-reviewed publications and they strictly complied with animal welfare regulations, which meant that all studies had at least two points (total score = 6 points). Additionally, 120 studies followed randomization principles (84.17%), 39 adopted blind methods (32.5%), 88 declared conflicts of interest among authors (73.33%), and only one study statistically calculated the sample size (0.83%) (Figure 2). Perhaps some researchers had calculated sample sizes before their studies, but this was not stated. After evaluations, bias risk scores for studies were in the 2–6 range: six studies scored 2 (5%), 29 scored 3 (24.17%), 56 scored 4 (46.67%), 28 scored 5 (23.33%), and one scored 6 (0.83%). Approximately half (46.67%) received four points, which proved that study quality was high. Bias risk evaluations for studies are shown (Table 7).

5 Toxicity

Unfortunately, many studies failed to provide NHE-related toxicity information. While drug toxicity studies are usually conducted at pre-experimental stages, researchers must articulate this. To complement the required NHE toxicity reports for this review, we performed additional NHE safety reviews by

TABLE 5 NHE therapeutic effects and mechanisms in *in vivo* CCI models.

Author(Year)	Extracts	Model	Species	Interventions	Positive control	Biological effects (experimental protocol)	Mechanism	Regulation
Zhang et al. (2017b)	SA	MCAO	C57BL/ 6 mice	SA (15/30 mg/kg) for 14 d	NA	Reduce neurological deficit (mNSS) Induce proliferation of neural progenitor cells (Westernblot)	SHH/BDNF NGF	Upregulated
Wan et al. (2022)	Triptolide	rUCCAO	C57BL/ 6 mice	Triptolide (5/20 ug/kg) for 28 d	NA	Improve cognitive impairment (new object recognition test, Morris water maze)	Src/Akt/GSK3β path	Upregulated
Feng et al. (2012)	LIG	2VO	SD rats	LIG (80 mg/kg) for 7 d	NA	Improve cognitive impairment (Morris Water Maze) Inhibit activation and proliferation of astrocytes (immunohistochemical)	NA	
Peng et al. (2022a)	LIG	2VO	SD rats	LIG (20/40 mg/kg) for 28 d	NA	Improve cognitive impairment (Morris Water Maze) Inhibit oxidative stress response (MDA assay)	SIRT1/IRE1α/XBP1s/ CHOP path	Upregulated
Yang et al. (2022a)	SAA	2VO	Wistar rats	SAA (5/10/20 mg/kg) for 56 d	nimodipine(10 mg/kg)	Improve cognitive impairment (Morris water maze, open field test) Inhibit apoptosis (TUNEL staining) Inhibit inflammatory response (immunofluorescence)	Drd2/Cryab/NF-κB path	Upregulated
Tan et al. (2022)	Que	BCAS	C57BL/ 6 mice	Que (60 mg/kg) for 14 d	NA	Improve cognitive impairment (Morris water maze, open field test, tail suspension test, forced swimming test, sucrose preference test)	NA	
Liu et al. (2019b)	CZ-7	2VO	Wistar rats	CZ-7 (10/20/40 mg/kg) for 25 d	nimodipine(20 mg/kg)	Improve cognitive impairment (Morris Water Maze) Inhibit oxidative stress response (MDA assay)	Nrf2	Upregulated
Zhang et al. (2023a)	Honokiol	BCAS	C57BL/ 6 mice	Honokiol (10 mg/kg) for 30 d	NA	Improve cognitive impairment (open field test, new object recognition test, fear conditioning, Y maze) Inhibit neuronal demyelination (immunohistochemical)	Akt/mTOR path	Upregulated
Chen et al. (2018a)	HAR	2VO	Wistar rats	HAR (15 mg/kg) for 60 d	NA	Improve cognitive impairment (Morris water maze, passive avoidance experiment)	PTEN/Akt/GSK3β	Downregulated
Lee et al. (2015)	Fructus extracts	BCCAo	Wistar rats	Fructus extracts (200 mg/kg) for 40 d	NA	Inhibit neuronal demyelination (immunohistochemical) Inhibit inflammatory response (Westernblot)	TLR4/ MyD88 p38 MAPK	Downregulated

(Continued on following page)

10.3389/fphar.2024.1424146

TABLE 5 (*Continued*) NHE therapeutic effects and mechanisms in *in vivo* CCI models.

Author(Year)	Extracts	Model	Species	Interventions	Positive control	Biological effects (experimental protocol)	Mechanism	Regulation
Li et al. (2012b)	Polydatin	4VO	SD rats	Polydatin (12.5/25/ 50 mg/kg) for 30 d	Ginkgo Tablets (25 mg/kg)	Improve cognitive impairment (Morris Water Maze) Inhibit oxidative stress response (MDA assay)	NA	
Shi et al. (2020)	Gas	2VO	SD rats	Gas (22.5/90 mg/kg) for 28 d	NA	Improve cognitive impairment (Morris water maze, attention diversion test)	NA	
Wu et al. (2023)	Gas	2VO	SD rats	Gas (25/50 mg/kg) for 28 d	NA	Improve cognitive impairment (Morris water maze, passive avoidance experiment) Reduce neuronal ischemic injury (immunohistochemical)	NA	
Yao et al. (2021)	EGB761	2VO	SD rats	EGB761(100 mg/kg) for 30 d	NA	Improve cognitive impairment (Morris water maze, new object recognition test) Inhibit neuronal demyelination (immunohistochemical)	mTOR	Upregulated
Kim et al. (2016)	GBE	BCCAo	Wistar rats	GBE (5/10/20/40 mg/kg) for 42 d	NA	Inhibit activation and proliferation of astrocytes (immunohistochemical) Inhibit inflammatory response (Westernblot)	NA	
Niu et al. (2020)	EF	2VO	SD rats	EF (50/100/200 mg/kg) for 84 d	nimodipine(10 mg/kg)	Improve cognitive impairment (new object recognition test, Y maze) Protect neuronal dendrites (immunohistochemical)	NRG1/ErbB4 BDNF/Fyn PI3K/Akt/CREB	Upregulated
Li et al. (2015b)	ICA	BCCAo	SD rats	ICA (10/40 mg/kg) for 23 d	NA	Improve cognitive impairment (Morris Water Maze)	BACE1 ADAM10 IDE	Downregulated(BACE1)、 Upregulated(ADAM10、IDE)
Wan et al. (2017)	GSRd	BCAS	C57BL/ 6 mice	GSRd (10/30 mg/kg) for 21 d	NA	Improve cognitive impairment (Morris water maze, open field test) Reduce neuronal ischemic injury (HE staining)	BDNF	Upregulated
Zong et al. (2019)	CK	2VO	SD rats	CK (50/100/200 mg/kg) for 56 d	donepezil(2 mg/kg)	Improve cognitive impairment (Morris Water Maze) Reduce neuronal ischemic injury (HE staining)	GSK3β IDE	Upregulated(IDE) Downregulated(GSK3β)
Zhu et al. (2018)	GSRg1	2VO	Wistar rats	GSRg1 (50/100 mg/kg) for 56 d	nimodipine(20 mg/kg)	Improve cognitive impairment (Morris water maze, balance beam test) Reduce neuronal ischemic damage (Westernblot)	Bcl-2/Bax VEGF	Upregulated
Hwang et al. (2011)	SB extracts	BCCAo	Wistar rats	SB extracts (100/ 200 mg/kg) for 40 d	donepezil(10 mg/kg)	Improve cognitive impairment (Morris Water Maze)	MAPKs	Upregulated

(Continued on following page)

10.3389/fphar.2024.1424146

TABLE 5 (*Continued*) NHE therapeutic effects and mechanisms in *in vivo* CCI models.

Author(Year)	Extracts	Model	Species	Interventions	Positive control	Biological effects (experimental protocol)	Mechanism	Regulation
Ahad et al. (2023)	CTRF	PBOCCA	SD rats	CTRF (10/20/40 mg/kg)	NA	Improve cognitive dysfunction (Morris water maze, passive avoidance test, open field test)	NA	
Damodaran et al. (2018)	CTRF	PBOCCA	SD rats	CTRF (100/200/ 300 mg/kg)	NA	Improve cognitive dysfunction (Morris water maze, passive avoidance test, open field test)	NA	
Tiang et al. (2020)	XEFGM α-MG	2VO	SD rats	XEFGM (25/50/ 100 mg/kg) for 40 d α-MG (25,50 mg/kg) for 40 d	NA	Improve cognitive dysfunction (Morris water maze, open field test)	NA	
Hosseinzadeh et al. (2012)	CSL extracts crocin	2VO	Wistar rats	CSL extracts (50/100/ 250 mg/kg) for 5 d Crocin (5/10/25 mg/kg) for 5 d	NA	Improve cognitive dysfunction (Morris water maze)	NA	
Kim et al. (2023)	AA	BCCAo	Wistar rats	AA (150/750 mg/kg) for 56 d	NA	Improve cognitive dysfunction (open field test, Y maze, eight-arm maze test) Inhibit microglial activation (immunohistochemical) Inhibit oxidative stress response (immunohistochemical)	Nrf2/Keap1/ARE path	Upregulated
Guang and Du. (2006)	pinocembrin	2VO	SD rats	Pinocembrin (0.5/5 mg/kg) for 14 d	NA	Improve regional cerebral blood flow disturbance (laser-Doppler) Improve cognitive impairment (Morris Water Maze) Inhibit oxidative stress response (Measurement of hydrogen peroxide production in mitochondria)	NA	
Zhou et al. (2021b)	PNS	MCAO	SD rats	PNS (72 mg/kg) for 14/28 d	nimodipine(14.4 mg/kg)	Reduce neurological deficit (Longa) Reduce infarct size (TTC)	ROCKII	Downregulated

10.3389/fphar.2024.1424146

TABLE 6 NHE therapeutic effects and mechanisms in *in vitro* CCI models.

Author(Year)	Extracts	Model	Cell types	Interventions	Positive control	Biological effects (experimental protocol)	Mechanism	Regulation
Peng et al. (2022a)	LIG	OGD	PC12	LIG (80 μM) for 2 h	NA	NA	SIRT1/IRE1α/XBP1s/CHOP path	Upregulated
Yang et al. (2022a)	SAA	OGD	SH-SY5Y	SAA (0.05/0.5/5/10/50 μM)	NA	Inhibit apoptosis (Flow Cytometry)	Drd2/Cryab/NF-κB path	Upregulated
Li et al. (2012b)	Polydatin	OGD	Primary neurons	Polydatin (12.5/5 μg/mL)	NA	Alleviate hypoxic damage (phase-contrast microscopy)	NA	
Wu et al. (2023)	Gas	Model of cell injury induced by H_2O_2	HT-22	Gas (100 μM)	NA	Enhance cell viability (MTT) Ameliorate mitochondrial dysfunction (oxygen consumption rate)	NA	

summarizing the toxicity reports in selected studies (Supplementary Table S2). However, not all NHEs have accompanying toxicity reports, which undoubtedly confirms a lack of safety studies in the natural herb research field. Reported that the LD50 (median lethal dose, the minimum amount of toxin required to kill half of an animal of a certain weight or age within a specified period of time) of SAA in mice (the dose required to kill half of cells/animal after a specific trial duration) was 1,161.2 mg/kg (Yang M.-Y. et al., 2022). *G. biloba* extracts may be carcinogenic and caution is recommended for their long-term use (Mei et al., 2017). ASIV is not toxic during maternal and embryonic development, but may inhibit fertility in female rats, suggesting its non-use in perinatal periods (Xuying et al., 2010). Luo et al. reported that emodin reduces and inhibits human sperm motility, suggesting some reproductive toxicity in these cells (Luo et al., 2015). LHA did not generate significant adverse reactions in toxicity tests in multiple experimental animals (Zhu et al., 2018). The main component of an ethanolic extract from *Erythrina velutina* Willd. (EEEV) is gallic acid, with *in vivo* studies showing that gallic acid at 210 mg/kg exerted no toxic effects in mice (Li et al., 2019). Ginkgolide A and ginkgolide B reduce mouse blastocyst viability and cause embryonic retardation in mice, leading to embryo death, suggesting caution when using these reagents during pregnancy (Mei et al., 2017). The main component of supercritical CO2 extracts from DanShen (SCED) is tanshinone IIA (TSA); it was found that at high TSA concentrations (25M), zebrafish embryo models exhibited severe growth inhibition, developmental malformations, and cardiotoxicity (Wang T. et al., 2017). Usually there are no obvious side effects when *Panax notoginseng* is supplemented to patients, but due to its estrogen effects, some patients have reported vaginal bleeding and distending breast pain. Those patients taking high *P. notoginseng* doses (>2.5 g/day) have central nervous system damaging effects such as insomnia, tachyarrhythmia, hypertension, and tension (Mancuso and Santangelo, 2017). *In vivo* betulinic acid studies showed no signs of systemic toxicity (Liu C. et al., 2019). Scutellarin has the lowest toxicity in rodents, and can even be said to be non-toxic. Quercetin (Que) toxicity is low; the organ weights and histopathology of rats treated with 400 mg/kg/d Que for 410 consecutive days showed no significant changes. Ginsenoside Rd, ginsenoside Rb1, and notoginsenoside promote cancer cell apoptosis and have significant effects in cancer treatment. Notoginsenoside R1 also inhibits cell proliferation, migration, invasion and angiogenesis, and promotes cell apoptosis at 150 μM. Shikonin is considered safe, but may cause skin allergies at very low doses. Luteolin exerts cytotoxicity at 5 μM and 10 μM doses, and its safety must be further evaluated in animal models and clinical trials. Hydroxysafflor yellow A is sensitive to interactions between herbs and drugs, resulting in no therapeutic effects at certain doses (Guo et al., 2023). Galangin has an IC50 (half-inhibitory concentration, the concentration at which a biological process or activity is inhibited by 50%) value of 275.48 μM in V79 cells, and does not produce genotoxic effects at all concentrations (Bacanlı et al., 2017). Similarly, echinocystic acid (EA) exerts no cytotoxic effects under any conditions in cell viability assays (Joh et al., 2012). Glycyrrhizin is moderately toxic and should be used with caution during pregnancy. It also has selective cytotoxic effects toward cancer cells, and its most important side effects are secondary diseases induced by hypertension and hypokalemia (Nazari et al., 2017). After the maternal application of 1.0 mg/kg ASIV for 28 consecutive days, ASIV delays development in young rats and should be used with caution in perinatal women (Zhang J. et al., 2020). Studies report serious adverse reactions to matrine, the most serious being hepatotoxicity, neurotoxicity, and reproductive toxicity (Wang X. et al., 2023). Acute and subacute toxicity studies report that breviscapine is a safe drug with a potential for widespread use in clinical settings (Wu et al., 2021). Icariin has an IC50 of 20 μM in HeLa cells, and its toxic effects in normal cells are relatively negligible (Huang et al., 2019).

6 Discussion

We comprehensively summarized the molecular mechanisms underlying CI treatment by NHEs (Figure 3). As mentioned, NHE therapeutic effects toward CI are roughly divided in two ways: one

TABLE 7 Summary of IR study characteristics.

In vivo		Quantity	*In vitro*		Quantity
Model			Model		
	MCAO/R	65		OGD/R	24
	4VO	1		Model of cell injury induced by H_2O_2	1
	2VO	2		Model of cell injury induced by glutamic acid	1
Species				EAN	1
	SD rats	41	Cell types		
	C57BL/6 mice	11		PC12	4
	Wistar rats	6		SH-SY5Y	5
	Swiss mice	1		Primary neurons	8
	ICR mice	7		BMEC	1
	Long-Evans rats	1		bEnd.3	2
	$Trpm8^{-/-}$ mice	2		Primary microglia	7
	Mongolian gerbils	1		Primary cortical capillary endothelial cells	1
	Kunming mice	1		HUVEC	1
Drug effect				HBMEC	1
	Reduce neurological deficit	40		BV2	2
	Reduce cerebral edema	11		N2A	1
	Inhibit oxidative stress response	11		Olineu	1
	Reduce infarct size	45		C17.2 cell	1
	Inhibition inflammatory response	17	Drug effect		
	Facilitate the production of new neurons	3		Enhance cell viability	14
	Protect the blood-brain barrier	8		Inhibit apoptosis	5
	Inhibit neuronal autophagy	4		Inhibit granulocyte adhesion	1
	Improve regional cerebral blood flow disturbance	3		Promote endothelial cell proliferation, migration and invasion	1
	Increase angiogenesis	4		Inhibit oxidative stress response	5
	Promote astrocyte activation and proliferation	3		Protect the blood-brain barrier	1
	Inhibit degradation of tight junctions in ischemic areas	1		Inhibit degradation of tight junctions in ischemic areas	1
	Inhibit brain infiltration by NK cells	1		Inhibition inflammatory response	7
	Promote M2 microglia/macrophage polarization	1		Promote neuronal proliferation and differentiation	1
	Promote neurotrophic factor expression	1		Inhibit autophagy	1
	Improve cognitive impairment	3		Alleviate glutamate-induced neuronal damage	1
				Inhibit microglial activation	2
				Inhibit glutamate-induced calcium increase	1

reduces damage, mainly by improving local blood flow disturbance, inhibiting oxidative stress, inflammatory responses and apoptosis, relieving cerebral edema, protecting the BBB, and inhibiting excitatory amino acid overexpression. The other way promotes injury recovery, mainly by promoting endothelial cell proliferation and migration, promoting neuron proliferation and differentiation, and promoting neurotrophic factor expression. NHEs may also act on molecules, such as SAA, *via* several pathways. SAA is a bioactive compound extracted from *Salvia miltiorrhiza Bunge*. Studies report that SAA has direct or indirect effects on toll-like receptor 2/4 (TLR2/4), phosphoinositide 3-kinase (PI3K), glycogen synthase kinase 3β (GSK3β), vascular endothelial

TABLE 8 NHE therapeutic effects and mechanisms in *in vivo* IR models.

Author(Year)	Extracts	Model	Cell types	Interventions	Positive control	Biological effects (experimental protocol)	Mechanism	Regulation
Zhang et al. (2017a)	LHA	OGD/R	bEnd.3	LHA(15 uM)	NA	Inhibit degradation of tight junctions in ischemic areas (immunofluorescence)	HDAC4/NOX4/MMP-9 path	Upregulated
Zhang et al. (2018)	DGMI GA GB GC	OGD/R	PC12	DGMI(1/10/20 ug/mL) GA, GB or GC (10 μmol/L)	N-Acetyl-L-cysteine	Enhance cell viability (MTT) Inhibit oxidative stress response (Westernblot)	PI3K/Akt/Nrf2/HO-1 path PI3K/Akt/CREB/Bcl-2/Bax/Caspase-3 path	Upregulated
Yang et al. (2018)	EGB761 GB	EAN	Primary microglia Primary cortical capillary endothelial cells	EGB761 (0.1 mg/mL) GB (100 mmol/L)	NA	Enhance cell viability (MTT) Protect the blood-brain barrier (Na-F analysis) Inhibit apoptosis (Westernblot)	Bax/Bcl-2 path	Downregulated
Tu et al. (2018)	NGR1	OGD/R	Primary neurons	NGR1 (10 μM)	NA	Enhance cell viability (MTT)	ER/PI3K/Akt/mTOR JNK path	Upregulated
Ling et al. (2021)	SAA	OGD/R	Primary neurons Primary microglia	SAA (62.5/125/250 μg/mL) for 15 m	NA	Inhibit inflammatory response (Westernblot)	TLR2/4	Downregulated
Jiang et al. (2011)	SAA	OGD/R	BMEC	SAA (0.025/0.25/2.5/25 mg/L) for 20 h	NA	Inhibit granulocyte adhesion (cone-plate rheometer)	ICAM-1	Downregulated
Song et al. (2019)	SAA	OGD/R	SH-SY5Y	SAA (0.05/0.5/5 μM) for 24 h	NA	Enhance cell viability (MTT)	Akt/FOXO3a/BIM	Upregulated
Luan et al. (2020)	SA	OGD/R	PC12	SA (5 μM) for 24 h	Edaravone	Enhance cell viability (CCK-8) Inhibit oxidative stress response (MDA assay) Inhibit apoptosis (Hoechst staining)	Caspase-3 path	Downregulated
Zhang et al. (2019)	GSF1	OGD/R	HUVEC HBMEC	GSF1 (20/40 μM) for 4/8/12/24 h	VEGF(80 ng/mL)	Promote endothelial cell proliferation, migration and invasion (Transwell assays)	IGF-1/IGF1R path	Upregulated
Yuan et al. (2020)	PF11	OGD/R	Primary neurons	PF11 (30/100/200 μM) for 24 h	Dl-3-n-Butylphthalide	Promote neuronal proliferation and differentiation (BrdU administration)	BDNF/TrKB path	Upregulated
Zhang et al. (2020a)	GSRd	OGD/R	Primary neurons	GSRd (1/3/10/30/100 μM)	NA	NA	DAPK/NR2b/NMDAR	Downregulated
Zhao et al. (2021)	Betulinic Acid	OGD/R	PC12	Betulinic Acid	NA	Inhibit autophagy (Flow Cytometry)	SIRT1/FOXO1	Upregulated
Wang et al. (2007)	Emodin-8-O-beta-D-glucoside	Model of cell injury induced by glutamic acid	Primary neurons	Emodin-8-O-beta-D-glucoside (2.5/5/10 mg/kg) for 1 d	MK-801(10 uM)	Alleviate glutamate-induced neuronal damage	NA	
Leung et al. (2020)	emodin	OGD/R	PC12	Emodin (1/10 μM) for 4 h	NA	Inhibit oxidative stress response (ROS assay)	GLT-1 ERK-1/2/Bcl-2/Caspase-3	Upregulated

(Continued on following page)

10.3389/fphar.2024.1424146

TABLE 8 (*Continued*) NHE therapeutic effects and mechanisms in *in vivo* IR models.

Author(Year)	Extracts	Model	Cell types	Interventions	Positive control	Biological effects (experimental protocol)	Mechanism	Regulation
Yang et al. (2020)	Procyanidins	OGD/R	BV2	Procyanidins (10 μM)	NA	Inhibit inflammatory response (Westernblot)	TLR4/p38/NF-κB/ NLRP3	Downregulated
Chen et al. (2020)	Glycyrrhizin	OGD/R	bEnd.3	Glycyrrhizin (10 μM)	rt-PA(20 ug/mL)	NA	ONOO-/HMGB1/ TLR2/MMP9	Downregulated
Wang et al. (2019)	EK100	OGD/R	N2A	EK100 (20/40 μM)	NA	Inhibit apoptosis (Annexin V/PI assay)	p65 NF-κB Caspase-3	Downregulated
Li et al. (2021c)	ASIV	OGD/R	Primary microglia Primary neurons	ASIV (50 μM)	NA	Inhibit inflammatory response (Westernblot)	STAT3/CCL2	Downregulated
Mao et al. (2017)	Gas-d	Model of cell injury induced by H_2O_2	SH-SY5Y	Gas-d (10 uM) for 24 h	NA	Enhance cell viability (MTT) Inhibit oxidative stress response (ROS assay) Inhibit inflammatory response (ELISA)	NA	
Bai et al. (2024)	PQS	OGD/R	Primary microglia	PQS (25/100 ug/mL)	NA	Inhibit microglial activation (ELISA)	Nrf2/miR-103-3p/ TANK	Upregulated
Zhang et al. (2024)	VOEX	OGD/R	Primary microglia	VOEX (6.25/12.5/25/50/ 100 μM) for 24 h	Dl-3-n-Butylphthalide(10uM)	Enhance cell viability (CCK-8)	IL17A	Downregulated
Zhou et al. (2021b)	PNS	OGD/R	SH-SY5Y	PNS (20/40/80/160/320/ 640 μg/mL)	NA	Enhance cell viability (CCK-8)	ROCKII	Downregulated
Qin et al. (2012)	PAL extracts	OGD/R	Primary neurons	PAL extracts (0.0156/0.0625/ 0.25 mg/mL)	NA	Enhance cell viability (MTT)	Caspase-9/3	Downregulated
Wan et al. (2022)	Triptolide	OGD/R	BV2 Olineu	Triptolide (0.001/0.01/ 0.1 nM) for 24 h	NA	Inhibit apoptosis (Hoechst staining) Inhibit inflammatory response (ELISA)	Src/Akt/GSK3β	Upregulated
Tan et al. (2022)	Que	OGD/R	Primary microglia	Que (30/60 μM) for 2 h	NA	Facilitate microglial phenotype switching (transmission electron microscopy) Inhibit inflammatory response (ELISA)	NA	
Wan et al. (2017)	GSRd	OGD/R	Primary neurons	GSRd (0.1/1/10 μM) for 2 h	NA	Enhance cell viability (MTT)	BDNF	Upregulated
Damodaran et al. (2018)	CTRF	OGD/R	Primary neurons	CTRF (2 μg/mL) for 24 h	NA	Inhibit glutamate-induced calcium increase (Fura-2 calcium imaging)	NA	
Wang et al. (2023b)	ASIV	OGD/R	SH-SY5Y	ASIV(10/20/40 μM) for 24 h	Ferrostatin-1(10 μM) for 24 h	Enhance cell viability (CCK-8) Inhibit peroxidation (ROS assay)	Nrf2	Upregulated

(Continued on following page)

10.3389/fphar.2024.1424146

TABLE 8 (*Continued*) NHE therapeutic effects and mechanisms in *in vivo* IR models.

Author(Year)	Extracts	Model	Cell types	Interventions	Positive control	Biological effects (experimental protocol)	Mechanism	Regulation
Li et al. (2024)	Sophoricoside	OGD/R	Primary neurons	Sophoricoside(25/50 μM)	NA	Enhance cell viability (CCK-8) Inhibit apoptosis (Westernblot, RT-qPCR) Inhibit inflammatory response (Westernblot, RT-qPCR)	Bax/Bcl-2 pAMPK	Upregulated(pAMPK) Downregulated(Bax/Bcl-2)
Park et al. (2009)	ESF	OGD/R	SH-SY5Y	ESF(0.4/2/10 ug/mL)	NA	Enhance cell viability (MTT)	Caspase-3	Downregulated
Chen et al. (2019)	ASIV	OGD/R	C17.2 cell	ASIV(100 μM)	Gefitinib(10 nM)	Enhance cell viability (MTT)	EGFR/MAPK	Upregulated

growth factor A (VEGFA), and intercellular adhesion molecule 1 (ICAM1), which means that SAA not only inhibits apoptosis, inflammation, and oxidative stress, and protects the BBB, but also promotes vascular proliferation and recovery (Jiang et al., 2011; Chien et al., 2016; Song et al., 2019; Liu C. et al., 2021; Ling et al., 2021). Additionally, some key factors involved in multiple pathways, such as VEGF, are activated by multiple NHEs. The discovery of VEGF has completely changed our understanding of blood vessel production during development and physiological homeostasis. The biological effects mediated by VEGF are mainly due to its impact on vascular permeability and new blood vessel generation. VEGF has important relationships with tumor growth and metastasis, hypertensive retinopathy, and other pathological conditions (Apte et al., 2019). T-VA is extracted from *Ligusticum sinense* (Li G. et al., 2015). Several studies report that T-VA, ginsenoside Rb1 (GSRb1), L-borneol, and DL-n-butylphthalide (DL-NBP) can also play a role through VEGF (Li G. et al., 2015; Zhu et al., 2018; Ma et al., 2021; Wang et al., 2020).

CI is a severe nerve injury caused by interrupted cerebral blood flow. The molecular mechanisms underpinning its pathological processes are extremely complex and cannot be fully explained at present. CI involves amino acid excitation, injury oxidative stress, inflammatory responses, BBB injury, mitochondrial dysfunction, cell necrosis, and apoptosis. Many studies report that key molecules are involved in these CI-mediated processes, such as hypoxia-inducible factor alpha (HIF-1α), VEGF, brain-derived neurotrophic factor (BDNF), protein kinase B (Akt), matrix metalloproteinases (MMPs), c-Jun N-terminal kinase (JNK), B-cell lymphoma-2-associated X (Bax), Caspase-3/9, mitogen-activated protein kinases (MAPKs) and nuclear factor kappa-B (NF-κB) (Wang et al., 2020; Li et al., 2022; Liu et al., 2023; Li et al., 2017; Chen H.-S. et al., 2018; Hu et al., 2020; Peng T. et al., 2022; Xu et al., 2021).

Blood flow disturbance is the most fundamental issue in CI, and appears to initiate several pathological conditions, such as BBB damage, mitochondrial dysfunction, cell necrosis, and apoptosis. To reduce the severity and prognosis of stroke onset, doctors must rapidly conduct clinical interventions such as intravenous thrombolysis and surgical thrombectomy to unblock cerebral blood vessels. Anticoagulant and antiplatelet therapies are recommended for patients without contraindications, but their harsh conditions of use and severe side effects have prompted scientists to explore better treatments. Thromboxane A2 (TXA2) is a potent vasoconstrictor and the main cyclooxygenase (COX) product of arachidonic acid (AA). The functional importance of this eicosanoid in acute coronary ischemic syndrome has been demonstrated as it activates platelets (Reilly and Fitzgerald, 1993). Fei et al. extracted natural compounds with TSA as the main component from *S. miltiorrhiza Bunge* (DanShen); this SCED inhibits platelet aggregation and improves regional blood flow disorders by inhibiting TXA2 activation (Fei et al., 2017). Although the specific molecular mechanisms have not been clarified, and to determine NHE biological effects on blood flow disorders, several studies have used laser speckle imaging to show that *P. notoginseng* saponins (PNS), GSRb1, L-borneol, and galangin can improve regional blood flow disorders after stroke (Li S. et al., 2012; Wang S. et al., 2017; Gao et al., 2022; Xie et al., 2023).

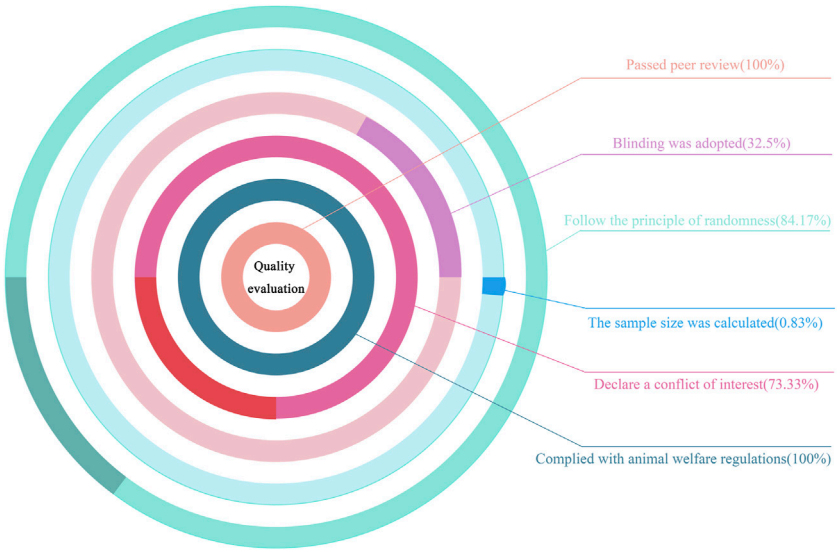

FIGURE 2
Quality evaluation chart.

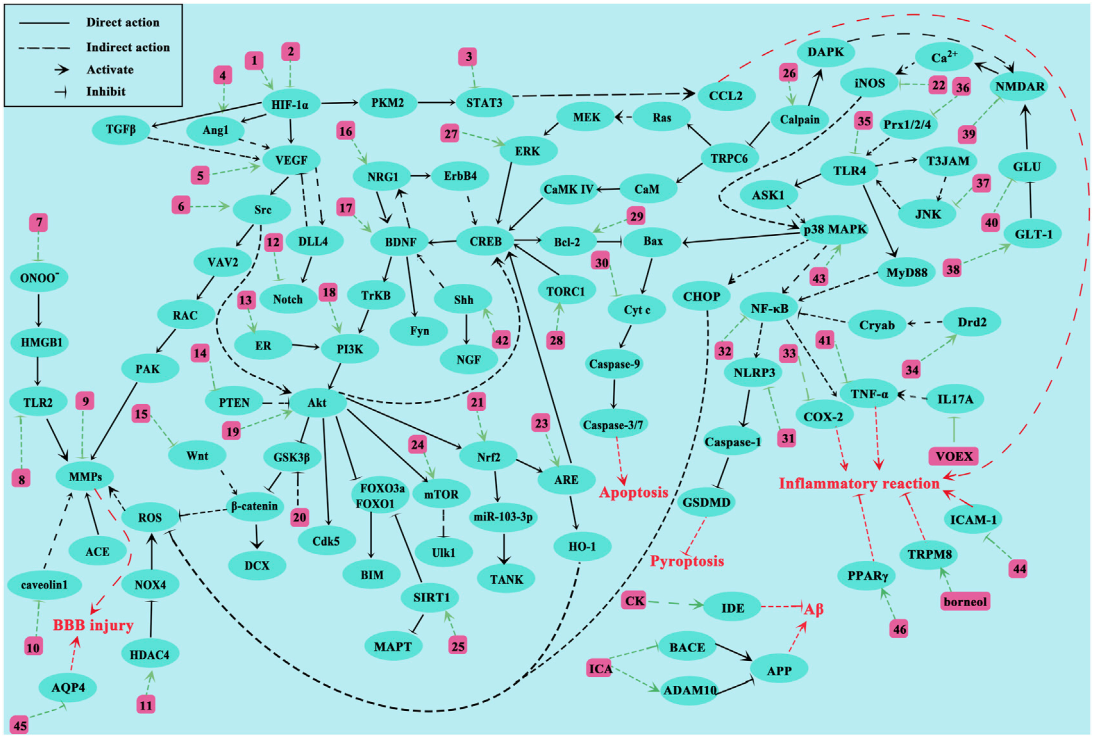

FIGURE 3
Proposed NHE molecular mechanisms for treating CI. The green line represents the interaction between NHEs and molecules. The red line represents the pathological effects caused by molecules. Numbers represent NHEs (1, DL-NBP; 2, PNS, SAA and SA; 3, ASIV and Formononetin; 4, L-borneol; 5, T-VA and GSRb1; 6, Triptolide; 7, Glycyrrhizin and SAA; 8, SAA; 9, ASIV and Methylophiopogonanone A; 10, NGR1; 11, LHA; 12, L-borneol; 13, NGR1; 14, HAR; 15, L-borneol; 16, EF; 17, GSRd, LHA, PF11, and SAA; 18, EK100, TFCJ, DGMI, and Formononetin; 19, Honokiol, L-NBP, HSYA, and GSF1; 20, CK; 21, Catalpol, KRGP, CZ-7, AA, Rus, PQS, and ASIV; 22, Honokiol; 23, EGB761; 24, EGB761 and Vitexin; 25, LIG, BA and ASIV; 26, Hyperforin and GSRd; 27, emodin; 28, TSA; 29, Catalpol, MO, SHPL-49, Galangin, KuA, Asiaticoside, GSRb1, OLE, EGB761, SA, GB, Sophoricoside and Matrine; 30, PAL extracts and GSRb1; 31, SB extracts; 32, T-VA, Silymarin, Storax, EK100 and Rus; 33, ES; 34, SAA; 35, Fructus extracts, Procyanidins and SAA; 36, Gas-d; 37, YZR extracts and EA; 38, GSRb1 and emodin; 39, GSRb1 and GSRd; 40, EEEV, scutellarin, EDAC and CTRF; 41, MO; 42, SA and PNS; 43, L-borneol, SB extracts and ASD extract; 44, ASIV and Vitexin; 45, GSRg1, ASIV and DSE; 46, Silymarin, SAA and ICA).

Amino acid excitotoxicity is due to the abnormal accumulation of some excitatory amino acids (such as glutamate) outside neurons after ischemia. Glutamate accumulation leads to sustained Ca^{2+} channel and N-methyl-D-aspartic acid receptor (NMDAR) activation on neuronal synaptic membranes. NMDAR is an ion channel regulated by glutamate on cell membranes. After glutamate activation, high Ca^{2+} levels are transported into membranes. Ca^{2+} accumulates in the cytoplasm and mitochondria, resulting in Ca^{2+} overload. This alteration affects many biological processes, such as calpain activation, oxidative stress responses, and mitochondrial damage, and also protease, kinase, phosphatase, and other enzyme activities, leading to cell death. As a major transporter of excitatory amino acids, glutamate transporter 1 (GLT-1) is mainly distributed in astrocytes. Usually, GLT-1 mediates glutamate uptake by glial cells to maintain extracellular glutamate concentrations. GLT-1 function is impaired during CI, resulting in high intersynaptic glutamate accumulation (Rao et al., 2001). GSRb1 and emodin reportedly activate GLT-1 receptors on astrocyte membranes, transferring glutamate into astrocytes to reduce its abnormal accumulation outside neurons (Wang S. et al., 2017; Leung et al., 2020). GSRb1 also has the same effects as ginsenoside Rd (GSRd) in inhibiting NMDAR expression (Zhang C. et al., 2020). Glutamine synthetase (GS) catalyzes glutamate conversion to glutamine *in vivo* and has important roles regulating glutamate levels. KRGP is an active substance extracted from Korean red ginseng(Liu L. et al., 2019). Liu et al. found that GS expression levels are significantly elevated after CI in KRGP-pretreated mice, while GS expression levels are not changed much in nuclear factor erythroid 2-related factor 2 (Nrf2) gene deletion mice, suggesting that the Nrf2 pathway has important roles in glutamate homeostasis after CI, and that KRGP may reduce amino acid excitation damage caused by CI *via* Nrf2 signaling (Liu L. et al., 2019).

Oxidative stress is a common phenomenon in hypoxic cells. Mitochondria are essential organelles which maintain energy homeostasis in cells. The state and function of mitochondria undergo significant changes during hypoxia, leading to increased intracellular reactive oxygen species (ROS) levels, which severely damage cells and brain tissue. Oxidative stress products directly attack biomacromolecules (amino acids and nucleic acids) to induce apoptosis and increase BBB permeability. Nrf2 has antioxidant and anti-inflammatory effects that activate heme oxygenase-1 (HO-1) after oxidative stress-inducer (e.g., inflammatory chemokines/cytokines) activation or tissue damage (Hassanein et al., 2023). HO-1 is an inducible homolog with antioxidant properties and has important roles regulating oxidative stress, with elevated HO-1 levels detected in almost all oxidatively stressed cells. catalpol, KRGP, CZ-7, AA, and ruscogenin (Rus) increase HO-1 expression by stimulating Nrf2 (Liu L. et al., 2019; Liu D.-D. et al., 2019; Wang et al., 2022; Zhang S. et al., 2023; Kim et al., 2023). Additionally, by detecting mitochondrial energy metabolism-related genes (*Atp12a* and *Atp6v1g3*), Liu et al. found that notoginsenoside R1 (NGR1) mitigates mitochondrial energy metabolism abnormalities (Liu et al., 2022). Three Nei-like DNA glycosylases exist in mammalian cells, which protect DNA by removing oxidative bases. GSRd protects neurons by activating Nei-like DNA glycosylase 1/3 (NEIL1/3) to promote DNA hydrolysis of oxidative stress-induced product damage (Yang et al., 2016).

Inflammatory responses are self-defense mechanisms; they are stimulated by endogenous and exogenous inflammatory factors and are closely related to different diseases. Neuroinflammation occurs at almost all stages of ischemic stroke and is caused by damage-associated molecular pattern release by damaged/dead cells. These patterns, including adenosine, heat shock proteins, and interleukin 33 (IL-33) are recognized by corresponding immune cells which trigger multiple downstream signaling pathways (Qin et al., 2022). Additionally, these patterns stimulate inflammation-related cytokine, interferon or chemokine production, leading to increased adhesion molecule expression, helping white blood cells adhere to blood vessel surfaces, and promoting immune cell infiltration. Therefore, for patients with CI, early anti-inflammatory treatment is an important method to reduce ischemic injury and improve prognosis. Pro-inflammatory cytokines induce chemokine secretion immediately after CI. Chemokine-chemokineligand2 (CCL2) and its receptors are involved in regulating inflammation in the ischemic state, and may be recruited to and adhere to cerebral vascular endothelial cells by immune cells. Signal transducer and activator of transcription 3 (STAT3) has positive regulatory effects on chemokines (such as CCL2) and acts as a key transcription factor during inflammation and immunity. Li et al. reports that ASIV inhibits CCL2 functions by inhibiting STAT3 expression and inhibiting NK cell infiltration (Li S. et al., 2021). JNK, TLR4, NF-κB, and MAPKs also have key roles in inflammatory signaling pathways *via* a vicious cycle between JNK and TLR4 (Cheng et al., 2021a). TLRs are expressed on cell surfaces and in intracellular spaces, and regulate the state and function of many immune cells. Fructus extracts, procyanidins, and SAA inhibit TLR4 expression (Lee et al., 2015; Yang et al., 2020; Ling et al., 2021), while *Alpinia oxyphylla* Miq. (YZR) extract and EA inhibit JNK activation (Yu et al., 2019; Cheng et al., 2021a). T-VA, silymarin, storax, and EK100 also suppress inflammatory responses by inhibiting NF-κB (Hou et al., 2010; Li G. et al., 2015; Wang et al., 2019; Zhou M. et al., 2021). The MAPK signaling pathway is activated shortly after ischemic injury onset. MAPK is composed of three major effectors, extracellular signal-related kinases (ERK1/2), JNK, and p38 MAPK. Among these, p38 MAPK regulates pro-inflammatory cytokine expression. The activation of MAPK/ERK signaling and the stimulating effects of MMP expression can aggravate BBB injury in ischemic stroke and further enhance pro-inflammatory factor expression. Interestingly, we found that different NHEs have opposite effects on p38 MAPK, but all were protective against CI injury, which we speculate might be due to the activation of different factors downstream of p38 MAPK. L-borneol and *Angelica sinensis* (Oliv.) Diels (ASD) extracts activate p38 MAPK (Cheng et al., 2021b; Xie et al., 2023), while Honokiol and *Scutellaria baicalensis* Georgi (SB) extracts inhibit its function (Hwang et al., 2011; Chen et al., 2014).

MMPs are essential for BBB function and structure, and mainly act on the tight junction component, ZO-1, between adjacent cells. Endothelial cells and their tight junction components are key factors maintaining BBB stability. MMPs disrupt the BBB *via* enzymatic ZO-1 hydrolysis, so they are potential therapeutic targets for CI

(Batra et al., 2010). Glycyrrhizin indirectly inhibits MMPs by reducing peroxynitrite ($ONOO^-$) production (Chen et al., 2020). NGR1 mitigates BBB disruption by MMPs by inhibiting caveolin 1 (Liu B. et al., 2021). LHA promotes histone deacetylase 4 (HDAC4) expression, leading to decreased NADPH oxidase 4 (NOX4) expression, which in turn inhibits MMP expression (Zhang Q.-Y. et al., 2017). Additionally, ginsenoside Rg1 (GSRg1), ASIV, and DSE prevent ischemic cerebral edema and BBB damage by inhibiting AQP4 (Lee K. et al., 2012; Li et al., 2013; Zhou et al., 2014).

Apoptosis is a normal physiological activity, but after CI, the process becomes overactivated and causes neuronal death, which leads to neurological deficits in patients with CI, and seriously affects neurological function recovery in later stages. Bax is a classical apoptosis-promoting gene that promotes cytochrome C (Cyt-C) transfer from the mitochondria to cells, and then activates the caspase cascade to eventually lead to apoptosis. B-cell lymphoma-2 (Bcl-2) is an apoptosis inhibitor protein, which binds to Bax and forms dimers to inhibit apoptosis. Therefore, the balance between Bcl-2 and Bax is key to neuronal survival. Several NHEs protect neurons from apoptosis, such as catalpol, MO, SHPL-49, galangin, KuA, asiaticoside, GSRb1, oleuropein (OLE), EGB761, salvianolic acid (SA), and GB, by increasing Bcl-2 levels (Li S. et al., 2012; Sun et al., 2015; Yu et al., 2016; Liu et al., 2017; Zhao et al., 2017; Yang et al., 2018; Zhang et al., 2018; Zhu et al., 2018; Luan et al., 2020; Wang et al., 2022; Zhang P. et al., 2023). Additionally, SAA also inhibits neuronal apoptosis *via* the Akt/FOXO3a/BIM pathway (Song et al., 2019).

7 Conclusion and prospects

With deepening research on NHEs, their mechanisms are becoming more complex and multifaceted. Complexity means that a single NHE, such as SAA, can simultaneously act on multiple molecular pathways. Multifaceted means that a NHE acting on the same key factor on a certain pathway may have different regulatory outcomes, such as L-borneol and Honokiol. In such cases, a deeper understanding of study conditions and results is required. Although too many pathways and factors are involved in these studies, key factors such as VEGF, BDNF, Akt, MMPs, JNK, Bax, Caspase-3/9, MAPKs, and NF-κB, may provide reference points for further research. Additionally, although CI pathogenesis is highly complex, the first and most important pathology is disturbed blood flow, which is why early CI treatments should rapidly restore blood supply. Therefore, more attention should be paid to NHEs (TSA or GSRb1) with antiplatelet or antithrombotic effects. For advanced CI treatments, selected studies should mainly focus on inhibiting neuroinflammation, inhibiting neuronal apoptosis, and protecting the BBB. This means that NHE treatment effects for CI are significant, and show how important neuroinflammation and neuronal apoptosis processes are in CI. In addition, the treatment of transient cerebral ischemia and permanent cerebral ischemia is also different. Transient cerebral ischemia is a sudden, transient cerebral vascular insufficiency, usually without brain tissue necrosis. The treatment of transient cerebral ischemia is mainly prevention, such as antiplatelet therapy. Permanent cerebral ischemia often has abnormal pathology such as thrombus, which leads to blood flow interruption and eventually brain cell death. If the vascular recanalization treatment cannot be carried out in time, serious sequelae will often be left.

Although strict review conditions were set, some flaws were identified in selected studies: 1) The elaboration of extraction protocols or NHE sources was not adequately detailed. Due to different NHE extraction methods, resultant NHEs may have different biological activities and effects, which makes the research data unreliable; 2) NHE toxicity was not adequately explored in selected studies. Even if some studies performed toxicity tests, they were *in vitro* and not *in vivo*; 3) Although considerable animal data were observed, it is uncertain if these NHEs can be eventually used in clinical practice; therefore, more pharmacological and pharmacological studies are required; and 4) NHE mechanisms were not fully explored. Most studies only explored one or several related factors, but did not examine complete NHE mechanisms.

Clinically observed NHE effects are the result of combined drug actions across a multitude of signaling pathways. Researchers are constantly exploring new treatment options to maximize treatment benefits while minimizing side effects. Traditional Chinese medicine efforts in this area are worthy of recognition, and the synergistic actions of multiple NHEs should be considered in future research. In addition, the reproducibility of drug efficacy is very critical, and it is an important factor affecting whether a drug can be transformed into clinical practice. In order to do this, we need to maintain a rigorous working attitude and record the experimental process in detail. We should strengthen our understanding of the various parts of the experiment and conduct sufficient pre-experiments. The factors affecting the transformation of medical achievements also include the lack of advanced medical equipment, insufficient attention to medical transformation, and lack of communication between the supply and demand sides.

In this review, we retrieved and screened high-quality NHE studies related to CI. We briefly summarized the potential therapeutic effects and mechanisms underpinning NHEs toward CI, which may promote NHE development and their applications in clinical settings. Selecting a clinical medication is a long and complicated process, and any possibilities, to combat CI, must be carefully and comprehensively considered.

Data availability statement

The original contributions presented in the study are included in the article/Supplementary Material, further inquiries can be directed to the corresponding author.

Author contributions

JY: Conceptualization, Data curation, Methodology, Visualization, Writing–original draft, Writing–review and editing. BY: Data curation, Supervision, Writing–review and editing. JZ: Conceptualization, Funding acquisition, Project administration, Supervision, Writing–review and editing.

Funding

The author(s) declare that financial support was received for the research, authorship, and/or publication of this article. This work is supported by the Education Department of Liaoning Provincial Basic Research Projects (JYTMS20230098); and the 30 Project Fund of Shengjing Hospital: M0269.

Conflict of interest

The authors declare that the research was conducted in the absence of any commercial or financial relationships that could be construed as a potential conflict of interest.

Supplementary material

The Supplementary Material for this article can be found online at: https://www.frontiersin.org/articles/10.3389/fphar.2024.1424146/full#supplementary-material

References

Ahad, M. A., Chear, N.J.-Y., Keat, L. G., Has, A. T. C., Murugaiyah, V., and Hassan, Z. (2023). Bio-enhanced fraction from Clitoria ternatea root extract ameliorates cognitive functions and *in vivo* hippocampal neuroplasticity in chronic cerebral hypoperfusion rat model. *Ageing Res. Rev.* 89, 101990. doi:10.1016/j.arr.2023.101990

Apte, R. S., Chen, D. S., and Ferrara, N. (2019). VEGF in signaling and disease: beyond discovery and development. *Cell.* 176, 1248–1264. doi:10.1016/j.cell.2019.01.021

Bacanlı, M., Başaran, A. A., and Başaran, N. (2017). The antioxidant, cytotoxic, and antigenotoxic effects of galangin, puerarin, and ursolic acid in mammalian cells. *Drug Chem. Toxicol.* 40, 256–262. doi:10.1080/01480545.2016.1209680

Bai, X., Qiu, Y., Wang, J., Dong, Y., Zhang, T., and Jin, H. (2024). Panax quinquefolium saponins attenuates microglia activation following acute cerebral ischemia-reperfusion injury via Nrf2/miR-103-3p/TANK pathway. *Cell. Biol. Int.* 48, 201–215. doi:10.1002/cbin.12100

Batra, A., Latour, L. L., Ruetzler, C. A., Hallenbeck, J. M., Spatz, M., Warach, S., et al. (2010). Increased plasma and tissue MMP levels are associated with BCSFB and BBB disruption evident on post-contrast FLAIR after experimental stroke. *J. Cereb. Blood Flow. Metab.* 30, 1188–1199. doi:10.1038/jcbfm.2010.1

Cao, Y., Mao, X., Sun, C., Zheng, P., Gao, J., Wang, X., et al. (2011). Baicalin attenuates global cerebral ischemia/reperfusion injury in gerbils via anti-oxidative and anti-apoptotic pathways. *Brain Res. Bull.* 85, 396–402. doi:10.1016/j.brainresbull.2011.05.002

Chen, C., Zhang, H., Xu, H., Xue, R., Zheng, Y., Wu, T., et al. (2018a). Harpagoside rescues the memory impairments in chronic cerebral hypoperfusion rats by inhibiting PTEN activity. *J. Alzheimers Dis.* 63, 445–455. doi:10.3233/JAD-171170

Chen, H., Guan, B., Wang, B., Pu, H., Bai, X., Chen, X., et al. (2020). Glycyrrhizin prevents hemorrhagic transformation and improves neurological outcome in ischemic stroke with delayed thrombolysis through targeting peroxynitrite-mediated HMGB1 signaling. *Stroke Res.* 11, 967–982. doi:10.1007/s12975-019-00772-1

Chen, H.-S., Chen, X., Li, W.-T., and Shen, J.-G. (2018b). Targeting RNS/caveolin-1/MMP signaling cascades to protect against cerebral ischemia-reperfusion injuries: potential application for drug discovery. *Acta Pharmacol. Sin.* 39, 669–682. doi:10.1038/aps.2018.27

Chen, J.-H., Kuo, H.-C., Lee, K.-F., and Tsai, T.-H. (2014). Magnolol protects neurons against ischemia injury via the downregulation of p38/MAPK, CHOP and nitrotyrosine. *Toxicol. Appl. Pharmacol.* 279, 294–302. doi:10.1016/j.taap.2014.07.005

Chen, X., Wu, H., Chen, H., Wang, Q., Xie, X.-J., and Shen, J. (2019). Astragaloside VI promotes neural stem cell proliferation and enhances neurological function recovery in transient cerebral ischemic injury via activating EGFR/MAPK signaling cascades. *Mol. Neurobiol.* 56, 3053–3067. doi:10.1007/s12035-018-1294-3

Cheng, C.-Y., Chiang, S.-Y., Kao, S.-T., and Huang, S.-C. (2021a). Alpinia oxyphylla Miq extract reduces cerebral infarction by downregulating JNK-mediated TLR4/T3JAM- and ASK1-related inflammatory signaling in the acute phase of transient focal cerebral ischemia in rats. *Chin. Med.* 16, 82. doi:10.1186/s13020-021-00495-2

Cheng, C.-Y., Huang, H.-C., Kao, S.-T., and Lee, Y.-C. (2021b). Angelica sinensis extract promotes neuronal survival by enhancing p38 MAPK-mediated hippocampal neurogenesis and dendritic growth in the chronic phase of transient global cerebral ischemia in rats. *J. Ethnopharmacol.* 278, 114301. doi:10.1016/j.jep.2021.114301

Chien, M.-Y., Chuang, C.-H., Chern, C.-M., Liou, K.-T., Liu, D.-Z., Hou, Y.-C., et al. (2016). Salvianolic acid A alleviates ischemic brain injury through the inhibition of inflammation and apoptosis and the promotion of neurogenesis in mice. *Free Radic. Biol. Med.* 99, 508–519. doi:10.1016/j.freeradbiomed.2016.09.006

Choi, M., Lim, C., Lee, B.-K., and Cho, S. (2022). Amelioration of Brain Damage after Treatment with the Methanolic Extract of Glycyrrhizae Radix et Rhizoma in Mice. *Pharmaceutics* 14, 2776. doi:10.3390/pharmaceutics14122776

Dai, J., Qiu, Y.-M., Ma, Z.-W., Yan, G.-F., Zhou, J., Li, S.-Q., et al. (2018). Neuroprotective effect of baicalin on focal cerebral ischemia in rats. *Neural Regen. Res.* 13, 2129–2133. doi:10.4103/1673-5374.241464

Damodaran, T., Tan, B. W. L., Liao, P., Ramanathan, S., Lim, G. K., and Hassan, Z. (2018). Clitoria ternatea L. root extract ameliorated the cognitive and hippocampal long-term potentiation deficits induced by chronic cerebral hypoperfusion in the rat. *J. Ethnopharmacol.* 224, 381–390. doi:10.1016/j.jep.2018.06.020

Dhamija, R. K., and Donnan, G. A. (2007). Time is brain--acute stroke management. *Aust. Fam. Physician* 36, 892–895.

Dong, X., Zhou, S., and Nao, J. (2023). Kaempferol as a therapeutic agent in Alzheimer's disease: evidence from preclinical studies. *Ageing Res. Rev.* 87, 101910. doi:10.1016/j.arr.2023.101910

Fatiha, A., Larbi, B., and Ahmed, M. (2023). Antifungal activity of the Pistacia atlantica tar against Fusarium oxysporum f. Sp. albedinis, the cause of the bayoud of the date palm in Southwest Algeria. *Adv. Biol. Earth Sci.* 8, 75–82.

Fei, Y.-X., Wang, S.-Q., Yang, L.-J., Qiu, Y.-Y., Li, Y.-Z., Liu, W.-Y., et al. (2017). Salvia miltiorrhiza Bunge (Danshen) extract attenuates permanent cerebral ischemia through inhibiting platelet activation in rats. *J. Ethnopharmacol.* 207, 57–66. doi:10.1016/j.jep.2017.06.023

Feng, Z., Lu, Y., Wu, X., Zhao, P., Li, J., Peng, B., et al. (2012). Ligustilide alleviates brain damage and improves cognitive function in rats of chronic cerebral hypoperfusion. *J. Ethnopharmacol.* 144, 313–321. doi:10.1016/j.jep.2012.09.014

Ferreira, R. S., Ribeiro, P. R., Silva, J. H. C. E., Hoppe, J. B., de Almeida, M. M. A., de Lima Ferreira, B. C., et al. (2023). Amburana cearensis seed extract stimulates astrocyte glutamate homeostatic mechanisms in hippocampal brain slices and protects oligodendrocytes against ischemia. *BMC Complement. Med. Ther.* 23, 154. doi:10.1186/s12906-023-03959-0

Ganieva, R., Galandarova, T., and Agalarov, R. (2023). Effect of chenopodium quinoa seed extract in protecting the thylakoid membrane under the influence of Cd and Na salts. *Adv. Biol. Earth Sci.* 8, 288–292.

Gao, J., Yao, M., Zhang, W., Yang, B., Yuan, G., Liu, J.-X., et al. (2022). Panax notoginseng saponins alleviates inflammation induced by microglial activation and protects against ischemic brain injury via inhibiting HIF-1α/PKM2/STAT3 signaling. *Biomed. Pharmacother.* 155, 113479. doi:10.1016/j.biopha.2022.113479

Guan, T., Liu, Q., Qian, Y., Yang, H., Kong, J., Kou, J., et al. (2013). Ruscogenin reduces cerebral ischemic injury via NF-κB-mediated inflammatory pathway in the mouse model of experimental stroke. *Eur. J. Pharmacol.* 714, 303–311. doi:10.1016/j.ejphar.2013.07.036

Guang, H.-M., and Du, G.-H. (2006). Protections of pinocembrin on brain mitochondria contribute to cognitive improvement in chronic cerebral hypoperfused rats. *Eur. J. Pharmacol.* 542, 77–83. doi:10.1016/j.ejphar.2006.04.054

Guo, C., Huang, Q., Wang, Y., Yao, Y., Li, J., Chen, J., et al. (2023). Therapeutic application of natural products: NAD+ metabolism as potential target. *Phytomedicine* 114, 154768. doi:10.1016/j.phymed.2023.154768

Hassanein, E. H. M., Ibrahim, I. M., Abd-Alhameed, E. K., Sharawi, Z. W., Jaber, F. A., and Althagafy, H. S. (2023). Nrf2/HO-1 as a therapeutic target in renal fibrosis. *Life Sci.* 334, 122209. doi:10.1016/j.lfs.2023.122209

Hosseinzadeh, H., Sadeghnia, H. R., Ghaeni, F. A., Motamedshariaty, V. S., and Mohajeri, S. A. (2012). Effects of saffron (Crocus sativus L.) and its active constituent,

crocin, on recognition and spatial memory after chronic cerebral hypoperfusion in rats. *Phytother. Res.* 26, 381–386. doi:10.1002/ptr.3566

Hou, Y.-C., Liou, K.-T., Chern, C.-M., Wang, Y.-H., Liao, J.-F., Chang, S., et al. (2010). Preventive effect of silymarin in cerebral ischemia-reperfusion-induced brain injury in rats possibly through impairing NF-κB and STAT-1 activation. *Phytomedicine* 17, 963–973. doi:10.1016/j.phymed.2010.03.012

Hu, W., Wu, X., Yu, D., Zhao, L., Zhu, X., Li, X., et al. (2020). Regulation of JNK signaling pathway and RIPK3/AIF in necroptosis-mediated global cerebral ischemia/reperfusion injury in rats. *Exp. Neurol.* 331, 113374. doi:10.1016/j.expneurol.2020.113374

Huai, Y., Dong, Y., Xu, J., Meng, N., Song, C., Li, W., et al. (2013). L-3-n-butylphthalide protects against vascular dementia via activation of the Akt kinase pathway. *Neural Regen. Res.* 8, 1733–1742. doi:10.3969/j.issn.1673-5374.2013.19.001

Huang, S., Xie, T., and Liu, W. (2019). Icariin inhibits the growth of human cervical cancer cells by inducing apoptosis and autophagy by targeting mTOR/PI3K/AKT signalling pathway. *J. BUON* 24, 990–996.

Huang, S.-S., Su, H.-H., Chien, S.-Y., Chung, H.-Y., Luo, S.-T., Chu, Y.-T., et al. (2022). Activation of peripheral TRPM8 mitigates ischemic stroke by topically applied menthol. *J. Neuroinflammation* 19, 192. doi:10.1186/s12974-022-02553-4

Hui, Z., Sha, D.-J., Wang, S.-L., Li, C.-S., Qian, J., Wang, J.-Q., et al. (2017). Panaxatriol saponins promotes angiogenesis and enhances cerebral perfusion after ischemic stroke in rats. *BMC Complement. Altern. Med.* 17, 70. doi:10.1186/s12906-017-1579-5

Hwang, Y. K., Jinhua, M., Choi, B.-R., Cui, C.-A., Jeon, W. K., Kim, H., et al. (2011). Effects of Scutellaria baicalensis on chronic cerebral hypoperfusion-induced memory impairments and chronic lipopolysaccharide infusion-induced memory impairments. *J. Ethnopharmacol.* 137, 681–689. doi:10.1016/j.jep.2011.06.025

Ipek, P., Atalar, M. N., Baran, A., Baran, M. F., Ommati, M. M., Karadag, M., et al. (2024). Determination of chemical components of the endemic species Allium turcicum L. plant extract by LC-MS/MS and evaluation of medicinal potentials. *Heliyon* 10, e27386. doi:10.1016/j.heliyon.2024.e27386

Jiang, J., Dai, J., and Cui, H. (2018b). Vitexin reverses the autophagy dysfunction to attenuate MCAO-induced cerebral ischemic stroke via mTOR/Ulk1 pathway. *Biomed. Pharmacother.* 99, 583–590. doi:10.1016/j.biopha.2018.01.067

Jiang, M., Liu, X., Zhang, D., Wang, Y., Hu, X., Xu, F., et al. (2018a). Celastrol treatment protects against acute ischemic stroke-induced brain injury by promoting an IL-33/ST2 axis-mediated microglia/macrophage M2 polarization. *J. Neuroinflammation* 15, 78. doi:10.1186/s12974-018-1124-6

Jiang, M., Wang, X.-Y., Zhou, W.-Y., Li, J., Wang, J., and Guo, L.-P. (2011). Cerebral protection of salvianolic acid A by the inhibition of granulocyte adherence. *Am. J. Chin. Med.* 39, 111–120. doi:10.1142/S0192415X11008683

Joh, E.-H., Gu, W., and Kim, D.-H. (2012). Echinocystic acid ameliorates lung inflammation in mice and alveolar macrophages by inhibiting the binding of LPS to TLR4 in NF-κB and MAPK pathways. *Biochem. Pharmacol.* 84, 331–340. doi:10.1016/j.bcp.2012.04.020

Kim, M.-S., Bang, J. H., Lee, J., Han, J.-S., Baik, T. G., and Jeon, W. K. (2016). Ginkgo biloba L. extract protects against chronic cerebral hypoperfusion by modulating neuroinflammation and the cholinergic system. *Phytomedicine* 23, 1356–1364. doi:10.1016/j.phymed.2016.07.013

Kim, S.-Y., Kim, Y.-J., Cho, S.-Y., Lee, H.-G., Kwon, S., Park, S.-U., et al. (2023). Efficacy of Artemisia annua Linné in improving cognitive impairment in a chronic cerebral hypoperfusion-induced vascular dementia animal model. *Phytomedicine* 112, 154683. doi:10.1016/j.phymed.2023.154683

Lee, D., Park, J., Yoon, J., Kim, M.-Y., Choi, H.-Y., and Kim, H. (2012a). Neuroprotective effects of Eleutherococcus senticosus bark on transient global cerebral ischemia in rats. *J. Ethnopharmacol.* 139, 6–11. doi:10.1016/j.jep.2011.05.024

Lee, K., Jo, I.-Y., Park, S. H., Kim, K. S., Bae, J., Park, J.-W., et al. (2012b). Defatted sesame seed extract reduces brain oedema by regulating aquaporin 4 expression in acute phase of transient focal cerebral ischaemia in rat. *Phytother. Res.* 26, 1521–1527. doi:10.1002/ptr.4599

Lee, K. M., Bang, J., Kim, B. Y., Lee, I. S., Han, J.-S., Hwang, B. Y., et al. (2015). Fructus mume alleviates chronic cerebral hypoperfusion-induced white matter and hippocampal damage via inhibition of inflammation and downregulation of TLR4 and p38 MAPK signaling. *BMC Complement. Altern. Med.* 15, 125. doi:10.1186/s12906-015-0652-1

Leung, S. W., Lai, J. H., Wu, J.C.-C., Tsai, Y.-R., Chen, Y.-H., Kang, S.-J., et al. (2020). Neuroprotective effects of emodin against ischemia/reperfusion injury through activating ERK-1/2 signaling pathway. *Int. J. Mol. Sci.* 21, 2899. doi:10.3390/ijms21082899

Li, D.-J., Li, Y.-H., Yuan, H.-B., Qu, L.-F., and Wang, P. (2017). The novel exercise-induced hormone irisin protects against neuronal injury via activation of the Akt and ERK1/2 signaling pathways and contributes to the neuroprotection of physical exercise in cerebral ischemia. *Metabolism* 68, 31–42. doi:10.1016/j.metabol.2016.12.003

Li, G., Li, G., Tian, Y., Zhang, Y., Hong, Y., Hao, Y., et al. (2015a). A novel ligustrazine derivative T-VA prevents neurotoxicity in differentiated PC12 cells and protects the brain against ischemia injury in MCAO rats. *Int. J. Mol. Sci.* 16, 21759–21774. doi:10.3390/ijms160921759

Li, L., Gan, H., Jin, H., Fang, Y., Yang, Y., Zhang, J., et al. (2021b). Astragaloside IV promotes microglia/macrophages M2 polarization and enhances neurogenesis and angiogenesis through PPARγ pathway after cerebral ischemia/reperfusion injury in rats. *Int. Immunopharmacol.* 92, 107335. doi:10.1016/j.intimp.2020.107335

Li, M., Ma, R. N., Li, L. H., Qu, Y. Z., and Gao, G. D. (2013). Astragaloside IV reduces cerebral edema post-ischemia/reperfusion correlating the suppression of MMP-9 and AQP4. *Eur. J. Pharmacol.* 715, 189–195. doi:10.1016/j.ejphar.2013.05.022

Li, N., Zhang, X., Zhai, J., Yin, J., Ma, K., Wang, R., et al. (2022). Isoflurane and Netrin-1 combination therapy enhances angiogenesis and neurological recovery by improving the expression of HIF-1α-Netrin-1-UNC5B/VEGF cascade to attenuate cerebral ischemia injury. *Exp. Neurol.* 352, 114028. doi:10.1016/j.expneurol.2022.114028

Li, R.-P., Wang, Z.-Z., Sun, M.-X., Hou, X.-L., Sun, Y., Deng, Z.-F., et al. (2012b). Polydatin protects learning and memory impairments in a rat model of vascular dementia. *Phytomedicine* 19, 677–681. doi:10.1016/j.phymed.2012.03.002

Li, S., Dou, B., Shu, S., Wei, L., Zhu, S., Ke, Z., et al. (2021c). Suppressing NK cells by astragaloside IV protects against acute ischemic stroke in mice via inhibiting STAT3. *Front. Pharmacol.* 12, 802047. doi:10.3389/fphar.2021.802047

Li, S., Wu, C., Zhu, L., Gao, J., Fang, J., Li, D., et al. (2012a). By improving regional cortical blood flow, attenuating mitochondrial dysfunction and sequential apoptosis galangin acts as a potential neuroprotective agent after acute ischemic stroke. *Molecules* 17, 13403–13423. doi:10.3390/molecules171113403

Li, S., Zhang, Y., and Yang, L. (2007). Improving effect of Ginkgolide B on mitochondrial respiration of ischemic neuron after cerebral thrombosis in tree shrews. *Chin. Med. J. (Engl.)* 120, 1529–1533. doi:10.1097/00029330-200709010-00012

Li, W.-X., Deng, Y.-Y., Li, F., Liu, B., Liu, H.-Y., Shi, J.-S., et al. (2015b). Icariin, a major constituent of flavonoids from Epimedium brevicornum, protects against cognitive deficits induced by chronic brain hypoperfusion via its anti-amyloidogenic effect in rats. *Pharmacol. Biochem. Behav.* 138, 40–48. doi:10.1016/j.pbb.2015.09.001

Li, Y., Xiang, L., Wang, C., Song, Y., Miao, J., and Miao, M. (2021a). Protection against acute cerebral ischemia/reperfusion injury by Leonuri Herba Total Alkali via modulation of BDNF-TrKB-PI3K/Akt signaling pathway in rats. *Biomed. Pharmacother.* 133, 111021. doi:10.1016/j.biopha.2020.111021

Li, Y., Yang, Q., Shi, Z.-H., Zhou, M., Yan, L., Li, H., et al. (2019). The anti-inflammatory effect of feiyangchangweiyan capsule and its main components on pelvic inflammatory disease in rats via the regulation of the NF-κB and BAX/BCL-2 pathway. *Evid. Based Complement. Altern. Med.* 2019, 9585727. doi:10.1155/2019/9585727

Li, Z., Zhang, M., Yang, L., Fan, D., Zhang, P., Zhang, L., et al. (2024). Sophoricoside ameliorates cerebral ischemia-reperfusion injury dependent on activating AMPK. *Eur. J. Pharmacol.* 971, 176439. doi:10.1016/j.ejphar.2024.176439

Liang, K., Ye, Y., Wang, Y., Zhang, J., and Li, C. (2014). Formononetin mediates neuroprotection against cerebral ischemia/reperfusion in rats via downregulation of the Bax/Bcl-2 ratio and upregulation PI3K/Akt signaling pathway. *J. Neurol. Sci.* 344, 100–104. doi:10.1016/j.jns.2014.06.033

Lin, M., Sun, W., Gong, W., Zhou, Z., Ding, Y., and Hou, Q. (2015). Methylophiopogonanone A protects against cerebral ischemia/reperfusion injury and attenuates blood-brain barrier disruption *in vitro*. *PLoS One* 10, e0124558. doi:10.1371/journal.pone.0124558

Lin, Y., Zhang, J.-C., Fu, J., Chen, F., Wang, J., Wu, Z.-L., et al. (2013). Hyperforin attenuates brain damage induced by transient middle cerebral artery occlusion (MCAO) in rats via inhibition of TRPC6 channels degradation. *J. Cereb. Blood Flow. Metab.* 33, 253–262. doi:10.1038/jcbfm.2012.164

Ling, Y., Jin, L., Ma, Q., Huang, Y., Yang, Q., Chen, M., et al. (2021). Salvianolic acid A alleviated inflammatory response mediated by microglia through inhibiting the activation of TLR2/4 in acute cerebral ischemia-reperfusion. *Phytomedicine* 87, 153569. doi:10.1016/j.phymed.2021.153569

Liu, B., Li, Y., Han, Y., Wang, S., Yang, H., Zhao, Y., et al. (2021a). Notoginsenoside R1 intervenes degradation and redistribution of tight junctions to ameliorate blood-brain barrier permeability by Caveolin-1/MMP2/9 pathway after acute ischemic stroke. *Phytomedicine* 90, 153660. doi:10.1016/j.phymed.2021.153660

Liu, B., Zhao, T., Li, Y., Han, Y., Xu, Y., Yang, H., et al. (2022). Notoginsenoside R1 ameliorates mitochondrial dysfunction to circumvent neuronal energy failure in acute phase of focal cerebral ischemia. *Phytother. Res.* 36, 2223–2235. doi:10.1002/ptr.7450

Liu, C., Chen, Y., Lu, C., Chen, H., Deng, J., Yan, Y., et al. (2019c). Betulinic acid suppresses Th17 response and ameliorates psoriasis-like murine skin inflammation. *Int. Immunopharmacol.* 73, 343–352. doi:10.1016/j.intimp.2019.05.030

Liu, C., Liu, N.-N., Zhang, S., Ma, G.-D., Yang, H.-G., Kong, L.-L., et al. (2021b). Salvianolic acid A prevented cerebrovascular endothelial injury caused by acute

ischemic stroke through inhibiting the Src signaling pathway. *Acta Pharmacol. Sin.* 42, 370–381. doi:10.1038/s41401-020-00568-2

Liu, D.-D., Yuan, X., Chu, S.-F., Chen, C., Ren, Q., Luo, P., et al. (2019b). CZ-7, a new derivative of Claulansine F, ameliorates 2VO-induced vascular dementia in rats through a Nrf2-mediated antioxidant responses. *Acta Pharmacol. Sin.* 40, 425–440. doi:10.1038/s41401-018-0078-7

Liu, J., Jiang, X., Zhang, Q., Lin, S., Zhu, J., Zhang, Y., et al. (2017). Neuroprotective effects of Kukoamine A against cerebral ischemia via antioxidant and inactivation of apoptosis pathway. *Neurochem. Int.* 107, 191–197. doi:10.1016/j.neuint.2016.12.024

Liu, L., Vollmer, M. K., Ahmad, A. S., Fernandez, V. M., Kim, H., and Doré, S. (2019a). Pretreatment with Korean red ginseng or dimethyl fumarate attenuates reactive gliosis and confers sustained neuroprotection against cerebral hypoxic-ischemic damage by an Nrf2-dependent mechanism. *Free Radic. Biol. Med.* 131, 98–114. doi:10.1016/j.freeradbiomed.2018.11.017

Liu, L., Zhang, X., Wang, L., Yang, R., Cui, L., Li, M., et al. (2010). The neuroprotective effects of Tanshinone IIA are associated with induced nuclear translocation of TORC1 and upregulated expression of TORC1, pCREB and BDNF in the acute stage of ischemic stroke. *Brain Res. Bull.* 82, 228–233. doi:10.1016/j.brainresbull.2010.04.005

Liu, X., Fan, L., Li, J., Bai, Z., Wang, Y., Liu, Y., et al. (2023). Mailuoning oral liquid attenuates convalescent cerebral ischemia by inhibiting AMPK/mTOR-associated apoptosis and promoting CREB/BDNF-mediated neuroprotection. *J. Ethnopharmacol.* 317, 116731. doi:10.1016/j.jep.2023.116731

Luan, P., Xu, J., Ding, X., Cui, Q., Jiang, L., Xu, Y., et al. (2020). Neuroprotective effect of salvianolate on cerebral ischaemia-reperfusion injury in rats by inhibiting the Caspase-3 signal pathway. *Eur. J. Pharmacol.* 872, 172944. doi:10.1016/j.ejphar.2020.172944

Luo, T., Li, N., He, Y., Weng, S., Wang, T., Zou, Q., et al. (2015). Emodin inhibits human sperm functions by reducing sperm [Ca(2+)]i and tyrosine phosphorylation. *Reprod. Toxicol.* 51, 14–21. doi:10.1016/j.reprotox.2014.11.007

Ma, R., Lu, D., Xie, Q., Yuan, J., Ren, M., Li, Y., et al. (2023). l-Borneol and d-Borneol promote transdifferentiation of astrocytes into neurons in rats by regulating Wnt/Notch pathway to exert neuroprotective effect during recovery from cerebral ischaemia. *Phytomedicine* 109, 154583. doi:10.1016/j.phymed.2022.154583

Ma, R., Xie, Q., Li, H., Guo, X., Wang, J., Li, Y., et al. (2021). l-Borneol exerted the neuroprotective effect by promoting angiogenesis coupled with neurogenesis via ang1-VEGF-BDNF pathway. *Front. Pharmacol.* 12, 641894. doi:10.3389/fphar.2021.641894

Mahmood, Q., Wang, G.-F., Wu, G., Wang, H., Zhou, C.-X., Yang, H.-Y., et al. (2017). Salvianolic acid A inhibits calpain activation and eNOS uncoupling during focal cerebral ischemia in mice. *Phytomedicine* 25, 8–14. doi:10.1016/j.phymed.2016.12.004

Mancuso, C., and Santangelo, R. (2017). Panax ginseng and Panax quinquefolius: from pharmacology to toxicology. *Food Chem. Toxicol.* 107, 362–372. doi:10.1016/j.fct.2017.07.019

Mao, X.-N., Zhou, H.-J., Yang, X.-J., Zhao, L.-X., Kuang, X., Chen, C., et al. (2017). Neuroprotective effect of a novel gastrodin derivative against ischemic brain injury: involvement of peroxiredoxin and TLR4 signaling inhibition. *Oncotarget* 8, 90979–90995. doi:10.18632/oncotarget.18773

Mei, N., Guo, X., Ren, Z., Kobayashi, D., Wada, K., and Guo, L. (2017a). Review of Ginkgo biloba-induced toxicity, from experimental studies to human case reports. *J. Environ. Sci. Health C Environ. Carcinog. Ecotoxicol. Rev.* 35, 1–28. doi:10.1080/10590501.2016.1278298

Mei, N., Guo, X., Ren, Z., Kobayashi, D., Wada, K., and Guo, L. (2017b). Review of Ginkgo biloba-induced toxicity, from experimental studies to human case reports. *J. Environ. Sci. Health C Environ. Carcinog. Ecotoxicol. Rev.* 35, 1–28. doi:10.1080/10590501.2016.1278298

Nazari, S., Rameshrad, M., and Hosseinzadeh, H. (2017). Toxicological effects of Glycyrrhiza glabra (licorice): a review. *Phytother. Res.* 31, 1635–1650. doi:10.1002/ptr.5893

Niu, H.-M., Ma, D.-L., Wang, M.-Y., Chen, X.-P., Zhang, Li, Li, Y.-L., et al. (2020). Epimedium flavonoids protect neurons and synapses in the brain via activating NRG1/ErbB4 and BDNF/Fyn signaling pathways in a chronic cerebral hypoperfusion rat model. *Brain Res. Bull.* 162, 132–140. doi:10.1016/j.brainresbull.2020.06.012

Park, S. J., Nam, K. W., Lee, H. J., Cho, E. Y., Koo, U., and Mar, W. (2009). Neuroprotective effects of an alkaloid-free ethyl acetate extract from the root of Sophora flavescens Ait. against focal cerebral ischemia in rats. *Phytomedicine* 16, 1042–1051. doi:10.1016/j.phymed.2009.03.017

Peng, D., Wang, Y.-X., Huang, T.-H., Luo, D., Qiao, L.-J., Wang, Q., et al. (2022a). Ligustilide improves cognitive impairment via regulating the SIRT1/ire1α/XBP1s/CHOP pathway in vascular dementia rats. *Oxid. Med. Cell. Longev.* 2022, 6664990. doi:10.1155/2022/6664990

Peng, T., Li, S., Liu, L., Yang, C., Farhan, M., Chen, L., et al. (2022b). Artemisinin attenuated ischemic stroke induced cell apoptosis through activation of ERK1/2/CREB/BCL-2 signaling pathway *in vitro* and *in vivo*. *Int. J. Biol. Sci.* 18, 4578–4594. doi:10.7150/ijbs.69892

Pengyue, Z., Tao, G., Hongyun, H., Liqiang, Y., and Yihao, D. (2017). Breviscapine confers a neuroprotective efficacy against transient focal cerebral ischemia by attenuating neuronal and astrocytic autophagy in the penumbra. *Biomed. Pharmacother.* 90, 69–76. doi:10.1016/j.biopha.2017.03.039

Powers, W. J. (2020). Acute ischemic stroke. *N. Engl. J. Med.* 383, 252–260. doi:10.1056/NEJMcp1917030

Qi, Z., Yan, F., Shi, W., Zhang, C., Dong, W., Zhao, Y., et al. (2014). AKT-related autophagy contributes to the neuroprotective efficacy of hydroxysafflor yellow A against ischemic stroke in rats. *Transl. Stroke Res.* 5, 501–509. doi:10.1007/s12975-014-0346-x

Qin, C., Yang, S., Chu, Y.-H., Zhang, H., Pang, X.-W., Chen, L., et al. (2022). Signaling pathways involved in ischemic stroke: molecular mechanisms and therapeutic interventions. *Signal Transduct. Target Ther.* 7, 215. doi:10.1038/s41392-022-01064-1

Qin, X., Li, L., Lv, Q., Yu, B., Yang, S., He, T., et al. (2012). Underlying mechanism of protection from hypoxic injury seen with n-butanol extract of Potentilla anserine L. in hippocampal neurons. *Neural Regen. Res.* 7, 2576–2582. doi:10.3969/j.issn.1673-5374.2012.33.002

Rao, V. L., Bowen, K. K., and Dempsey, R. J. (2001). Transient focal cerebral ischemia down-regulates glutamate transporters GLT-1 and EAAC1 expression in rat brain. *Neurochem. Res.* 26, 497–502. doi:10.1023/a:1010956711295

Reilly, M., and Fitzgerald, G. A. (1993). Cellular activation by thromboxane A2 and other eicosanoids. *Eur. Heart J.* 14 (Suppl. K), 88–93.

Rodrigues, F. T. S., de Sousa, C. N. S., Ximenes, N. C., Almeida, A. B., Cabral, L. M., Patrocínio, C. F. V., et al. (2017). Effects of standard ethanolic extract from Erythrina velutina in acute cerebral ischemia in mice. *Biomed. Pharmacother.* 96, 1230–1239. doi:10.1016/j.biopha.2017.11.093

Saleem, S., Zhuang, H., Biswal, S., Christen, Y., and Doré, S. (2008). Ginkgo biloba extract neuroprotective action is dependent on heme oxygenase 1 in ischemic reperfusion brain injury. *Stroke* 39, 3389–3396. doi:10.1161/STROKEAHA.108.523480

Seo, H.-W., Ha, T.-Y., Ko, G., Jang, A., Choi, J.-W., Lee, D.-H., et al. (2023). Scutellaria baicalensis attenuated neurological impairment by regulating programmed cell death pathway in ischemic stroke mice. *Cells* 12, 2133. doi:10.3390/cells12172133

Shi, R., Zheng, C.-B., Wang, H., Rao, Q., Du, T., Bai, C., et al. (2020). Gastrodin alleviates vascular dementia in a 2-VO-vascular dementia rat model by altering amyloid and tau levels. *Pharmacology* 105, 386–396. doi:10.1159/000504056

Shi, Y.-H., Zhang, X.-L., Ying, P.-J., Wu, Z.-Q., Lin, L.-L., Chen, W., et al. (2021). Neuroprotective effect of astragaloside IV on cerebral ischemia/reperfusion injury rats through sirt1/mapt pathway. *Front. Pharmacol.* 12, 639898. doi:10.3389/fphar.2021.639898

Song, J., Zhang, W., Wang, J., Yang, H., Zhou, Q., Wang, H., et al. (2019). Inhibition of FOXO3a/BIM signaling pathway contributes to the protective effect of salvianolic acid A against cerebral ischemia/reperfusion injury. *Acta Pharm. Sin. B* 9, 505–515. doi:10.1016/j.apsb.2019.01.010

Sun, T., Liu, B., and Li, P. (2015). Nerve protective effect of asiaticoside against ischemia-hypoxia in cultured rat cortex neurons. *Med. Sci. Monit.* 21, 3036–3041. doi:10.12659/MSM.894024

Talman, A. M., Clain, J., Duval, R., Ménard, R., and Ariey, F. (2019). Artemisinin bioactivity and resistance in malaria parasites. *Trends Parasitol.* 35, 953–963. doi:10.1016/j.pt.2019.09.005

Tan, Z., Yang, G., Qiu, J., Yan, W., Liu, Y., Ma, Z., et al. (2022). Quercetin alleviates demyelination through regulating microglial phenotype transformation to mitigate neuropsychiatric symptoms in mice with vascular dementia. *Mol. Neurobiol.* 59, 3140–3158. doi:10.1007/s12035-021-02712-3

Teixeira, L. L., Alencar, H. M. N. da S., Ferreira, L. O., Rodrigues, J. C. M., de Souza, R. D., Celestino Pinto, L., et al. (2023). Oral treatment with the extract of euterpe oleracea mart. Improves motor dysfunction and reduces brain injury in rats subjected to ischemic stroke. *Nutrients* 15, 1207. doi:10.3390/nu15051207

Tiang, N., Ahad, M. A., Murugaiyah, V., and Hassan, Z. (2020). Xanthone-enriched fraction of Garcinia mangostana and α-mangostin improve the spatial learning and memory of chronic cerebral hypoperfusion rats. *J. Pharm. Pharmacol.* 72, 1629–1644. doi:10.1111/jphp.13345

Tu, L., Wang, Y., Chen, D., Xiang, P., Shen, J., Li, Y., et al. (2018). Protective effects of notoginsenoside R1 via regulation of the PI3K-Akt-mTOR/JNK pathway in neonatal cerebral hypoxic-ischemic brain injury. *Neurochem. Res.* 43, 1210–1226. doi:10.1007/s11064-018-2538-3

Wan, Q., Ma, X., Zhang, Z.-J., Sun, T., Xia, F., Zhao, G., et al. (2017). Ginsenoside reduces cognitive impairment during chronic cerebral hypoperfusion through brain-derived neurotrophic factor regulated by epigenetic modulation. *Mol. Neurobiol.* 54, 2889–2900. doi:10.1007/s12035-016-9868-4

Wan, Y.-S., You, Y., Ding, Q.-Y., Xu, Y.-X., Chen, H., Wang, R.-R., et al. (2022). Triptolide protects against white matter injury induced by chronic cerebral hypoperfusion in mice. *Acta Pharmacol. Sin.* 43, 15–25. doi:10.1038/s41401-021-00637-0

Wang, C., Chen, H., Jiang, H.-H., Mao, B.-B., and Yu, H. (2021). Total flavonoids of chuju decrease oxidative stress and cell apoptosis in ischemic stroke rats: network and experimental analyses. *Front. Neurosci.* 15, 772401. doi:10.3389/fnins.2021.772401

Wang, C., Liu, Y., Liu, X., Zhang, Y., Yan, X., Deng, X., et al. (2023a). Scutellarin alleviates ischemic brain injury in the acute phase by affecting the activity of neurotransmitters in neurons. *Molecules* 28, 3181. doi:10.3390/molecules28073181

Wang, C., Zhang, D., Ma, H., and Liu, J. (2007). Neuroprotective effects of emodin-8-O-beta-D-glucoside *in vivo* and *in vitro*. *Eur. J. Pharmacol.* 577, 58–63. doi:10.1016/j.ejphar.2007.08.033

Wang, J., Zhang, Y., Zhang, M., Sun, S., Zhong, Y., Han, L., et al. (2022). Feasibility of catalpol intranasal administration and its protective effect on acute cerebral ischemia in rats via anti-oxidative and anti-apoptotic mechanisms. *Drug Des. devel. Ther.* 16, 279–296. doi:10.2147/DDDT.S343928

Wang, L., Liu, C., Wang, L., and Tang, B. (2023b). Astragaloside IV mitigates cerebral ischaemia-reperfusion injury via inhibition of P62/Keap1/Nrf2 pathway-mediated ferroptosis. *Eur. J. Pharmacol.* 944, 175516. doi:10.1016/j.ejphar.2023.175516

Wang, S., Li, M., Guo, Y., Li, C., Wu, L., Zhou, X.-F., et al. (2017a). Effects of Panax notoginseng ginsenoside Rb1 on abnormal hippocampal microenvironment in rats. *J. Ethnopharmacol.* 202, 138–146. doi:10.1016/j.jep.2017.01.005

Wang, T., Wang, C., Wu, Q., Zheng, K., Chen, J., Lan, Y., et al. (2017b). Evaluation of tanshinone IIA developmental toxicity in zebrafish embryos. *Molecules* 22, 660. doi:10.3390/molecules22040660

Wang, X., Zhu, W., Xing, M., Zhu, H., Chen, E., and Zhou, J. (2023c). Matrine disrupts Nrf2/GPX4 antioxidant system and promotes hepatocyte ferroptosis. *Chem. Biol. Interact.* 384, 110713. doi:10.1016/j.cbi.2023.110713

Wang, Y., Shen, Y., Liu, Z., Gu, J., Xu, C., Qian, S., et al. (2019). Dl-NBP (Dl-3-N-butylphthalide) treatment promotes neurological functional recovery accompanied by the upregulation of white matter integrity and HIF-1α/VEGF/Notch/Dll4 expression. *Front. Pharmacol.* 10, 1595. doi:10.3389/fphar.2019.01595

Wang, Y.-H., Chern, C.-M., Liou, K.-T., Kuo, Y.-H., and Shen, Y.-C. (2019). Ergostatrien-7,9(11),22-trien-3β-ol from Antrodia camphorata ameliorates ischemic stroke brain injury via downregulation of p65NF-κ-B and caspase 3, and activation of Akt/GSK3/catenin-associated neurogenesis. *Food Funct.* 10, 4725–4738. doi:10.1039/c9fo00908f

Wang, Z., Liu, T., Gan, L., Wang, T., Yuan, X., Zhang, B., et al. (2010). Shikonin protects mouse brain against cerebral ischemia/reperfusion injury through its antioxidant activity. *Eur. J. Pharmacol.* 643, 211–217. doi:10.1016/j.ejphar.2010.06.027

Wu, R., Liang, Y., Xu, M., Fu, K., Zhang, Y., Wu, L., et al. (2021). Advances in chemical constituents, clinical applications, pharmacology, pharmacokinetics and toxicology of Erigeron breviscapus. *Front. Pharmacol.* 12, 656335. doi:10.3389/fphar.2021.656335

Wu, S., Huang, R., Zhang, R., Xiao, C., Wang, L., Luo, M., et al. (2023). Gastrodin and gastrodigenin improve energy metabolism disorders and mitochondrial dysfunction to antagonize vascular dementia. *Molecules* 28, 2598. doi:10.3390/molecules28062598

Xie, Q., Lu, D., Yuan, J., Ren, M., Li, Y., Wang, J., et al. (2023). l-borneol promotes neurovascular unit protection in the subacute phase of transient middle cerebral artery occlusion rats: p38-MAPK pathway activation, anti-inflammatory, and anti-apoptotic effect. *Phytother. Res.* 37, 4166–4184. doi:10.1002/ptr.7878

Xiong, D., Deng, Y., Huang, B., Yin, C., Liu, B., Shi, J., et al. (2016). Icariin attenuates cerebral ischemia-reperfusion injury through inhibition of inflammatory response mediated by NF-κB, PPARα and PPARγ in rats. *Int. Immunopharmacol.* 30, 157–162. doi:10.1016/j.intimp.2015.11.035

Xu, D., Kong, T., Shao, Z., Liu, M., Zhang, R., Zhang, S., et al. (2021). Orexin-A alleviates astrocytic apoptosis and inflammation via inhibiting OX1R-mediated NF-κB and MAPK signaling pathways in cerebral ischemia/reperfusion injury. *Biochim. Biophys. Acta Mol. Basis Dis.* 1867, 166230. doi:10.1016/j.bbadis.2021.166230

Xuying, W., Jiangbo, Z., Yuping, Z., Xili, M., Yiwen, Z., Tianbao, Z., et al. (2010). Effect of astragaloside IV on the general and peripartum reproductive toxicity in Sprague-Dawley rats. *Int. J. Toxicol.* 29, 505–516. doi:10.1177/1091581810376840

Yang, B., Sun, Y., Lv, C., Zhang, W., and Chen, Y. (2020). Procyanidins exhibits neuroprotective activities against cerebral ischemia reperfusion injury by inhibiting TLR4-NLRP3 inflammasome signal pathway. *Psychopharmacol. (Berl.)* 237, 3283–3293. doi:10.1007/s00213-020-05610-z

Yang, L.-X., Zhang, X., and Zhao, G. (2016). Ginsenoside Rd attenuates DNA damage by increasing expression of DNA glycosylase endonuclease VIII-like proteins after focal cerebral ischemia. *Chin. Med. J. (Engl.)* 129, 1955–1962. doi:10.4103/0366-6999.187851

Yang, M.-Y., Song, Z.-Y., Gan, H.-L., Zheng, M.-H., Liu, Q., Meng, X.-T., et al. (2022b). Non-clinical safety evaluation of salvianolic acid A: acute, 4-week intravenous toxicities and genotoxicity evaluations. *BMC Pharmacol. Toxicol.* 23, 83. doi:10.1186/s40360-022-00622-1

Yang, X., Zheng, T., Hong, H., Cai, N., Zhou, X., Sun, C., et al. (2018). Neuroprotective effects of Ginkgo biloba extract and Ginkgolide B against oxygen-glucose deprivation/reoxygenation and glucose injury in a new *in vitro* multicellular network model. *Front. Med.* 12, 307–318. doi:10.1007/s11684-017-0547-2

Yang, Y., Song, J., Liu, N., Wei, G., Liu, S., Zhang, S., et al. (2022a). Salvianolic acid A relieves cognitive disorder after chronic cerebral ischemia: involvement of Drd2/Cryab/NF-κB pathway. *Pharmacol. Res.* 175, 105989. doi:10.1016/j.phrs.2021.105989

Yao, Z.-H., Wang, J., Yuan, J.-P., Xiao, K., Zhang, S.-F., Xie, Y.-C., et al. (2021). EGB761 ameliorates chronic cerebral hypoperfusion-induced cognitive dysfunction and synaptic plasticity impairment. *Aging (Albany NY)* 13, 9522–9541. doi:10.18632/aging.202555

Yu, H., Li, W., Cao, X., Wang, X., Zhao, Y., Song, L., et al. (2019). Echinocystic acid, a natural plant extract, alleviates cerebral ischemia/reperfusion injury via inhibiting the JNK signaling pathway. *Eur. J. Pharmacol.* 861, 172610. doi:10.1016/j.ejphar.2019.172610

Yu, H., Liu, P., Tang, H., Jing, J., Lv, X., Chen, L., et al. (2016). Oleuropein, a natural extract from plants, offers neuroprotection in focal cerebral ischemia/reperfusion injury in mice. *Eur. J. Pharmacol.* 775, 113–119. doi:10.1016/j.ejphar.2016.02.027

Yu, L., Zhang, Y., Chen, Q., He, Y., Zhou, H., Wan, H., et al. (2022). Formononetin protects against inflammation associated with cerebral ischemia-reperfusion injury in rats by targeting the JAK2/STAT3 signaling pathway. *Biomed. Pharmacother.* 149, 112836. doi:10.1016/j.biopha.2022.112836

Yuan, L., Sun, S., Pan, X., Zheng, L., Li, Y., Yang, J., et al. (2020). Pseudoginsenoside-F11 improves long-term neurological function and promotes neurogenesis after transient cerebral ischemia in mice. *Neurochem. Int.* 133, 104586. doi:10.1016/j.neuint.2019.104586

Zhang, C., Liu, X., Xu, H., Hu, G., Zhang, X., Xie, Z., et al. (2020a). Protopanaxadiol ginsenoside Rd protects against NMDA receptor-mediated excitotoxicity by attenuating calcineurin-regulated DAPK1 activity. *Sci. Rep.* 10, 8078. doi:10.1038/s41598-020-64738-2

Zhang, J., Liu, M., Huang, M., Chen, M., Zhang, D., Luo, L., et al. (2019). Ginsenoside F1 promotes angiogenesis by activating the IGF-1/IGF1R pathway. *Pharmacol. Res.* 144, 292–305. doi:10.1016/j.phrs.2019.04.021

Zhang, J., Wu, C., Gao, L., Du, G., and Qin, X. (2020b). Astragaloside IV derived from Astragalus membranaceus: a research review on the pharmacological effects. *Adv. Pharmacol.* 87, 89–112. doi:10.1016/bs.apha.2019.08.002

Zhang, P., Xu, J., Cui, Q., Lin, G., Wang, F., Ding, X., et al. (2023b). Multi-pathway neuroprotective effects of a novel salidroside derivative SHPL-49 against acute cerebral ischemic injury. *Eur. J. Pharmacol.* 949, 175716. doi:10.1016/j.ejphar.2023.175716

Zhang, Q.-Y., Wang, Z.-J., Sun, D.-M., Wang, Y., Xu, P., Wu, W.-J., et al. (2017a). Novel therapeutic effects of leonurine on ischemic stroke: new mechanisms of BBB integrity. *Oxid. Med. Cell. Longev.* 2017, 7150376. doi:10.1155/2017/7150376

Zhang, S., Song, Z., Shi, L., Zhou, L., Zhang, J., Cui, J., et al. (2021). A dandelion polysaccharide and its selenium nanoparticles: structure features and evaluation of anti-tumor activity in zebrafish models. *Carbohydr. Polym.* 270, 118365. doi:10.1016/j.carbpol.2021.118365

Zhang, S., Yu, Y., Sheng, M., Chen, X., Wu, Q., Kou, J., et al. (2023c). Ruscogenin timing administration mitigates cerebral ischemia-reperfusion injury through regulating circadian genes and activating Nrf2 pathway. *Phytomedicine* 120, 155028. doi:10.1016/j.phymed.2023.155028

Zhang, W., Song, J.-K., Yan, R., Li, L., Xiao, Z.-Y., Zhou, W.-X., et al. (2018). Diterpene ginkgolides protect against cerebral ischemia/reperfusion damage in rats by activating Nrf2 and CREB through PI3K/Akt signaling. *Acta Pharmacol. Sin.* 39, 1259–1272. doi:10.1038/aps.2017.149

Zhang, W., Zhang, P., Xu, L.-H., Gao, K., Zhang, J.-L., Yao, M.-N., et al. (2024). Ethanol extract of Verbena officinalis alleviates MCAO-induced ischaemic stroke by inhibiting IL17A pathway-regulated neuroinflammation. *Phytomedicine* 123, 155237. doi:10.1016/j.phymed.2023.155237

Zhang, W., Zhang, Q., Deng, W., Li, Y., Xing, G., Shi, X., et al. (2014). Neuroprotective effect of pretreatment with ganoderma lucidum in cerebral ischemia/reperfusion injury in rat hippocampus. *Neural Regen. Res.* 9, 1446–1452. doi:10.4103/1673-5374.139461

Zhang, Y., Zhang, X., Cui, L., Chen, R., Zhang, C., Li, Y., et al. (2017b). Salvianolic Acids for Injection (SAFI) promotes functional recovery and neurogenesis via sonic hedgehog pathway after stroke in mice. *Neurochem. Int.* 110, 38–48. doi:10.1016/j.neuint.2017.09.001

Zhang, Y.-C., Gan, F.-F., Shelar, S. B., Ng, K.-Y., and Chew, E.-H. (2013). Antioxidant and Nrf2 inducing activities of luteolin, a flavonoid constituent in Ixeris sonchifolia Hance, provide neuroprotective effects against ischemia-induced cellular injury. *Food Chem. Toxicol.* 59, 272–280. doi:10.1016/j.fct.2013.05.058

Zhang, Z., Shu, X., Cao, Q., Xu, L., Wang, Z., Li, C., et al. (2023a). Compound from magnolia officinalis ameliorates white matter injury by promoting oligodendrocyte maturation in chronic cerebral ischemia models. *Neurosci. Bull.* 39, 1497–1511. doi:10.1007/s12264-023-01068-z

Zhao, G.-C., Yuan, Y.-L., Chai, F.-R., and Ji, F.-J. (2017). Effect of Melilotus officinalis extract on the apoptosis of brain tissues by altering cerebral thrombosis and inflammatory mediators in acute cerebral ischemia. *Biomed. Pharmacother.* 89, 1346–1352. doi:10.1016/j.biopha.2017.02.109

Zhao, P., Zhou, R., Zhu, X.-Y., Hao, Y.-J., Li, N., Wang, J., et al. (2015). Matrine attenuates focal cerebral ischemic injury by improving antioxidant activity and inhibiting apoptosis in mice. *Int. J. Mol. Med.* 36, 633–644. doi:10.3892/ijmm.2015.2260

Zhao, Y., Shi, X., Wang, J., Mang, J., and Xu, Z. (2021). Betulinic acid ameliorates cerebral injury in middle cerebral artery occlusion rats through regulating autophagy. *ACS Chem. Neurosci.* 12, 2829–2837. doi:10.1021/acschemneuro.1c00198

Zheng, M., Zhou, M., Chen, M., Lu, Y., Shi, D., Wang, J., et al. (2021). Neuroprotective effect of daidzein extracted from pueraria lobate radix in a stroke model via the akt/mTOR/BDNF channel. *Front. Pharmacol.* 12, 772485. doi:10.3389/fphar.2021.772485

Zhou, D., Cen, K., Liu, W., Liu, F., Liu, R., Sun, Y., et al. (2021b). Xuesaitong exerts long-term neuroprotection for stroke recovery by inhibiting the ROCKII pathway, *in vitro* and *in vivo*. *J. Ethnopharmacol.* 272, 113943. doi:10.1016/j.jep.2021.113943

Zhou, M., Li, D., Li, L., Zhao, P., Yue, S., Li, X., et al. (2021a). Post-stroke treatment of storax improves long-term outcomes of stroke in rats. *J. Ethnopharmacol.* 280, 114467. doi:10.1016/j.jep.2021.114467

Zhou, Y., Li, H., Lu, L., Fu, D., Liu, A., Li, J., et al. (2014). Ginsenoside Rg1 provides neuroprotection against blood brain barrier disruption and neurological injury in a rat model of cerebral ischemia/reperfusion through downregulation of aquaporin 4 expression. *Phytomedicine* 21, 998–1003. doi:10.1016/j.phymed.2013.12.005

Zhu, J.-D., Wang, J.-J., Zhang, X.-H., Yu, Y., and Kang, Z.-S. (2018). Panax ginseng extract attenuates neuronal injury and cognitive deficits in rats with vascular dementia induced by chronic cerebral hypoperfusion. *Neural Regen. Res.* 13, 664–672. doi:10.4103/1673-5374.230292

Zhu, Y. Z., Wu, W., Zhu, Q., and Liu, X. (2018). Discovery of Leonuri and therapeutical applications: from bench to bedside. *Pharmacol. Ther.* 188, 26–35. doi:10.1016/j.pharmthera.2018.01.006

Zong, W., Zeng, X., Chen, S., Chen, L., Zhou, L., Wang, X., et al. (2019). Ginsenoside compound K attenuates cognitive deficits in vascular dementia rats by reducing the Aβ deposition. *J. Pharmacol. Sci.* 139, 223–230. doi:10.1016/j.jphs.2019.01.013

Glossary

CI	cerebral ischemia
ACI	acute cerebral ischemia
CCI	chronic cerebral ischemia
IR	ischemia-reperfusion
BBB	blood-brain barrier
NHE	natural herbal extract
rt-PA	recombinant tissue plasminogen activator
LHA	*Leonurus japonicus* Houtt. total alkaloids
KuA	kukoamine A
ICA	icariin
ASIV	astragaloside IV
SAA	salvianolic acid A
BA	betulinic acid
LIG	ligustilide
GB	ginkgolide B
TSA	tanshinone IIA
SCED	supercritical CO_2 extracts from *DanShen*
NGR1	notoginsenoside R1
GSRb1	ginsenoside Rb1
GSRg1	ginsenoside Rg1
GSF1	ginsenoside F1
GSRd	ginsenoside Rd
PF11	pseudoginsenoside-F11
SA	salvianolic acid
Que	quercetin
HAR	harpagoside
GBE	*Ginkgo biloba* L. extract
EF	epimedium flavonoids
SB	*Scutellaria baicalensis* Georgi
Gas	gastrodin
CTRF	*Clitoria ternatea* L. root extract
XEFGM	xanthone-enriched fraction of *Garcinia mangostana* L.
CSL	*Crocus sativus* L.
EEEV	ethanolic extract from *Erythrina velutina* Willd.
YZR	*Alpinia oxyphylla* Miq.
GA	ginkgolide A
GC	ginkgolide C
OLE	oleuropein
PQS	*Panax quinquefolius* L. saponins
VOEX	*Verbena officinalis* L. ethanol extracts
Rus	ruscogenin
TFCJ	total flavonoids of *Chuju*
NBP	n-butylphthalide
L-NBP	L-n-butylphthalide
DL-NBP	DL-n-butylphthalide
GL	*Ganoderma lucidum*
HSYA	Hydroxysafflor Yellow A
PNS	*Panax notoginseng* saponins
ES	*Eleutherococcus senticosus*
GRex	*Glycyrrhiza uralensis* Fisch. methanolic extracts
EO	*Euterpe oleracea* Mart.
ASD	*Angelica sinensis* (Oliv.) Diels
ESF	EtOAc extract of *Sophora flavescens* Aiton
MCAO	middle cerebral artery occlusion
PT	photothrombosis
rUCCAO	right unilateral common carotid artery occlusion
2VO	bilateral carotid artery ligation
BCAS	bilateral common carotid artery stenosis
BCCAo	bilateral common carotid artery occlusion
4VO	4-vessel occlusion
PBOCCA	permanent bilateral occlusion of common carotid arteries
MCAO/R	middle cerebral artery occlusion and reperfusion
mNSS	modified Neurological Severity Score
EB	evans blue
OGD	oxygen-glucose deprivation
OGD/R	oxygen-glucose deprivation/re-oxygenation
Nrf2	nuclear factor erythroid 2-related factor 2
HO-1	heme oxygenase-1
Bax	B-cell lymphoma-2-Associated X
Bcl-2	B-cell lymphoma-2
6-keto-PGF1α	6-keto Prostaglandin F1α
TXB2	thromboxane B2
TXA2	thromboxane A2
PAFR	platelet-activating factor receptor
PLC	phospholipase C
PKC	protein kinase C
TORC1	target of Rapamycin Complex 1
CREB	cAMP-response element binding protein
BDNF	brain-derived neurotrophic factor
VEGF	vascular endothelial growth factor
VEGFA	vascular endothelial growth factor A
Src	tyrosine kinase Src
VAV2	vav guanine nucleotide exchange factor 2

Rac	Ras-related C3 botulinum toxin substrate
PAK	p21 activated kinase
MMPs	matrix metalloproteinases
MMP2/9	matrix metalloproteinase 2/9
HIF-1α	hypoxia-inducible factor alpha
PKM2	pyruvate kinase isozyme type M2
STAT3	signal transducer and activator of transcription 3
GLT-1	glutamate transporter 1
NMDAR	N-methyl-D-aspartic acid receptor
NR2b	N-methyl-D-aspartic acid receptor 2b
Cyt-C	cytochrome C
NEIL1/3	Nei Like DNA Glycosylase 1/3
Ang1	Angiopoietin-1
NF-κB	nuclear factor kappa-B
COX-2	cyclooxygenase-2
IL-33	interleukin 33
IL-17A	interleukin 17A
ICAM1	intercellular adhesion molecule 1
ST2	growth stimulation expressed gene 2
SHH	Sonic hedgehog
NGF	nerve growth factor
Drd2	dopamine D2 receptor
Cryab	αB-crystallin
Akt	protein kinase B
GSK3β	glycogen synthase kinase 3β
SIRT1	sirtuin 1
IRE1α	inositol-requiring enzyme-1α
XBP1s	X-box binding protein 1
CHOP	C/EBP-homologous protein
mTOR	mammalian target of rapamycin
PTEN	phosphatase and tensin homolog
TLR4	toll-like receptor 4
TLR2	toll-like receptor 2
MyD88	myeloid differentiation factor 88
MAPK	mitogen-activated protein kinase
p38 MAPK	p38 mitogen-activated protein kinase
NRG1	neuregulin1
ErbB4	epidermal growth factor receptor
PI3K	phosphoinositide 3-kinase
BACE1	beta-secretase 1
ADAM10	a disintegrin and metalloproteinase domain 10
IDE	insulin-degrading enzyme
Keap1	kelch-like ECH-associated protein 1
ARE	antioxidant response element
ROCKII	Rho-associated protein kinase II
$ONOO^-$	peroxynitrite
TrKB	tyrosine kinase receptor B
HDAC4	histone deacetylase 4
NOX4	NADPH oxidase 4
HPLC	high performance liquid chromatography
JNK	c-Jun N-terminal kinase
T3JAM	TRAF3-interacting JNK-activating modulator
ER	estrogen receptor
RIPK1/3	receptor-interacting protein kinase 1/3
NLRP3	NOD-like receptor family pyrin domain-containing 3
HMGB1	high mobility group box 1
Dll4	delta-like ligand 4
TRPC6	transient receptor potential channel 6
IGF-1	insulin-like growth factor 1
IGF1R	insulin-like growth factor 1 receptor
DAPK	death-associated protein kinase
ERK1/2	extracellular signal-related kinases 1/2.

frontiers | Frontiers in Neuroscience

TYPE Original Research
PUBLISHED 13 August 2024
DOI 10.3389/fnins.2024.1432969

OPEN ACCESS

EDITED BY
Giuseppe Di Giovanni,
Cardiff University, United Kingdom

REVIEWED BY
Shaista Chaudhary,
NewYork-Presbyterian, United States
B. S. Mamatha,
NITTE University Center for Science Education and Research (NUCSER), India

*CORRESPONDENCE
Bin Li
leebin009@163.com
Hanyong Jin
jinhanyong@ybu.edu.cn

†These authors have contributed equally to this work and share first authorship

RECEIVED 15 May 2024
ACCEPTED 26 July 2024
PUBLISHED 13 August 2024

CITATION
Li Z, Cao Z, Chen F, Li B and Jin H (2024) Lutein inhibits glutamate-induced apoptosis in HT22 cells via the Nrf2/HO-1 signaling pathway.
Front. Neurosci. 18:1432969.
doi: 10.3389/fnins.2024.1432969

Lutein inhibits glutamate-induced apoptosis in HT22 cells via the Nrf2/HO-1 signaling pathway

Zhenhua Li[1†], Zhuohua Cao[1†], Fangmei Chen[2†], Bin Li[3,4*] and Hanyong Jin[1*]

[1]Key Laboratory of Natural Medicines of the Changbai Mountain, Ministry of Education, College of Pharmacy, Yanbian University, Yanji, Jilin, China, [2]Institute of Science and Technology Information Research of Tibet Autonomous Region, Lhasa, China, [3]Key Laboratory of Pharmaceutical Research for Metabolic Diseases, Department of Pharmacy, Qingdao University of Science and Technology, Qingdao, China, [4]Department of Medicament, College of Medicine, Tibet University, Lhasa, China

Introduction: Excessive glutamate levels induce oxidative stress, resulting in neuronal damage, and cell death. While natural antioxidants show promise for neuroprotection, their effectiveness in the central nervous system (CNS) is limited by the blood -brain barrier. Lutein, a neuroprotective carotenoid, has gained attention for its ability to traverse this barrier and accumulate in various brain regions. This study aimed to elucidate the mechanisms underlying the protective effects of lutein against glutamateinduced cell death in HT22 cells.

Methods: HT22 cells were treated with lutein (1.25-20 μM) for 24 hours. Cell viability, ROS levels, apoptosis, and mitochondrial membrane potential were assessed following lutein pretreatment and glutamate exposure. Protein expression of apoptotic markers was analyzed using Western blotting.

Results: Lutein effectively attenuated glutamate-induced apoptosis due to its antioxidant properties. Additionally, lutein inhibited glutamate-induced mitochondrial-mediated apoptosis. We observed that lutein modulated the nuclear translocation of nuclear factor erythroid 2 -related factor 2 (Nrf2) and upregulated the expression of heme oxygenase-1 (HO-1). Inhibition of HO-1 by tin protoporphyrin (SnPP), a synthetic inhibitor, weakened the protective effect of lutein. Furthermore, we demonstrated that lutein prevented the aberrant activation of MAPKs induced by glutamate, including ERK1/2, p38, and JNK, thereby conferring oxidative protection.

Discussion: Our study highlights the potent antioxidant properties of lutein, which effectively safeguards against glutamate-induced mitochondrial apoptotic cell death through the Nrf2/HO-1 signaling pathway and inhibition of MAPK activation. These findings demonstrate that lutein exerts a neuroprotective effect against glutamate-induced neuronal cell damage.

KEYWORDS

lutein, glutamate, neuroprotective effects, oxidative stress, apoptosis

1 Introduction

Glutamate, a crucial endogenous excitatory neurotransmitter in the central nervous system, mediates synaptic transmission through the activation of both metabotropic and ionotropic glutamate receptors (iGluRs) on neurons. It regulates various physiological functions in the cerebral cortex and hippocampus, significantly influencing synaptic plasticity, cognition, learning, and memory (Haroon et al., 2017). However, elevated extracellular glutamate concentrations can induce neuronal cell death through excitotoxicity (Bano et al., 2005), thereby contributing to the pathogenesis of neurodegenerative diseases such as

Alzheimer's, Parkinson's, and amyotrophic lateral sclerosis (Barnham et al., 2004), as well as the onset and progression of mental illnesses like depression and anxiety disorders (Salim, 2014; Black et al., 2015). Many studies have described glutamate-induced cytotoxicity occurring through both receptor-mediated and non-receptor-mediated pathways. iGluRs are classified into four subtypes based on their ligand binding properties and sequence similarity, including α-amino-3-hydroxy-5-methyl-4-isoxazolepropionic acid (AMPA), kainate, N-methyl-d-aspartate (NMDA), and delta receptors (Collingridge et al., 2009), which predominantly mediate most of the fast excitatory neurotransmission in the brain. In non-receptor-mediated cytotoxicity, excess extracellular glutamate inhibits the neuronal glutamate/cystine antiporter (Murphy et al., 1989). This inhibition results in decreased cystine uptake, leading to reduced levels of glutathione, impaired clearance of reactive oxygen species (ROS), and the subsequent accumulation of these species, causing oxidative stress toxicity (Murphy et al., 1989). HT22 neuronal cells are advantageous for studying non-receptor-mediated cytotoxicity and oxidative stress responses induced by glutamate due to their lack of ionotropic glutamate receptors (Murphy et al., 1989; Maher and Davis, 1996).

The dynamic levels of ROS within mitochondria are closely associated with essential cellular functions. However, the disruption of mitochondrial redox balance in cells from various tissues can lead to pathological developments (Sies and Jones, 2020).This impairment compromises cellular function and disrupts the organism's normal physiological activities, ultimately inducing oxidative stress. Consequently, lipid peroxidation, cellular damage, and the opening of mitochondrial permeability transition pores (MPTP) are triggered, thereby facilitating apoptosis in various tissue cells (Sies and Jones, 2020). Neuronal cells in the central nervous system, characterized by their heightened metabolism, lipid richness, and lower antioxidant levels, are notably prone to oxidative stress damage compared to other tissue cells (Floyd and Carney, 1992). Oxidative stress, whether induced by an overproduction of mitochondrial ROS or impairment of antioxidant defenses, results in mitochondrial dysfunction and initiates the cellular death cascade (Islam, 2017). Mitochondrial dysfunction-induced cell death typically begins with mitochondrial outer membrane permeabilization (MOMP), a process activated by pro-apoptotic effectors, Bax and Bak. The loss of membrane integrity results in the release of cytochrome c into the cytosol, where it forms a complex known as the apoptosome along with the proapoptotic cytosolic factor *APAF1*. This apoptosome complex then activates caspase 9, which subsequently cleaves caspases 3 and 7 leading to rapid cellular demolition (Bock and Tait, 2020).

Scavenging ROS through Nrf2-mediated induction of antioxidant enzymes is essential for maintaining cellular redox homeostasis (Loboda et al., 2016). Heme oxygenase-1 (HO-1) is a major target gene regulated by Nrf2, playing a critical role in cellular protection against harmful stimuli from both endogenous and exogenous sources (Winyard et al., 2005). Its antioxidant function involves preventing free heme from engaging in oxidative reactions and, along with its enzymatic products biliverdin and carbon monoxide (CO), conferring antioxidant, anti-inflammatory, anti-apoptotic, and vasodilatory effects, as well as enhancing tissue microcirculation. Under normal conditions, Nrf2 is bound to its cytoplasmic inhibitor Keap1. Upon external stimulation, Nrf2 dissociates, translocates to the nucleus, and binds to the HO-1 promoter antioxidant response element (ARE), thereby activating HO-1 gene expression and providing cellular protection. Previous studies have shown that the Nrf2/HO-1 signaling pathway prevents glutamate-induced oxidative stress in HT22 cell death (Wang et al., 2016; Huang et al., 2018; Cuadrado et al., 2019; Song et al., 2019b; Gao et al., 2023; Wang et al., 2024).

Intracellular oxidative stress can also be induced by the mitogen-activated protein kinase (MAPK) signaling pathway, leading to the production of reactive oxygen species (ROS) (Son et al., 2011). The MAPK protein belongs to the serine/threonine protein kinase family and plays an important role in the expression of various proteins involved in cell differentiation, inflammation, and apoptosis (Yue and López, 2020). MAPKs, such as ERK1/2, p38, and JNK, serve as key mediators in converting extracellular signals into a multitude of cellular responses, encompassing cell growth, migration, proliferation, differentiation, and apoptosis (Yue and López, 2020). Several studies have demonstrated that oxidative stress resulting from glutamate exposure can activate MAPKs, leading to hippocampal neuronal apoptosis (Fukui et al., 2009; Ortuño-Sahagún et al., 2014; Park et al., 2019; Song et al., 2019a,b; Baek et al., 2021).

Lutein has beneficial effects in delaying the progression of age-related eye conditions and shows promise in protecting against neurodegenerative diseases by enhancing antioxidant enzyme activity in the brain (Ahn and Kim, 2021). Several studies have reported that lutein exhibits protective effects against neuronal damage caused by glutamate, enhancing antioxidant enzyme activity and reducing inflammation in both neuroblastoma and microglial cells (Pap et al., 2022; Phoraksa et al., 2023). However, further research is necessary to fully comprehend its effectiveness against glutamate-induced excitotoxicity, particularly concerning metabotropic glutamate receptors. In this study, we demonstrated that lutein prevents glutamate-induced apoptosis in HT22 cells by reducing oxidative stress and mitochondrial damage. This protective effect is mediated through the Nrf2/HO-1 and MAPKs pathways, suggesting significant neuroprotective potential.

2 Materials and methods

2.1 Reagents

Lutein (purity of >98%) was purchased from Chengdu Must Bio-technology Co., Ltd. (Chengdu, China). All chemicals used in this study were purchased from Gibco BRL Co. (Grand Island, NY, United States). The following kits were purchased: Reactive Oxygen Species Assay Kit, Mitochondrial Membrane Potential Assay Kit with JC-1, and One Step of TUNEL Apoptosis Assay Kit were purchased from Beyotime Biotechnology Co., Ltd. (Shanghai, China). MTT [3-(4,5-Dimethylthiazol-2-yl)-2,5-diphenyltetrazolium bromide] were purchased from Beijing Solarbio Science & Technology Co., Ltd. (Beijing, China). Cobalt protoporphyrin (CoPP) and tin protoporphyrin (SnPP) were obtained from Sigma-Aldrich Life Science & Technology Co., Ltd. (St. Louis, MO, United States).

2.2 Cell culture

Mouse hippocampal HT22 cells were obtained from the Chinese Type Culture Collection Center (Wuhan, China) and were cultured

in DMEM medium containing 10% heat-inactivated FBS (BDBIO, Hangzhou, China) at 37°C in an incubator with 5% carbon dioxide.

2.3 Cell viability assay

Cell viability was evaluated by a 3-[4,5-Dimethylthiazol-2-yl]-2,5-diphenyltetrazolium bromide (MTT) assay. Cells (8×10^3 cells/well in 96-well plates) were incubated with MTT at a final concentration of 0.5 mg/mL for 4 h Dimethyl sulfoxide (DMSO) (Sigma-Aldrich) was added to dissolve dark blue formazan crystals formed in the viable cells. Optical density was measured at 490 nm using a microplate reader (Thermo Multiskan Sky, Waltham, MA, United States). The optical density of formazan formed in the control (untreated) cells was considered as 100% cell viability.

2.4 Analyses of ROS levels in cells

According to the directions provided by the manufacturer, the intracellular ROS level was assayed with the fluorescent probe 2,7-dichlorodi-hydrofluorescein diacetate (DCF-DA; Solarbio, Beijing, China). HT22 cells (1.0×10^4 cells/well) were cultured in 24-well plates. After 20 min of incubation at 37°C with a diluted DCFH-DA probe, serum-free medium was used to wash the cells three times. The cells were then collected after being washed three times with PBS. With the use of a spectrofluorometer (Spectramax Gemini XS; Molecular Devices, Sunnyvale, San Jose, CA, United States), the fluorescence intensity was detected at wavelengths of 530 nm for the emission and 484 nm for the excitation.

2.5 Mitochondrial membrane potential assay

Changes in mitochondrial membrane potential in HT22 cells were measured using the mitochondrial membrane potential assay kit with JC-1 (Beyotime, Shanghai, China). After being cultivated in a 6-well plate and treated with glutamate and/or lutein, the cells were washed with PBS. The JC-1 staining solution was added to each well and incubated for 30 min at 37°C. Mitochondria were visualized using a fluorescence microscope (Provis AX70, Olympus Optical Co., Tokyo, Japan) after cells were rinsed with JC-1 staining solution (1 ×). Green fluorescence indicates mitochondrial depolarization, while red fluorescence indicates normal mitochondria. The red/green fluorescence intensity ratio is utilized to assess mitochondrial depolarization.

2.6 Cell apoptosis assay

One step of TUNEL Apoptosis Assay Kit (Beyotime, Shanghai, China) was used to investigate the apoptosis of HT22 cells. Briefly, cells were treated with 0.3% Triton X-100 and the TUNEL detection solution at 37°C in the absence of light after being fixed in 4% paraformaldehyde for 60 min. Subsequently, the nuclei were stained with DAPI staining solution, sealed with a microscope cover glass, and observed under a fluorescence microscope (Olympus Optical Co.) after being washed three times with PBS buffer solution.

2.7 Western blotting

The samples (40 μg protein) were electrophoresed by 10% SDS-polyacrylamide gel electrophoresis (SDS-PAGE) and transferred to a nitrocellulose membrane (Pall Corporation, NY, United States). The membrane was sealed for 2 h in TBST with 5% nonfat dry milk. The primary antibodies, including p-JNK antibody (Cat: #AF3318, 1:1000), JNK antibody (Cat: #AF6318, 1:1000), p-ERK antibody (Cat: #AF1015, 1:1000), ERK antibody (Cat: #AF0155, 1:1000), p-p38 antibody (Cat: #AF6456, 1:1000), p-p38 antibody (Cat: #AF4001, 1:1000), HO-1 antibody (Cat: #AF5393, 1:1000), Nrf2 antibody (Cat: #AF0639, 1:1000), caspase 3 antibody (Cat: #AF6311, 1:1000), caspase 9 antibody (Cat: #AF6348, 1:1000), cleaved caspase 3 antibody (Cat: #AF7022, 1:1000), cleaved caspase 9 antibody (Cat: #AF5240, 1:1000), β-Actin antibody (Cat: #AF7018, 1:1000), Lamin B1 antibody (Cat: #AF5161, 1:1000), and HRP-conjugated Affifinipure Goat Anti-Rabbit IgG (H + L) secondary antibodies (#S0001, 1:10000) were obtained from Affinity Biosciences (OH, United States). An Ultra High Sensitivity ECL Kit (MCE, State of New Jersey, United States) and ChemiDoc image analyzer (Tanon 4,600, Tanon, China) are used to display protein imprinting. Finally, protein quantitative analysis was used by an ImageJ analysis program (National Institutes of Health, United States).

2.8 Subcellular fractionation

HT22 cells were lysed with a mixture of RIPA lysis buffer [50 mM Tris (pH 7.4), 150 mM NaCl, 1% Triton X-100, 1% sodium deoxycholate, 0.1% SDS, and general protease and phosphatase inhibitors] (MCE, State of New Jersey, United States) and 1 mM phenylmethylsulfonyl fluoride (PMSF; Solarbio, Beijing, China) for 10 min at 4°C, and the supernatant was collected by centrifugation to extract total protein. The extraction of nuclear and cytosolic proteins was performed using the Nuclear Protein Extraction Kit (Solarbio, Beijing, China) from HT22 cells. Bradford Protein Assay Kit (Solarbio, Beijing, China) was used to measure the protein extracts.

2.9 Nrf2 immunofluorescence

For the nuclear translocation of Nrf2, immunofluorescence experiments were performed. HT22 cells were permeabilized with 0.5% Triton X-100 after being treated with lutein (10 μM) and fixed with 4% paraformaldehyde. After blocking non-specific binding sites with 1% FBS for an hour, cells were incubated with a Nrf2 antibody (1,200) at 4°C for an overnight period and were incubated with the secondary conjugated antibodies (Alexa Fluor 488; Invitrogen, Carlsbad, CA, United States) at 4°C for 10 min. In order to see the nuclei, DAPI (1 μg/mL) labeling was completed. A Provis AX70 fluorescent microscope (Olympus Optical, Tokyo, Japan) was used to view and capture stained cells.

2.10 Statistical analysis

All data described in this study were replicated at least three times and are presented as the mean ± standard error of mean (S.E.M).

Statistical analyses were conducted using GraphPad Prism 7 software (San Diego, CA, United States), and group differences were assessed using one-way ANOVA. A significance level of $p < 0.05$ was considered as indicating statistically significant.

3 Results

3.1 Effect of lutein on cell viability in glutamate-induced cytotoxicity

To assess the impact of lutein on HT22 cells, cell viability was determined using the MTT assay after incubation with various concentrations of lutein (1.25, 2.5, 5, 10, 20 μM) for 24 h (Figure 1). The results indicated that lutein did not induce cytotoxicity in HT22 cells except at the highest concentration (20 μM) (Figure 1). Consequently, the maximum concentration of lutein was restricted to 10 μM in all subsequent experiments. Next, we evaluated the ability of lutein to counteract glutamate-induced cytotoxicity in HT22 cells. To determine the neuroprotective effect of lutein against glutamate-induced cytotoxicity in HT22 cells, the cells were treated with 20 mM glutamate with or without varying concentrations of lutein (1.25, 2.5, 5, and 10 μM) for 24 h (Figure 2A). Treatment with 20 mM glutamate significantly reduced the cell viability of HT22 neuronal cells compared to the control, which was reversed by pretreatment with 10 μM of Lutein (Figure 2A). Consequently, it was observed that lutein significantly inhibited HT22 cell death induced by glutamate at a level similar to that of the positive control, Trolox. Consistent with this findings, quantitative fluorescence intensity results demonstrated that glutamate exposure elevated increased intracellular ROS levels, a phenomenon significantly attenuated by pretreatment with 10 μM lutein and Trolox (Figure 2B). These findings suggest that the antioxidant properties of lutein may mitigate oxidative stress-mediated neuronal cell death induced by glutamate.

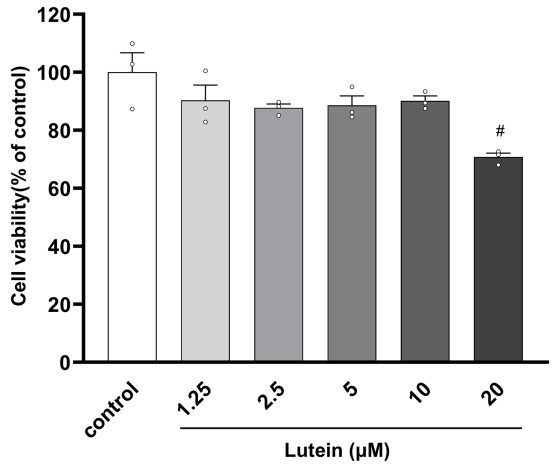

FIGURE 1
Effect of Lutein on the viability of HT22 cells. HT22 cells were incubated with various concentrations of Lutein for 24 h, and cell viability was evaluated. Data are means ± S.E.M of three independent experiments. Statistical significance is denoted as follows: $^{\#}p < 0.05$, vs. control group.

3.2 Effects of lutein against glutamate-induced mitochondrial apoptotic death in HT22 cells

Previous studies have indicated that glutamate-induced cell death in HT22 cells primarily proceeds through the apoptotic pathway (Kritis et al., 2015; Huang et al., 2018; Song et al., 2019a; Gao et al., 2023). In this study, we aimed to investigate the impact of lutein on glutamate-induced apoptotic cell death. HT22 cells were treated with increasing concentrations of lutein in the presence of glutamate to assess its effects. DAPI staining demonstrated a reduction in glutamate-induced nuclear condensation following lutein treatment (Figure 3A). Additionally, the number of FITC-positive HT22 cells induced by glutamate decreased significantly with increasing doses of lutein (Figure 3A). Glutamate exposure led to elevated intracellular ROS levels, contributing to neuronal cell death through oxidative stress mechanisms (Figures 2A,B). To explore lutein's potential antiapoptotic mechanisms, we conducted a JC-1 staining assay to evaluate its ability to counteract glutamate-induced apoptosis by preventing mitochondrial dysfunction triggered by oxidative stress. Glutamate markedly induced mitochondrial membrane potential depolarization in HT22 cells (Figure 3B). However, pretreatment with lutein dose-dependently attenuated glutamate-induced MOMP depolarization (Figure 3B). Additionally, immunoblot analysis revealed the activation of caspase 9 and caspase 3 due to glutamate-induced disruption of mitochondrial membranes (Figure 3C). Conversely, lutein treatment dose-dependently inhibited apoptosis induction by preventing the formation of cleaved caspase 9 and caspase 3 (Figure 3C). These findings indicate that lutein exerts anti-apoptotic effects by inhibiting glutamate-induced mitochondrial apoptotic death in HT22 cells.

3.3 Protective effects of lutein on glutamate-induced oxidative stress

Previous studies have demonstrated that glutamate-induced oxidative stress can trigger aberrant activation of MAPK pathways, leading to neuronal cell death (Xia et al., 1995; Horstmann et al., 1998; Stanciu et al., 2000; Szydlowska et al., 2010). To investigate whether lutein can inhibit the aberrant activation of MAPKs by glutamate, we treated HT22 neuronal cells with increasing concentrations of lutein in the presence or absence of glutamate and conducted immunoblotting analysis (Figure 4A). The results showed that the activation of MAPKs, including the phosphorylation of ERK, p38, and JNK induced by glutamate, was significantly reduced in a dose–response manner upon treatment with increasing concentrations of lutein (Figures 4A–D). These findings suggest that the inhibition of MAPKs is a molecular mechanism underlying lutein-mediated neuroprotection against glutamate-induced cell death in HT22 cells.

3.4 Antioxidant properties of lutein on HT22 cells by regulating Nrf2/HO-1 axis

The Nrf2/HO-1 signaling pathway has been implicated in the progression of various neurological complications, including

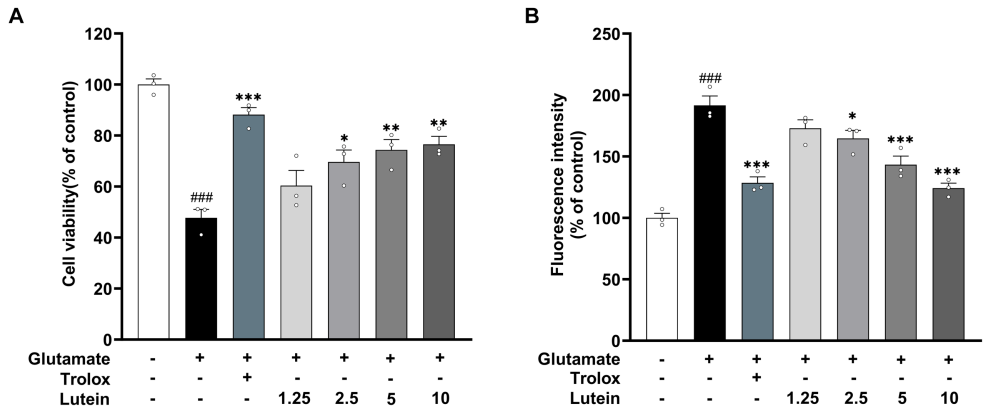

FIGURE 2
Neuroprotective effects of Lutein on glutamate-induced toxicity in HT22 cells. (**A,B**) HT22 cells were stimulated with glutamate (20 mM) for 24 h after pretreatment with an increasing concentrations of Lutein or Trolox (50 μM) for 12 h. Cell viability **(A)** and intracellular ROS levels **(B)** were measured. Data are means ± S.E.M of three independent experiments. Statistical significance is denoted as follows: $^{###}p < 0.001$ vs. control group; $^{*}p < 0.05$, $^{**}p < 0.01$, $^{***}p < 0.001$ vs. glutamate treated group.

glutamate-induced oxidative cell death (Sacks et al., 2018). Previous studies have suggested that lutein activates Nrf2, leading to the expression of antioxidant genes such as HO-1. To investigate the potential of lutein as a modulator of the Nrf2/HO-1 signaling pathway in different neurodegenerative disorders, we examined its impact on Nrf2 translocation and HO-1 expression in HT22 cells. Immunofluorescence and immunoblot analysis revealed a significant increase in Nrf2 accumulation within the nucleus after a 2 h treatment with 10 μM lutein, compared to the control group (Figures 5A–C). Conversely, the levels of cytosolic Nrf2 were notably decreased (Figure 5A), indicating that lutein effectively enhanced the translocation of Nrf2 to the nucleus in HT22 neuronal cells, leading to the activation of Nrf2 downstream target gene expression.

Given the demonstrated role of Nrf2-driven antioxidant gene expression of HO-1 in protecting against glutamate-induced oxidative damage in HT22 neuronal cells (Kim et al., 2012), we aimed to investigate the effects of lutein on HO-1 expression in HT22 neuronal cells. Immunoblot analysis showed that HO-1 expression significantly increased with lutein treatment in a dose- and time-dependent manner (Figures 6A,B). Cobalt protoporphyrin (CoPP), an HO-1 inducer, also significantly increased HO-1 expression, comparable to the level induced by 10 μM lutein (Figure 6A). Next, we further elucidated whether the increase in Nrf2 nuclear translocation and HO-1 expression by lutein contributed to the protection of HT22 neuronal cells from glutamate-induced oxidative cell death. To validate the role of HO-1, we utilized tin protoporphyrin (SnPP), a synthetic inhibitor of HO-1, to inhibit its activity. In Figure 6C, we observed that the presence of 50 μM SnPP partially blocked the protective effect of lutein against glutamate-induced HT22 cell death. Consistently, treatment with SnPP also partially prevented the reduction of intracellular ROS levels induced by lutein in HT22 neuronal cells (Figure 6D). These findings suggest that lutein modulation of Nrf2-mediated expression of HO-1 could be a potential molecular mechanism for eliminating glutamate-induced oxidative stress by lutein, thereby partially inhibiting glutamate-induced oxidative cell death.

4 Discussion

Naturally occurring antioxidants have garnered significant attention due to their neuroprotective effects against oxidative stress (Pérez-Torres et al., 2021). However, their efficacy in the central nervous system (CNS) is often limited by the blood–brain barrier. Lutein, capable of crossing this barrier and accumulating in various brain regions, significant accumulation has been observed in the hippocampal regions of both humans and non-human primates, presents a promising candidate for neuroprotection against degenerative diseases (Lieblein-Boff et al., 2015; Mohn et al., 2017; Iyer et al., 2024). Although extensively studied, the specific neuroprotective effects of lutein in hippocampal neurons had not been investigated prior to our research. HT22 hippocampal neuron cells, selected for their resistance to glutamate receptor-mediated excitotoxicity, are commonly used as an *in vitro* model to investigate the neuroprotective properties of natural compounds against oxidative stress induced by non-receptor glutamate pathways. Glutamate-induced oxidative stress in neuronal cells results from altered cystine/glutamate antiporter activity and other pathological factors such as ischemia and trauma (Newcomb et al., 1997).

Lutein, a naturally occurring carotenoid obtained through dietary intake (Berendschot et al., 2000), has shown significant neuroprotective effects in both clinical trials and experimental studies (Yuan et al., 2021; Agarwal et al., 2022). It accumulates in critical areas like the retina and the CNS, offering protection against oxidative stress-induced damage, which is particularly relevant in neurodegenerative disorders such as Alzheimer's and Parkinson's diseases (Feart et al., 2016; Mullan et al., 2017). The primary mechanism underlying lutein's neuroprotection is its antioxidant properties (Iyer et al., 2024). Although studies have shown lutein's ability to mitigate ROS generation induced by various factors in CNS cells, such as b.END.3, PC12, SH-SY5Y, and BV-2 cells (Liu et al., 2017; Singhrang et al., 2018; Pap et al., 2021), research has primarily focused on its role in countering oxidative stress in neuronal cells triggered by amyloid deposition and external oxidants. Excitotoxicity, induced by glutamate, is recognized as a crucial factor in the development and progression of neurodegenerative diseases. Addressing glutamate-induced excitotoxicity and oxidative stress with

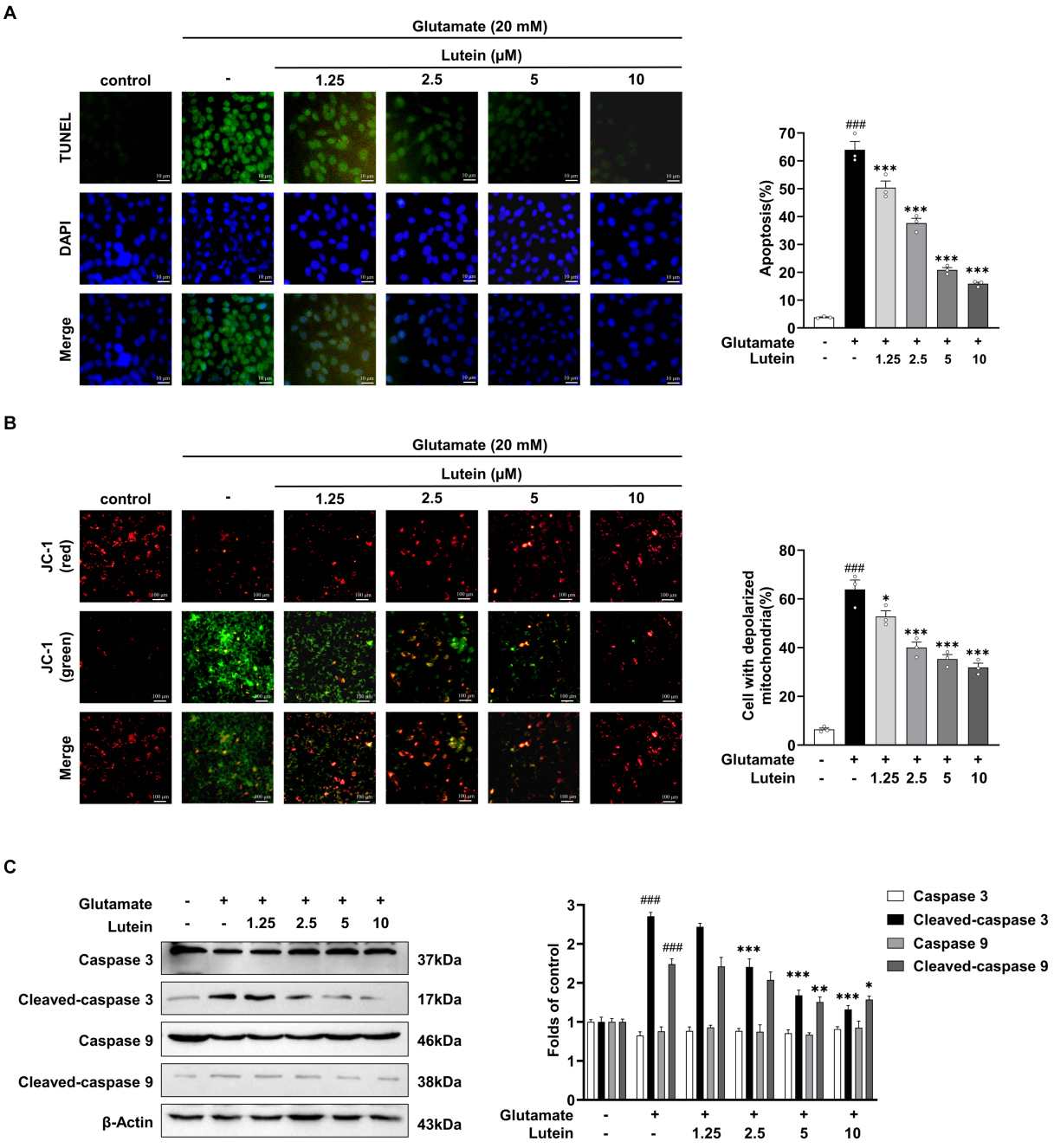

FIGURE 3
Lutein participates in early cell apoptosis by inhibiting glutamate mediated mitochondrial membrane potential destruction. **(A)** HT22 cells were exposed to 20 mM glutamate with varying concentrations of lutein (1.25, 2.5, 5, and 10 μM) and subjected to the FITC test (one-step TUNEL apoptosis test kit) to assess the number of apoptotic and dead cells, respectively. The bar graph indicates the percentage of apoptotic cells. Data are presented as the mean value ± S.E.M of three independent experiments. **(B)** Representative images of JC-1 staining were detected using fluorescence microscopy. The bar graph indicates the percentage of cells exhibiting mitochondrial depolarization. Data are presented as the mean value ± S.E.M of three independent experiments. **(C)** Western blot analysis was conducted. β-Actin serving as a loading control. The bars represent the fold-increase in the levels of cleaved caspase 3 and cleaved caspase 9 compared to control cells. Data are presented as the mean value ± S.E.M of three independent experiments. Statistical significance is denoted as follows: $^{###}p < 0.001$ vs. control cells; $^{*}p < 0.05$, $^{**}p < 0.01$, $^{***}p < 0.001$ vs. glutamate treated group.

safe and effective natural compounds is thus crucial in treating such conditions. This study aims to enrich our understanding of lutein's pharmacological properties, thereby broadening our comprehension of its specific mechanisms underlying therapeutic potential for neurodegenerative diseases. Therefore, in this study, we constructed an *in vitro* glutamate-induced HT22 cell injury model to explore the neuroprotective mechanism of lutein in mouse hippocampal neuronal cell lines. We found that lutein can decrease the cytotoxicity of glutamate-induced HT22 cells in a concentration-dependent manner (Figure 2A), depends on its antioxidant properties (Figure 2B).

Excessive extracellular glutamate levels can trigger neuronal death through excitotoxicity, ferroptosis, and mitochondrial dysfunction, all

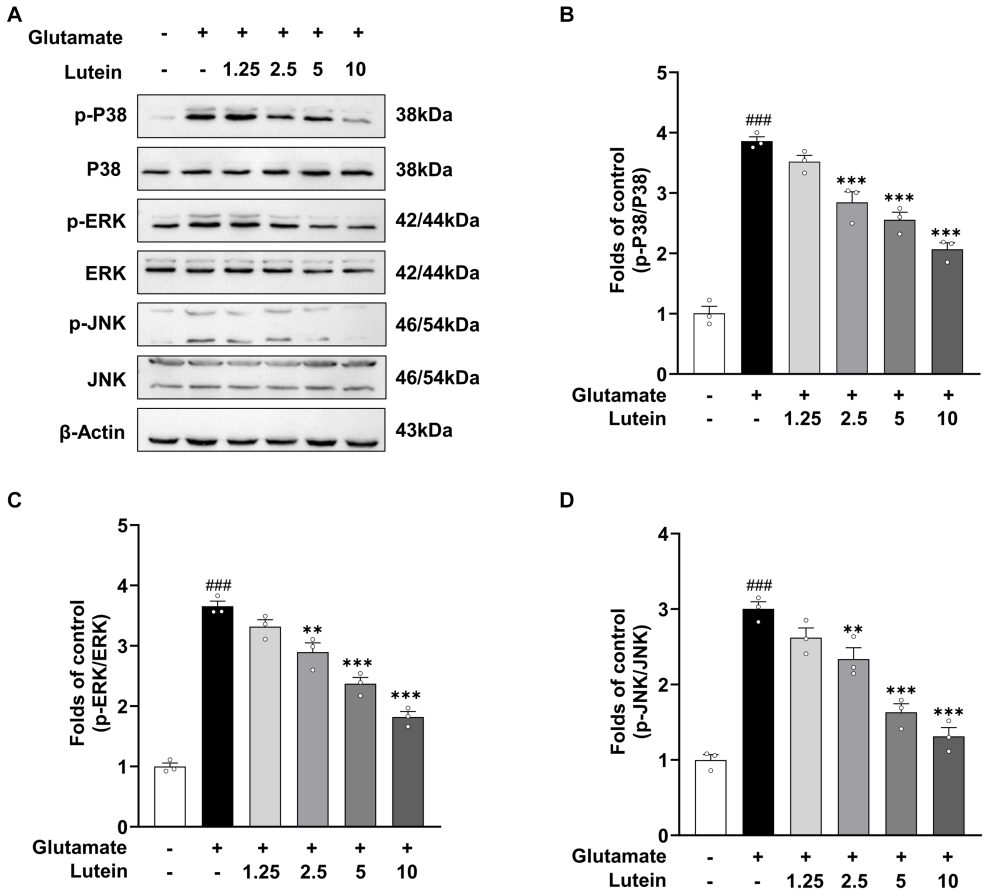

FIGURE 4
Lutein inhibits glutamate-induced MAPK activation in HT22 cells. **(A)** HT22 cells were exposed to 20 mM glutamate in the presence or absence of indicated concentrations for 8 h. Western blot analysis was performed using indicated antibodies, with β-Actin serving as a loading control. **(B–D)** The bars represent the fold-increases of P38, ERK, and JNK phosphorylation levels compared to the control cells. Data are presented as the mean value ± S.E.M of three independent experiments. Statistical significance is denoted as follows: $^{###}p < 0$ 0.001 vs. control group; $^{**}p < 0.01$, $^{***}p < 0.001$ vs. glutamate treated group.

of which disrupt intracellular redox balance (Vaglio-Garro et al., 2024). Our study, consistent with prior research, highlights the association between neuronal apoptosis and oxidative stress-induced accumulation of ROS within mitochondria, leading to mitochondrial damage and caspase-mediated apoptosis (Figure 3). In our investigation, lutein demonstrated notable protective effects against glutamate-induced MOMP depolarization in HT22 cells in a dose-dependent manner (Figure 3B). Moreover, lutein effectively inhibited the activation of caspase 3 and caspase 9, thereby mitigating apoptosis (Figure 3C). The precise mechanism underlying glutamate-induced cell death in HT22 cells remains debated, with evidence suggesting alternative pathways at lower concentrations. For instance, lower glutamate concentrations (≤ 5 mM) can induce caspase-independent DNA fragmentation (Fukui et al., 2009), while specific concentrations can trigger ferroptosis, a process attenuated by compounds like quercetin through the SIRT1/Nrf2/SLC7A11/GPX4 pathway (Xie et al., 2022). Furthermore, in other cell lines like the human neuroblastoma cell line SH-SY5Y, glutamate treatments induce oxidative stress, inflammation, iron accumulation, and lipid peroxidation. Lutein counteracts these effects by reducing ROS, suppressing pro-inflammatory cytokines, preventing iron accumulation, and downregulating lipid peroxidation-associated gene expression, thus inhibiting ferroptosis (Xie et al., 2022). Our findings suggest that lutein protects against caspase-dependent apoptosis following 20 mM glutamate treatment in HT22 cells. However, further research is needed to explore whether lutein's protective effects extend to other cell death pathways in HT22 cells.

Mitogen-activated protein kinases (MAPKs) play crucial roles in various cellular processes, including cell proliferation, differentiation, inflammation, and apoptosis. Oxidative stress triggers the activation of MAPK pathways, such as JNK and p38, through apoptosis signal-regulating kinase 1 (ASK1), ultimately inducing apoptosis (Saitoh et al., 1998). Although studies have linked JNK, p38, and ERK activation to glutamate-induced apoptosis in HT22 cells, lutein inhibits MAPK activation under oxidative stress, providing cellular protection. For instance, lutein suppresses ERK1/2, JNK1, and p38 activation in cells exposed to oxidative stress inducers (Hu et al., 2021), and reduces lipid peroxidation and JNK and p38 activation in human lens epithelial cells exposed to UVB radiation (Silván et al., 2016). Similarly, our research shows that lutein inhibits JNK, p38, and ERK activation in HT22 cells under oxidative stress induced by glutamate, thereby reducing apoptosis (Figure 4). Overall, high concentrations of glutamate induce MAPK and caspase activation, leading to apoptotic cell death, which is dependent on mitochondrial dysfunction caused by oxidative stress-induced ROS accumulation.

Nrf2, a transcription factor, plays a crucial role in regulating antioxidant stress proteins. Normally, Nrf2 levels are kept low by Keap1,

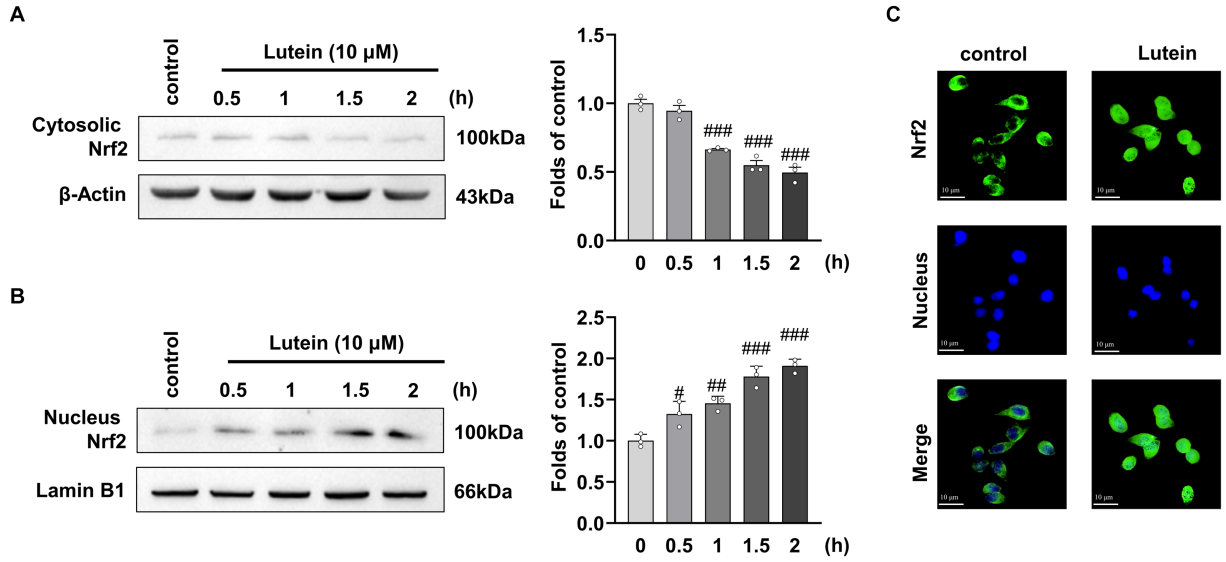

FIGURE 5
Lutein increases Nrf2 nuclear translocation in HT22 cells. (**A,B**) Translocation of cytosolic Nrf2 into the nucleus was assessed in HT22 cells incubated with 10 μM Lutein for indicated times. The cytosolic and nucleus fractions were isolated and analyzed by western blotting with β-Actin and Lamin B1, respectively. Bars indicate fold-increases compared to the control cells. Data are mean ± S.E.M of three independent experiments. Statistical significance is denoted as follows: $^{\#}p < 0.05$, $^{\#\#}p < 0.01$, $^{\#\#\#}p < 0.001$ vs. control cells. (**C**) Representative immunofluorescence of Nrf2 expression in HT22 cells is shown. Representative immunofluorescence of Nrf2 expression in HT22 cells is shown. Staining of Nrf2 (green labeled) and the nucleus (blue labeled) was detected using fluorescent microscopy.

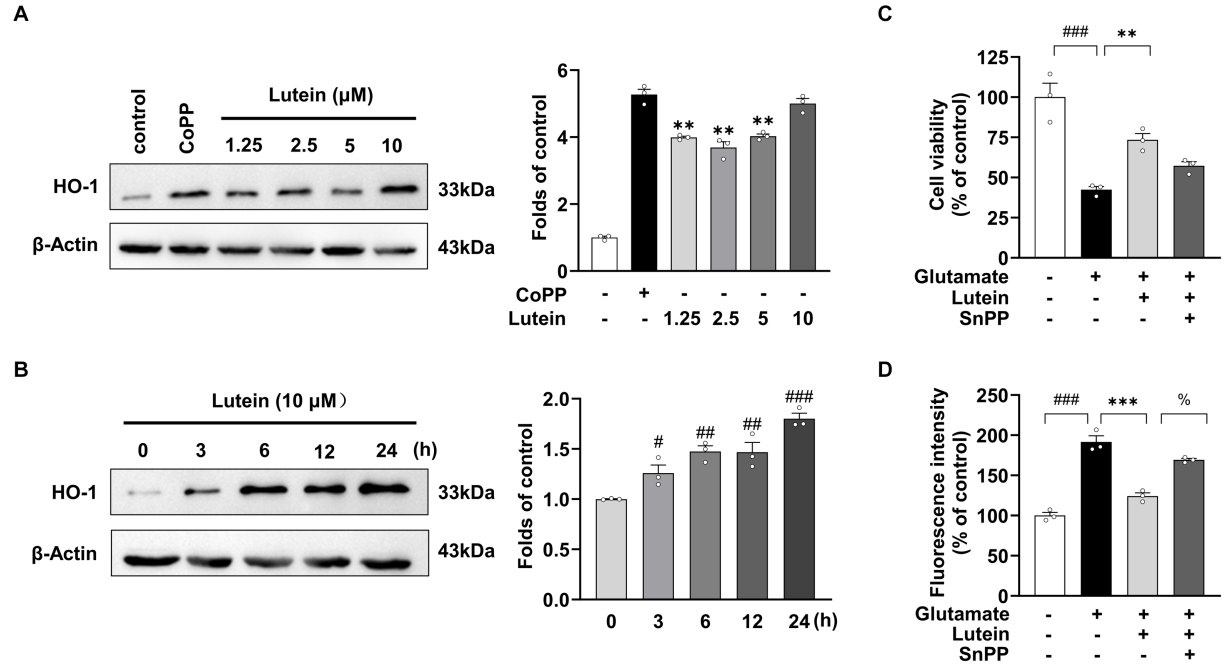

FIGURE 6
Effects of Lutein on HO-1 expression in HT22 cells. (**A**) HO-1 expression was evaluated in the presence of varying concentrations of Lutein and compared to 20 μM CoPP after 12 h. Western blot analysis was conducted with β-Actin as the control. Bars represent fold-increases in HO-1 expression. Data are presented as the mean value ± S.E.M of three independent experiments. Statistical significance is denoted as follows: $^{**}p < 0.001$ vs. CoPP treated group. (**B**) Western blot analysis was performed after incubation with 10 μM Lutein for indicated times, with β-Actin as a loading control. Data are presented as the mean value ± S.E.M of three independent experiments. Statistical significance is denoted as follows: $^{\#}p < 0.05$, $^{\#\#}p < 0.01$, $^{\#\#\#}p < 0.001$ vs. CoPP treated cells group. (**C,D**) HT22 cells were treated with 20 mM glutamate and subsequently incubated with either 50 μM SnPP or 10 μM Lutein, followed by the assessment of cell viability (**C**) and intracellular ROS levels (**D**). Data are presented as the mean value ± S.E.M of three independent experiments. Statistical significance is denoted as follows: $^{\%}p < 0.05$, $^{***}p < 0.001$, $^{\#\#\#}p < 0.001$ vs. corresponding group.

which promotes its degradation via ubiquitination. However, exposure to ROS or electrophilic agents causes Nrf2 to dissociate from Keap1 and translocate to the nucleus. There, it binds to antioxidant response element (ARE) sequences, activating the transcription of various antioxidant enzymes like HO-1, GST, SOD, and NQO-1, which help detoxify ROS (Huang et al., 2002). Lutein has been found to enhance the nuclear translocation of Nrf2, leading to increased expression of Nrf2-targeted antioxidant enzymes and exerting an antioxidant effect. Studies show that lutein activates Nrf2, resulting in elevated expression of protective enzymes like HO-1 and NQO1, which mitigates oxidative stress in microglial cells exposed to lipopolysaccharide (Wu et al., 2015) Additionally, lutein reverses H_2O_2-induced down-regulation of HO-1 mRNA in PC12 cells (Hu et al., 2021). Our research confirms these findings, demonstrating that lutein boosts the nuclear translocation of Nrf2 and upregulates HO-1 expression in HT22 cells (Figure 5). The antioxidant properties of lutein may stem from the upregulation of Nrf2-dependent antioxidant genes and its phenolic hydroxyl structure's inherent reductive capacity against ROS. Moreover, we observed that the HO-1 inhibitor, SnPP, significantly diminishes lutein's antioxidant efficacy, highlighting the crucial role of HO-1 upregulation in protecting HT22 cells from glutamate-induced oxidative stress (Figure 6).

In undifferentiated HT22 cells devoid of glutamate receptors, we have confirmed that lutein confers protection against non-receptor-mediated glutamate neurotoxicity via its antioxidant properties. Non-receptor-mediated glutamate neurotoxicity is pivotal in inducing neuronal cell toxicity under pathological states, including hypoxia and neuronal injury, characterized by the release and accumulation of intracellular glutamate in the synaptic cleft at elevated concentrations. The *in vivo* hippocampus consists of differentiated neurons with glutamate and cholinergic receptors, operating at lower synaptic cleft glutamate levels, further research is needed to elucidate lutein's protective effect against NMDA receptor-mediated excitotoxicity. Reports indicate that the antioxidant dithiothreitol (DTT) exhibits a diminished capacity to reverse the decrease in cell viability in differentiated HT22 cells with NMDA receptors treated with glutamate, in comparison to undifferentiated HT22 cells (He et al., 2013). Conversely, another study demonstrated that lutein significantly mitigated the upregulation of Bax, cytochrome c, p-p38 MAPK, and p-c-Jun in the retinal ganglion cells of rats administered NMDA, ameliorating neuronal damage from excitotoxicity (Zhang et al., 2016). Despite the diminished role of oxidative stress in glutamate receptor-mediated excitotoxicity, lutein might still afford protection against neuronal excitotoxicity via mechanisms distinct from its antioxidant activity.

In summary, our research underscores lutein's potential as a neuroprotective agent against glutamate-induced oxidative stress and apoptosis in HT22 cells. Lutein demonstrates significant efficacy in reducing cytotoxicity, primarily through its antioxidant properties, which mitigate ROS accumulation within mitochondria and inhibit caspase-mediated apoptosis. Moreover, lutein modulates MAPK pathways and activates Nrf2-mediated antioxidant responses, particularly by upregulating HO-1 expression (Figure 7). These findings highlight lutein's multifaceted neuroprotective effects and its

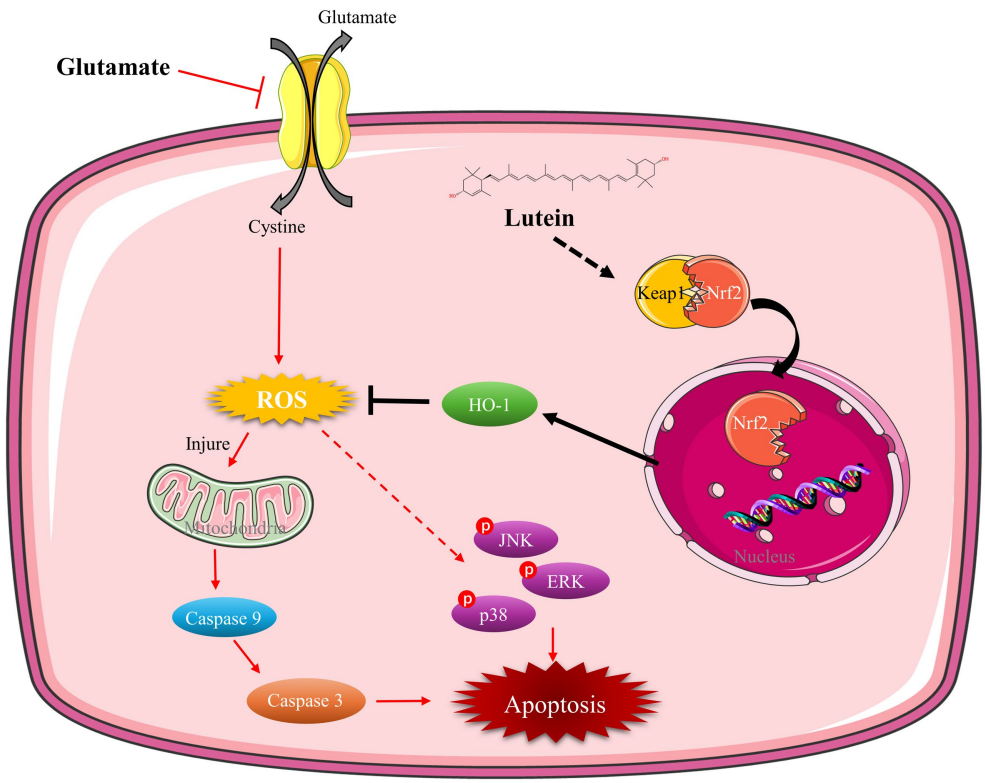

FIGURE 7
Mechanism of lutein mitigating oxidative stress and apoptosis in glutamate-induced HT22 cells. Lutein facilitates the nuclear translocation of Nrf2, upregulates HO-1 expression, diminishes ROS levels, mitigates mitochondrial damage caused by oxidative stress, inhibits caspase and MAPK activation, and alleviates oxidative stress and apoptosis in HT22 cells.

promise for therapeutic intervention in neurodegenerative diseases characterized by oxidative damage.

Data availability statement

The original contributions presented in the study are included in the article/Supplementary material, further inquiries can be directed to the corresponding authors.

Author contributions

ZL: Data curation, Formal analysis, Writing – original draft. ZC: Data curation, Formal analysis, Validation, Writing – review & editing. FC: Data curation, Formal analysis, Validation, Writing – review & editing. BL: Conceptualization, Validation, Writing – review & editing. HJ: Conceptualization, Formal analysis, Funding acquisition, Validation, Writing – original draft, Writing – review & editing.

Funding

The author(s) declare that financial support was received for the research, authorship, and/or publication of this article. This research was funded by the Higher Education Discipline Innovation Project (111 Project, D18012) and the Jilin Province Science and Technology Development Plan Project (YDZJ202201ZYTS200).

Conflict of interest

The authors declare that the research was conducted in the absence of any commercial or financial relationships that could be construed as a potential conflict of interest.

Publisher's note

All claims expressed in this article are solely those of the authors and do not necessarily represent those of their affiliated organizations, or those of the publisher, the editors and the reviewers. Any product that may be evaluated in this article, or claim that may be made by its manufacturer, is not guaranteed or endorsed by the publisher.

Supplementary material

The Supplementary material for this article can be found online at: https://www.frontiersin.org/articles/10.3389/fnins.2024.1432969/full#supplementary-material

References

Agarwal, P., Wang, Y., Buchman, A. S., Holland, T. M., Bennett, D. A., and Morris, M. C. (2022). Dietary antioxidants associated with slower progression of parkinsonian signs in older adults. *Nutr. Neurosci.* 25, 550–557. doi: 10.1080/1028415x.2020.1769411

Ahn, Y. J., and Kim, H. (2021). Lutein as a modulator of oxidative stress-mediated inflammatory diseases. *Antioxidants* 10:1488. doi: 10.3390/antiox10091448

Baek, J. Y., Jung, K., Kim, Y. M., Kim, H. Y., Kang, K. S., and Chin, Y. W. (2021). Protective effect of γ-mangostin isolated from the Peel of *Garcinia mangostana* against glutamate-induced cytotoxicity in HT22 hippocampal neuronal cells. *Biomol. Ther.* 11:170. doi: 10.3390/biom11020170

Bano, D., Young, K. W., Guerin, C. J., Lefeuvre, R., Rothwell, N. J., Naldini, L., et al. (2005). Cleavage of the plasma membrane Na+/Ca^{2+} exchanger in excitotoxicity. *Cell* 120, 275–285. doi: 10.1016/j.cell.2004.11.049

Barnham, K. J., Masters, C. L., and Bush, A. I. (2004). Neurodegenerative diseases and oxidative stress. *Nat. Rev. Drug Discov.* 3, 205–214. doi: 10.1038/nrd1330

Berendschot, T. T., Goldbohm, R. A., Klöpping, W. A., van de Kraats, J., van Norel, J., and van Norren, D. (2000). Influence of lutein supplementation on macular pigment, assessed with two objective techniques. *Invest. Ophthalmol. Vis. Sci.* 41, 3322–3326

Black, C. N., Bot, M., Scheffer, P. G., Cuijpers, P., and Penninx, B. W. (2015). Is depression associated with increased oxidative stress? A systematic review and meta-analysis. *Psychoneuroendocrinology* 51, 164–175. doi: 10.1016/j.psyneuen.2014.09.025

Bock, F. J., and Tait, S. W. G. (2020). Mitochondria as multifaceted regulators of cell death. *Nat. Rev. Mol. Cell Biol.* 21, 85–100. doi: 10.1038/s41580-019-0173-8

Collingridge, G. L., Olsen, R. W., Peters, J., and Spedding, M. (2009). A nomenclature for ligand-gated ion channels. *Neuropharmacology* 56, 2–5. doi: 10.1016/j.neuropharm.2008.06.063

Cuadrado, A., Rojo, A. I., Wells, G., Hayes, J. D., Cousin, S. P., Rumsey, W. L., et al. (2019). Therapeutic targeting of the NRF2 and KEAP1 partnership in chronic diseases. *Nat. Rev. Drug Discov.* 18, 295–317. doi: 10.1038/s41573-018-0008-x

Feart, C., Letenneur, L., Helmer, C., Samieri, C., Schalch, W., Etheve, S., et al. (2016). Plasma carotenoids are inversely associated with dementia risk in an elderly French cohort. *J. Gerontol. A Biol. Sci. Med. Sci.* 71, 683–688. doi: 10.1093/gerona/glv135

Floyd, R. A., and Carney, J. M. (1992). Free radical damage to protein and DNA: mechanisms involved and relevant observations on brain undergoing oxidative stress. *Ann. Neurol.* 32, S22–S27. doi: 10.1002/ana.410320706

Fukui, M., Song, J. H., Choi, J., Choi, H. J., and Zhu, B. T. (2009). Mechanism of glutamate-induced neurotoxicity in HT22 mouse hippocampal cells. *Eur. J. Pharmacol.* 617, 1–11. doi: 10.1016/j.ejphar.2009.06.059

Gao, L., Wang, T., Zhuoma, D., Yuan, R., Huang, S., and Li, B. (2023). Farrerol attenuates glutamate-induced apoptosis in HT22 cells via the Nrf2/heme oxygenase-1 pathway. *Biosci. Biotechnol. Biochem.* 87, 1009–1016. doi: 10.1093/bbb/zbad084

Haroon, E., Miller, A. H., and Sanacora, G. (2017). Inflammation, glutamate, and glia: a trio of trouble in mood disorders. *Neuropsychopharmacology* 42, 193–215. doi: 10.1038/npp.2016.199

He, M. C., Liu, J., Cheng, S. W., Xing, Y. G., and Suo, W. Z. (2013). Differentiation renders susceptibility to excitotoxicity in HT22 neurons. *Neural Regen. Res.* 8, 1297–1306. doi: 10.3969/j.issn.1673-5374.2013.14.006

Horstmann, S., Kahle, P. J., and Borasio, G. D. (1998). Inhibitors of p38 mitogen-activated protein kinase promote neuronal survival in vitro. *J. Neurosci. Res.* 52, 483–490. doi: 10.1002/(sici)1097-4547(19980515)52:4<483::Aid-jnr12>3.0.Co;2-4

Hu, Y., Zhang, X., Lian, F., Yang, J., and Xu, X. (2021). Combination of lutein and DHA alleviate H(2)O(2) induced cytotoxicity in PC12 cells by regulating the MAPK pathway. *J. Nutr. Sci. Vitaminol.* 67, 234–242. doi: 10.3177/jnsv.67.234

Huang, S., Meng, N., Liu, Z., Guo, L., Dong, L., Li, B., et al. (2018). Neuroprotective effects of *Taraxacum officinale* Wigg. Extract on glutamate-induced oxidative stress in HT22 cells via HO-1/Nrf2 pathways. *Nutrients* 10. doi: 10.3390/nu10070926

Huang, H. C., Nguyen, T., and Pickett, C. B. (2002). Phosphorylation of Nrf2 at Ser-40 by protein kinase C regulates antioxidant response element-mediated transcription. *J. Biol. Chem.* 277, 42769–42774. doi: 10.1074/jbc.M206911200

Islam, M. T. (2017). Oxidative stress and mitochondrial dysfunction-linked neurodegenerative disorders. *Neurol. Res.* 39, 73–82. doi: 10.1080/01616412.2016.1251711

Iyer, S., Bhat, I., and Bangera Sheshappa, M. (2024). Lutein and the underlying neuroprotective promise against neurodegenerative diseases. *Mol. Nutr. Food Res.* 68:2300409. doi: 10.1002/mnfr.202300409

Kim, H. J., Lim, S. S., Park, I. S., Lim, J. S., Seo, J. Y., and Kim, J. S. (2012). Neuroprotective effects of dehydroglyasperin C through activation of heme oxygenase-1 in mouse hippocampal cells. *J. Agric. Food Chem.* 60, 5583–5589. doi: 10.1021/jf300548b

Kritis, A. A., Stamoula, E. G., Paniskaki, K. A., and Vavilis, T. D. (2015). Researching glutamate - induced cytotoxicity in different cell lines: a comparative/collective analysis/study. *Front. Cell. Neurosci.* 9:91. doi: 10.3389/fncel.2015.00091

Lieblein-Boff, J. C., Johnson, E. J., Kennedy, A. D., Lai, C. S., and Kuchan, M. J. (2015). Exploratory metabolomic analyses reveal compounds correlated with lutein concentration in frontal cortex, Hippocampus, and occipital cortex of human infant brain. *PLoS One* 10:e0136904. doi: 10.1371/journal.pone.0136904

Liu, T., Liu, W. H., Zhao, J. S., Meng, F. Z., and Wang, H. (2017). Lutein protects against β-amyloid peptide-induced oxidative stress in cerebrovascular endothelial cells through modulation of Nrf-2 and NF-κb. *Cell Biol. Toxicol.* 33, 57–67. doi: 10.1007/s10565-016-9360-y

Loboda, A., Damulewicz, M., Pyza, E., Jozkowicz, A., and Dulak, J. (2016). Role of Nrf2/HO-1 system in development, oxidative stress response and diseases: an evolutionarily conserved mechanism. *Cell. Mol. Life Sci.* 73, 3221–3247. doi: 10.1007/s00018-016-2223-0

Maher, P., and Davis, J. B. (1996). The role of monoamine metabolism in oxidative glutamate toxicity. *J. Neurosci.* 16, 6394–6401. doi: 10.1523/jneurosci.16-20-06394.1996

Mohn, E. S., Erdman, J. W., Kuchan, M. J., Neuringer, M., and Johnson, E. J. (2017). Lutein accumulates in subcellular membranes of brain regions in adult rhesus macaques: relationship to DHA oxidation products. *PLoS One* 12:e0186767. doi: 10.1371/journal.pone.0186767

Mullan, K., Williams, M. A., Cardwell, C. R., McGuinness, B., Passmore, P., Silvestri, G., et al. (2017). Serum concentrations of vitamin E and carotenoids are altered in Alzheimer's disease: a case-control study. *Alzheimers Dement.* 3, 432–439. doi: 10.1016/j.trci.2017.06.006

Murphy, T. H., Miyamoto, M., Sastre, A., Schnaar, R. L., and Coyle, J. T. (1989). Glutamate toxicity in a neuronal cell line involves inhibition of cystine transport leading to oxidative stress. *Neuron* 2, 1547–1558. doi: 10.1016/0896-6273(89)90043-3

Newcomb, R., Sun, X., Taylor, L., Curthoys, N., and Giffard, R. G. (1997). Increased production of extracellular glutamate by the mitochondrial glutaminase following neuronal death. *J. Biol. Chem.* 272, 11276–11282. doi: 10.1074/jbc.272.17.11276

Ortuño-Sahagún, D., González, R. M., Verdaguer, E., Huerta, V. C., Torres-Mendoza, B. M., Lemus, L., et al. (2014). Glutamate excitotoxicity activates the MAPK/ERK signaling pathway and induces the survival of rat hippocampal neurons in vivo. *J. Mol. Neurosci.* 52, 366–377. doi: 10.1007/s12031-013-0157-7

Pap, R., Pandur, E., Jánosa, G., Sipos, K., Agócs, A., and Deli, J. (2021). Lutein exerts antioxidant and anti-inflammatory effects and influences Iron utilization of BV-2 microglia. *Antioxidants* 10:363. doi: 10.3390/antiox10030363

Pap, R., Pandur, E., Jánosa, G., Sipos, K., Nagy, T., Agócs, A., et al. (2022). Lutein decreases inflammation and oxidative stress and prevents Iron accumulation and lipid peroxidation at glutamate-induced neurotoxicity. *Antioxidants* 11:269. doi: 10.3390/antiox11112269

Park, J. S., Park, J. H., and Kim, K. Y. (2019). Neuroprotective effects of myristargenol A against glutamate-induced apoptotic HT22 cell death. *RSC Adv.* 9, 31247–31254. doi: 10.1039/c9ra05408a

Pérez-Torres, I., Castrejón-Téllez, V., Soto, M. E., Rubio-Ruiz, M. E., Manzano-Pech, L., and Guarner-Lans, V. (2021). Oxidative stress, plant natural antioxidants, and obesity. *Int. J. Mol. Sci.* 22:1786. doi: 10.3390/ijms22041786

Phoraksa, O., Chimkerd, C., Thiyajai, P., Judprasong, K., Tuntipopipat, S., Tencomnao, T., et al. (2023). Neuroprotective effects of *Albizia lebbeck* (L.) Benth. Leaf extract against glutamate-induced endoplasmic reticulum stress and apoptosis in human microglial cells. *Pharmaceuticals* 16:989. doi: 10.3390/ph16070989

Sacks, D., Baxter, B., Campbell, B. C. V., Carpenter, J. S., Cognard, C., Dippel, D., et al. (2018). Multisociety consensus quality improvement revised consensus statement for endovascular therapy of acute ischemic stroke. *Int. J. Stroke* 13, 612–632. doi: 10.1177/1747493018778713

Saitoh, M., Nishitoh, H., Fujii, M., Takeda, K., Tobiume, K., Sawada, Y., et al. (1998). Mammalian thioredoxin is a direct inhibitor of apoptosis signal-regulating kinase (ASK) 1. *EMBO J.* 17, 2596–2606. doi: 10.1093/emboj/17.9.2596

Salim, S. (2014). Oxidative stress and psychological disorders. *Curr. Neuropharmacol.* 12, 140–147. doi: 10.2174/1570159x11666131120230309

Sies, H., and Jones, D. P. (2020). Reactive oxygen species (ROS) as pleiotropic physiological signalling agents. *Nat. Rev. Mol. Cell Biol.* 21, 363–383. doi: 10.1038/s41580-020-0230-3

Silván, J. M., Reguero, M., and de Pascual-Teresa, S. (2016). A protective effect of anthocyanins and xanthophylls on UVB-induced damage in retinal pigment epithelial cells. *Food Funct.* 7, 1067–1076. doi: 10.1039/c5fo01368b

Singhrang, N., Tocharus, C., Thummayot, S., Sutheerawattananonda, M., and Tocharus, J. (2018). Protective effects of silk lutein extract from *Bombyx mori* cocoons on β-amyloid peptide-induced apoptosis in PC12 cells. *Biomed. Pharmacother.* 103, 582–587. doi: 10.1016/j.biopha.2018.04.045

Son, Y., Cheong, Y. K., Kim, N. H., Chung, H. T., Kang, D. G., and Pae, H. O. (2011). Mitogen-activated protein kinases and reactive oxygen species: how can ROS activate MAPK pathways? *J. Signal. Transduct.* 2011:792639. doi: 10.1155/2011/792639

Song, J. H., Kim, S. Y., Hwang, G. S., Kim, Y. S., Kim, H. Y., and Kang, K. S. (2019a). Sanguiin H-11 from Sanguisorbae radix protects HT22 murine hippocampal cells against glutamate-induced death. *Bioorg. Med. Chem. Lett.* 29, 252–256. doi: 10.1016/j.bmcl.2018.11.042

Song, J. H., Lee, H. J., and Kang, K. S. (2019b). Procyanidin C1 activates the Nrf2/HO-1 signaling pathway to prevent glutamate-induced apoptotic HT22 cell death. *Int. J. Mol. Sci.* 20:142. doi: 10.3390/ijms20010142

Stanciu, M., Wang, Y., Kentor, R., Burke, N., Watkins, S., Kress, G., et al. (2000). Persistent activation of ERK contributes to glutamate-induced oxidative toxicity in a neuronal cell line and primary cortical neuron cultures. *J. Biol. Chem.* 275, 12200–12206. doi: 10.1074/jbc.275.16.12200

Szydlowska, K., Gozdz, A., Dabrowski, M., Zawadzka, M., and Kaminska, B. (2010). Prolonged activation of ERK triggers glutamate-induced apoptosis of astrocytes: neuroprotective effect of FK506. *J. Neurochem.* 113, 904–918. doi: 10.1111/j.1471-4159.2010.06656.x

Vaglio-Garro, A., Kozlov, A. V., Smirnova, Y. D., and Weidinger, A. (2024). Pathological interplay between inflammation and mitochondria aggravates glutamate toxicity. *Int. J. Mol. Sci.* 25:2276. doi: 10.3390/ijms25042276

Wang, T., Gao, L., Tan, J., Zhuoma, D., Yuan, R., Li, B., et al. (2024). The neuroprotective effect of Sophocarpine against glutamate-induced HT22 cell cytotoxicity. *J. Oleo Sci.* 73, 359–370. doi: 10.5650/jos.ess23089

Wang, B., Liu, H., Yue, L., Li, X., Zhao, L., Yang, X., et al. (2016). Neuroprotective effects of pterostilbene against oxidative stress injury: involvement of nuclear factor erythroid 2-related factor 2 pathway. *Brain Res.* 1643, 70–79. doi: 10.1016/j.brainres.2016.04.048

Winyard, P. G., Moody, C. J., and Jacob, C. (2005). Oxidative activation of antioxidant defence. *Trends Biochem. Sci.* 30, 453–461. doi: 10.1016/j.tibs.2005.06.001

Wu, W., Li, Y., Wu, Y., Zhang, Y., Wang, Z., and Liu, X. (2015). Lutein suppresses inflammatory responses through Nrf2 activation and NF-κB inactivation in lipopolysaccharide-stimulated BV-2 microglia. *Mol. Nutr. Food Res.* 59, 1663–1673. doi: 10.1002/mnfr.201500109

Xia, Z., Dickens, M., Raingeaud, J., Davis, R. J., and Greenberg, M. E. (1995). Opposing effects of ERK and JNK-p38 MAP kinases on apoptosis. *Science* 270, 1326–1331. doi: 10.1126/science.270.5240.1326

Xie, R., Zhao, W., Lowe, S., Bentley, R., Hu, G., Mei, H., et al. (2022). Quercetin alleviates kainic acid-induced seizure by inhibiting the Nrf2-mediated ferroptosis pathway. *Free Radic. Biol. Med.* 191, 212–226. doi: 10.1016/j.freeradbiomed.2022.09.001

Yuan, C., Chen, H., Wang, Y., Schneider, J. A., Willett, W. C., and Morris, M. C. (2021). Dietary carotenoids related to risk of incident Alzheimer dementia (AD) and brain AD neuropathology: a community-based cohort of older adults. *Am. J. Clin. Nutr.* 113, 200–208. doi: 10.1093/ajcn/nqaa303

Yue, J., and López, J. M. (2020). Understanding MAPK signaling pathways in apoptosis. *Int. J. Mol. Sci.* 21:2346. doi: 10.3390/ijms21072346

Zhang, C. J., Wang, Z., Zhao, J. Y., Li, Q., Huang, C. Q., Zhu, L. H., et al. (2016). Neuroprotective effect of lutein on NMDA-induced retinal ganglion cell injury in rat retina. *Cell. Mol. Neurobiol.* 36, 531–540. doi: 10.1007/s10571-015-0231-5

Frontiers in Pharmacology

Explores the interactions between chemicals and living beings

The most cited journal in its field, which advances access to pharmacological discoveries to prevent and treat human disease.

Discover the latest Research Topics

See more →

Frontiers

Avenue du Tribunal-Fédéral 34
1005 Lausanne, Switzerland
frontiersin.org

Contact us

+41 (0)21 510 17 00
frontiersin.org/about/contact